Disseny, síntesi, avaluació farmacològica i modelatge molecular de nous inhibidors de l'acetilcolinesterasa de lloc d'unió dual

Carlos Galdeano Cantador

Farmacologia i Química Terapèutica
acia

dicina de la Universitat de Barcelona

rcelona

Disseny, síntesi , avaluació farmacològica i modelatge molecular de nous inhibidors de l'acetilcolinesterasa de lloc d'unió dual

Carlos
Galdeano

DISSENY SÍNTESI AVALUACIÓ FARMACOLÒGICA I MODELATGE MOLECULAR DE NOUS INHIBIDORS DE L'AChE DE LLOC D'UNIÓ DUAL

CARLOS GALDEANO CANTADOR

2012

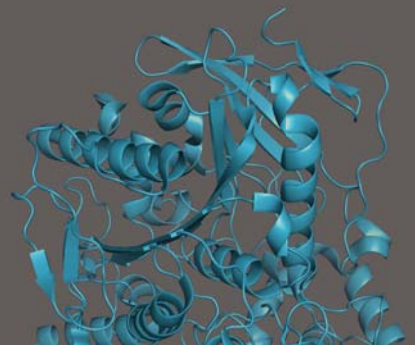

LABORATORI DE QUÍMICA FARMACÈUTICA
DEPARTAMENT DE FARMACOLOGIA I QUÍMICA TERAPÈUTICA
FACULTAT DE FARMÀCIA
I
INSTITUT DE BIOMEDICINA DE LA UNIVERSITAT DE BARCELONA (IBUB)

DISSENY, SÍNTESI, AVALUACIÓ FARMACOLÒGICA I MODELATGE MOLECULAR DE NOUS INHIBIDORS DE L'ACETILCOLINESTERASA DE LLOC D'UNIÓ DUAL

Carlos Galdeano Cantador

Barcelona, 2012

LABORATORI DE QUÍMICA FARMACÈUTICA
DEPARTAMENT DE FARMACOLOGIA I QUÍMICA TERAPÈUTICA
FACULTAT DE FARMÀCIA
I
INSTITUT DE BIOMEDICINA DE LA UNIVERSITAT DE BARCELONA (IBUB)

Programa de Doctorat:
Química Orgànica en la Indústria Químico-Farmacèutica
Bienni 2006-2008

DISSENY, SÍNTESI, AVALUACIÓ FARMACOLÒGICA I MODELATGE MOLECULAR DE NOUS INHIBIDORS DE L'ACETILCOLINESTERASA DE LLOC D'UNIÓ DUAL

Memòria presentada per Carlos Galdeano Cantador per a optar al títol de Doctor per la Universitat de Barcelona

Dirigida per:

Dr. Diego Muñoz-Torrero López-Ibarra **Dr. F. Javier Luque Garriga**

Carlos Galdeano Cantador
Barcelona, 2012

Als meus pares

AGRAÏMENTS

Fa quasi bé 10 anys que vaig trucar a la porta del Laboratori de Química Farmacèutica per intentar fer un Treball Dirigit, feia segon de carrera, mai hagués imagina't que un dia com avui estaria escribint aquesta pàgina donant gràcies a tanta gent. El camí ha estat molt llarg, potser massa i tot, i segur que em deixaré molta gent, segur! No obstant, als que esteu nombrats i als que no: GRÀCIES!

Abans de res m'agradaria agrair el suport incondicional dels meus Directors de Tesi, Diego Muñoz-Torrero i Javi Luque. És molt difícil expressar tota la gratitud que tinc cap a Diego i Javi. Diego ha estat el millor jefe que podia tenir, el millor exemple a seguir com a persona i com a científic, *gracias.* Javi em va acollir al seu grup com un "computacional" més. *Gràcies Javi per inculcar-me aquesta passió pel treball ben fet i per la ciència i per la teva implicació personal en tot moment tant professional com personal.*

Tampoc m'agradaria oblidar-me aquí d'altres "professors" als quals dec molt professionalment. Pelayo Camps, per la confiança dipositada i per introduir-me al món de la química amb tanta passió; Santi Vazquez, per tenir la porta del despatx sempre oberta per a donar *un consejo inteligente,* ja sigui químic o personal; Carmen Escolano, *porque eres muy grande*!; Ramon Pouplana, perque és un petit geni (*ile-pu*) i a Xavi Barril, un altre exemple a seguir.

És important nombrar a tots aquells grups de recerca que d'una forma o altra han col·laborat amb aquest projecte. Al grup del Dr. Rodolfo Lavilla, al grup de la Dra. Maria Isabel Rodríguez-Franco, al grup de les Dres. Vincenza Andrisano i Manuela Bartolini, al grup dels Drs. Antoni Camins i Merce Pallàs, al grup de la Dra. Cristina Minguillón i finalment, i molt especialment, al grup dels Drs. Victòria Clos i Albert Badia.

Escriure una Tesi Doctoral no és només cosa d'un sol, hi ha molta gent que en algun moment, amb la seva feina, fa més fàcil la teva. Aquí m'agradaria agrair el treball i el suport de les nostres secretàries: Manolita (un mite), Cati i finalment Maite. L'ajuda de Javier. I como no de Rita, por sus "buenos días" sin igual. També m'agradaria agrair aquí l'ajuda de tota la gent dels Serveis Científico-Tècnics de la UB i del CSIC.

Aquest camí tan llarg m'ha permès conèixer altres Laboratoris. Gràcies a tota la gent de l'Autònoma per la seva col·laboració i acollida, especialment a Victòria Clos, Albert Badia, Belén Perez, Miriam Ratia i Júlia Relat. És molt difícil nombrar a tothom amb qui he compartit alguna cosa al Laboratori de Farmacologia de la UAB, però *gràcies a tots*. Également à remercier tous ceux qui m'ont aidé dans mon séjour à Gif sur Yvette, especialment Catherine, Thierry, Zoila et Manuel. And thanks to all group members of Carlier's group in the Virginia Tech, specially to Paul and his family, Dawn Wong, Ming Ma and Eeeeugene.

També m'agradaria agrair l'ajuda dels que em van acompanyar als inicis del doctorat, concretament als cursos de València: Carlos, Slavo, Lucia & Lucia, Laura, Pau i Sara. I tota aquella gent del Laboratori de Química Orgànica, de la Facultat de Farmàcia, de LIDQO i de Salvat que m'he anat trobant durant aquesta Tesi Doctoral.

Amb tants anys al Laboratori de Química Farmacèutica he conegut molta gent, tots, en algun moment o altre han estat importants per aquesta Tesi. La primera persona que m'agradaria nombrar és a Xavi Formosa, el meu "mentor", ell em va deixar la flama del nostre tema i jo la vaig agafar molt orgullós, *gràcies Xavi!.* No em puc oblidar aquí d'Elena, Laura, Carles Ayats, Michelle i especialment Loli, Rosa i Jose, *gracias a los tres por vuestra amistat en el tiempo*. També m'agradaria agrair a Jordi Rull els bons moments que hem tingut al lab. i fora d'ell.

Si avancem en el temps ens trobarem amb la Lorena, que voy a decir de la Paye*, sabes que te quiero mucho;* Tània, no ho negaré, té una mica de mala llet a vegades, però també té un cor que no li cap en metre i….*gràcies Tània per la teva ajuda*!!; a Evo m'agradaria agrair-li la seva sinceritat i amistat, *i els teus cantics de sirena, mec mec*!; Irene, quantes coses podria dir de la Irene, la més important es *que confio molt amb tu*; Ornella, tan tranquila, tan callada, però siempre dispuesta a ayudar, y que pizzas hace!; Matu, *m'encantes Matu*!; Elena, se fue pero volvió*, ahora aguanta con nosotros*!; Marta, *això no serveix per res, jajaja*!; i com no als més nous: Ane, vull dir Aneeeeee.. l'alegria de la casa; David, per la teva discreta xafarderia, el millor hereu que podia tenir en aquest aspecte i Euge, *que bueno que viniste!*. També al Toni, per ser tant bona persona i un gran cunyat. No m'agradaria oblidar-me de cap estudiant que ha passat pel lab, i dels quals es pot apendre molt: Paramgit, Diana, Silvia S., Sabin, Silvia M., Aïna, Valentina, Xavi, Aleix, Lenuta, Francesca, Magda, Stephanie, Ilaria, Marisa, Mattia, Marta (II), Rosana, Silvia C., Albert, Marc, Andrés, Claudio, Edu, Emma, Roser…..especialment a Matteo, per ser tant bona persona! Tampoc no puc oblidar-me de l'Arnau, jeje, *saps que t'aprecio molt i que has fet un amic*!

El meu pas pel "palomar" de Física també ha deixat una empremta molt important. M'agradaria agrair l'ajuda en tot moment de la gent de quart pis: Ignasi, Òscar, Peter, Moussumi, Juana, vull dir Montse, Jesús, Dani, Patricio, Sergi, Adrián Roitberg, Carolina, Carles Curu i molt especialment als que m'han acompanyat en el meu dia a dia. M'agradaria agrair a l'Axel la seva ajuda inestimable i la seva amistat, *m'ha agradat molt treballlar amb tu*!; a Flavio, perque sense ell aquest laboratori no seria el mateix; a la *mama* Assumpta, perque jo de gran vull ser com ella!; a Ana, *por tu simpatía*; a Salomé, sempre disposada a ajudar, una gran persona; i finalment a Jodi, perque si no li tens en compte que li falta caràcter (ironia) i que és el meu marit, jo el considero un gran amic, yeah!

Finalment encara que no estiguin directament involucrats en aquesta Tesi només tinc paraules d'agraïment per als meus amics, els de la Uni (que després de tants anys no té sentit que encara ens diguem els de la Uni), els d'Alella i els de Tortosa. També agrair molt sincerament el suport que sempre he sentit de la meva familia, especialment del meus pares, el meu germà i "els meus sogres", Eli i Toni.

I ara si, per acabar m'agradaria agrair-li tot a la persona més especial, l'Eli. No tinc paraules per descriure tot el suport, ajuda i comprensió que m'ha donat durant aquests anys, és impossible. *Només m'agradaria que aquest camí que vam començar, en part gràcies a aquesta Tesi, no s'acabi mai*!

El treball experimental recollit en aquesta memòria s'ha realitzat al Laboratori de Química Farmacèutica de la Facultat de Farmàcia de la Universitat de Barcelona sota la direcció del Dr. Diego Muñoz-Torrero i al Departament de Fisicoquímica de la Facultat de Farmàcia de la Universitat de Barcelona sota la direcció del Dr. F. Javier Luque. La part d'avaluació farmacològica s'ha realitzat al Departament de Farmacologia, Terapèutica i Toxicologia de la Facultat de Medicina de la Universitat Autònoma de Barcelona sota la direcció dels Drs. Albert Badia i M. Victòria Clos.

Aquesta Tesi Doctoral ha estat possible gràcies a la concessió d'una *Beca de Col·laboració en Projectes de Recerca* per a estudiants de tercer cicle per part de l'Institut de Biomedicina de la Universitat de Barcelona (IBUB), al qual m'agradaria expressar la meva gratitud.

El present treball ha estat finançat pel *Ministerio de Ciencia e Innovación* (projectes CTQ2005-02192/BQU, CTQ2008-03768/PPQ i SAF2008-05595) i per l'AGAUR de la *Generalitat de Catalunya* (2005SGR00180, 2009SGR1396 i 2009SGR00249). Els càlculs computacionals han estat realitzats a la Supercomputadora Mare Nostrum del *Barcelona Supercomputing Centre*.

Pròleg

Aquesta Tesi Doctoral es presenta com a *Compendi de publicacions*. S'ha dividit en 6 capítols que d'acord amb la normativa vigent, inclouen un apartat d'introducció, uns objectius, la discussió dels resultats, les còpies completes de les publicacions i un resum global i conclusions. La discussió dels resultats es mostra abans de la publicació corresponent i exposa el treball realitzat per mi mateix en la publicació a la qual precedeix.

El Capítol 1 consisteix en una introducció general de la malatia d'Alzheimer i de les actuals estratègies terapèutiques per combatre-la. S'explica d'una forma més extensa el paper de l'enzim acetilcolinesterasa, proteïna clau en aquesta Tesi Doctoral. També trobem aquí una breu descripció dels antecedents del nostre grup en aquesta línia de recerca.

En el Capítol 2 es plantejen els objectius d'aquesta Tesi Doctoral per a cadascun dels treballs, els quals queden recollits en els següents quatre capítols.

En el Capítol 3 s'inclou la publicació "*Novel Donepezil-Based Inhibitors of Acetyl- and Butyrylcholinesterase and Acetylcholinesterase-Induced β-Amyloid Aggregation*" (*J. Med. Chem.* **2008**, *51*, 3588–3598). Els objectius d'aquest treball se centren únicament en la part sintètica dels compostos. El Capítol 4 recull la síntesi química i la farmacologia de la publicació "*Pyrano[3,2-c]quinoline-6-Chlorotacrine Hybrids as a Novel Family of Acetylcholinesterase- and β-Amyloid-Directed Anti-Alzheimer Compounds*" (*J. Med. Chem.* **2009**, *52*, 5365–5379). En canvi, el Capítol 5 gira en tot moment sobre els estudis de modelatge molecular que es van realitzar per a la publicació "*Novel Huprine Derivatives with Inhibitory Activity toward β-Amyloid Aggregation and Formation as Disease- Modifying Anti-Alzheimer Drug Candidates*" (*ChemMedChem* **2010**, 5, 1855–1870). L'última publicació s'adjunta en el Capítol 6 i se centra en la síntesi enantiopura i el modelatge molecular d'heterodímers huprina–tacrina; "*Huprine–Tacrine Heterodimers as Anti-Amyloidogenic Compounds of Potential Interest against Alzheimer's and Prion Diseases*" (*J. Med. Chem.* **2012***, 55,* 661–669).

La memòria també inclou un apartat amb les conclusions finals en forma de resum i dos apartats annexos on es descriuen els mètodes en química computacional emprats i altres publicacions que han sorgit d'aquesta Tesi Doctoral.

Abreviatures

aa	aminoàcid
ACh	Acetilcolina
AChE	Acetilcolinesterasa
ApoE	Apoliproteïna E
APP	Proteïna precursora de l'amiloide
ATCh	Acetiltiocolina
βA	β-amiloide
βA_{42}	β-amiloide de 42 aminoàcids
bAChE	Acetilcolinesterasa bovina
BACE-1	β-secretasa
BB	*Backbone*
BChE	Butirilcolinesterasa
BHE	Barrera hematoencefàlica
BS	*Binding site*
BTCh	Butiriltiocolina
CG	*Conjugate gradient*
DEA	Dietilamina
DDQ	2,3-dicloro-5,6-dicianobenzoquinona
DM	Dinàmica molecular
DTNB	àcid 5,5'-ditio*bis*(2-nitrobenzoic)
EDC	1-etil-3-(3'-dimetilaminopropil)carbodiïmida
Eq.	Equació
FDA	*Food and Drug Administration*
hAChE	Acetilcolinesterasa humana
hBChE	Butirilcolinesterasa humana
HOBt	Hidroxibenzotriazol
HPLC	Cromatografia líquida d'alta pressió
IC_{50}	concentració que inhibeix el 50% de l'activitat enzimàtica

iMAO	inhibidor de la monoamino oxidasa
Ki	Constant d'inhibició
MA	Malaltia d'Alzheimer
mAChE	Acetilcolinesterasa de ratolí
min	minut
MM/PBSA	Molecular Mechanics / Poisson-Boltzman Surface Area
MPLC	Cromatografia líquida de pressió mitjana
MRI	*Magnetic resonance imaging*
MRS	*Proton magnetic resonance spectroscopy*
QM	*Quantum mechanics*
PDB	*Protein Data Bank*
PET	*Positron emission tomography*
PKC	Protein–quinasa C
PrP	Pèptid priònic
RESP	*Restrained electrostatic potential*
RMN	Ressonància Magnètica Nuclear
RMSD	*Root-mean square desviation*
SD	*Steepest-descent*
SIE	*Solvent interaction energies*
SNC	Sistema nerviós central
*Tc*AChE	Acetilcolinesterasa de *Torpedo californica*
t_r	Temps de retenció

Índex

Capítol 1: Introducció

A principis de l'any 1901 el psiquiatra i neurobiòleg de l'Hospital de Frankfurt Alois Alzheimer va assistir per primer cop Auguste D., una dona de 51 anys que durant 5 anys va anar perdent gradualment la memòria. La complicació del quadre clínic que presentava aquella senyora va ser analitzada per Alzheimer i altres facultatius. Cinc anys després del seu ingrés a l'hospital, la pacient va morir per una septicèmia. Una nova malaltia s'havia descobert…

1.1 La malaltia d'Alzheimer

El 4 de novembre de 1906 el Dr. Alois Alzheimer va presentar en la XXXVII Conferència de Psiquiatria a Tübingen la comunicació: "*Sobre una malaltia específica severa de l'escorça cerebral*"[1] en la qual per primer cop es descrivia una inusual malaltia caracteritzada per pèrdua de memòria, desorientació, al·lucinacions i demència.

En l'actualitat, la incidència de la Malaltia d'Alzheimer (MA) ha anat augmentant dràsticament fins a esdevenir la causa més comuna de deterioració mental entre la gent d'edat avançada, representant més del 50% de tots els casos de demència en persones majors de 65 anys en els països occidentals.[2] Estudis recents mostren que actualment la MA afecta al voltant de 36 milions de persones a tot el món,[3] i que el 6% de la població major de 65 anys i el 30% de la població major de 85 anys pateix la malaltia,[4] depenent dels països i de les ètnies. Tot i així no s'espera que aquest creixement pari, es preveu que l'any 2030 hi hagi 66 milions d'afectats, i que l'any 2050 aquesta xifra arribi fins als 115 milions.[3] Així, la MA constitueix, junt amb els accidents cardiovasculars i el càncer, un dels majors problemas socio-sanitaris en països desenvolupats.

Clínicament, la MA es caracteritza per un notable deteriorament de les funcions cognitives, una pèrdua progressiva de la memòria i un descens en la capacitat d'aprenentatge, juntament amb desorientació temporal i espacial, reducció de l'habilitat per dur a terme les activitats bàsiques diàries, i un ampli ventall de símptomes neuropsiquiàtrics tals com apatia, irritabilitat, agressivitat, ansietat, depressió i al·lucinacions.[5] Tot i que no és mortal, el pacient acostuma a morir degut a infeccions víriques o bacterianes associades.[6]

La MA és essencialment un trastorn relacionat amb l'edat. Fins i tot en persones amb

---

[1]Alzheimer A. *Allegemeine Zeitschrift für Psychiatrie und Psychisch-Gerichtliche Medizin* **1907**, *64*, 146. [2] Launer, L.J.; Fratiglioni, L.; Andersen, K.; Breteler, M.M.B.; Copeland, R.J.M.; Dartigues, J.-F.; Lobo, A.; Martinez-Lage, J.; Soininen, H.; Hofman, A. En "*Alzheimer's Disease and Related Disorders: Etiology, Pathogenesis and Therapeutics*"; Iqbal, K.; Swaab, D.F.; Winblad, B.; Wisniewski, H.M. Eds. John Wiley & Sons, New York, **1999**. [3]Alzheimer's Disease International. *World Alzheimer Report: The benefits of early diagnosis and intervention* **2011**. [4]Walsh, D.M.; Selkoe, D.J. *Neuron* **2004**, *44*, 181. [5]Cummings, J.L.; Askin-Edgar, S. *CNS Drugs* **2000**, *13*, 385. [6]Leonard, B.E. *Hum. Psychopharmacol.* **1998**, *13*, 83.

antecedents familiars de MA (MA familiar), la seva probabilitat de desenvolupar la malaltia és mínima. En realitat, la predisposició genètica s'associa tan sols amb un 3% dels pacients amb MA.[7] Es coneixen tres tipus principals de mutacions sobre gens que codifiquen la formació de proteïnes transmembrana que condueixen a una aparició ràpida de la MA: el gen que codifica la proteïna precursora del β-amiloide (APP) sobre el cromosoma 21,[8] la presenilina-1 sobre el cromosoma 14,[9] i la presenilina-2 sobre el cromosoma 1.[10] No obstant això, és important emfatitzar que la majoria de pacients amb MA no presenten antecedents familiars de la malaltia ni mostren mutacions patològiques en aquests gens. Per tant, en la majoria dels casos (MA esporàdica), la malaltia no sembla estar causada per defectes genètics.

Tot i la gran quantitat d'estudis científics desenvolupats, la MA continua sent un enigma, però gràcies als descobriments realitzats en el camp de la biologia molecular en els darrers 25 anys ha augmentat en gran mesura el coneixement d'aquest trencaclosques molecular.

1.2 La malaltia d'Alzheimer: una malaltia multifactorial amb constants descobriments. Patogènia.

Els dos signes neuropatològics més característics de la MA són les plaques senils i els cabdells degeneratius neurofibril·lars, formats fonamentalment per pèptid β-amiloide (βA) i per proteïna *tau* hiperfosforilada, respectivament. Aquestes dues proteïnes semblen ser la base de la patogènesi de la malaltia.[11] Existeix un debat entre quina de les dues proteïnes és la desencadenant i quina la conseqüència del procés neurodegeneratiu de la MA, i fins i tot si ambdues són lesions que representen un efecte més causat per la malaltia.[12] Tot i així, fins el moment, la hipòtesi més acceptada sobre la causa de la MA és la hipòtesi de la cascada de l'amiloide. Aquesta hipòtesi col·loca el pèptid βA a l'inici de la cascada de processos neurotòxics que condueixen a una degeneració neuronal generalitzada i a la simptomatologia clínica de la demència.[13,14]

---

[7] Lahiri, D.K.; Farlow, M.R.; Sambamurti, K.; Greig, N.H.; Giacobini, E.; Schneider, L.S. *Curr. Drug Targets* **2003**, *4*, 97. [8]Goate, A.; Chartier-Harlin, N.C.; Mullan, M.; Brown, J.; Crawford, F.; Fidani, L.; Giuffra, L.; Haynes, A.; Irving, N.; James, L.; Mant, R.; Newton, P.; Rooke, K.; Roques, P.; Talbot, C.; Pericak-Vance, M.; Roses, A.; Williamson, R.; Rossor, M.; Owen, M.; Hardy, J. *Nature* **1991**, *349*, 704. [9]Sherrington, R.; Rogaev, E.I.; Liang, Y.; Rogaeva, E.A.; Levesque, G.; Ikeda, M.; Chi, H.; Lin, C.; Li, G.; Holman, K.; Tsuda, T.; Mar, L.; Foncin, J.-F.; Bruni, A.C.; Montesi, M.P.; Sorbi, S.; Rainero, I.; Pinessi, L.; Nee, L.; Chumakov, I.; Pollen, D.; Brookes, A.; Sanseau, P.; Polinsky, R.J.; Wasco, W.; Da Silva, H.A.R.; Haines, J.L.; Pericak-Vance, M.A.; Tanzi, R.E.; Roses, A.D.; Fraser, P.E.; Rommens, J.M.; St George-Hyslop, P.H. *Nature* **1995**, *375*, 754. [10]Levy-Lehad, E.; Wijsman, E.M.; Nemens, E.; Anderson, A.L.; Goddard, K.A.B.; Weber, J.L.; Bird, T.D.; Schellenberg, G.D. *Science* **1995**, *269*, 970. [11]Klafki, H-W.; Staufenbiel, M.; Kornhuber, J.; Wiltfang, J. *Brain* **2006**, *129*, 743. [12]Castellani, R.J.; Zhu, X.; Lee, H-G.; Moreira, P.I.; Perry, G.; Smith, M.A. *Expert Rev. Neurother*. **2007**, 7, 473. [13]Hardy, J.; Allsop, D.; *Trends Pharm. Sci.* **1991**, *12*, 383. [14]Hardy, J. *Curr. Alzheimer Res*. **2006**, *3*, 71.

El βA és un pèptid de 38 a 42 aminoàcids, que prové de la ruptura proteolítica de l'APP. L'APP, de forma natural, és degradat per l'acció seqüencial dels enzims α- i γ-secretasa, proporcionant pèptids no amiloidogènics amb propietats neurotròfiques i neuroprotectores.[15] De forma alternativa, però, l'APP és processat per l'acció seqüencial dels enzims β- i γ-secretasa, donant lloc a la formació del pèptid βA (Figura 1.1).

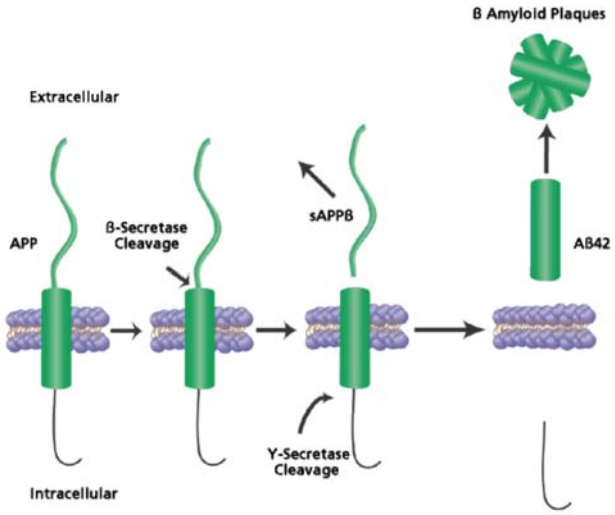

Figura 1.1 Esquema sobre la via patològica de ruptura proteolítica de l'APP. (Font de l'imatge: www.sigma-aldrich.com)

En els pacients amb MA, la formació del pèptid βA, en particular la forma de 42 aminoàcids (βA_{42}), que és la més neurotòxica i insoluble, es troba anormalment augmentada. Aquest pèptid experimenta un canvi conformacional cap a una estructura rica en làmines β, amb major tendència a formar agregats insolubles.[15] La seva posterior deposició sobre les neurones en forma de plaques d'amiloide (plaques senils) dispara una cascada de processos neurotòxics que finalment condueix a una disfunció i mort neuronal generalitzada (Figura 1.1 i 1.2), provocant un dèficit de neurotransmissors en el sistema nerviós central (SNC). En particular, les neurones colinèrgiques i glutamatèrgiques semblen ser les més vulnerables als efectes neurotòxics desencadenats pel pèptid βA.

Les plaques senils són estructures extracel·lulars compactes i esfèriques de 60 μm de diàmetre aproximadament, localitzades al parèmquima del teixit cerebral. Al microscopi electrònic s'observa que les plaques senils estan formades per un material central, d'aspecte dens i constituït per elements proteics insolubles, i per una regió perifèrica constituïda per terminacions nervioses, tant dendrítiques com axonals, en degeneració.

[15]Coughlan, C.M.; Breen, K.C; *Pharmacol. Therapeut* **2000**, *86*, 111.

No obstant, dins la placa d'amiloide no només trobem el pèptid βA, sinó que també apareixen una sèrie d'altres proteïnes, tant en el nucli central com en la perifèria, que corresponen a factors involucrats en l'agregació del pèptid βA, les quals podem anomenar-se "xaperones moleculars".[16] Entre aquests components, hi ha alguns que són comuns a tots els tipus d'amiloide, com és el cas dels proteoglicans. També s'observen proteïnes típiques de matrius extracel·lulars com el col·lagen de tipus IV, l'entactina i la laminina. A més, principalment a la regió central de la placa, trobem altres proteïnes com l'α_1-antiquimiotripsina, la ubiqüitina, les proteïnes lisosomals, l'acetilcolinesterasa (AChE) i l'apoliproteïna E (apoE).[16] La funció d'aquestes "xaperones moleculars" sembla estar relacionada amb la modulació positiva o negativa de l'agregació del pèptid en oligòmers, protofibres o fibres d'amiloide.

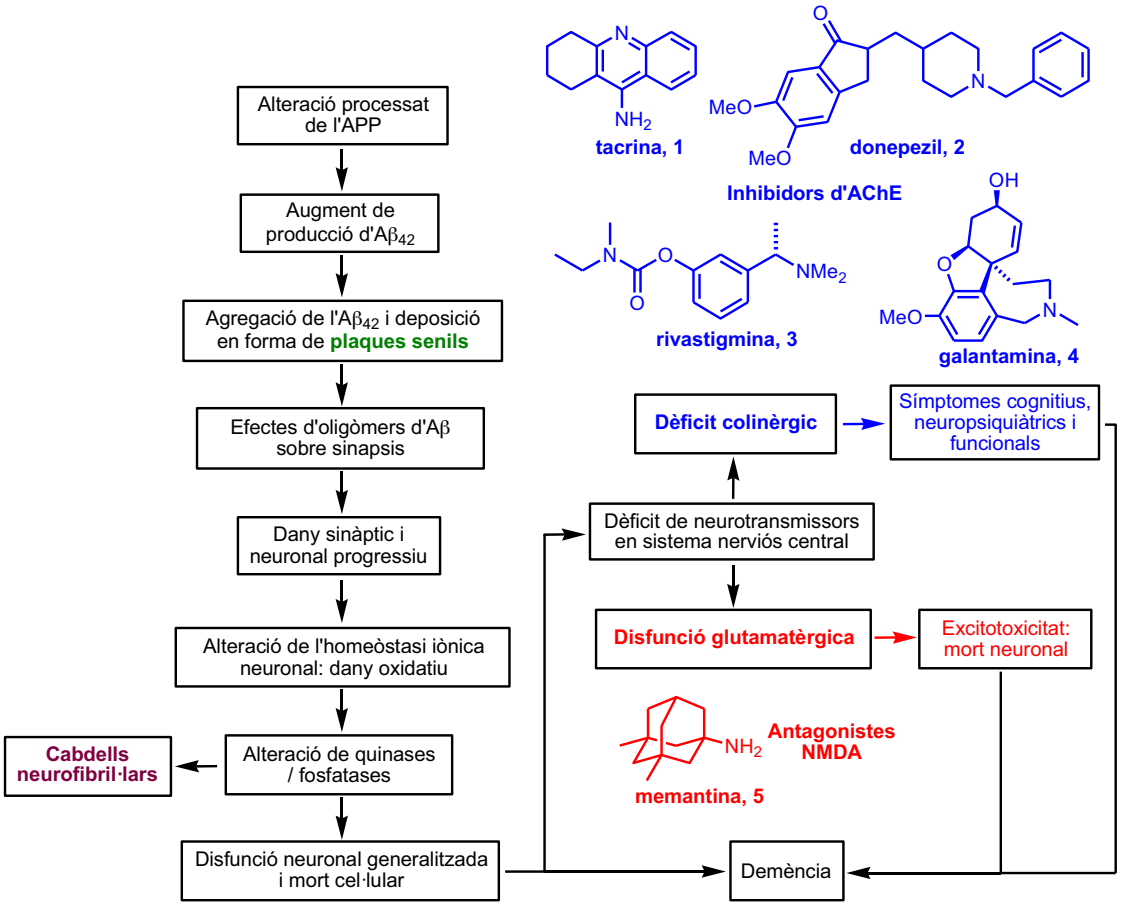

Figura 1.2 Cascada de neurodegeneració de la MA i fàrmacs aprovats que actuen sobre el dèficit de neurotransmissors que provoca la disfunció neuronal.

Els cabdells neurofibril·lars són el segon tipus de lesió cerebral present en els pacients amb MA. Aquests cabdells són filaments intracel·lulars que mesuren 20 nm en la seva zona més ampla i 8 nm en el seu punt més estret i estan constituïts majoritàriament per la proteïna *tau*.

[16] Inestrosa, N.C., *Las incomunicaciones del Alzheimer*, Atenea Impresores Ltda. **2007**.

La proteïna *tau* és una de les proteïnes que associa els microtúbuls entre ells per tal que s'estabilitzin. La fosforilació i desfosforilació reversible de la proteïna *tau* regula la seva unió als microtúbuls. En els cabdells neurofibril·lars aquesta proteïna es troba anormalment hiperfosforilada.[17]

A la MA totes les isoformes de la *tau* poden fosforilar-se excessivament i, en lloc de lligar-se als microtúbuls, poden lligar-se les unes a les altres, desestabilitzant el citoesquelet neuronal i acumular-se en agregats intracel·lulars per formar els cabdells característics.

Encara que la majoria d'hipòtesis se centren al voltant del pèptid βA com el causant principal que dispara el procés degeneratiu, l'etiologia de la malaltia és encara desconeguda. La MA és una malaltia multifactorial causada per diferents factors genètics, ambientals i endògens. Dins aquests factors endògens també podríem incloure un plegament erroni i agregació de diverses proteïnes, sovint relacionades amb el sistema ubiqüitina-proteosoma, estrés oxidatiu i formació de radicals lliures,[18] anormalitats en el processos energètics del mitocondri[19] i diferents procesos de neuroinflamació.[20] Aquestes evidències i el coneixement sobre la patogènesi de la malatia mostren el camí per a l'obtenció de teràpies racionals per atacar directament les causes moleculars de la MA.

1.3 Estratègies terapèutiques de la MA

De cara a retardar o prevenir el procés neurodegeneratiu de la MA, el pèptid βA constitueix la principal diana biològica. Així, en els darrers anys s'han estat duent a terme grans esforços en investigació per tal de desenvolupar fàrmacs anti-Alzheimer modificadors de la malaltia, sobretot, a nivell de formació i agregació del βA.[21,22]

Els assaigs clínics inicials amb els agents dirigits a inhibir el pèptid βA han estat bastant decebedors. El desenvolupament de la vacuna AN1792 i del tramiprosat, un inhibidor de l'agregació del βA i de la formació de plaques amiloides, es van suspendre a causa de problemes de seguretat i eficàcia, respectivament. Mentre que trobar el primer agent terapèutic modificador de la malaltia segueix sent difícil d'assolir, els enfocaments alternatius estan avançant en els estudis clínics, incloent la segona generació de vacunes de βA amb

[17]Goedert, M. *Trends Neurosci.* **1993**, *16,* 460. [18]Schubert, S.; Behl, C.; Lesley, R.; Brack, A.; Dargusch, R.; Sagara, Y.; Kumura, H. *Proc. Natl. Acad. Sci. USA* **1995**, *92*, 1989. [19]Olanow, C.W. *Trends Neurosci.* **1993**, *16*, 439. [20]Eikelenboom, P.; Zhan, S.-S.; van Gool, W.A.; Allsop, D. *Trends Pharmacol. Sci.* **1994**, *15*, 447. [21]Melnikova, I. *Nat. Rev. Drug Discovery* **2007**, *6*, 341. [22]Skovronsky, D.M.; Lee, V.M.-Y.; Trojanowski, J.Q. *Annu. Rev. Pathol. Mech. Dis*. **2006**, *1*, 151

perfils de seguretat millorats en relació a l'AN1792, com les vacunes CAD-106 i la V-950 (fase I), els anticossos monoclonals anti-βA com el bapineuzumab (fase III) o el LY2062430 (fase II),[23] inhibidors de la β-secretasa (BACE-1), com el CTS-21166 (fase I),[24] i moduladors de la α-secretasa com el LY450139 i el MK 0752 (fase II) o l'E2012 (fase I),[25] entre altres.

Apart de les estratègies dirigides al pèptid βA, s'han intentat explorar altres vies per obtenir un fàrmac eficaç per al tractament de la MA. Tot i que per a la formació dels cabdells neurofibril·lars són diverses les quinases involucrades en la hiperfosforilació de la proteïna *tau*, diverses evidències han assenyalat la desregulació de les quinases Cdk5 i GSK-3β com a agents responsables.[26] Així doncs, una de les estratègies terapèutiques alternatives és la recerca d'inhibidors d'aquestes quinases amb l'objectiu de limitar la hiperfosforilació característica.

La monoamino oxidasa (MAO) és una flavoproteïna present a la membrana mitocondrial externa de les cèl·lules neuronals i glials. La MAO pot existir en dues isoformes, la MAO-A i la MAO-B. S'ha descrit que l'activitat de la MAO-B augmenta amb l'edat i es troba en concentracions elevades al voltant de les plaques senils.[27,28] A més, en el trancurs de la desaminació oxidativa de les amines biògenes, la MAO-B produeix peròxid d'hidrogen i altres espècies oxigenades reactives, fet que ha suggerit la seva possible implicació en l'estrés oxidatiu associat a la MA.[29] Degut a la seva capacitat per inhibir el dany oxidatiu, els inhibidors de la MAO-B (iMAO-B) s'han presentat com a potencials candidats en la farmacoteràpia anti-Alzheimer.[30] Clars exemples són la selegilina, **6**, i la rasagilina, **7** (Figura 1.3).

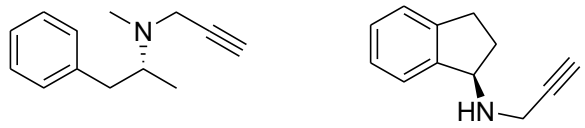

selegilina, **6** rasagilina, **7**

Figura 1.3

D'ençà que la Unió Europea va aprovar la memantina (Figura 1.2), diversos antagonistes no competitius de baixa afinitat han estat descrits per la seva capacitat de bloquejar el receptor NMDA de glutamat, evitant el flux de calci dins la cèl·lula.[31] Malauradament, cap d'ells ha superat la memantina ni ha estat capaç de revertir el procés degeneratiu.

---

[23]Yamin, G.; Ono, K.; Inayathullah, M.; Teplow, D.B. *Curr. Pharm. Design* **2008**, *14*, 3231. [24]Ghosh, A.K.; Gemma, S.; Tang, J. *Neurotherapeutics* **2008**, *5*, 399. [25]Silvestri R. *Med. Res. Rev.* **2009**, *29*, 295. [26]Buee, L.; Bussiere, T.; Buee-Scherrer, V.; Delacourte, A.; Hof, P.R. *Brain Res. Rev.* **2000**, *33*, 95. [27]Carreiras, M.C.; Marco, J.L. *Curr. Pharm. Design* **2004**, *10*, 3167. [28]Saura, J.; Luque, J.L.; Cesura, A.M.; Da Prada, M.; Chan-Palay, V.; Huber, G.; Loffler, J.; Richards, J.G. *Neurosci.* **1994**, *62*, 15. [29]Good, P.F.; Werner, P.; Hsu, A.; Olanow, C.W.; Perl, D.P. *Am. J. Pathol.* **1996**, *149*, 21. [30]Ebadi, M.; Sharma, S.; Shavadi, S.; El Refaey, K. *J. Neurosci. Res.* **2002**, *67*, 285. [31]Rogawski, M.A. *Amino Acids* **2000**, *19*, 133.

Apart de les estratègies terapèutiques esmentades, actualment existeixen diversos compostos que es troben en fase pre-clínica o en fase clínica inicial, i que poseeixen diferents perfils farmacològics basats en els coneixements adquirits els últims anys en relació a les bases moleculars de la MA. Així s'estan desenvolupant noves teràpies basades en agents anti-inflamatoris, antioxidants, estròg ens, estatines, neuroprotectors, agents neurotròfics, anti-hipertensius i queladors de zinc i de coure.[32,33]

No obstant, tenint en compte l'etiologia multifactorial de la MA, les noves estratègies terapèutiques van dirigides al desenvolupament de "compostos multipotents o multidiana". Així, el clàssic paradigma en química mèdica d'"un fàrmac, una diana" s'està canviant pel d'"un fàrmac, diverses dianes".[34] Seguint aquesta estratègia s'estan desenvolupant noves famílies estructurals de compostos capaços d'unir en una sola molècula diferents accions farmacològiques.

Fins el moment, però, l'estratègia terapèutica més rellevant per al tractament de la MA es basa en un grup de fàrmacs que van ser desenvolupats per a tractar els símptomes de la demència associada, els quals apareixen anys després de l'inici del procés neurodegeneratiu. Aquesta estratègia es basa en l'anomenada hipòtesi colinèrgica, la qual defensa que la major part de la simptomatologia associada a la MA és una causa directa d'una marcada davallada dels nivells del neurotransmissor acetilcolina (ACh) al SNC, com a conseqüència de la pèrdua de neurones alliberadores, les quals es troben situades principalment al nucli basal i projecten els seus axons cap a l'escorça cerebral i l'hipocamp. Així, és d'esperar que l'ús d'agents colinomimètics capaços de compensar aquest dèficit en el SNC puguin millorar la simptomatologia de la malaltia.[35]

L'acetilcolinesterasa (AChE) és un enzim que es troba a la sinapsi de les neurones colinèrgiques i s'encarrega de la degradació de l'ACh mitjançant la seva hidròlisi. L'estructura tridimensional de raigs X de l'enzim AChE de *Torpedo californica* va ser elucidada l'any 1991 pel grup dels Drs. Sussman i Silman (Weizman Institute, Israel).[36] El lloc actiu de l'enzim està constituït per una tríade catalítica (Ser200, His440 i Glu327, numeració corresponent a l'AChE de *Torperdo californica* (*Tc*AChE)) responsable de la hidròlisi del neurotransmissor, i per un sublloc de caràcter aniònic i hidrofòbic pròxim al lloc actiu (Trp84, Tyr130, Tyr330 i Phe330) que estabilitza la càrrega positiva del grup amoni quaternari de l'ACh, facilitant el posicionament de l'èster al lloc actiu (Figura 1.4).

---

[32]Cutler, N.R.; Sramek, J.J. *Prog. Neuro-Psychopharmacol. Biol. Psychiat.* **2001**, *25*, 27. [33]Knopman, D. *Clin. Neuropharmacol.* **2003**, *26*, 93. [34]Youdim, M.B.; Buccafusco, J.J. *Trends Pharmacol. Sci.* **2005**, *26*, 27. [35]Camps, P.; Muñoz-Torrero, D. *Mini-Rev. Med. Chem* **2002**, *2*, 11. [36]Sussman, J.L.; Harel, M.; Frolow, F.; Oefner, C.; Goldman, A.; Toker, L.; Silman, I. *Science* **1991**, *253*, 872.

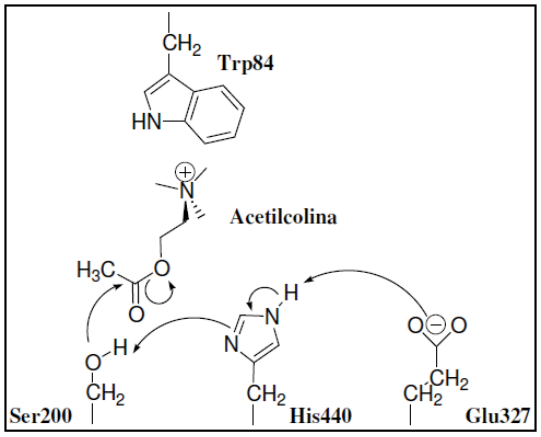

Figura 1.4 Lloc actiu de l'AChE. Esquema dels residus que intervenen en la hidròlisi de l'ACh. Tríade catalítica (Ser200, His440 i Glu327) i residu característic del sublloc aniònic (Trp84). Font de l'imatge: Introducció a la Química Terapeutica, Ediciones Díaz de Santos, Madrid, 2004.

El centre actiu o catalític, on té lloc el procés d'hidròlisi, es troba al fons d'una cavitat o gorja d'uns 20 Å de profunditat, alineada majoritàriament per residus aromàtics. És en aquesta zona central on trobem els residus Phe288 i Phe290, responsables de la selectivitat dels substrats. A l'entrada de la gorja es troba l'anomenat lloc perifèric de l'enzim (Tyr70, Asp72, Tyr121, Trp279 i Tyr334), que actua com a lloc d'unió inicial del substrat, guiant la seva entrada cap al centre actiu.[36] Així, una possible interacció amb el Trp84, residu característic del lloc actiu, o amb el Trp279, residu característic del lloc perifèric, podria ser important per a un disseny racional d'inhibidors de l'AChE (Figura 1.5).

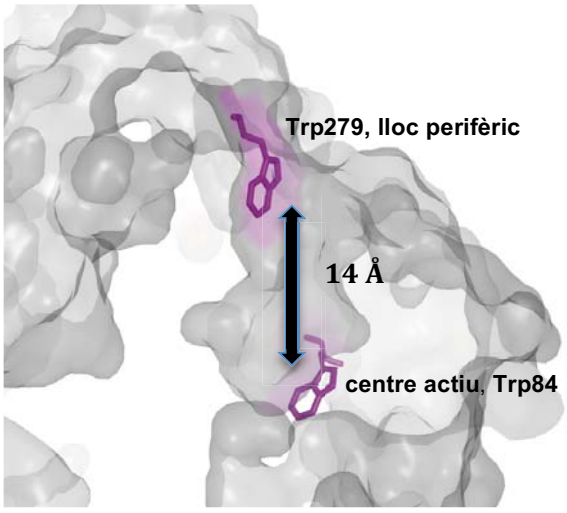

Figura 1.5 Gorja catalítica de l'AChE amb el residus característics del centre actiu i del lloc perifèric de l'enzim.

[36]Sussman, J.L.; Harel, M.; Frolow, F.; Oefner, C.; Goldman, A.; Toker, L.; Silman, I. *Science* **1991**, *253*, 872

1.3.1 Inhibidors de l'acetilcolinesterasa

Amb l'única excepció del recentment aprovat antagonista de receptors de NMDA de glutamat, memantina, els altres 4 fàrmacs anti-Alzheimer aprovats per la *U.S. Food and Drug Administration* (FDA): la tacrina, **1**, el donepezil, **2**, la rivastigmina, **3** i la galantamina, **4**, (Figura 1.2) són un grup de colinomimètics amb el perfil farmacològic d'inhibidors de l'enzim AChE. Estudis de difracció de raigs-X de monocristalls dels complexes de cadascun dels 4 inhibidors amb *Tc*AChE han permès conéixer el seu mode d'unió a l'AChE.[37,38] D'una banda, la tacrina (codi Protein Data Bank (PDB): 1ACJ), la galantamina (codi PDB: 1QTI i 1DX6) i la rivastigmina (codi PDB: 1GQR) es col·loquen en el centre actiu de l'enzim. Els dos primers duen a terme interaccions no covalents amb diferents residus característics del centre actiu, com el Trp84 (Figura 1.6). La rivastigmina també es col·loca clarament en el centre actiu de l'AChE, però a diferència dels dos anteriors, modifica covalentment el residu de Ser200, al qual transfereix el seu grup *N*-etil-*N*-metilcarbamoïl, mentre que la resta de l'inhibidor estableix interaccions amb altres residus del centre actiu de l'enzim. L'AChE carbamoïlada acaba regenerant-se per hidròlisi. Aquesta regeneració però és més lenta que en el cas de l'enzim acetilat per l'ACh, per la qual cosa la rivastigmina és considerada un inhibidor *pseudoirreversible*. El donepezil (codi PDB: 1EVE) es un inhibidor mixt i presenta un mode d'unió clarament diferenciat. Així, la molècula de donepezil ocupa tota la gorja catalítica de l'AChE, interaccionant amb residus del centre actiu i de la gorja de l'enzim, i amb el residu Trp279, característic del lloc perifèric (Figura 1.6).

tacrina, 1 (taronja)
donepezil, 2 (blau)
rivastigmina, 3 (verd)
galantamina, 4 (vermell)

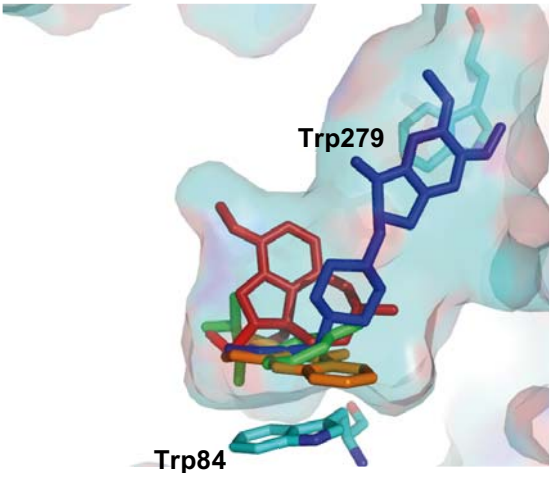

Figura 1.6 Mode d'unió dels 4 inhibidors d'acetilcolinesterasa aprovats per la FDA amb *Tc*AChE.

[37]Harel, M.; Schalk, I.; Ehret-Sabatier, L.; Bouet, F.; Goeldner, M.; Hirth, C.; Axelsen, P.; Silman, I.; Sussman, J.L. *Proc. Natl. Acad. Sci. U.S.A.* **1993**, *90*, 9031. [38]Greenblatt, H.M.; Kryger, G.; Lewis, T.; Silman, I.; Sussman, J. *FEBS Lett.* **1999**, *463*, 321.

1.3.2 Evidències d'efectes neuroprotectors dels inhibidors d'AChE

En els últims anys, l'ús dels inhibidors d'AChE ha experimentat una sèrie d'alts i baixos. Aquests fàrmacs constitueixen actualment la medicació més efectiva per a la millora a curt termini (de 6 a 12 mesos) de l'activitat cognitiva i funcional i presenten perfils de seguretat i tolerabilitat favorables.[6] Malgrat això, s'ha criticat que els resultats globals són generalment modestos, afectant només a una tercera part dels pacients tractats, i que l'ús d'aquests fàrmacs va acompanyat de freqüents, encara que suaus, efectes secundaris gastrointestinals de tipus colinèrgic.[39] No obstant, la principal objecció és que sempre han estat contemplats com un tractament merament simptomàtic de la MA, en contraposició a les teràpies dirigides al βA, per a les quals s'espera un paper modificador de la malaltia.

Tanmateix, nombrosos estudis preclínics, radiològics i clínics han evidenciat efectes neuroprotectors associats a l'ús d'inhibidors d'AChE que apunten a un paper modificador de la malaltia per part d'aquests fàrmacs.[40] Els 4 inhibidors d'AChE esmentats, i en particular el donepezil, amb el qual s'han dut a terme la majoria d'estudis, presenten algun tipus d'efecte neuroprotector en assaigs *in vitro* i *in vivo* enfront una varietat d'estímuls neurotòxics. Per exemple, s'han descrit efectes neuroprotectors d'aquests fàrmacs enfront la toxicitat induïda per glutamat[41,42] o NMDA en cultius primaris de neurones corticals de rata,[43] i enfront la toxicitat induïda per βA en cultius primaris de neurones colinèrgiques septals de rata,[44,45] cèl·lules SH-SY5Y,[46] ratolins[47] o enfront altres agents neurotòxics com el peròxid d'hidrogen[48] o el monòxid de carboni.[49] Així mateix, s'han descrit efectes neuroprotectors d'aquests fàrmacs en models de dany neuronal induït per privació d'oxigen i glucosa.[41,50-52] Anàlogament, hi ha evidències clíniques que suggereixen un efecte modificador de la malaltia per part dels inhibidors d'AChE, que semblen tenir efectes prolongats i sostinguts en el temps.[53] Diferents assaigs clínics a llarg termini (rivastigmina i donepezil fins a 5 anys, galantamina fins a 4 anys) suggereixen un enlentiment, tot i que no interrupció, del deteriorament cognitiu quan el pacient és tractat amb inhibidors d'AChE.[54]

---

[6]Leonard, B.E. *Hum. Psychopharmacol.* **1998**, *13*, 83. [39]Giacobini, E. *Neurochem. Res.* **2000**, *25*, 1185. [40]Muñoz-Torrero, D. *Neuroprotección en la enfermedad de Alzheimer*; Edicomplet **2007**, Madrid. [41]Akaike, A. *Alzheimer Dis. Assoc. Disord.* **2006**, *20(Suppl. 1)*, S8. [42]Geerts, H. *Brain. Res. Bull.* **2005**, *64*, 519. [43]Akasofu, S.; Kimura, M.; Kosasa, T.; Ogura, H.; Sawada, K. *Eur. J. Pharmacol.* **2006**, *530*, 215. [44]Kimura, M.; Akasofu, S.; Ogura, H.; Sawada, K. *Brain Res.* **2005**, *1047*, 72. [45]Kimura, M.; Komatsu, H.; Ogura, H.; Sawada, K. *Neurosci. Lett.* **2005**, *391*, 17. [46]Arias, E.; Gallego-Sandín, S.; Villarroya, M.; García, A.G.; López, M.G. *J. Pharmacol. Exp. Ther.* **2005**, *315*, 1346. [47]Meunier, J.; Ieni, J.; Maurice, T. *Br. J. Pharmacol.* **2006**, *149*, 998. [48]Zhang, H.Y.; Tang, X.C. *Neurosci. Lett.* **2000**, *292*, 41. [49]Meunier, J.; Ieni, J.; Maurice, T. *J. Pharmacol. Exp. Ther.* **2006**, *317*, 1307. [50]Riepe, M.W. *Eur. J. Neurol.* **2005**, *12(Suppl. 3)*, 3. [51]Zhou, J.; Fu, Y. ; Tang, X.C. *Neurosci. Lett.* **2001**, *306*, 53. [52]Sobrado, M.; Roda, J.M.; López, M.G.; Egea, J.; García, A.G. *Neurosci. Lett.* **2004**, *365*, 132. [53]Sabbagh, M.N.; Farlow, M.R.; Relkin, N.; Beach, T.G. *Alzheimers & Dementia* **2006**, *2*, 118. [54]Bullock, R.; Dengiz, A. *Int. J. Clin. Pract.* **2005**, *59*, 817.

L'efecte neuroprotector dels inhibidors d'AChE durant assaigs clínics ha estat també demostrat utilitzant tècniques neuroradiològiques com MRI (*Magnetic Resonance Imaging*), MRS (*proton Magnetic Resonance Spectroscopy*) i PET (*Positron Emission Tomography*).[55]

També s'ha proposat el seguiment de l'atròfia hipocampal com a marcador quantificable per comprovar l'eficàcia de fàrmacs en la modificació de la MA.[56,57] Precisament, entre les dades clíniques que suggereixen un possible efecte neuroprotector dels inhibidors d'AChE, l'evidència més convincent s'obtingué en dos estudis de MRI en els quals es va comparar el volum hipocampal de pacients tractats amb donepezil durant un any amb el de pacients no tractats. En un d'aquests estudis la proporció mitjana d'atròfia hipocampal va resultar ser d'un 3,82% en el grup tractat amb donepezil enfront el 5,04% del grup control,[58] mentre que en un altre estudi es va observar que els pacients tractats amb donepezil presentaven descensos més petits del volum hipocampal total (–0,4%) que els pacients del grup placebo (–8,2%).[59]

1.3.3 Mecanismes de neuroprotecció dels inhibidors d'AChE

Des dels primers estudis preclínics de neuroprotecció efectuats sobre els inhibidors d'AChE, va semblar que aquests fàrmacs exercien el seu efecte neuroprotector a través d'un mode d'acció diferent a la inhibició de l'enzim. El coneixement del mode d'acció responsable de l'efecte neuroprotector dels inhibidors d'AChE resulta de gran interès, sobretot de cara al disseny i desenvolupament de nous fàrmacs, que exhibint aquest mateix mode d'acció puguin presentar un efecte modificador de la malaltia optimitzat.[40]

S'han proposat diferents mecanismes a través dels quals alguns dels inhibidors d'AChE podrien exercir efectes neuroprotectors, que inclouen el bloqueig de la excitotoxicitat induïda per glutamat mitjançant antagonisme dels receptors NMDA,[60] la sobreexpressió de la proteïna antiapoptòtica *bcl*-2 mitjançant estimulació de receptors nicotínics $\alpha 7$ i $\alpha 4\beta 2$,[42,46,61] o la mobilització des del retícul endoplasmàtic de dipòsits de calci mitjançant activació de receptors σ_1.[47,49] No obstant això, les evidències més interessants sobre un mode d'acció

---

[40]Muñoz-Torrero, D. *Neuroprotección en la enfermedad de Alzheimer*; Edicomplet **2007**, Madrid. [42]Geerts, H. *Brain. Res. Bull.* **2005**, *64*, 519. [46]Arias, E.; Gallego-Sandín, S.; Villarroya, M.; García, A.G.; López, M.G. *J. Pharmacol. Exp. Ther.* **2005**, *315*, 1346. [47]Meunier, J.; Ieni, J.; Maurice, T. *Br. J. Pharmacol.* **2006**, *149*, 998. [49]Meunier, J.; Ieni, J.; Maurice, T. *J. Pharmacol. Exp. Ther.* **2006**, *317*, 1307. [55]Modrego, P.J. *Curr. Med. Chem.* **2006**, *13*, 3417. [56]Jack, C.R. Jr.; Petersen, R.C.; Xu, Y.; O-Brien, P.C.; Smith, G.E.; Ivnik, R.J.; Tangalos, E.G.; Kokmen, E. *Neurology* **1998**, *51*, 993. [57] Mori, E.; Lee, K.; Yasuda, M.; Hashimoto, M.; Kazui, H.; Hirono, N.; Matsui, M.. *Ann. Neurol.* **2002**, *51*, 209. [58]Hashimoto, M.; Kazui, H.; Matsumoto, K.; Nakano, Y.; Yasuda, M.; Mori, E. *Am. J. Psychiatry* **2005**, *162*, 676. [59]Krishnan, K.R.; Charles, H.C.; Doraiswamy, P.M.; Mintzer, J.; Weiler, R.; Yu, X.; Perdomo, C.; Ieni, J.R.; Rogers, S. *Am. J. Psychiatry* **2003**, *160*, 2003. [60] Wang, X.-D.; Chen, X.-Q.; Yang, H.-H.; Hu, G.-Y. *Neurosci. Lett.* **1999**, *272*, 21. [61]Takada-Takatori, Y.; Kume, T.; Sugimoto, M.; Katsui, H.; Sugimoto, H.; Akaike, A. *Neuropharmacology* **2006**, *51*, 474.

secundari responsable dels efectes neuroprotectors són les que suggereixen que la formació i l'agregació del βA podrien estar sota control colinèrgic. La interferència d'aquests agents en la part més alta de la cascada de neurodegeneració de la MA (Figura 1.2) té un interès evident pel que respecta a la modificació del curs de la malaltia.

Diferents estudis han establert connexions entre el sistema colinèrgic i el metabolisme de l'APP. És conegut que el carbacol, un agonista muscarínic no selectiu, augmenta la secreció del fragment no amiloidogènic sAPPα en cèl·lules que expressen receptors muscarínics M_1 i M_3, però no en cèl·lules que expressen receptors M_2 o M_4.[62] Aquest efecte és molt important si es té en compte que la formació del sAPPα implica la ruptura proteolítica de l'APP per la α-secretasa, via no patològica. En ser mútuament excloents el processat de l'APP per la α- o per la β-secretasa, l'activació de la via de la α-secretasa implicada en aquest efecte es tradueix en un bloqueig de la síntesi de pèptid βA. L'activació directa de receptors M_1 i M_3 per part d'agonistes muscarínics selectius o indirecta per part d'inhibidors d'AChE, i l'activació resultant de la protein quinasa C (PKC) pot estimular el processat de l'APP per generar components no amiloidogènics. Els efectes mostrats pels diferents inhibidors d'AChE sobre els nivells de sAPPα difereixen entre tipus cel·lulars, depenent del fàrmac específic, de la duració del tractament i de la dosi assajada.[63] L'augment dels nivells de sAPPα per part de la tacrina i el donepezil ha estat demostrat en diferents estudis *in vitro*.[64,65] Així mateix, s'han observat canvis en el processat de l'APP en estudis amb pacients tractats amb donepezil, que sembla ser capaç de restablir el balanç entre l'activitat de la α- i β-secretasa.[66,67]

1.4 Els descobriments d'Inestrosa. Connexió entre les hipòtesis amiloide i colinèrgica

Fa 15 anys, el Dr. Nibaldo Inestrosa i col·laboradors (Universidad Pontificia Católica de Chile, Chile) van descubrir una interacció directa entre l'enzim AChE i el pèptid βA, que ha guiat en bona part el disseny d'inhibidors d'AChE en l'última dècada. En efecte, s'ha demostrat que l'enzim AChE, que és un component de les plaques senils, es pot unir directament al βA. En aquesta interacció, l'AChE actua com a "xaperona patològica" induint un canvi conformacional

[62]Nitsch, R.M.; Slack, B.E.; Wurtman, R.J.; Growdon, J.H. *Science* **1992**, *258*, 304. [63]Lahiri, D.K.; Rogers, J.T.; Greig, N.H.; Sambamurti, K. *Curr. Pharm. Des.* **2004**, *10*, 3111. [64]Chong, Y.H.; Suh, Y.H. *Life Sci.* **1996**, *59*, 545. [65]Zimmermann, M.; Gardoni, F.; Marcello, E.; Colciaghi, F.; Borroni, B.; Padovani, A.; Cattabeni, F.; DiLuca, M. *J. Neurochem.* **2004**, *90*, 1489. [66]Borroni, B.; Colciaghi, F.; Pastorino, L.; Pettenati, C.; Cottini, E.; Rozzini, L.; Monastero, R.; Lenzi, G.L.; Cattabeni, F.; DiLuca, M.; Padovani, A. *Arch. Neurol.* **2001**, *58*, 442. [67]Zimmermann, M.; Borroni, B.; Cattabeni, F.; Padovani, A.; Di Luca, M. *Neurobiol. Dis.* **2005**, *19*, 237.

en el βA des d'una conformació no amiloidogènica cap a una conformació amiloidogènica amb major tendència a formar agregats (Figura 1.7).[68]

L'efecte accelerador de l'AChE sobre l'agregació del βA en fibres d'amiloide sembla tenir lloc ja en les fases inicials de l'agregació del pèptid. A més, el complex macromolecular AChE–βA resulta més neurotòxic que els agregats de βA sol tant *in vitro* (cèl·lules PC12 i cèl·lules de retina primàries) com *in vivo* (hipocamp de rata).[69,70]

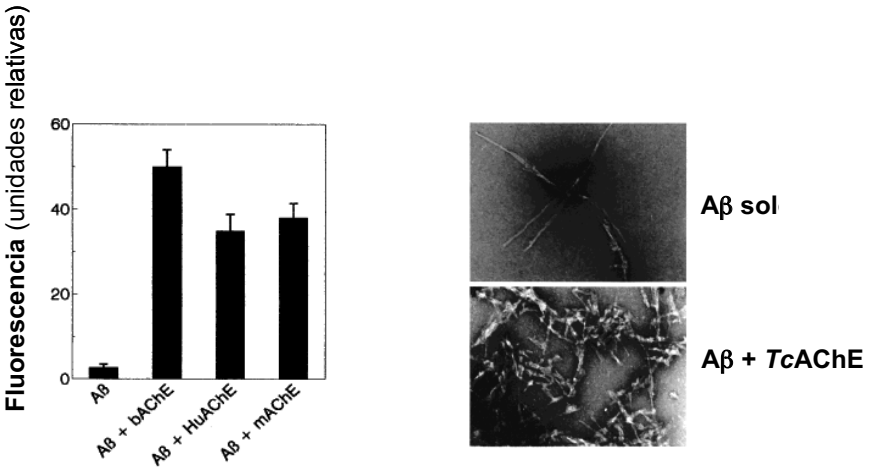

Figura 1.7 Esquerra. Agregació del βA en presència d'AChE bovina (bAChE), humana (hAChE) o de ratolí (mAChE), quantificada per l'augment en la fluorescència de la tioflavina T, un compost que s'uneix al βA quan està en forma agregada d'amiloide, rica en làmines β, augmentant així la seva fluorescència (βA 240 μM, AChE 2,4-9,6 μM, temperatura ambient, 48 h). Dreta. Micrografies electròniques de preparacions de fibrilles de βA agregades soles o en presència de *Tc*AChE (55000×).

Els resultats del Dr. Inestrosa han estat confirmats independentment pels treballs del Dr. Stephen Brimijoin (Mayo Clinic, USA) *in vivo* utilitzant ratolins doblement transgènics que expressaven APP humà i AChE humana (hAChE) al cervell. L'expressió simultània en aquests ratolins d'APP, i consegüentment, de βA, i d'hAChE va accelerar i incrementar l'aparició de plaques d'amiloide al còrtex cerebral en relació a ratolins transgènics que expressaven exclusivament APP humà.[71] A més, el Dr. Stephen Brimijoin i la Dra. Hermona Soreq (The Hebrew University of Jerusalem, Israel) van descobrir que la càrrega d'amiloide incrementada en ratolins doblement transgènics estava estretament correlacionada amb els dèficits cognitius observats en estudis de comportament amb aquests animals.[72]

[68]Inestrosa, N.C.; Alvarez, A.; Pérez, C.A.; Moreno, R.D.; Vicente, M.; Linker, C.; Casanueva, O.I.; Soto, C.; Garrido, C. *Neuron.* **1996**, *16*, 81. [69]Alvarez, A.; Alarcón, R.; Opazo, C.; Campos, E.O.; Muñoz, F.J.; Calderón, F.H.; Dajas, F.; Gentry, M.K.; Doctor, B.P.; De Mello, F.G.; Inestrosa, N.C. S *J. Neurosci.* **1998**, *18*, 3213. [70]Reyes, A.E.; Chacón, M.A.; Dinamarca, M.C.; Cerpa, W.; Morgan, C.; Inestrosa, N.C. *Am. J. Pathol.* **2004**, *164*, 2163. [71]Rees, T.; Hammond, P.I.; Soreq, H.; Younkin, S.; Brimijoin, S. *Neurobiol. Aging* **2003**, *24*, 777. [72]Rees, T.M.; Berson, A.; Sklan, E.H.; Younkin, S.; Brimiojin, S.; Soreq, H. *Curr. Alzheimer Res.* **2005**, *2*, 291.

Aquestes observacions col·loquen l'enzim AChE en la part més alta de la cascada neurotòxica de la MA (Figura 1.2) i obren les portes al desenvolupament d'inhibidors d'AChE capaços de bloquejar aquesta interacció directa entre l'enzim i el βA, i amb això l'agregació del pèptid. Aquest tipus d'inhibidors d'AChE tindrien un evident potencial modificador de la malaltia en tallar, en gran part, la cascada de neurodegeneració des del seu inici.

El lloc proposat de reconeixement o interacció del pèptid βA amb l'AChE és el lloc perifèric de l'enzim,[73] el qual es troba a l'entrada de la gorja catalítica, a una distància d'uns 14 Å del centre actiu de l'enzim. Donat que el lloc perifèric de l'AChE és el lloc a través del qual es produeix la interacció amb el βA, el bloqueig d'aquesta zona de l'enzim mitjançant un inhibidor específic hauria de resultar en la inhibició de l'agregació del pèptid βA. El primer compost descrit amb elevada capacitat per bloquejar l'agregació del βA induïda per AChE ha estat el propidi, **8** (Figura 1.8),[74] un inhibidor no competitiu descrit anys enrera amb capacitat d'interaccionar exclusivament amb el lloc perifèric. Malauradament, la seva baixa potència inhibitòria de l'AChE, i la seva naturalesa dicatiònica han fet descartar el seu ús en la farmacoteràpia anti-Alzheimer.

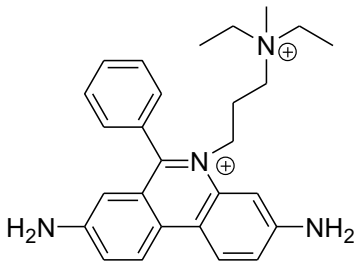

propidi, **8**

Figura 1.8

Aprofitant la particularitat estructural de la gorja catalítica que connecta el lloc perifèric amb el centre actiu de l'enzim, una alternativa a l'ús d'inhibidors d'AChE específics del lloc perifèric és el desenvolupament d'inhibidors que siguin capaços d'interaccionar simultàniament, a través de diferents parts de la seva estructura, amb els dos llocs d'unió de l'enzim. Aquest tipus particular de compostos s'anomenen inhibidors d'AChE de lloc d'unió dual.

L'avantatge associat a l'ús dels inhibidors de lloc d'unió dual és doble. En primer lloc, l'activitat d'un fàrmac depèn de la seva capacitat per a establir tota una sèrie d'interaccions químiques amb la seva diana biològica. En general, quant major sigui el nombre d'interaccions o punts de contacte entre fàrmac i diana biològica, major serà l'afinitat cap a la seva diana. El segon avantatge és molt més important. El bloqueig del lloc perifèric de l'AChE exercit per aquests

[73]De Ferrari, G.V.; Canales, M.A.; Shin, I.; Weiner, L.M.; Silman, I.; Inestrosa, N.C. *Biochemistry* **2001**, *40*, 10447.
[74]Taylor, P., Lappi, S. *Biochemistry* **1975**, *14,* 1989

compostos hauria de permetre'ls inhibir l'agregació del pèptid βA induïda per AChE, tallant la cascada de neurodegeneració des del seu inici. Aquesta interferència hauria de permetre prevenir o retardar el procés de neurodegeneració, modificant així positivament el progrés de la malaltia.

Com s'ha comentat anteriorment, el donepezil es pot considerar un inhibidor d'AChE de lloc d'unió dual, fet que podria explicar el seu excel·lent perfil farmacològic.[75] De fet, per al donepezil s'ha descrit un efecte antiagregant del βA *in vitro* (22% d'inhibició a una concentració 100 μM), que si bé està lluny del percentatge d'inhibició de l'inhibidor específic de lloc perifèric propidi (82% d'inhibició a una concentració 100 μM), és clarament superior al percentatge d'inhibició dels inhibidors del centre actiu com la tacrina (7% d'inhibició).[76]

1.5. Desenvolupament d'inhibidors de l'AChE de lloc d'unió dual

El potencial modificador de la malaltia esperat per als inhibidors de l'AChE de lloc d'unió dual ha propiciat intensos esforços per dissenyar i desenvolupar nous compostos amb aquest mode d'unió. Principalment, s'estan utilitzant aproximacions conjuntives, basades en combinar en una mateixa molècula una unitat o fragment estructural d'un conegut inhibidor de l'AChE per a la interacció amb el centre actiu i una segona unitat o fragment estructural del mateix (dimerització molecular) o d'un altre (hibridació molecular) conegut inhibidor per a la interacció amb el lloc perifèric, conectant les dues unitats constituents del dímer o de l'híbrid amb una cadena espaiadora o *linker* de longitud adecuada per permetre la interacció simultània amb ambdues zones d'unió de l'enzim.

El primer dels inhibidors d'AChE de lloc d'unió dual específicament dissenyat com a tal va ser la denominada *bis*(7)-tacrina (**9**, Esquema 1.10), constituït per dues unitats de tacrina connectades per una cadena espaiadora de 7 grups metilens, la qual proporciona la distància ideal per permetre la interacció simultània de les dues unitats de tacrina amb els dos llocs d'unió de l'AChE.[77,78] La *bis*(7)-tacrina col·loca una de les seves unitats de tacrina exactament en la mateixa posició que la pròpia tacrina, mentre que la cadena espaiadora ocupa tota la

[75]Muñoz-Torrero. D.; Camps, P. *Curr. Med. Chem.* **2006**, *13*, 399. [76]Bartolini, M.; Bertucci, C.; Cavrini, V.; Andrisano, V. *Biochem. Pharmacol.* **2003**, *65*, 407. [77]Pang. Y.-P.; Quiram. P.; Jelacic. T.; Hong. F.; Brimijoin. S. *J. Biol. Chem.* **1996**, *271*, 23646. [78]Carlier, P.R.; Han, Y.F.; Chow, E.S.-H.; Li, C.P.-L.; Wang, H.; Lieu, T.X.; Wong, H.S.; Pang, Y.-P. *Bioorg. Med. Chem.* **1999**, *7*, 351.

longitud de la gorja de l'enzim, col·locant la segona unitat de tacrina suficientment a prop del residu de Trp279 com per poder interaccionar amb ell (Esquema 1.9).[79]

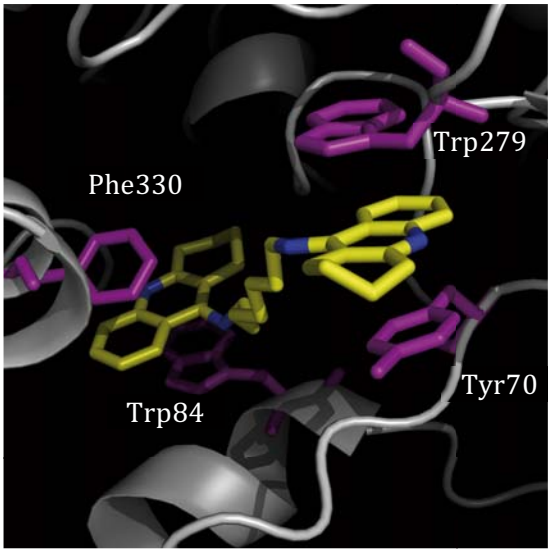

Figura 1.9 Unió de la *bis*(7)-tacrina, **9**, a *Tc*AChE (codi PDB: 2CKM).

La potència inhibitòria de la *bis*(7)-tacrina és unes 150 vegades superior a la de la tacrina, mostrant així un dels avantatges associats als inhibidors de lloc d'unió dual. A més, mostra una notable inhibició de l'agregació del pèptid βA induïda per AChE (68% d'inhibició a 100 μM).[80] Aquest efecte podria ser responsable de l'àmplia varietat d'efectes neuroprotectors mostrats per aquest compost, que inclouen la protecció de neurones enfront a l'apoptosi induïda per diferents agents neurotòxics com el peròxid d'hidrogen,[81] el glutamat,[82] el pèptid βA,[83] així com la protecció en diferents condicions d'isquèmia.[84]

Seguint el disseny de la *bis*(7)-tacrina, s'han desenvolupat altres famílies estructurals d'inhibidors d'AChE de lloc d'unió dual.[75,85-93] Alguns dels nous compostos són exemples molt clars dels dos avantatges associats a aquest tipus de compostos.

---

[75]Muñoz-Torrero. D.; Camps, P. *Curr. Med. Chem.* **2006**, *13*, 399. [79]Rydberg, E.H.; Brumshtein, B.; Greenblatt, H.M.; Harry, M.; Wong, D.M.; Shaya, D.; Williams, L.D.; Carlier, P.R.; Pang, Y.-P.; Silman, I.; Sussman, J.L. *J. Med. Chem.* **2006**, *49*, 5491. [80]Bolognesi, M.L.; Cavalli, A.; Valgimigli, L.; Bartolini, M.; Rosini, M.; Andrisano, V.; Recanatini, M.; Mechiorre, C. *J. Med. Chem.* **2007**, *50*, 6446. [81]Xiao, X.Q.; Lee, N.T.-K.; Carlier, P.R.; Pang, Y.-P.; Han, Y.F. *Neurosci. Lett.* **2000**, *290*, 197. [82]Li, W.; Pi, R.; Chan, H.H.N.; Fu, H.; Lee, N.T.K.; Tsang, H.W.; Pu, Y.; Chang, D.C.; Li, C.; Luo, J.; Xiong, K.; Li, Z.; Xue, H.; Carlier, P.R.; Pang, Y.-P.; Tsim, K.W.K.; Li, M.; Han, Y. *J. Biol. Chem.* **2005**, *280*, 18179. [83]Fu, H.; Li. W.; Lao, Y.; Luo, J.; Lee, N.T.K.; Kan, K.K.W.; Tsang, H.W.; Tsim, K.W.K.; Pang, Y.-P.; Li, Z.; Chang, D.C.; Li, M.; Han, Y. *J. Neurochem.* **2006**, *98*, 1400. [84]Han, Y.-F.; Wu, D.-C.; Xiao, X.-Q.; Chen, P.M.Y.; Chung, W.; Lee, N.T.K.; Pang, Y.-P.; Carlier, P.R. *Neurosci. Lett.* **2000**, *288*, 95. *Corrigendum in Neurosci. Lett.* **2000**, *290*, 84. [85]Castro, A.; Martinez, A. *Mini-Rev. Med. Chem.* **2001**, *1*, 267. [86]Du, D.-M.; Carlier, P.R. *Curr. Pharm. Des.* **2004**, *10*, 3141. [87]Li, W.M.; Kan, K.K.W.; Carlier, P.R.; Pang, Y.P.; Han, Y.F. *Curr. Alzheimer Res.* **2007**, *4*, 386. [88]Recanatini, M.; Valenti, P. *Curr. Pharm. Des.* **2004**, *10*, 3157. [89]Castro, A.; Martinez, A. *Curr. Pharm. Des.* **2006**, *12*, 4377. [90]Holzgrabe, U.; Kapková, P.; Alptüzün, V.; Scheiber, J.; Kugelmann, E. *Expert Opin. Ther. Targets* **2007**, *11*, 161. [91]Musial, A.; Bajda, M.; Malawska, B. *Curr. Med. Chem.* **2007**, *14*, 2654. [92]Haviv, H.; Wong, D.M.; Silman, I.; Sussman, J.L. *Curr. Top. Med. Chem.* **2007**, *7*, 375. [93]Cavalli, A.; Bolognesi, M.L.; Minarini, A.; Rosini, M.; Tumiatti, V.; Recanatini, M.; Melchiorre, C. *J. Med. Chem.* **2008**, *51*, 347.

D'una banda, la major part dels inhibidors d'AChE de lloc d'unió dual presenten valors d'IC_{50} en el rang nanomolar baix o fins i tot picomolar. D'altra banda, alguns d'aquests compostos són capaços d'inhibir *in vitro* de forma molt important l'agregació del pèptid βA induïda per AChE, utilitzant concentracions 100 μM d'inhibidor. Per a aquesta activitat inhibitòria, els valors d'IC_{50} dels inhibidors de lloc d'unió dual són en el rang micromolar baix.

L'AP2238 (**10**, Figura 1.10), desenvolupat pels Drs. Valenti i Recanatini (Università di Bologna, Itàlia), va ser el primer inhibidor de l'AChE de lloc d'unió dual dissenyat racionalment per bloquejar l'agregació del βA induïda per AChE. En la seva estructura es combina un fragment *N*-bencilamino, present en molts inhibidors coneguts d'AChE com el mateix donepezil, per a la interacció amb el centre actiu, un sistema de cumarina per a la interacció amb el lloc perifèric i un fragment *p*-fenilè per a la interacció amb els residus aromàtics localitzats a meitat de la gorja catalítica de l'enzim.[94] Aquest compost va presentar una potent activitat inhibitòria de l'hAChE (IC_{50} = 45 nM) i una moderada activitat inhibitòria de l'agregació del βA induïda per AChE (35% d'inhibició a 100 μM).[94] A més el seu anàleg *N*-etil substituït (l'AP2243) hi suma una potent inhibició de la BACE-1 (IC_{50} = 238 nM).[95]

El compost **11** (Figura 1.10), desenvolupat per la Dra. Ana Martínez, pertany a una de las famílies d'inhibidors de l'AChE de lloc d'unió dual més interessants pel seu perfil farmacològic que combina una extremada potent activitat inhibitòria de l'AChE amb valors d'IC_{50} en el rang picomolar (IC_{50} = 20 pM en aquest cas) i una inhibició quasi bé completa de l'agregació del pèptid βA induïda per AChE a concentració 100 μM (96% d'inhibició, IC_{50} = 6 μM).[96]

La memoquina (**12**, Figura 1.10), desenvolupada pels Drs. Melchiorre i Bolognesi (Università di Bologna, Itàlia), és un inhibidor d'AChE de lloc d'unió dual que constitueix un dels candidats a fàrmacs anti-Alzheimer modificadors de la malaltia més prometedors. Aquest compost combina una potent activitat inhibitòria enfront l'hAChE (IC_{50} = 1,55 nM), amb una elevada activitat inhibitòria enfront l'agregació del pèptid βA induïda per AChE (87% d'inhibició a 100 μM, IC_{50} = 28 μM) i enfront l'agregació del βA espontània (96% d'inhibició a 50 μM, IC_{50} = 6 μM), i amb una elevada activitat inhibitòria enfront BACE-1 (IC_{50} = 108 nM), a més d'efectes

[94]Piazzi, L.; Rampa, A.; Bisi, A.; Gobbi, S.; Belluti, F.; Cavalli, A.; Bartolini, M.; Andrisano, V.; Valenti, P.; Recanatini, M. *J. Med. Chem.* **2003**, *46*, 2279. [95]Piazzi, L.; Cavalli, A.; Colizzi, F.; Belluti, F.; Bartolini, M.; Mancini, F.; Recanatini, M.; Andrisano, V.; Rampa, A. *Bioorg. Med. Chem. Lett.* **2008**, *18*, 423. [96]Muñoz-Ruiz, P.; Rubio, L.; García-Palomero, E.; Dorronsoro, I.; del Monte-Millán, M.; Valenzuela, R.; Usán, P.; de Austria, C.; Bartolini, M.; Andrisano, V.; Bidon-Chanal, A.; Orozco, M.; Luque, F.J.; Medina, M.; Martínez, A. *J. Med. Chem.* **2005**, *48*, 7223.

neuroprotectors en cèl·lules SH-SY5Y que expressen alts nivells de NAD(P)H:quinona oxidoreductasa contra a l'estrès oxidatiu.[97,98]

En estudis *in vivo* realitzats amb la memoquina i amb el NP-61, un inhibidor d'AChE de lloc d'unió dual desenvolupat per la companyia Neuropharma S.A (actualment Noscira), s'ha obtingut la prova de concepte de la utilitat terapèutica de l'efecte antiagregant del βA mostrat *in vitro* pels inhibidors d'AChE de lloc d'unió dual. La memoquina és capaç de reduir significativament els dipòsits de βA i de millorar la cognició en un model de ratolí transgènic que desenvolupa el conjunt complet de signes histopatològics característics de la MA.[97] Per la seva part, el NP-61, després de l'administració oral durant 3 mesos, és capaç de reduir el nombre i la grandària de les plaques d'amiloide en el còrtex i l'hipocamp de ratolins transgènics que expressen APP humà, conduïnt la càrrega d'amiloide reduïda a una significativa millora cognitiva.[99] En la primera meitat de 2007, el NP-61 va entrar en assaigs clínics de fase I al Regne Unit,[100] i al llarg de 2009 es van descartar efectes adversos rellevants. Els resultats d'aquests estudis constitueix en una clara evidència del prometedor paper dels inhibidors d'AChE de lloc d'unió dual en el tractament de la MA.

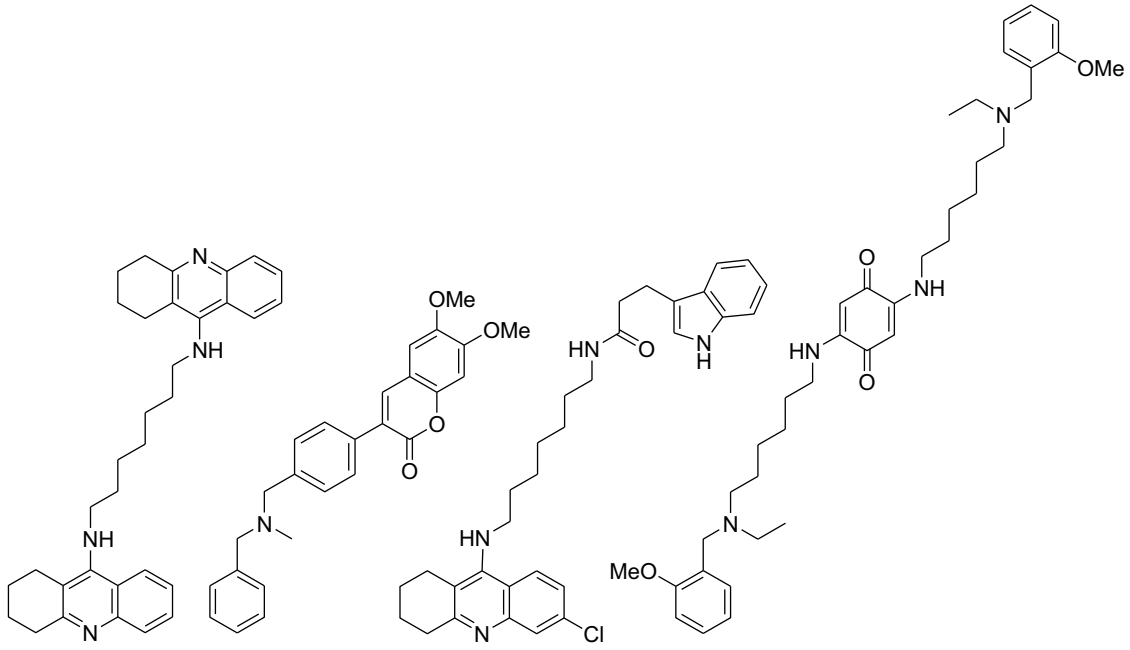

bis(7)-tacrina, **9** AP2238, **10** **11** memoquina, **12**

Figura 1.10 Estructura d'alguns inhibidors de l'AChE de lloc d'unió dual representatius dissenyats racionalment.

[97]Cavalli, A.; Bolognesi, M.L.; Capsoni, S.; Andrisano, V.; Bartolini, M.; Margotti, E.; Cattaneo, A.; Recanatini, M.; Melchiorre, C. *Angew. Chem. Int. Ed.* **2007**, *46*, 3689. [98]Bolognesi, M.L.; Banzi, R.; Bartolini, M.; Cavalli, A.; Tarozzi, A.; Andrisano, V.; Minarini, A.; Rosini, M.; Tumiatti, V.; Bergamini, C.; Fato, R.; Lenaz, G.; Hrelia, P.; Cattaneo, A.; Recanatini, M.; Melchiorre, C. *J. Med. Chem.* **2007**, *50*, 4882. [99]Vericat, J.A.; Muñoz, P.; Windisch, M.; Hutter-Paier, B.; Medina, M.; Martinez, A. *5th Neurobiology of Aging Conference*, San Diego, USA, 2004. [100]http://www.noscira.es.

1.6 Antecedents del disseny d'inhibidors d'AChE en el nostre grup de recerca, les huprines.

L'equip d'investigació dels Drs. Pelayo Camps i Diego Muñoz-Torrero va iniciar fa uns 15 anys un treball multidisciplinar dirigit al disseny, síntesi i avaluació farmacològica d'una família d'inhibidors d'AChE de centre actiu anomenats huprines, les quals es troben entre els inhibidors reversibles de més elevada potència desenvolupats fins el moment. Les huprines combinen a la mateixa molècula el sistema de 4-aminoquinolina de la tacrina, **1**, i el sistema carbobicíclic d'un altre conegut inhibidor d'AChE de lloc actiu d'origen natural, la (–)-huperzina A, **13** (Figura 1.11). Entre més de 30 huprines diferents, resultants de la modificació de tres parts de l'estructura general de la huprina model **14**: el pont metilènic entre les posicions 7 i 11, el pont insaturat de tres carbonis entre les posicions 7 i 11, i l'anell benzènic del sistema quinolínic, les huprines amb millor perfil farmacològic són les anomenades (–)-huprina Y, (–)-**15**, i (–)-huprina X, (–)-**16**.[101,102]

A més a més, experiments *ex vivo* van demostrar que aquestes huprines són capaces de travessar la barrera hematoencefàlica (BHE) i inhibir l'AChE del cervell de rates amb una potència molt superior a la de la tacrina, la (−)-huperzina A i el donepezil.[103,104]

Estudis cinètics duts a terme en col·laboració amb el grup del Dr. Terrone L. Rosenberry (Mayo Clinic, USA), van demostrar que les huprines (−)-**15** i (−)-**16** presenten una constant d'inhibició (*K*i) d'uns 30 pM, posant de manifest que l'afinitat d'aquests compostos per l'AChE humana (hAChE) recombinant és fins a 1200 cops superior a la de la tacrina, 180 cops superior a la de la (−)-huperzina A, i 40 cops superior a la del donepezil.[105]

L'excel·lent perfil farmacològic de les huprines es complementa amb altres característiques funcionals addicionals que s'han observat en la huprina Y racèmica, com l'acció agonista sobre el receptor muscarínic M1 en cervell de rata,[106] i l'efecte neuroprotector per antagonisme sobre els receptors NMDA de glutamat. Estudis *in vitro* i *in vivo* van demostrar que la (±)-huprina Y evita la mort neuronal induïda per excés de glutamat mitjançant el bloqueig directe dels receptors de NMDA,[107] mimetitzant així, addicionalment, els efectes de l'únic fàrmac anti-Alzheimer que no és un inhibidor de l'AChE, la memantina.

---

[101]Badia, A.; Baños, J.E.; Camps, P.; Contreras, J.; Görbig, D.M.; Muñoz-Torrero, D.; Simon, M.; Vivas, N.M. *Bioorg. Med. Chem.* **1998**, *6*, 427. [102]Muñoz-Torrero, D.; Camps, P. *Expert Opin. Drug Discovery* **2008**, *3*, 65. [103]Camps, P.; El Achab, R.; Morral, J.; Muñoz-Torrero, D.; Badia, A.; Baños, J.E.; Vivas, N.M.; Barril, X.; Orozco, M.; Luque, F.J. *J. Med. Chem.* **2000**, *43*, 4657. [104]Alcalá, M.M.; Vivas, N.M.; Hospital, S.; Camps, P.; Muñoz-Torrero, D.; Badia, A. *Neuropharmacol.* **2003**, *44*, 749. [105]Camps, P.; Cusack, B.; Mallender, W.D.; El Achab, R.; Morral, J.; Muñoz-Torrero, D.; Rosenberry, T.L. *Mol. Pharmacol.* **2000**, *57*, 409. [106]Roman, S.; Vivas, N.M.; Badia, A.; Clos, M.V. *Neurosci. Lett.* **2002**, *325*, 103. [107]Canudas, A.M.; Pubill, D.; Sureda, F.X.; Verdaguer, E.; Camps, P.; Muñoz-Torrero, D.; Jiménez, A.; Camins, A.; Pallàs, M. *Exp. Neurol.* **2003**, *180*, 123.

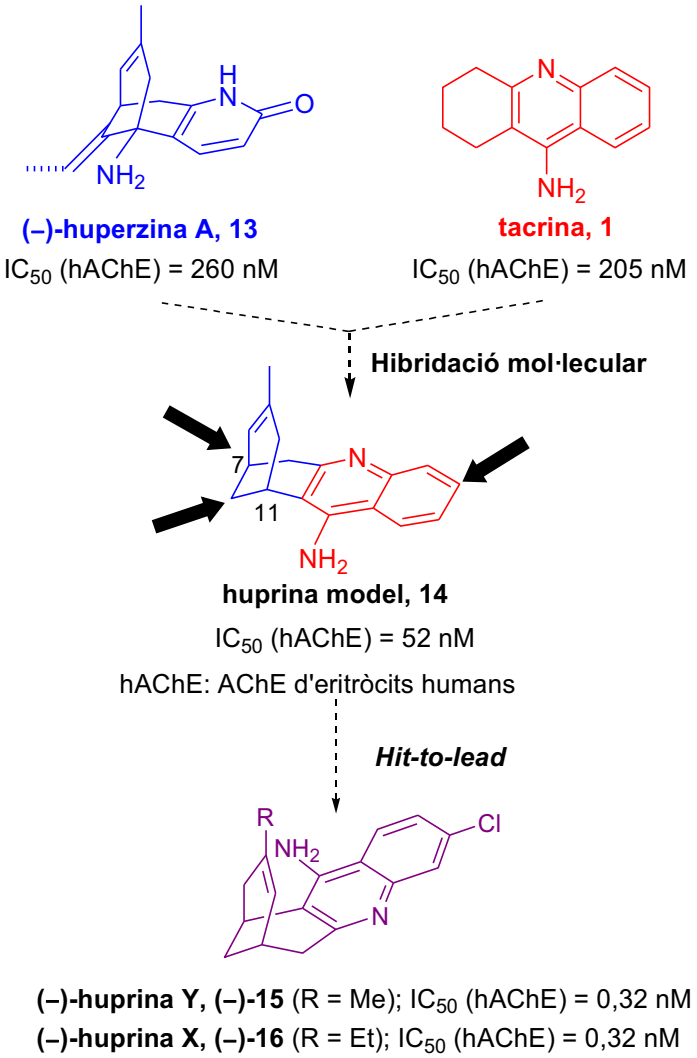

Figura 1.11 Disseny i farmacomodulació de les huprines.

Tal com es va predir mitjançant estudis de modelatge molecular duts a terme per l'equip del Dr. F. Javier Luque, confirmats posteriorment amb la resolució de l'estructura tridimensional de raigs-X del complex (–)-huprina X–*Tc*AChE (codi PDB: 1E66) per l'equip del Dr. Joel L. Sussman (Weizmann Institute of Science, Israel), les huprines actuen veritablement com a híbrids huperzina A–tacrina.[108] Les huprines s'uneixen al lloc aniònic catalític de l'enzim, impedint l'accés de l'ACh al lloc esteràtic (Figura 1.12). El sistema de 4-aminoquinolina de la (–)-huprina X, ocupa el mateix lloc d'unió que el corresponent sistema aromàtic de la tacrina, empaquetant-se a través d'interaccions π-stacking entre els anells aromàtics del Trp84 i de la Phe330, i establint interaccions per pont d'hidrogen entre el nitrogen piridínic, protonat a pH

[108]Dvir, H.; Wong, D.M.; Harel, M.; Barril, X.; Orozco, M.; Luque, F.J.; Muñoz-Torrero, D.; Camps, P.; Rosenberry, T.L.; Silman, I.; Sussman, J.L. *Biochemistry* **2002**, *41*, 2970.

fisiològic i l'oxigen carbonílic de la His440, i altres enllaços d'hidrogen, mediats per molècules d'aigua entre el grup amino exocíclic i els residus Asp72, Tyr121 i Tyr334. Addicionalment, la part carbobicíclica de (–)-**16** es col·loca a la mateixa butxaca hidrofòbica que la corresponent subunitat de la (–)-huperzina A (codi PDB: 1VOT), tot i que els ponts metilènics d'aquests apunten en direccions contràries.

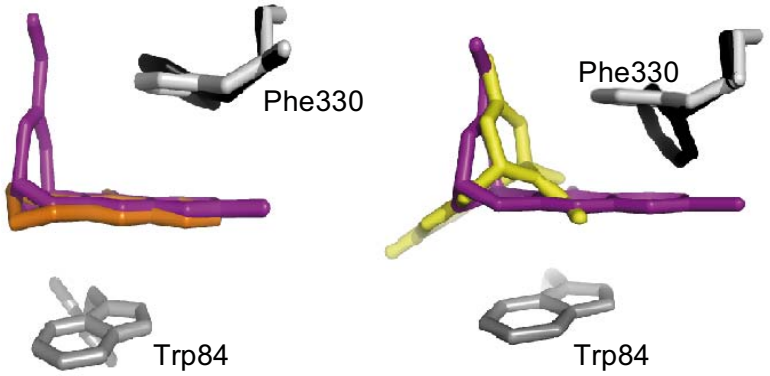

Figura 1.12 Esquerra: Comparació de la disposició de la tacrina, **1** (taronja) i la (–)-huprina X, (–)-**16** (lila) al lloc actiu de *Tc*AChE. Dreta: Superposició de la disposició de la (–)-huperzina A, **13** (groga) i de (–)-**16**, al lloc actiu de *Tc*AChE. Els residus Trp84 i Phe330 del complex (–)-**16**–*Tc*AChE es representen en gris clar. El residu Phe330 en els complexos amb tacrina i (–)-huperzina A es representa en negre.

A més de les interaccions corresponents a les subestructures de tacrina, i de (–)-huperzina A, la (–)-huprina X, també presenta les interaccions addicionals corresponents a l'àtom de clor, que es disposa en una butxaca hidrofòbica on interacciona amb els anells dels residus aromàtics del Trp432 i de la Phe330, i amb els grups metil de la Met436 i la Ile439 (Figura 1.13).

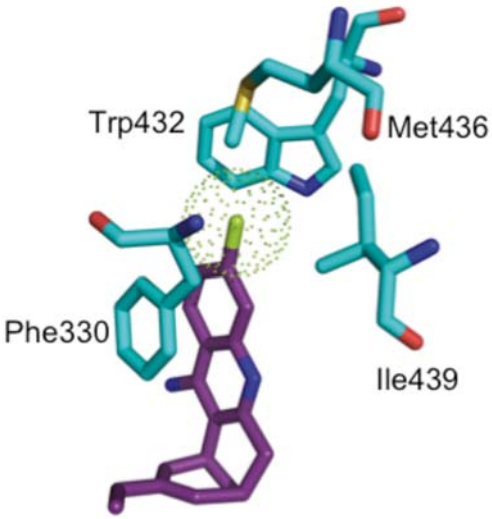

Figura 1.13 Interaccions corresponents a l'àtom de clor de la (–)-huprina X, (–)-**16** (lila), amb el centre actiu de l'AChE (residus en color blau clar).

Finalment, s'ha demostrat que la huprina X és capaç de disminuir els nivells de pèptid βA en cervells de ratolins *3xTg*-AD, a més d'incrementar de forma clara els nivells de sinaptofisina.[109] Aquestes accions poden ser degudes, bé a l'interacció amb el lloc perifèric de l'enzim, o bé a l'activació de diversos receptors colinèrgics involucrats en la MA. No obstant, aquests resultats no s'han pogut observar en ratolins *APPswe*, possiblement a causa de les diferències neuropatològiques dels cervells entre els dos models assatjats.[109]

[109]Hedberg, M.M; Clos, M.V.; Ratia, M.; Gonzalez, D.; Unger Lithner, C.; Camps, P.; Muñoz-Torrero, D.; Badia, A.; Giménez-Llort, L.; Nordberg, A. *Neurodegener. Dis.* **2010***, 7*, 379.

Capítol 2: Objectius

2.1 Objectius del Capítol 3. Síntesi d'híbrids donepezil–tacrina com a agents anticolinesteràsics i antiagregants del pèptid βA. (*J. Med. Chem.* **2008,** *51*, 3588–3598).

Els híbrids donepezil-tacrina d'estructura general **I** (figura 2.1) havien estat sintetitzats al nostre grup de recerca en quantitats bastant reduïdes (al voltant dels 50–100 mg dels corresponents dihidroclorurs en la majoria dels casos), que havien permès completar la caracterització química però no la caracterització farmacològica. En la majoria dels casos no quedava una quantitat de mostra analítica suficient per poder dur a terme els estudis farmacològics addicionals que ens havíem plantejat.

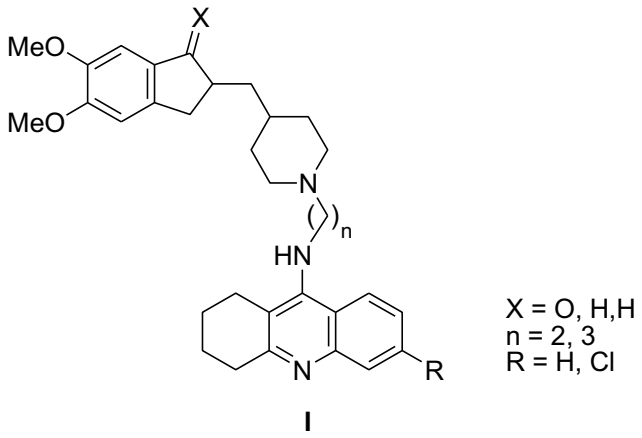

I

Figura 2.1

Aprofitant el fet que havíem de resintetitzar alguns híbrids donepezil–tacrina seleccionats i tenint en compte els problemes metodològics associats a algunes de les etapes de síntesi de la seqüència desenvolupada prèviament al nostre grup de recerca, en la present Tesi doctoral es va plantejar l'accés a aquests híbrids a través de dos procediments alternatius:

1. D'una banda es va plantejar la preparació d'alguns híbrids a través de la mateixa seqüència sintètica desenvolupada anteriorment al nostre grup, però intentant millorar els rendiments d'obtenció dels intermedis i productes finals.
2. En la seqüència sintètica desenvolupada anteriorment, la unitat de tacrina s'introduïa aprofitant l'electrofília d'un precursor de tipus 4-cloroquinolina. Disposant al nostre laboratori de quantitats importants de tacrina i de 6-clorotacrina, i tenint en compte la nucleofília del seu grup amino primari després de la desprotonació en medi bàsic, ens vam plantejar l'accés alternatiu a alguns híbrids donepezil–tacrina a través d'una metodologia alternativa en la qual tant el fragment piperidínic derivat del donepezil com la unitat derivada de tacrina s'enllacessin al *linker* reaccionant com a nucleòfils.

2.2 Objectius del Capítol 4. Disseny, síntesi i avaluació farmacològica d'híbrids pirano[3,2-c]quinolina–6-clorotacrina com a una nova família de compostos anti–Alzheimer.

(*J. Med. Chem.* **2009,** *52*, 5365–5379).

Aquest capítol s'emmarca dins d'una col·laboració amb el grup de treball del Dr. Rodolfo Lavilla, de la Unitat de Química Orgànica de la Facultat de Farmàcia i del Parc Científic de Barcelona, amb àmplia experiència en la síntesi de sistemes tricíclics nitrogenats a través de reaccions multicomponent. En concret, en aquest treball:

1. Es va plantejar la síntesi d'una nova sèrie d'híbrids d'estructura general **II** (Figura 2.2) com a inhibidors d'AChE de lloc d'unió dual, constituïts per una unitat de 6-clorotacrina per a la interacció amb el lloc actiu de l'enzim i un d'aquests sistemes policíclics aromàtics nitrogenats amb estructura reminiscent a la de l'inhibidor d'AChE específic del lloc perifèric, propidi, amb potencial per establir interaccions amb el residu Trp279 del lloc perifèric de l'AChE, utilitzant com a productes de partida èsters que havien estat sintetitzats prèviament pel grup del Dr. Lavilla. Les dues unitats constituents dels nous híbrids es connectarien a través d'un *linker* de longitud variable.

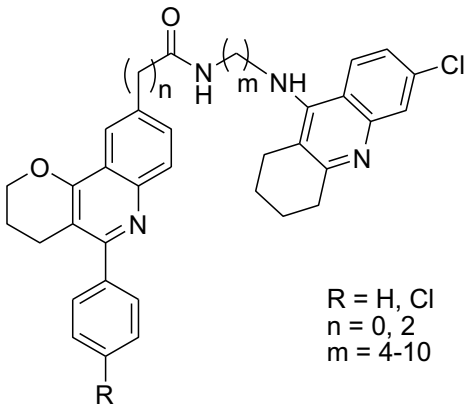

II

Figura 2.2

2. Un cop obtinguts els híbrids desitjats, es va plantejar l'avaluació de l'activitat inhibidora d'AChE i de la butirilcolinesterasa (BChE) dels nous híbrids per mi mateix sota la supervisió dels Drs. Albert Badia i Victòria Clos del Departament de Famacologia, de Terapèutica i de Toxicologia de la Universitat Autònoma de Barcelona.
3. Per tal de verificar l'estabilitat del grup amida present en aquests compostos, es va plantejar un estudi d'estabilitat d'un dels membres de la sèrie sota condicions fisiològiques.

2.3 Objectius del Capítol 5. Estudis de modelatge molecular d'híbrids donepezil–huprina amb activitat inhibitòria enfront la formació i l'agregació del pèptid βA. (*ChemMedChem* **2010**, *5*, 1855–1870).

En vista de l'excel·lent perfil farmacològic dels híbrids donepezil−tacrina, dins del Màster Experimental d'Elisabet Viayna es va sintetitzar una sèrie d'híbrids donepezil–huprina d'estructura general **III** com a una nova família d'inhibidors d'AChE de lloc d'unió dual (Figura 2.3), constituïts per una unitat d'huprina Y o d'huprina X racèmica o enantiopura per a la interacció amb el centre actiu de l'AChE i el fragment 5,6-dimetoxi-2[(4-piperidinil)metil]indà derivat del donepezil per a interaccionar amb la gorja catalítica i el lloc perifèric, separats per una cadena espaiadora de 2 o 3 grups metilens. Després de la seva caracterització farmacològica es va plantejar l'exploració del mode d'unió d'aquests nous híbrids a l'AChE per confirmar el caràcter d'inhibidors de lloc d'unió dual de l'AChE i justificar les relacions estructura–activitat trobades en aquesta família.

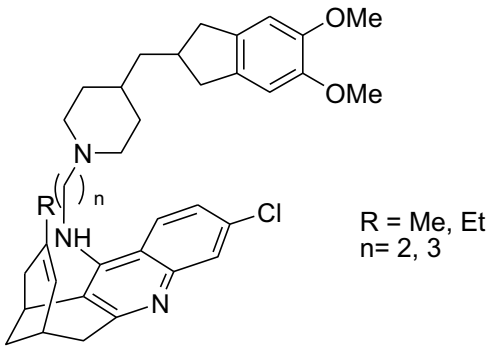

III

Figura 2.3

2.4 *Objectius del Capítol 6. Síntesi i modelatge molecular d'híbrids huprina–tacrina com a compostos anti-amilodiogènics amb potencial interès enfront la malaltia d'Alzheimer i les malalties priòniques.* (*J. Med. Chem.* **2012,** *55,* 661–669).

En la Tesi Doctoral del Dr. Xavier Formosa es va dur a terme el disseny, la síntesi i l'avaluació farmacològica d'una sèrie d'inhibidors de l'AChE de lloc d'unió dual constituïts per una molècula d'huprina Y, una cadena amb diferents longituds i funcionalitzacions i una unitat de tacrina o 6-clorotacrina. La naturalesa quiral de les huprines va fer que el nostre grup de recerca es plantegés abordar la preparació dels enantiòmers d'alguns d'aquests híbrids amb l'objectiu de determinar si existien diferències d'activitat entre ells. En aquest context, en la present tesi doctoral es va plantejar:

1. La síntesi enantiopura dels híbrids huprina–tacrina contenint una cadena heptametilènica, una unitat de tacrina; 6-clorotacrina i una unitat d'huprina Y enantiopura (estuctura general **IV**, figura 2.4). La consecució d'aquest objectiu requeria la síntesi de la huprina Y en forma racèmica i la seva posterior resolució cromatogràfica a escala preparativa mitjançant cromatografia líquida de pressió mitjana (MPLC). Per tal de determinar l'excés enantiomèric de les fraccions obtingudes per MPLC calia posar a punt un mètode analític mitjançant HPLC quiral.
2. Avaluar la capacitat d'inhibir l'AChE i la BChE dels híbrids enantiopurs sintetitzats i comparar les dades obtingudes entre ells i amb els seus corresponents racèmics.
3. Un cop obtingudes les dades farmacològiques dels híbrids enantiopurs sintetitzats es va plantejar explorar el mode d'unió dels nous híbrids per justificar les diferències d'activitat amb les diferències estructurals.

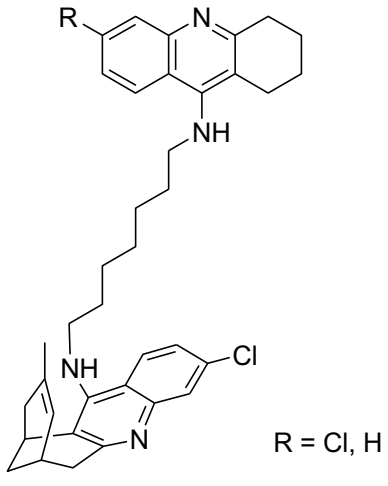

IV

Figura 2.4

Capítol 3: ***Síntesi d'híbrids donepezil–tacrina com a agents anticolinesteràsics i antiagregants del pèptid βA.***

(J. Med. Chem. **2008,** *51,* 3588–3598).

3.1 Antecedents sobre el desenvolupament del híbrids donepezil–tacrina

Donat que el donepezil és pot considerar un inhibidor d'AChE de lloc d'unió dual, el seu perfil farmacològic ha propiciat el desenvolupament d'altres inhibidors de lloc d'unió dual que incorporessin algun fragment del donepezil. Així, s'han desenvolupat diferents famílies d'inhibidors que combinen un fragment de donepezil amb una unitat de tacrina. El grup del Dr. Yuanchao Li (Shanghai Institute of Materia Medica, Xina) va desenvolupar una família d'híbrids donepezil–tacrina que combinaven el fragment de benzilpiperidina del donepezil amb una unitat de tacrina.[110] El compost més potent de la sèrie, **17** (Figura 3.1), inhibeix l'AChE de rata amb una potència similar a la del donepezil. Estudis de modelatge molecular van demostrar el seu caràcter d'inhibidor de lloc d'unió dual. El grup de la Dra. Ana Martínez (Instituto de Química Médica, Madrid) va desenvolupar una altra sèrie d'híbrids donepezil–tacrina, com **18**, en els quals es combinava el fragment de 5,6-dimetoxi-1-indanona del donepezil amb una unitat de tacrina (Figura 3.1).[111] El compost **18**, tot i ser un potent inhibidor d'AChE, és dues vegades menys potent que donepezil com a inhibidor de l'hAChE. Tanmateix, en un estudi de competició amb propidi com a assaig indirecte per comprovar el seu caràcter d'inhibidor de lloc d'unió dual, i en particular, la seva interacció amb el lloc perifèric, el compost **18** no va ser capaç de desplaçar el propidi del lloc perifèric de l'enzim. Cal destacar, però, que el compost **18** és un dels inhibidors més potents de la butirilcolinesteresa (BChE) descrits fins el moment, sent més de 12.000 vegades més potent que el donepezil enfront aquest enzim.

En un treball contemporani als anteriors, en el Màster Experimental de Michele Scapellini[112] i en la Tesi Doctoral del Dr. Xavier Formosa,[113] del nostre grup de recerca, es va desenvolupar una família d'híbrids donepezil–tacrina, d'estructura **19**–**22** (Figura 3.1), en què es preservava molt més que en les altres aproximacions l'estructura del donepezil i se substituïa el grup benzil del donepezil per una unitat d'alquiltacrina.[114] D'una banda, aquesta substitució havia de conduir a una major interacció amb el centre actiu de l'AChE, alhora que s'haurien de mantenir les interaccions amb els residus de la gorja catalítica. D'altra banda, la modulació de la longitud de la cadena oligometilènica que connectava el fragment derivat del donepezil i la unitat de tacrina havia de permetre millorar la interacció amb el lloc perifèric de l'enzim i amb això superar el modest efecte antiagregant del pèptid βA mostrat pel donepezil.

---

[110]Shao, D.; Zou, C.; Luo, C.; Tang, X.; Li, Y. *Bioorg. Med. Chem. Lett.* **2004**, *14*, 4639. [111]Alonso, D.; Dorronsoro, I.; Rubio, L.; Muñoz, P.; García-Palomero, E.; Del Monte, M.; Bidon-Chanal, A.; Orozco, M.; Luque, F.J.; Castro, A.; Medina, M.; Martínez, A. *J. Med. Chem.* **2005**, *48*, 7223. [112]Scarpellini, M. *Màster Experimental*, Universitat de Barcelona, **2006**. [113]Xavier Formosa, *Tesi Doctoral*, Universitat de Barcelona, **2006**. [114]Camps, P.; Muñoz-Torrero, D.; Formosa, X.; Scarpellini, M. Patent P200601045, WO2007/122274A1.

A més, en aquests compostos es va estudiar l'efecte que tenia sobre l'activitat la introducció d'un àtom de clor a la posició 6 de la unitat de tacrina d'aquests híbrids, substitució que en altres derivats de tacrina condueix a un important augment de la potència inhibitòria enfront l'AChE.[115] També es va estudiar l'efecte que tenia la substitució del sistema d'indanona característic del donepezil pel corresponent sistema indànic. Quant a la longitud de la cadena espaidora o *linker,* es va plantejar la utilització de cadenes de dos i tres grups metilè.

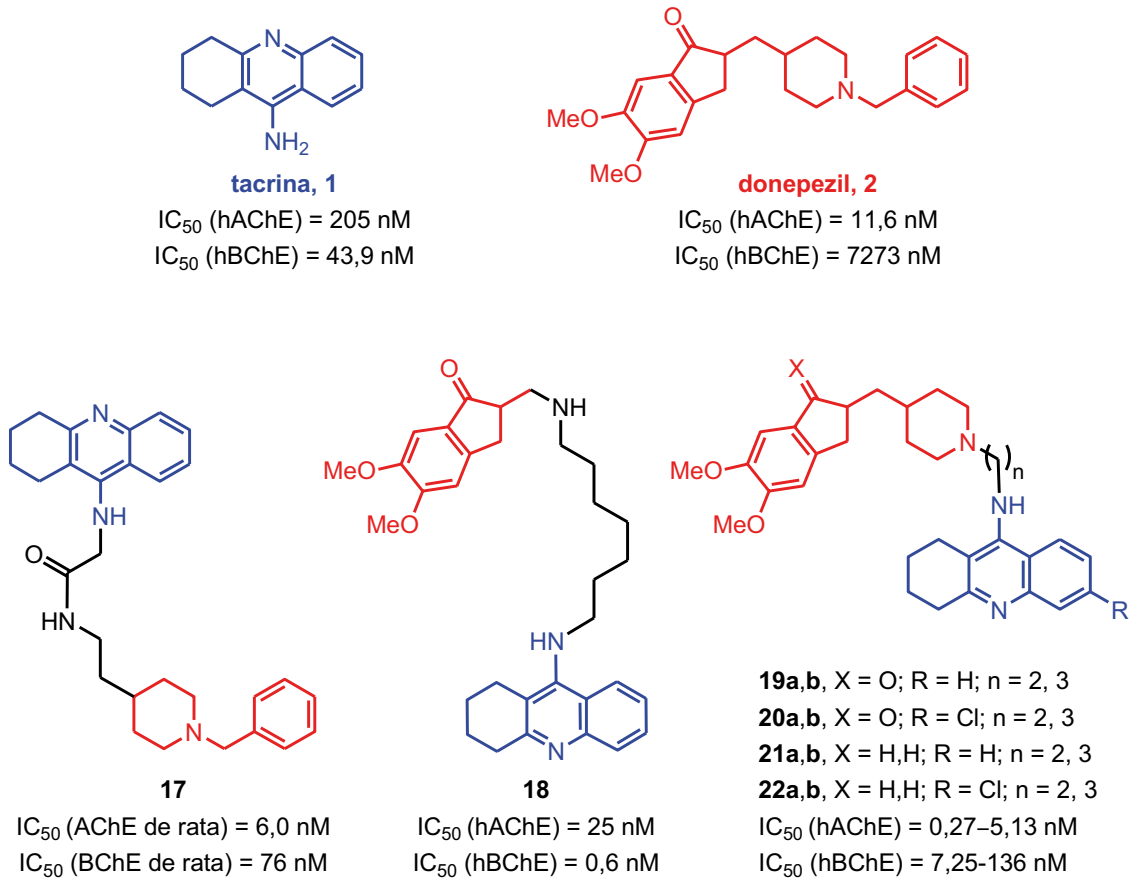

Figura 3.1 Híbrids donepezil–tacrina desenvolupats fins el moment.

La síntesi d'aquests híbrids donepezil–tacrina implicava una seqüència en tres etapes basada en la substitució nucleòfila aromàtica inicial de les conegudes 4-cloroquinolines **23 i 24** amb 2-aminoetanol, **25a**, o 3-amino-1-propanol, **25b**, seguit de conversió dels alcohols resultants en els corresponents mesilats i substitució nucleòfila dels mateixos amb les conegudes piperidines **30** o **31** (Esquema 3.1). Les dues primeres etapes van transcórrer amb rendiments excel·lents, mentre que a l'última etapa els rendiments van ser de baixos a moderats (18–69%), amb la qual cosa els rendiments globals d'obtenció dels híbrids **19**–**22** voltaven entre el 17% i el 66%.

[115]Kawakami, H.; Ohuchi, R.; Kitano, M.; Ono, K. EP 0 268 871 A1, 1988.

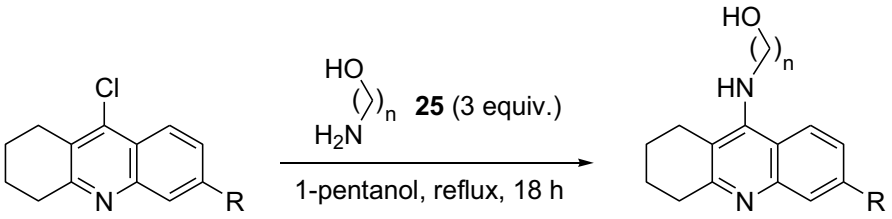

23, R = H
24, R = Cl

26a, R = H, n = 2
26b, R = H, n = 3
27a, R = Cl, n = 2
27b, R = Cl, n = 3

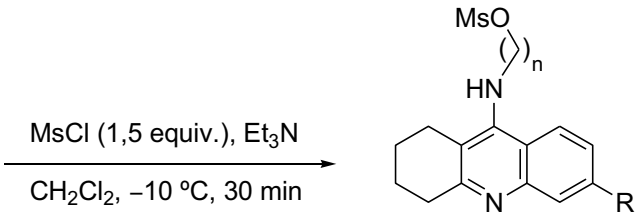

28a, R = H, n = 2
28b, R = H, n = 3
29a, R = Cl, n = 2
29b, R = Cl, n = 3

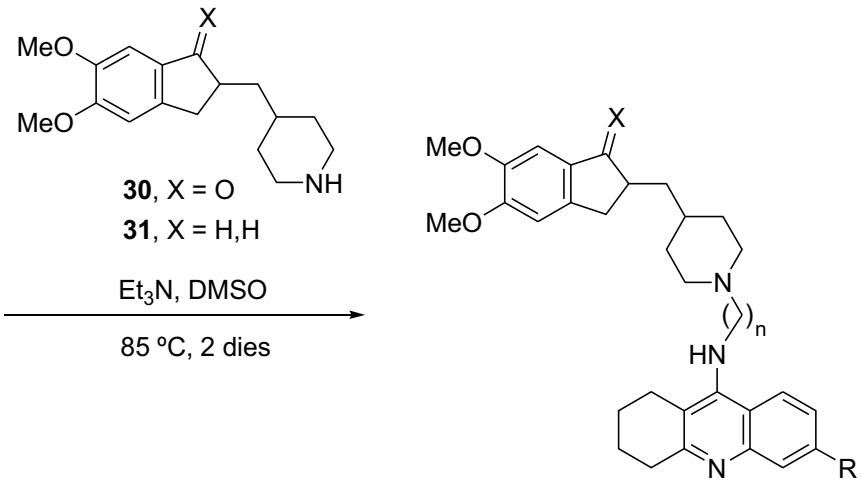

19a, X = O, R = H, n = 2 (18% global)
19b, X = O, R = H, n = 3 (66% global)
20a, X = O, R = Cl, n = 2 (36% global)
20b, X = O, R = Cl, n = 3 (26% global)
21a, X = H,H, R = H, n = 2 (31% global)
21b, X = H,H, R = H, n = 3 (17% global)
22a, X = H,H, R = Cl, n = 2 (26% global)
22b, X = H,H, R = Cl, n = 3 (31% global)

Esquema 3.1

Aquesta seqüència sintètica implicava una única purificació cromatogràfica, la dels productes finals. Tanmateix, aquesta separació cromatogràfica va resultar bastant difícil i molt tediosa. També va resultar molt llarg i tediós l'aïllament dels alcohols **26**,**27**, que implicava l'eliminació del dissolvent (1-pentanol) i l'excés d'aminoalcohol mitjançant microdestil·lació en un forn de boles giratori a 85 ^{o}C / 0,8 Torr, fent difícil l'escalat de la reacció de preparació d'aquests alcohols.

Els híbrids donepezil–tacrina sintetitzats al nostre grup van resultar ser molt potents inhibidors de l'AChE bovina i humana, amb valors subnanomolars d'IC_{50} en molts casos. Les característiques estructurals que comporten una activitat inhibidora d'AChE òptima inclouen la presència del sistema d'indanona, un àtom de clor a la posició 6 de la subunitat de tacrina i una cadena espaidora de tres metilens. Així mateix, alguns d'aquests híbrids són també potents inhibidors de la BChE humana, amb valors d'IC_{50} en el rang nanomolar baix, la qual cosa representa un important valor afegit de cara al tractament de la MA, sobretot en etapes avançades en què els nivells d'AChE al SNC disminueixen mentre que els nivells de BChE es mantenen o fins i tot augmenten fins a esdevenir el principal responsable de la hidròlisi de l'ACh.[116]

Estudis de modelatge molecular duts a terme en el marc de la Tesi Doctoral del Dr. Axel Bidón-Chanal, del grup del Dr. F. Javier Luque, van confirmar el caràcter d'inhibidors de lloc d'unió dual dels híbrids donepezil–tacrina preparats al nostre grup i van justificar la seva elevada potència inhibitòria no només com a conseqüència de la interacció simultània amb el centre actiu i el lloc perifèric, sinó també d'interaccions addicionals amb residus de la gorja catalítica de l'AChE.

El caràcter d'inhibidors de lloc d'unió dual dels nostres híbrids donepezil–tacrina, i en particular la seva capacitat d'interacció amb el lloc perifèric també es va fer palès mitjançant un assaig de competició amb tioflavina T, un lligand que pot unir-se al lloc perifèric de l'AChE donant lloc a un augment de fluorescència més gran que el que es produeix quan s'uneix el propidi.[117]

L'excel·lent activitat inhibitòria de l'AChE i de la BChE exhibida pels nostres híbrids donepezil–tacrina, juntament amb la seva capacitat d'interacció amb el lloc perifèric demostrada en l'assaig de competició amb tioflavina T com a prova indirecta del seu potencial per inhibir l'agregació del pèptid βA induïda per AChE, feien molt interessant la determinació directa del seu efecte antiagregant de βA. A més, de cara a completar l'estudi del perfil

[116]Giacobini, E. *Neurochem. Res.* **2003**, *28*, 515. [117]De Ferrari, G.V.; Mallender, W.D.; Inestrosa, N.C.; Rosenberry, T.L. *J. Biol. Chem.* **2001**, *276*, 23282.

farmacològic d'aquests híbrids també ens vam plantejar estudiar la seva possible activitat inhibidora de la BACE-1, un efecte que presenten altres inhibidors d'AChE de lloc d'unió dual.
En aquest context, el primer objectiu de la present Tesi Doctoral consistia en resintetitzar els híbrids donepezil–tacrina **20a**,**b**–**22a**,**b** a través de la via sintètica ja desenvolupada, intentant resoldre els problemes metodològics comentats, sobretot els relacionats amb l'aïllament dels alcohols intermedis **26a**,**b** i **27a**,**b**

3.2 Optimització de la via de síntesi dels híbrids donepezil–tacrina desenvolupada anteriorment al grup de recerca

3.2.1 Síntesi dels mesilats 28a,b i 29a,b

En el moment d'iniciar aquest projecte, al nostre laboratori hi havia disponible una quantitat important de 4-cloroquinolina **23**, però no del seu anàleg 6-clorosubstituït, **24**, el qual es va haver de sintetitzar. La preparació de **24** es va dur a terme amb rendiment quasi quantitatiu seguint un procediment descrit consistent en fer reaccionar l'àcid 4-cloroantranílic, **33**, amb ciclohexanona i excés de $POCl_3$ a reflux durant 2 h (Esquema 3.2).[118,119]

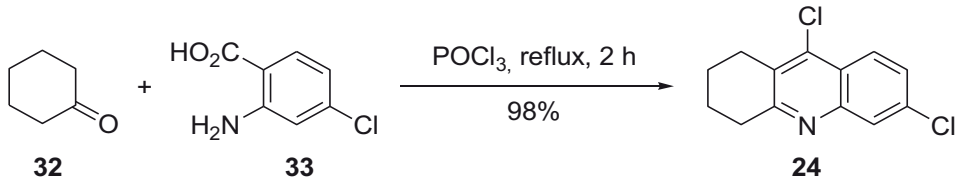

32 **33** **24**

Esquema 3.2

El tractament separat de les 4-cloroquinolines **23 i 24** amb 3 equiv. de 2-aminoetanol o de 3-amino-1-propanol en el si d'1-pentanol a reflux (punt d'ebullició de l'1-pentanol 136–138 ^{o}C) durant 18 h, seguit d'una extracció àcid–base, va permetre l'obtenció dels alcohols **26a,b** i **27a**,**b** amb molt bons rendiments (Esquema 3.3). No només van ser els rendiments d'obtenció d'aquests alcohols lleugerament superiors als obtinguts anteriorment al nostre grup, sinó que l'aïllament dels alcohols mitjançant extraccions àcid–base era molt més fàcil i ràpid que com s'havia fet anteriorment al grup, per eliminació de l'excés d'aminoalcohol i del dissolvent per microdestil·lació a pressió reduïda, i feia més fàcilment escalables aquestes reaccions.

[118]Hu, M.-K.; Lu, C.-F. *Tetrahedron Lett.* **2000**, *41*, 1815. [119]Hu, M.-K.; Wu, L.-J.; Hsiao, G.; Yen, M.-H. *J. Med. Chem.* **2002**, *45*, 2277.

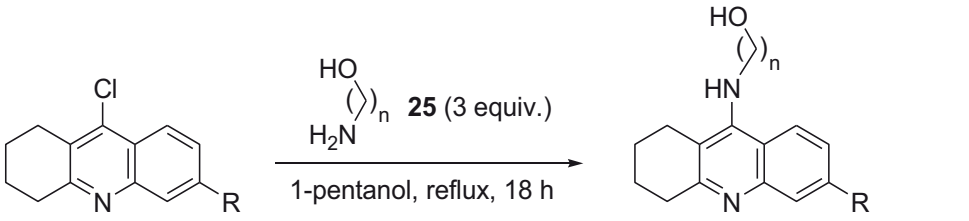

23, R = H
24, R = Cl

26a, R = H, n = 2 (95%)
26b, R = H, n = 3 (quantitatiu)
27a, R = Cl, n = 2 (85%)
27b, R = Cl, n = 3 (92%)

Esquema 3.3

Els alcohols **26a**,**b** i **27a**,**b** es convertiren en els corresponents mesilats per reacció amb clorur de mesil i Et_3N en el si de diclorometà a –10 °C durant 30 min,[120] amb rendiments pràcticament quantitatius (Esquema 3.4).

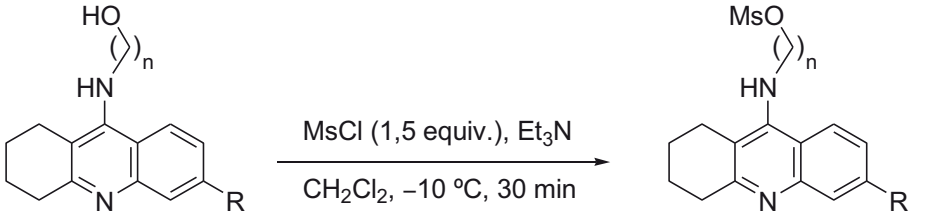

26a, R = H, n = 2
26b, R = H, n = 3
27a, R = Cl, n = 2
27b, R = Cl, n = 3

28a, R = H, n = 2 (95%)
28b, R = H, n = 3 (99%)
29a, R = Cl, n = 2 (97%)
29b, R = Cl, n = 3 (92%)

Esquema 3.4

3.2.2 Síntesi de les piperidines 30 i 31

Un cop es disposava dels mesilats **28a**,**b** i **29a**,**b** s'abordà la preparació de la piperidina **30** i del seu anàleg indànic **31**. La piperidina **30** és un precursor immediat en algunes síntesis del donepezil i derivats.[121,122] Les síntesis descrites de **30** impliquen només dos o tres etapes a partir de la 5,6-dimetoxi-1-indanona, comercialment assequible: condensació aldòlica de la 5,6-dimetoxi-1-indanona amb 1-benzoïl-4-piperidinacarboxaldehid seguit d'hidrogenació catalítica i hidròlisi àcida de la funció amida,[121] o alternativament, condensació aldòlica de la

[120]Crossland, R.K.; Servis, K.L. *J. Org. Chem.* **1970**, *35*, 3195. [121]Sugimoto, H.; Iimura, Y.; Yamanishi, Y.; Yamatsu, K. *J. Med. Chem.* **1995**, *38*, 4821. [122]Elati, C.R.; Kolla, N.; Chalamala, S.R.; Vankawala, P.J.; Sundaram, V.; Vurimidi, H.; Mathad, V.T. *Synth. Commun.* **2006**, *36*, 169.

5,6-dimetoxi-1-indanona amb piridina-4-carboxaldehid seguit d'hidrogenació catalítica.[122,123] Per la seva part, la síntesi descrita de la piperidina **31** implica una reducció del derivat indanònic **30** amb $LiAlH_4$.[123]

No obstant això, una donació de donepezil per part de l'empresa Medichem® en el moment en què abordàvem els treballs inicials ens havia permès dur a terme la síntesi de la piperidina **30** en només una etapa: per desbenzilació del propi donepezil. A més, en el Máster Experimental de Michele Scarpellini s'observà que quan la desbenzilació per hidrogenòlisi del donepezil s'efectuava en medi àcid, la reacció de desbenzilació cursava amb reducció simultània del grup carbonil d'indanona a un grup metilè.

Així amb les quantitats de donepezil de què es disposava, en la present Tesi Doctoral es van preparar les piperidines **30** i **31** utilitzant les condicions d'hidrogenòlisi posades a punt anteriorment al nostre grup. Per hidrogenació del donepezil en presència de Pd/C al 5% en MeOH a pressió atmosfèrica i temperatura ambient durant 3 dies, es va obtenir la piperidina **30** amb rendiment quantitatiu (Esquema 3.5).

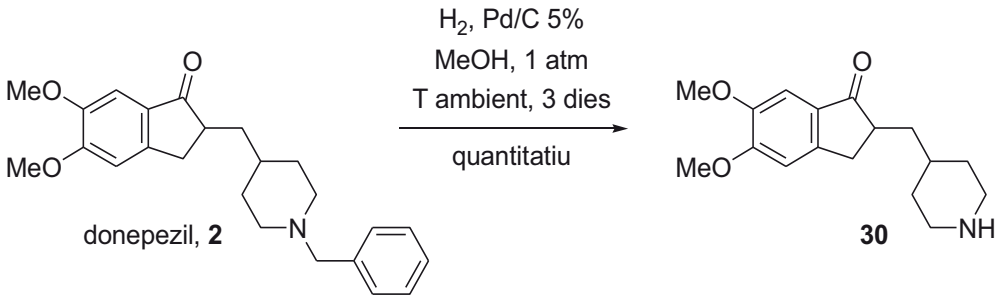

Esquema 3.5

La hidrogenació de l'hidroclorur del donepezil en presència de Pd/C al 5% i HCl 1 N en MeOH a 14 atm de pressió i a 50 °C durant 3 dies va proporcionar en diferents ocasions mescles de **30** i **31**, que s'havien de tornar a hidrogenar fins a obtenir **31** com a únic producte. Quan es va apujar la pressió de la hidrogenació a 28 atm, la temperatura a 65 °C i es va allargar el temps de reacció fins a 6 dies es va obtenir directament la piperidina **31** amb un 82% de rendiment, sense que es detectés la presència de producte de reducció parcial (Esquema 3.6).

[122]Elati, C.R.; Kolla, N.; Chalamala, S.R.; Vankawala, P.J.; Sundaram, V.; Vurimidi, H.; Mathad, V.T. *Synth. Commun.* **2006**, *36*, 169. [123]Reddy, K.V.S.R.K.; Babu, J.M.; Kumar, P.A.; Chandrashekar, E.R.R.; Mathad, V.T.; Eswaraiah, S.; Reddy, M.S.; Vyas, K. *J. Pharm. Biomed. Anal.* **2004**, *35*, 1047.

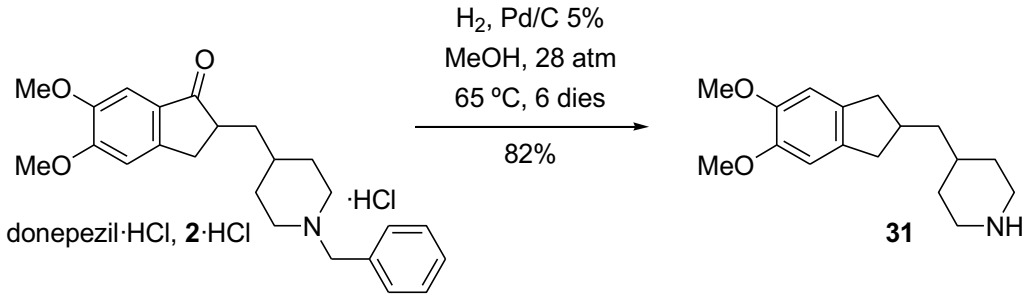

Esquema 3.6

En vista de les dificultats que plantejava la hidrogenació directa del donepezil i per no dependre de les donacions externes del mateix, es va desenvolupar un procediment alternatiu de síntesi de la piperidina **31** per modificació d'una de les metodologies descrites per a la preparació de **30**: condensació aldòlica de la 5,6-dimetoxi-1-indanona amb piridina-4-carboxaldehid, seguit d'hidrogenació catalítica a pressió, en calent i en medi àcid. Així, per reacció de la 5,6-dimetoxi-1-indanona, **34**, amb piridina-4-carboxaldehid, **35**, sota catàlisi d'àcid *p*-toluensulfònic en toluè a reflux durant 6 h amb destil·lació azeotròpica d'aigua, es va obtenir el compost **36** amb excel·lent rendiment (Esquema 3.7). El compost **36** es va sotmetre a hidrogenació catalítica en presència de Pd/C al 5% i HCl conc. en MeOH a 30 atm de pressió i a 65 °C. Analitzant alíquotes de la mescla de reacció cada 6–7 dies, es va observar la presència de la piperidina **31** desitjada juntament amb producte de reducció parcial, **30**, el qual va desaparèixer definitivament al cap de 20 dies. Així, després de 20 dies en aquestes condicions de reacció, es va obtenir la piperidina **31** amb un rendiment gairebé quantitatiu (Esquema 3.7).

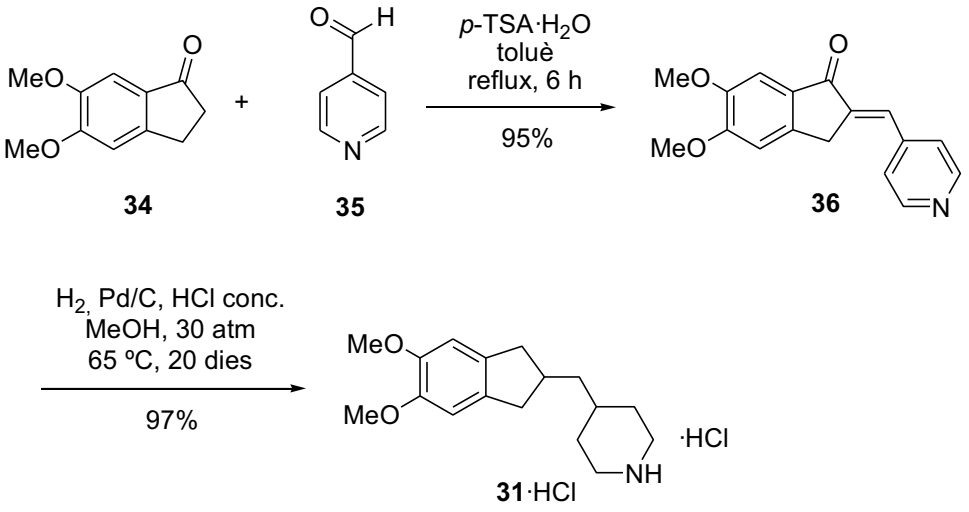

Esquema 3.7

3.2.3 Síntesi dels híbrids donepezil–tacrina 20a,b–22a,b

Finalment, es va dur a terme la síntesi dels híbrids donepezil–tacrina **20a**,**b**–**22a**,**b** per reacció de les piperidines **30** i **31** amb els mesilats **28a**,**b** i **29a**,**b** en presència de Et_3N en el si de DMSO a 85 ^oC durant 2 dies (Esquema 3.8), seguit d'una tediosa purificació dels corresponents crus de reacció per cromatografia en columna a través de gel de sílice. Així, s'obtingueren els híbrids donepezil–tacrina plantejats amb rendiments baixos a moderats (28–56%), però en qualsevol cas, en el mateix rang que els rendiments descrits per altres grups de recerca en alquilacions de la piperidina **30** en el context de la síntesi de derivats del donepezil (24–63%).[121] Els rendiments d'obtenció dels híbrids **20a**,**b** i **22a**,**b** van ser gairebé idèntics als obtinguts prèviament al grup, mentre que en el cas dels híbrids **21a**,**b**, gairebé es va doblar el rendiment descrit prèviament. Aquests híbrids es van transformar en els seus corresponents dihidroclorurs per tractament amb una dissolució metanòlica d'HCl, es purificaren per cristal·lització de MeOH, i es caracteritzaren completament a través de les seves dades espectroscòpiques i anàlisi elemental.

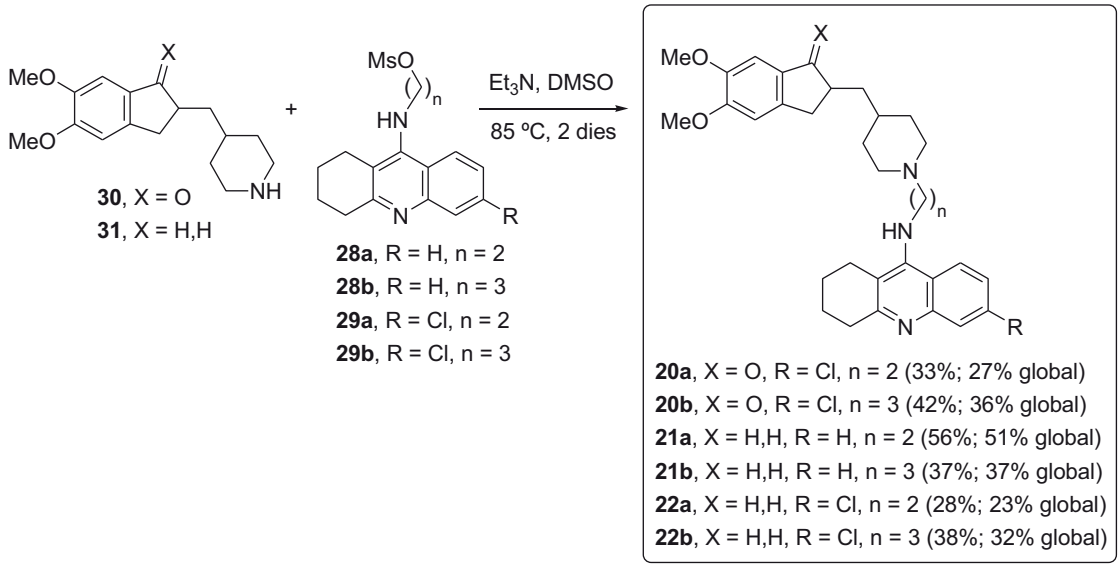

Esquema 3.8

3.3 Mètode alternatiu de síntesi dels híbrids donepezil–tacrina

El segon objectiu de la present Tesi Doctoral consistia en desenvolupar una via alternativa d'accés als híbrids donepezil–tacrina, en la qual tant el fragment piperidínic derivat del

[121] Sugimoto, H.; Iimura, Y.; Yamanishi, Y.; Yamatsu, K. *J. Med. Chem.* **1995**, *38*, 4821

donepezil com la unitat derivada de tacrina s'enllacessin al *linker* reaccionant com a nucleòfils. Al Màster Experimental de Michele Scarpellini s'havia fet un intent d'accés als híbrids donepezil–tacrina per alquilació seqüencial de la 6-clorotacrina i de la piperidina derivada del donepezil. Tanmateix, els intents inicials d'alquilació de la 6-clorotacrina amb 1,3-dibromopropà, 1,3-dicloropropà o 3-cloro-1-propanol van resultar infructuosos.

Tenint en compte que l'alquilació del nitrogen nucleofílic del fragment piperidínic derivat del donepezil el convertiria en un nitrogen terciari, fent menys probables els problemes observats anteriorment en l'alquilació del grup amino primari de la 6-clorotacrina (dialquilació per dues substitucions nucleòfiles intermoleculars o per una intermolecular i una altra intramolecular i/o reaccions d'eliminació), en la present Tesi Doctoral ens vam plantejar reintentar l'accés a alguns dels híbrids donepezil–tacrina (**20a**,**b** i **22a,b**), però duent a terme en primer lloc l'alquilació del fragment piperidínic derivat del donepezil.

Diferents intents d'alquilació de la piperidina **30** amb 1,3-dibromopropà utilitzant Et_3N o una mescla Na_2CO_3 / K_2CO_3 com a base en DMSO a 85 ^oC, en THF a reflux o en EtOH a reflux o en absència de base en el si d'acetonitril van resultar infructuosos, obtenint-se mescles complexes que no semblaven contenir el producte desitjat (^{1}H-RMN) o recuperant-se en part la piperidina de partida inalterada. En vista d'aquests resultats negatius, ens vam plantejar utilitzar un ω-haloalcohol com a espècie electrofílica, en comptes de l'α,ω-dihaloalcà plantejat inicialment. El grup hidroxil de l'alcohol resultant de la reacció d'alquilació es podria transformar després en un bon grup sortint (halogen, mesilat, tosilat) permetent així l'alquilació de la unitat derivada de tacrina. Afortunadament, l'alquilació de les piperidines **30** i **31** amb 2 equivalents de 2-bromoetanol o 3-cloro-1-propanol en 1-pentanol a reflux durant 2 dies, seguida d'aïllament dels alcohols resultants per extracció àcid–base i purificació mitjançant cromatografia en columna a través de gel de sílice va permetre obtenir els alcohols **38a**,**b** i **39a**,**b** amb rendiments moderats (Esquema 3.9). Cal destacar que aquests alcohols són compostos nous, els quals van ser completament caracteritzats a través de les seves dades espectroscòpiques i anàlisis elementals.

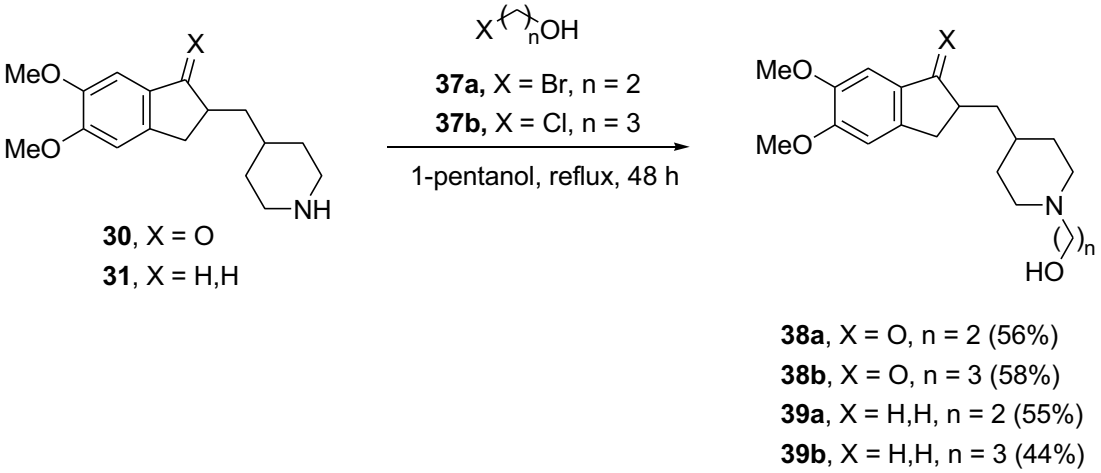

Esquema 3.9

Els alcohols **38a**,**b** i **39a**,**b** es van intentar transformar en els corresponents mesilats utilitzant la mateixa metodologia emprada per a la conversió dels alcohols **26a**,**b** i **27a**,**b** en els mesilats **28a**,**b** i **29a**,**b**, que implica la reacció de l'alcohol amb 1,5 equivalents de clorur de metanosulfonil en presència de 1,7 equivalents de Et_3N en el si de CH_2Cl_2 anhidre a –10 ^{o}C, seguit de tractament amb dissolució aquosa de NaOH 2 N en el final de reacció, per eliminar l'excés de clorur de metanosulfonil i l'acid metanosulfònic format i aïllar el mesilat en forma de base. Tanmateix, el tractament de l'alcohol **39a** amb excés de clorur de metanosulfonil sota aquestes condicions de reacció no va proporcionar el mesilat desitjat, recuperant-se en bona part l'alcohol de partida. El mesilat que s'hauria de formar en aquesta reacció, contenint el grup electròfil en posició β respecte al nitrogen terciari de la piperidina alquilada podria estar en equilibri amb la corresponent sal d'aziridini formada per substitució nucleòfila intramolecular, per reacció de la qual amb els anions hidròxid de la dissolució de NaOH utilitzada en el final de reacció es podria formar fàcilment l'alcohol de partida. Anàlogament, diferents intents de transformació de l'alcohol **39b** en el corresponent tosilat o cloroderivat, per reacció amb clorur de tionil o clorur de *p*-toluensulfonil, seguit de tractament bàsic en el final de reacció tampoc no van proporcionar els compostos desitjats.

En vista d'aquests resultats, ens vam plantejar efectuar la transformació dels alcohols **38a**,**b** i **39a**,**b** en els seus cloroderivats, prescindint del tractament bàsic del final de reacció. Així, per reacció de **38a**,**b** i **39a**,**b** amb excés de clorur de tionil (50 equivalents) en el si de CH_2Cl_2 a reflux durant 4 h, seguit directament d'evaporació de la mescla resultant a pressió reduïda i de cinc cicles de redissolució del cru en CH_2Cl_2 / evaporació a pressió reduïda per tal d'acabar d'arrossegar els components volàtils, es van obtenir crus de reacció constituïts

fonamentalment pels cloroderivats desitjats, en forma d'hidroclorurs (Esquema 3.10), que van ser utilitzats directament en la següent reacció d'alquilació de la 6-clorotacrina.

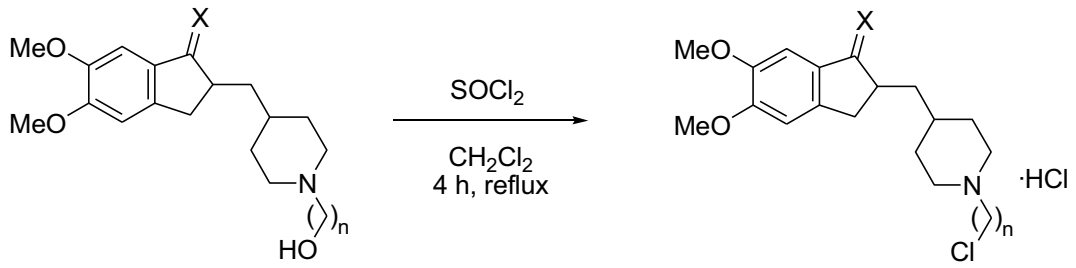

38a, X = O, n = 2
38b, X = O, n = 3
39a, X = H,H, n = 2
39b, X = H,H, n = 3

40a, X = O, n = 2
40b, X = O, n = 3
41a, X = H,H, n = 2
41b, X = H,H, n = 3

Esquema 3.10

La 6-clorotacrina, **43** es va sintetitzar amb rendiment excel·lent per condensacio de tipus Friedländer amb la cicloohexanona, **32**, i el 4-cloro-2-aminobenzonitril, **42**. Tanmateix, la reacció de 1,2 equivalents dels cloroderivats indanònics crus **40a**,**b** amb l'anió de la 6-clorotacrina, **43**, format prèviament per desprotonació del grup amino primari amb excés de KOH (aproximadament 5 equivalents), en el si de DMSO a temperatura ambient durant 3 dies no va proporcionar els híbrids desitjats **20a**,**b**, recuperant-se majoritàriament la 6-clorotacrina de partida inalterada (^{1}H-RMN) (Esquema 3.11).

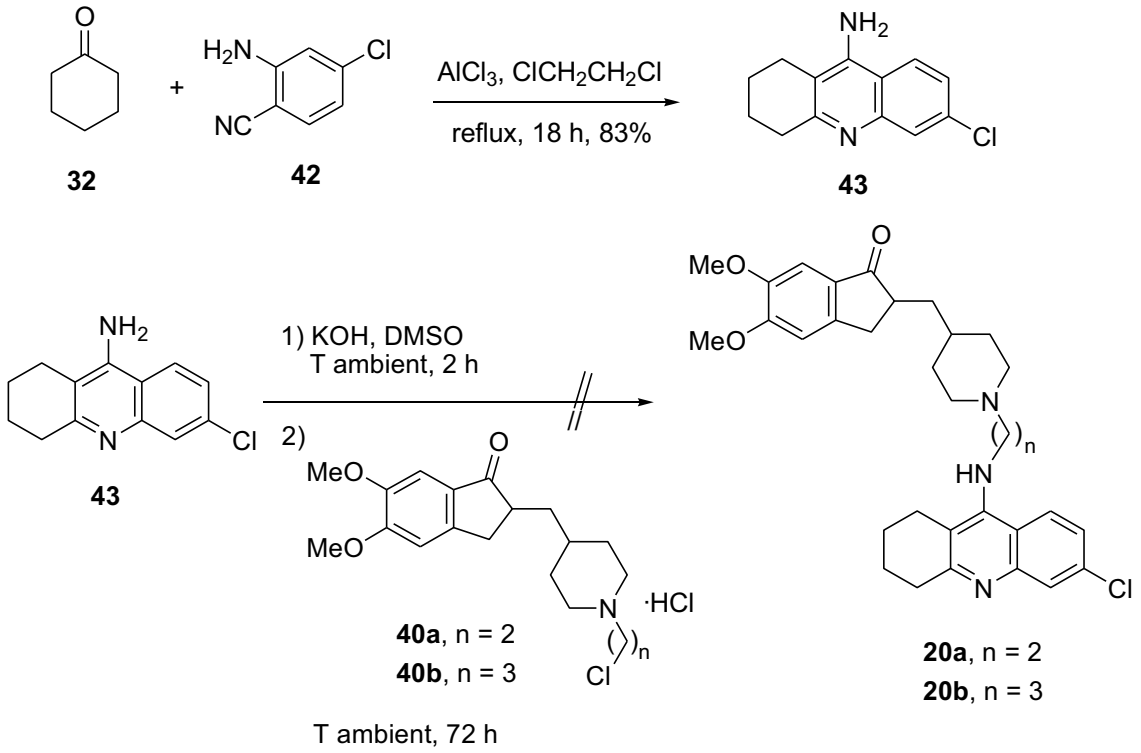

32 **42** **43** **43** **40a**, n = 2 **40b**, n = 3 **20a**, n = 2 **20b**, n = 3

Esquema 3.11

En contrast amb aquests resultats, el tractament dels cloroderivats indànics crus **41a**,**b** amb la 6-clorotacrina en les mateixes condicions de reacció sí que va proporcionar els híbrids desitjats **22a**,**b** amb rendiments moderats, després de purificació dels crus de reacció per cromatografia en columna a través de gel de sílice (Esquema 3.12).

El diferent comportament dels cloroderivats amb sistema d'indanona respecte als derivats amb sistema d'indà podria ser degut a la protonació de l'anió de la 6-clorotacrina (pK_a ≈ 23 com a àcid) per cessió del protó àcid de la posició α-carbonílica del sistema d'indanona dels primers cloroderivats, la qual esdevindria un centre nucleòfil que podria ser alquilat amb una segona molècula de cloroderivat, consumint així l'espècie electrofílica. Això explicaria que es recuperés intacta la 6-clorotacrina de partida, però no el cloroderivat indanònic que podria anar polimeritzant.

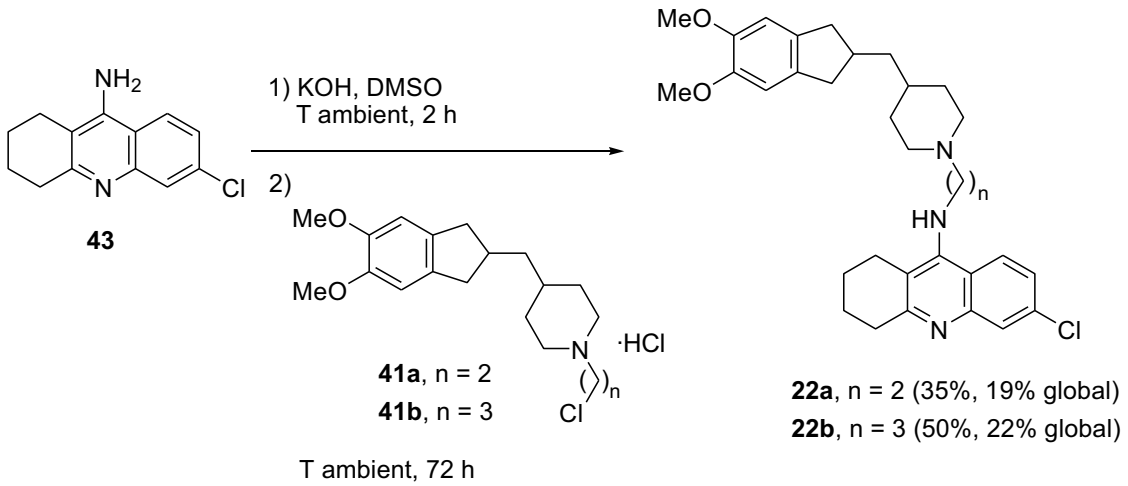

Esquema 3.12

Globalment, aquesta via alternativa sembla vàlida només per a la síntesi d'híbrids donepezil–tacrina amb sistema de 5,6-dimetoxiindà i proporciona aquests compostos amb rendiments lleugerament inferiors als obtinguts amb la via original modificada en aquesta Tesi Doctoral (Esquema 3.8).

Novel Donepezil-Based Inhibitors of Acetyl- and Butyrylcholinesterase and Acetylcholinesterase-Induced β-Amyloid Aggregation

Pelayo Camps,*[,†] Xavier Formosa,[†] Carles Galdeano,[†] Tània Gómez,[†] Diego Muñoz-Torrero,*[,†] Michele Scarpellini,[†] Elisabet Viayna,[†] Albert Badia,[‡] M. Victòria Clos,[‡] Antoni Camins,[§] Mercè Pallàs,[§] Manuela Bartolini,[#] Francesca Mancini,[#] Vincenza Andrisano,[#] Joan Estelrich,[||,⊥] Mònica Lizondo,[||,⊥] Axel Bidon-Chanal,[||] and F. Javier Luque[||]

Laboratori de Química Farmacèutica (Unitat Associada al CSIC), Facultat de Farmàcia, and Institut de Biomedicina (IBUB), Universitat de Barcelona, Av. Diagonal 643, E-08028, Barcelona, Spain, Departament de Farmacologia, de Terapèutica i de Toxicologia, Facultat de Medicina, Universitat Autònoma de Barcelona, E-08193-Bellaterra, Barcelona, Spain, Unitat de Farmacologia i Farmacognòsia, Facultat de Farmàcia, Universitat de Barcelona, Av. Diagonal 643, E-08028, Barcelona, Spain, Department of Pharmaceutical Sciences, Alma Mater Studiorum, Bologna University, Via Belmeloro 6, I-40126 Bologna, Italy, Departament de Fisicoquímica, Facultat de Farmàcia, and Institut de Biomedicina (IBUB), Universitat de Barcelona, Av. Diagonal 643, E-08028, Barcelona, Spain, and Institut de Nanociència i Nanotecnologia, Universitat de Barcelona, Barcelona, Spain

Received February 7, 2008

A novel series of donepezil−tacrine hybrids designed to simultaneously interact with the active, peripheral and midgorge binding sites of acetylcholinesterase (AChE) have been synthesized and tested for their ability to inhibit AChE, butyrylcholinesterase (BChE), and AChE-induced Aβ aggregation. These compounds consist of a unit of tacrine or 6-chlorotacrine, which occupies the same position as tacrine at the AChE active site, and the 5,6-dimethoxy-2-[(4-piperidinyl)methyl]-1-indanone moiety of donepezil (or the indane derivative thereof), whose position along the enzyme gorge and the peripheral site can be modulated by a suitable tether that connects tacrine and donepezil fragments. All of the new compounds are highly potent inhibitors of bovine and human AChE and BChE, exhibiting IC_{50} values in the subnanomolar or low nanomolar range in most cases. Moreover, six out of the eight hybrids of the series, particularly those bearing an indane moiety, exhibit a significant Aβ antiaggregating activity, which makes them promising anti-Alzheimer drug candidates.

Introduction

Since bis(7)-tacrine, a heptamethylene-linked dimer of the first marketed anti-Alzheimer drug tacrine (**1**, Chart 1), was developed 1 decade ago,[1–3] the search for inhibitors of acetylcholinesterase (AChE[a]) able to simultaneously bind to its catalytic and peripheral binding sites has become an area of very active research. Several classes of dual binding site AChE inhibitors have been developed by connecting through a suitable linker the two interacting units, which are generally derived from known AChE inhibitors either commercialized or under development.[2–8] The success of the dual binding site strategy is evidenced by the large increase in AChE inhibitory potency of these dimers or hybrids relative to the parent compounds from which they have been designed. Further interest comes from the fact that some of these dual binding site AChE inhibitors have been shown to inhibit the aggregation of β-amyloid peptide (Aβ),[9–18] which is a key event in the neurotoxic cascade of Alzheimer's disease (AD).[19] This effect, which has been related to the blockade of the AChE peripheral site[20] by dual binding site AChE inhibitors, makes these compounds very promising disease-modifying anti-Alzheimer drug candidates.

Chart 1. Structures of Tacrine, Donepezil, and the Known Donepezil−Tacrine Hybrids **3** and **4**

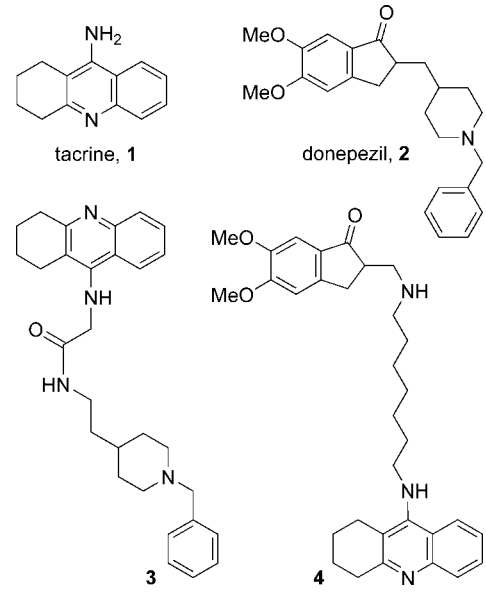

To date, the sole dual binding site AChE inhibitor approved for the treatment of AD is donepezil (**2**, Chart 1), though it was not specifically designed as such.[21] The X-ray crystallographic structure of the complex between *Torpedo californica* AChE (*Tc*AChE) and donepezil (PDB entry 1EVE)[22] shows that the

* To whom correspondence should be addressed. For P.C.: phone, +34 + 934024536; fax, + 34 + 934035941; e-mail, camps@ub.edu. For D.M.-T.: phone, +34 + 934024536; fax, + 34 + 934035941; e-mail, dmunoztorrero@ub.edu.

† Laboratori de Química Farmacèutica and IBUB, Universitat de Barcelona.

‡ Universitat Autònoma de Barcelona.

§ Unitat de Farmacologia i Farmacognòsia, Universitat de Barcelona.

Bologna University.

|| Departament de Fisicoquímica, Universitat de Barcelona.

⊥ Institut de Nanociència i Nanotecnologia, Universitat de Barcelona.

[a] Abbreviations: Aβ, β-amyloid peptide; AChE, acetylcholinesterase; AChEI, acetylcholinesterase inhibitor; AD, Alzheimer's disease; APP, amyloid precursor protein; BChE, butyrylcholinesterase; DTNB, 5,5′-dithiobis(2-nitrobenzoic) acid; HFIP, 1,1,1,3,3,3-hexafluoro-2-propanol; MD, molecular dynamics; PDB, protein data bank; PTFE, polytetrafluoroethylene; rmsd, root-mean square deviation

10.1021/jm8001313 CCC: $40.75
Published on Web 06/03/2008

elongated structure of donepezil spans the entire length of the enzyme active-site gorge forming a variety of interactions with specific residues, such as aromatic stacking interactions between the benzyl and indanone moieties and the indole rings of Trp84 and Trp279 (Trp86 and Trp286 in human AChE) at the catalytic and peripheral sites, respectively, and the cation−π interaction between the protonated piperidine nitrogen and the phenyl ring of Phe330. As a result of its dual binding site character, donepezil at 100 μM is able to inhibit by 22% the AChE-induced aggregation of Aβ.[23] As bis(7)-tacrine, most of the dual binding site AChE inhibitors developed so far contain at least one unit related to tacrine, probably because of its ease of synthesis and its affinity for both the active and peripheral sites of AChE.[10–12,17,24–34] Conversely, to the best of our knowledge, only two classes of donepezil-based hybrids have been purposely designed as dual binding site AChE inhibitors by combining different fragments of donepezil with tacrine.[30,31] Among these donepezil−tacrine hybrids, compounds **3** and **4** (Chart 1), which retain the *N*-benzylpiperidine and the 5,6-dimethoxy-1-indanone moieties of donepezil, respectively, are the most potent, they being 37- and 7-fold more potent than tacrine but nearly equipotent to donepezil, while their Aβ-antiaggregating effect has not been assessed.

Herein, we describe the synthesis, pharmacological evaluation (AChE and butyrylcholinesterase (BChE) inhibition and Aβ-antiaggregating effect), and molecular modeling of a novel class of highly potent donepezil−tacrine hybrids. On the basis of the binding modes of donepezil[22] and tacrine[35] within *Tc*AChE, these novel hybrids were designed by combining the 5,6-dimethoxy-2-[(4-piperidinyl)methyl]-1-indanone moiety of donepezil with tacrine, which would thus replace the benzyl moiety of donepezil. In contrast to the preceding approaches,[30,31] the strategy adopted here largely preserves the chemical skeleton of donepezil, which should allow the new hybrid compounds not only to mimic the interactions of tacrine at the catalytic site and of the indanone ring at the peripheral one but also to preserve the contacts of the piperidine moiety with the residues that are lining the wall of the AChE gorge as a third binding site within the enzyme.

Chemistry

The structures of the novel donepezil−tacrine hybrids **14**−**15a**,**b** are shown in Scheme 1. The linker was selected taking into account the sizable increase in AChE inhibitory potency observed in tacrine-based homo- and heterodimers upon introduction in the tether of a protonatable amino group at a distance equivalent to three methylene groups.[28,29] Because this protonatable amino group could be the piperidine nitrogen atom of these donepezil−tacrine hybrids, a length of two to three methylenes for the linker was considered. Moreover, introduction of a chlorine atom at position 6 of the tacrine skeleton should lead to additional interactions within the active site of the enzyme.[36–38]

The synthesis of the novel donepezil−tacrine hybrids **14**−**15a**,**b** was carried out through a three-step sequence involving amination of the known 9-chloro-1,2,3,4-tetrahydroacridines **5** or **6**[39,40] with an ω-aminoalcohol **7**, followed by mesylation of the resulting alcohol **8** or **9** and subsequent reaction with the known piperidine **12**[21,41,42] (Scheme 1). Taking into account that both enantiomers of donepezil display similar pharmacologic and pharmacokinetic profiles and span the entire AChE gorge with a common pattern of interactions,[43] compounds **14**−**15a**,**b**, which bear the stereocenter-containing indanone unit of donepezil, were prepared in racemic form.

Scheme 1. Synthesis of the Donepezil−Tacrine Hybrids **14**−**17a**,**b**

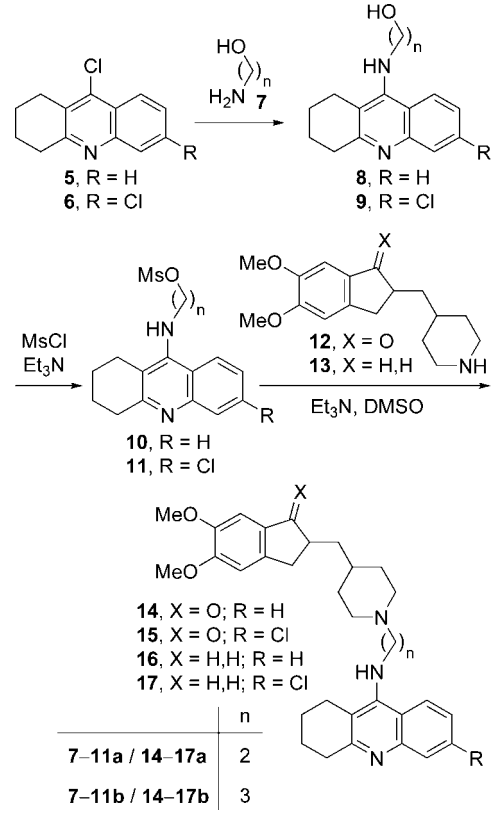

Moreover, because the indane derivative **13** is readily available,[44] the synthesis of a parallel series of achiral hybrids **16**−**17a**,**b** was also carried out by following the same methodology but using piperidine **13** in the last step instead of **12** (Scheme 1).

In a first approach, the amination of the chloroquinolines **5** and **6** was carried out on reaction with 3 equiv of 2-aminoethanol (**7a**) or 3-amino-1-propanol (**7b**) in refluxing 1-pentanol[45,46] for 18 h, followed by removal of the solvent and excess of aminoalcohol by distillation under reduced pressure. Alternatively, the change of this tedious microdistillation workup by a standard acid−base extraction turned out to be much more convenient for the isolation of the desired alcohols. In this way, the new alcohols **8a** and **9a**,**b** and the known alcohol **8b**[40] were obtained in excellent yields and used directly in the next reaction without further purification. However, for characterization purposes, the new alcohols **8a** and **9a**,**b** were transformed into their hydrochlorides and recrystallized from MeOH/AcOEt mixtures.

Mesylation of **8**-**9a**,**b** proceeded almost quantitatively, affording pure mesylates **10a**,**b** and **11a** and slightly impure **11b**, which were used directly in the following reaction.

Piperidine **12** was prepared in quantitative yield following a described procedure[42] based on the catalytic hydrogenation of donepezil in MeOH at 1 atm and room temperature for 72 h, while piperidine **13** was prepared in 82% yield by a new procedure involving the catalytic hydrogenation of donepezil hydrochloride in MeOH in the presence of 1 N HCl at 28 atm and 65 °C for 6 days (Scheme 2). Alternatively, **13** was prepared in better yield (92% overall) through a two-step procedure involving aldol condensation of 5,6-dimethoxy-1-indanone with pyridine-4-carboxaldehyde in the presence of *p*-TsOH·H_2O in refluxing toluene,[41] followed by catalytic hydrogenation of the resulting compound **18** under forcing conditions (Scheme 2).

Scheme 2. Synthesis of Piperidine **13** and the Indane Derivative of Donepezil **19**

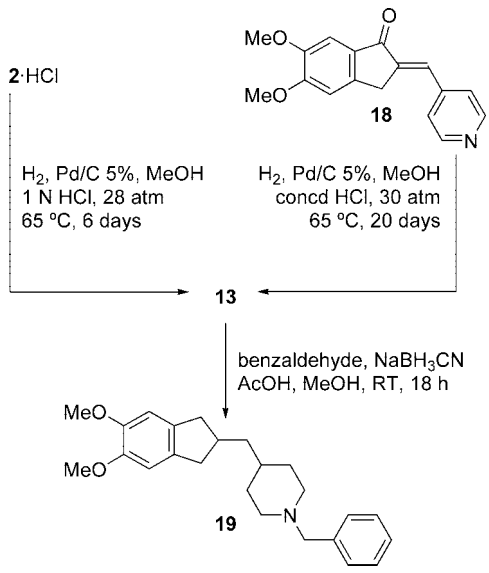

Finally, alkylation of piperidines **12** and **13** with a stoichiometric amount of mesylates **10**−**11a**,**b** in the presence of excess of Et_3N in DMSO at 85 °C for 2 days afforded the desired donepezil−tacrine hybrids **14**−**15a**,**b** and the indane derivatives **16**−**17a**,**b** in low to moderate yields (Scheme 1) after a tedious purification of the crude products by silica gel column chromatography.

For comparison purposes, the indane derivative of donepezil, **19** (Scheme 2), was also prepared. This compound can be prepared directly from donepezil by reduction with borane in THF.[44] However, in our hands this reaction failed. Other attempts to prepare **19** involving Wolff−Kishner reduction of donepezil or benzylation of piperidine **13** afforded intractable mixtures containing the desired product together with starting materials and some byproduct, as those arising from demethylation of the 5-methoxy group, in the first case, or from *N*,*N*-dibenzylation, in the latter. Finally, we prepared **19** in 53% yield by $NaBH_3CN$ reductive alkylation of piperidine **13** with benzaldehyde (Scheme 2), followed by purification by silica gel column chromatography.

The novel hybrids **14**−**17a**,**b** were fully characterized as dihydrochlorides through their spectroscopic data and elemental analyses (C, H, N, Cl), while the known indane analogue of donepezil **19** was characterized by spectroscopic data and HRMS analyses.

Pharmacology

AChE and BChE Inhibition. To determine the potential interest of the new donepezil−tacrine hybrids **14**−**15a**,**b** and the indane derivatives **16**−**17a**,**b** for the treatment of AD, their AChE inhibitory activity was assayed by the method of Ellman et al.[47] on AChE from bovine (bAChE) and human (hAChE) erythrocytes. Recent evidence has shown that in advanced AD patients, AChE activity is greatly reduced in specific brain regions while BChE activity increases, likely as compensation for AChE decrease.[48] The increasing role of BChE in the hydrolysis of acetylcholine as the ratio AChE/BChE gradually decreases in these patients suggests that inhibition of BChE might be valuable in the search for anti-Alzheimer agents.[48,49] Consequently, the inhibitory activity on human serum BChE (hBChE) was also assayed by the same method.

Table 1. Pharmacological Data of the Hydrochlorides of Tacrine, 6-Chlorotacrine, Donepezil, Compound **19**, and the Dihydrochlorides of the Donepezil−Tacrine Hybrids **14**−**15a,b** and Their Indane Derivatives **16**−**17a**,**b**[a]

	IC_{50} (nM)		
compd	bAChE	hAChE	hBChE
14a·2HCl	1.74 ± 0.02	4.04 ± 0.06	12.4 ± 0.6
14b·2HCl	0.29 ± 0.03	0.88 ± 0.04	12.3 ± 0.6
15a·2HCl	0.57 ± 0.05	0.67 ± 0.06	136 ± 9
15b·2HCl	0.09 ± 0.01	0.27 ± 0.03	66.3 ± 4.0
16a·2HCl	2.28 ± 0.06	5.13 ± 0.52	8.06 ± 0.32
16b·2HCl	0.82 ± 0.06	2.16 ± 0.21	7.25 ± 0.33
17a·2HCl	1.86 ± 0.07	2.60 ± 0.23	88.7 ± 0.2
17b·2HCl	0.82 ± 0.08	1.06 ± 0.05	72.7 ± 4.2
tacrine·HCl	130 ± 10	205 ± 18	43.9 ± 1.7
6-chlorotacrine·HCl	5.73 ± 0.44	8.32 ± 0.75	916 ± 19
donepezil·HCl	8.12 ± 0.26	11.6 ± 1.6	7273 ± 621
19·HCl	1451 ± 33	not determined	6401 ± 119

[a] Values are expressed as mean ± standard error of the mean of at least four experiments. IC_{50} inhibitory concentration (nM) of AChE (from bovine or human erythrocytes) or BChE (from human serum) activity.

Table 1 summarizes the data for the new compounds, as well as for tacrine·HCl, 6-chlorotacrine·HCl, and donepezil·HCl as reference compounds. Although the indane analogue of donepezil **19** is a known compound,[44] its biological activity has not been determined. In order to extend the comparison of activity between indanone and indane derivatives planned for the novel hybrids, the cholinesterase inhibitory activity of this indane derivative of donepezil was also assessed. All of the new hybrids are highly potent bAChE inhibitors, exhibiting IC_{50} values in the subnanomolar range in most cases and being clearly more potent than the parent compounds tacrine (57- to 1440-fold), 6-chlorotacrine (3- to 65-fold), donepezil (4- to 90-fold), and **19** (640- to 16100-fold). Hybrids **14**−**15**, which bear the indanone system of donepezil, are more potent bAChE inhibitors (1.3- to 9-fold more potent) than their indane analogues **16**−**17**, although the difference is much more pronounced in the case of donepezil and **19** (180-fold). The presence of a chlorine atom in the tacrine moiety enhances the inhibitory potency by 3-fold in indanone hybrids, while it has less effect in indane hybrids. Moreover, the three-methylene tether in the hybrids of the **b** series makes them 6- and 3-fold more potent than their indanone and indane counterparts of the **a** series, respectively. Overall, compound **15b** is the most active compound with an IC_{50} of 90 pM.

The new hybrids result in less potent inhibitors of human than bovine AChE (1.2- to 3-fold less potent), as it is the case for the parent compounds (around 1.5-fold less potent). Nevertheless, they are highly potent hAChE inhibitors, being more active than tacrine (40- to 760-fold), 6-chlorotacrine (2-to 30-fold), and donepezil (2- to 45-fold). As observed for bAChE, the best substitution pattern involves the presence of a chlorine atom at position 6 of the tacrine unit, the indanone ring of donepezil, and a tether length of three methylenes. As a result, **15b** is also the most active hAChE inhibitor (IC_{50} = 0.27 nM).

Moreover, the new hybrids are potent inhibitors of hBChE, though their activity is lower than that shown for hAChE. Thus, these compounds are 1.6- to 246-fold more potent toward hAChE than hBChE, as it is found for 6-chlorotacrine and donepezil (110- and 627-fold more potent toward AChE) but in contrast with tacrine (4.7-fold more potent toward BChE). When hBChE inhibitory activity is considered, the structure−activity relationships in this novel class of compounds reveal trends different from those observed for the AChE inhibitory activity. Thus, the indane hybrids **16**−**17** are 1.5-fold more potent than their analogues **14**−**15** bearing the indanone system of donepezil

(with the only exception of **17b**, which is slightly less potent than **15b**), which agrees with the 1.1-fold increase in potency of indane analogue **19** relative to donepezil. Moreover, a chlorine atom at position 6 of the tacrine unit is detrimental for the hBChE inhibitory activity, the unsubstituted hybrids **14** and **16** being 10-fold more potent than their 6-chloro derivatives **15** and **17**, which agrees with the 21-fold increase in potency of tacrine relative to 6-chlorotacrine and with the results reported for other tacrine-based dual binding site AChE inhibitors.[12,26] The effect of the tether length on the BChE inhibitory activity is much lower than that observed when the AChE inhibitory activity is considered, the hybrids of the **b** series being equipotent or slightly more potent (up to 2-fold) than their counterparts of the **a** series. Overall, the most active BChE inhibitor is **16b** (IC_{50} = 7.25 nM), which is 6-, 125-, 1000-, and 880-fold more potent than tacrine, 6-chlorotacrine, donepezil, and **19**, respectively.

Although the higher AChE vs BChE inhibitory activity of the first tacrine-based homo- and heterodimers was initially ascribed to the lack of a peripheral binding site in BChE,[1,46] recent studies have suggested that Phe278 would be responsible for $\pi-\pi$ interactions with aromatic moieties of tacrine-based heterodimers.[28] The higher BChE inhibitory activity of bis(7)-tacrine and several tacrine-based heterodimers,[28,29] as well as that of some of the new donepezil−tacrine hybrids herein described, relative to tacrine seems to validate this hypothesis. At this point, the high inhibitory activity toward both AChE and BChE of most of the donepezil−tacrine hybrids should not be detrimental for an anti-Alzheimer agent because dual inhibition of AChE and BChE could increase the efficacy of treatment and broaden the indications.[49]

The novel compounds reported in this study compare quite favorably with the previously known donepezil−tacrine hybrids.[30,31] Thus, hybrids **14**−**17a**,**b** are more potent AChE inhibitors than compounds **3** (IC_{50} = 6.0 nM, using rat cortex AChE; IC_{50} = 223 and 5.7 nM[21] for tacrine and donepezil, respectively, with the same enzyme source) and **4** (IC_{50} = 25 nM, using bovine erythrocyte AChE; IC_{50} = 167 and 19 nM for tacrine and donepezil, respectively, in the same assay). Regarding the BChE inhibitory activity, compounds **14a**,**b** and **16a**,**b** are more potent than **3** (IC_{50} = 76 nM, using rat serum BChE; IC_{50} = 92 and 7138 nM[21] for tacrine and donepezil, respectively, with the same enzyme source), though none of them is as potent as **4** (IC_{50} = 0.6 nM, using hBChE; IC_{50} = 24 and 930 nM for tacrine and donepezil, respectively).

Thioflavin T Competition Assay. Inestrosa et al. reported that AChE binds, through its peripheral site, to Aβ, thereby inducing amyloid fibril formation,[20,50,51] thus making blockade of the AChE peripheral site an interesting pharmacological target to develop disease-modifying anti-Alzheimer drug candidates. Since propidium, a selective inhibitor of the AChE peripheral site, exhibits an increase in fluorescence upon binding to AChE, it has been used as a probe for competitive ligand binding to the enzyme.[31,52,53] Thioflavin T is another fluorescent probe widely used to detect amyloid structures,[54] though it can also bind to other proteins.[55,56] In particular, thioflavin T binds to the AChE peripheral site, and the fluorescence enhancement reported for thioflavin T upon binding to AChE is much greater than that observed with propidium.[56] Therefore, we chose thioflavin T to study the interaction of selected donepezil−tacrine hybrids (compounds **15a** and **15b**) at the AChE peripheral site.

Table 2 shows the reduction of thioflavin T fluorescence arising from the competition with **15a** and **15b**, as well as tacrine, 6-chlorotacrine, and donepezil as reference compounds.

Table 2. Thioflavin T Competition Assay Results with the Dihydrochlorides of the Donepezil−Tacrine Hybrids **15a** and **15b** and with the Hydrochlorides of Tacrine, 6-Chlorotacrine, and Donepezil[a]

compd	reduction of fluorescence (%)
15a·2HCl	79.4 ± 3.5
15b·2HCl	57.0 ± 2.0
tacrine·HCl	12.6 ± 3.8
6-chlorotacrine·HCl	12.4 ± 1.9
donepezil·HCl	26.0 ± 3.5

[a] Percentage of thioflavin T fluorescence reduction by effect of several AChE inhibitors at 100 μM concentration. Values are expressed as the mean ± standard error of the mean of three experiments.

Table 3. Inhibition of hAChE-Induced Aggregation of Aβ_{1-40} by Donepezil−Tacrine Hybrids **15**−**17a**,**b** and Tacrine, 6-Chlorotacrine, Donepezil, and **19** as Reference Compounds[a]

compd	inhibition at 100 μM ± SEM (%)
15a·2HCl	37.6 ± 8.8
15b·2HCl	46.1 ± 9.0
16a·2HCl	60.0 ± 3.2
16b·2HCl	65.9 ± 2.5
17a·2HCl	61.6 ± 1.8
17b·2HCl	63.5 ± 6.2
tacrine·HCl	7[b]
6-chlorotacrine·HCl	8.5 ± 1.6
donepezil·HCl	22[b]
19·HCl	17.5 ± 2.5

[a] Values are the mean of two independent measurements, each performed in duplicate (SEM = standard error of the mean). [b] Data from ref 23.

Since the excitation wavelength of propidium is very close to the emission wavelength of thioflavin T, this compound was not included in the assay. The active site inhibitors tacrine and 6-chlorotacrine reduce thioflavin T fluorescence, on average, by 12%, an effect that might be ascribed to changes in the local conformation at the peripheral site induced upon binding at the AChE active site.[56] The dual binding site AChE inhibitor donepezil led to a 2-fold greater reduction in fluorescence (26% reduction) relative to the preceding active site inhibitors, as expected from the direct interaction of the indanone moiety with the AChE peripheral site. Finally, the novel donepezil−tacrine hybrids **15a** and **15b** produced the highest reductions in thioflavin T fluorescence among all the tested compounds (79% and 57% reduction, respectively), which could be ascribed to the displacement of the fluorophore at the peripheral site of the enzyme. Moreover, the 3- and 2-fold greater effect obtained for **15a** and **15b** relative to donepezil suggests a larger occupancy of the AChE peripheral site by the indanone unit of the novel hybrids.

Inhibiton of AChE-Induced Aβ Aggregation. The results of the thioflavin T competition assay provide indirect evidence of the ability of these donepezil−tacrine hybrids to interfere with the AChE-induced Aβ aggregation. A direct measure involving AChE and Aβ was therefore required to assess the potential disease-modifying role of these hybrids. Thus, the inhibitory activity of hybrids **15**−**17a**,**b** on the AChE-induced aggregation of Aβ_{1-40} was determined by a thioflavin T fluorescent method.[23] Also, the Aβ-antiaggregating effect of 6-chlorotacrine and the indane derivative of donepezil **19** was determined, while those of tacrine and donepezil were already described.[23]

Table 3 summarizes the Aβ-antiaggregating activity of the novel hybrids and reference compounds. The six tested donepezil−tacrine hybrids exhibit, at a 100 μM concentration, a significant Aβ-antiaggregating effect with percentages of inhibition ranging from 38% to 66%, being 5.4- to 9.4-fold more potent than tacrine, 4.4- to 7.8-fold more potent than 6-chlorotacrine, 1.7- to 3-fold more potent than donepezil, and 2.1-

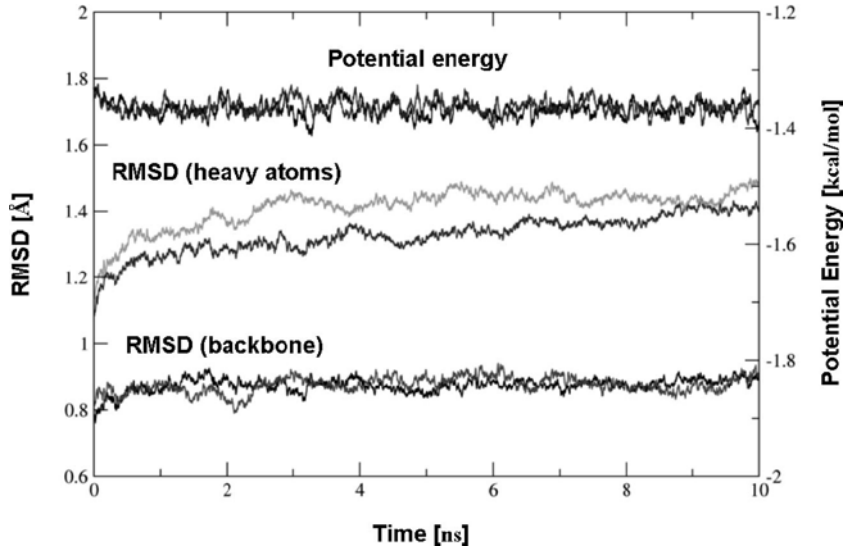

Figure 1. Time dependence of the potential energy ($\times 10^5$, kcal/mol) and the positional root-mean-squared deviation (rmsd, Å) determined for the backbone and heavy atoms in the mobile part of the simulation system for the hAChE complexes with **15a** (gray) and **15b** (black). The profiles were smoothed in 50 ps windows for the sake of clarity.

to 3.8-fold more potent than **19**. Indane derivatives **16**−**17a**,**b** are clearly more potent than indanone derivatives **15a**,**b** (about 1.5-fold), in contrast with the similar effect determined for donepezil and its indane derivative **19**. The length of the linker and the substitution at the active site interacting unit, i.e., the presence or absence of the chlorine atom at position 6 of the tacrine unit, have little effect on the Aβ-antiaggregating activity of the hybrids, observing only a slightly increased effect in the hybrids bearing the trimethylene linker. The Aβ-antiaggregating effects exhibited by these donepezil−tacrine hybrids are in the same range as those of known dual binding site AChE inhibitors such as lipocrine,[11] xanthostigmine derivatives,[13] and bis-(7)-tacrine derivatives,[17] while other families with lower[9,14] or higher[10,12,15,16] potencies have been developed.

The ability of dual binding site AChE inhibitors to block the AChE-induced Aβ aggregation constitutes their most interesting property because of the derived potential to interfere upstream in the neurotoxic cascade of AD. However, some concerns exist about the biological relevance of the results of the in vitro Aβ antiaggregating effects of these compounds. Indeed, these assays are performed using much higher concentrations of AChE and Aβ than those present in brain, but they are necessary to accelerate the aggregation process up to a reasonable extent for analytical purposes. Also, the concentration of inhibitor used in these assays is much higher (usually 100 μM) than those necessary to inhibit AChE (in the nanomolar or picomolar range). However, as pointed out elsewhere,[23] these high concentration values should be normalized in order to compare the inhibition data. Thus, if the inhibitor/AChE concentration ratio in both the Ellman's assay for determination of the AChE inhibitory activity and in the thioflavin T-based fluorometric assay for determination of the Aβ antiaggregating effect is taken into account, the resulting values are indeed of the same magnitude. Thus, it would seem reasonable that similar amounts of a given inhibitor might afford both inhibitory activities.

Moreover, the proof-of-concept of the therapeutic usefulness of the in vitro Aβ antiaggregating effect of dual binding site AChEIs has been recently obtained in in vivo studies. Thus, memoquin, a dual binding site AChEI that in vitro blocked by 87% the AChE-induced Aβ aggregation at 100 μM,[15,16] has been shown to delay Aβ expression to significantly reduce Aβ deposits and to rescue behavioral deficits linked to attention and memory in 15-month-old AD11 mice, a kind of transgenic mice that display a full set of hallmarks of AD.[15] Also, Neuropharma's NP-61 (formerly NP-0361), a dual binding site AChEI that in vitro inhibited the AChE-induced Aβ aggregation with an IC_{50} value 1 order of magnitude lower than that of propidium, reduced the number, surface area, and size of amyloid plaques in the cortex and hippocampus in human amyloid precursor protein (hAPP) transgenic mice (Swedish and London mutation) after oral administration during 3 months, and the reduced brain amyloid burden resulted in a significantly increased cognition (spatial learning and memory in the Morris water maze test).[57] In the first half of 2007, NP-61 entered phase I clinical trials for Alzheimer's disease in the U.K.,[58] which constitutes clear evidence of the promising role of these compounds as anti-Alzheimer disease-modifying agents.

Molecular Modeling Studies

To gain insight into the molecular determinants that modulate the inhibitory activity of the novel donepezil−tacrine hybrids, the binding modes of **15a** and **15b** were explored by means of 10 ns molecular dynamics (MD) simulations performed for their complexes to hAChE. In the two cases the potential energy dropped smoothly during the first nanosecond, but it remained nearly constant for the rest of the trajectory (Figure 1). Indeed, the stability of the trajectories is supported by the small positional root-mean-squared deviations determined for the backbone and heavy atoms, which amount to around 0.9 and 1.4 Å, respectively (Figure 1).

The position of **15a** with respect to selected key residues in the binding site is shown in Figure 2. The tacrine moiety is firmly bound to the catalytic site of hAChE, it being stacked against the aromatic rings of Trp86 and Tyr337 (average distances from the central ring of tacrine of 3.73 and 4.35 Å, respectively, and numbering of residues corresponding to hAChE). The aromatic nitrogen of tacrine, protonated at physiological pH, is hydrogen-bonded to the main chain carbonyl oxygen of His447 (average N···O distance of 2.81 Å). Finally, the chlorine atom occupies a small hydrophobic pocket formed by Trp439, Met443, and Pro446, which parallels the interaction observed between the chlorine atom at position 3 of huprine X, a hybrid compound whose structure contains a

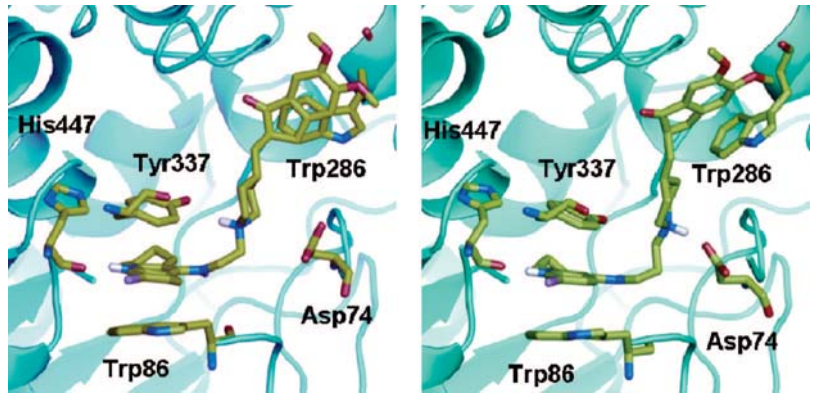

Figure 2. Representation of the heterodimers **15a** (left) and **15b** (right) in the binding site of hAChE highlighting selected residues that form the main interactions with tacrine, piperidine, and indanone units of the inhibitors. Most hydrogen atoms are omitted for the sake of clarity.

6-chlorotacrine moiety, and *Tc*AChE,[38,59] though in this latter case Pro446 is replaced by Ile439. The occupancy of such hydrophobic pocket by the chlorine atom contributes to the higher potency of heterodimers having the 6-chlorotacrine unit relative to their unsubstituted counterparts. As noted previously,[12,28] in hBChE, Met437 replaces Pro446 of hAChE and Ile439 of *Tc*AChE, which makes the terminal methyl group of Met437 to be around 1.2 Å closer to the chlorine atom. The larger steric hindrance due to the greater proximity of the chlorine atom to Met437 could account for the detrimental influence of this substituent on the hBChE inhibitory activity.

Regarding the linker, which is aligned along the gorge, the most relevant features come from the interactions formed by the piperidine ring. This unit occupies a position slightly shifted from that found in the X-ray crystallographic structure of the *Tc*AChE-donepezil complex (PDB entry 1EVE), although it still retains the electrostatic interaction with the carboxylate group of Asp74 (average N(piperidine)···O(carboxylate) distance of 4.72 Å). In turn, this latter residue is hydrogen-bonded to the hydroxyl group of Tyr72 (average O···O distance of 2.87 Å). Moreover, the protonated piperidine nitrogen is hydrogen-bonded to the hydroxyl group of Tyr337 (average N(piperidine)···O distance of 3.20 Å). Thus, a network of interactions that couple several residues in the gorge and the catalytic binding site is formed. Finally, the indanone ring is stacked onto the aromatic ring of Trp286 (average distance between the centers of indanone and indole rings of 4.38 Å), whose orientation resembles that found in the *Tc*AChE−donepezil complex. Moreover, the carbonyl group of the indanone unit forms water-mediated contacts with the backbone N−H groups of Phe295 and Arg296 and the C═O groups of Pro290 and Ser293, which should contribute to the higher AChE inhibitory activity of indanone derivatives relative to the indane analogues.

The binding mode of **15b** at the catalytic site of hAChE closely mimics the interactions noted above for **15a** (Figure 2). Thus, the tacrine ring is stacked against Trp86 and Tyr337 (average distances between rings of 3.63 and 4.44 Å, respectively), the protonated quinoline nitrogen is hydrogen-bonded to the main chain carbonyl oxygen of His447 (average N···O distance of 2.82 Å), and the chlorine atom fills the hydrophobic pocket formed by Trp439, Met443, and Pro446. The enlargement of the tether length, however, leads to differences in the interactions found along the gorge and at the peripheral site. First, the protonated piperidine N−H group points directly to the carboxylate group of Asp74 (average N···O distance of 2.73 Å), which would strengthen the electrostatic interaction. The hydrogen bonds between Asp74 and Tyr72 and between the piperidine N−H unit and Tyr337 observed in the binding of **15a** are lost in the complex with **15b**. Thus, Asp74 forms a hydrogen-bond interaction with the backbone N−H unit of Leu76 and the hydroxyl group of Tyr337 establishes a hydrogen-bond contact with Tyr124. Second, though at the beginning of the simulation the indanone ring was stacked onto the indole ring of Trp286, its orientation changed along the first nanosecond of MD simulation and adopted an arrangement roughly normal to the indole ring (Figure 3). This change was accompanied by a conformational change in the indole ring of Trp286, whose position differed from that found in the X-ray structure by a rotation around the $C_\alpha-C_\beta-C3_{indole}-C3a_{indole}$ from −83° (in 1EVE) to +32°. This finding, therefore, supports the conformational plasticity of this residue in the peripheral site of the enzyme already noted by other studies.[12,60–62]

Comparison of the binding mode of compounds **15a** and **15b** with that of tacrine and donepezil (taken from X-ray structures 1ACJ and 1EVE, respectively) shows that the tacrine unit in the dual binding site inhibitors closely matches the position occupied by tacrine in the catalytic site (Figure 4). There are, however, notable differences in the relative arrangement of the indanone units of **15a** and **15b**. Thus, in **15a** this unit is shifted compared to the position occupied by the corresponding moiety of donepezil, leading to a more efficient $\pi-\pi$ stacking interaction between the indanone ring of **15a** and the indole ring of Trp286 (Figure 4). In **15b** the strong electrostatic interaction formed between the protonated piperidine and Asp74 explains the distinct orientation of the indanone unit relative to donepezil and the conformational change adopted by the indole ring of Trp286, which impedes the formation of a $\pi-\pi$ stacking interaction (Figure 4).

Conclusion

We have synthesized a new series of donepezil−tacrine hybrids, designed to simultaneously interact with the active, peripheral, and mid-gorge binding sites of AChE. In contrast to previous approaches, the conjunctive strategy adopted here largely preserves the chemical skeleton of donepezil while its benzyl moiety is replaced by a tacrine unit. The length of the tether that connects the two constituting fragments of the novel hybrids, i.e., the 5,6-dimethoxy-2-[(4-piperidinyl)methyl]-1-indanone moiety of donepezil (or its corresponding indane derivative) and the tacrine (or 6-chlorotacrine) unit, has a relevant effect on the arrangement of the hybrid along the gorge, leading to different orientations of the piperidine ring and the indanone system within the enzyme gorge and at the peripheral site, respectively, while their tacrine unit closely matches the position occupied by tacrine within the AChE active site. Thus,

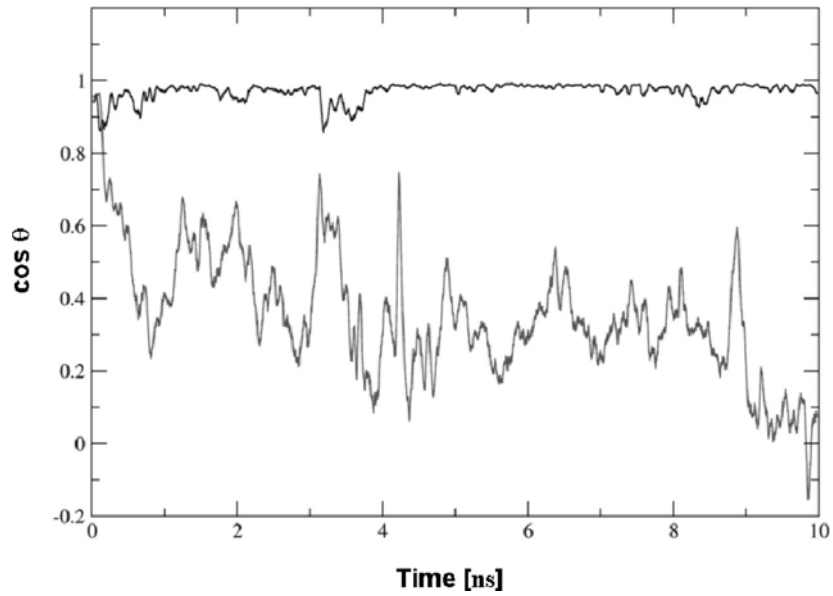

Figure 3. Time dependence of the relative orientation of the indanone ring of heterodimers **15a** (black) and **15b** (gray) and the indole ring of Trp286 at the peripheral site. The relative orientation was measured from the cosine function of the angle formed by the vectors normal to the indanone and indole rings. Accordingly, a perfect stacking would correspond to cos $\theta = 1$, while a perpendicular arrangement is denoted by cos $\theta = 0$.

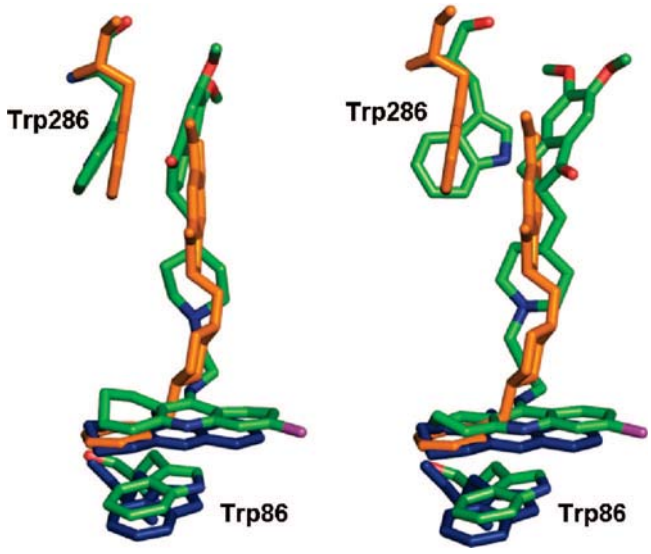

Figure 4. Superposition of the heterodimers **15a** (left) and **15b** (right) with tacrine (taken from the 1ACJ X-ray structure of the *Tc*AChE−tacrine complex, blue) and donepezil (from the 1EVE X-ray structure of the *Tc*AChE−donepezil complex, orange), showing the relative positions of Trp86 (Trp84 in 1ACJ) and Trp286 (Trp279 in 1EVE) at the catalytic and peripheral sites, respectively. Compounds **15a** and **15b** are colored by atom.

enlargement of the linker from two to three methylenes permits the piperidine ring to form a direct electrostatic interaction with Asp74, though at the expense of a less efficient $\pi-\pi$ interaction between the indanone unit and the indole ring of Trp286. In spite of these structural differences, all of the new hybrids are highly potent bovine and human AChE inhibitors, exhibiting IC_{50} values in the subnanomolar range in most cases and being clearly more potent than the parent compounds from which they were designed and the previously described donepezil−tacrine hybrids. The most potent AChE inhibitors are those bearing an indanone system, a chlorine atom at the tacrine unit and a tether length of three methylenes. Though all of the new hybrids are less potent toward hBChE, the most active compounds, i.e., those bearing an unsubstituted tacrine unit irrespective of the presence of an indanone or indane system and the tether length, are also more potent hBChE inhibitors than the parent compounds. Following some interesting results arising from a thioflavin T competition assay to assess their interaction with the AChE peripheral site, six out of the eight hybrids of the series were tested for their ability to block the AChE-induced Aβ-aggregation. All the tested hybrids exhibited a significant Aβ antiaggregating activity, being more potent than the parent compounds, including the dual binding site inhibitor donepezil. Overall, these results suggest that the novel donepezil−tacrine hybrids herein reported may have a potential disease-modifying role in the treatment of AD.

Experimental Section

Chemistry. General Methods. Melting points were determined in open capillary tubes with a MFB 595010 M Gallenkamp melting point apparatus. The 300 MHz ^{1}H/75.4 MHz ^{13}C NMR spectra, 400 MHz ^{1}H/100.6 MHz ^{13}C NMR spectra, and 500 MHz ^{1}H NMR spectra were recorded on Varian Gemini 300, Varian Mercury 400, and Varian Inova 500 spectrometers, respectively. The chemical shifts are reported in ppm (δ scale) relative to internal tetramethylsilane, and coupling constants are reported in hertz (Hz). Assignments given for the NMR spectra of the new compounds have been carried out by comparison with the NMR data of **15a**, **16a**, **17b**, and 6-chlorotacrine, as model compounds, which in turn were assigned on the basis of DEPT, COSY ^{1}H/^{1}H (standard procedures), NOESY ^{1}H/^{1}H, and COSY ^{1}H/^{13}C (gHSQC and gHMBC sequences) experiments. IR spectra were run on a Perkin-Elmer Spectrum RX I spectrophotometer. Absorption values are expressed as wavenumbers (cm^{-1}); only significant absorption bands are given. Column chromatography was performed on silica gel 60 AC.C (35−70 mesh, SDS, no. 2000027). Thin-layer chromatography was performed with aluminum-backed sheets with silica gel 60 F_{254} (Merck, no. 1.05554), and spots were visualized with UV light and 1% aqueous solution of $KMnO_4$. Analytical grade solvents were used for crystallization, while pure for synthesis solvents were used in the reactions, extractions, and column chromatography. For characterization purposes, the new donepezil−tacrine hybrids were transformed into the corresponding dihydrochlorides and recrystallized. Worthy of note, as previously reported for some tacrine-related dimeric compounds,[63] the new donepezil−tacrine

hybrids have the ability to retain molecules of water, which cannot be removed after drying the analytical samples at 80 °C/30 Torr for 2 days. Thus, the elemental analyses of these compounds showed the presence of variable amounts of water. NMR spectra of all of the new compounds were performed at the Serveis Científico-Tècnics of the University of Barcelona, while elemental analyses and high resolution mass spectra were carried out at the Microanalysis Service of the IIQAB (CSIC, Barcelona, Spain) with a Carlo Erba model 1106 analyzer and at the Mass Spectrometry Laboratory of the University of Santiago de Compostela (Spain) with a Micromass Autospec spectrometer, respectively.

General Procedure for the Reaction of 9-Chloro-1,2,3,4-tetrahydroacridine, 5, or 6,9-Dichloro-1,2,3,4-tetrahydroacridine, 6, with ω-Aminoalcohols. A mixture of **5** or **6** (1 mmol) and an excess of the aminoalcohol **7** (3 mmol) in 1-pentanol (1 mL) was heated under reflux with magnetic stirring for 18 h. The resulting mixture was cooled to room temperature, diluted with AcOEt (5 mL), and extracted with 1 N HCl (4 × 3 mL). The combined aqueous extracts were washed with AcOEt (3 × 3 mL), alkalinized with NaOH pellets (until pH 12), and extracted with CH_2Cl_2 (3 × 8 mL). The combined organic extracts were dried with anhydrous Na_2SO_4 and concentrated in vacuo to give alcohol **8** or **9** as a pale-brown solid or oily residue, which was used in the next step without further purification.

For characterization purposes, analytical samples of the hydrochlorides of **8** and **9** were prepared as follows: The alcohol **8** or **9** (1 mmol) was dissolved in MeOH (10 mL). The solution was filtered through a 0.45 μm polytetrafluoroethylene (PTFE) filter and treated with an excess of a methanolic solution of HCl (3 mmol), and the resulting solution was concentrated in vacuo to dryness. The solid was recrystallized from a mixture MeOH/AcOEt in a ratio of 1:4 (5 mL) and dried at 80 °C/30 Torr for 48 h to give the 9-(ω-hydroxyalkylamino)tetrahydroacridine hydrochloride **8**·HCl or **9**·HCl as a light-brown solid.

9-[(2-Hydroxyethyl)amino]-1,2,3,4-tetrahydroacridine Hydrochloride (8a·HCl). From **5** (3.34 g, 15.4 mmol) and 2-aminoethanol **7a** (2.48 mL, 2.83 g, 46.4 mmol), alcohol **8a** (3.52 g, 95% yield, free base) was obtained: R_f = 0.38 (CH_2Cl_2/MeOH/25% aqueous NH_4OH, 9:1:0.1). **8a**·HCl: mp 184−185 °C (MeOH/AcOEt, 1:4); IR (KBr) ν 3700−2400 (max at 3358, 3142, 3058, 3016, 2938, 2872, O−H, N−H, $^+$N−H, and C−H st), 1633, 1592, 1577, and 1524 (ar−C−C and ar−C−N st) cm^{-1}; ^{1}H NMR (300 MHz, CD_3OD) δ 1.90−2.04 (complex signal, 4H, 2-H_2 and 3-H_2), 2.74 (m, 2H, 1-H_2), 3.01 (m, 2H, 4-H_2), 3.86 (t, J = 5.4 Hz, 2H, 2′-H_2), 4.01 (t, J = 5.4 Hz, 2H, 1′-H_2), 4.87 (s, OH, NH and $^+$NH), 7.54 (ddd, J = 8.4 Hz, J' = 6.0 Hz, J'' = 2.4 Hz, 1H, 7-H), 7.76−7.84 (complex signal, 2H, 5-H and 6-H), 8.40 (d, J = 8.4 Hz, 1H, 8-H); ^{13}C NMR (75.4 MHz, CD_3OD) δ 21.1 (CH_2, C3), 23.1 (CH_2, C2), 24.8 (CH_2, C1), 30.1 (CH_2, C4), 51.2 (CH_2, C1′), 61.7 (CH_2, C2′), 113.7 (C, C9a), 117.7 (C, C8a), 121.2 (CH, C5), 126.0 (CH, C8), 126.1 (CH, C7), 133.3 (CH, C6), 140.9 (C, C10a), 152.8 (C, C4a), 157.4 (C, C9). HRMS calcd for ($C_{15}H_{18}N_2O$ + H^+) 243.1497, found 243.1494.

General Procedure for the Mesylation of Alcohols 8 and 9. To a cold solution (−10 °C, ice−salt bath) of the alcohol **8** or **9** (1 mmol) and anhydrous Et_3N (1.7 mmol) in anhydrous CH_2Cl_2 (6 mL), methanesulfonyl chloride (1.5 mmol) was added dropwise, and the reaction mixture was stirred for 30 min at this temperature. The mixture was concentrated in vacuo, the residue was taken in CH_2Cl_2 (4 mL), and the resulting organic solution was washed with 2 N NaOH (3 × 3 mL) until the aqueous phase remained basic (pH > 10), dried with anhydrous Na_2SO_4, and concentrated in vacuo to give the corresponding mesylate **10** or **11** as a brown oily residue, which was used in the next step without further purification.

For characterization purposes, analytical samples of the mesylates were obtained by extraction of the oily crude product with hot AcOEt except in the case of **11a**, whose analytical sample was prepared by recrystallization of the corresponding hydrochloride, obtained in a similar way to that described for the hydrochlorides of alcohols **8** and **9**.

9-[(2-Methanesulfonyloxyethyl)amino]-1,2,3,4-tetrahydroacridine (10a). From alcohol **8a**(3.52 g, 14.5 mmol), mesylate **10a** (4.41 g, 95% yield) was obtained: R_f = 0.67 (CH_2Cl_2/MeOH/25% aqueous NH_4OH, 9:1:0.1); IR (NaCl) ν 3391 and 3339 (N−H st), 1638, 1586, and 1524 (ar−C−C and ar−C−N st), 1352 (SO_2 st as), 1178 (SO_2 st s) cm^{-1}; ^{1}H NMR (300 MHz, $CDCl_3$) δ 1.88−1.98 (complex signal, 4H, 2-H_2 and 3-H_2), 2.76 (m, 2H, 1-H_2), 2.97 (s, 3H, OSO_2CH_3), 3.08 (m, 2H, 4-H_2), 3.81 (m, 2H, 1′-H_2), 4.34 (t, J = 4.9 Hz, 2H, 2′-H_2), 4.54 (broad s, 1H, NH), 7.39 (ddd, J = 8.4 Hz, J' = 6.8 Hz, J'' = 1.5 Hz, 1H, 7-H), 7.57 (ddd, J = 8.4 Hz, J' = 6.8 Hz, J'' = 1.5 Hz, 1H, 6-H), 7.91−7.95 (complex signal, 2H, 5-H and 8-H); ^{13}C NMR (75.4 MHz, $CDCl_3$) δ 22.4 (CH_2) and 22.7 (CH_2) (C2 and C3), 24.7 (CH_2, C1), 33.3 (CH_2, C4), 37.3 (CH_3, OSO_2CH_3), 47.4 (CH_2, C1′), 69.0 (CH_2, C2′), 117.7 (C, C9a), 120.7 (C, C8a), 122.2 (CH), 124.3 (CH), 127.8 (CH), 128.7 (CH) (C5, C6, C7, and C8), 146.2 (C, C10a), 149.6 (C, C4a), 158.2 (C, C9). HRMS calcd for ($C_{16}H_{20}N_2O_3S$ + H^+) 321.127, found 321.128.

General Procedure for the Coupling of Mesylates 10 and 11 with 5,6-Dimethoxy-2-[(4-piperidinyl)methyl]indan-1-one (12) or 5,6-Dimethoxy-2-[(4-piperidinyl)methyl]indane (13). A solution of the mesylate **10** or **11** (1 mmol), the piperidine **12** or **13** (1 mmol), and anhydrous Et_3N (2.5 mmol) in DMSO (8 mL) was heated at 85 °C for 48 h. The resulting solution was allowed to cool to room temperature and was concentrated in vacuo. The brown oily residue was treated with aqueous 2 N NaOH (25 mL) and extracted with CH_2Cl_2 (3 × 35 mL). The combined organic extracts were washed with water (6 × 40 mL) and brine (4 × 30 mL), dried with anhydrous Na_2SO_4, filtered, and evaporated under reduced pressure to give an oily residue, which was submitted to column chromatography (35−70 μm silica gel, CH_2Cl_2/MeOH/25% aqueous NH_4OH mixtures as eluent).

The isolated donepezil−tacrine hybrids **14**−**17** were transformed into the corresponding dihydrochlorides as follows: A solution of the free base (1 mmol) in MeOH (40 mL) was filtered through a 0.45 μm PTFE filter and treated with excess of a methanolic solution of HCl (5 mmol). The solution was concentrated in vacuo to dryness, and the solid residue was recrystallized from MeOH (20 mL) and dried at 80 °C/30 Torr for 48 h.

9-[(2-{4-[(5,6-Dimethoxy-1-oxoindan-2-yl)methyl]piperidin-1-yl}ethyl)amino]-1,2,3,4-tetrahydroacridine Dihydrochloride (14a·2HCl). From mesylate **10a** (276 mg, 0.86 mmol) and piperidine **12** (249 mg, 0.86 mmol), compound **14a** (87 mg, 20% yield) was obtained as a pale-brown solid on elution with a mixture of CH_2Cl_2/MeOH/25% aqueous NH_4OH, 99.5:0.5:0.4: R_f = 0.91 (CH_2Cl_2/MeOH/25% aqueous NH_4OH, 90:10:0.1). **14a**·2HCl: mp 190−191 °C (MeOH); IR (KBr) ν 3700−2400 (max at 3401, 2928, 2871, 2718, N−H, $^+$N−H, and C−H st), 1685, 1672 (C=O st), 1636, 1588, 1523, and 1500 (ar−C–C and ar−C–N st) cm^{-1}; ^{1}H NMR (500 MHz, CD_3OD) δ 1.45 (m, 1H, indanone-2-CH_a), 1.62−1.73 (broad signal, 2H, piperidine 3-H_{ax} and 5-H_{ax}), 1.86 (m, 1H, indanone-2-CH_b), 1.90−2.02 (broad signal, 1H, piperidine 4-H), superimposed 1.99 (complex signal, 4H, acridine 2-H_2 and 3-H_2), 2.02 (broad d, J = 14.5 Hz, 1H) and 2.14 (broad d, J = 14.0 Hz, 1H) (piperidine 3-H_{eq} and 5-H_{eq}), 2.74−2.80 (complex signal, 2H, indanone 2-H and 3-H_a), 2.84 (m, 2H, acridine 1-H_2), 3.08 (m, 2H, acridine 4-H_2), 3.12 (broad signal, 2H, piperidine 2-H_{ax} and 6-H_{ax}), superimposed in part 3.34 (dd, J = 18.0 Hz, J' = 8.5 Hz, 1H, indanone 3-H_b), 3.60 (broad signal, 2H, $NHCH_2CH_2N$), 3.72 (broad signal, 2H, piperidine 2-H_{eq} and 6-H_{eq}), 3.85 (s, 3H, 6-OCH_3), 3.94 (s, 3H, 5-OCH_3), 4.42 (t, J = 7.7 Hz, 2H, $NHCH_2CH_2N$), 4.85 (s, NH and $^+$NH), 7.07 (s, 1H, indanone 4-H), 7.15 (s, 1H, indanone 7-H), 7.68 (ddd, J = 8.5 Hz, J' = 7.0 Hz, J'' = 1.0 Hz, 1H, acridine 7-H), 7.83 (dd, J = 8.5 Hz, J' = 1.0 Hz, 1H, acridine 5-H), 7.91 (ddd, J = 8.5 Hz, J' = 7.0 Hz, J'' = 1.0 Hz, 1H, acridine 6-H), 8.43 (d, J = 8.5 Hz, 1H, acridine 8-H); ^{13}C NMR (100.6 MHz, CD_3OD) δ 21.7 (CH_2, acridine C3), 23.0 (CH_2, acridine C2), 25.7 (CH_2, acridine C1), 29.5 (CH_2, acridine C4), 30.3 (CH_2) and 31.1 (CH_2) (piperidine C3 and C5), 33.0 (CH, piperidine C4), 34.2 (CH_2, indanone C3), 39.0 (CH_2, indanone-2-CH_2), 43.1 (CH_2, $NHCH_2CH_2N$), 46.1 (CH, indanone C2), 54.1 (2 CH_2, piperidine

C2 and C6), 56.5 (CH_3, 6-OCH_3), 56.7 (CH_3, 5-OCH_3), 57.4 (CH_2, $NHCH_2CH_2N$), 105.3 (CH, indanone C7), 109.0 (CH, indanone C4), 114.4 (C, acridine C9a), 117.6 (C, acridine C8a), 120.3 (CH, acridine C5), 125.9 (CH, acridine C8), 127.2 (CH, acridine C7), 129.8 (C, indanone C7a), 134.3 (CH, acridine C6), 139.4 (C, acridine C10a), 151.1 (C, indanone C6), 151.3 (C, indanone C3a), 153.1 (C, acridine C4a), 157.8 (C) and 158.0 (C) (indanone C5 and acridine C9), 209.7 (C, indanone C1). Anal. ($C_{32}H_{39}N_3O_3 \cdot 2HCl \cdot 1.5H_2O$) C, H, N, Cl.

Biochemical Studies. AChE inhibitory activity was evaluated spectrophotometrically at 25 °C by the method of Ellman,[47] using AChE from bovine or human erythrocytes and acetylthiocholine iodide (0.53 and 0.13 mM for bovine and human AChE, respectively) as substrate. The reaction took place in a final volume of 3 mL of 0.1 M phosphate-buffered solution, pH 8.0, containing 0.025 or 0.04 unit of bovine or human AChE, respectively, and 333 μM 5,5′-dithiobis(2-nitrobenzoic) acid (DTNB) solution used to produce the yellow anion of 5-thio-2-nitrobenzoic acid. Inhibition curves were performed in triplicate by incubating at least 12 concentrations of inhibitor for 15 min. One triplicate sample without inhibitor was always present to yield 100% of AChE activity. The reaction was stopped by the addition of 100 μL of 1 mM eserine, and the color production was measured at 414 nm. BChE inhibitory activity determinations were carried out similarly, using 0.035 unit of human serum BChE and 0.56 mM butyrylthiocholine, instead of AChE and acetylthiocholine, in a final volume of 1 mL.

Data from concentration−inhibition experiments of the inhibitors were calculated by nonlinear regression analysis, using the GraphPad Prism program package (GraphPad Software; San Diego, CA), which gave estimates of the IC_{50} (concentration of drug producing 50% of enzyme activity inhibition). Results are expressed as the mean ± SEM of at least four experiments performed in triplicate. DTNB, acetylthiocholine, butyrylthiocholine, and the enzymes were purchased from Sigma, and eserine was purchased from Fluka.

Thioflavin T Competition Assay. Fluorescence measurements were carried out at room temperature in a SFM-25 spectrofluorimeter (Biotek, Italy) using a 1 mL quartz cell. Fluorescence was monitored at 448 and 488 nm for excitation and emission, respectively. An aqueous solution of hAChE at 2.3 μM was stirred at room temperature for 24 h. After incubation, an amount of 50 μL of the enzyme solution was mixed with 750 μL of 50 mM glycine−NaOH buffer (pH 8.5) containing 15 μM thioflavin T. The resulting solution was stirred for 1 h, and the fluorescence of the sample was recorded (F_1). To check the ability of reducing the fluorescence arising from the interaction of AChE and thioflavin T, the enzyme, at a final concentration of 2.3 μM, was mixed with the inhibitor (final concentration of 100 μM), and the solution was stirred for 24 h. After incubation, an amount of 50 μL of the protein solution was mixed with 750 μL of fluorophore solution, as indicated above, and the corresponding fluorescence was recorded (F_2). Finally, the fluorescence of a solution formed by 750 μL of the buffer containing the dye and 50 μL of water was recorded (F_0). The percentage of reduction of ThT fluorescence was determined as

$$\% = 1 - \frac{F_2 - F_0}{F_1 - F_0} \quad (1)$$

Inhibition of AChE-Induced Aβ_{40} Aggregation Assay. Thioflavin T (Basic Yellow 1), human recombinant AChE lyophilized powder, and 1,1,1,3,3,3-hexafluoro-2-propanol (HFIP) were purchased from Sigma Chemicals. Buffers and other chemicals were of analytical grade. Absolute DMSO over molecular sieves was from Fluka. Water was deionized and doubly distilled. β-Amyloid 1−40 (Aβ_{40}), supplied as trifluoroacetate salt, was purchased from Bachem AG (Bubendorf, Switzerland). Aβ_{40} (2 mg mL^{-1}) was dissolved in HFIP and lyophilized. The 1 mM solutions of tested inhibitors were prepared by dissolution in MeOH.

Aliquots of 2 μL of Aβ_{40} peptide, lyophilized from 2 mg mL^{-1} HFIP solution and dissolved in DMSO, were incubated for 24 h at room temperature in 0.215 M sodium phosphate buffer (pH 8.0) at a final concentration of 230 μM. For co-incubation experiments, aliquots (16 μL) of hAChE (final concentration of 2.30 μM, Aβ/AChE molar ratio of 100:1) and AChE in the presence of 2 μL of the tested inhibitor (final inhibitor concentration 100 μM) in 0.215 M sodium phosphate buffer, pH 8.0, solution were added. Blanks containing Aβ_{1-40} alone, human recombinant AChE alone, and Aβ_{1-40} plus tested inhibitors in 0.215 M sodium phosphate buffer (pH 8.0) were prepared. The final volume of each vial was 20 μL. Each assay was run in duplicate. To quantify amyloid fibril formation, the thioflavin T fluorescence method was then applied.[23] The fluorescence intensities due to β-sheet conformation were monitored for 300 s at $\lambda_{em} = 490$ nm ($\lambda_{exc} = 446$ nm). The percent inhibition of the AChE-induced aggregation due to the presence of the tested compound was calculated by the following expression: $100 - [(IF_i/IF_o) \times 100]$ where IF_i and IF_o are the fluorescence intensities obtained for Aβ plus AChE in the presence and in the absence of inhibitor, respectively, minus the fluorescence intensities due to the respective blanks.

Molecular Modeling Methods. The binding modes of compounds **15a** and **15b** were explored by means of 10 ns molecular dynamics simulations performed for their complexes to human acetylcholinesterase (hAChE). To this end, models of the bonded ligands were built up using the X-ray crystallographic structure of the hAChE−fasciculin complex (PDB code 1B41).[64] Fasciculin was removed from the structure, truncated residues were reconstructed, and missing residues were modeled using InsightII graphics package.[65] The starting pose of the ligands was determined by means of docking computations with GOLD[66] (using GoldScore scoring function), which was successful for predicting the docking of donepezil in the enzyme (see Supporting Information), and was later refined by inspection of the X-ray crystallographic structures of the *Tc*AChE complexes with tacrine (1ACJ),[35] huprine X (1E66),[38] and donepezil (1EVE)[22] and the final structures of previous heterodimer studies.[12,31] The system was hydrated by centering a sphere of 50 Å of TIP3P[67] water molecules at the inhibitor, paying attention to filling the position of crystallographic waters inside the binding cavity. Finally, six Na^+ cations were added to neutralize the negative charge of the system with the xleap module of AMBER8.[68]

Molecular dynamics simulations were run using the sander module of AMBER8 and the parm98 parameters for the protein. The charge distribution of the inhibitor was determined from a fit to the HF/6s-31G(d) electrostatic potential obtained with Gaussian'03[69] using the RESP procedure,[70] and the van der Waals parameters were taken from those defined for related atoms in the AMBER force field. The system was partitioned into a mobile region, which included the ligand, all the protein residues containing at least one atom within 20 Å from the ligand, and all the water molecules and Na^+ cations. The geometry of the system was minimized in four steps. First, the position of hydrogen atoms was optimized using 3000 steps of steepest descent algorithm. Then water molecules were refined through 2000 steps of steepest descent followed by 3000 steps of conjugate gradient. Next, the ligand, water molecules, and counterions were optimized with 2000 steps of steepest descent and 4000 steps of conjugate gradient, and finally the whole system was optimized with 3000 steps of steepest descent and 7000 steps of conjugate gradient. Thermalization of the mobile part of the system was performed in five steps of 20 ps, incrementing the temperature up to 298 K. At this point, a 10 ns molecular dynamics simulation was carried out using a time step of 1 fs. SHAKE was used for those bonds containing hydrogen atoms, and a cutoff of 11 Å was used for nonbonded interactions.

The analysis of the structural features that mediate the binding mode to the enzyme was determined by averaging the parameters for the snapshots (saved every picosecond) sampled along the last 5 ns of the molecular dynamics simulations.

Acknowledgment. Financial support from Dirección General de Investigación of Ministerio de Ciencia y Tecnología and FEDER (Projects CTQ2005-02192/BQU, SAF2006-04339, CTQ2005-09365, and SAF2005-01604) and Comissionat per a

Universitats i Recerca of the Generalitat de Catalunya (Projects 2005-SGR00180, 2001-SGR00216, and 2005-SGR00893) are gratefully acknowledged. We also thank the Serveis Científico-Tècnics of the University of Barcelona for NMR facilities, and we thank P. Domènech from the IIQAB (CSIC, Barcelona, Spain) for carrying out the elemental analyses.

Supporting Information Available: Experimental procedures, spectral and analytical characterization data of all of the new compounds (except for **8a**, **10a**, and **14a**) and the known compounds **13** and **19**, and the predicted pose of donepezil obtained by using GOLD. This material is available free of charge via the Internet at http://pubs.acs.org.

References

(1) Pang, Y.-P.; Quiram, P.; Jelacic, T.; Hong, F.; Brimijoin, S. Highly Potent, Selective, and Low Cost Bis-tetrahydroaminacrine Inhibitors of Acetylcholinesterase. *J. Biol. Chem.* **1996**, *271*, 23646–23649.

(2) Du, D.-M.; Carlier, P. R. Development of Bivalent Acetylcholinesterase Inhibitors as Potential Therapeutic Drugs for Alzheimer's Disease. *Curr. Pharm. Des.* **2004**, *10*, 3141–3156.

(3) Li, W. M.; Kan, K. K. W.; Carlier, P. R.; Pang, Y. P.; Han, Y. F. Easts Meets West in the Search for Alzheimer's Therapeutics. Novel Dimeric Inhibitors from Tacrine and Huperzine A. *Curr. Alzheimer Res.* **2007**, *4*, 386–396.

(4) Recanatini, M.; Valenti, P. Acetylcholinesterase Inhibitors as a Starting Point towards Improved Alzheimer's Disease Therapeutics. *Curr. Pharm. Des.* **2004**, *10*, 3157–3166.

(5) Muñoz-Torrero, D.; Camps, P. Dimeric and Hybrid Anti-Alzheimer Drug Candidates. *Curr. Med. Chem.* **2006**, *13*, 763–771.

(6) Castro, A.; Martinez, A. Targeting Beta-Amyloid Pathogenesis through Acetylcholinesterase Inhibitors. *Curr. Pharm. Des.* **2006**, *12*, 4377–4387.

(7) Holzgrabe, U.; Kapková, P.; Alptüzün, V.; Scheiber, J.; Kugelmann, E. Targeting Acetylcholinesterase To Treat Neurodegeneration. *Expert Opin. Ther. Targets* **2007**, *11*, 161–179.

(8) Cavalli, A.; Bolognesi, M. L.; Minarini, A.; Rosini, M.; Tumiatti, V.; Recanatini, M.; Melchiorre, C. Multi-Target-Directed Ligands To Combat Neurodegenerative Diseases. *J. Med. Chem.* **2008**, *51*, 347–372.

(9) Piazzi, L.; Rampa, A.; Bisi, A.; Gobbi, S.; Belluti, F.; Cavalli, A.; Bartolini, M.; Andrisano, V.; Valenti, P.; Recanatini, M. 3-(4-{[Benzyl(methyl)amino]methyl}phenyl)-6,7-dimethoxy-2*H*-2-chromenone (AP2238) Inhibits Both Acetylcholinesterase and Acetylcholinesterase-Induced β-Amyloid Aggregation: A Dual Function Lead for Alzheimer's Disease Therapy. *J. Med. Chem.* **2003**, *46*, 2279–2282.

(10) Bolognesi, M. L.; Andrisano, V.; Bartolini, M.; Banzi, R.; Melchiorre, C. Propidium-Based Polyamine Ligands as Potent Inhibitors of Acetylcholinesterase and Acetylcholinesterase-Induced Amyloid-β Aggregation. *J. Med. Chem.* **2005**, *48*, 24–27.

(11) Rosini, M.; Andrisano, V.; Bartolini, M.; Bolognesi, M. L.; Hrelia, P.; Minarini, A.; Tarozzi, A.; Melchiorre, C. Rational Approach To Discover Multipotent Anti-Alzheimer Drugs. *J. Med. Chem.* **2005**, *48*, 360–363.

(12) Muñoz-Ruiz, P.; Rubio, L.; García-Palomero, E.; Dorronsoro, I.; del Monte-Millán, M.; Valenzuela, R.; Usán, P.; de Austria, C.; Bartolini, M.; Andrisano, V.; Bidon-Chanal, A.; Orozco, M.; Luque, F. J.; Medina, M.; Martínez, A. Design, Synthesis, and Biological Evaluation of Dual Binding Site Acetylcholinesterase Inhibitors: New Disease-Modifying Agents for Alzheimer's Disease. *J. Med. Chem.* **2005**, *48*, 7223–7233.

(13) Belluti, F.; Rampa, A.; Piazzi, L.; Bisi, A.; Gobbi, S.; Bartolini, M.; Andrisano, V.; Cavalli, A.; Recanatini, M.; Valenti, P. Cholinesterase Inhibitors: Xanthostigmine Derivatives Blocking the Acetylcholinesterase-Induced β-Amyloid Aggregation. *J. Med. Chem.* **2005**, *48*, 4444–4456.

(14) Piazzi, L.; Cavalli, A.; Belluti, F.; Bisi, A.; Gobbi, S.; Rizzo, S.; Bartolini, M.; Andrisano, V.; Recanatini, M.; Rampa, A. Extensive SAR and Computational Studies of 3-{4-[(Benzylmethylamino)methyl]phenyl}-6,7-dimethoxy-2*H*-2-chromenone (AP2238) Derivatives. *J. Med. Chem.* **2007**, *50*, 4250–4254.

(15) Cavalli, A.; Bolognesi, M. L.; Capsoni, S.; Andrisano, V.; Bartolini, M.; Margotti, E.; Cattaneo, A.; Recanatini, M.; Melchiorre, C. A Small Molecule Targeting the Multifactorial Nature of Alzheimer's Disease. *Angew. Chem., Int. Ed.* **2007**, *46*, 3689–3692.

(16) Bolognesi, M. L.; Banzi, R.; Bartolini, M.; Cavalli, A.; Tarozzi, A.; Andrisano, V.; Minarini, A.; Rosini, M.; Tumiatti, V.; Bergamini, C.; Fato, R.; Lenaz, G.; Hrelia, P.; Cattaneo, A.; Recanatini, M.; Melchiorre, C. Novel Class of Quinone-Bearing Polyamines as Multi-Target-Directed Ligands To Combat Alzheimer's Disease. *J. Med. Chem.* **2007**, *50*, 4882–4897.

(17) Bolognesi, M. L.; Cavalli, A.; Valgimigli, L.; Bartolini, M.; Rosini, M.; Andrisano, V.; Recanatini, M.; Melchiorre, C. Multi-Target-Directed Drug Design Strategy: From a Dual Binding Site Acetylcholinesterase Inhibitor to a Trifunctional Compound against Alzheimer's Disease. *J. Med. Chem.* **2007**, *50*, 6446–6449.

(18) Kwon, Y. E.; Park, J. Y.; No, K. T.; Shin, J. H.; Lee, S. K.; Eun, J. S.; Yang, J. H.; Shin, T. Y.; Kim, D. K.; Chae, B. S.; Leem, J.-Y.; Kim, K. H. Synthesis, in Vitro Assay, and Molecular Modeling of New Piperidine Derivatives Having Dual Inhibitory Potency against Acetylcholinesterase and $A\beta_{1-42}$ Aggregation for Alzheimer's Disease Therapeutics. *Bioorg. Med. Chem.* **2007**, *15*, 6596–6607.

(19) Skovronsky, D. M.; Lee, V. M.-Y.; Trojanowski, J. Q. Neurodegenerative Diseases: New Concepts of Pathogenesis and Their Therapeutic Implications. *Annu. Rev. Pathol. Mech. Dis.* **2006**, *1*, 151–170.

(20) De Ferrari, G. V.; Canales, M. A.; Shin, I.; Weiner, L. M.; Silman, I.; Inestrosa, N. C. A Structural Motif of Acetylcholinesterase That Promotes Amyloid Beta-Peptide Fibril Formation. *Biochemistry* **2001**, *40*, 10447–10457.

(21) Sugimoto, H.; Iimura, Y.; Yamanishi, Y.; Yamatsu, K. Synthesis and Structure−Activity Relationships of Acetylcholinesterase Inhibitors: 1-Benzyl-4-[(5,6-dimethoxy-1-oxoindan-2-yl)methyl]piperidine Hydrochloride and Related Compounds. *J. Med. Chem.* **1995**, *38*, 4821–4829.

(22) Kryger, G.; Silman, I.; Sussman, J. L. Structure of Acetylcholinesterase Complexed with E2020 (Aricept): Implications for the Design of New Anti-Alzheimer Drugs. *Structure* **1999**, *7*, 297–307.

(23) Bartolini, M.; Bertucci, C.; Cavrini, V.; Andrisano, V. β-Amyloid Aggregation Induced by Human Acetylcholinesterase: Inhibition Studies. *Biochem. Pharmacol.* **2003**, *65*, 407–416.

(24) Carlier, P. R.; Du, D. -M.; Han, Y.; Liu, J.; Pang, Y.-P. Potent, Easily Synthesized Huperzine A-Tacrine Hybrid Acetylcholinesterase Inhibitors. *Bioorg. Med. Chem. Lett.* **1999**, *9*, 2335–2338.

(25) Savini, L.; Campiani, G.; Gaeta, A.; Pellerano, C.; Fattorusso, C.; Chiasserini, L.; Fedorko, J. M.; Saxena, A. Novel and Potent Tacrine-Related Hetero- and Homobivalent Ligands for Acetylcholinesterase and Butyrylcholinesterase. *Bioorg. Med. Chem. Lett.* **2001**, *11*, 1779–1782.

(26) Hu, M.-K.; Wu, L.-J.; Hsiao, G.; Yen, M.-H. Homodimeric Tacrine Congeners as Acetylcholinesterase Inhibitors. *J. Med. Chem.* **2002**, *45*, 2277–2282.

(27) Lewis, W. G.; Green, L. G.; Grynszpan, F.; Radić, Z.; Carlier, P. R.; Taylor, P.; Finn, M. G.; Sharpless, K. B. Click Chemistry in Situ: Acetylcholinesterase as a Reaction Vessel for the Selective Assembly of a Femtomolar Inhibitor from an Array of Building Blocks. *Angew. Chem., Int. Ed.* **2002**, *41*, 1053–1057.

(28) Savini, L.; Gaeta, A.; Fattorusso, C.; Catalanotti, B.; Campiani, G.; Chiasserini, L.; Pellerano, C.; Novellino, E.; McKissic, D.; Saxena, A. Specific Targeting of Acetylcholinesterase and Butyrylcholinesterase Recognition Sites. Rational Design of Novel, Selective, and Highly Potent Cholinesterase Inhibitors. *J. Med. Chem.* **2003**, *46*, 1–4.

(29) Camps, P.; Formosa, X.; Muñoz-Torrero, D.; Petrignet, J.; Badia, A.; Clos, M. V. Synthesis and Pharmacological Evaluation of Huprine−Tacrine Heterodimers: Subnanomolar Dual Binding Site Acetylcholinesterase Inhibitors. *J. Med. Chem.* **2005**, *48*, 1701–1704.

(30) Shao, D.; Zou, C.; Luo, C.; Tang, X.; Li, Y. Synthesis and Evaluation of Tacrine-E2020 Hybrids as Acetylcholinesterase Inhibitors for the Treatment of Alzheimer's Disease. *Bioorg. Med. Chem. Lett.* **2004**, *14*, 4639–4642.

(31) Alonso, D.; Dorronsoro, I.; Rubio, L.; Muñoz, P.; García-Palomero, E.; Del Monte, M.; Bidon-Chanal, A.; Orozco, M.; Luque, F. J.; Castro, A.; Medina, M.; Martínez, A. Donepezil−Tacrine Hybrid Related Derivatives as New Dual Binding Site Inhibitors of AChE. *Bioorg. Med. Chem.* **2005**, *13*, 6588–6597.

(32) Gemma, S.; Gabellieri, E.; Huleatt, P.; Fatorusso, C.; Borriello, M.; Catalanotti, B.; Butini, S.; De Angelis, M.; Novellino, E.; Nacci, V.; Belinskaya, T.; Saxena, A.; Campiani, G. Discovery of Huperzine A-Tacrine Hybrids as Potent Inhibitors of Human Cholinesterases Targeting Their Midgorge Recognition Sites. *J. Med. Chem.* **2006**, *49*, 3421–3425.

(33) Elsinghorst, P. W.; González Tanarro, C. M.; Gütschow, M. Novel Heterobivalent Tacrine Derivatives as Cholinesterase Inhibitors with Notable Selectivity Toward Butyrylcholinesterase. *J. Med. Chem.* **2006**, *49*, 7540–7544.

(34) Elsinghorst, P. W.; Cieslik, J. S.; Mohr, K.; Tränkle, C.; Gütschow, M. First Gallamine−Tacrine Hybrid: Design and Characterization at Cholinesterases and the M_2 Muscarinic Receptor. *J. Med. Chem.* **2007**, *50*, 5685–5695.

(35) Harel, M.; Schalk, I.; Ehret-Sabatier, L.; Bouet, F.; Goeldner, M.; Hirth, C.; Axelsen, P.; Silman, I.; Sussman, J. L. Quaternary Ligand Binding to Aromatic Residues in the Active-Site Gorge of Acetylcholinesterase. *Proc. Natl. Acad. Sci. U.S.A.* **1993**, *90*, 9031–9035.
(36) Wlodek, S. T.; Antosiewicz, J.; McCammon, J. A.; Straatsma, T. P.; Gilson, M. K.; Briggs, J. M.; Humblet, C.; Sussman, J. L. Binding of Tacrine and 6-Chlorotacrine by Acetylcholinesterase. *Biopolymers* **1996**, *38*, 109–117.
(37) Recanatini, M.; Cavalli, A.; Belluti, F.; Piazzi, L.; Rampa, A.; Bisi, A.; Gobbi, S.; Valenti, P.; Andrisano, V.; Bartolini, M.; Cavrini, V. SAR of 9-Amino-1,2,3,4-tetrahydroacridine-Based Acetylcholinesterase Inhibitors: Synthesis, Enzyme Inhibitory Activity, QSAR, and Structure-Based CoMFA of Tacrine Analogues. *J. Med. Chem.* **2000**, *43*, 2007–2018.
(38) Dvir, H.; Wong, D. M.; Harel, M.; Barril, X.; Orozco, M.; Luque, F. J.; Muñoz-Torrero, D.; Camps, P.; Rosenberry, T. L.; Silman, I.; Sussman, J. L. 3D Structure of *Torpedo californica* Acetylcholinesterase Complexed with Huprine X at 2.1 Å Resolution: Kinetic and Molecular Dynamic Correlates. *Biochemistry* **2002**, *41*, 2970–2981.
(39) Hu, M.-K.; Lu, C.-F. A Facile Synthesis of Bis-Tacrine Isosteres. *Tetrahedron Lett.* **2000**, *41*, 1815–1818.
(40) Michalson, E. T.; D'Andrea, S.; Freeman, J. P.; Szmuszkovicz, J. The Synthesis of 9-(1-Azetidinyl)-1,2,3,4-tetrahydroacridine. *Heterocycles* **1990**, *30*, 415–425.
(41) Elati, C. R.; Kolla, N.; Chalamala, S. R.; Vankawala, P. J.; Sundaram, V.; Vurimidi, H.; Mathad, V. T. New Synthesis of Donepezil through Palladium-Catalyzed Hydrogenation Approach. *Synth. Commun.* **2006**, *36*, 169–174.
(42) Lee, S.-Y.; Choe, Y. S.; Sugimoto, H.; Kim, S. E.; Hwang, S. H.; Lee, K.-H.; Choi, Y.; Lee, J.; Kim, B.-T. Synthesis and Biological Evaluation of 1-(4-[^{18}F]Fluorobenzyl-4-[5,6-dimethoxy-1-oxoindan-2-yl)methyl]piperidine for in Vivo Studies of Acetylcholinesterase. *Nuclear Med. Biol.* **2000**, *27*, 741–744.
(43) Inoue, A.; Kawai, T.; Wakita, M.; Iimura, Y.; Sugimoto, H.; Kawakami, Y. The Simulated Binding of (±)-2,3-Dihydro-5,6-dimethoxy-2-[[1-(phenylmethyl)-4-piperidinyl]methyl]-1*H*-inden-1-one Hydrochloride (E2020) and Related Inhibitors to Free and Acylated Acetylcholinesterases and Corresponding Structure−Activity Analyses. *J. Med. Chem.* **1996**, *39*, 4460–4470.
(44) Reddy, K. V. S. R. K.; Babu, J. M.; Kumar, P. A.; Chandrashekar, E. R. R.; Mathad, V. T.; Eswaraiah, S.; Reddy, M. S.; Vyas, K. Identification and Characterization of Potential Impurities of Donepezil. *J. Pharm. Biomed. Anal.* **2004**, *35*, 1047–1058.
(45) Galanakis, D.; Davis, C. A.; Ganellin, C. R.; Dunn, P. M. Synthesis and Quantitative Structure−Activity Relationship of a Novel Series of Small Conductance Ca^{2+}-Activated K^+ Channel Blockers Related to Dequalinium. *J. Med. Chem.* **1996**, *39*, 359–370.
(46) Carlier, P. R.; Chow, E. S.-H.; Han, Y.; Liu, J.; El Yazal, J.; Pang, Y.-P. Heterodimeric Tacrine-Based Acetylcholinesterase Inhibitors: Investigating Ligand-Peripheral Site Interactions. *J. Med. Chem.* **1999**, *42*, 4225–4231.
(47) Ellman, G. L.; Courtney, K. D.; Andres, B., Jr.; Featherstone, R. M. A New and Rapid Colorimetric Determination of Acetylcholinesterase Activity. *Biochem. Pharmacol.* **1961**, *7*, 88–95.
(48) Giacobini, E. Cholinesterase Inhibitors: New Roles and Therapeutic Alternatives. *Pharmacol. Res.* **2004**, *50*, 433–440.
(49) Lane, R. M.; Potkin, S. G.; Enz, A. Targeting Acetylcholinesterase and Butyrylcholinesterase in Dementia. *Int. J. Neuropsychopharmacol.* **2005**, *9*, 1–24.
(50) Inestrosa, N. C.; Alvarez, A.; Pérez, C. A.; Moreno, R. D.; Vicente, M.; Linker, C.; Casanueva, O. I.; Soto, C.; Garrido, J. Acetylcholinesterase Accelerates Assembly of Amyloid-β-Peptides into Alzheimer's Fibrils: Possible Role of the Peripheral Site of the Enzyme. *Neuron* **1996**, *16*, 881–891.
(51) Alvarez, A.; Alarcón, R.; Opazo, C.; Campos, E. O.; Muñoz, F. J.; Calderón, F. H.; Dajas, F.; Gentry, M. K.; Doctor, B. P.; De Mello, F. G.; Inestrosa, N. C. Stable Complexes Involving Acetylcholinesterase and Amyloid-β-Peptide Change the Biochemical Properties of the Enzyme and Increase the Neurotoxicity of Alzheimer's Fibrils. *J. Neurosci.* **1998**, *18*, 3213–3223.
(52) Taylor, P.; Lappi, S. Interaction of Fluorescence Probes with Acetylcholinesterase. The Site and Specificity of Propidium Binding. *Biochemistry* **1975**, *14*, 1989–1997.
(53) Camps, P.; Cusack, B.; Mallender, W. D.; El Achab, R.; Morral, J.; Muñoz-Torrero, D.; Rosenberry, T. L. Huprine X Is a Novel High-Affinity Inhibitor of Acetylcholinesterase That Is of Interest for Treatment of Alzheimer's Disease. *Mol. Pharmacol.* **2000**, *57*, 409–417.
(54) LeVine, H., III. Quantification of β-Sheet Amyloid Fibril Structures with Thioflavin T. *Methods Enzymol.* **1999**, *309*, 274–284.
(55) Eisert, R.; Felau, L.; Brown, L. R. Methods for Enhancing the Accuracy and Reproducibility of Congo Red and Thioflavin T Assays. *Anal. Biochem.* **2006**, *353*, 144–146.
(56) De Ferrari, G. V.; Mallender, W. D.; Inestrosa, N. C.; Rosenberry, T. L. Thioflavin T Is a Fluorescent Probe of the Acetylcholinesterase Peripheral Site That Reveals Conformational Interactions between the Peripheral and Acylation Sites. *J. Biol. Chem.* **2001**, *276*, 23282–23287.
(57) Vericat, J. A.; Muñoz, P.; Windisch, M.; Hutter-Paier, B.; Medina, M.; Martinez, A. Presented at the 5th Neurobiology of Aging Conference, San Diego, CA, 2004.
(58) http://www.neuropharma.es.
(59) Camps, P.; El Achab, R.; Morral, J.; Muñoz-Torrero, D.; Badia, A.; Baños, J. E.; Vivas, N. M.; Barril, X.; Orozco, M.; Luque, F. J. New Tacrine−Huperzine A Hybrids (Huprines): Highly Potent Tight-Binding Acetylcholinesterase Inhibitors of Interest for the Treatment of Alzheimer's Disease. *J. Med. Chem.* **2000**, *43*, 4657–4666.
(60) Senapati, S.; Bui, J. M.; McCammon, J. A. Induced Fit in Mouse Acetylcholinesterase upon Binding a Femtomolar Inhibitor: A Molecular Dynamics Study. *J. Med. Chem.* **2005**, *48*, 8155–8162.
(61) Bourne, Y.; Radic, Z.; Kolb, H. C.; Sharpless, K. B.; Taylor, P.; Marchot, P. Structural Insights into Conformational Flexibility at the Peripheral Site and within the Active Center Gorge of AChE. *Chem.-Biol. Interact.* **2005**, *157−158*, 159–165.
(62) Colletier, J. Ph.; Sanson, B.; Nachon, F.; Gabellieri, E.; Fattorusso, C.; Campiani, G.; Weik, M. Conformational Flexibility in the Peripheral Site of *Torpedo californica* Acetylcholinesterase Revealed by the Complex Structure with a Bifunctional Inhibitor. *J. Am. Chem. Soc.* **2006**, *128*, 4526–4527.
(63) Aguado, F.; Badía, A.; Baños, J. E.; Bosch, F.; Bozzo, C.; Camps, P.; Contreras, J.; Dierssen, M.; Escolano, C.; Görbig, D. M.; Muñoz-Torrero, D.; Pujol, M. D.; Simón, M.; Vázquez, M. T.; Vivas, N. M. Synthesis and Evaluation of Tacrine-Related Compounds for the Treatment of Alzheimer's Disease. *Eur. J. Med. Chem.* **1994**, *29*, 205–221.
(64) Kryger, G.; Harel, M.; Giles, K.; Toker, L.; Velan, B.; Lazar, A.; Kronman, C.; Barak, D.; Ariel, N.; Shafferman, A.; Silman, I.; Sussman, J. L. Structures of Recombinant Native and E202Q Mutant Human Acetylcholinesterase Complexed with the Snake-Venom Toxin Fasciculin-II. *Acta Cystallogr., Sect. D: Biol. Crystallogr.* **2000**, *56*, 1385–1394.
(65) *InsightII*; Accelrys Inc.: San Diego, CA, 1996.
(66) Jones, G.; Willet, P.; Glen, R. C.; Leach, A. R.; Taylor, R. Development and Validation of a Genetic Algorithm for Flexible Docking. *J. Mol. Biol.* **1997**, *267*, 727–748.
(67) Jorgensen, W. L.; Chandrasekhar, J.; Madura, J. D.; Impey, R. W.; Klein, M. L. Comparison of Simple Potential Functions for Simulating Liquid Water. *J. Chem. Phys.* **1983**, *79*, 926–935.
(68) Case, D. A.; Darden, T. A.; Cheatham, T. E.; Pearlman, D. A.; Simmerling, C. L.; Wang, J.; Duke, R. E.; Luo, R.; Merz, K. M.; Pearlman, D. A.; Crowley, M. ; Brozell, S.; Tsui, V.; Gohlke, H.; Mongan, J.; Hornak, V.; Cui, G.; Beroza, P.; Schafmeister, P.; Caldwell, J. W.; Ross, W. S.; Kollman, P. A. *AMBER8*; University of California: San Francisco, CA, 2004.
(69) Frisch, M. J.; Trucks, G. W.; Schlegel, H. B.; Scuseria, G. E.; Robb, M. A.; Cheeseman, J. R.; Montgomery, J. A., Jr.; Vreven, T.; Kudin, K. N.; Burant, J. C.; Millam, J. M.; Iyengar, S. S.; Tomasi, J.; Barone, V.; Mennucci, B.; Cossi, M.; Scalmani, G.; Rega, N.; Petersson, G. A.; Nakatsuji, H.; Hada, M.; Ehara, M.; Toyota, K.; Fukuda, R.; Hasegawa, J.; Ishida, M.; Nakajima, T.; Honda, Y.; Kitao, O.; Nakai, H.; Klene, M.; Li, X.; Knox, J. E.; Hratchian, H. P.; Cross, J. B.; Adamo, C.; Jaramillo, J.; Gomperts, R.; Stratmann, R. E.; Yazyev, O.; Austin, A. J.; Cammi, R.; Pomelli, C.; Ochterski, J. W.; Ayala, P. Y.; Morokuma, K.; Voth, G. A.; Salvador, P.; Dannenberg, J. J.; Zakrzewski, V. G.; Dapprich, S.; Daniels, A. D.; Strain, M. C.; Farkas, O.; Malick, D. K.; Rabuck, A. D.; Raghavachari, K.; Foresman, J. B.; Ortiz, J. V.; Cui, Q.; Baboul, A. G.; Clifford, S.; Cioslowski, J.; Stefanov, B. B.; Liu, G.; Liashenko, A.; Piskorz, P.; Komaromi, I.; Martin, R. L.; Fox, D. J.; Keith, T.; Al-Laham, M. A.; Peng, C. Y.; Nanayakkara, A.; Challacombe, M.; Gill, P. M. W.; Johnson, B.; Chen, W.; Wong, M. W.; Gonzalez, C.; Pople, J. A. *Gaussian 03*, revision B.04; Gaussian, Inc.: Pittsburgh, PA, 2003.
(70) Bayly, C. I.; Cieplak, P.; Cornell, W. D.; Kollman, P. A. A Well-Behaved Electrostatic Potential Based Method Using Charge Restraints for Deriving Atomic Charges. *J. Phys. Chem.* **1993**, *97*, 10269–10280.

JM8001313

Supporting Information for

Novel Donepezil–Based Inhibitors of Acetyl- and Butyrylcholinesterase and Acetylcholinesterase-Induced β-Amyloid Aggregation

Pelayo Camps,[*,†] *Xavier Formosa,*[†] *Carles Galdeano,*[†] *Tània Gómez,*[†] *Diego Muñoz-Torrero,*[*,†] *Michele Scarpellini,*[†] *Elisabet Viayna,*[†] *Albert Badia,*[‡] *M. Victòria Clos,*[‡] *Antoni Camins,*[§] *Mercè Pallàs,*[§] *Manuela Bartolini,*[#] *Francesca Mancini,*[#] *Vincenza Andrisano*[#] *Joan Estelrich,*[//,⊥] *Mònica Lizondo,*[//,⊥] *Axel Bidon-Chanal,*[//] *and F. Javier Luque,*[//]

[†] Laboratori de Química Farmacèutica (Unitat Associada al CSIC), Facultat de Farmàcia, and Institut de Biomedicina (IBUB), Universitat de Barcelona, Av. Diagonal 643, E-08028, Barcelona, Spain

[‡] Departament de Farmacologia, de Terapèutica i de Toxicologia, Institut de Neurociències, Universitat Autònoma de Barcelona, E-08193-Bellaterra, Barcelona, Spain

[§] Unitat de Farmacologia i Farmacognòsia, Facultat de Farmàcia, Universitat de Barcelona, Av. Diagonal 643, E-08028, Barcelona, Spain

[#] Department of Pharmaceutical Sciences, Alma Mater Studiorum, Bologna University, Via Belmeloro 6, I-40126 Bologna, Italy

[//] Departament de Fisicoquímica, Facultat de Farmàcia, and Institut de Biomedicina (IBUB), Universitat de Barcelona, Av. Diagonal 643, E-08028, Barcelona, Spain

[⊥] Institut de Nanociència i Nanotecnologia, Universitat de Barcelona

Table of Contents

9-[(3-Hydroxypropyl)amino]-1,2,3,4-tetrahydroacridine hydrochloride (8b·HCl). From **5** (3.39 g, 15.6 mmol) and 3-amino-1-propanol, **7b** (3.58 mL, 3.52 g, 46.8 mmol), alcohol **8b** (3.99 g, quantitative yield, free base) was obtained: R_f 0.27 (CH_2Cl_2 / MeOH / 25% aqueous NH_4OH 9:1:0.1). **8b**·HCl: mp 125–126 ºC (MeOH / AcOEt 1:4) [described 130–133 ºC].[1]

6-Chloro-9-[(2-hydroxyethyl)amino]-1,2,3,4-tetrahydroacridine hydrochloride (9a·HCl). From **6** (2.80 g, 11.1 mmol) and 2-aminoethanol, **7a** (2.2 mL, 2.23 g, 36.5 mmol), alcohol **9a** (2.61 g, 85% yield, free base) was obtained: R_f 0.42 (CH_2Cl_2 / MeOH / 25% aqueous NH_4OH 9:1:0.1). **9a**·HCl: mp 221–222 ºC (MeOH / AcOEt 1:4); IR (KBr) ν 3600–2400 (max. at 3372, 3291, 3136, 3052, 3009, 2939, 2872, 2784, O–H, N–H, $^{+}$N–H and C–H st), 1632, 1588, 1573, and 1518 (ar–C–C and ar–C–N st) cm^{-1}; ^{1}H NMR (500 MHz, CD_3OD) δ 1.93–2.02 (complex signal, 4H, 2-H_2 and 3-H_2), 2.71 (m, 2H, 1-H_2), 3.00 (m, 2H, 4-H_2), 3.89 (t, J = 5.2 Hz, 2H, 2'-H_2), 4.07 (t, J = 5.2 Hz, 2H, 1'-H_2), 4.85 (s, OH, NH and $^{+}$NH), 7.56 (dd, J = 9.0 Hz, J' = 2.0 Hz, 1H, 7-H), 7.77 (d, J = 2.0 Hz, 1H, 5-H),

8.49 (d, J = 9.0 Hz, 1H, 8-H); ^{13}C NMR (75.4 MHz, CD_3OD) δ 21.8 (CH_2, C3), 22.8 (CH_2, C2), 24.6 (CH_2, C1), 29.3 (CH_2, C4), 51.2 (CH_2, C1'), 61.4 (CH_2, C2'), 113.5 (C, C9a), 115.4 (C, C8a), 119.0 (CH, C5), 126.6 (CH, C7), 128.7 (CH, C8), 139.9 (C, C6), 140.3 (C, C10a), 152.2 (C, C4a), 158.2 (C, C9). Anal. ($C_{15}H_{17}ClN_2O$·HCl·1/4H_2O) C, H, N, Cl.

6-Chloro-9-[(3-hydroxypropyl)amino]-1,2,3,4-tetrahydroacridine hydrochloride (9b·HCl). From **6** (2.80 g, 11.1 mmol) and 3-amino-1-propanol, **7b** (2.5 mL, 2.46 g, 32.7 mmol), alcohol **9b** (2.96 g, 92% yield, free base) was obtained: R_f 0.32 (CH_2Cl_2 / MeOH / 25% aqueous NH_4OH 9:1:0.1). **9b**·HCl: mp 164–165 ºC (MeOH / AcOEt 1:4); IR (KBr) ν 3500–2400 (max. at 3353, 3314, 3263, 3131, 3051, 3014, 2936, 2907, 2875, 2845, 2803, O–H, N–H, $^+$N–H and C–H st), 1630, 1572, and 1526 (ar–C–C and ar–C–N st) cm^{-1}; ^{1}H NMR (500 MHz, CD_3OD) δ 1.92–2.00 (complex signal, 4H, 2-H_2 and 3-H_2), 2.03 (m, 2H, 2'-H_2), 2.64 (m, 2H, 1-H_2), 2.99 (m, 2H, 4-H_2), 3.83 (t, J = 5.5 Hz, 2H, 3'-H_2), 4.14 (t, J = 6.0 Hz, 2H, 1'-H_2), 4.85 (s, OH, NH and $^+$NH), 7.54 (dd, J = 9.0 Hz, J' = 2.0 Hz, 1H, 7-H), 7.76 (d, J = 2.0 Hz, 1H, 5-H), 8.46 (d, J = 9.0 Hz, 1H, 8-H); ^{13}C NMR (75.4 MHz, CD_3OD) δ 21.8 (CH_2, C3), 22.8 (CH_2, C2), 24.6 (CH_2, C1), 29.3 (CH_2, C4), 33.0 (CH_2, C2'), 48.6 (CH_2, C1'), 61.5 (CH_2, C3'), 113.1 (C, C9a), 115.1 (C, C8a), 118.9 (CH, C5), 126.1 (CH, C7), 129.0 (CH, C8), 139.9 (C, C6), 140.5 (C, C10a), 151.6 (C, C4a), 157.5 (C, C9). Anal. ($C_{16}H_{19}ClN_2O$·HCl·1/4H_2O) C, H, N, Cl.

9-[(3-Methanesulfonyloxypropyl)amino]-1,2,3,4-tetrahydroacridine (10b). From alcohol **8b** (3.99 g, 15.6 mmol), mesylate **10b** (5.15 g, 99% yield) was obtained: R_f 0.95 (CH_2Cl_2 / MeOH / 25% aqueous NH_4OH 9:1:0.1); IR (NaCl) ν 3282 (N-H st), 1639, 1586, 1524 and 1501 (ar–C–C and ar–C–N st), 1352 (SO_2 st as), 1174 (SO_2 st s) cm^{-1}; ^1H NMR (300 MHz, $CDCl_3$) δ 1.84–1.94 (complex signal, 4H, 2-H_2 and 3-H_2), 2.06 (m, 2H, 2'-H_2), 2.71 (m, 2H, 1-H_2), 2.96 (s, 3H, OSO_2CH_3), 3.04 (m, 2H, 4-H_2), 3.60 (m, 2H, 1'-H_2), 4.33 (t, J = 5.8 Hz, 2H, 3'-H_2), 7.35 (pseudo t, J = 7.6 Hz, 1H, 7-H), 7.54 (pseudo t, J = 7.6 Hz, 1H, 6-H), 7.88–7.92 (complex signal, 2H, 5-H and 8-H) (the signal corresponding to the NH group was not observed); ^{13}C NMR (75.4 MHz, $CDCl_3$) δ 22.5 (CH_2) and 22.8 (CH_2) (C2 and C3), 24.7 (CH_2, C1), 30.6 (CH_2, C2'), 33.5 (CH_2, C4), 37.2 (CH_3, OSO_2CH_3), 44.7 (CH_2, C1'), 67.4 (CH_2, C3'), 116.7 (C, C9a), 120.1 (C, C8a), 122.2 (CH), 124.0 (CH), 128.1 (CH), and 128.4 (CH) (C5, C6, C7, and C8), 146.6 (C, C10a), 150.2 (C, C4a), 158.2 (C, C9). HRMS calcd for $[C_{17}H_{22}N_2O_3S + H]^+$ 335.142, found 335.141.

6-Chloro-9-[(2-methanesulfonyloxyethyl)amino]-1,2,3,4-tetrahydroacridine (11a). From alcohol **9a** (2.61 g, 9.44 mmol), mesylate **11a** (3.23 g, 97% yield) was obtained: R_f 0.63 (CH_2Cl_2 / MeOH / 25% aqueous NH_4OH 9:1:0.1). **11a**·HCl: mp: 149–150 ºC (MeOH); IR (KBr) ν 3700–2500 (max. at 3426, 3234, 3114, 3012, 2925, 2798, N–H, $^+$N–H and C–H st), 1630, 1606, 1582 and 1572 (ar–C–C and ar–C–N st), 1354 (SO_2 st as), 1161 (SO_2 st s) cm^{-1}; ^1H NMR (500 MHz, CD_3OD) δ 1.94–2.00 (complex signal, 4H, 2-H_2 and 3-H_2), 2.76 (m, 2H, 1-H_2), 3.03 (m, 2H, 4-H_2), 3.08 (s, 3H, OSO_2CH_3), 4.31 (t, J = 5.0 Hz, 2H, 1'-H_2),

4.57 (t, J = 5.0 Hz, 2H, 2'-H_2), 4.85 (s, NH and $^{+}$NH), 7.59 (dd, J = 9.0 Hz, J' = 2.0 Hz, 1H, 7-H), 7.82 (d, J = 2.0 Hz, 1H, 5-H), 8.39 (d, J = 9.0 Hz, 1H, 8-H); ^{13}C NMR (75.4 MHz, CD_3OD) δ 21.7 (CH_2, C3), 22.8 (CH_2, C2), 25.1 (CH_2, C1), 29.5 (CH_2, C4), 37.4 (CH_3, OSO_2CH_3), 48.3 (CH_2, C1'), 69.7 (CH_2, C2'), 114.7 (C, C9a), 116.0 (C, C8a), 119.2 (CH, C5), 127.2 (CH, C7), 128.3 (CH, C8), 140.2 (2 C, C6 and C10a), 153.2 (C, C4a), 158.6 (C, C9). HRMS calcd for $[C_{16}H_{19}ClN_2O_3S + H]^+$ 355.0878, found 355.0889.

6-Chloro-9-[(3-methanesulfonyloxypropyl)amino]-1,2,3,4-tetrahydroacridine (11b). From alcohol **9b** (2.96 g, 10.2 mmol), impure mesylate **11b** (3.47 g, 92% yield) was obtained, and directly used in the next step without further purification: R_f 0.70 (CH_2Cl_2 / MeOH / 25% aqueous NH_4OH 9:1:0.1).

5,6-Dimethoxy-2-[(4-piperidinyl)methyl]indane (13).

Procedure A. A mixture of donepezil hydrochloride (2.00 g, 4.81 mmol), 1 N HCl (7 mL, 7 mmol) and 5% Pd/C (50% content in water, 801 mg) in MeOH (24 mL) was hydrogenated in a Parr reactor at 28 atm and 65 ºC for 6 days. The resulting suspension was filtered and the filtrate was evaporated under reduced pressure. The resulting residue was diluted with CH_2Cl_2 (30 mL) and 2 N NaOH (15 mL). The organic phase was collected and the aqueous one was extracted with CH_2Cl_2 (3×30 mL). The combined organic phases were washed with H_2O (4×30 mL), dried with anhydrous Na_2SO_4 and concentrated in vacuo to give

piperidine **13** (1.09 g, 82% yield) as a light brown solid: R_f 0.26 (CH_2Cl_2 / MeOH / 25% aqueous NH_4OH 90:10:0.1).

An analytical sample of **13**·HCl was prepared by treatment of a solution of **13** (50 mg, 0.18 mmol) in CH_2Cl_2 (2 mL) with a methanolic solution of HCl (1.81 N, 0.3 mL), followed by evaporation in vacuo. After drying at 80 ºC / 30 Torr for 2 days, **13**·HCl (57 mg) was obtained as a white solid: mp 243–244 ºC (MeOH); IR (KBr) ν 3500–2100 (max. at 3436, 2944, 2884, 2836, 2801, 2764, 2641, 2504, $^{+}$N–H and C–H st), 1609, 1591 and 1504 (ar–C–C st) cm^{-1}; ^{1}H NMR (500 MHz, CD_3OD) δ 1.41 [m, 2H, piperidine 3(5)-H_{ax}], 1.50 (t, J = 7.0 Hz, 2H, indane-2-CH_2), 1.74 (m, 1H, piperidine 4-H), 1.99 [broad d, J = 14.5 Hz, 2H, piperidine 3(5)-H_{eq}], 2.48–2.60 [complex signal, 3H, indane 2-H and 1(3)-H_{cis}], 2.97–3.03 [complex signal, 4H, indane 1(3)-H_{trans} and piperidine 2(6)-H_{ax}], 3.39 [broad d, J = 13.0 Hz, 2H, piperidine 2(6)-H_{eq}], 3.78 [s, 6H, 5(6)-OCH_3], 4.85 (s, $^{+}NH_2$), 6.80 [s, 2H, indane 4(7)-H]; ^{13}C NMR (100.6 MHz, CD_3OD) δ 30.2 [CH_2, piperidine C3(5)], 33.6 (CH, piperidine C4), 38.7 (CH, indane C2), 40.3 [CH_2, indane C1(3)], 43.3 (CH_2, indane-2-CH_2), 45.3 [CH_2, piperidine C2(6)], 56.7 [CH_3, 5(6)-OCH_3], 109.7 [CH, indane C4(7)], 136.3 [C, indane C3a(7a)], 149.4 [C, indane C5(6)].

Procedure B. A mixture of compound **18** (17.8 g, 63.3 mmol), concd. HCl (8.2 mL, 35%, 78.6 mmol) and 5% Pd/C (50% content in water, 10.7 g) in MeOH (300 mL) was hydrogenated in a Parr reactor at 30 atm and 65 ºC for 20 days. The resulting suspension was filtered and the filtrate was evaporated in vacuo to give **13**·HCl (19.2 g, 97% yield) as a brown solid.

9-[(3-{4-[(5,6-Dimethoxy-1-oxoindan-2-yl)methyl]piperidin-1-yl}propyl)amino]-1,2,3,4-tetrahydroacridine dihydrochloride (14b·2HCl). From mesylate **10b** (80 mg, 0.24 mmol) and piperidine **12** (82 mg, 0.28 mmol), compound **14b** (87 mg, 69% yield) was obtained as a pale brown solid, on elution with a mixture of CH_2Cl_2 / MeOH / 25% aqueous NH_4OH 98:2:0.5: R_f 0.46 (CH_2Cl_2 / MeOH / 25% aqueous NH_4OH 9:1:0.1). **14b**·2HCl: mp 198–199 ºC (MeOH); IR (KBr) ν 3700–2400 (max. at 3435, 2930, 2706, N–H, $^{+}$N–H and C–H st), 1690 (C=O st), 1636, 1590, 1522 and 1500 (ar–C–C and ar–C–N st) cm^{-1}; ^{1}H NMR (500 MHz, CD_3OD) δ 1.44 (m, 1H, indanone-2-CH_a), 1.50–1.62 (broad signal, 2H, piperidine 3-H_{ax} and 5-H_{ax}), 1.80–1.96 (broad signal, 2H, piperidine 4-H and indanone-2-CH_b), 1.96–2.05 (complex signal, 5H, acridine 2-H_2 and 3-H_2, and piperidine 3-H_{eq} or 5-H_{eq}), 2.10 (broad d, J = 13.0 Hz, piperidine 5-H_{eq} or 3-H_{eq}), 2.31 (complex signal, 2H, $NHCH_2CH_2CH_2N$), 2.72-2.80 (complex signal, 4H, acridine 1-H_2, indanone 2-H and 3-H_a), 2.95–3.03 (broad signal, 2H, piperidine 2-H_{ax} and 6-H_{ax}), 3.05 (m, 2H, acridine 4-H_2), 3.25 (complex signal, 2H, $NHCH_2CH_2CH_2N$), superimposed in part 3.34 (dd, J = 17.5 Hz, J' = 8.0 Hz, 1H, indanone 3-H_b), 3.56–3.68 (broad signal, 2H, piperidine 2-H_{eq} and 6-H_{eq}), 3.85 (s, 3H, 6-OCH_3), 3.93 (s, 3H, 5-OCH_3), 4.08 (t, J = 7.0 Hz, 2H, $NHCH_2CH_2CH_2N$), 4.85 (s, NH and $^{+}$NH), 7.06 (s, 1H, indanone 4-H), 7.15 (s, 1H, indanone 7-H), 7.64 (ddd, J = 9.0 Hz, J' = 7.0 Hz, J'' = 1.0 Hz, 1H, acridine 7-H), 7.80 (dd, J = 8.5 Hz, J' = 1.0 Hz, 1H, acridine 5-H), 7.88 (ddd, J = 8.5 Hz, J' = 7.0 Hz, J'' = 1.0 Hz, 1H, acridine 6-H), 8.43 (d, J = 9.0 Hz, 1H, acridine 8-H); ^{13}C NMR (100.6 MHz, CD_3OD) δ 21.7 (CH_2, acridine C3),

23.0 (CH_2, acridine C2), 25.2 (CH_2, acridine C1), 26.3 (CH_2, $NHCH_2\mathit{C}H_2CH_2N$), 29.4 (CH_2, acridine C4), 30.3 (CH_2) and 31.2 (CH_2) (piperidine C3 and C5), 33.1 (CH, piperidine C4), 34.1 (CH_2, indanone C3), 39.0 (CH_2, indanone-2-CH_2), 45.9 (CH_2, $NH\mathit{C}H_2CH_2CH_2N$), 46.1 (CH, indanone C2), 54.1 (CH_2) and 54.2 (CH_2) (piperidine C2 and C6), 55.3 (CH_2, $NHCH_2CH_2\mathit{C}H_2N$), 56.5 (CH_3, 6-OCH_3), 56.8 (CH_3, 5-OCH_3), 105.2 (CH, indanone C7), 109.0 (CH, indanone C4), 113.5 (C, acridine C9a), 117.2 (C, acridine C8a), 120.2 (CH, acridine C5), 126.3 (CH, acridine C8), 126.8 (CH, acridine C7), 129.7 (C, indanone C7a), 134.2 (CH, acridine C6), 139.6 (C, acridine C10a), 151.0 (C, indanone C6), 151.4 (C, indanone C3a), 152.3 (C, acridine C4a), 157.7 (C) and 157.9 (C) (indanone C5 and acridine C9), 209.9 (C, indanone C1). Anal. ($C_{33}H_{41}N_3O_3\cdot 2HCl\cdot 2.5H_2O$) C, H, N, Cl.

6-Chloro-9-[(2-{4-[(5,6-dimethoxy-1-oxoindan-2-yl)methyl]piperidin-1-yl}ethyl)amino]-1,2,3,4-tetrahydroacridine dihydrochloride (15a·2HCl). From mesylate **11a** (1.02 g, 2.88 mmol) and piperidine **12** (0.82 g, 2.84 mmol), compound **15a** (514 mg, 33% yield) was obtained as a pale brown solid, on elution with a mixture of CH_2Cl_2 / MeOH / 50% aqueous NH_4OH 95:5:0.4: R_f = 0.53 (CH_2Cl_2 / MeOH / 50% aqueous NH_4OH 9:1:0.05). **15a**·2HCl: mp 187−189 ºC (MeOH); IR (KBr) ν 3600–2500 (max. at 3401, 3258, 3054, 3005, 2926, 2862, 2791, N–H, $^+$N–H and C–H st), 1687, 1675 (C=O st), 1629, 1583 and 1500 (ar–C–C and ar–C–N st) cm^{-1}; ^1H NMR (500 MHz, CD_3OD) δ 1.44 (m, 1H, indanone-2-CH_a), 1.64–1.78 (m, 2H, piperidine 3-H_{ax} and 5-H_{ax}), 1.86 (m, 1H, indanone-2-CH_b), 1.92–2.02 (complex signal, 5H, acridine 2-H_2 and 3-H_2, and piperidine 4-H), 2.05

(broad d, J = 14.0 Hz, 1H) and 2.12 (broad d, J = 14.0 Hz, 1H) (piperidine 3-H_{eq} and 5-H_{eq}), 2.71-2.78 (complex signal, 2H, indanone 2-H and 3-H_a), 2.82 (m, 2H, acridine 1-H_2), 3.06 (m, 2H, acridine 4-H_2), 3.15 (broad dd, $J \approx J' \approx$ 12.0 Hz, 2H, piperidine 2-H_{ax} and 6-H_{ax}), superimposed in part 3.33 (dd, J = 18.0 Hz, J' = 8.0 Hz, 1H, indanone 3-H_b), 3.62 (t, J = 6.5 Hz, 2H, $NHCH_2CH_2N$), 3.70–3.79 (complex signal, 2H, piperidine 2-H_{eq} and 6-H_{eq}), 3.84 (s, 3H, 6-OCH_3), 3.93 (s, 3H, 5-OCH_3), 4.43 (t, J = 6.5 Hz, 2H, $NHCH_2CH_2N$), 4.85 (s, NH and $^+$NH), 7.05 (s, 1H, indanone 4-H), 7.12 (s, 1H, indanone 7-H), 7.63 (dd, J = 9.0 Hz, J' = 2.0 Hz, 1H, acridine 7-H), 7.83 (d, J = 2.0 Hz, 1H, acridine 5-H), 8.44 (d, $J \approx$ 9.0 Hz, 1H, acridine 8-H); ^{13}C NMR (100.6 MHz, CD_3OD) δ 21.6 (CH_2, acridine C3), 22.9 (CH_2, acridine C2), 25.6 (CH_2, acridine C1), 29.5 (CH_2, acridine C4), 30.3 (CH_2) and 31.1 (CH_2) (piperidine C3 and C5), 33.1 (CH, piperidine C4), 34.2 (CH_2, indanone C3), 39.0 (CH_2, indanone-2-CH_2), 43.1 (CH_2, $NHCH_2CH_2N$), 46.1 (CH, indanone C2), 54.8 (2 CH_2, piperidine C2 and C6), 56.5 (CH_3, 6-OCH_3), 56.7 (CH_3, 5-OCH_3), 57.3 (CH_2, $NHCH_2CH_2N$), 105.2 (CH, indanone C7), 109.0 (CH, indanone C4), 114.8 (C, acridine C9a), 116.0 (C, acridine C8a), 119.4 (CH, acridine C5), 127.7 (CH, acridine C7), 128.2 (CH, acridine C8), 129.8 (C, indanone C7a), 140.1 (C, acridine C6), 140.3 (C, acridine C10a), 151.1 (C, indanone C6), 151.3 (C, indanone C3a), 153.6 (C, acridine C4a), 157.7 (C) and 157.9 (C) (indanone C5 and acridine C9), 209.6 (C, indanone C1). Anal. ($C_{32}H_{38}ClN_3O_3 \cdot 2HCl \cdot 3H_2O$) C, H, N, Cl.

6-Chloro-9-[(3-{4-[(5,6-Dimethoxy-1-oxoindan-2-yl)methyl]piperidin-1-yl}propyl)amino]-1,2,3,4-tetrahydroacridine dihydrochloride (15b·2HCl). From crude mesylate **11b** (1.00 g, 2.71 mmol) and piperidine **12** (784 mg, 2.71 mmol), compound **15b** (634 mg, 42% yield) was obtained as a light yellow solid, on elution with a mixture of CH_2Cl_2 / MeOH / 50% aqueous NH_4OH 95:5:0.4: R_f = 0.24 (CH_2Cl_2 / MeOH / 50% aqueous NH_4OH 9:1:0.05). **15b**·2HCl: mp 177 ºC (dec.) (MeOH); IR (KBr) ν 3600–2500 (max. at 3411, 3258, 3131 3060, 2931, 2879, N–H, $^{+}$N–H and C–H st), 1686 (C=O st), 1654, 1630, 1586, and 1499 (ar–C–C and ar–C–N st) cm^{-1}; ^{1}H NMR (500 MHz, CD_3OD) δ 1.45 (m, 1H, indanone-2-CH_a), 1.50–1.65 (complex signal, 2H, piperidine 3-H_{ax} and 5-H_{ax}), 1.84 (m, 1H, indanone-2-CH_b), 1.90–2.00 (complex signal, 5H, acridine 2-H_2 and 3-H_2, and piperidine 4-H), 2.04 (broad d, J = 14.0 Hz, 1H) and 2.11 (broad d, J = 13.5 Hz, 1H) (piperidine 3-H_{eq} and 5-H_{eq}), 2.32 (m, 2H, $NHCH_2C\mathit{H}_2CH_2N$), 2.73–2.78 (complex signal, 4H, acridine 1-H_2, indanone 2-H and 3-H_a) 2.99–3.05 (complex signal, 4H, acridine 4-H_2, piperidine 2-H_{ax} and 6-H_{ax}), 3.26 (broad t, J = 7.5 Hz, 2H, $NHCH_2CH_2C\mathit{H}_2N$), superimposed in part 3.34 (dd, J = 17.5 Hz, J' = 8.0 Hz, 1H, indanone 3-H_b), 3.60–3.66 (broad signal, 2H, piperidine 2-H_{eq} and 6-H_{eq}), 3.85 (s, 3H, 6-OCH_3), 3.94 (s, 3H, 5-OCH_3), 4.07 (t, J = 7.0 Hz, 2H, $NHC\mathit{H}_2CH_2CH_2N$), 4.85 (s, NH and $^{+}$NH), 7.07 (s, 1H, indanone 4-H), 7.15 (s, 1H, indanone 7-H), 7.62 (dd, J = 9.5 Hz, J' = 2.0 Hz, 1H, acridine 7-H), 7.80 (d, $J \approx$ 2.0 Hz, 1H, acridine 5-H), 8.43 (d, $J \approx$ 9.5 Hz, 1H, acridine 8-H); ^{13}C NMR (100.6 MHz, CD_3OD) δ 22.5 (CH_2, acridine C3), 23.2 (CH_2, acridine C2), 25.8 (CH_2, acridine C1), 27.1 (CH_2, $NHCH_2\mathit{C}H_2CH_2N$), 31.4 (CH_2), 31.5 (CH_2) and 32.7 (CH_2) (acridine C4

and piperidine C3 and C5), 34.1 (CH_2, indanone C3), 34.4 (CH, piperidine C4), 39.5 (CH_2, indanone-2-CH_2), 46.4 (CH, indanone C2), 48.2 (CH_2, NH*C*$H_2CH_2CH_2N$), 54.7 (2 CH_2, piperidine C2 and C6), 56.4 (CH_3, 6-OCH_3), 56.7 (CH_3, 5-OCH_3), 57.1 (CH_2, $NHCH_2CH_2$*C*H_2N), 105.2 (CH, indanone C7), 108.9 (CH, indanone C4), 115.0 (C, acridine C9a), 117.1 (C, acridine C8a), 122.2 (CH, acridine C5), 126.1 (CH, acridine C7), 127.9 (CH, acridine C8), 129.7 (C, indanone C7a), 138.1 (C) and 143.8 (C) (acridine C6 and C10a), 151.0 (C, indanone C6), 151.2 (C, indanone C3a), 155.4 (C), 155.6 (C) and 157.6 (C) (acridine C4a and C9, and indanone C5), 209.9 (C, indanone C1). Anal. ($C_{33}H_{40}ClN_3O_3 \cdot 2HCl \cdot 2.5H_2O$) C, H, N, Cl.

9-[(2-{4-[(5,6-Dimethoxyindan-2-yl)methyl]piperidin-1-yl}ethyl)amino]-1,2,3,4-tetrahydroacridine dihydrochloride (16a·2HCl). From mesylate **10a** (500 mg, 1.56 mmol) and piperidine **13** (430 mg, 1.56 mmol), compound **16a** (436 mg, 56% yield) was obtained as a pale brown solid, on elution with a mixture of CH_2Cl_2 / MeOH / 50% aqueous NH_4OH 97:3:0.2: R_f 0.45 (CH_2Cl_2 / MeOH / 50% aqueous NH_4OH 90:10:0.05). **16a**·2HCl: mp 176–178 ºC (MeOH); IR (KBr) ν 3600–2500 (max. at 3401, 3263, 3065, 2927, 2835, 2725, 2670, N–H, $^+$N–H and C–H st), 1635, 1604, 1585, 1525 and 1501 (ar–C–C and ar–C–N st) cm^{-1}; ^{1}H NMR (500 MHz, CD_3OD) δ 1.53 (t, J = 6.7 Hz, 2H, indane-2-CH_2), 1.63 [m, 2H, piperidine 3(5)-H_{ax}], 1.76 (m, 1H, piperidine 4-H), 1.96–2.00 (complex signal, 4H, acridine 2-H_2 and 3-H_2), 2.06 [broad d, J = 14.5 Hz, 2H, piperidine 3(5)-H_{eq}], 2.48-2.61 [complex signal, 3H, indane 2-H and 1(3)-H_{cis}], 2.84 (m, 2H, acridine 1-H_2), 3.00 [dd, J =

14.0 Hz, *J'* = 7.5 Hz, 2H, indane 1(3)-H_{trans}], 3.06–3.15 [complex signal, 4H, acridine 4-H_2 and piperidine 2(6)-H_{ax}], 3.59 (t, *J* = 6.7 Hz, 2H, $NHCH_2CH_2N$), 3.71 [broad d, *J* = 12.0 Hz, 2H, piperidine 2(6)-H_{eq}], 3.78 [s, 6H, 5(6)-OCH_3], 4.42 (t, *J* = 6.7 Hz, 2H, $NHCH_2CH_2N$), 4.85 (s, NH and ^{+}NH), 6.79 [s, 2H, indane 4(7)-H], 7.68 (ddd, *J* = 8.0 Hz, *J'* = 7.0 Hz, *J''* = 1.0 Hz, 1H, acridine 7-H), 7.83 (broad d, *J* = 8.0 Hz, 1H, acridine 5-H), 7.91 (ddd, *J* = 8.0 Hz, *J'* = 7.0 Hz, *J''* = 1.0 Hz, 1H, acridine 6-H), 8.42 (d, *J* = 8.0 Hz, 1H, acridine 8-H); ^{13}C NMR (100.6 MHz, CD_3OD) δ 21.7 (CH_2, acridine C3), 23.0 (CH_2, acridine C2), 25.6 (CH_2, acridine C1), 29.5 (CH_2, acridine C4), 31.0 [broad CH_2, piperidine C3(5)], 33.5 (broad CH, piperidine C4), 38.9 (CH, indane C2), 40.3 [CH_2, indane C1(3)], 43.0 (broad CH_2, $NHCH_2CH_2N$), 43.2 (CH_2, indane-2-CH_2), 54.7 [broad CH_2, piperidine C2(6)], 56.7 [CH_3, 5(6)-OCH_3], 57.4 (broad CH_2, $NHCH_2CH_2N$), 109.7 [CH, indane C4(7)], 114.3 (C, acridine C9a), 117.6 (C, acridine C8a), 120.3 (CH, acridine C5), 126.0 (CH, acridine C8), 127.2 (CH, acridine C7), 134.3 (CH, acridine C6), 136.3 [C, indane C3a(7a)], 139.5 (C, acridine C10a), 149.4 [C, indane C5(6)], 153.0 (C, acridine C4a), 158.0 (C, acridine C9). Anal. ($C_{32}H_{41}N_3O_2 \cdot 2HCl \cdot 1.75H_2O$) C, H, N. Cl, calcd, 11.74; found, 11.22.

9-[(3-{4-[(5,6-dimethoxyindan-2-yl)methyl]piperidin-1-yl}propyl)amino]-1,2,3,4-tetrahydroacridine dihydrochloride (16b·2HCl). From mesylate **10b** (480 mg, 1.44 mmol) and piperidine **13** (440 mg, 1.60 mmol), compound **16b** (274 mg, 37% yield) was obtained as a white solid, on elution with a mixture of CH_2Cl_2 / MeOH / 50% aqueous

NH_4OH 96:4:0.2: R_f 0.31 (CH_2Cl_2 / MeOH / 50% aqueous NH_4OH 9:1:0.05). **16b**·2HCl: mp 67–69 ºC (MeOH); IR (KBr) ν 3600–2500 (max. at 3401, 3060, 2926, 2857, 2840, 2725, N–H, $^{+}$N–H and C–H st), 1630, 1585, 1522 and 1502 (ar–C–C and ar–C–N st) cm^{-1}; ^{1}H NMR (500 MHz, CD_3OD) δ 1.49–1.60 [complex signal, 4H, indane-2-CH_2 and piperidine 3(5)-H_{ax}], 1.74 (m, 1H, piperidine 4-H), 1.99 (complex signal, 4H, acridine 2-H_2 and 3-H_2), 2.05 [broad d, J = 14.0 Hz, 2H, piperidine 3(5)-H_{eq}], 2.33 (m, 2H, $NHCH_2C\mathit{H}_2CH_2N$), 2.49–2.60 [complex signal, 3H, indane 2-H and 1(3)-H_{cis}], 2.78 (m, 2H, acridine 1-H_2), 2.97–3.07 [complex signal, 6H, indane 1(3)-H_{trans}, acridine 4-H_2 and piperidine 2(6)-H_{ax}], 3.25 (m, 2H, $NHCH_2CH_2C\mathit{H}_2N$), 3.62 [broad d, J = 12.5 Hz, 2H, piperidine 2(6)-H_{eq}], 3.78 [s, 6H, 5(6)-OCH_3], 4.08 (t, J = 7.0 Hz, 2H, $NHC\mathit{H}_2CH_2CH_2N$), 4.85 (s, NH and $^{+}$NH), 6.78 [s, 2H, indane 4(7)-H], 7.64 (ddd, J = 8.0 Hz, J' = 7.0 Hz, J'' = 1.0 Hz, 1H, acridine 7-H), 7.80 (dd, J = 8.0 Hz, J' = 1.0 Hz, 1H, acridine 5-H), 7.88 (ddd, J = 8.0 Hz, J' = 7.0 Hz, J'' = 1.0 Hz, 1H, acridine 6-H), 8.43 (d, J = 8.0 Hz, 1H, acridine 8-H); ^{13}C NMR (100.6 MHz, CD_3OD) δ 21.8 (CH_2, acridine C3), 23.0 (CH_2, acridine C2), 25.3 (CH_2, acridine C1), 26.3 (CH_2, $NHCH_2\mathit{C}H_2CH_2N$), 29.4 (CH_2, acridine C4), 30.9 [CH_2, piperidine C3(5)], 33.6 (CH, piperidine C4), 38.8 (CH, indane C2), 40.3 [CH_2, indane C1(3)], 43.1 (CH_2, indane-2-CH_2), 45.9 (CH_2, $NH\mathit{C}H_2CH_2CH_2N$), 54.3 [CH_2, piperidine C2(6)], 55.3 (CH_2, $NHCH_2CH_2\mathit{C}H_2N$), 56.7 [CH_3, 5(6)-OCH_3], 109.7 [CH, indane C4(7)], 113.5 (C, acridine C9a), 117.3 (C, acridine C8a), 120.2 (CH, acridine C5), 126.3 (CH, acridine C8), 126.8 (CH, acridine C7), 134.2 (C, acridine C6), 136.3 [C,

indane C3a(7a)], 139.6 (C, acridine C10a), 149.4 [C, indane C5(6)], 152.3 (C, acridine C4a), 157.9 (C, acridine C9). Anal. ($C_{33}H_{43}N_3O_2 \cdot 2HCl \cdot 2.5H_2O$) C, H, N, Cl.

6-Chloro-9-[(2-{4-[(5,6-dimethoxyindan-2-yl)methyl]piperidin-1-yl}ethyl)amino]-1,2,3,4-tetrahydroacridine dihydrochloride (17a·2HCl). From mesylate **11a** (520 mg, 1.47 mmol) and piperidine **13** (400 mg, 1.45 mmol), compound **17a** (216 mg, 28% yield) was obtained as a pale brown solid, on elution with a mixture of CH_2Cl_2 / MeOH / 50% aqueous NH_4OH 95:5:0.4: R_f 0.45 (CH_2Cl_2 / MeOH / 50% aqueous NH_4OH 9:1:0.05). **17a**·2HCl: mp 218–220 ºC (MeOH); IR (KBr) ν 3600–2500 (max. at 3421, 3274, 3060, 2926, 2835, N–H, $^+$N–H and C–H st), 1629, 1617, 1578 and 1500 (ar–C–C and ar–C–N st) cm^{-1}; ^{1}H NMR (500 MHz, CD_3OD) δ 1.53 (t, J = 7.0 Hz, 2H, indane-2-CH_2), 1.63 [pseudo q, $J \approx$ 12.0 Hz, 2H, piperidine 3(5)-H_{ax}], 1.70–1.80 (broad signal, 1H, piperidine 4-H), 1.94–2.04 (complex signal, 4H, acridine 2-H_2 and 3-H_2), 2.06 [broad d, J = 14.0 Hz, 2H, piperidine 3(5)-H_{eq}], 2.50-2.61 [complex signal, 3H, indane 2-H and 1(3)-H_{cis}], 2.81 (m, 2H, acridine 1-H_2), 2.98–3.14 [complex signal, 6H, acridine 4-H_2, indane 1(3)-H_{trans}, and piperidine 2(6)-H_{ax}], 3.58 (m, 2H, $NHCH_2CH_2N$), 3.71 [broad d, J = 11.5 Hz, 2H, piperidine 2(6)-H_{eq}], 3.78 [s, 6H, 5(6)-OCH_3], 4.41 (t, J = 6.5 Hz, 2H, $NHCH_2CH_2N$), 4.85 (s, NH and $^+$NH), 6.79 [s, 2H, indane 4(7)-H], 7.65 (dd, J = 9.5 Hz, J' = 2.0 Hz, 1H, acridine 7-H), 7.83 (d, J = 2.0 Hz, 1H, acridine 5-H), 8.43 (d, $J \approx$ 9.5 Hz, 1H, acridine 8-H); ^{13}C NMR (100.6 MHz, CD_3OD) δ 21.6 (CH_2, acridine C3), 22.9 (CH_2, acridine C2), 25.6 (CH_2, acridine C1), 29.6 (CH_2, acridine C4), 30.9 [CH_2, piperidine C3(5)], 33.4 (CH,

piperidine C4), 38.8 (CH, indane C2), 40.3 [CH_2, indane C1(3)], 43.1 (2 CH_2, indane-2-CH_2 and NH*C*H_2CH_2N), 54.9 [broad CH_2, piperidine C2(6)], 56.7 [CH_3, 5(6)-OCH_3], 57.3 (broad CH_2, NHCH_2*C*H_2N), 109.6 [CH, indane C4(7)], 114.6 (C, acridine C9a), 115.8 (C, acridine C8a), 119.2 (CH, acridine C5), 127.5 (CH, acridine C7), 128.2 (CH, acridine C8), 136.2 [C, indane C3a(7a)], 140.0 (C, acridine C6), 140.1 (C, acridine C10a), 149.3 [C, indane C5(6)], 153.5 (C, acridine C4a), 157.7 (C, acridine C9). Anal. ($C_{32}H_{40}ClN_3O_2$·2HCl·2.25H_2O) C, H, N, Cl.

6-Chloro-9-[(3-{4-[(5,6-dimethoxyindan-2-yl)methyl]piperidin-1-yl}propyl)amino]-1,2,3,4-tetrahydroacridine dihydrochloride (17b·2HCl). From crude mesylate **11b** (490 mg, 1.33 mmol) and piperidine **13** (370 mg, 1.35 mmol), compound **17b** (274 mg, 38% yield) was obtained as a white solid, on elution with a mixture of CH_2Cl_2 / MeOH / 50% aqueous NH_4OH 95:5:0.4: R_f 0.29 (CH_2Cl_2 / MeOH / 50% aqueous NH_4OH 9:1:0.05). **17b**·2HCl: mp 158–160 ºC (dec.) (MeOH); IR (KBr) ν 3600–2450 (max. at 3412, 3054, 2929, 2835, N–H, $^+$N–H and C–H st), 1629, 1578 and 1501 (ar–C–C and ar–C–N st) cm^{-1}; ^{1}H NMR (500 MHz, CD_3OD) δ 1.51 (t, J = 7.0 Hz, 2H, indane-2-CH_2), superimposed in part 1.57 [broad pseudo q, J = 13.0 Hz, 2H, piperidine 3(5)-H_{ax}], 1.74 (m, 1H, piperidine 4-H), 1.96–2.00 (complex signal, 4H, acridine 2-H_2 and 3-H_2), 2.05 [broad d, J = 14.0 Hz, 2H, piperidine 3(5)-H_{eq}], 2.33 (m, 2H, NHCH_2C*H*$_2$CH_2N), 2.48-2.60 [complex signal, 3H, indane 2-H and 1(3)-H_{cis}], 2.75 (m, 2H, acridine 1-H_2), 2.97–3.04 [complex signal, 6H, acridine 4-H_2, indane 1(3)-H_{trans}, and piperidine 2(6)-H_{ax}], 3.25 (m, 2H, NHCH_2CH_2C*H*$_2$N),

3.62 [broad d, J = 12.5 Hz, 2H, piperidine 2(6)-H_{eq}], 3.78 [s, 6H, 5(6)-OCH_3], 4.07 (t, J = 7.5 Hz, 2H, NHC$H_2$$CH_2CH_2N$), 4.85 (s, NH and $^+$NH), 6.78 [s, 2H, indane 4(7)-H], 7.62 (dd, J = 9.5 Hz, J' = 2.0 Hz, 1H, acridine 7-H), 7.80 (d, J = 2.0 Hz, 1H, acridine 5-H), 8.43 (d, $J \approx$ 9.5 Hz, 1H, acridine 8-H); ^{13}C NMR (100.6 MHz, CD_3OD) δ 21.7 (CH_2, acridine C3), 22.8 (CH_2, acridine C2), 25.1 (CH_2, acridine C1), 26.2 (CH_2, NHC$H_2$$CH_2CH_2N$), 29.4 ($CH_2$, acridine C4), 30.9 [$CH_2$, piperidine C3(5)], 33.6 (CH, piperidine C4), 38.8 (CH, indane C2), 40.3 [CH_2, indane C1(3)], 43.1 (CH_2, indane-2-CH_2), 46.0 (CH_2, NH$CH_2CH_2CH_2N$), 54.3 [CH_2, piperidine C2(6)], 55.3 (CH_2, $NHCH_2CH_2CH_2N$), 56.7 [CH_3, 5(6)-OCH_3], 109.7 [CH, indane C4(7)], 114.0 (C, acridine C9a), 115.7 (C, acridine C8a), 119.2 (CH, acridine C5), 127.7 (CH, acridine C7), 128.6 (CH, acridine C8), 136.3 [C, indane C3a(7a)], 140.2 (C, acridine C6), 140.4 (C, acridine C10a), 149.4 [C, indane C5(6)], 152.7 (C, acridine C4a), 157.9 (C, acridine C9). Anal. ($C_{33}H_{42}ClN_3O_2 \cdot 2HCl \cdot 3H_2O$) C, H, N, Cl.

2-[(1-benzylpiperidin-4-yl)methyl]-5,6-dimethoxyindane hydrochloride (19·HCl). To a solution of piperidine **13**·HCl (300 mg, 0.96 mmol) in MeOH (8 mL), $NaBH_3CN$ (130 mg, 2.07 mmol), AcOH (0.12 mL, 126 mg, 2.10 mmol), and freshly distilled benzaldehyde (0.15 mL, 153 mg, 1.44 mmol) were added. The reaction mixture was stirred at room temperature for 3 h and treated with additional $NaBH_3CN$ (65 mg, 1.03 mmol), and benzaldehyde (0.08 mL, 77 mg, 0.72 mmol). The resulting mixture was stirred at room temperature for 15 h and was evaporated under reduced pressure. The resulting residue was

diluted with H_2O (35 mL) and was extracted with CH_2Cl_2 (4×15 mL). The combined organic extracts were washed successively with 2 N NaOH (3×15 mL) and brine (2×15 mL), were dried with anhydrous Na_2SO_4 and evaporated in vacuo, to give a brown solid residue (477 mg), which was submitted to column chromatography (35–70 μm, silica gel, CH_2Cl_2 / MeOH / 50% aqueous NH_4OH mixtures as eluent). On elution with CH_2Cl_2 / MeOH 99.5:0.5, benzyl alcohol (186 mg) was separated. On elution with CH_2Cl_2 / MeOH / 50% aqueous NH_4OH 98:2:0.2 to 90:10:0.2, compound **19** (185 mg, 53% yield) was isolated as a white solid: R_f 0.12 (CH_2Cl_2 / MeOH 98:2).

The hydrochloride of **19** was prepared by treatment of a 0.45 μm-PTFE filtered solution of **19** (171 mg, 0.47 mmol) in CH_2Cl_2 (3 mL) with a methanolic solution of HCl (3.5 N, 0.9 mL), followed by evaporation in vacuo, and trituration of the resulting solid (172 mg) with Et_2O (6×1 mL). After drying at 80 ºC / 30 Torr for 2 days, **19**·HCl (161 mg) was obtained as a white solid: mp 211–213 ºC (MeOH); IR (KBr) ν 3500–2100 (max. at 3430, 3059, 3037, 2998, 2923, 2836, 2630, 2614, 2589, 2498, 2423, $^+$N–H and C–H st), 1607 and 1506 (ar–C–C st) cm^{-1}; ^{1}H NMR (400 MHz, CD_3OD) δ 1.40–1.52 [complex signal, 4H, indane-2-CH_2 and piperidine 3(5)-H_{ax}], 1.70 (m, 1H, piperidine 4-H), 2.01 [broad d, J = 14.4 Hz, 2H, piperidine 3(5)-H_{eq}], 2.46–2.58 [complex signal, 3H, indane 2-H and 1(3)-H_{cis}], 2.97 [dd, J = 13.6 Hz, J' = 6.8 Hz, 2H, indane 1(3)-H_{trans}], superimposed in part 3.02 [broad dd, $J \approx J' \approx$ 12.8 Hz, 2H, piperidine 2(6)-H_{ax}], 3.49 [broad d, J = 12.8 Hz, 2H, piperidine 2(6)-H_{eq}], 3.77 [s, 6H, 5(6)-OCH_3], 4.31 (s, 2H, N–CH_2–Ph), 4.85 (s, $^+$NH), 6.78 [s, 2H, indane 4(7)-H], 7.48–7.57 (complex signal, 5H, Ar–H); ^{13}C NMR (100.6 MHz, CD_3OD) δ 30.8

[CH_2, piperidine C3(5)], 33.6 (CH, piperidine C4), 38.8 (CH, indane C2), 40.2 [CH_2, indane C1(3)], 43.0 (CH_2, indane-2-CH_2), 53.9 [CH_2, piperidine C2(6)], 56.7 [CH_3, 5(6)-OCH_3], 61.8 (CH_2, N–CH_2–Ph), 109.7 [CH, indane C4(7)], 130.3 [CH, phenyl C2(6)], 130.5 (C, phenyl C1), 131.2 (CH, phenyl C4), 132.4 [CH, phenyl C3(5)], 136.3 [C, indane C3a(7a)], 149.4 [C, indane C5(6)]. HRMS calcd for $[C_{24}H_{32}NO_2 + H]^+$ 366.2427, found 366.2426.

Predicted pose of donepezil obtained by using GOLD

Top: View of the X-ray crystallographic structure of the AChE enzyme complexed to donepezil (gray) and the docked ligand (colored by atom).
Bottom: View of the X-ray and docked ligands in the binding site.

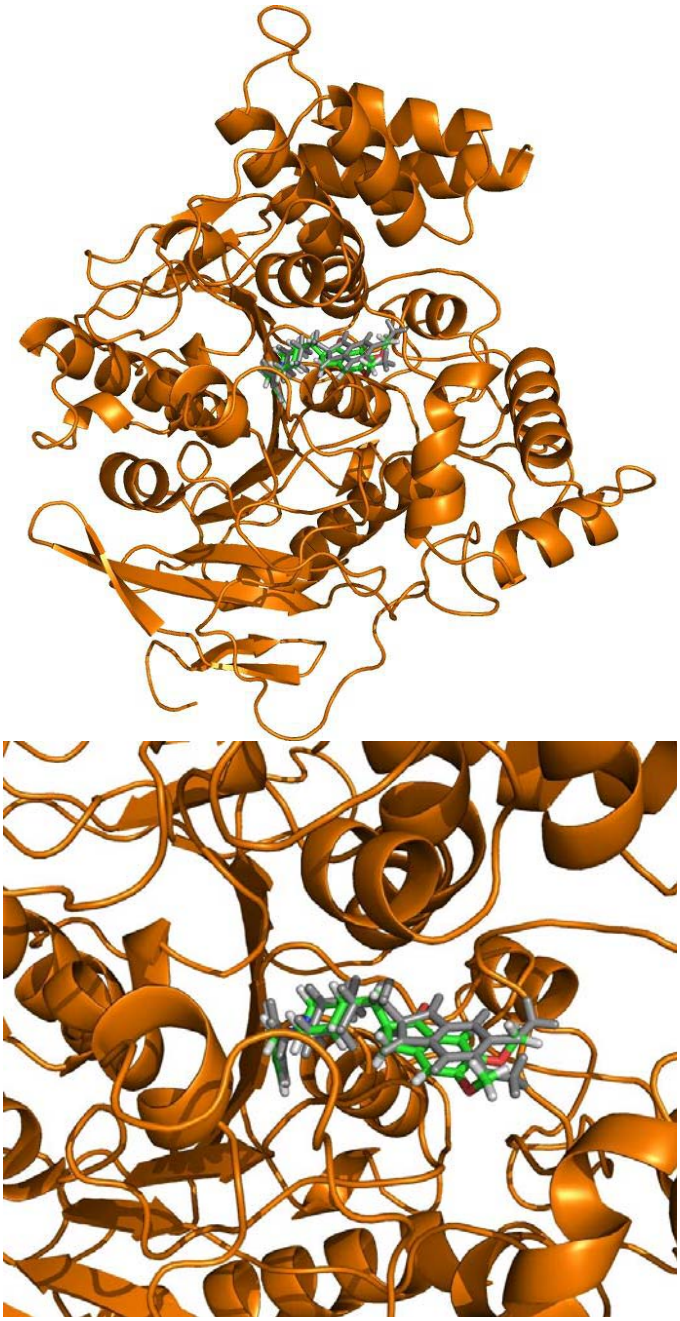

References

(1) Michalson, E. T.; D'Andrea, S.; Freeman, J. P.; Szmuszkovicz, J. The Synthesis of 9-(1-Azetidinyl)-1,2,3,4-tetrahydroacridine. *Heterocycles* **1990**, *30*, 415–425.

(2) Mancini, F.; Naldi, M.; Cavrini, V.; Andrisano, V. Multiwell Fluorometric and Colorimetric Microassays for the Evaluation of Beta-Secretase (BACE-1) Inhibitors. *Anal. Bioanal. Chem*. **2007**, *388*, 1175–1183.

Appendix

Compound	**Molecular Formula**	**Calculated**				**Found**			
		C	H	N	Cl	C	H	N	Cl
9a·HCl·0.25H_2O	$C_{15}H_{17}ClN_2O$·HCl·0.25H_2O	56.70	5.87	8.82	22.32	56.58	5.85	8.85	22.09
9b·HCl·0.25H_2O	$C_{16}H_{19}ClN_2O$·HCl·0.25H_2O	57.93	6.23	8.44	21.37	58.03	6.31	8.41	21.23
14a·2HCl·1.5H_2O	$C_{32}H_{39}N_3O_3$·2HCl·1.5H_2O	62.64	7.23	6.85	11.56	62.64	7.05	6.59	11.59
14b·2HCl·2.5H_2O	$C_{33}H_{41}N_3O_3$·2HCl·2.5H_2O	61.39	7.49	6.51	10.98	61.60	7.24	6.31	11.16
15a·2HCl·3H_2O	$C_{32}H_{38}ClN_3O_3$·2HCl·3H_2O	56.93	6.87	6.22	15.75	57.16	6.90	5.89	15.41
15b·2HCl·2.5H_2O	$C_{33}H_{40}ClN_3O_3$·2HCl·2.5H_2O	58.28	6.97	6.18	15.64	58.18	7.08	5.92	15.33
16a·2HCl·1.75H_2O	$C_{32}H_{41}N_3O_2$·2HCl·1.75H_2O	63.62	7.76	6.96	11.74	63.67	7.58	6.80	11.22
16b·2HCl·2.5H_2O	$C_{33}H_{43}N_3O_2$·2HCl·2.5H_2O	62.75	7.98	6.65	11.22	62.50	7.93	6.45	11.48
17a·2HCl·2.25H_2O	$C_{32}H_{40}ClN_3O_2$·2HCl·2.25H_2O	59.35	7.24	6.49	16.42	59.00	7.14	6.40	16.17
17b·2HCl·3H_2O	$C_{33}H_{42}ClN_3O_2$·2HCl·3H_2O	58.71	7.46	6.22	15.75	58.46	7.70	6.14	16.04

Capítol 4: ***Disseny, síntesi i avaluació farmacològica d'híbrids pirano[3,2-c]quinolina–6-clorotacrina com a una nova família de compostos anti–Alzheimer.***

(*J. Med. Chem* **2009**, *52,* 5365–5379).

4.1 Disseny d'una nova família d'inhibidors de l'AChE de lloc d'unió dual

La síntesi d'inhibidors de l'AChE de lloc d'unió dual en els quals s'incorpora una unitat de l'inhibidor específic de lloc perifèric propidi, **8** (Figura 4.1), ha interessat a diferents grups de recerca fins al moment.[124,125] Encara que des d'un punt de vista mecanístic o com a eina farmacològica aquests nous compostos basats en propidi poden ser de gran utilitat, des d'un punt de vista d'aplicació mèdica tenen poc interès ja que en contenir dos nitrògens quaternaris difícilment podran travessar la BHE.

El grup de treball del Dr. Rodolfo Lavilla va desenvolupar una metodologia[126] que permet un fàcil accés a compostos tricíclics d'estructura similar a la del compost **44** (Figura 4.1), que és reminiscent a la del propidi.

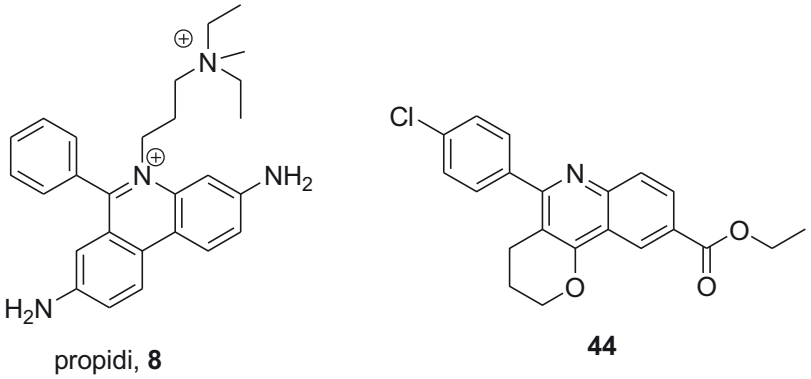

Figura 4.1 Estructura del propidi, **8**, i del compost tricíclic **44**.

En la Figura 4.2 es mostra la disposició del propidi en el lloc perifèric de l'AChE, extreta de l'estructura tridimensional de raigs-X del complex entre l'AChE de ratolí i el propidi (codi PDB 1N5R)[127] i se superposa l'estructura de **44** amb la del propidi. La superposició entre aquests dos compostos no és perfecta. Per un costat, els nitrògens quinolínics i els carbonis susbtituïts amb el grup fenil estarien intercanviats. Una altra diferència important és que el propidi presenta una càrrega positiva sobre l'àtom de nitrogen fenantridínic, mentre sembla bastant probable que el nitrogen quinolínic de **44** no estarà protonat a pH fisiològic. El pK_a calculat amb el software ACD/Labs V8.14 en un compost model com la 2-fenil-4-metoxiquinolina és de 5,8. Així doncs, sembla raonable que el pK_a de **44** sigui semblant, sent aquest nitrogen quinolínic no suficientment bàsic com per estar protonat en una proporció important a pH

[124]Bolognesi, M.L.; Andrisano, V.; Bartolini, M.; Banzi, R.; Melchiorre, C. *J. Med. Chem*. **2005**, *48,* 24. [125]Bourne, Y.; Kolb, H.C.; Radic, Z.; Sharpless, K.B.; Taylor, P.; Marchot, P. *Proc. Natl. Acad. Sci. U.S.A* **2004**, *101*, 1449. [126]Jiménez, O.; de la Rosa, G.; Lavilla, R. *Angew. Chem. Int. Ed.* **2005**, *44*, 6521. [127]Bourne, Y.; Taylor, P.; Radic, Z.; Marchot, P. *EMBO J.* **2003**, *22*, 1.

fisiològic. Tot i que aquest tipus d'estructura no podria establir interaccions de tipus catió–π amb el triptòfan característic del lloc perifèric, el seu sistema aromàtic sí que podria establir interaccions de tipus π-stacking. Per això, ens va semblar adequat utilizar aquest tipus d'estructura com a unitat d'interacció amb el lloc perifèric de l'AChE en una nova família d'inhibidors de lloc d'unió dual. A més, el grup funcional èster i la seva colocació en la posició 9 del sistema tricíclic semblaven adequades per a l'ancoratge del *linker* mitjançant la formació d'un enllaç amida i per a la seva extensió al llarg de la gorja catalítica de l'enzim (Figura 4.2). Finalment, vam escollir una unitat de 6-clorotacrina com a unitat d'interacció amb el lloc actiu per la seva facilitat de síntesi i per la seva major afinitat pel centre actiu en relació amb la unitat de tacrina sense substituir, present en una gran quantitat de famílies d'inhibidors d'AChE de lloc d'unió dual.

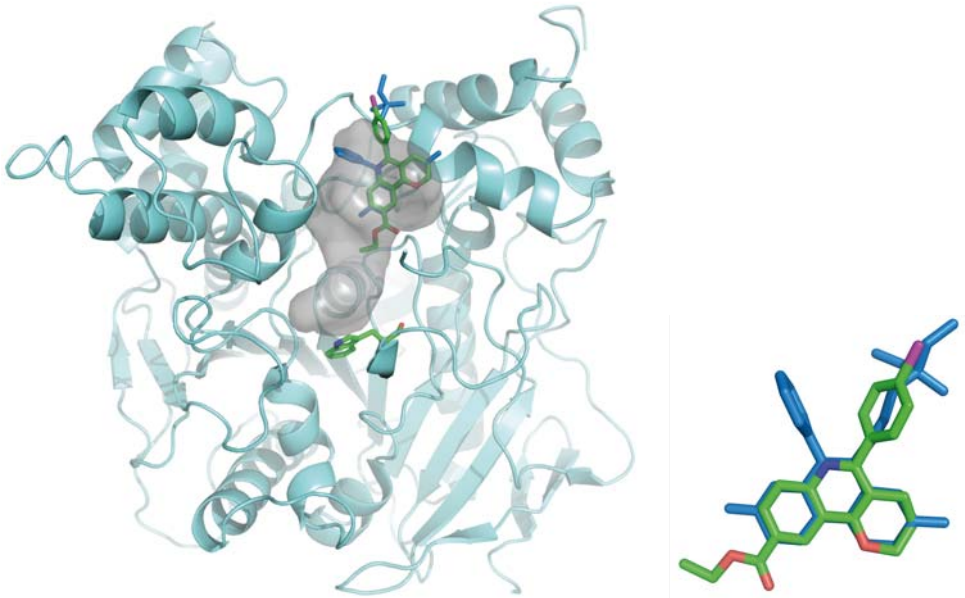

Figura 4.2 Superposició del propidi (blau) i del compost **44** (verd) en el lloc perifèric de l'AChE. En color gris, es representa la gorja catalítica de l'enzim.

D'altra banda, en una família d'inhibidors d'AChE de lloc d'unió dual desenvolupada per la Dra. Ana Martínez (Instituto de Química Médica, Madrid), que combinen un sistema d'indol per a la interacció amb el lloc perifèric de l'AChE i una unitat de 6-clorotacrina per a la interacció amb el centre actiu a través d'un *linker* que conté un grup amida, la posició d'aquest grup amida dins del *linker* va resultar crítica per a l'activitat inhibitòria de l'AChE.[111] Així, el desplaçament en dues posicions del grup amido del compost **46** (Figura 4.3) per a donar el compost **47**, que

[111] Alonso, D.; Dorronsoro, I.; Rubio, L.; Muñoz, P.; García-Palomero, E.; Del Monte, M.; Bidon-Chanal, A.; Orozco, M.; Luque, F.J.; Castro, A.; Medina, M.; Martínez, A. *J. Med. Chem.* **2005**, *48*, 7223.

globalment presenta la mateixa longitud de *linker* que **46,** condueix a un augment de 9 cops en la potència inhibitòria enfront l'AChE bovina, mentre que el mateix desplaçament per passar del compost **48** al **49** va tenir resultats encara més dramàtics en la potència del compost resultant (2300 cops més potent). En vista d'aquests resultats, també es va plantejar la utilització del derivat homologat de **44** amb dos metilens entre l'èster i el sistema tricíclic com a subunitat d'interacció amb el lloc perifèric de l'AChE.

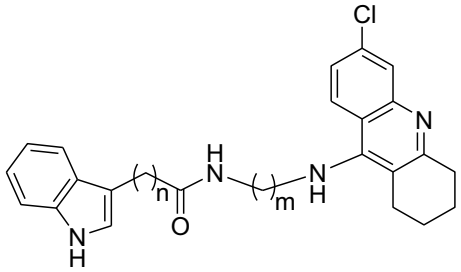

n = 0, m = 7, **46** [IC_{50} (bAChE) = 36 nM] ----------→ n = 2, m = 5, **47** [IC_{50} (bAChE) = 4 nM]

n = 0, m = 8, **48** [IC_{50} (bAChE) = 46 nM] ----------→ n = 2, m = 6, **49** [IC_{50} (bAChE) = 0,02 nM]

Figura 4.3 Efecte de la posició del grup amido en el *linker* d'híbrids indol–tacrina sobre la potència inhibitòria de l'AChE.

A l'esquema 4.1 es detalla la seqüència retrosintètica que es va plantejar per a la preparació dels híbrids d'estructura general **II**. Aquests compostos es podien sintetitzar per reacció dels èsters obtinguts **44** i **45**, preparats pel grup del Dr. Rodolfo Lavilla, amb les aminoalquiltacrines **50**, que es poden preparar fàcilment per substitució nucleòfila aromàtica de la coneguda cloroacridina **24** amb diferents diaminoalcans comercials.

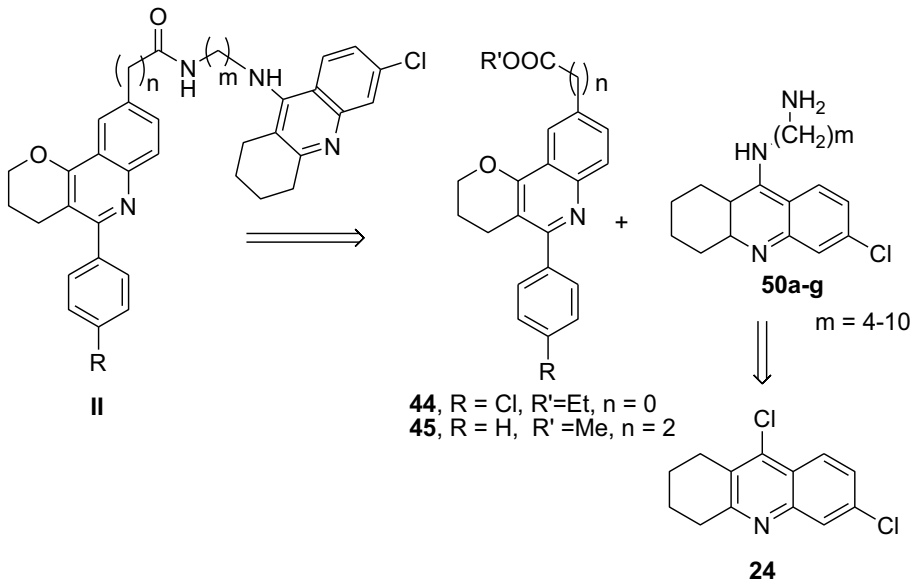

II

44, R = Cl, R'=Et, n = 0
45, R = H, R' =Me, n = 2

50a-g

m = 4-10

24

Esquema 4.1

4.2 Síntesi dels nous híbrids pirano[3,2-c]quinolina–6-clorotacrina

4.2.1 Síntesi dels èsters tricíclics 44 i 45

La preparació dels èsters tricíclics **la va abordar l'equip del Dr. Rodolfo Lavilla**. La reacció de Povarov entre l'èter d'enol, **51**, el *p*-aminobenzoat d'etil, **52**, i el *p*-clorobenzaldehid, **53**, sota catàlisi de $Y(OTf)_3$ en el si d'acetonitril va proporcionar una mescla diastereomèrica de les corresponents tetrahidroquinolines **54**. La posterior oxidació amb DDQ va donar l'èster desitjat **44** (Esquema 4.2).

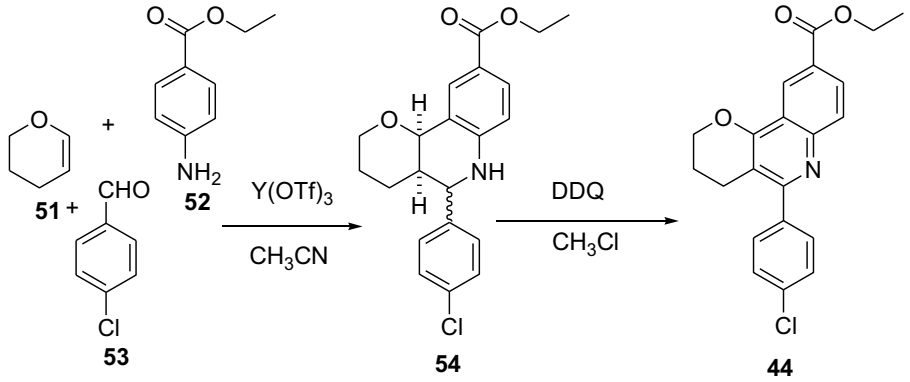

Esquema 4.2

Anàlogament, la reacció de Povarov entre l'èter d'enol **51**, el *p*-clorobenzaldehid, **53**, i el 3-(4-aminofenil)propanoat de metil, **55**, i sota catàlisi de $Sc(OTf)_3$, seguit d'oxidació amb DDQ de la mescla diastereomèrica de les tetrahidroquinolines **56** va donar lloc a l'èster tricíclic homologat **57**, juntament amb el corresponent derivat cinnàmic **58**, resultant de la sobreoxidació de la cadena lateral etilènica. Després d'una tediosa purificació d'aquesta mescla per cromatografia en columna es va poder aïllar **57** amb un baix rendiment. Alternativament, de cara a augmentar el rendiment d'obtenció de **57**, es va assajar la hidrogenació catalítica d'aquesta mescla, amb la idea de convertir el derivat cinnàmic **58** obtingut en **57**. No obstant, a l'efectuar la hidrogenació catalítica d'aquesta mescla, la reducció del doble enllaç exocíclic va anar acompanyada de deshalogenació, obtenint-se l'èster tricíclic **45** com a producte de reacció (Esquema 4.3). En vista d'aquests resultats i tenint en compte que la presència o absència de l'àtom de clor en l'estructura tricíclica no semblava crítica per a la interacció amb el lloc perifèric de l'AChE, es va decidir utilitzar l'èster tricíclic deshalogenat **45** com a precursor de la nova sèrie d'híbrids (Esquema 4.3).

El grup del Dr. Rodolfo Lavilla va optimitzar la síntesi de l'èster tricíclic **45**, efectuant també la reacció de Povarov directament amb l'aldehid deshalogenat **59** (Esquema 4.3).

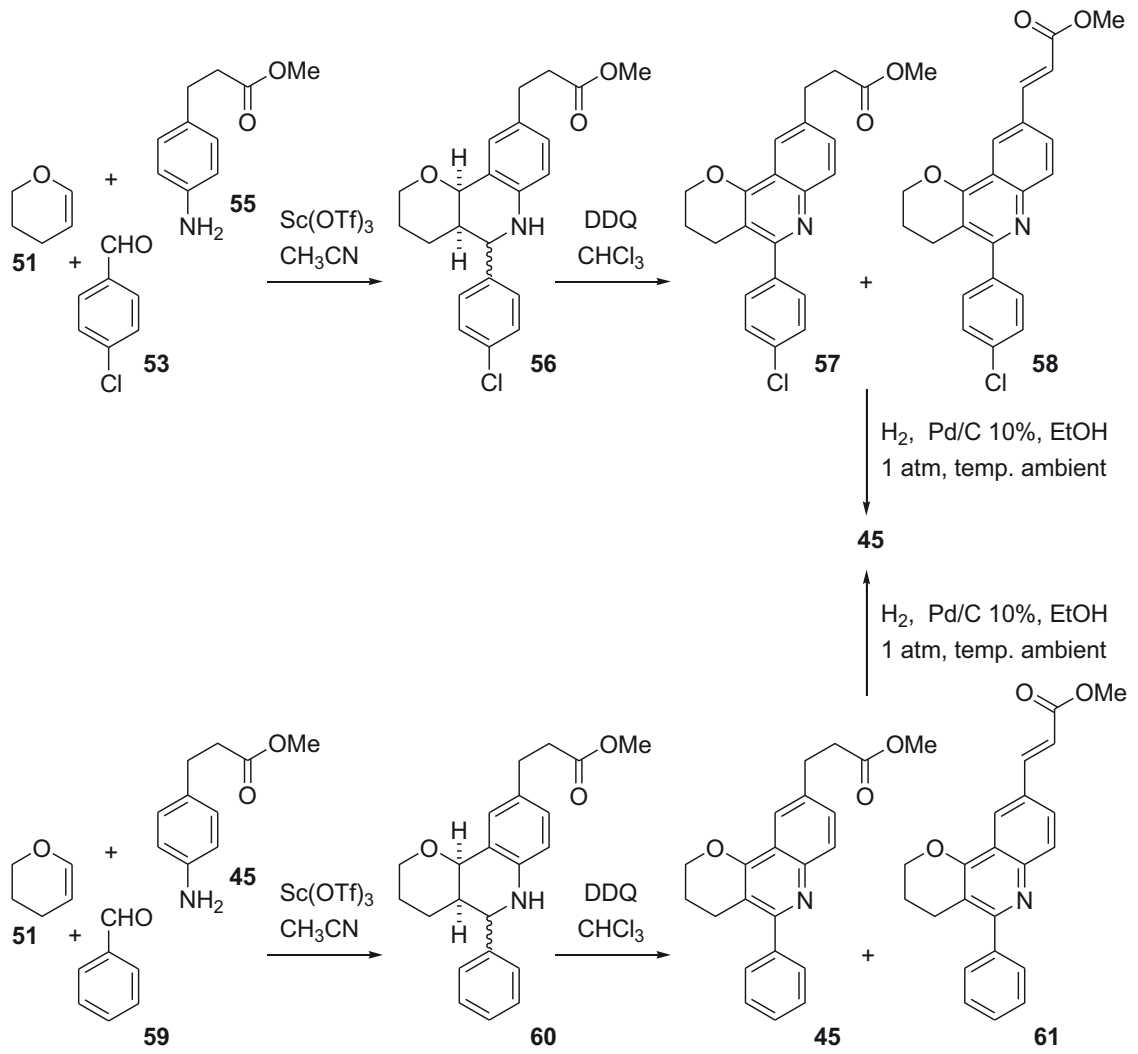

Esquema 4.3

4.2.2 Síntesi de les aminoalquiltacrines 50a–g

Una cop es disposava dels èsters tricíclics **44** i **45**, en la present Tesi Doctoral es va abordar la preparació de les aminoalquiltacrines **50a**–**g**, contenint *linkers* de 4 a 10 grups metilens, a partir de la coneguda 6,9-dicloro-1,2,3,4-tetrahidroacridina, **24**[118] i les diamines **62a**–**g**, comercialment assequibles.

Tal com s'ha indicat al Capítol 3, la dicloroquinolina es va preparar amb un rendiment quantitatiu seguint un procediment descrit[118,119] basat en la reacció de la ciclohexanona, amb un lleuger excés d'àcid 4-cloroantranílic, **33**, i 10 equivalents de $POCl_3$ a reflux durant 2 h-

[118]Hu, M.-K.; Lu, C.-F. *Tetrahedron Lett.* **2000**, *41*, 1815. [119] Hu, M.-K.; Wu, L.-J.; Hsiao, G.; Yen, M.-H. *J. Med. Chem.* **2002**, *45*, 2277.

El tractament de la dicloroquinolina **24** amb 4 equivalents de les diamines **62a**–**g** es va dur a terme utilitzant les condicions descrites pels Drs. Carlier i Pang per a la síntesi de vàries famílies d'inhibidors de l'AChE de lloc d'unió dual basats en tacrina, que impliquen l'ús d'1-pentanol com a disolvent a reflux (punt d'ebullició de l'1-pentanol = 136–138 °C).[87,128] Els crus de reacció obtinguts es van purificar per cromatografia en columna a través de gel de sílice, el que va permetre aïllar les aminoalquiltacrines desitjades amb rendiments de moderats a bons (35–78%) (Esquema 4.4). Cal destacar que tot i utilitzar excés de diamina (4 equivalents), en aquestes reaccions es van formar els subproductes resultants de la dimerització de la 6-cloroquinolina (compostos **63a**–**g**), amb rendiments baixos (6–11%), excepte en el cas de **63e** i **63f** que es van obtenir amb rendiments lleugerament superiors als de les corresponents aminoalquiltacrines (46% i 53%, respectivament) (Esquema 4.4).

A efectes de caracterització, tant les aminoalquiltacrines **50a**–**g** com les *bis*-tacrines **63a**–**g** es van transformar, per tractament amb dissolucions metanòliques d'HCl, en els corresponents dihidroclorurs, els quals es van cristal·litzar de mescles MeOH / AcOEt per a obtenir les mostres analítiques. Cal destacar que l'aminoalquiltacrina **50a** i la *bis*-tacrina **63b** són compostos nous, per la qual cosa van ser completament caracteritzats a través de les seves dades espectroscòpiques i anàlisi elemental. La resta d'aminoalquiltacrines i *bis*-tacrines són compostos coneguts, per la qual cosa es van caracteritzar únicament a través de les seves dades espectroscòpiques, excepte en el cas de les *bis*-tacrines **63a** i **63d**, que no es van poder obtenir en forma suficientment pura ni després de cromatografia en columna ni en els posteriors intents de cristal·lització dels corresponents dihidroclorurs.

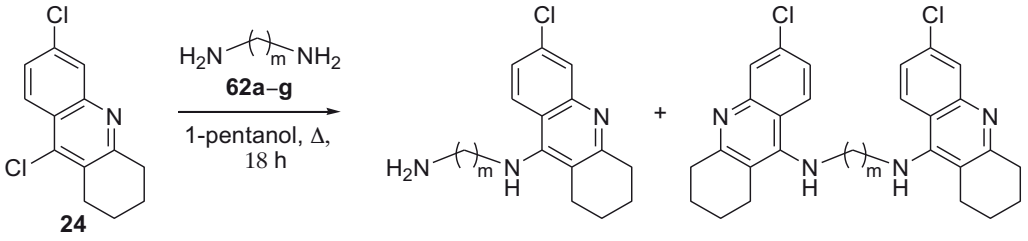

m = 4, **50a** (63%)
m = 5, **50b** (70%)
m = 6, **50c** (78%)
m = 7, **50d** (78%)
m = 8, **50e** (35%)
m = 9, **50f** (35%)
m=10, **50g** (38 %)

m = 4, **63a** (11%)
m = 5, **63b** (6%)
m = 6, **63c** (8%)
m = 7, **63d** (10%)
m = 8, **63e** (46%)
m = 9, **63f** (53%)
m = 10, **63g** (15%)

Esquema 4.4

[87]Li, W.M.; Kan, K.K.W.; Carlier, P.R.; Pang, Y.P.; Han, Y.F. *Curr. Alzheimer Res.* **2007**, *4*, 386. [128]Carlier, P.R.; Chow, E.S.-H.; Han, Y.; Liu, J.; El Yazal, J.; Pang, Y.-P. *J. Med. Chem.* **1999**, *42*, 4225.

4.2.3 Síntesi dels nous híbrids 64c–g i 65a–e

Una vegada es disposava de les aminoalquiltacrines **50a**–**g** i dels èsters **44** i **45**, en la present Tesi Doctoral es va abordar la preparació dels nous híbrids d'estructura **64** i **65**. La formació de l'enllaç amida dels híbrids va resultar una tasca difícil. Diferents intents inicials de formació de **64c** per reacció directa de l'èster **44** amb l'amina **50c** van resultar infructuosos. Així, la reacció de l'èster **44** amb 1 equiv. de l'aminoalquiltacrina **50c** i 2 equiv. de *t*-BuOK en el si de toluè a reflux durant 6 dies va deixar els productes de partida inalterats (Esquema 4.5). El mateix resultat es va obtenir en diferents intents d'acoblament de l'èster **44** amb 1 equiv. de l'aminoalquiltacrina **50c** en presència d'1 equiv. de *t*-BuOK sota irradiació de microones en el si de DMSO (200 ^{o}C durant 3 min), toluè (150 ^{o}C durant 3 min), 1,2-dicloroetà (120 ^{o}C durant 3 min) o en presència d'una quantitat catalítica de NaCN sota irradiació de microones en EtOH (120 ^{o}C durant 3 min) (Esquema 4.5).

En vista d'aquests resultats, es va plantejar alternativament la formació de l'enllaç amida de **64c** mitjançant la hidròlisi de l'èster **44**, seguida d'activació de l'àcid resultant i reacció amb l'amina **50c**. La hidròlisi de **44** es va dur a terme per reacció amb NaOH 5 N en MeOH a reflux durant 16 h, seguit d'acidificació amb dissolució aquosa d'HCl 2 N, evaporació a pressió reduïda de la mescla i extracció del residu sòlid resultant amb MeOH. D'aquesta forma es va aïllar l'àcid desitjat **66** en forma d'hidroclorur (Esquema 4.5), probablement acompanyat de petites quantitats de NaCl format durant la neutralització i extretes en part amb el MeOH. Aquest producte cru es va utilitzar directament en la següent etapa sense cap purificació posterior. El tractament de **66**·HCl amb excés de $SOCl_2$ durant 1 h, seguit d'evaporació dels productes volàtils i reacció del clorur d'àcid resultant amb 1 equiv. de l'aminoalquiltacrina **50c** i 2,5 equiv. de Et_3N en CH_2Cl_2 a temperatura ambient durant 61 h tampoc no va proporcionar l'amida desitjada **64c**, recuperant-se l'amina de partida **50c** inalterada després d'un final de reacció bàsic (Esquema 4.5). Sortosament, la reacció de l'àcid **66**·HCl cru amb 1 equiv. de cloroformiat d'etil i 2,1 equiv. de Et_3N en CH_2Cl_2 a 0 ^{o}C durant 30 min, seguit de reacció de l'anhídrid mixt format amb l'aminoalquiltacrina **50c** a temperatura ambient durant 64 h va conduir a l'híbrid desitjat **64c** amb un 23% de rendiment global (rendiment global a partir de l'èster **44**), després de purificació per cromatografia en columna a través de gel de sílice (Esquema 4.5).

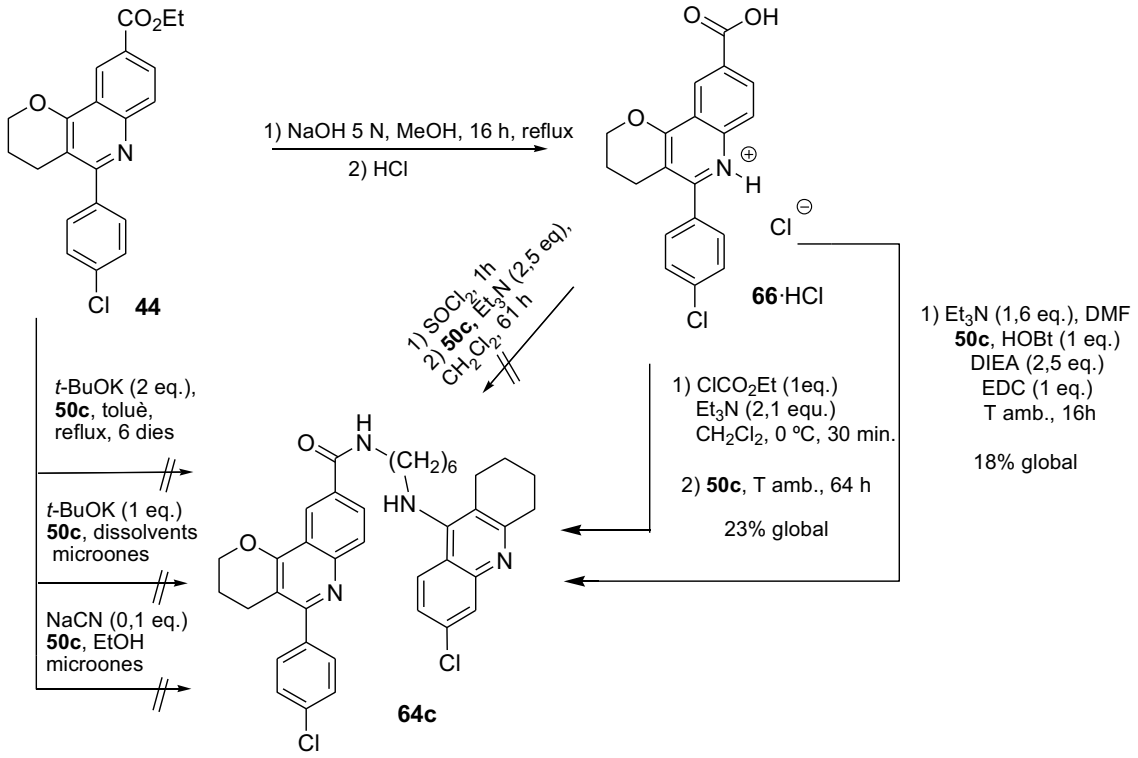

Esquema 4.5

El baix rendiment d'obtenció de l'híbrid **64c** a través d'aquesta metodologia ens va fer plantejar una altra via d'activació d'àcids, d'utilització freqüent en la química de pèptids. Així, es va fer reaccionar l'aminoalquiltacrina **50c** amb 1 equiv. d'àcid **66**·HCl, 1 equiv. d'1-hidroxibenzotriazol (HOBt) i 1 equiv. de l'hidroclorur d'1-etil-3-(3'-dimetilaminopropil)carbodiïmida (EDC) en presència d'excés de Et_3N i diisopropiletilamina en el si de DMF a temperatura ambient durant 16 h, obtenint-se l'híbrid desitjat **64c** amb menor rendiment que per la via anterior (15%), després de purificació del cru de reacció per cromatografia en columna a través de gel de sílice.

En vista d'aquest resultat, els híbrids **64d**–**g** es van preparar a partir de les corresponents aminoalquiltacrines **50d**–**g**, via formació de l'anhídrid mixt de l'acid **66**·HCl amb el cloroformiat d'etil, amb rendiments comparables a l'obtingut en la preparació de **64c** (Esquema 4.6).

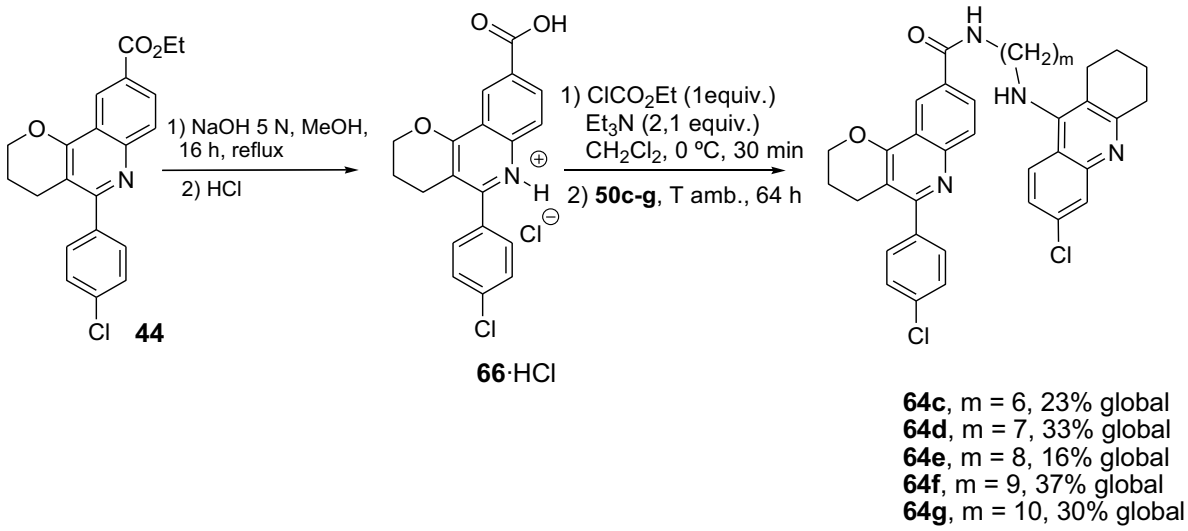

Esquema 4.6

Amb l'experiència adquirida en la preparació d'aquests híbrids ens vam plantejar l'accés als híbrids d'estructura **65** utilitzant la mateixa metodologia. La hidròlisi de l'èster **45**, preparat pel grup del Dr. Lavilla, es va dur a terme per tractament amb NaOH 5 N en el si de MeOH a reflux durant 16 h. A diferència del que va passar a la hidròlisi de l'èster **44**, la hidròlisi de l'èster **45** va resultar incompleta. Així es va tractar la mescla d'èster i d'àcid resultant amb KOH en MeOH a reflux durant 64 h, seguit d'acidificació amb una dissolució metanòlica d'HCl, evaporació a pressió reduïda de la mescla i extracció del residu sòlid resultant amb MeOH, obtenint-se l'àcid desitjat **67** en forma d'hidroclorur (Esquema 4.7), probablement impurificat per petites quantitats de NaCl. No obstant, aquests resultats no es van poder reproduir en assaigs posteriors en els quals l'acidificació amb HCl–MeOH produïa l'esterificació parcial de l'àcid, fins i tot efectuant l'acidificació i l'evaporació en fred i el més ràpidament possible. Finalment, es va poder optimizar el procediment d'aïllament de l'àcid evaporant a sequetat la mescla de reacció alcalina i tractant el residu sòlid resultant amb una dissolució de HCl en Et_2O durant 30 min. L'àcid **67**·HCl cru obtingut per evaporació de la dissolució etèrea àcida es va usar directament per a l'acoblament amb les amines **50a**–**e**.

Així, el tractament de l'àcid **67**·HCl cru amb 1 equiv. de cloroformiat d'etil i 2,1 equiv. de Et_3N en CH_2Cl_2 a 0 ^{o}C durant 30 min, seguit de reacció de l'anhídrid mixt format amb les aminoalquiltacrines **50a**–**e** a temperatura ambient durant 64 h va conduir als híbrids desitjats **65a**–**e** amb rendiments moderats, després de purificació dels crus de reacció per cromatografia en columna a través de gel de sílice (Esquema 4.7).

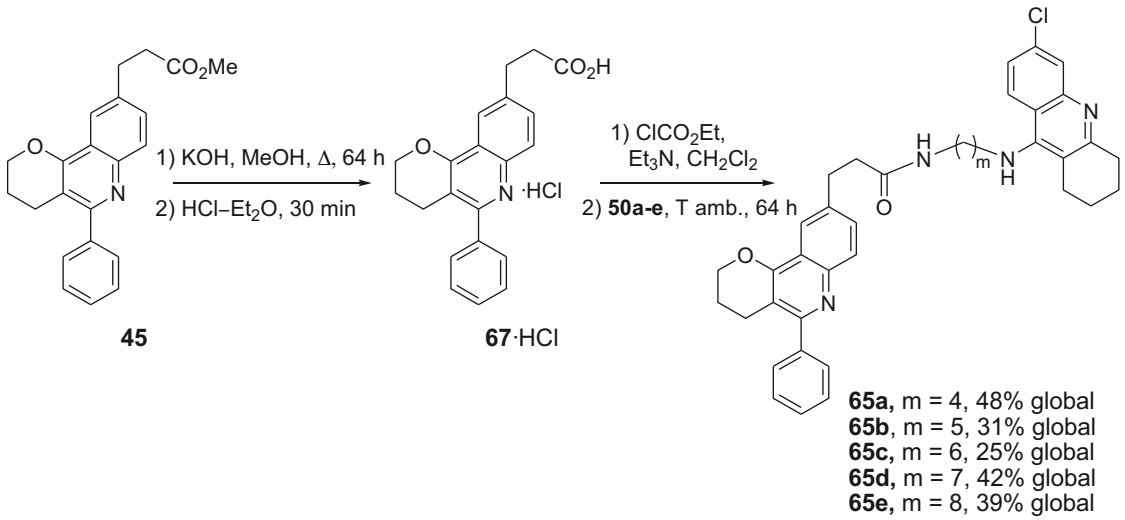

Esquema 4.7

Tots els nous híbrids sintetitzats en aquest capítol van ser transformats en els corresponents dihidroclorurs per tractament amb excés de dissolució metanòlica d'HCl, i en forma de dihidroclorurs van ser completament caracteritzats a través de les seves dades espectroscòpiques i anàlisi elemental.

4.3 Avaluació de la inhibició sobre diferents colinesterases dels nous híbrids

L'avaluació de l'activitat inhibidora de l'AChE i de la BChE dels nous híbrids **64c–g** i **65a–e** preparats en el present capítol va ser realitzada per mi mateix sota la supervisió del Dr. Albert Badia i la Dra. Victòria Clos, del Departament de Farmacologia, de Terapèutica i de Toxicologia de la Facultat de Medicina de la Universitat Autònoma de Barcelona. L'activitat inhibitòria de l'AChE dels nous híbrids, en forma de dihidroclorurs, es va determinar espectrofotomètricament mitjançant el mètode d'Ellman.[129]

4.3.1 El mètode d'Ellman

Nombrosos mètodes han estat descrits fins al moment per determinar l'activitat i la inhibició de les diferents colinesterases. La majoria d'ells mesuren les diferències de pH o bé usen mètodes basats en tècniques calorimètriques, espectrofotomètriques, fluoromètriques, radiomètriques o electroquímiques.[130] A més, noves tècniques basades en nous materials i

[129]Ellman, G.L.; Courtney, K.D.; Andres, B., Jr.; Featherstone, R.M. *Biochem. Pharmacol.* **1961**, *7*, 88. [130]Miao, Y.; He, N.; Zhu, J.-J. *Chem. Rev.* **2010**, *110,* 5216.

nanotecnologia han fet una important contribució en el desenvolupament dels diferents assaigs. No obstant, el tipus de mètode que encara avui preval és el basat en tècniques espectrofotomètriques.[130]

El mètode espectrofotomètric més usat és el mètode d'Ellman.[129] El principal avantatge d'aquest mètode és la simplicitat, la precisió i el relatiu baix cost que té.[131] A més, és fàcilment adaptable a analitzadors automàtics o lectors de plaques per a un ràpid processat de les mostres. Aquest assaig usa tioèsters com l'acetiltiocolina (ATCh) o la butiriltiocolina (BTCh) en lloc dels substrats naturals, acetilcolina o butirilcolina. L'AChE o la BChE hidrolitza l'ATCh o la BTCh produïnt tiocolina, la qual reacciona amb l'àcid 5,5'-ditiobis(2-nitrobenzoic) (DTNB) per donar un producte de color groc, l'àcid 5-mercapto-2-nitrobenzoic. La diferència en el color que produeix aquest producte es mesura en un espectrofotometre a 412 nm (Figura 4.4). La mesura espectrofotomètrica de l'absorbància es troba directament relacionada amb la quantitat d'ATCh degradada, i en conseqüència directament relacionada amb l'activitat enzimàtica mostrada per l'AChE en presència del fàrmac inhibidor.

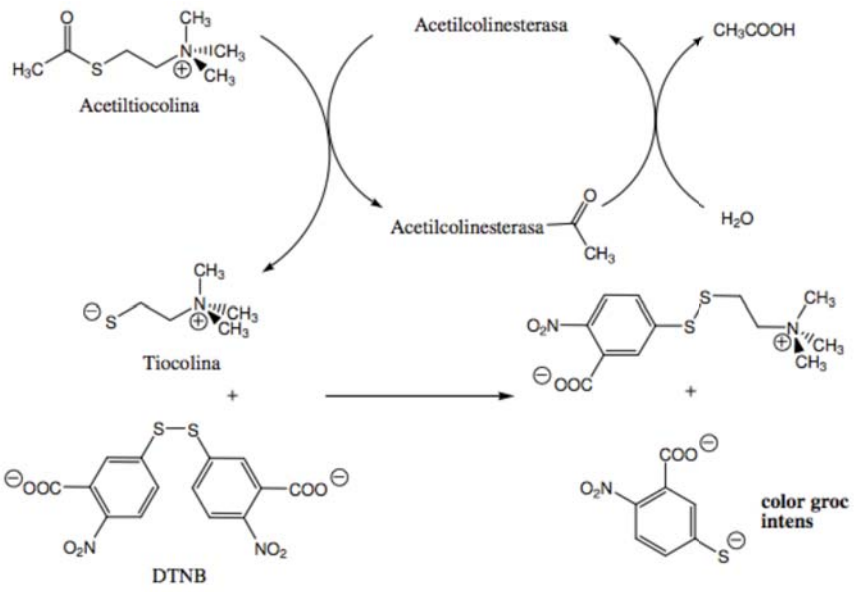

Figura 4.4

Així, experimentalment, es van afegir concentracions creixents de cada inhibidor a una dissolució que contenia DTNB (a una concentració 333 µM), i 0,025 *U.I.* d'enzim en tampó

[129]Ellman, G.L.; Courtney, K.D.; Andres, B., Jr.; Featherstone, R.M. *Biochem. Pharmacol.* **1961**, *7*, 88. [130]Miao, Y.; He, N.; Zhu, J.-J. *Chem. Rev.* **2010,** *110,* 5216. [131]Rackonczay, Z. *Neuromethods, Neurotransmitter Enzymes*; Humana Press: NJ, **1986;** p. 319**.**

fosfat 0,1 M de pH = 8, i ATCh com a substrat (fins a arribar a una concentració 0,53 mM o 0,27 mM per a AChE bovina o humana, respectivament, concentracions determinades en estudis cinètics previs). La reacció va tenir lloc en un volum final de 3 mL. Les corbes d'inhibició es van realitzar per duplicat incubant la dissolució descrita com a mínim amb 8 concentracions diferents de cadascun dels inhibidors durant 15 min a 25 ^{o}C. Un dels duplicats es va incubar en absència d'inhibidor per a permetre aconseguir el 100% d'activitat enzimàtica i actuar així com a control. La reacció es va aturar afegint-hi 100 μL de fisostigmina 1 mM, i el color obtingut es va mesurar a una longitud d'ona de 412 nm, mitjançant un espectrofotòmetre Multiskan Labsystems MS type 352. Així, es van realitzar com a mínim 3 experiments per a cada inhibidor. La determinació de l'activitat inhibidora de la BChE es va dur a terme de manera similar, utilitzant 0,035 *U.I.* d'enzim de sèrum humà i una dissolució 0,56 mM de butiriltiocolina com a substrat, arribant a un volum final d'1 mL.

Les dades obtingudes van permetre construir les corbes concentració–inhibició per als diferents híbrids mitjançant anàlisi de regressió no lineal utilitzant el programa GraphPad Prism4®, i a partir d'elles es va donar una estimació de la IC_{50}. Els resultats es van expressar com a la mitjana ± error estàndard de la mitjana.

En un treball posterior a l'avaluació dels híbrids d'estructura **64** i **65**, i amb la col·laboració de la Dra. Míriam Ratia del Departament de Farmacologia, de Terapèutica i de Toxicologia de la Facultat de Medicina de la Universitat Autònoma de Barcelona, es va optimitzar l'assaig que es duia a terme fins al moment. Així vam desenvolupar una metodologia per dur a terme aquesta mateixa avaluació en paral·lel i de manera miniaturitzada fent servir plaques de 96 pous, optimitzant les concentracions de l'enzim, el fàrmac i el substrat per portar-ho a un volum final de 300 μL per pou.[132] Això va suposar un estalvi tant econòmic com de temps de realització de l'assaig molt considerable, augmentant així l'eficiència del mètode.

4.3.2 Inhibició de l'AChE i la BChE

En la Taula 4.1 s'indiquen els valors d'IC_{50} enfront l'AChE bovina i humana i enfront la BChE humana dels nous híbrids preparats en la present Tesi Doctoral, així com els dels èsters tricíclics precursors i de la 6-clorotacrina i el propidi com a compostos de referència.

[132]Viayna, E.; Gómez, T.; Galdeano, C.; Ramírez, L.; Ratia, M.; Badia, A.; Clos, M. V.; Verdaguer, E.; Junyent, F.; Camins, A.; Pallàs, M.; Bartolini, M.; Mancini, F.; Andrisano, V.; Arce, M. P.; Rodríguez-Franco, M. I.; Bidon-Chanal, A.; Luque, F. J.; Camps, P.; Muñoz-Torrero, D. *ChemMedChem* **2010**, *5*, 1855.

Els compostos de la primera sèrie (**64**) són en general potents inhibidors de l'AChE bovina i humana, amb valors d'IC_{50} en el rang nanomolar baix. No hi ha importants diferències d'activitat en funció de la font de l'AChE. L'activitat inhibidora de l'AChE tampoc sembla dependre de forma important de la longitud del *linker*, si bé els compostos **64d** i **64e**, amb el *linker* de 7 i 8 grups metilens, respectivament, són lleugerament més potents que la resta de la sèrie. Una excepció seria el compost **64g**, amb un linker de 10 grups metilens que sí que és clarament menys potent inhibidor de l'bAChE que la resta. Tots els compostos d'aquesta sèrie són clarament més potents inhibidors de l'AChE que l'èster tricíclic precursor **44** i que el propidi, però són menys potents que l'inhibidor model de centre actiu 6-clorotacrina, amb l'única excepció del compost **64e**, que és pràcticament equipotent amb la 6-clorotacrina.

Taula 4.1 Activitat inhibitòria dels nous híbrids, la 6-clorotacrina, el propidi i els èsters tricíclics **44** i **45**.

Compost	**IC_{50} (nM)** **AChE bovina**	**IC_{50} (nM)** **AChE humana**	**IC_{50} (nM)** **BChE humana**
64c	20,4 ± 0,9	19,2 ± 1,5	1074 ± 178
64d	10,3 ± 0,4	18,3 ± 2,6	1931 ± 47
64e	10,4 ± 0,7	7,03 ± 0,3	331 ± 42
64f	24,0 ± 1,6	24,9 ± 1,5	1391 ± 31
64g	93,7 ± 3,2	50,0 ± 3,0	1622 ± 117
65a	48,1 ± 2,0	16,6 ± 1,0	586 ± 16
65b	23,9 ± 1,3	9,64 ± 1,4	290 ± 10
65c	30,8 ± 1,9	11,1 ± 0,1	218 ± 3
65d	29,9 ± 0,6	14,4 ± 1,4	234 ± 8
65e	34,1 ± 1,0	14,0 ± 1,2	1076 ± 78
44	> 10.000	> 10.000	> 10.000
45	> 10.000	no det.	no det.
propidi	6289 ± 377	32300 ± 2200	13200 ± 400
6-clorotacrina	5,7 ± 0,44	8,32 ± 0,7	916 ± 19

Per la seva part, els compostos de la segona sèrie (**65**), són lleugerament menys potents que els compostos de la primera sèrie d'igual longitud total de *linker* enfront l'bAChE, però són lleugerament més potents enfront l'hAChE. En aquest cas, sí que sembla haver una certa diferència de potència inhibitòria en funció de la font de l'enzim, sent els compostos **65a**–**e** 2–3 cops més potents enfront l'hAChE que enfront l'bAChE. Tal com s'ha indicat abans, en aquesta segona sèrie tampoc varia excessivament la potència inhibitòria de l'AChE bovina o humana amb la longitud del *linker*, sent els compostos **65b** i **65c**, equivalents quant a longitud del *linker* a **64d** i **64e** de la primera sèrie, els més potents. Els híbrids **65a**–**e** són clarament més

potents inhibidors de l'AChE que l'èster tricíclic precursor **45** i més potents inhibidors de l'bAChE que el propidi però són menys potents que el model 6-clorotacrina.

De forma anàloga al que passa amb el model de 6-clorotacrina, que presenta una inhibició 110 cops més potent enfront l'AChE que enfront la BChE humanes, els híbrids de les dues sèries són selectius enfront l'hAChE, presentant selectivitats de 47–106 cops en la primera sèrie i de 16–77 cops en la segona. Els híbrids de la primera sèrie presenten en general una baixa potència inhibitòria de la BChE, amb valors d'IC_{50} en el rang micromolar, excepte en el cas de l'híbrid **64e**, l'IC_{50} del qual està en el rang nanomolar. Els híbrids de la segona sèrie (**65**) són inhibidors de la BChE humana 2–7 cops més potents que els corresponents compostos de la primera sèrie amb una longitud total de *linker* equivalent, presentant quasi bé tots valors nanomolars d'IC_{50}.

L'elevada potència inhibitòria enfront l'AChE d'aquests híbrids, en relació sobretot als èsters tricíclics precursors, tot i que no tant en relació amb el model 6-clorotacrina, és indicativa del seu caràcter d'inhibidors de lloc d'unió dual, què també ha estat demostrat amb la determinació del seu efecte inhibidor de l'agregació del pèptid βA induïda per AChE *in vitro*, dut a terme per la Dra. Vincenza Andrisano i la Dra. Manuela Bartolini del Dipartimento di Scienze Farmaceutiche de la Universitat de Bologna (Itàlia) i pels estudis de modelatge molecular emmarcats en la Tesi Doctoral de l'Òscar Huertas del grup de treball del Dr. F. Javier Luque.

4.5 Avaluació de l'estabilitat del grup amida de l'híbrid 65a

La investigació de l'estabilitat dels compostos sintetitzats representa un important aspecte a l'hora d'avaluar-los com a possibles fàrmacs. Hi ha diferents condicions tant ambientals, calor i llum, com químiques, que poden acabar produint reaccions d'hidròlisi o d'oxidació.[133] La hidròlisi és una de les reaccions més comunes de degradació. Així, per tal d'avaluar la possible hidròlisi del grup amida característic dels híbrids **64** i **65** a pH fisiològic ens vam plantejar dur a terme un estudi d'estabilitat de l'híbrid **65a** a pH 7,4 durant 4 dies a 37 ^{o}C seguint una metodologia ja descrita[134] on es mesurava la descomposició del compost estudiat amb l'ajut d'un HPLC a diferents temps. Aquesta anàlisi va concluir que en cap dels temps estudiats es va observar degradació de l'amida (Figura 4.5).

[133] *Stability testing of New Drugs Substances and Products* (**2002**) Proceedings of the International Conference on Harmonization (ICH), IFPMA, Geneva, Switzerland. [134] Álvarez-Lueje, A.; Valenzuela, C.; Squella, J.A.; Nuñez-Vergara, J.L. *J. AOAC Int.* **2005**, *88*, 1631

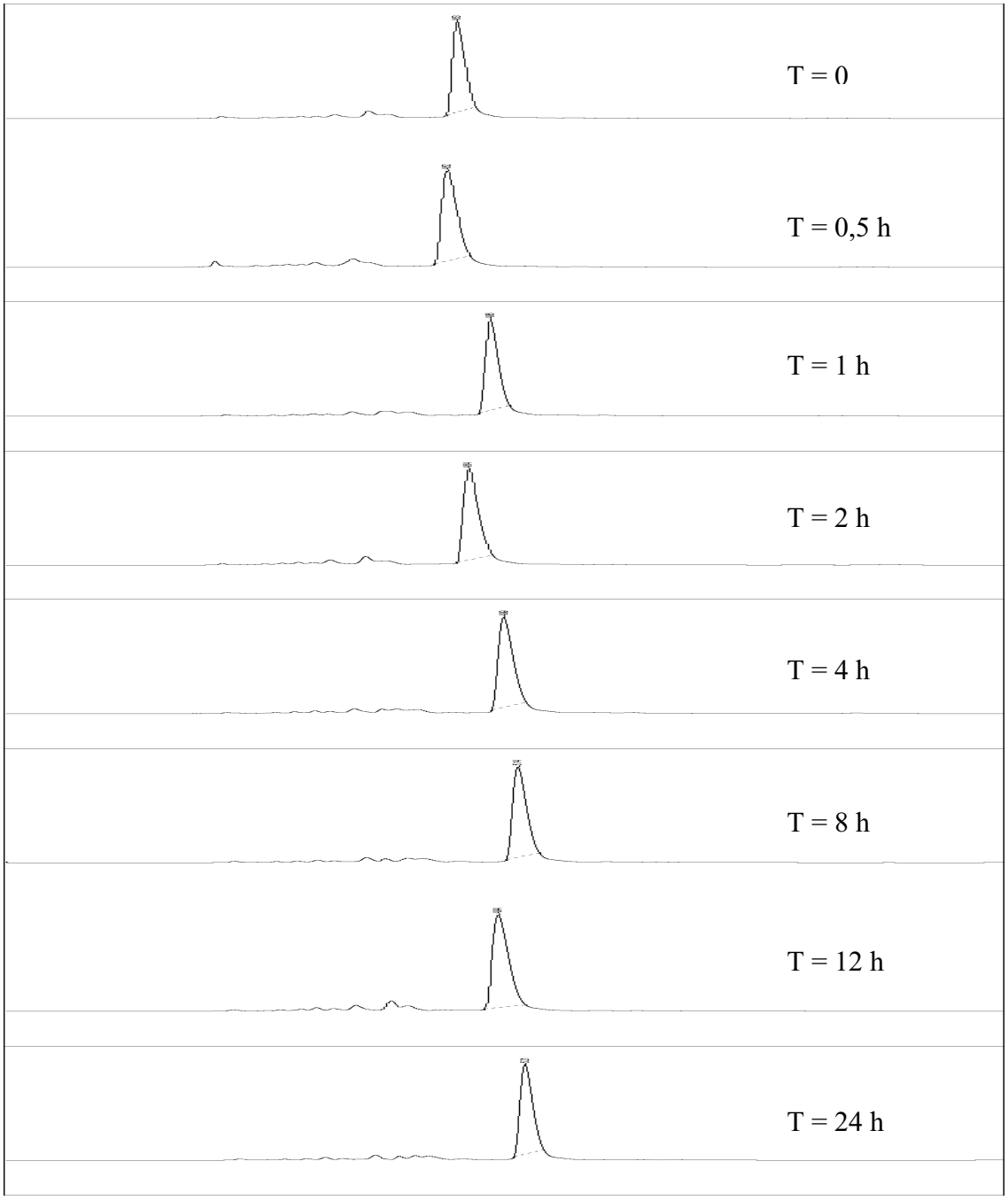

Figura 4.5 Evolució dels cromatogrames d'HPLC de l'híbrid durant les primeres 24 hores d'assaigs

4.5.1 Metodologia

L'híbrid **65a** es va dissoldre per duplicat en una dissolució 1:1 d'acetonitril i tampó fosfat Sörensen a pH 7.4 a una concentració de 1 mg/mL. Aquestes dissolucions es van dividir en 10 aliqüotes de 100 μL i es van incubar a 37 ^{o}C. L'estabilitat del compost va ser mesurada per duplicat a diferents temps (t = 0, 0,5, 1, 2, 4, 8, 12, 24, 48 i 96 hores) injectant 5 μL de la corresponent dissolució incubada en un cromatògraf d'HPLC (cromatògraf Perkin Elmer series

200 equipat amb un detector de longitud d'ona variable, usant una columna Kromasil® C-18 [5 μm, 25x0,46 cm] i amb una fase mòbil 35:65:0.2 acetonitril/aigua/àcid trifluoroacètic, flux 1 $mL \cdot min^{-1}$, λ = 254 nM) i comparant les dades cromatogràfiques a diferents temps de l'híbrid **65a** a t = 0 (t_r = 5,05 min) amb una mostra del producte de la hidròlisi pur (t_r = 2.33 min).

Journal of Medicinal Chemistry Article

J. Med. Chem. **2009,** *52,* 5365–5379 **5365**
DOI: 10.1021/jm900859q

Pyrano[3,2-*c*]quinoline−6-Chlorotacrine Hybrids as a Novel Family of Acetylcholinesterase- and β-Amyloid-Directed Anti-Alzheimer Compounds

Pelayo Camps,[†] Xavier Formosa,[†] Carles Galdeano,[†] Diego Muñoz-Torrero,*[,†] Lorena Ramírez,[†] Elena Gómez,[‡] Nicolás Isambert,[‡] Rodolfo Lavilla,[‡,⊥] Albert Badia,[§] M. Victòria Clos,[§] Manuela Bartolini,[#] Francesca Mancini,[#] Vincenza Andrisano,[#] Mariana P. Arce,[∞] M. Isabel Rodríguez-Franco,[∞] Óscar Huertas,[∥] Thomai Dafni,[∥] and F. Javier Luque[∥]

[†]*Laboratori de Química Farmacèutica* (*Unitat Associada al CSIC*), *Facultat de Farmàcia, and Institut de Biomedicina* (*IBUB*), *Universitat de Barcelona, Av. Diagonal 643, E-08028, Barcelona, Spain,* [‡]*Institute for Research in Biomedicine, Barcelona Science Park, Baldiri Reixac 10-12, E-08028, Barcelona, Spain,* [⊥]*Laboratori de Química Orgànica, Facultat de Farmàcia, Universitat de Barcelona, Av. Joan XXIII, s/n, E-08028, Barcelona, Spain,* [§]*Departament de Farmacologia, Terapèutica i Toxicologia, Institut de Neurociències, Universitat Autònoma de Barcelona, E-08193, Bellaterra, Barcelona, Spain,* [#]*Department of Pharmaceutical Sciences, Alma Mater Studiorum, Bologna University, Via Belmeloro 6, I-40126, Bologna, Italy,* [∞]*Instituto de Química Médica* (*CSIC*), *Juan de la Cierva, 3, E-28006, Madrid, Spain, and* [∥]*Departament de Fisicoquímica, Facultat de Farmàcia, and Institut de Biomedicina* (*IBUB*), *Universitat de Barcelona, Av. Diagonal 643, E-08028, Barcelona, Spain*

Received March 16, 2009

Two isomeric series of dual binding site acetylcholinesterase (AChE) inhibitors have been designed, synthesized, and tested for their ability to inhibit AChE, butyrylcholinesterase, AChE-induced and self-induced β-amyloid (Aβ) aggregation, and β-secretase (BACE-1) and to cross blood−brain barrier. The new hybrids consist of a unit of 6-chlorotacrine and a multicomponent reaction-derived pyrano[3,2-*c*]-quinoline scaffold as the active-site and peripheral-site interacting moieties, respectively, connected through an oligomethylene linker containing an amido group at variable position. Indeed, molecular modeling and kinetic studies have confirmed the dual site binding of these compounds. The new hybrids, and particularly **27**, retain the potent and selective human AChE inhibitory activity of the parent 6-chlorotacrine while exhibiting a significant in vitro inhibitory activity toward the AChE-induced and self-induced Aβ aggregation and toward BACE-1, as well as ability to enter the central nervous system, which makes them promising anti-Alzheimer lead compounds.

Introduction

In the past decade, the design of novel classes of inhibitors of the enzyme acetylcholinesterase (AChE[a]) as therapeutic interventions for Alzheimer's disease (AD) has been mostly driven by the pivotal finding that AChE can bind the β-amyloid peptide (Aβ), thereby promoting Aβ aggregation as an early event in the neurodegenerative cascade of AD.[1,2] The Aβ proaggregating effect of AChE results in cognitive impairment in doubly transgenic mice expressing human amyloid precursor protein (APP) and human AChE.[3,4] Blockade of the peripheral site of AChE, the Aβ recognition zone within the enzyme,[5] was therefore expected to affect the AChE-induced Aβ aggregation and could be a potential strategy to modulate the progression of AD.

On the basis of these premises, novel classes of AChE inhibitors (AChEIs) targeting the peripheral site have emerged as promising disease-modifying anti-Alzheimer drug candidates.[6] Of particular interest are those AChEIs able to simultaneously bind to both peripheral and catalytic sites, which are separated by about 14 Å, as they are located at the mouth and at the bottom of the gorge leading to the active site.[7] Apart from the Aβ antiaggregating effects arising from blockade of the peripheral site, dual binding site AChEIs are usually endowed with a potent AChE inhibitory activity because of the increased number of drug−target interactions, thus overcoming the low activity of selective peripheral site AChEIs.[8−18] Indeed, in vitro inhibitory activities of AChE and AChE-induced Aβ aggregation have been reported for different families of dual binding site AChEIs,[19−34] which in cases such as memoquin[26,27] and NP-61[35] have been shown to reduce brain amyloid burden and increase cognition in animal models of AD. Some dual binding site AChEIs such as memoquin[26,27] or bis(7)-tacrine[9,13,36,37] are undergoing preclinical evaluation, while NP-61 entered phase I clinical trials for AD in the U.K. in April 2007.[38] Prompted by these results and the tremendous potential of dual binding site AChEIs to impact both the course of AD and its symptomatology, the design and synthesis of novel families of dual binding site AChEIs have been actively pursued in the past years.[39−52]

The design of dual binding site AChEIs is carried out by linking through a tether of suitable length an active-site interacting unit, usually derived from a known active site AChEI, with a peripheral-site interacting unit suited to interact with Trp286 (human AChE (hAChE) numbering), the

*To whom correspondence should be addressed. Phone: +34 + 934024533. Fax: +34 + 934035941. E-mail: dmunoztorrero@ub.edu.

[a] Abbreviations: Aβ, β-amyloid peptide; AChE, acetylcholinesterase; AChEI, acetylcholinesterase inhibitor; AD, Alzheimer's disease; APP, amyloid precursor protein; bAChE, bovine acetylcholinesterase; BACE-1, β-secretase; BBB, blood−brain barrier; BChE, butyrylcholinesterase; CNS, central nervous system; DDQ, 2,3-dichloro-5,6-dicyano-1,4-benzoquinone; DTNB, 5,5′-dithiobis(2-nitrobenzoic) acid; hAChE, human acetylcholinesterase; hBChE, human butyrylcholinesterase; HFIP, 1,1,1,3,3,3-hexafluoro-2-propanol; PAMPA, parallel artificial membrane permeation assay; PBS, phosphate buffered saline; PDB, Protein Data Bank; PTFE, polytetrafluoroethylene; *Tc*AChE, *Torpedo californica* acetylcholinesterase.

Published on Web 08/07/2009

characteristic residue of the peripheral site. With a few exceptions in which a peripheral-site interacting unit containing an aliphatic amine, protonated at physiological pH, or a quaternary ammonium group establishes cation−π interactions with Trp286, in most cases the peripheral-site interacting unit contains aromatic moieties able to establish $\pi-\pi$ stacking interactions with Trp286, in some cases reinforced by concomitant cation−π interactions due to the presence of protonatable or quaternary nitrogen atoms in the aromatic system. The prototype of peripheral site AChEI is propidium (**1**, Chart 1), which binds the AChE peripheral site in two orientations related by a flip of 180° around the phenanthridinium pseudosymmetry axis.[53,54] The driving force for the binding of **1** to the peripheral site is the $\pi-\pi$ stacking, reinforced by cation−π interactions, between the phenanthridinium moiety and Trp286, which is supplemented by a hydrogen bond between one of the aromatic amino groups and His287.

Some of us recently reported the synthesis of the multicomponent reaction-derived pyrano[3,2-*c*]quinoline scaffold **2** (Chart 1).[55] We thought that a 5-phenyl-substituted derivative thereof would resemble the 6-phenylphenanthridinium moiety of propidium and could serve as the peripheral-site interacting unit of a novel family of dual binding site AChEIs. Because the nitrogen atom of this tricyclic moiety is not expected to be protonated at physiological pH (Table S1, Supporting Information), this aromatic system should establish $\pi-\pi$ stacking with Trp286. Noteworthy, the neutral character of this moiety could result in a better penetration into the central nervous system (CNS).

Herein, we describe the synthesis, pharmacological evaluation, and molecular modeling of a novel family of potent dual binding site AChEIs that combine a 5-phenylpyrano[3,2-*c*]quinoline moiety with 6-chlorotacrine, **3** (Chart 1), a potent AChEI already used in other dual binding site AChEIs,[22,23,31,32,39,44,52,56,57] through an amido-containing oligomethylene linker. The pharmacological evaluation of these novel compounds includes AChE and butyrylcholinesterase (BChE) inhibition, as well as inhibition of the AChE- and self-induced Aβ aggregation and inhibition of β-secretase (BACE-1), which altogether comprises an interesting set of effects shared by some dual binding site AChEIs. To prove the starting hypothesis on a good blood−brain barrier (BBB) permeability, the brain penetration of the novel hybrids has been assessed using an artificial membrane assay.

Chemistry

The structures of the novel 5-phenylpyrano[3,2-*c*]-quinoline−6-chlorotacrine hybrids **18**−**27** are shown in Scheme 2. Alignment of the 5-phenylpyrano[3,2-*c*]quinoline system with the phenanthridinium moiety of propidium in its complex with mouse AChE[53] (Figure S1, Supporting Information) revealed that if the novel hybrids were to interact with AChE by placing the tricyclic system in a way similar to that of the tricyclic system of propidium, position 9 of the pyrano[3,2-*c*]quinoline system would be suitable for attachment of the linker, which from this point could snake down the active site gorge. An ester group at position 9 was chosen as a suitable functionalization to allow attachment of the linker by reaction with an appropriate aminoalkyltacrine. Thus, tricyclic ester **11** (Scheme 1) was designed as the precursor of the peripheral-site interacting unit of the novel hybrids **18**−**22** (Scheme 2).

Chart 1. Structures of Propidium, Scaffold **2**, and 6-Chlorotacrine

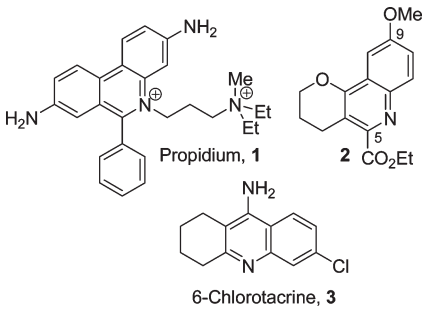

Scheme 1. Synthesis of Tricyclic Esters **11** and **12** and Carboxylic Acids **13** and **14**

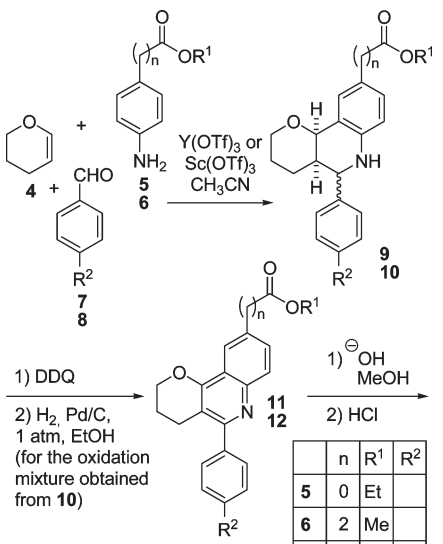

	n	R^1	R^2
5	0	Et	
6	2	Me	
7			Cl
8			H
9	0	Et	Cl
10	2	Me	H
11	0	Et	Cl
12	2	Me	H
13	0		Cl
14	2		H

Recently, Martínez and co-workers developed a novel series of indole−tacrine hybrids as dual binding site AChEIs, which contained an amido group within the linker either directly bound to the indole system (i.e., the peripheral-site interacting unit) or separated by one to three atoms (methylene groups in most cases), and reported important differences in the AChE inhibitory activity upon shift of the amido group within the tether chain while keeping the same total length of the linker.[23] Specifically, separation of the amide from the indole ring by two methylene groups increased up to 2300-fold the AChE inhibitory potency relative to the indole directly bound counterpart. In view of these results, we designed the tricyclic ester **12** (Scheme 1) as the precursor of the parallel series of hybrids **23**−**27** (Scheme 2), containing linkers of the same total length as **18**−**22** but with the amido group shifted two positions within the tether. Regarding the length of the linker, oligomethylene chains of 6−10 and 4−8 members for hybrids **18**−**22** and **23**−**27**, respectively, were considered suitable to provide the dual site binding.

Scheme 2. Synthesis of Hybrids **18**−**27**

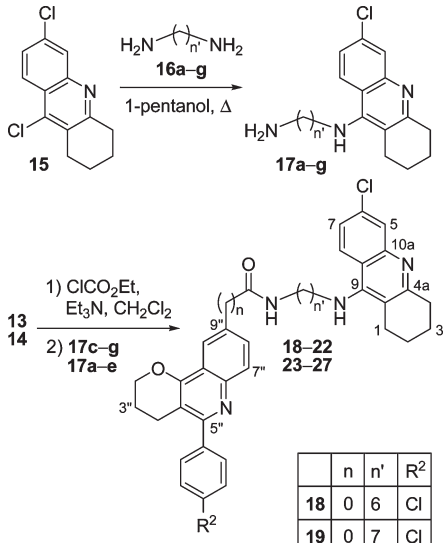

16, 17	n'
a	4
b	5
c	6
d	7
e	8
f	9
g	10

	n	n'	R^2
18	0	6	Cl
19	0	7	Cl
20	0	8	Cl
21	0	9	Cl
22	0	10	Cl
23	2	4	H
24	2	5	H
25	2	6	H
26	2	7	H
27	2	8	H

The synthesis of hybrids **18**−**27** was envisaged through the coupling of tricyclic esters **11** and **12** with readily available aminoalkyltacrines **17**.[23] A straightforward access to **11** and **12** was carried out through a Povarov multicomponent reaction.[58] Thus, reaction of 3,4-dihydro-2*H*-pyran, **4**, with ethyl *p*-aminobenzoate, **5**, and *p*-chlorobenzaldehyde, **7**, under $Y(OTf)_3$ catalysis in CH_3CN afforded in 76% yield a 1.3:1 diastereomeric mixture of pyranotetrahydroquinolines **9**, whose 2,3-dichloro-5,6-dicyano-1,4-benzoquinone (DDQ) oxidation[55] yielded the desired tricyclic ester **11** in 75% yield. The Povarov reaction of methyl 3-(4-aminophenyl)propanoate **6**[59] with **4** and benzaldehyde **8** under $Sc(OTf)_3$ catalysis, followed by DDQ oxidation of the diastereomeric mixture of pyranotetrahydroquinolines **10** and catalytic hydrogenation of the unseparable mixture of the desired ester **12** and its cinnamate derivative, formed by the competitive oxidation of the ethylene bridge, afforded in 82% overall yield the tricyclic ester **12** (Scheme 1). This latter compound lacked the chlorine atom at the phenyl substituent, present in **11**. However, this chlorine atom, easily removable in the catalytic hydrogenation conditions, was not expected to play a major role in the interaction of this moiety with the AChE peripheral site.

Aminoalkyltacrines **17a**−**g** were synthesized in 35−78% yield following a procedure[23,60,61] that involves amination of dichloroacridine **15**[62] with commercially available α,ω-diamines **16a**−**g** in refluxing 1-pentanol (Scheme 2). In this reaction, significant amounts of dimers of 6-chlorotacrine, **28a**−**g**,[56,62,63] were formed despite the fact that an excess of diamines (4 equiv) was used.

Hydrolysis of esters **11** and **12** (Scheme 1), followed by treatment of the corresponding carboxylic acids **13** and **14** with 1 equiv of ethyl chloroformate and 2.2 equiv of Et_3N in CH_2Cl_2, and reaction of the resulting mixed anhydrides with 1 equiv of aminoalkyltacrines **17c**−**g** and **17a**−**e**, respectively, afforded hybrids **18**−**22** and **23**−**27** in low to moderate yields (19−37% and 25−48% yield, respectively). The novel hybrids **18**−**27** were fully characterized as dihydrochlorides through their spectroscopic data, HRMS, and elemental analyses. Not unexpectedly, in a study to assess the potential chemical instability at physiological pH of the new hybrids due to the presence of a hydrolyzable amido group, hybrid **23** did not undergo any noticeable decomposition in 1:1 acetonitrile/Sorensen phosphate buffer at pH 7.4 up to 4 days at 37 °C (see Supporting Information).

Pharmacology and Molecular Modeling

Cholinesterase Inhibition. AChE Inhibition. The AChE inhibitory activity of hybrids **18**−**27** was assayed by the method of Ellman et al.[64] on AChE from bovine (bAChE) and human (hAChE) erythrocytes (Table 1). The hybrids of the first series (**18**−**22**) are potent inhibitors of both bAChE and hAChE, with IC_{50} values in the low nanomolar range in most cases. The most potent hAChE inhibitor was **20**, and shortening or lengthening of the linker led to a 3- to 7-fold decrease of inhibitory activity. The hybrids of the second series (**23**−**27**) are also potent inhibitors of both enzymes. In contrast with the first series, hybrids **23**−**27** turned out to be 2- to 3-fold more potent toward the human enzyme. Also, unlike the first series, no significant dependency on the length of the linker was found for the hAChE inhibitory activity of **23**−**27**. Hybrids **24** and **25** were the most potent hAChE inhibitors of the second series, they being roughly equipotent to compound **20**, in which the total length of the linker is equivalent to that of **25**. Although dual site binding to AChE is expected to increase the inhibitory potency relative to the monomeric parent compounds from which they were designed, this assumption is not always fulfilled.[65,66] Indeed, the hAChE inhibitory activity of hybrids **20**, **24**, and **25** is comparable with that of the parent 6-chlorotacrine and is clearly higher than the activity measured for propidium and the tricyclic ester precursors **11** and **12**.

Molecular Modeling Studies. To gain insight into the molecular determinants that modulate the hAChE inhibitory activity of the novel hybrids, the binding mode of compounds **20**, **25**, and **27** was investigated by means of docking computations.

The conformation of the active site gorge appears to be highly conserved in different X-ray crystallographic structures. In particular, the observed structural changes at the catalytic binding site are small except for those of Tyr337 (in hAChE; Phe330 in *Torpedo californica* AChE, *Tc*AChE).[67,68] Accordingly, the binding mode of the 6-chlorotacrine unit of these hybrids can be inferred from the X-ray crystallographic structures of *Tc*AChE complexes with tacrine[7] and its structurally related analogue huprine X,[69] where the 9-aminotetrahydroacridine unit is stacked against Trp86 and Tyr337 (Trp84 and Phe330 in *Tc*AChE), the protonated pyridine nitrogen atom is hydrogen-bonded to His447 (His440 in *Tc*AChE), and the chlorine atom fits a hydrophobic pocket formed by Trp439, Met443, and Pro446 (Trp432, Met436, and Ile439 in *Tc*AChE). In fact, a common pose is found for the tacrine moiety in the X-ray structures of a variety of dual binding site inhibitors, including bis(5)-tacrine and bis(7)-tacrine,[70] tacrine(8)-4-aminoquinoline,[70] NF595,[71] tacrine(10)-hupyridone,[72] and TZ2PA6.[73] The structural features of the binding of the pyrano[3,2-*c*]-quinoline moiety of the hybrids at the peripheral site are

Table 1. AChE and BChE Inhibitory Activities of the Hydrochlorides of 6-Chlorotacrine and Tricyclic Esters **11** and **12**, Propidium Iodide, and the Dihydrochlorides of the Pyrano[3,2-*c*]quinoline−6-Chlorotacrine Hybrids[a]

	IC_{50} (nM)			
compd	bAChE	hAChE	hBChE	AChE selectivity[b]
18·2HCl	20.4 ± 0.9	19.2 ± 1.5	1074 ± 178	56
19·2HCl	10.3 ± 0.4	18.3 ± 2.6	1931 ± 47	106
20·2HCl	10.4 ± 0.7	7.03 ± 0.3	331 ± 42	47
21·2HCl	24.0 ± 1.6	24.9 ± 1.5	1391 ± 31	56
22·2HCl	93.7 ± 3.2	50.0 ± 3.0	1622 ± 117	32
23·2HCl	48.1 ± 2.0	16.6 ± 1.0	586 ± 16	35
24·2HCl	23.9 ± 1.3	9.64 ± 1.4	290 ± 9.8	30
25·2HCl	30.8 ± 1.9	11.1 ± 0.1	218 ± 3.2	20
26·2HCl	29.9 ± 0.6	14.4 ± 1.4	234 ± 7.8	16
27·2HCl	34.1 ± 1.0	14.0 ± 1.2	1076 ± 78	77
11·HCl	> 10000	> 10000	> 10000	nd[c]
12·HCl	> 10000	nd[c]	nd[c]	nd[c]
propidium iodide	6289 ± 377	32300 ± 2200[d]	13200 ± 400[d]	0.4
6-chlorotacrine·HCl	5.73 ± 0.4	8.32 ± 0.7	916 ± 19	110

[a] Values are expressed as the mean ± standard error of the mean of at least four experiments. IC_{50} inhibitory concentration (nM) of AChE (from bovine or human erythrocytes) or BChE (from human serum) activity. [b] IC_{50}(hBChE)/IC_{50}(hAChE). [c] Not determined. [d] Data from ref 21.

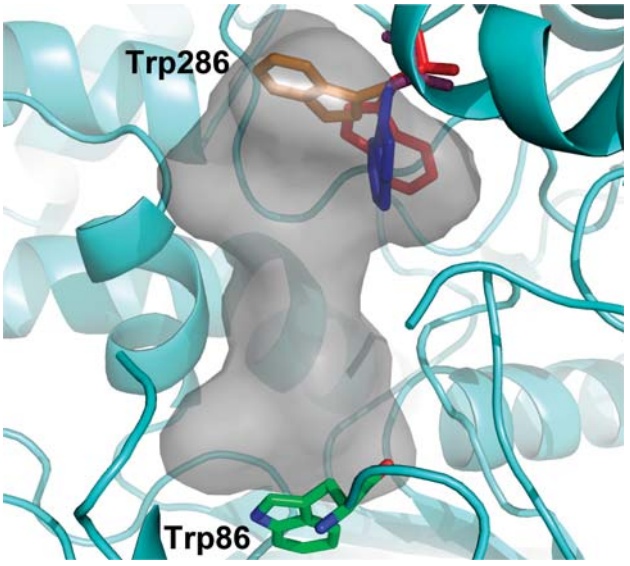

Figure 1. Representation of the three orientations adopted by Trp286 in targets A (blue), B (red), and C (orange) of hAChE (χ_1 and χ_2 amount to −60° and −80° for A, to −120° and +50° for B, and to −160° and −120° for C; see text). The backbone of hAChE is shown in ribbon (light-blue). Trp86 at the catalytic site is colored by atom, and the gorge leading from the peripheral site to the catalytic pocket is shown in gray.

more delicate because of the conformational flexibility of Trp286 (Trp279 in *Tc*AChE), as noted in the X-ray structures available for several peripheral site ligands,[53] including propidium, and dual binding site inhibitors[70−73] as well as from molecular dynamics simulations.[23,31,74] In fact, three main arrangements of the indole ring of Trp286 can be identified upon inspection of the X-ray structures (Table S2, Supporting Information). The first orientation is characterized by dihedral angles χ_1 (N−C_α−C_β−C_γ) and χ_2 (C_α−C_β−C_γ−$C_{\delta 2}$) close to −60°and −80°, respectively, as found in the apo form of the enzyme,[53,75] and in complexes with catalytic (tacrine,[7] huprine X,[69] and (−)-huperzine A[76]) and peripheral (propidium, decidium, and gallamine)[53] binding site inhibitors. Moreover, this arrangement is found in complexes with dual binding site inhibitors (decamethonium,[7] donepezil,[77] bis(5)-tacrine,[70] tacrine(10)-hupyridone,[72] and anti-TZ2PA6[73]) and in the complex with fasciculin.[78] Dihedral angles close to −120° (χ_1) and +50° (χ_2) are found in complexes with bis(7)-tacrine,[70] tacrine(8)-4-aminoquinoline,[70] and NF595.[71] At this point, it is worth stressing how the different lengths of the tether in bis(5)-tacrine and bis(7)-tacrine lead to a distinct arrangement of the indole ring of Trp286.[70] Finally, an alternative orientation defined by dihedral angles close to −160° (χ_1) and −120° (χ_2) is found in the complex with *syn*-TZ2PA6.[73] Overall, this analysis stresses the conformational plasticity of Trp286 and its capability to adopt different orientations depending on the chemical features of the ligand.

On the basis of the preceding discussion, the binding modes of **20**, **25**, and **27** were investigated using three models of hAChE, in which Trp286 was imposed to adopt each one of the three above-mentioned conformational orientations (denoted as A, B, and C; Figure 1). Moreover, suitable restraints were introduced to fix the orientation of the 6-chlorotacrine moiety, thus enhancing the conformational sampling of the ligand at the peripheral binding site and along the gorge. Noteworthy, this restrained docking protocol was able to predict the X-ray binding mode of bis(5)-tacrine, bis(7)-tacrine, tacrine(8)-4-aminoquinoline, (*R*)- and (*S*)-tacrine(10)-hupyridone, and *syn*- and *anti*-TZ2PA6 within the first 10 poses and with root-mean square deviations less than 1.8 Å (Table S3, Supporting Information).

Following previous studies in the literature,[79−81] the relative stabilities of the first 50 poses obtained in the docking of every ligand on each one of the targets were reranked using MM−PBSA calculations (Table S4, Supporting Information). In all cases the most favorable binding is found for target C, as this binding mode is favored by 4.3−7.6 and 2.4−9.9 kcal/mol when dielectric permittivities of 2 and 4 are considered for the interior of the ligand−hAChE complex, respectively, relative to the second most stable complex. Moreover, the results also show that there are small differences in the affinities estimated for the binding of hybrids **20**, **25**, and **27** to target C. Keeping in mind the range of uncertainty expected for MM−PBSA calculations,[80,82] this finding is in agreement with the similar inhibitory potencies measured for these compounds (IC_{50} values ranging from 7 to 14 nM, Table 1).

Inspection of the best poses found for hybrid **20** bound to target C shows that the 6-chlorotacrine moiety roughly matches the tacrine unit of *syn*-TZ2PA6. The slight

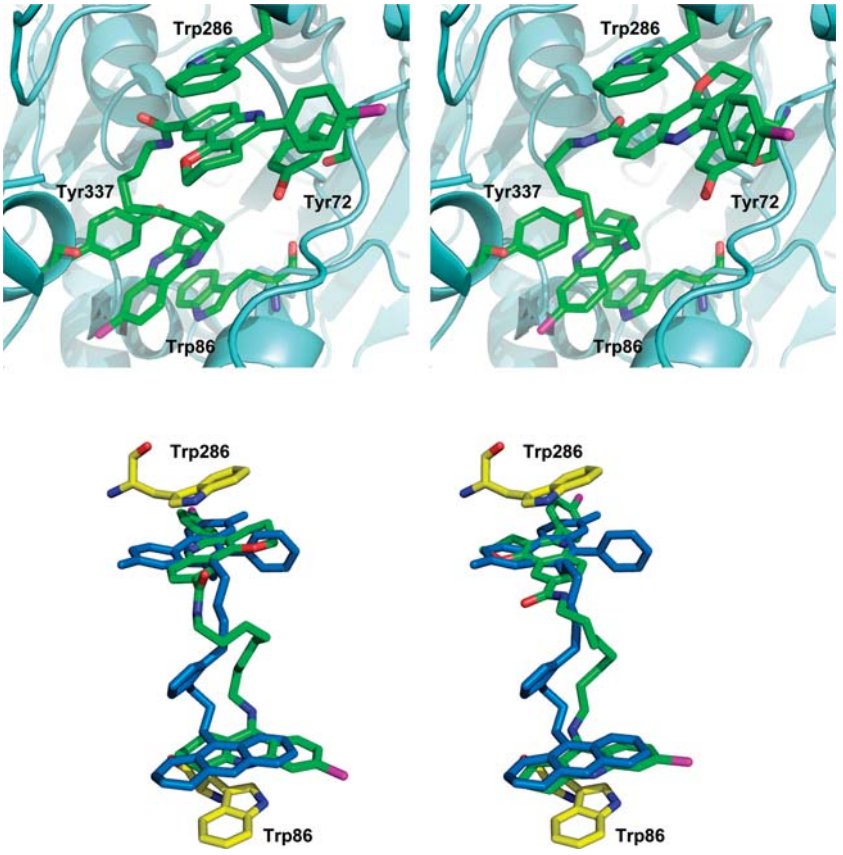

Figure 2. (Top) Representation of the most favorable binding mode of hybrid **20** (colored by atom) determined from MM-PBSA computations performed with internal permittivities of 2 (left) and 4 (right). Relevant residues at the catalytic (Trp86 and Tyr337) and peripheral (Trp286 and Tyr72) binding sites are colored by atom. (Bottom) Representation of the poses predicted for hybrid **20** from MM-PBSA computations and the orientation of *syn*-TZ2PA6 (blue) in the X-ray crystallographic structure of mouse AChE (PDB entry 1Q83).

displacement observed for the tetrahydroacridine systems can be ascribed to the positioning of the chlorine atom in **20** in the hydrophobic pocket formed by Trp439, Met443, and Pro446 (see above) and particularly to the active role played by the triazole ring in the tether of *syn*-TZ2PA6 in mediating interactions with specific residues along the gorge (see Figure 2),[73] which also explain the different arrangement of the linker observed for *syn*-TZ2PA6 and for the two poses of **20**. At the peripheral binding site the pyrano[3,2-*c*]-quinoline moiety adopts two main orientations (Figure 2), which can be roughly interconverted by a 180° rotation through the C5−C9 axis. At first sight, this finding might be surprising, keeping in mind the well-defined arrangement observed for the phenanthridinium moiety of *syn*-TZ2PA6 in the X-ray structure,[73] but this can be ascribed to additional interactions involving the buried phenanthridinium amino group that are absent in the case of the pyrano[3,2-*c*]-quinoline moiety. Accordingly, the stacking of the pyrano-[3,2-*c*]quinoline moiety might involve distinct arrangements provided that there exists a significant overlap with the aromatic rings of Trp286 and Tyr72 and that steric clashes with neighboring residues are avoided. Similar overall arrangements are found for hybrids **25** and **27** (see Figures S2 and S3, Supporting Information).

To further explore the proposed binding mode, a series of 10 ns molecular dynamics simulations were run for compounds **20** and **25**, which were chosen as representative members of the two series of dual binding site inhibitors. The simulations were run for each of the two potential binding modes shown in Figure 2 for compound **20** (and Figures S2 and S3 for **25**). Only the trajectories run for the ligand with the pyran ring oriented toward the bulk solvent yielded stable trajectories, as noted by inspection of the time dependence of both the potential energy and the root-mean-square deviation of selected atoms in the protein backbone, the binding site, and the ligand in the ligand−receptor complexes (Figure S4, Supporting Information). There is a large resemblance between the snapshots collected at the end of the trajectories and those used as starting structures (Figure 3). The main difference lies in the orientation of the tether, which adopts a more extended conformation at the end of the trajectories. Nevertheless, the tacrine unit remains stacked between the aromatic rings of Trp86 and Tyr337, and the pyrano[3,2-*c*]quinoline unit retains the $\pi-\pi$ stacking with Trp286 and Tyr72. Finally, a well-defined interaction pattern between the amido functionality and residues lining the entrance of the gorge is not observed. This finding is in contrast with the binding mode reported from modeling studies for a series of structurally related indole−tacrine hybrids containing an amido group within the linker,[23] where this group was proposed to participate in hydrogen-bond interactions with several residues in the gorge. These distinct features could presumably stem from the different arrangement of the pyrano[3,2-*c*]quinoline and indole units at the peripheral binding site.

Kinetic Analysis of AChE Inhibition. The mechanism of AChE inhibition was investigated in vitro using compound **20**, the most potent inhibitor of the two series. Graphical

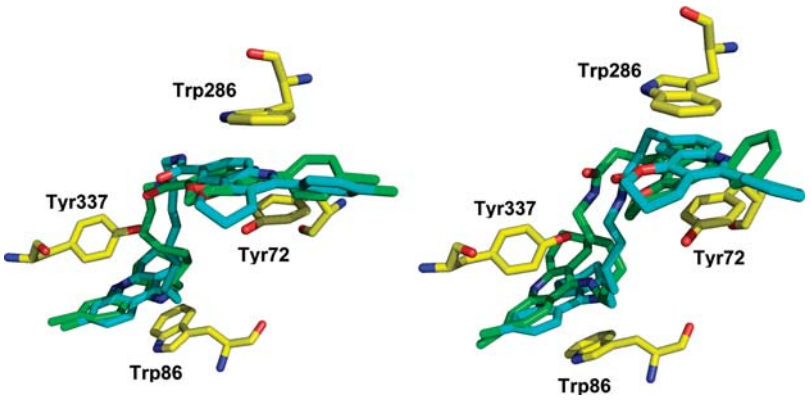

Figure 3. Representation of the structures (blue) collected at the end of the 10 ns molecular dynamics simulations of compounds **20** (left) and **25** (right) bound to AChE showing the stacking of the tacrine moiety with Trp86 and Tyr337 and of the phenylpyrano[3,2-*c*]quinoline unit with Trp286 and Tyr72 (yellow). The starting structure used in molecular dynamics simulations is shown in green.

analysis of the overlaid reciprocal Lineweaver−Burk plots (Figure 4) showed both increasing slopes (decreased V_{max}) and increasing intercepts (higher K_m) at increasing inhibitor concentration. This pattern indicates mixed-type inhibition. Therefore, in agreement with molecular modeling studies, the pattern in Figure 4 shows that **20** is able to bind the peripheral site as well as the active site of hAChE. Replots of the slope versus concentration of **20** give an estimate of the competitive inhibition constant, K_i, of 1.91 nM.

BChE Inhibition. Recent evidence has shown that inhibition of BChE might be valuable in the search for anti-Alzheimer agents.[83,84] Consequently, the inhibitory activity on human serum BChE (hBChE) was also assayed by the method of Ellman et al. (Table 1).[64] 6-Chlorotacrine inhibits hAChE 110-fold more potently than hBChE.[31] The presence of the chlorine atom at the tacrine unit, which leads to an increased AChE inhibitory activity relative to unsubstituted tacrine,[85−87] becomes detrimental for hBChE inhibition. A steric hindrance due to the proximity of the chlorine atom to the terminal methyl group of Met437 in the hBChE active site seems to account for the detrimental influence of this substituent on the hBChE inhibitory activity relative to tacrine,[23,65] which is 21-fold more potent toward hBChE than 6-chlorotacrine.[31] As expected, hybrids **18**−**27** are more potent inhibitors of hAChE than hBChE (32- to 106-fold and 16- to 77-fold in the first and second series, respectively). Hybrids **23**−**27** exhibit IC_{50} values in the nanomolar range, they being 1.5- to 7-fold more potent than their counterparts of the first series and up to 3- to 4-fold more potent than 6-chlorotacrine.

Inhibition of Aβ Aggregation and Formation. Inhibition of AChE-Induced Aβ Aggregation. With the design of this novel family of dual binding site AChEIs, an interference with the AChE-induced Aβ aggregation was also pursued. Thus, the new hybrids were tested for their ability to inhibit the AChE-induced aggregation of $A\beta_{1-40}$, by using a thioflavin T fluorescence method.[88] Also, the Aβ-antiaggregating effect of one of the tricyclic ester precursors, **12**, was determined, while those of propidium[88] and 6-chlorotacrine[31] were already described. The new hybrids significantly inhibit, at 100 μM, the hAChE-induced Aβ aggregation, with percentages of inhibition ranging from 23% to 46% (Table 2), while 6-chlorotacrine and **12** were the almost inactive. Most of the new hybrids could be classified as weak inhibitors of the AChE-induced Aβ aggregation, with expected IC_{50} values in the high micromolar range, while the most potent described inhibitors display potencies in the low micromolar range.[21,23,26,27,30,33] Nevertheless, the inhibitory activity of the most potent hybrids, **26** and **27**, is in the same range as that of other known dual binding site AChEIs.[20,22,24,28,29,31,32]

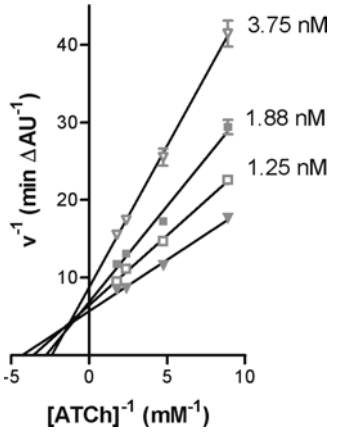

Figure 4. Kinetic study on the mechanism of AChE inhibition by **20**. Overlaid Lineweaver−Burk reciprocal plots of AChE initial velocity at increasing substrate concentration (ATCh, 0.56−0.11 mM) in the absence of inhibitor and in the presence of **20** (1.25−3.75 nM) are shown. Lines were derived from a weighted least-squares analysis of the data points.

The Aβ antiaggregating effect of the novel hybrids seems to depend on the position of the amido group within the linker, the hybrids of the second series being more potent than their counterparts of the first series. Moreover, the Aβ antiaggregating effect seems to be independent of the length of the linker within the first series, while a slightly increased effect is observed upon lengthening of the linker in the second series. Overall, the most potent AChE-induced Aβ aggregation inhibitors within both series were hybrids **26** and **27**. The higher Aβ antiaggregating activity of the novel hybrids relative to 6-chlorotacrine and **12** seems to be indicative of their dual binding site character. In turn, their lower Aβ antiaggregating activity relative to propidium could be ascribed to the different binding mode of the pyrano[3,2-*c*]quinoline moiety of these hybrids at the AChE peripheral site and/or to a less efficient interaction with Trp286 due to the lack of cation−π interaction in our hybrids, which are not protonated at the quinoline nitrogen atom of this moiety at physiological pH.

Table 2. Aβ Aggregation and BACE-1 Inhibitory Activities of the Hydrochlorides of 6-Chlorotacrine and Tricyclic Ester **12**, Propidium Iodide, and the Dihydrochlorides of the Pyrano[3,2-*c*]quinoline−6-Chlorotacrine Hybrids[a]

compd	AChE-induced $A\beta_{1-40}$ aggregation[b] (%)	$A\beta_{1-42}$ self-induced aggregation[c] (%)	BACE-1 activity[d] (%)
18·2HCl	27.2 ± 7.1	16.4 ± 2.6	na[e]
19·2HCl	22.9 ± 3.2	28.6 ± 3.3	14.5 ± 5.7
20·2HCl	28.6 ± 0.5	21.5 ± 1.8	18.5 ± 7.6
21·2HCl	nd[f]	nd[f]	nd[f]
22·2HCl	27.9 ± 5.2	20.5 ± 1.1	na[e]
23·2HCl	34.4 ± 1.0	45.3 ± 0.9	na[e]
24·2HCl	37.9 ± 3.4	12.2 ± 1.1	na[e]
25·2HCl	38.9 ± 2.6	30.8 ± 8.6	19.6 ± 5.1
26·2HCl	45.9 ± 2.8	49.1 ± 15.1	34.4 ± 3.6
27·2HCl	45.7 ± 0.3	47.3 ± 8.8	77.8 ± 6.4
12·HCl	10.5 ± 4.7	na[e]	na[e]
propidium iodide	82.0 ± 2.5[g]	89.8 ± 0.9	nd[f]
6-chlorotacrine·HCl	8.5 ± 1.6[h]	7.1 ± 1.2	na[e]

[a] Values are expressed as mean ± standard error of the mean from two independent measurements, each performed in duplicate. [b] A 100 μM concentration of the inhibitor was used. [c] A 50 μM concentration of the inhibitor was used ([Aβ]/[I] = 1/1). [d] A 2.5 μM concentration of the inhibitor was used. [e] Not active. [f] Not determined. [g] Data from ref 88. [h] Data from ref 31.

Inhibition of Spontaneous Aβ Aggregation. A number of dual binding site AChE inhibitors exhibit a significant inhibitory activity on Aβ self-aggregation.[23,26,27,29,32−34] The new hybrids significantly inhibit the self-induced Aβ aggregation when tested at equimolar ratio with Aβ, with percentages of inhibition ranging from 12% to 49% (Table 2). In the same assay conditions, 6-chlorotacrine and the tricyclic ester **12** turned out to be, respectively, almost and completely inactive, while propidium was more potent than the new hybrids. Hybrids of the second series were generally more potent than their counterparts of the first series, with the sole exception of **24** which was 2-fold less potent than **19**. A clear dependency of the spontaneous Aβ antiaggregating activity on the length of the linker was not observed. Compounds **23**, **26**, and **27** were the most potent hybrids. It might be hypothesized that a two-methylene linker between the amido group and the phenylpirano[3,2-*c*]quinoline moiety facilitates the formation of hydrogen bonds, with Aβ leading to an increased affinity. The expected IC_{50} values for the most potent hybrids must be around 50 μM, while the strongest inhibitors of spontaneous Aβ aggregation among known dual binding site AChEIs show potencies in the low micromolar range.[26,27,33,34] Thus, **23**, **26**, and **27** can be considered moderate inhibitors of $A\beta_{1-42}$ self-aggregation.

Inhibition of BACE-1. BACE-1 has been largely investigated as a therapeutic target for disease-modifying agents in AD, since BACE-1 is involved in the proteolytic cleavage of APP to Aβ and BACE-1 knockout mice did not show any adverse phenotype. Although highly active in vitro peptide inhibitors with poor pharmacokinetics are known, potent brain permeable inhibitors have not been developed yet. Therefore, there is an increasing need for small organic BACE-1 inhibitors able to cross the BBB.[89] The ability of the novel hybrids to inhibit in vitro human recombinant BACE-1 was also investigated. Some dual binding site AChEIs such as donepezil,[90] bis(7)-tacrine,[91] lipocrine,[92] memoquin,[26] and AP2243[93] exhibit BACE-1 inhibitory activity, which increases their potential as disease-modifying anti-Alzheimer drug candidates. In particular, since the new hybrids might structurally resemble to some extent bis(7)-tacrine, which showed in vitro and in vivo activity,[91] their BACE-1 inhibitory activity was first screened at a single concentration (2.5 μM) by a fluorometric assay.[94]

Hybrid **27** was the most potent BACE-1 inhibitor, exhibiting a 78% inhibition. Compounds **19**, **20**, **25**, and **26** were less active than **27** (15−34% inhibition), and the rest of the hybrids, the tricyclic ester **12**, and 6-chlorotacrine were inactive (Table 2). In general the BACE-1 inhibitory activity of the hybrids of the second series was higher than that of their counterparts of the first series. For the second series, the inhibitory activity increased along with the tether length. The IC_{50} value of the most active hybrid (**27**) was 1.81 ± 0.48 μM, it being more active than bis(7)-tacrine in vitro (IC_{50} = 7.5 μM).[91] Thus, **27** emerged as a promising anti-Alzheimer drug candidate endowed with a potent hAChE inhibitory activity (nanomolar range) and a significant in vitro inhibitory effect on both Aβ formation and AChE-induced and self-induced Aβ aggregation.

In Vitro Blood−Brain Barrier Permeation Assay. Brain penetration is a major issue for successful CNS drugs. In the past years, several in silico/in vitro methods have been used to predict the BBB permeation potential of test compounds. Among them, the parallel artificial membrane permeation assay (PAMPA-BBB) described by Di et al.[95] predicts passive BBB permeation with high success, high throughput, and reproducibility. To evaluate the brain penetration of the pyrano[3,2-*c*]quinoline−6-chlorotacrine hybrids herein described, we used the PAMPA-BBB assay, which was successfully applied by some of us to different compounds.[39,52,96−98] The in vitro permeability (P_e) of selected hybrids (**18**, **19**, and **23**−**27**), the tricyclic ester **12**, and 6-chlorotacrine through a lipid extract of porcine brain was determined by using phosphate buffered saline (PBS)/EtOH (80:20 or 70:30, depending on the solubility of compounds). At each solvent mixture, assay validation was made by comparing the experimental permeability with the reported values of 15 commercial drugs that gave a good lineal correlation: $P_e(\text{exp}) = 1.48P_e(\text{bibl}) + 1.91$ ($R^2 = 0.95$) for PBS/EtOH (80:20) and $P_e(\text{exp}) = 1.99\ P_e(\text{bibl}) + 1.07$ ($R^2 = 0.92$) for PBS/EtOH (70:30). From these equations and taking into account the limits established by Di et al. for BBB permeation,[95] we established that compounds with permeability values over 7.8×10^{-6} cm s^{-1} (PBS/EtOH, 80:20) or 9.0×10^{-6} cm s^{-1} (PBS/EtOH, 70:30) should cross the BBB. All tested hybrids showed permeability values over the above limits (Table 3; see also Table S5, Supporting Information), pointing out that they could cross the BBB and reach their pharmacological targets located in the CNS.

Table 3. Permeability Results from the PAMPA-BBB Assay for Selected Pyrano[3,2-*c*]quinoline−6-Chlorotacrine Hybrids (P_e, 10^{-6} cm s^{-1}) with Their Predictive Penetration into the CNS

compd	P_e (10^{-6} cm s^{-1})[a]	prediction
18·2HCl[b]	14.9 ± 1.1	CNS+
19·2HCl[b]	17.7 ± 0.2	CNS+
23·2HCl[c]	15.1 ± 0.2	CNS+
24·2HCl[b]	10.6 ± 0.4	CNS+
25·2HCl[c]	13.2 ± 0.4	CNS+
26·2HCl[b]	10.2 ± 0.3	CNS+
27·2HCl[b]	10.1 ± 0.4	CNS+
12[c]	21.4 ± 0.6	CNS+
6-chlorotacrine·HCl[c]	19.8 ± 0.4	CNS+

[a] Values are expressed as the mean ± standard deviation of three independent experiments. [b] Compound dissolved in PBS/EtOH (70:30). [c] Compound dissolved in PBS/EtOH (80:20).

Conclusion

We have synthesized a new series of pyrano[3,2-*c*]-quinoline−6-chlorotacrine hybrids as a novel class of dual binding site AChEIs. Variation of the position of an amido group within the oligomethylene linker gives rise to two parallel isomeric series. In general, the new hybrids are potent AChEIs, with IC_{50} values in the low nanomolar range and with slight differences between both series. The results indicate that linkage of a 5-phenylpyrano[3,2-*c*]quinoline moiety to a unit of the highly potent AChE active site inhibitor 6-chlorotacrine through an amido-containing tether does not result in an increased potency, as the most potent hybrids are equipotent to 6-chlorotacrine. Moreover, the AChE inhibitory potency of the hybrids shows a modest dependence on the length of the linker and the position of the amido group. Molecular modeling and kinetic studies have confirmed the dual site binding of these hybrids to hAChE. Apart from the characteristic interactions of the 6-chlorotacrine unit of these hybrids within the active site of AChE, the pyranoquinoline moiety is proposed to interact at the peripheral site forming a double near-parallel stacking with Trp286 and Tyr72, respectively, which are positioned in a way similar to the arrangement found in the complex of the enzyme with *syn*-TZ2PA6. The presence of a chlorine atom at position 6 of the tacrine unit, known to be detrimental for BChE inhibition, not unexpectedly accounts for the hAChE/hBChE selectivity of these hybrids.

Because of their dual binding site character, the new hybrids are able to inhibit the AChE-induced $A\beta_{1-40}$ aggregation. Also, these compounds exhibit a significant ability to inhibit the self-induced $A\beta_{1-42}$ aggregation, and some of them can also inhibit BACE-1. In general, these effects seem to be sensitive to the position of the amido group of the linker, the hybrids of the second series being more potent than their counterparts of the first series. Moreover, in the second series the activities increase along with the tether length. Finally, these hybrids seem to be able to cross BBB. Overall, **27** emerges as a promising anti-Alzheimer drug candidate able to hit both AChE (catalytic and noncatalytic activities) and Aβ (aggregation and production) and, therefore, with potential symptomatic and disease-modifying effects.

Experimental Section

Chemistry. General Methods. Melting points were determined in open capillary tubes with a MFB 595010M Gallenkamp or a Büchi B-540 melting point apparatus. 300 MHz ^{1}H/75.4 MHz ^{13}C NMR spectra, 400 MHz ^{1}H/100.6 MHz ^{13}C NMR spectra, and 500 MHz ^{1}H NMR spectra were recorded on Varian Gemini 300, Varian Mercury 400, and Varian Inova 500 spectrometers, respectively. The chemical shifts are reported in ppm (δ scale) relative to internal tetramethylsilane, and coupling constants are reported in hertz (Hz). Assignments given for the NMR spectra of the new compounds have been carried out by comparison with the NMR data of **18**, **27**, and 6-chlorotacrine, as model compounds, which in turn were assigned on the basis of DEPT, COSY ^{1}H/^{1}H (standard procedures), and COSY ^{1}H/^{13}C (gHSQC and gHMBC sequences) experiments. IR spectra were run on Perkin-Elmer Spectrum RX I or Thermo Nicolet Nexus spectrophotometers. Absorption values are expressed as wavenumbers (cm^{-1}); only significant absorption bands are given. Column chromatography was performed on silica gel 60 AC.C (35−70 mesh, SDS, ref 2000027). Thin-layer chromatography was performed with aluminum-backed sheets with silica gel 60 F_{254} (Merck, ref 1.05554), and spots were visualized with UV light and 1% aqueous solution of $KMnO_4$. The analytical samples of all of the new hybrids that were subjected to pharmacological evaluation possess a purity of ≥95%, as evidenced by results of their elemental analyses.

(4a*RS*,5*RS*,10b*RS*)- and (4a*RS*,5*SR*,10b*RS*)-Ethyl 5-(4-Chlorophenyl)-3,4,4a,5,6,10b-hexahydro-2*H*-pyrano[3,2-*c*]quinoline-9-carboxylate (9). $Y(OTf)_3$ (295 mg, 0.55 mmol, 0.2 equiv) was added to a solution of *p*-chlorobenzaldehyde, **7** (385 mg, 2.74 mmol, 1 equiv), and ethyl *p*-aminobenzoate, **5** (453 mg, 2.74 mmol, 1 equiv), in dry CH_3CN (20 mL). A solution of 3,4-dihydro-2*H*-pyran, **4** (250 μL, 231 mg, 2.74 mmol, 1 equiv), in dry CH_3CN (3 mL) was then added, and the reaction mixture was stirred at room temperature under inert atmosphere for 12 h. Saturated aqueous $NaHCO_3$ (20 mL) was added, and the resulting mixture was extracted with AcOEt (3 × 10 mL). The combined organic extracts were dried with anhydrous Na_2SO_4, filtered, and concentrated under reduced pressure to give a residue (1.1 g), which was subjected to column chromatography [35−70 μm silica gel (40 g), hexane/AcOEt mixtures]. On elution with hexane/AcOEt, 20:80, the desired product **9** (722 mg, 71% yield) was isolated as a 1.3:1 mixture of diastereoisomers as a waxy solid. A single diastereoisomer was obtained as a waxy solid in pure form from fractions isolated from the flash chromatography (51 mg, 5% yield) and characterized as the all-cis isomer (4a*RS*,5*RS*,10b*RS*): IR (NaCl) ν 3346 (N−H st), 1685 (C=O st) cm^{-1}; ^{1}H NMR (400 MHz, $CDCl_3$) δ 1.27−1.62 (m, 4H, 3-H_2 and 4-H_2), 1.37 (t, J = 7.1 Hz, 3H, CH_2-CH_3), 2.16 (m, 1H, 4a-H), 3.43 (dt, J = 12.0, J' = 1.9 Hz, 1H, 2-H_{ax}), 3.63 (broad d, $J \approx$ 12.0 Hz, 1H, 2-H_{eq}), 4.26 (s, 1H, NH), 4.33 (m, 2H, CH_2-CH_3), 4.73 (d, J = 1.7 Hz, 1H, 10b-H), 5.28 (d, J = 5.4 Hz, 1H, 5-H), 6.58 (d, J = 8.4 Hz, 1H, 7-H), 7.30−7.40 (complex signal, 4H, 5-ArH), 7.79 (d, J = 8.4 Hz, 1H, 8-H), 8.11 (s, 1H, 10-H); ^{13}C NMR (100.6 MHz, $CDCl_3$) δ 14.5 (CH_3, CH_2-CH_3), 18.1 (CH_2, C3), 25.3 (CH_2, C4), 38.4 (CH, C4a), 58.6 (CH, C5), 60.3 (CH_2, CH_2-CH_3), 60.7 (CH_2, C2), 72.1 (CH, C10b), 113.6 (CH, C7), 118.7 (C, C9), 120.3 (C, C10a), 128.0 (CH, C8), 128.7 (CH, 5-Ar-C_{meta}), 129.8 (CH, 5-Ar-C_{ortho}), 130.1 (CH, C10), 133.5 (C, 5-Ar-C_{para}), 138.7 (C, 5-Ar-C_{ipso}), 148.7 (C, C7a), 166.8 (C, CO). HRMS calcd for (C_{21}-$H_{22}{}^{35}ClNO_3$ + H^+) 372.1361, found 372.1370.

Ethyl 5-(4-Chlorophenyl)-3,4-dihydro-2*H*-pyrano[3,2-*c*]quinoline-9-carboxylate (11). To a solution of the diastereomeric mixture of tetrahydroquinolines **9** (408 mg, 1.11 mmol) in $CHCl_3$ (15 mL), DDQ (498 mg, 2.19 mmol, 2 equiv) was added, and the reaction mixture was stirred at room temperature for 24 h. Saturated aqueous Na_2CO_3 (50 mL) was added, the organic phase was separated, and the aqueous one was extracted with CH_2Cl_2 (3 × 10 mL). The combined organic phase and extracts were dried with anhydrous Na_2SO_4 and evaporated under reduced pressure to give a crude residue (870 mg), which was subjected to column chromatography [35−70 μm silica gel (20 g), hexane/AcOEt mixtures]. On elution with hexane/AcOEt, 50:50, pyranoquinoline **11** (305 mg, 75% yield) was obtained as an off-white solid: mp 197−199 °C (hexane/AcOEt, 1:1); IR (NaCl) ν 1715 (C=O st), 1623 (ar−C−C and ar−C−N st) cm^{-1}; ^{1}H NMR (400 MHz, CD_3OD) δ 1.36 (t, J = 7.1 Hz, 3H, CH_2-CH_3),

2.09 (m, 2H, 3-H_2), 2.76 (t, J = 6.3 Hz, 2H, 4-H_2), 4.39 (q, J = 7.1 Hz, 2H, CH_2-CH_3), 4.60 (m, 2H, 2-H_2), 7.60−7.70 (complex signal, 4H, 5-ArH), 8.04 (dd, J = 8.9 Hz, J' = 0.5 Hz, 1H, 7-H), 8.46 (dd, J = 8.9 Hz, J' = 1.8 Hz, 1H, 8-H), 8.93 (dd, J = 1.8 Hz, J' = 0.5 Hz, 1H, 10-H); ^{13}C NMR (100.6 MHz, CD_3OD) δ 13.4 (CH_3, CH_2-CH_3), 20.3 (CH_2, C3), 22.3 (CH_2, C4), 62.0 (CH_2, CH_2−CH_3), 70.3 (CH_2, C2), 114.5 (C, C4a), 119.3 (C, C10a), 120.8 (CH, C10), 125.1 (C, C9), 129.4 (CH, C7), 130.1 (CH, C8), 130.3 (CH, 5-Ar-C_{ortho}), 130.8 (CH, 5-Ar-C_{meta}), 133.3 (C, 5-Ar-C_{para}), 138.0 (C, 5-Ar-C_{ipso}), 140.6 (C, C6a), 157.2 (C, C10b), 165.0 (C, C5), 166.3 (C, CO). HRMS calcd for ($C_{21}H_{18}{}^{35}ClNO_3 + H^+$) 368.1048, found 368.1056.

Methyl 3-(3,4-Dihydro-5-phenyl-2*H*-pyrano[3,2-*c*]quinolin-9-yl)propanoate (12). A. Synthesis of the Diastereomeric Mixture of Tetrahydroquinolines 10. To a solution of 3,4-dihydro-2*H*-pyran (508 μL, 468 mg, 5.58 mmol, 1 equiv), benzaldehyde (566 μL, 591 mg, 5.58 mmol, 1 equiv), and the aniline **6** (1.00 g, 5.58 mmol, 1 equiv) in CH_3CN (40 mL) was added $Sc(OTf)_3$ (550 mg, 1.12 mmol, 0.2 equiv), and the reaction mixture was stirred overnight under inert atmosphere at room temperature. Saturated aqueous $NaHCO_3$ (40 mL) was added, and the resulting mixture was extracted with AcOEt (3 × 30 mL). The combined organic extracts were dried with anhydrous $MgSO_4$ and concentrated under reduced pressure to give a residue (1.9 g), which was subjected to column chromatography [35−70 μm silica gel (40 g), hexane/AcOEt/Et_3N mixtures]. On elution with hexane/AcOEt/Et_3N, 74:25:1, the expected adduct **10** (1.68 g, 86% yield) was obtained as a diastereomeric mixture.

B. DDQ Oxidation of 10 to 12: Overoxidation of 12 to Its Cinnamic Derivative. To a solution of the mixture of diastereoisomers **10** (4.75 g, 13.5 mmol, 1 equiv) in $CHCl_3$ (50 mL) were added Et_3N (5.70 mL, 4.14 g, 40.8 mmol, 3 equiv) and DDQ (3.10 g, 13.6 mmol, 1 equiv). The reaction mixture was heated to reflux for 3 h and concentrated in vacuo. The resulting solid residue (7.90 g) was subjected to column chromatography [35−70 μm silica gel (200 g), hexane/AcOEt mixtures]. On elution with hexane/AcOEt, 20:80, the desired pyranoquinoline **12** (1.60 g) was obtained together with its cinnamic derivative (1.60 g, 35% combined yield).

C. Hydrogenation of the Mixture of 12 and Its Cinnamic Derivative. The previous mixture (100 mg) was subjected to hydrogenation at atmospheric pressure in EtOH (10 mL) in the presence of 10% w/w Pd/C (20 mg) for 12 h. The resulting mixture was filtered, and the filtrate was concentrated in vacuo. The resulting residue was taken up in AcOEt (15 mL) and washed with saturated aqueous $NaHCO_3$ (20 mL), and the organic phase was dried with anhydrous $MgSO_4$ and evaporated at reduced pressure to yield the desired pyranoquinoline **12** (98 mg, 95% overall yield from **10**), which was obtained as a glassy white solid: mp 93−94 °C (AcOEt); IR (NaCl) ν 1736 (C=O st) cm^{-1}; ^{1}H NMR (400 MHz, $CDCl_3$) δ 1.99 (m, 2H, 3-H_2), 2.73 (complex signal, 4H, 4-H_2 and 9-CH_2-CH_2-COO), 3.13 (t, J = 7.8 Hz, 2H, 9-CH_2-CH_2-COO), 3.67 (s, 3H, $COOCH_3$), 4.42 (t, J = 5.2 Hz, 2H, 2-H_2), 7.43 (complex signal, 4H, 8-H, 5-ArH_{meta}, and 5-ArH_{para}), 7.55 (dd, J = 8.4 Hz, J' = 1.5 Hz, 2H, 5-ArH_{ortho}), 7.94 (d, J = 1.5 Hz, 1H, 10-H), 7.97 (d, J = 8.4 Hz, 1H, 7-H); ^{13}C NMR (100.6 MHz, $CDCl_3$) δ 21.7 (CH_2, C3), 23.6 (CH_2, C4), 31.0 (CH_2, 9-CH_2-CH_2-COO), 35.5 (CH_2, 9-CH_2-CH_2-COO), 51.5 (CH_3, COOCH_3), 66.9 (CH_2, C2), 110.6 (C, C4a), 119.6 (C, C10a), 119.7 (CH, C10), 128.0 (CH, C7), 128.1 (CH, 5-Ar-C_{para}), 128.6 (CH, 5-Ar-C_{ortho}), 129.0 (CH, 5-Ar-C_{meta}), 130.1 (CH, C8), 137.5 (C, C9), 140.3 (C, 5-Ar-C_{ipso}), 146.0 (C, C6a), 156.9 (C, C10b), 160.2 (C, C5), 173.1 (C, COO). HRMS calcd for ($C_{22}H_{21}NO_3 + H^+$) 348.1594, found 348.1588.

General Procedure for the Reaction of 6,9-Dichloro-1,2,3,4-tetrahydroacridine, 15, with α,ω-Alkanediamines. A mixture of **15** (1 mmol) and an excess of the diamine **16** (4 mmol) in 1-pentanol (1.3 mL) was heated under reflux with magnetic stirring for 18 h. The resulting mixture was cooled to room temperature, diluted with CH_2Cl_2 (3 mL), and washed successively with aqueous 2 N NaOH (3 × 3 mL) and water (2 × 3 mL). The organic phase was dried with anhydrous Na_2SO_4 and concentrated in vacuo to give a brown oily residue, from which 1-pentanol and the excess of diamine were removed by distillation at 100 °C/1 Torr and 140 °C/1 Torr, respectively. The distillation residue was taken in CH_2Cl_2 (1.3 mL), filtered, and concentrated in vacuo to give a brown oily residue which was subjected to column chromatography (35−70 μm silica gel, CH_2Cl_2/MeOH/25% or 50% aqueous NH_4OH or AcOEt/MeOH/Et_3N mixtures as eluent) to afford, separately, bis-6-chlorotacrine **28** and the desired amine **17** as a brown and yellowish oil, respectively.

For characterization purposes, analytical samples of the dihydrochlorides of **17** and **28** were prepared as follows: the amine **17** or the dimer **28** (1 mmol) were dissolved in MeOH (2−10 mL), the solution was filtered through a polytetrafluoroethylene (PTFE) 0.45 μm filter and treated with an excess of a methanolic solution of HCl (6−9 mmol), and the resulting solution was concentrated in vacuo to dryness. The solid was recrystallized from MeOH/AcOEt mixtures, triturated with Et_2O, and dried at 65 °C/15 Torr for 4 days to give **17**·2HCl or **28**·2HCl as yellowish solids.

9-[(6-Aminohexyl)amino]-6-chloro-1,2,3,4-tetrahydroacridine Dihydrochloride (17c·2HCl). From **15** (4.00 g, 15.9 mmol) and 1,6-diaminohexane, **16c** (7.52 g, 64.8 mmol), a brown oily residue (7.30 g) was obtained and subjected to column chromatography [35−70 μm silica gel (88 g), CH_2Cl_2/MeOH/25% aqueous NH_4OH mixtures]. On elution with CH_2Cl_2/MeOH/25% aqueous NH_4OH, 99:1:0.05, bis(6)-6-chlorotacrine, **28c** (246 mg), a mixture **28c**/**17c** in the approximate ratio of 20:80 (^{1}H NMR) (614 mg, 8% total yield of **28c**), and amine **17c** (3.61 g, 78% total yield) were consecutively isolated as brown-yellow oils: $R_{f(\mathbf{17c})}$ = 0.39; $R_{f(\mathbf{28c})}$ = 0.80 (CH_2Cl_2/MeOH/25% aqueous NH_4OH, 9:1:0.01).

17c·2HCl: mp 157−158 °C (MeOH); IR (KBr) ν 3500−2500 (max at 3413, 2935, 2864, N−H, $^+$N−H, and C−H st), 1630, 1573, and 1513 (ar−C−C and ar−C−N st) cm^{-1}; ^{1}H NMR (300 MHz, CD_3OD, presat/Watergate) δ 1.39−1.52 (complex signal, 4H, 3′-H_2 and 4′-H_2), 1.66 (tt, $J \approx J' \approx$ 7.5 Hz, 2H, 5′-H_2), 1.80 (tt, $J \approx J' \approx$ 7.5 Hz, 2H, 2′-H_2), 1.88−1.98 (complex signal, 4H, 2-H_2 and 3-H_2), 2.69 (m, 2H, 1-H_2), 2.90 (t, J = 7.5 Hz, 2H, 6′-H_2), 2.98 (m, 2H, 4-H_2), 3.83 (t, J = 7.5 Hz, 2H, 1′-H_2), 7.48 (dd, J = 9.3 Hz, J' = 2.1 Hz, 1H, 7-H), 7.75 (d, J = 2.1 Hz, 2H, 5-H), 8.30 (d, J = 9.3 Hz, 1H, 8-H); ^{13}C NMR (75.4 MHz, CD_3OD) δ 22.3 (CH_2, C3), 23.2 (CH_2, C2), 25.2 (CH_2, C1), 27.1 (CH_2) and 27.3 (CH_2) (C3′ and C4′), 28.5 (CH_2), 30.9 (CH_2) and 31.4 (CH_2) (C4, C2′, and C5′), 40.6 (CH_2, C6′), 49.1 (CH_2, C1′), 114.3 (C, C9a), 116.5 (C, C8a), 121.3 (CH, C5), 126.1 (CH, C7), 128.0 (CH, C8), 138.5 (C, C6), 142.8 (C, C10a), 154.5 (C, C4a), 156.2 (C, C9).

28c·2HCl [*N*,*N*′-Bis(6-chloro-1,2,3,4-tetrahydroacridin-9-yl)-1,6-hexanediamine]: mp 126−127 °C (MeOH); IR (KBr) ν 3500−2500 (max at 3254, 3049, 2933, 2859, 2792, N−H, $^+$N−H, and C−H st), 1631, 1603, 1574, 1557, and 1514 (ar−C−C and ar−C−N st) cm^{-1}; ^{1}H NMR (300 MHz, CD_3OD) δ 1.50 (m, 4H, 3′-H_2), 1.80−2.00 (complex signal, 12H, 2-H_2, 3-H_2, and 2′-H_2), 2.66 (m, 4H, 1-H_2), 2.98 (m, 4H, 4-H_2), 3.91 (t, $J \approx$ 7.0 Hz, 4H, 1′-H_2), 4.87 (s, NH and $^+$NH), 7.51 (dd, J = 9.6 Hz, J' = 2.2 Hz, 2H, 7-H), 7.75 (d, J = 2.2 Hz, 2H, 5-H), 8.35 (d, $J \approx$ 9.6 Hz, 2H, 8-H); ^{13}C NMR (75.4 MHz, CD_3OD) δ 22.5 (CH_2, C3), 23.3 (CH_2, C2), 25.3 (CH_2, C1), 27.4 (CH_2), 31.4 (CH_2), and 31.6 (CH_2) (C4, C2′, and C3′), 49.2 (CH_2, C1′), 114.6 (C, C9a), 116.9 (C, C8a), 122.1 (CH, C5), 125.9 (CH, C7), 127.7 (CH, C8), 138.0 (C, C6), 143.6 (C, C10a), 155.3 (C), and 155.6 (C) (C4a and C9).

9-[(8-Aminooctyl)amino]-6-chloro-1,2,3,4-tetrahydroacridine Dihydrochloride (17e·2HCl). From **15** (4.00 g, 15.9 mmol) and 1,8-diaminooctane, **16e** (8.24 g, 57.2 mmol), a brown oily residue (9.56 g) was obtained and subjected to column chromatography [35−70 μm silica gel (115 g), CH_2Cl_2/MeOH/25% aqueous NH_4OH mixtures]. On elution with CH_2Cl_2/MeOH/

25% aqueous NH_4OH, 96:4:0.1 to 85:15:0.2, bis(8)-6-chlorotacrine, **28e** (2.11 g, 46% yield) and amine **17e** (2.00 g, 35% yield) were consecutively isolated as brown-yellow oils: $R_{f(\mathbf{17e})} = 0.33$; $R_{f(\mathbf{28e})} = 0.88$ (CH_2Cl_2/MeOH/25% aqueous NH_4OH, 9:1:0.01).

17e·2HCl: mp 109−110 °C (MeOH/AcOEt, 1:1); IR (KBr) ν 3500−2500 (max at 3344, 2929, 2855, N−H, $^+$N−H, and C−H st), 1630, 1605, 1574, 1558, and 1512 (ar−C−C and ar−C−N st) cm^{-1}; ^{1}H NMR (300 MHz, CD_3OD) δ 1.24−1.44 (complex signal, 8H, 3′-H_2, 4′-H_2, 5′-H_2, and 6′-H_2), 1.63 (tt, $J \approx J' \approx 7.5$ Hz, 2H, 7′-H_2), 1.71 (tt, $J \approx J' \approx 7.5$ Hz, 2H, 2′-H_2), 1.84−1.94 (complex signal, 4H, 2-H_2 and 3-H_2), 2.66 (m, 2H, 1-H_2), 2.89 (t, $J = 7.5$ Hz, 2H, 8′-H_2), 2.94 (m, 2H, 4-H_2), 3.69 (t, $J = 7.5$ Hz, 2H, 1′-H_2), 4.89 (s, NH, $^+$NH and $^+NH_3$), 7.36 (dd, $J = 9.0$ Hz, $J' = 2.1$ Hz, 1H, 7-H), 7.71 (d, $J = 2.1$ Hz, 1H, 5-H), 8.16 (d, $J =$ 9.0 Hz, 1H, 8-H); ^{13}C NMR (75.4 MHz, CD_3OD) δ 22.8 (CH_2, C3), 23.5 (CH_2, C2), 25.5 (CH_2, C1), 27.4 (CH_2) and 27.7 (CH_2) (C3′ and C6′), 28.6 (CH_2), 30.1 (2 CH_2), 31.8 (CH_2), and 32.1 (CH_2) (C4, C2′, C4′, C5′, and C7′), 40.8 (CH_2, C8′), 49.4 (CH_2, C1′), 115.1 (C, C9a), 117.6 (C, C8a), 123.3 (CH, C5), 125.6 (CH, C7), 127.4 (CH, C8), 137.3 (C, C6), 144.9 (C, C10a), 155.0 (C, C4a), 156.6 (C, C9).

28e·2HCl [*N,N*′-Bis(6-chloro-1,2,3,4-tetrahydroacridin-9-yl)-1,8-octanediamine]: mp 134−135 °C (MeOH/AcOEt, 1:1); IR (KBr) ν 3500−2500 (max at 3229, 3046, 2926, 2853, 2768, N−H, $^+$N−H, and C−H st), 1630, 1570, and 1515 (ar−C−C and ar−C−N st) cm^{-1}; ^{1}H NMR (300 MHz, CD_3OD, presat/Watergate) δ 1.37−1.48 (complex signal, 8H, 3′-H_2 and 4′-H_2), 1.83 (tt, $J \approx J' \approx 7.2$ Hz, 4H, 2′-H_2), 1.90−1.98 (complex signal, 8H, 2-H_2 and 3- H_2), 2.66 (m, 4H, 1-H_2), 2.99 (m, 4H, 4-H_2), 3.92 (t, $J =$ 7.2 Hz, 4H, 1′-H_2), 7.54 (dd, $J = 9.3$ Hz, $J' = 2.1$ Hz, 2H, 7-H), 7.77 (d, $J \approx 2.1$ Hz, 2H, 5-H), 8.37 (d, $J \approx 9.3$ Hz, 2H, 8-H); ^{13}C NMR (75.4 MHz, CD_3OD) δ 21.8 (CH_2, C3), 22.9 (CH_2, C2), 24.8 (CH_2, C1), 27.6 (CH_2, C3′), 29.4 (CH_2, C4), 30.2 (CH_2) and 31.3 (CH_2) (C2′ and C4′), 49.2 (CH_2, C1′), 113.2 (C, C9a), 115.3 (C, C8a), 119.0 (CH, C5), 126.6 (CH, C7), 128.7 (CH, C8), 139.9 (C, C6), 140.3 (C, C10a), 152.0 (C, C4a), 157.5 (C, C9).

General Procedure for the Preparation of Amides 18−27 from Esters 11 or 12 and Amines 17. A.1. Hydrolysis of Ester 11. A solution of ester **11** (1 mmol) and aqueous 5 N NaOH (1.2 mL, 6 equiv) in MeOH (56 mL) was heated under reflux with magnetic stirring for 16 h. The resulting mixture was cooled to 0 °C (ice−water bath), treated with aqueous 2 N HCl (5.5 mL, 11 equiv), and concentrated in vacuo. The obtained solid residue was extracted with MeOH (18 mL), and the organic extract was evaporated at reduced pressure to give the hydrochloride of the corresponding carboxylic acid, **13**, as a white solid, which was used in the next step without further purification.

A.2. Hydrolysis of Ester 12. A solution of ester **12** (1 mmol) and KOH pellets (240 mg of 85% purity reagent, 3.6 equiv) in MeOH (25 mL) was heated under reflux with magnetic stirring for 24 h. The resulting mixture was cooled to room temperature and evaporated in vacuo. The obtained solid residue was treated with a solution of HCl in Et_2O (20 equiv) with stirring for 30 min, and the suspension was evaporated in vacuo to give the hydrochloride of the corresponding carboxylic acid, **14**, as a white solid, which was used in the next step without further purification.

B. Reaction of Carboxylic Acids 13 or 14 with Amines 17. To a cold solution (0 °C, ice−water bath) of **13** or **14** (crude product arising from 1 mmol of the starting ester **11** or **12**) and anhydrous Et_3N (2.2 mmol) in anhydrous CH_2Cl_2 (50 mL), ethyl chloroformate (1 mmol) was added and the mixture was thoroughly stirred at 0 °C for 30 min. To the resulting solution, a cold solution (0 °C, ice−water bath) of amine **17** (1 mmol) in anhydrous CH_2Cl_2 (50 mL) was added, and the reaction mixture was stirred at room temperature for 64−72 h and treated with 10% aqueous Na_2CO_3 until pH 10 (95 mL). The organic phase was separated, and the aqueous one was extracted with CH_2Cl_2 (3 × 40 mL). The organic phase and combined extracts were washed with water (2 × 80 mL), dried with anhydrous Na_2SO_4, and evaporated at reduced pressure to give a yellow oily residue, which was subjected to column chromatography (35−70 μm silica gel, hexane/AcOEt/Et_3N or heptane/AcOEt/Et_3N mixtures as eluent) to afford the amides **18**−**27** as yellowish oils.

The isolated hybrids **18**−**27** were transformed into the corresponding dihydrochlorides as follows: A solution of the free base (1 mmol) in CH_2Cl_2 (10−60 mL) was filtered through a 0.45 μm PTFE filter and treated with excess of a methanolic solution of HCl (6 mmol). The solution was concentrated in vacuo to dryness, and the solid residue was, in general, recrystallized from MeOH/AcOEt mixtures and dried at 65 °C/15 Torr for 4 days.

6-Chloro-9-{{6-[5-(4-chlorophenyl)-3,4-dihydro-2*H*-pyrano[3,2-*c*]quinoline-9-carboxamido]hexyl}amino}-1,2,3,4-tetrahydroacridine Dihydrochloride (18·2HCl). From crude **13** [173 mg of the crude product obtained from 136 mg (0.37 mmol) of ester **11**] and amine **17c** (126 mg, 0.37 mmol), a brown oily residue (212 mg) was obtained and subjected to column chromatography [35−70 μm silica gel (20 g), hexane/AcOEt/Et_3N mixtures]. On elution with hexane/AcOEt/Et_3N, 20:80:0.05 to 0:100:0.05, hybrid **18** (56 mg, 23% yield) was isolated as a yellowish oil: $R_f = 0.52$ (AcOEt/Et_3N, 10:0.05). **18**·2HCl: mp 194−195 °C (CH_2Cl_2). IR (KBr) ν 3500−2500 (max at 3393, 3253, 3056, 2928, 2856, N−H, $^+$N−H, O−H, and C−H st), 1633 and 1575 (C=O, ar−C−C and ar−C−N st) cm^{-1}; ^{1}H NMR (500 MHz, CD_3OD) δ 1.46−1.56 (complex signal, 4H, 3′-H_2 and 4′-H_2), 1.70 (tt, $J \approx J' \approx 7.0$ Hz, 2H, 5′-H_2), 1.88 (tt, $J = J' = 7.0$ Hz, 2H, 2′-H_2), 1.92−1.99 (complex signal, 4H, 2-H_2 and 3-H_2), 2.16 (tt, $J = J' = 6.0$ Hz, 2H, 3″-H_2), 2.68 (t, $J = 6.0$ Hz, 2H, 1-H_2), 2.85 (t, $J = 6.0$ Hz, 2H, 4″-H_2), 2.98 (t, $J = 6.0$ Hz, 2H, 4-H_2), 3.45 (t, $J = 7.0$ Hz, 2H, 6′-H_2), 3.96 (t, $J = 7.0$ Hz, 2H, 1′-H_2), 4.76 (t, $J \approx 6.0$ Hz, 2H, 2″-H_2), 4.85 (s, NH and $^+$NH), 7.53 (dd, $J = 9.5$ Hz, $J' = 2.0$ Hz, 1H, 7-H), 7.69 [dm, $J = 8.5$ Hz, 2H, 3(5)-H *p*-chlorophenyl], superimposed in part 7.73 [dm, $J = 8.5$ Hz, 2H, 2(6)-H *p*-chlorophenyl], 7.74 (d, $J = 2.0$ Hz, 1H, 5-H), 8.09 (d, $J \approx 9.0$ Hz, 1H, 7″-H), 8.34 (dd, $J = 9.0$ Hz, $J' = 2.0$ Hz, 1H, 8″-H), 8.38 (d, $J = 9.5$ Hz, 1H, 8-H), 8.79 (d, $J = 2.0$ Hz, 1H, 10″-H); ^{13}C NMR (100.6 MHz, CD_3OD) δ 21.72 (CH_2, C3″), 21.74 (CH_2, C3), 22.9 (CH_2, C2), 23.7 (CH_2, C4″), 24.7 (CH_2, C1), 27.2 (CH_2) and 27.5 (CH_2) (C3′and C4′), 29.3 (CH_2, C4), 30.2 (CH_2, C5′), 31.2 (CH_2, C2′), 40.9 (CH_2, C6′), 49.1 (CH_2, C1′), 70.9 (CH_2, C2″), 113.4 (C, C9a), 115.2 (C, C4a″), 115.4 (C, C8a), 119.1 (CH, C5), 120.5 (C, C10a″), 122.9 (CH, C7″), 123.3 (CH, C10″), 126.7 (CH, C7), 128.8 (CH, C8), 130.4 [CH, C3(5) *p*-chlorophenyl], 132.0 [CH, C2(6) *p*-chlorophenyl], 132.7 (CH + C, C8″ and C1 *p*-chlorophenyl), 135.0 (C, C9″), 138.7 (C, C4 *p*-chlorophenyl), 140.0 (C, C6), 140.5 (C, C10a), 142.2 (C, C6a″), 152.1 (C, C4a), 157.8 (C, C9), 158.6 (C, C5″), 166.2 (C, C10b″), 168.0 (C, CONH). HRMS calcd for ($C_{38}H_{38}{}^{35}Cl_2N_4O_2 + H^+$) 653.2450, found 653.2432. Anal. ($C_{38}H_{38}Cl_2N_4O_2 \cdot 2HCl \cdot 2.4H_2O$) C, H, N.

6-Chloro-9-{{8-[3-(3,4-dihydro-5-phenyl-2*H*-pyrano[3,2-*c*]quinolin-9-yl)propanamido]octyl}amino}-1,2,3,4-tetrahydroacridine Dihydrochloride (27·2HCl). From crude **14** [126 mg of the crude product obtained from 122 mg (0.35 mmol) of ester **12**] and amine **17e** (126 mg, 0.35 mmol), a yellow oily residue (198 mg) was obtained and subjected to column chromatography [35−70 μm silica gel (19 g), heptane/AcOEt/Et_3N mixtures]. On elution with heptane/AcOEt/Et_3N, 20:80:0.1, hybrid **27** (91 mg, 39% yield) was isolated as a yellowish oil: $R_f = 0.68$ (AcOEt/MeOH/Et_3N, 90:10:0.1). **27**·2HCl: mp 190−191 °C (MeOH). IR (KBr) ν 3500−2500 (max at 3389, 3245, 3056, 2925, 2853, N−H, $^+$N−H, O−H, and C−H st), 1633 and 1576 (C=O, ar−C−C, and ar−C−N st) cm^{-1}; ^{1}H NMR (500 MHz, CD_3OD) δ 1.20−1.36 (complex signal, 6H, 4′-H_2, 5′-H_2, and 6′-H_2), 1.37−1.45 (complex signal, 4H, 3′-H_2, and 7′-H_2), 1.81 (quint, $J = 7.5$ Hz, 2H, 2′-H_2), 1.91−1.99 (complex signal, 4H, 2-H_2, and 3-H_2), 2.15 (quint, $J \approx 6.0$ Hz, 2H, 3″-H_2), 2.62 (t, $J = 7.5$ Hz, 2H, 9″-CH_2−CH_2-CONH), 2.66 (t, $J = 6.0$ Hz, 2H, 1-H_2), 2.83

(t, J = 6.5 Hz, 2H, 4″-H_2), 2.99 (t, J = 6.0 Hz, 2H, 4-H_2), 3.10 (t, J = 7.5 Hz, 2H, 8′-H_2), 3.18 (t, J = 7.5 Hz, 2H, 9″-CH_2-CH_2−CONH), 3.92 (t, J = 7.5 Hz, 2H, 1′-H_2), 4.76 (t, J = 5.0 Hz, 2H, 2″-H_2), 4.84 (s, NH and $^+$NH), 7.55 (dd, J = 9.5 Hz, J' = 2.0 Hz, 1H, 7-H), 7.65−7.74 [complex signal, 5H, Ar-H phenyl], 7.77 (d, J = 2.0 Hz, 1H, 5-H), 7.94 (dd, J = 9.0 Hz, J' = 1.5 Hz, 1H, 8″-H), 8.00 (d, J = 9.0 Hz, 1H, 7″-H), 8.21 (d, J = 1.5 Hz, 1H, 10″-H), 8.37 (d, $J \approx$ 9.5 Hz, 1H, 8-H); ^{13}C NMR (100.6 MHz, CD_3OD) δ 21.8 (CH_2, C3″), 21.9 (CH_2, C3), 22.9 (CH_2, C2), 23.8 (CH_2, C4″), 24.7 (CH_2, C1′), 27.6 (CH_2, C3′), 27.7 (CH_2, C6′), 29.3 (CH_2, C4), 30.1 (CH_2) and 30.2 (CH_2) (C4′ and C5′), 30.3 (CH_2, C7′), 31.3 (CH_2, C2′), 32.8 (CH_2, 9″-CH_2-CH_2-CONH), 38.1 (CH_2, 9″-CH_2-CH_2-CONH), 40.3 (CH_2, C8′), 49.2 (CH_2, C1′), 70.6 (CH_2, C2″), 113.3 (C, C9a), 114.2 (C, C4a″), 115.4 (C, C8a), 119.1 (CH, C5), 121.0 (C, C10a″), 122.3 (2 CH, C7″ and C10″), 126.8 (CH, C7), 128.8 (CH, C8), 130.2 (CH) and 132.2 (CH + C) [C1, C2(6), C3(5), and C4 phenyl], 135.9 (CH, C8″), 139.7 (C, C6a″), 140.1 (C, C6), 140.5 (C, C10a), 142.9 (C, C9″), 152.1 (C, C4a), 157.8 (C, C5″), 157.9 (C, C9), 165.1 (C, C10b″), 174.3 (C, CONH). HRMS calcd for ($C_{42}H_{47}{}^{35}ClN_4O_2$ + H^+) 675.3460, found 675.3457. Anal. ($C_{42}H_{47}ClN_4O_2 \cdot 2HCl \cdot 2.25H_2O$) C, H, N.

Biochemical Studies. AChE and BChE Inhibition Assay. AChE inhibitory activity was evaluated spectrophotometrically at 25 °C by the method of Ellman,[64] using AChE from bovine or human erythrocytes and acetylthiocholine iodide (0.53 or 0.13 mM for bAChE and hAChE, respectively) as substrate. The reaction took place in a final volume of 3 mL of 0.1 M phosphate-buffered solution, pH 8.0, containing 0.025 or 0.04 units of bAChE or hAChE, respectively, and 333 μM 5,5′-dithiobis(2-nitrobenzoic) acid (DTNB) solution used to produce the yellow anion of 5-thio-2-nitrobenzoic acid. Inhibition curves were performed in triplicate by incubating at least 12 concentrations of inhibitor for 15 min. One triplicate sample without inhibitor was always present to yield 100% of AChE activity. The reaction was stopped with 100 μL of 1 mM eserine, and the color production was measured at 414 nm. BChE inhibitory activity determinations were carried out similarly, using 0.035 unit of human serum BChE and 0.56 mM butyrylthiocholine, instead of AChE and acetylthiocholine, in a final volume of 1 mL.

Data from concentration−inhibition experiments of the inhibitors were calculated by nonlinear regression analysis, using the GraphPad Prism program package (GraphPad Software; San Diego, CA), which gave estimates of the IC_{50} (concentration of drug producing 50% of enzyme activity inhibition). Results are expressed as the mean ± SEM of at least four experiments performed in triplicate. DTNB, acetylthiocholine, butyrylthiocholine, and enzymes were purchased from Sigma, and eserine was purchased from Fluka.

Kinetic Analysis of AChE Inhibition. To obtain estimates of the mechanism of action of **20**, reciprocal plots of 1/velocity versus 1/[substrate] were constructed at relatively low concentration of substrate (0.56−0.11 mM) by using Ellman's method[64] and human recombinant AChE (Sigma, Milan, Italy). Three concentrations of **20** were selected for this study: 1.25, 1.88, and 3.75 nM. The plots were assessed by a weighted least-squares analysis that assumed the variance of the velocity (v) to be a constant percentage of v for the entire data set. Data analysis was performed with GraphPad Prism 4.03 software (GraphPad Software Inc.).

Slopes of the obtained reciprocal plots were then plotted against **20** concentration in a similar weighted analysis, and K_i was determined as the intercept on the negative x-axis.

AChE-Induced Aβ_{1-40} Aggregation Inhibition Assay. Thioflavin T (Basic Yellow 1), human recombinant AChE lyophilized powder, 1,1,1,3,3,3-hexafluoro-2-propanol (HFIP), were purchased from Sigma Chemicals. Absolute DMSO over molecular sieves was from Fluka. Water was deionized and doubly distilled. Aβ_{1-40}, supplied as trifluoroacetate salt, was purchased from Bachem AG (Bubendorf, Switzerland). Aβ_{1-40} (2 mg mL^{-1}) was dissolved in HFIP and lyophilized. The 1 mM solutions of tested inhibitors were prepared by dissolution in MeOH.

Aliquots of 2 μL Aβ_{1-40} peptide, lyophilized from 2 mg mL^{-1} HFIP solution and dissolved in DMSO, were incubated for 24 h at room temperature in 0.215 M sodium phosphate buffer (pH 8.0) at a final concentration of 230 μM. For co-incubation experiments aliquots (16 μL) of hAChE (final concentration 2.30 μM, Aβ/AChE molar ratio 100:1) and AChE in the presence of 2 μL of the tested inhibitor (final inhibitor concentration 100 μM) in 0.215 M sodium phosphate buffer, pH 8.0, solution were added. Blanks containing Aβ_{1-40} alone, human recombinant AChE alone, and Aβ_{1-40} plus tested inhibitors in 0.215 M sodium phosphate buffer (pH 8.0) were prepared. The final volume of each vial was 20 μL. Each assay was run in duplicate. To quantify amyloid fibril formation, the thioflavin T fluorescence method was then applied.[88] The fluorescence intensities due to β-sheet conformation were monitored for 300 s at λ_{em} = 490 nm (λ_{exc} = 446 nm). The percent inhibition of the AChE-induced aggregation due to the presence of the tested compound was calculated by the following expression: 100 − [(IF_i/IF_o) × 100)] where IF_i and IF_o are the fluorescence intensities obtained for Aβ plus AChE in the presence and in the absence of inhibitor, respectively, minus the fluorescence intensities due to the respective blanks.

Aβ_{1-42} Self-Aggregation Inhibition Assay. As reported in a previously published protocol,[99] HFIP pretreated Aβ_{1-42} samples (Bachem AG, Switzerland) were solubilized with a CH_3CN/Na_2CO_3/NaOH (48.4:48.4:3.2) mixture. Experiments were performed by incubating the peptide in 10 mM phosphate buffer (pH 8.0) containing 10 mM NaCl at 30 °C for 24 h (final Aβ concentration 50 μM) with and without inhibitor (50 μM, Aβ/inhibitor = 1/1). Blanks containing the tested inhibitors were also prepared and tested. To quantify amyloid fibrils formation, the thioflavin T fluorescence method was used.[88] After incubation, samples were diluted to a final volume of 2.0 mL with 50 mM glycine−NaOH buffer (pH 8.5) containing 1.5 μM thioflavin T. A 300 s time scan of fluorescence intensity was carried out (λ_{exc} = 446 nm; λ_{em} = 490 nm, FP-6200 fluorometer, Jasco Europe), and values at plateau were averaged after subtracting the background fluorescence of 1.5 μM thioflavin T solution. The fluorescence intensities were compared, and the percent inhibition due to the presence of the inhibitor was calculated by the following formula 100 − [(IF_i/IF_o) × 100] where IF_i and IF_o are the fluorescence intensities obtained for Aβ_{1-42} in the presence and in the absence of inhibitor, respectively.

β-Secretase (BACE-1) Inhibition Assay. β-Secretase (BACE-1, Sigma) inhibition studies were performed by employing a peptide mimicking APP sequence as substrate (M-2420, Bachem). The following procedure was employed: an amount of 5 μL of test compound (or DMSO) was preincubated with 175 μL of the enzyme (c = 17.2 nM) for 1 h at room temperature. The substrate (3 μM) was then added and left to react for 15 min. The fluorescence signal was read at λ_{em} = 405 nm (λ_{exc} = 320 nm). The fluorescence intensities with and without inhibitor were compared, and the percent inhibition due to the presence of test compounds was calculated. The % inhibition due to the presence of increasing test compound concentration was calculated by the following expression: 100 − [(IF_i/IF_o) × 100], where IF_i and IF_o are the fluorescence intensities obtained for BACE-1 in the presence and in the absence of inhibitor, respectively. Inhibition curve was obtained for **27** by plotting the % inhibition versus the logarithm of inhibitor concentration in the assay sample. The linear regression parameters were determined and the IC_{50} was extrapolated, when possible (GraphPad Prism 4.0, GraphPad Software Inc.).

To demonstrate inhibition of BACE-1 activity, a peptidomimetic inhibitor (β-secretase inhibitor IV, Calbiochem) was serially diluted into the reactions' wells (IC_{50} = 0.013 μM).

Molecular Modeling. Docking was performed with the program rDock, which is an extension of the program RiboDock,[100] using an empirical scoring function calibrated on the basis of protein−ligand complexes.[101] The reliability of rDock was assessed by docking a set of known dual binding site AChEIs taking advantage of the X-ray crystallographic structures of their complexes with AChE (PDB entries 1Q83, 1Q84, 1ODC, 1ZGB, 1ZGC, 2CKM, and 2CMF), which was also chosen to identify three different orientations of the indole ring of Trp286 in the peripheral binding site in hAChE (see Molecular Modeling Studies and also Tables S2 and S3 in Supporting Information).

The docking of compounds **20**, **25**, and **27** in hAChE was then explored using the three structural models of the target hAChE (named A, B, and C). Structural water molecules that mediate relevant interactions between the tacrine moiety and the enzyme were retained in the target models. The docking volume was defined as the space within 10 Å of the ligands spanning both catalytic and peripheral binding sites. The ligands were considered in their monocationic form on the basis of the pK_a estimated using ACD software.[102] The structure of the ligands was initially energy minimized at the AM1[103] level using Gaussian 03.[104] Suitable restraints were introduced to position the tacrine moiety of the hybrids in the catalytic site, as inspection of the X-ray crystallographic structures of several tacrine-based dual binding site AChEIs reveals that the tacrine unit shares a common binding mode, which in turn mimics the pose found for AChE complexes with tacrine[7] and huprine X[69] (see text). This allowed us to focus the sampling effort on the orientation of the pyrano[3,2-*c*]quinoline unit of the hybrids at the peripheral binding site and the linker along the gorge. Each compound was subjected to 100 docking runs, and the output docking modes were analyzed by visual inspection in conjunction with the docking scores.

The ligand−protein poses were reranked using the MM−PBSA approach (Table S4, Supporting Information). An energy minimization of the complexes was first carried out in order to reduce steric clashes that might arise from docking calculations. All minimizations and MM-PBSA calculations were performed with the parmm99 force field of the Amber-9 package.[105] The relative binding affinities of the best poses of the ligands were determined by using eq 1.

$$\Delta G_{\text{binding}} = \Delta G_{\text{MM}} + \Delta G^{\text{sol}}_{\text{ele}} + \Delta G^{\text{sol}}_{\text{nonpolar}} - T\Delta S \qquad (1)$$

The partial atomic charges for the compounds were derived using the RESP protocol[106] by fitting to the molecular electrostatic potential calculated at the HF/6-31G* level with Gaussian 03. The internal conformational energy (ΔG_{MM}) was determined using the standard formalism and parameters implemented in AMBER. The electrostatic contribution ($\Delta G^{\text{sol}}_{\text{ele}}$) was computed using a dielectric constant of 78.4 for the aqueous environment, while values of 2 and 4 were considered for the ligand−enzyme complex. The electrostatic potentials were calculated using a grid spacing of 0.25 Å. The interior of the solutes was defined as the volume inaccessible to a solvent probe sphere of radius 1.4 Å. The nonpolar contribution ($\Delta G^{\text{sol}}_{\text{nonpolar}}$) was calculated using a linear dependence with the solvent-accessible surface.[107] Finally, entropy changes upon complexation were assumed to cancel out in the comparison of the binding affinities of **20** and **25**, as the number of rotatable bonds is the same in both compounds. However, since the spacer of **27** is larger by two methylene units, its binding affinity was corrected for the entropic penalty associated with the freezing of the two extra internal degrees of freedom using an empirical correction of 0.6 kcal/mol per rotatable bond.[108,109]

Finally, molecular dynamics simulations were run to further check the stability of the proposed binding mode for compounds **20** and **25**. Simulations were performed using the same protocol adopted in our previous studies,[31,109] which also enabled us to predict the binding mode of huprines to AChE.[110] Briefly, the enzyme was immersed in a pre-equilibrated box of TIP3P[111] water molecules. The final systems contained the protein−ligand complex and around 16 000 water molecules (about 57 000 atoms). After thermatilization at 298 K, a series of 10 ns trajectories were sampled for the different compounds in the receptor−ligand complex. The system was simulated in the NPT ensemble using periodic boundary conditions and Ewald sums for treating long-range electrostatic interactions (with the default Amber-9 parameters). All simulations were performed with the parmm99 force field of the Amber-9 package. The structural analysis was performed using in-house software and standard codes (PTRAJ module) of Amber-9.

In Vitro BBB Permeation Assay. Prediction of the brain penetration was evaluated using a parallel artificial membrane permeation assay (PAMPA) in a similar manner as described previously.[39,52,95−98] Commercial drugs, phosphate buffered saline solution at pH 7.4 (PBS), and dodecane were purchased from Sigma, Aldrich, Acros, and Fluka. Millex filter units (PVDF membrane, diameter 25 mm, pore size 0.45 μm) were acquired from Millipore. The porcine brain lipid (PBL) was obtained from Avanti Polar Lipids. The donor microplate was a 96-well filter plate (PVDF membrane, pore size 0.45 μm), and the acceptor microplate was an indented 96-well plate, both from Millipore. The acceptor 96-well microplate was filled with 180 μL of PBS/EtOH (80:20 or 70:30), and the filter surface of the donor microplate was impregnated with 4 μL of PBL in dodecane (20 mg mL^{-1}). Compounds were dissolved in PBS/EtOH (80:20 or 70:30) at 1 mg mL^{-1}, filtered through a Millex filter, and then added to the donor wells (180 μL). The donor filter plate was carefully put on the acceptor plate to form a sandwich, which was left undisturbed for 120 min at 25 °C. After incubation, the donor plate was carefully removed and the concentration of compounds in the acceptor wells was determined by UV spectroscopy. Every sample was analyzed at five wavelengths, in four wells, and at least in three independent runs, and the results are given as the mean ± standard deviation. In each experiment, 15 quality control standards of known BBB permeability were included to validate the analysis set.

Acknowledgment. Financial support from the Ministerio de Ciencia y Tecnología (MCT) and FEDER (Grants CTQ2008-03768/PPQ, BQU2006-03794, SAF2008-05595, SAF2006-04339, SAF2006-01249), Generalitat de Catalunya (Grants 2005-SGR00180, 2005-SGR00662), MIUR (Grant PRIN 2007) (Rome, Italy), and EU's 7FP funding (BISNES, Grants NMP-2007-1.1-1 and GA n. 214538) and fellowships for C.G. (IBUB) and Ó.H. (MCT) are acknowledged.

Supporting Information Available: Experimental procedures, spectral and analytical data of synthesized compounds (except for **9**−**14**, **17c**,**e**, and **28c**,**e**, **18**, and **27**, herein described); solution stability study with **23**; table with pK_a values of selected compounds; tables and figures with additional data on docking and molecular dynamics; PAMPA-BBB studies. This material is available free of charge via the Internet at http://pubs.acs.org.

References

(1) Inestrosa, N. C.; Alvarez, A.; Pérez, C. A.; Moreno, R. D.; Vicente, M.; Linker, C.; Casanueva, O. I.; Soto, C.; Garrido, J. Acetylcholinesterase Accelerates Assembly of Amyloid-**β**-peptides into Alzheimer's Fibrils: Possible Role of the Peripheral Site of the Enzyme. *Neuron* **1996**, *16*, 881–891.

(2) Inestrosa, N. C.; Dinamarca, M. C.; Alvarez, A. Amyloid−Cholinesterase Interactions. Implications for Alzheimer's Disease. *FEBS J.* **2008**, *275*, 625–632.

(3) Rees, T.; Hammond, P. I.; Soreq, H.; Younkin, S.; Brimijoin, S. Acetylcholinesterase Promotes Beta-Amyloid Plaques in Cerebral Cortex. *Neurobiol. Aging* **2003**, *24*, 777–787.

(4) Rees, T. M.; Berson, A.; Sklan, E. H.; Younkin, L.; Younkin, S.; Brimijoin, S.; Soreq, H. Memory Deficits Correlating with Acetylcholinesterase Splice Shift and Amyloid Burden in Doubly Transgenic Mice. *Curr. Alzheimer Res.* **2005**, *2*, 291–300.

(5) De Ferrari, G. V.; Canales, M. A.; Shin, I.; Weiner, L. M.; Silman, I.; Inestrosa, N. C. A Structural Motif of Acetylcholinesterase That Promotes Amyloid Beta-Peptide Fibril Formation. *Biochemistry* **2001**, *40*, 10447–10457.

(6) Johnson, G.; Moore, S. W. The Peripheral Anionic Site of Acetylcholinesterase: Structure, Functions and Potential Role in Rational Drug Design. *Curr. Pharm. Des.* **2006**, *12*, 217–225.

(7) Harel, M.; Schalk, I.; Ehret-Sabatier, L.; Bouet, F.; Goeldner, M.; Hirth, C.; Axelsen, P. H.; Silman, I.; Sussman, J. L. Quaternary Ligand Binding to Aromatic Residues in the Active-Site Gorge of Acetylcholinesterase. *Proc. Natl. Acad. Sci. U.S.A.* **1993**, *90*, 9031–9035.

(8) Castro, A.; Martinez, A. Peripheral and Dual Binding Site Acetylcholinesterase Inhibitors: Implications in Treatment of Alzheimer's Disease. *Mini-Rev. Med. Chem.* **2001**, *1*, 267–272.

(9) Du, D.-M.; Carlier, P. R. Development of Bivalent Acetylcholinesterase Inhibitors as Potential Therapeutic Drugs for Alzheimer's Disease. *Curr. Pharm. Des.* **2004**, *10*, 3141–3156.

(10) Recanatini, M.; Valenti, P. Acetylcholinesterase Inhibitors as a Starting Point towards Improved Alzheimer's Disease Therapeutics. *Curr. Pharm. Des.* **2004**, *10*, 3157–3166.

(11) Muñoz-Torrero, D.; Camps, P. Dimeric and Hybrid Anti-Alzheimer Drug Candidates. *Curr. Med. Chem.* **2006**, *13*, 763–771.

(12) Castro, A.; Martinez, A. Targeting Beta-Amyloid Pathogenesis through Acetylcholinesterase Inhibitors. *Curr. Pharm. Des.* **2006**, *12*, 4377–4387.

(13) Li, W. M.; Kan, K. K. W.; Carlier, P. R.; Pang, Y. P.; Han, Y. F. East Meets West in the Search for Alzheimer's Therapeutics—Novel Dimeric Inhibitors from Tacrine and Huperzine A. *Curr. Alzheimer Res.* **2007**, *4*, 386–396.

(14) Holzgrabe, U.; Kapková, P.; Alptüzün, V.; Scheiber, J.; Kugelmann, E. Targeting Acetylcholinesterase To Treat Neurodegeneration. *Expert Opin. Ther. Targets* **2007**, *11*, 161–179.

(15) Musial, A.; Bajda, M.; Malawska, B. Recent Developments in Cholinesterases Inhibitors for Alzheimer's Disease Treatment. *Curr. Med. Chem.* **2007**, *14*, 2654–2679.

(16) Haviv, H.; Wong, D. M.; Silman, I.; Sussman, J. L. Bivalent Ligands Derived from Huperzine A as Acetylcholinesterase Inhibitors. *Curr. Top. Med. Chem.* **2007**, *7*, 375–387.

(17) Cavalli, A.; Bolognesi, M. L.; Minarini, A.; Rosini, M.; Tumiatti, V.; Recanatini, M.; Melchiorre, C. Multi-Target-Directed Ligands To Combat Neurodegenerative Diseases. *J. Med. Chem.* **2008**, *51*, 347–372.

(18) Muñoz-Torrero, D. Acetylcholinesterase Inhibitors as Disease-Modifying Therapies for Alzheimer's Disease. *Curr. Med. Chem.* **2008**, *15*, 2433–2455.

(19) Piazzi, L.; Rampa, A.; Bisi, A.; Gobbi, S.; Belluti, F.; Cavalli, A.; Bartolini, M.; Andrisano, V.; Valenti, P.; Recanatini, M. 3-(4-{[Benzyl(methyl)amino]methyl}phenyl)-6,7-dimethoxy-2*H*-2-chromenone (AP2238) Inhibits Both Acetylcholinesterase and Acetylcholinesterase-Induced β-Amyloid Aggregation: A Dual Function Lead for Alzheimer's Disease Therapy. *J. Med. Chem.* **2003**, *46*, 2279–2282.

(20) Tumiatti, V.; Andrisano, V.; Banzi, R.; Bartolini, M.; Minarini, A.; Rosini, M.; Melchiorre, C. Structure−Activity Relationships of Acetylcholinesterase Noncovalent Inhibitors Based on a Polyamine Backbone. 3. Effect of Replacing the Inner Polymethylene Chain with Cyclic Amines. *J. Med. Chem.* **2004**, *47*, 6490–6498.

(21) Bolognesi, M. L.; Andrisano, V.; Bartolini, M.; Banzi, R.; Melchiorre, C. Propidium-Based Polyamine Ligands as Potent Inhibitors of Acetylcholinesterase and Acetylcholinesterase-Induced Amyloid-β Aggregation. *J. Med. Chem.* **2005**, *48*, 24–27.

(22) Rosini, M.; Andrisano, V.; Bartolini, M.; Bolognesi, M. L.; Hrelia, P.; Minarini, A.; Tarozzi, A.; Melchiorre, C. Rational Approach To Discover Multipotent Anti-Alzheimer Drugs. *J. Med. Chem.* **2005**, *48*, 360–363.

(23) Muñoz-Ruiz, P.; Rubio, L.; García-Palomero, E.; Dorronsoro, I.; del Monte-Millán, M.; Valenzuela, R.; Usán, P.; de Austria, C.; Bartolini, M.; Andrisano, V.; Bidon-Chanal, A.; Orozco, M.; Luque, F. J.; Medina, M.; Martínez, A. Design, Synthesis, and Biological Evaluation of Dual Binding Site Acetylcholinesterase Inhibitors: New Disease-Modifying Agents for Alzheimer's Disease. *J. Med. Chem.* **2005**, *48*, 7223–7233.

(24) Belluti, F.; Rampa, A.; Piazzi, L.; Bisi, A.; Gobbi, S.; Bartolini, M.; Andrisano, V.; Cavalli, A.; Recanatini, M.; Valenti, P. Cholinesterase Inhibitors: Xanthostigmine Derivatives Blocking the Acetylcholinesterase-Induced β-Amyloid Aggregation. *J. Med. Chem.* **2005**, *48*, 4444–4456.

(25) Piazzi, L.; Cavalli, A.; Belluti, F.; Bisi, A.; Gobbi, S.; Rizzo, S.; Bartolini, M.; Andrisano, V.; Recanatini, M.; Rampa, A. Extensive SAR and Computational Studies of 3-{4-[(Benzylmethylamino)methyl]phenyl}-6,7-dimethoxy-2*H*-2-chromenone (AP2238) Derivatives. *J. Med. Chem.* **2007**, *50*, 4250–4254.

(26) Cavalli, A.; Bolognesi, M. L.; Capsoni, S.; Andrisano, V.; Bartolini, M.; Margotti, E.; Cattaneo, A.; Recanatini, M.; Melchiorre, C. A Small Molecule Targeting the Multifactorial Nature of Alzheimer's Disease. *Angew. Chem., Int. Ed.* **2007**, *46*, 3689–3692.

(27) Bolognesi, M. L.; Banzi, R.; Bartolini, M.; Cavalli, A.; Tarozzi, A.; Andrisano, V.; Minarini, A.; Rosini, M.; Tumiatti, V.; Bergamini, C.; Fato, R.; Lenaz, G.; Hrelia, P.; Cattaneo, A.; Recanatini, M.; Melchiorre, C. Novel Class of Quinone-Bearing Polyamines as Multi-Target-Directed Ligands To Combat Alzheimer's Disease. *J. Med. Chem.* **2007**, *50*, 4882–4897.

(28) Bolognesi, M. L.; Cavalli, A.; Valgimigli, L.; Bartolini, M.; Rosini, M.; Andrisano, V.; Recanatini, M.; Melchiorre, C. Multi-Target-Directed Drug Design Strategy: From a Dual Binding Site Acetylcholinesterase Inhibitor to a Trifunctional Compound against Alzheimer's Disease. *J. Med. Chem.* **2007**, *50*, 6446–6449.

(29) Kwon, Y. E.; Park, J. Y.; No, K. T.; Shin, J. H.; Lee, S. K.; Eun, J. S.; Yang, J. H.; Shin, T. Y.; Kim, D. K.; Chae, B. S.; Leem, J.-Y.; Kim, K. H. Synthesis, in Vitro Assay, and Molecular Modeling of New Piperidine Derivatives Having Dual Inhibitory Potency against Acetylcholinesterase and Aβ_{1-42} Aggregation for Alzheimer's Disease Therapeutics. *Bioorg. Med. Chem.* **2007**, *15*, 6596–6607.

(30) Xie, Q.; Wang, H.; Xia, Z.; Lu, M.; Zhang, W.; Wang, X.; Fu, W.; Tang, Y.; Sheng, W.; Li, W.; Zhou, W.; Zhu, X.; Qiu, Z.; Chen, H. Bis-(−)-nor-meptazinols as Novel Nanomolar Cholinesterase Inhibitors with High Inhibitory Potency on Amyloid-β Aggregation. *J. Med. Chem.* **2008**, *51*, 2027–2036.

(31) Camps, P.; Formosa, X.; Galdeano, C.; Gómez, T.; Muñoz-Torrero, D.; Scarpellini, M.; Viayna, E.; Badia, A.; Clos, M. V.; Camins, A.; Pallàs, M.; Bartolini, M.; Mancini, F.; Andrisano, V.; Estelrich, J.; Lizondo, M.; Bidon-Chanal, A.; Luque, F. J. Novel Donepezil-Based Inhibitors of Acetyl- and Butyrylcholinesterase and Acetylcholinesterase-Induced β-Amyloid Aggregation. *J. Med. Chem.* **2008**, *51*, 3588–3598.

(32) Rosini, M.; Simoni, E.; Bartolini, M.; Cavalli, A.; Ceccarini, L.; Pascu, N.; McClymont, D. W.; Tarozzi, A.; Bolognesi, M. L.; Minarini, A.; Tumiatti, V.; Andrisano, V.; Mellor, I. R.; Melchiorre, C. Inhibition of Acetylcholinesterase, β-Amyloid Aggregation, and NMDA Receptors in Alzheimer's Disease: A Promising Direction for the Multi-Target-Directed Ligands Gold Rush. *J. Med. Chem.* **2008**, *51*, 4381–4384.

(33) Tumiatti, V.; Milelli, A.; Minarini, A.; Rosini, M.; Bolognesi, M. L.; Micco, M.; Andrisano, V.; Bartolini, M.; Mancini, F.; Recanatini, M.; Cavalli, A.; Melchiorre, C. Structure−Activity Relationships of Acetylcholinesterase Noncovalent Inhibitors Based on a Polyamine Backbone. 4. Further Investigation on the Inner Spacer. *J. Med. Chem.* **2008**, *51*, 7308–7312.

(34) Bolognesi, M. L.; Bartolini, M.; Rosini, M.; Andrisano, V.; Melchiorre, C. Structure−Activity Relationships of Memoquin: Influence of the Chain Chirality in the Multi-Target Mechanism of Action. *Bioorg. Med. Chem. Lett.* **2009**, *19*, 4312–4315.

(35) García-Palomero, E.; Muñoz, P.; Usan, P.; Garcia, P.; De Austria, C.; Valenzuela, R.; Rubio, L.; Medina, M.; Martínez, A. Potent β-Amyloid Modulators. *Neurodegener. Dis.* **2008**, *5*, 153–156.

(36) Pang, Y.-P.; Quiram, P.; Jelacic, T.; Hong, F.; Brimijoin, S. Highly Potent, Selective, and Low Cost Bis-tetrahydroaminacrine Inhibitors of Acetylcholinesterase. *J. Biol. Chem.* **1996**, *271*, 23646–23649.

(37) Zhang, L.; Yu, H.; Li, W. M.; Cheung, M. C.; Pang, Y. P.; Gu, Z. M.; Chan, K.; Wang, Y. T.; Zuo, Z.; Han, Y. F. Preclinical Characterization of Intestinal Absorption and Metabolism of Promising Anti-Alzheimer's Dimer Bis(7)-tacrine. *Int. J. Pharm.* **2008**, *357*, 85–94.

(38) http://www.noscira.com.

(39) Rodríguez-Franco, M. I.; Fernández-Bachiller, M. I.; Pérez, C.; Hernández-Ledesma, B.; Bartolomé, B. Novel Tacrine−Melatonin Hybrids as Dual-Acting Drugs for Alzheimer Disease, with Improved Acetylcholinesterase Inhibitory and Antioxidant Properties. *J. Med. Chem.* **2006**, *49*, 459–462.

(40) Gemma, S.; Gabellieri, E.; Huleatt, P.; Fattorusso, C.; Borriello, M.; Catalanotti, B.; Butini, S.; De Angelis, M.; Novellino, E.; Nacci, V.; Belinskaya, T.; Saxena, A.; Campiani, G. Discovery of Huperzine A−Tacrine Hybrids as Potent Inhibitors of Human Cholinesterases Targeting Their Midgorge Recognition Sites. *J. Med. Chem.* **2006**, *49*, 3421–3425.

(41) Decker, M. Homobivalent Quinazolinimines as Novel Nanomolar Inhibitors of Cholinesterases with Dirigible Selectivity toward Butyrylcholinesterase. *J. Med. Chem.* **2006**, *49*, 5411–5413.
(42) Elsinghorst, P. W.; González Tanarro, C. M.; Gütschow, M. Novel Heterobivalent Tacrine Derivatives as Cholinesterase Inhibitors with Notable Selectivity toward Butyrylcholinesterase. *J. Med. Chem.* **2006**, *49*, 7540–7544.
(43) Sauvaïtre, T.; Barlier, M.; Herlem, D.; Gresh, N.; Chiaroni, A.; Guenard, D.; Guillou, C. New Potent Acetylcholinesterase Inhibitors in the Tetracyclic Triterpene Series. *J. Med. Chem.* **2007**, *50*, 5311–5323.
(44) Elsinghorst, P. W.; Cieslik, J. S.; Mohr, K.; Tränkle, C.; Gütschow, M. First Gallamine−Tacrine Hybrid: Design and Characterization at Cholinesterases and the M_2 Muscarinic Receptor. *J. Med. Chem.* **2007**, *50*, 5685–5695.
(45) He, X.-C.; Feng, S.; Wang, Z.-F.; Shi, Y.; Zheng, S.; Xia, Y.; Jiang, H.; Tang, X.-C.; Bai, D. Study on Dual-Site Inhibitors of Acetylcholinesterase: Highly Potent Derivatives of Bis- and Bifunctional Huperzine B. *Bioorg. Med. Chem.* **2007**, *15*, 1394–1408.
(46) Butini, S.; Campiani, G.; Borriello, M.; Gemma, S.; Panico, A.; Persico, M.; Catalanotti, B.; Ros, S.; Brindisi, M.; Agnusdei, M.; Fiorini, I.; Nacci, V.; Novellino, E.; Belinskaya, T.; Saxena, A.; Fattorusso, C. Exploiting Protein Fluctuations at the Active-Site Gorge of Human Cholinesterases: Further Optimization of the Design Strategy To Develop Extremely Potent Inhibitors. *J. Med. Chem.* **2008**, *51*, 3154–3170.
(47) Pan, L.; Tan, J.-H.; Hou, J.-Q.; Huang, S.-L.; Gu, L.-Q.; Huang, Z.-S. Design, Synthesis and Evaluation of Isaindigotone Derivatives as Acetylcholinesterase and Butyrylcholinesterase Inhibitors. *Bioorg. Med. Chem. Lett.* **2008**, *18*, 3790–3793.
(48) Butini, S.; Guarino, E.; Campiani, G.; Brindisi, M.; Coccone, S. S.; Fiorini, I.; Novellino, E.; Belinskaya, T.; Saxena, A.; Gemma, S. Tacrine Based Human Cholinesterase Inhibitors: Synthesis of Peptidic-Tethered Derivatives and Their Effect on Potency and Selectivity. *Bioorg. Med. Chem. Lett.* **2008**, *18*, 5213–5216.
(49) Bembenek, S. D.; Keith, J. M.; Letavic, M. A.; Apodaca, R.; Barbier, A. J.; Dvorak, L.; Aluisio, L.; Miller, K. L.; Lovenberg, T. W.; Carruthers, N. I. Lead Identification of Acetylcholinesterase Inhibitors−Histamine H_3 Receptor Antagonists from Molecular Modeling. *Bioorg. Med. Chem.* **2008**, *16*, 2968–2973.
(50) Leonetti, F.; Catto, M.; Nicolotti, O.; Pisani, L.; Cappa, A.; Stefanachi, A.; Carotti, A. Homo- and Hetero-Bivalent Edrophonium-Like Ammonium Salts as Highly Potent, Dual Binding Site AChE Inhibitors. *Bioorg. Med. Chem.* **2008**, *16*, 7450–7456.
(51) Shen, Y.; Sheng, R.; Zhang, J.; He, Q.; Yang, B.; Hu, Y. 2-Phenoxy-indan-1-one Derivatives as Acetylcholinesterase Inhibitors: A Study on the Importance of Modifications at the Side Chain on the Activity. *Bioorg. Med. Chem.* **2008**, *16*, 7646–7653.
(52) Fernández-Bachiller, M. I.; Pérez, C.; Campillo, N. E.; Páez, J. A.; González-Muñoz, G. C.; Usán, P.; García-Palomero, E.; López, M. G.; Villarroya, M.; García, A. G.; Martínez, A.; Rodríguez-Franco, M. I. Tacrine−Melatonin Hybrids as Multifunctional Agents for Alzheimer's Disease, with Cholinergic, Antioxidant, and Neuroprotective Properties. *ChemMedChem* **2009**, *4*, 828–841.
(53) Bourne, Y.; Taylor, P.; Radić, Z.; Marchot, P. Structural Insights into Ligand Interactions at the Acetylcholinesterase Peripheral Anionic Site. *EMBO J.* **2003**, *22*, 1–12.
(54) Cavalli, A.; Bottegoni, G.; Raco, C.; De Vivo, M.; Recanatini, M. A Computational Study of the Binding of Propidium to the Peripheral Anionic Site of Human Acetylcholinesterase. *J. Med. Chem.* **2004**, *47*, 3991–3999.
(55) Jiménez, O.; de la Rosa, G.; Lavilla, R. Straightforward Access to a Structurally Diverse Set of Oxacyclic Scaffolds through a Four-Component Reaction. *Angew. Chem., Int. Ed.* **2005**, *44*, 6521–6525.
(56) Hu, M.-K.; Wu, L.-J.; Hsiao, G.; Yen, M.-H. Homodimeric Tacrine Congeners as Acetylcholinesterase Inhibitors. *J. Med. Chem.* **2002**, *45*, 2277–2282.
(57) Alonso, D.; Dorronsoro, I.; Rubio, L.; Muñoz, P.; García-Palomero, E.; Del Monte, M.; Bidon-Chanal, A.; Orozco, M.; Luque, F. J.; Castro, A.; Medina, M.; Martínez, A. Donepezil−Tacrine Hybrid Related Derivatives as New Dual Binding Site Inhibitors of AChE. *Bioorg. Med. Chem.* **2005**, *13*, 6588–6597.
(58) Povarov, L. S. **α,β**-Unsaturated Ethers and Their Analogues in Reactions of Diene Synthesis. *Russ. Chem. Rev.* **1967**, *36*, 656–670.
(59) Jakobsen, C. M.; Denmeade, S. R.; Isaacs, J. T.; Gady, A.; Olsen, C. E.; Christensen, S. B. Design, Synthesis, and Pharmacological Evaluation of Thapsigargin Analogues for Targeting Apoptosis to Prostatic Cancer Cells. *J. Med. Chem.* **2001**, *44*, 4696–4703.
(60) Carlier, P. R.; Han, Y. F.; Chow, E. S.-H.; Li, C. P.-L.; Wang, H.; Lieu, T. X.; Wong, H. S.; Pang, Y.-P. Evaluation of Short-Tether Bis-THA AChE Inhibitors. A Further Test of the Dual Binding Site Hypothesis. *Bioorg. Med. Chem.* **1999**, *7*, 351–357.
(61) Carlier, P. R.; Chow, E. S.-H.; Han, Y.; Liu, J.; El Yazal, J.; Pang, Y.-P. Heterodimeric Tacrine-Based Acetylcholinesterase Inhibitors: Investigating Ligand−Peripheral Site Interactions. *J. Med. Chem.* **1999**, *42*, 4225–4231.
(62) Hu, M. -K.; Lu, C.-F. A Facile Synthesis of Bis-Tacrine Isosteres. *Tetrahedron Lett.* **2000**, *41*, 1815–1818.
(63) Hu, M.-K.; Shaw, J. Tacrine Derivatives for Treating Alzheimer's Disease. WO 01/17529 A1, 2001.
(64) Ellman, G. L.; Courtney, K. D.; Andres, B., Jr.; Featherstone, R. M. A New and Rapid Colorimetric Determination of Acetylcholinesterase Activity. *Biochem. Pharmacol.* **1961**, *7*, 88–95.
(65) Savini, L.; Gaeta, A.; Fattorusso, C.; Catalanotti, B.; Campiani, G.; Chiasserini, L.; Pellerano, C.; Novellino, E.; McKissic, D.; Saxena, A. Specific Targeting of Acetylcholinesterase and Butyrylcholinesterase Recognition Sites. Rational Design of Novel, Selective, and Highly Potent Cholinesterase Inhibitors. *J. Med. Chem.* **2003**, *46*, 1–4.
(66) Savini, L.; Campiani, G.; Gaeta, A.; Pellerano, C.; Fattorusso, C.; Chiasserini, L.; Fedorko, J. M.; Saxena, A. Novel and Potent Tacrine-Related Hetero- and Homobivalent Ligands for Acetylcholinesterase and Butyrylcholinesterase. *Bioorg. Med. Chem. Lett.* **2001**, *11*, 1779–1782.
(67) Muñoz-Muriedas, J.; López, J. M.; Orozco, M.; Luque, F. J. Molecular Modelling Approaches to the Design of Acetylcholinesterase Inhibitors: New Challenges for the Treatment of Alzheimer's Disease. *Curr. Pharm. Des.* **2004**, *10*, 3131–3140.
(68) Silman, I.; Sussman, J. L. Acetylcholinesterase: "Classical" and "Non-Classical" Functions and Pharmacology. *Curr. Opin. Pharmacol.* **2005**, *5*, 293–302.
(69) Dvir, H.; Wong, D. M.; Harel, M.; Barril, X.; Orozco, M.; Luque, F. J.; Muñoz-Torrero, D.; Camps, P.; Rosenberry, T. L.; Silman, I.; Sussman, J. L. 3D Structure of *Torpedo californica* Acetylcholinesterase Complexed with Huprine X at 2.1 Å Resolution: Kinetic and Molecular Dynamics Correlates. *Biochemistry* **2002**, *41*, 2970–2981.
(70) Rydberg, E. H.; Brumshtein, B.; Greenblatt, H. M.; Wong, D. M.; Shaya, D.; Williams, L. D.; Carlier, P. R.; Pang, Y.-P.; Silman, I.; Sussman, J. L. Complexes of Alkylene-Linked Tacrine Dimers with *Torpedo californica* Acetylcholinesterase: Binding of Bis(5)-Tacrine Produces a Dramatic Rearrangement in the Active-Site Gorge. *J. Med. Chem.* **2006**, *49*, 5491–5500.
(71) Colletier, J. P.; Sanson, B.; Nachon, F.; Gabellieri, E.; Fattorusso, C.; Campiani, G.; Weik, M. Conformational Flexibility in the Peripheral Site of *Torpedo californica* Acetylcholinesterase Revealed by the Complex Structure with a Bifunctional Inhibitor. *J. Am. Chem. Soc.* **2006**, *128*, 4526–4527.
(72) Haviv, H.; Wong, D. M.; Greenblatt, H. M.; Carlier, P. R.; Pang, Y.-P.; Silman, I.; Sussman, J. L. Crystal Packing Mediates Enantioselective Ligand Recognition at the Peripheral Site of Acetylcholinesterase. *J. Am. Chem. Soc.* **2005**, *127*, 11029–11036.
(73) Bourne, Y.; Kolb, H. C.; Radic, Z; Sharpless, K. B.; Taylor, P.; Marchot, P. Freeze-Frame Inhibitor Captures Acetylcholinesterase in a Unique Conformation. *Proc. Natl. Acad. Sci. U.S.A.* **2004**, *101*, 1449–1454.
(74) Senapati, S.; Bui, J. M.; McCammon, J. A. Induced Fit in Mouse Acetylcholinesterase upon Binding a Femtomolar Inhibitor: A Molecular Dynamics Study. *J. Med. Chem.* **2005**, *48*, 8155–8162.
(75) Sussman, J. L.; Harel, M.; Frolow, F.; Oefner, C.; Goldman, A.; Toker, L.; Silman, I. Atomic Structure of Acetylcholinesterase from *Torpedo californica*: A Prototypic Acetylcholine-Binding Protein. *Science* **1991**, *253*, 872–879.
(76) Raves, M. L.; Harel, M.; Pang, Y.-P.; Silman, I.; Kozikowski, A. P.; Sussman, J. L. Structure of Acetylcholinesterase Complexed with the Nootropic Alkaloid, (−)-Huperzine A. *Nat. Struct. Biol.* **1997**, *4*, 57–63.
(77) Kryger, G.; Silman, I.; Sussman, J. L. Structure of Acetylcholinesterase Complexed with E2020 (Aricept): Implications for the Design of New Anti-Alzheimer Drugs. *Structure* **1999**, *7*, 297–307.
(78) Kryger, G.; Harel, M.; Giles, K.; Toker, L.; Velan, B.; Lazar, A.; Kronman, C.; Barak, D.; Ariel, N.; Shafferman, A.; Silman, I.; Sussman, J. L. Structures of Recombinant Native and E202Q Mutant Human Acetylcholinesterase Complexed with the Snake-Venom Toxin Fasciculin-II. *Acta Crystallogr., Sect. D: Biol. Crystallogr.* **2000**, *56*, 1385–1394.
(79) Lyne, P. D.; Lamb, M.; Saeh, J. C. Accurate Prediction of the Relative Potencies of Members of a Series of Kinase Inhibitors Using Molecular Docking and MM-GBSA Scoring. *J. Med. Chem.* **2006**, *49*, 4805–4808.
(80) Weis, A.; Katebzadeh, K.; Soderhjelm, P.; Nilsson, I.; Ryde, U. Ligand Affinities Predicted with the MM/PBSA Method: Dependence

on the Simulation Method and the Force Field. *J. Med. Chem.* **2006**, *49*, 6596–6606.
(81) Stoica, I.; Sadiq, S. K.; Coveney, P. V. Rapid and Accurate Prediction of Binding Free Energies for Saquinavir-Bound HIV-1 Proteases. *J. Am. Chem. Soc.* **2008**, *130*, 2639–2648.
(82) Barril, X.; Gelpí, J. L.; López, J. M.; Orozco, M.; Luque, F. J. How Accurate Can Molecular Dynamics/Linear Response and Poisson−Boltzmann/Solvent Accessible Surface Calculations Be for Predicting Relative Binding Affinities? Acetylcholinesterase Huprine Inhibitors as a Test Case. *Theor. Chem. Acc.* **2001**, *106*, 2–9.
(83) Giacobini, E. Cholinesterase Inhibitors: New Roles and Therapeutic Alternatives. *Pharmacol. Res.* **2004**, *50*, 433–440.
(84) Lane, R. M.; Potkin, S. G.; Enz, A. Targeting Acetylcholinesterase and Butyrylcholinesterase in Dementia. *Int. J. Neuropsychopharmacol.* **2005**, *9*, 1–24.
(85) Gregor, V. E.; Emmerling, M. R.; Lee, C.; Moore, C. J. The Synthesis and in Vitro Acetylcholinesterase and Butyrylcholinesterase Inhibitory Activity of Tacrine (Cognex) Derivatives. *Bioorg. Med. Chem. Lett.* **1992**, *2*, 861–864.
(86) Wlodek, S. T.; Antosiewicz, J.; McCammon, J. A.; Straatsma, T. P.; Gilson, M. K.; Briggs, J. M.; Humblet, C.; Sussman, J. L. Binding of Tacrine and 6-Chlorotacrine by Acetylcholinesterase. *Biopolymers* **1996**, *38*, 109–117.
(87) Recanatini, M.; Cavalli, A.; Belluti, F.; Piazzi, L.; Rampa, A.; Bisi, A.; Gobbi, S.; Valenti, P.; Andrisano, V.; Bartolini, M.; Cavrini, V. SAR of 9-Amino-1,2,3,4-tetrahydroacridine-Based Acetylcholinesterase Inhibitors: Synthesis, Enzyme Inhibitory Activity, QSAR, and Structure-Based CoMFA of Tacrine Analogues. *J. Med. Chem.* **2000**, *43*, 2007–2018.
(88) Bartolini, M.; Bertucci, C.; Cavrini, V.; Andrisano, V. β-Amyloid Aggregation Induced by Human Acetylcholinesterase: Inhibition Studies. *Biochem. Pharmacol.* **2003**, *65*, 407–416.
(89) Jakob-Roetne, R.; Jacobsen, H. Alzheimer's Disease: From Pathology to Therapeutic Approaches. *Angew. Chem., Int. Ed.* **2009**, *48*, 3030–3059.
(90) Mancini, F.; Naldi, M.; Cavrini, V.; Andrisano, V. Multiwell Fluorometric and Colorimetric Microassays for the Evaluation of Beta-Secretase (BACE-1) Inhibitors. *Anal. Bioanal. Chem.* **2007**, *388*, 1175–1183.
(91) Fu, H.; Li, W.; Luo, J.; Lee, N. T. K.; Li, M.; Tsim, K. W. K.; Pang, Y.; Youdim, M. B. H.; Han, Y. Promising Anti-Alzheimer's Dimer Bis(7)-tacrine Reduces β-Amyloid Generation by Directly Inhibiting BACE-1 Activity. *Biochem. Biophys. Res. Commun.* **2008**, *366*, 631–636.
(92) Rosini, M.; Andrisano, V.; Bartolini, M.; Melchiorre, C. Organic Compounds Useful for the Treatment of Alzheimer's Disease, Their Use and Method of Preparation. WO 2006/080043 A2, 2006.
(93) Piazzi, L.; Cavalli, A.; Colizzi, F.; Belluti, F.; Bartolini, M.; Mancini, F.; Recanatini, M.; Andrisano, V.; Rampa, A. Multi-Target-Directed Coumarin Derivatives: hAChE and BACE1 Inhibitors as Potential Anti-Alzheimer Compounds. *Bioorg. Med. Chem.* **2008**, *18*, 423–426.
(94) Hanessian, S.; Yun, H.; Hou, Y.; Yang, G.; Bayrakdarian, M.; Therrien, E.; Moitessier, N.; Roggo, S.; Veenstra, S.; Tintelnot-Blomley, M.; Rondeau, J.-M.; Ostermeier, C.; Strauss, A.; Ramage, P.; Paganetti, P.; Neumann, U.; Betschart, C. Structure-Based Design, Synthesis, and Memapsin 2 (BACE) Inhibitory Activity of Carbocyclic and Heterocyclic Peptidomimetics. *J. Med. Chem.* **2005**, *48*, 5175–5190.
(95) Di, L.; Kerns, E. H.; Fan, K.; McConnell, O. J.; Carter, G. T. High Throughput Artificial Membrane Permeability Assay for Blood−Brain Barrier. *Eur. J. Med. Chem.* **2003**, *38*, 223–232.
(96) Reviriego, F.; Rodríguez-Franco, M. I.; Navarro, P.; García-España, E.; Liu-González, M.; Verdejo, B.; Domènech, A. The Sodium Salt of Diethyl 1*H*-Pyrazole-3,5-dicarboxylate as an Efficient Amphiphilic Receptor for Dopamine and Amphetamines. Crystal Structure and Solution Studies. *J. Am. Chem. Soc.* **2006**, *128*, 16458–16459.
(97) Pavón, F. J.; Hernández-Folgado, L.; Bilbao, A.; Cippitelli, A.; Jagerovic, N.; Abellán, G.; Rodríguez-Franco, M. I.; Serrano, A.; Macías, M.; Navarro, M.; Goya, P.; Rodríguez de Fonseca, F. Antiobesity Effects of the Novel in Vivo Neutral Cannabinoid Receptor Antagonist 5-(4-Chlorophenyl)-1-(2,4-dichlorophenyl)-3-hexyl-1*H*-1,2,4-triazole—LH 21. *Neuropharmacology* **2006**, *51*, 358–366.
(98) Marco-Contelles, J.; León, R.; de los Ríos, C.; Samadi, A.; Bartolini, M.; Andrisano, V.; Huertas, O.; Barril, X.; Luque, F. J.; Rodríguez-Franco, M. I.; López, B.; López, M. G.; García, A. G.; Carreiras, M. C.; Villarroya, M. Tacripyrines, the First Tacrine−Dihydropyridine Hybrids, as Multitarget-Directed Ligands for the Treatment of Alzheimer's Disease. *J. Med. Chem.* **2009**, *52*, 2724–2732.
(99) Bartolini, M.; Bertucci, C.; Bolognesi, M. L.; Cavalli, A.; Melchiorre, C.; Andrisano, V. Insight into the Kinetic of Amyloid Beta (1−42) Peptide Self-Aggregation: Elucidation of Inhibitors' Mechanism of Action. *ChemBioChem* **2007**, *8*, 2152–2161.
(100) Morley, S. D.; Afshar, M. Validation of an Empirical RNA-Ligand Scoring Function for Fast Flexible Docking Using Ribo-Dock. *J. Comput.-Aided Mol. Des.* **2004**, *18*, 189–208.
(101) Barril, X.; Hubbard, R. E.; Morley, S. D. Virtual Screening in Structure-Based Drug Discovery. *Mini-Rev. Med. Chem.* **2004**, *4*, 779–791.
(102) *ACD/pKa*, version 8.02; Advanced Chemistry Development, Inc.: Toronto, Ontario, Canada, 2006; www.acdlabs.com.
(103) Dewar, M. J. S.; Zoebisch, E. G.; Healy, E. F.; Stewart, J. J. P. AM1: A New General Purpose Quantum Mechanical Molecular Model. *J. Am. Chem. Soc.* **1985**, *107*, 3902–3909.
(104) Frisch, M. J.; Trucks, G. W.; Schlegel, H. B.; Scuseria, G. E.; Robb, M. A.; Cheeseman, J. R.; Montgomery, J. A., Jr.; Vreven, T.; Kudin, K. N.; Burant, J. C.; Millam, J. M.; Iyengar, S. S.; Tomasi, J.; Barone, V.; Mennucci, B.; Cossi, M.; Scalmani, G.; Rega, N.; Petersson, G. A.; Nakatsuji, H.; Hada, M.; Ehara, M.; Toyota, K.; Fukuda, R.; Hasegawa, J.; Ishida, M.; Nakajima, T.; Honda, Y.; Kitao, O.; Nakai, H.; Klene, M.; Li, X.; Knox, J. E.; Hratchian, H. P.; Cross, J. B.; Adamo, C.; Jaramillo, J.; Gomperts, R.; Stratmann, R. E.; Yazyev, O.; Austin, A. J.; Cammi, R.; Pomelli, C.; Ochterski, J. W.; Ayala, P. Y.; Morokuma, K.; Voth, G. A.; Salvador, P.; Dannenberg, J. J.; Zakrzewski, V. G.; Dapprich, S.; Daniels, A. D.; Strain, M. C.; Farkas, O.; Malick, D. K.; Rabuck, A. D.; Raghavachari, K.; Foresman, J. B.; Ortiz, J. V.; Cui, Q.; Baboul, A. G.; Clifford, S.; Cioslowski, J.; Stefanov, B. B.; Liu, G.; Liashenko, A.; Piskorz, P.; Komaromi, I.; Martin, R. L.; Fox, D. J.; Keith, T.; Al-Laham, M. A.; Peng, C. Y.; Nanayakkara, A.; Challacombe, M.; Gill, P. M. W.; Johnson, B.; Chen, W.; Wong, M. W.; Gonzalez, C.; Pople, J. A. *Gaussian 03*, revision B.04, Gaussian, Inc.: Pittsburgh PA, 2003.
(105) Case, D. A.; Darden, T. A.; Cheatham, T. E., III; Simmerling, C. L.; Wang, J.; Duke, R. E.; Luo, R.; Merz, K. M.; Pearlman, D. A.; Crowley, M.; Walker, R. C.; Zhang, W.; Wang, B.; Hayik, S.; Roitberg, A.; Seabra, G.; Wong, K. F.; Paesani, F.; Wu, X.; Brozell, S.; Tsui, V.; Gohlke, H.; Yang, L.; Tan, C.; Mongan, J.; Hornak, V.; Cui, G.; Beroza, P.; Mathews, D. H.; Schafmeister, C.; Ross, W. S.; Kollman, P. A. *AMBER*, version 9; University of California: San Francisco, CA, 2006.
(106) Bayly, C. I.; Cieplak, P.; Cornell, W. D.; Kollman, P. A. A Well-Behaved Electrostatic Potential Based Method Using Charge Restraints for Deriving Atomic Charges. *J. Phys. Chem.* **1993**, *97*, 10269–10280.
(107) Sitkoff, D.; Sharp, K. A.; Honig, B. Accurate Calculation of Hydration Free Energies Using Macroscopic Solvent Models. *J. Phys. Chem.* **1994**, *98*, 1978–1988.
(108) Eldridge, M. D.; Murray, C. W.; Auton, T. R.; Paolini, G. V.; Mee, R. P. Empirical Scoring Functions: I. The Development of a Fast Empirical Scoring Function To Estimate the Binding Affinity of Ligands in Receptor Complexes. *J. Comput.-Aided Mol. Des.* **1997**, *11*, 425–445.
(109) Camps, P.; Gómez, E.; Muñoz-Torrero, D.; Badia, A.; Clos, M. V.; Curutchet, C.; Muñoz-Muriedas, J.; Luque, F. J. Binding of 13-Amidohuprines to Acetylcholinesterase: Exploring the Ligand-Induced Conformational Change of the Gly117−Gly118 Peptide Bond in the Oxyanion Hole. *J. Med. Chem.* **2006**, *49*, 6833–6840.
(110) Barril, X.; Orozco, M.; Luque, F. J. Predicting Relative Binding Free Energies of Tacrine−Huperzine A Hybrids as Inhibitors of Acetylcholinesterase. *J. Med. Chem.* **1999**, *42*, 5110–5119.
(111) Jorgensen, W. L.; Chandrasekhar, J.; Madura, J. D.; Impey, R. W.; Klein, M. L. Comparison of Simple Potential Functions for Simulating Liquid Water. *J. Chem. Phys.* **1983**, *79*, 926–935.

Supporting Information for

Pyrano[3,2-c]quinoline–6-Chlorotacrine Hybrids as a Novel Family of Acetylcholinesterase- and β-Amyloid-Directed Anti-Alzheimer Compounds

Pelayo Camps,[†] Xavier Formosa,[†] Carles Galdeano,[†] Diego Muñoz-Torrero,[,†] Lorena Ramírez,[†] Elena Gómez,[‡] Nicolás Isambert,[‡] Rodolfo Lavilla,[‡,⊥] Albert Badia,[§] M. Victòria Clos,[§] Manuela Bartolini,[#] Francesca Mancini,[#] Vincenza Andrisano,[#] Mariana P. Arce,[◊] M. Isabel Rodríguez-Franco,[◊] Óscar Huertas,[//] Thomai Dafni,[//] and F. Javier Luque[//]*

[†] Laboratori de Química Farmacèutica (Unitat Associada al CSIC), Facultat de Farmàcia, and Institut de Biomedicina (IBUB), Universitat de Barcelona, Av. Diagonal 643, E-08028, Barcelona, Spain; [‡] Institute for Research in Biomedicine, Barcelona Science Park, Baldiri Reixac 10–12, E-08028, Barcelona, Spain; [⊥] Laboratori de Química Orgànica, Facultat de Farmàcia, Universitat de Barcelona, Av. Joan XXIII, s/n, E-08028, Barcelona, Spain; [§] Departament de Farmacologia, Terapèutica i Toxicologia, Institut de Neurociències, Universitat Autònoma de Barcelona, E-08193, Bellaterra, Barcelona, Spain; [#] Department of Pharmaceutical Sciences, Alma Mater Studiorum, Bologna University, Via Belmeloro 6, I-40126, Bologna, Italy; [◊] Instituto de Química Médica (CSIC), Juan de la Cierva, 3, E-28006, Madrid, Spain; [//] Departament de Fisicoquímica, Facultat de Farmàcia, and Institut de Biomedicina (IBUB), Universitat de Barcelona, Av. Diagonal 643, E-08028, Barcelona, Spain

Table of Contents

Experimental details and characterization data of new compounds

9-[(4-Aminobutyl)amino]-6-chloro-1,2,3,4-tetrahydroacridine Dihydrochloride (17a·2HCl). It was prepared following the general procedure, from **15** (1.00 g, 3.97 mmol) and 1,4-diaminobutane, **16a** (1.6 mL, 1.40 g, 15.9 mmol), but the suspension obtained after heating under reflux with magnetic stirring for 18 h, once cooled to room temperature, was diluted with AcOEt (25 mL), and extracted with aq 1N HCl (4×30 mL). The combined aqueous extracts were washed with AcOEt (5×50 mL), alkalinized with NaOH pellets and extracted with CH_2Cl_2 (4×70 mL). The combined organic extracts were dried with anhyd Na_2SO_4 and concentrated in vacuo to give a brown oily residue (1.05 g), which was subjected to column chromatography [35–70 μm silica gel (31 g), CH_2Cl_2/MeOH/50% aq NH_4OH mixtures]. On elution with CH_2Cl_2/MeOH/50% aq NH_4OH 90:10:0.2, slightly impure *bis*(4)-6-chlorotacrine, **28a** (112 mg, 11% yield), and amine **17a** (764 mg, 63% yield) were consecutively isolated as a brown and a yellow oil, respectively: $R_{f(\mathbf{17a})}$ 0.25; $R_{f(\mathbf{28a})}$ 0.75 (CH_2Cl_2/MeOH/50% aq NH_4OH 9:1:0.2).

17a·2HCl: mp 127–128 ºC (MeOH/AcOEt 1:3); IR (KBr) ν 3500–2500 (max at 3402, 3257, 3050 2935, N–H, $^+$N–H, O–H, and C–H st), 1633, 1576, and 1526 (ar–C–C and ar–C–N st) cm^{-1}; ^{1}H NMR (300 MHz, CD_3OD) δ 1.80 (m, 2H) and 1.86–2.02 (complex signal, 6H, 2-H_2, 3-H_2, 2'-H_2, and 3'-H_2), 2.71 (m, 2H, 1-H_2), 2.94–3.06 (complex signal, 4H, 4-H_2 and 4'-H_2), 4.00 (t, J = 6.6 Hz, 2H, 1'-H_2), 4.84 (s, NH, $^+$NH, and $^+NH_3$), 7.57 (broad d, $J \approx$ 9.3 Hz, 1H, 7-H), 7.79 (broad s, 1H, 5-H), 8.41 (d, J = 9.3 Hz, 1H, 8-H); ^{13}C NMR (75.4 MHz, CD_3OD) δ 21.7 (CH_2, C3), 22.9 (CH_2, C2), 25.0 (CH_2, C1), 25.7 (CH_2) and 28.3 (CH_2) (C2' and C3'), 29.4 (CH_2, C4), 40.3 (CH_2, C4'), 48.4 (CH_2, C1'), 113.6 (C, C9a), 115.5 (C, C8a), 119.1 (CH, C5), 126.9 (CH, C7), 128.7 (CH, C8), 140.0 (C, C6), 140.4 (C, C10a), 152.3 (C, C4a), 157.8 (C, C9). Anal. ($C_{17}H_{22}ClN_3$·2HCl·1.5H_2O) C, H, N.

9-[(5-Aminopentyl)amino]-6-chloro-1,2,3,4-tetrahydroacridine Dihydrochloride (17b·2HCl). It was prepared as described for **17a**, from **15** (1.00 g, 3.97 mmol) and 1,5-diaminopentane, **16b** (1.9 mL, 1.66 g, 16.3 mmol), a brown oily residue (1.42 g) was obtained and subjected to column chromatography [35–70 μm silica gel (43 g), CH_2Cl_2/MeOH/50% aq NH_4OH mixtures]. On elution with CH_2Cl_2/MeOH/50% aq NH_4OH 90:10:0.2, *bis*(5)-6-chlorotacrine, **28b** (61 mg, 6% yield), and amine **17b** (880 mg, 70% yield) were consecutively isolated as a brown and a yellow oil, respectively: $R_{f(\mathbf{17b})}$ 0.13; $R_{f(\mathbf{28b})}$ 0.82 (CH_2Cl_2/MeOH/50% aq NH_4OH 9:1:0.2).

17b·2HCl: mp 132–133 ºC (MeOH/AcOEt 1:3); IR (KBr) ν 3500–2500 (max at 3401, 3260, 3046, 2932, 2861, N–H, $^+$N–H and C–H st), 1629, 1575, 1570, and 1508 (ar–C–C and ar–C–N st) cm^{-1}; ^{1}H NMR (300 MHz, CD_3OD) δ 1.52 (m, 2H) and 1.73 (tt, $J = J' =$ 7.5 Hz, 2H) (3'-H_2 and 4'-H_2), 1.89 (tt, $J \approx J' \approx$ 7.5 Hz, 2H, 2'-H_2), superimposed in part 1.88–2.02 (complex signal, 4H, 2-H_2 and 3-H_2), 2.69 (m, 2H, 1-H_2), 2.95 (t, J = 7.5 Hz, 2H, 5'-H_2), superimposed in part 3.00 (m, 2H, 4-H_2), 3.97 (t, J = 7.2 Hz, 2H, 1'-H_2), 4.84 (s, NH, $^+$NH, and $^+NH_3$), 7.57 (dd, J = 9.6 Hz, J' = 2.1 Hz, 1H, 7-H), 7.78 (d, J = 2.1 Hz, 1H,

5-H), 8.40 (d, J = 9.6 Hz, 1H, 8-H); ^{13}C NMR (75.4 MHz, CD_3OD) δ 21.8 (CH_2, C3), 22.9 (CH_2, C2), 24.6 (CH_2, C1), 24.9 (CH_2, C3'), 28.2 (CH_2, C4'), 29.4 (CH_2, C4), 30.9 (CH_2, C2'), 40.6 (CH_2, C5'), 48.5 (CH_2, C1'), 113.4 (C, C9a), 115.5 (C, C8a), 119.1 (CH, C5), 126.8 (CH, C7), 128.8 (CH, C8), 140.1 (C, C6), 140.5 (C, C10a), 152.2 (C, C4a), 157.8 (C, C9).

28b·2HCl [*N*,*N'*-*bis*(6-chloro-1,2,3,4-tetrahydroacridin-9-yl)-1,5-pentanediamine]: mp 139–140 ºC (MeOH/AcOEt 1:5); IR (KBr) ν 3500–2500 (max at 3382, 3230, 3047, 2931, 2860, N–H, $^+$N–H, O–H, and C–H st), 1629, 1570, and 1508 (ar–C–C and ar–C–N st) cm^{-1}; ^{1}H NMR (300 MHz, CD_3OD) δ 1.57 (quint, J = 6.6 Hz, 2H, 3'-H_2), 1.84–2.02 (complex signal, 12H, 2-H_2, 3-H_2, and 2'-H_2), 2.66 (m, 4H, 1-H_2), 2.98 (m, 4H, 4-H_2), 3.96 (t, J = 6.9 Hz, 4H, 1'-H_2), 4.85 (s, NH and $^+$NH), 7.51 (broad d, $J \approx$ 9.3 Hz, 2H, 7-H), 7.76 (broad s, 2H, 5-H), 8.36 (d, J = 9.3 Hz, 2H, 8-H); ^{13}C NMR (75.4 MHz, CD_3OD) δ 21.8 (CH_2, C3), 22.9 (CH_2, C2), 24.88 (CH_2) and 24.94 (CH_2) (C1 and C3'), 29.4 (CH_2, C4), 30.9 (CH_2, C2'), 48.9 (CH_2, C1'), 113.4 (C, C9a), 115.4 (C, C8a), 119.1 (CH, C5), 126.8 (CH, C7), 128.7 (CH, C8), 140.0 (C, C6), 140.4 (C, C10a), 152.2 (C, C4a), 157.7 (C, C9). Anal. ($C_{31}H_{34}Cl_2N_4$·2HCl·2.75H_2O) C, H, N.

9-[(7-Aminoheptyl)amino]-6-chloro-1,2,3,4-tetrahydroacridine Dihydrochloride (17d·2HCl). From **15** (4.00 g, 15.9 mmol) and 1,7-diaminoheptane, **16d** (8.46 g, 65.1 mmol), a brown oily residue (6.31 g) was obtained and subjected to column chromatography [35–70 μm silica gel (76 g), CH_2Cl_2/MeOH/25% aq NH_4OH mixtures]. On elution with CH_2Cl_2/MeOH/25% aq NH_4OH 98:2:0.1, slightly impure *bis*(7)-6-chlorotacrine, **28d** (437 mg, 10% yield) was isolated as a brown oil. On elution with CH_2Cl_2/MeOH/25% aq NH_4OH 96:4:0.1 to 80:20:0.3, amine **17d** (4.30 g, 78% yield) was isolated as a yellow oil. R_f(**17d**) 0.33; R_f(**28d**) 0.81 (CH_2Cl_2/MeOH/25% aq NH_4OH 9:1:0.01).

17d·2HCl: mp 164–165 ºC (MeOH); IR (KBr) ν 3500–2500 (max at 3411, 3255, 2931, 2859, N–H, $^+$N–H and C–H st), 1629, 1572, and 1514 (ar–C–C and ar–C–N st) cm^{-1}; ^{1}H NMR (300 MHz, CD_3OD, presat/Watergate) δ 1.38–1.53 (complex signal, 6H, 3'-H_2, 4'-H_2, and 5'-H_2), 1.66 (tt, $J \approx J' \approx$ 7.5 Hz, 2H, 6'-H_2), 1.85 (tt, $J \approx J' \approx$ 7.5 Hz, 2H, 2'-H_2), 1.92–1.99 (complex signal, 4H, 2-H_2 and 3-H_2), 2.68 (m, 2H, 1-H_2), 2.91 (t, J = 7.5 Hz, 2H, 7'-H_2), 3,00 (m, 2H, 4-H_2), 3.94 (t, $J \approx$ 7.5 Hz, 2H, 1'-H_2), 7.56 (dd, J = 9.3 Hz, J' = 2.1 Hz, 1H, 7-H), 7.78 (d, J = 2.1 Hz, 1H, 5-H), 8.39 (d, J = 9.3 Hz, 1H, 8-H); ^{13}C NMR (75.4 MHz, CD_3OD) δ 21.8 (CH_2, C3), 22.9 (CH_2, C2), 24.8 (CH_2, C1), 27.3 (CH_2) and 27.5 (CH_2) (C3' and C5'), 29.4 (CH_2, C4), 28.5 (CH_2), 29.8 (CH_2), and 31.3 (CH_2) (C2', C4', and C6'), 40.7 (CH_2, C7'), 49.1 (CH_2, C1'), 113.3 (C, C9a), 115.3 (C, C8a), 119.1 (CH, C5), 126.7 (CH, C7), 128.7 (CH, C8), 139.9 (C, C6), 140.4 (C, C10a), 152.0 (C, C4a), 157.6 (C, C9).

9-[(9-Aminononyl)amino]-6-chloro-1,2,3,4-tetrahydroacridine Dihydrochloride (17f·2HCl). From **15** (1.00 g, 3.97 mmol) and 1,9-diaminononane, **16f** (2.51 g, 15.9 mmol), a brown oily residue (1.83 g) was obtained and subjected to column chromatography [35–70 μm silica gel (73 g), AcOEt/MeOH/Et_3N mixtures]. On elution with AcOEt/MeOH/Et_3N

100:0:0.1 to 85:15:0.1, *bis*(9)-6-chlorotacrine, **28f** (69 mg) and a mixture **28f**/**17f** (1.24 g) were consecutively isolated. This mixture was subjected to column chromatography [35–70 μm silica gel (18 g), CH_2Cl_2/MeOH/25% aq NH_4OH mixtures]. On elution with CH_2Cl_2/MeOH/25% aq NH_4OH 90:10:0.2, **28f** (542 mg), a mixture **28f**/**17f** in an approximate ratio 8:92 (^{1}H NMR) (173 mg, 53% total yield of **28f**), and amine **17f** (363 mg, 35% total yield of **17f**) were consecutively isolated as brown-yellow oils: $R_{f(\mathbf{17f})}$ 0.18; $R_{f(\mathbf{28f})}$ 0.56 (AcOEt/MeOH/Et_3N 9:1:0.01).

17f·2HCl: mp 179–180 ºC (MeOH/AcOEt 3:8); IR (KBr) ν 3500–2500 (max at 3405, 3253, 2926, 2853, N–H, $^+$N–H and C–H st), 1629, 1570, and 1515 (ar–C–C and ar–C–N st) cm^{-1}; ^{1}H NMR (300 MHz, CD_3OD) δ 1.28–1.48 (complex signal, 10H, 3'-H_2, 4'-H_2, 5'-H_2, 6'-H_2, and 7'-H_2), 1.65 (tt, $J \approx J' \approx 7.5$ Hz, 2H, 8'-H_2), 1.83 (tt, $J \approx J' \approx 7.5$ Hz, 2H, 2'-H_2), 1.90–2.00 (complex signal, 4H, 2-H_2 and 3-H_2), 2.67 (m, 2H, 1-H_2), 2.91 (t, J = 7.5 Hz, 2H, 9'-H_2), 3.00 (m, 2H, 4-H_2), 3.94 (t, J = 7.5 Hz, 2H, 1'-H_2), 4.84 (s, NH, $^+$NH, and $^+NH_3$), 7.55 (dd, J = 9.3 Hz, J' = 2.1 Hz, 1H, 7-H), 7.79 (d, $J \approx$ 2.1 Hz, 5-H), 8.38 (d, J = 9.3 Hz, 1H, 8-H); ^{13}C NMR (75.4 MHz, CD_3OD) δ 21.8 (CH_2, C3), 22.9 (CH_2, C2), 24.8 (CH_2, C1), 27.4 (CH_2) and 27.7 (CH_2) (C3' and C7'), 29.3 (CH_2, C4), 28.6 (CH_2), 30.1 (CH_2), 30.2 (CH_2), 30.4 (CH_2), and 31.4 (CH_2) (C2', C4', C5', C6', and C8'), 40.8 (CH_2, C9'), 113.3 (C, C9a), 115.4 (C, C8a), 119.1 (CH, C5), 126.7 (CH, C7), 128.8 (CH, C8), 140.1 (C, C6), 140.5 (C, C10a), 152.1 (C, C4a), 157.8 (C, C9), the signal corresponding to C1', probably superimposed to those of CD_3OD, was not observed.

28f·2HCl [*N*,*N'*-*bis*(6-chloro-1,2,3,4-tetrahydroacridin-9-yl)-1,9-nonanediamine]: mp 141–142 ºC (MeOH/AcOEt 1:3); IR (KBr) ν 3500–2500 (max at 3231, 3047, 2926, 2853, N–H, $^+$N–H, O–H, and C–H st), 1630, 1571, and 1515 (ar–C–C and ar–C–N st) cm^{-1}; ^{1}H NMR (300 MHz, CD_3OD) δ 1.30–1.48 (complex signal, 10H, 3'-H_2, 4'-H_2, and 5'-H_2), 1.82 (tt, $J \approx J \approx 7.5$ Hz, 4H, 2'-H_2), 1.90–2.00 (complex signal, 8H, 2-H_2 and 3-H_2), 2.66 (m, 4H, 1-H_2), 2.99 (m, 4H, 4-H_2), 3.92 (t, J = 7.5 Hz, 4H, 1'-H_2), 4.84 (s, NH and $^+$NH), 7.54 (dd, J = 9.0 Hz, J' = 2.1 Hz, 2H, 7-H), 7.76 (d, J = 2.1 Hz, 2H, 5-H), 8.37 (d, J = 9.0 Hz, 2H, 8-H); ^{13}C NMR (75.4 MHz, CD_3OD) δ 21.8 (CH_2, C3), 22.9 (CH_2, C2), 24.8 (CH_2, C1), 27.7 (CH_2, C3'), 29.3 (CH_2, C4) 30.2 (CH_2), 30.4 (CH_2), and 31.4 (CH_2) (C2', C4', and C5'), 49.2 (CH_2, C1'), 113.3 (C, C9a), 115.4 (C, C8a), 119.1 (CH, C5), 126.7 (CH, C7), 128.7 (CH, C8), 140.0 (C, C6), 140.4 (C, C10a), 152.1 (C, C4a), 157.7 (C, C9). Anal. ($C_{35}H_{42}Cl_2N_4$·2HCl·1.25H_2O) C, H, N.

9-[(10-Aminodecyl)amino]-6-chloro-1,2,3,4-tetrahydroacridine Dihydrochloride (17g·2HCl). From **15** (1.00 g, 3.97 mmol) and 1,10-diaminodecane, **16g** (2.73 g, 15.9 mmol), a brown oily residue (2.34 g) was obtained and subjected to column chromatography [35–70 μm silica gel (33 g), CH_2Cl_2/MeOH/25% aq NH_4OH mixtures]. On elution with CH_2Cl_2/MeOH/25% aq NH_4OH 90:10:0.2, a mixture of *bis*(10)-6-chlorotacrine, **28g** and **17g** in an approximate ratio 90:10 (^{1}H NMR) (399 mg, 15% yield of **28g**), and amine **17g** (549 mg, 38% total yield of **17g**) were consecutively isolated as brown oils: $R_{f(\mathbf{17g})}$ 0.21; $R_{f(\mathbf{28g})}$ 0.71 (CH_2Cl_2/MeOH/25% aq NH_4OH 9:1:0.01).

17g·2HCl: mp 164–165 ºC (MeOH/AcOEt 5:13); IR (KBr) ν 3500–2500 (max at 3401, 3254, 2926, 2853, N–H, $^{+}$N–H and C–H st), 1629, 1572, and 1516 (ar–C–C and ar–C–N st) cm^{-1}; ^{1}H NMR (300 MHz, CD_3OD) δ 1.28–1.50 (complex signal, 12H, 3'-H_2, 4'-H_2, 5'-H_2, 6'-H_2, 7'-H_2, and 8'-H_2), 1.64 (tt, $J \approx J' \approx$ 7,5 Hz, 2H, 9'-H_2), 1.83 (tt, $J \approx J' \approx$ 7.5 Hz, 2H, 2'-H_2), 1.90–2.00 (complex signal, 4H, 2-H_2 and 3-H_2), 2.67 (m, 2H, 1-H_2), 2.90 (t, $J \approx$ 7.5 Hz, 2H, 10'-H_2), 2.99 (m, 2H, 4-H_2), 3.93 (t, J = 7.5 Hz, 2H, 1'-H_2), 4.84 (s, NH, $^{+}$NH, and $^{+}NH_3$), 7.56 (dd, J = 9.3 Hz, J' = 2.1 Hz, 1H, 7-H), 7.77 (d, J = 2.1 Hz, 1H, 5-H), 8.38 (d, $J \approx$ 9.3 Hz, 1H, 8-H); ^{13}C NMR (75.4 MHz, CD_3OD) δ 21.8 (CH_2, C3), 22.9 (CH_2, C2), 24.8 (CH_2, C1), 27.4 (CH_2) and 27,7 (CH_2) (C3' and C8'), 29.3 (CH_2, C4), 28.5 (CH_2), 30.2 (CH_2), 30.3 (CH_2), 30.4 (CH_2), 30.5 (CH_2), and 31.4 (CH_2) (C2', C4', C5', C6', C7', and C9'), 40.8 (CH_2, C10'), 49.2 (CH_2, C1'), 113.3 (C, C9a), 115.4 (C, C8a), 119.1 (CH, C5), 126.7 (CH, C7), 128.7 (CH, C8), 140.0 (C, C6), 140.4 (C, C10a), 152.1 (C, C4a), 157.7 (C, C9).

6-Chloro-9-{{7-[5-(4-chlorophenyl)-3,4-dihydro-2*H*-pyrano[3,2-*c*]quinoline-9-carboxamido]heptyl}amino}-1,2,3,4-tetrahydroacridine Dihydrochloride (19·2HCl). From crude **13** [aliquot of 243 mg of a total amount of 486 mg of the crude product obtained from 403 mg (1.10 mmol) of ester **11**] and amine **17d** (173 mg, 0.50 mmol), a yellow oily residue (230 mg) was obtained and subjected to column chromatography [35–70 μm silica gel (20 g), hexane/AcOEt/Et_3N mixtures]. On elution with hexane/AcOEt/Et_3N 50:50:0.5, hybrid **19** (122 mg, 37% yield) was isolated as a yellowish oil: R_f = 0.40 (CH_2Cl_2/MeOH/Et_3N 98:2:0.5). **19**·2HCl: mp 182–183 ºC (CH_2Cl_2). IR (KBr) ν 3500–2500 (max at 3233, 3050, 2927, 2855, N–H, $^{+}$N–H, O–H, and C–H st), 1631, 1577, and 1542 (C=O, ar–C–C and ar–C–N st) cm^{-1}; ^{1}H NMR (500 MHz, CD_3OD) δ 1.43–1.51 (complex signal, 6H, 3'-H_2, 4'-H_2, and 5'-H_2), 1.68 (tt, $J \approx J' \approx$ 6.0 Hz, 2H, 6'-H_2), 1.86 (tt, $J \approx J' \approx$ 7.0 Hz, 2H, 2'-H_2), 1.90−1.99 (complex signal, 4H, 2-H_2 and 3-H_2), 2.17 (tt, $J \approx J' \approx$ 5.6 Hz, 2H, 3"-H_2), 2.67 (t, J = 5.5 Hz, 2H, 1-H_2), 2.85 (t, J = 6.0 Hz, 2H, 4"-H_2), 2.99 (t, J = 5.5 Hz, 2H, 4-H_2), 3.44 (dt, $J = J'$ = 6.0 Hz, 2H, 7'-H_2), 3.94 (t, J = 7.0 Hz, 2H, 1'-H_2), 4.77 (t, J = 5.5 Hz, 2H, 2"-H_2), 4.87 (s, NH and $^{+}$NH), 7.54 (dd, J = 9.0 Hz, J' = 2.0 Hz, 1H, 7-H), 7.69 [broad d, J = 8.5 Hz, 2H, 3(5)-H *p*-chlorophenyl], 7,74 [broad d, J = 8.5 Hz, 2H, 2(6)-H *p*-chlorophenyl], 7.76 (d, $J \approx$ 2.0 Hz, 1H, 5-H), 8.10 (d, J = 9.0 Hz, 1H, 7"-H), superimposed in part 8.35 (dd, $J \approx$ 9.0 Hz, $J' \approx$ 2.0 Hz, 1H, 8"-H), 8.37 (d, J = 9.0 Hz, 1H, 8-H), 8.80 (d, J = 2.0 Hz, 1H, 10"-H), 8.91 (t, J = 6.0 Hz, CONH); ^{13}C NMR (100.6 MHz, CD_3OD) δ 21.7 (CH_2, C3"), 21.8 (CH_2, C3), 22.9 (CH_2, C2), 23.7 (CH_2, C4"), 24.7 (CH_2, C1), 27.6 (CH_2) and 27.9 (CH_2) (C3' and C5'), 29.3 (CH_2, C4), 29.9 (CH_2, C4'), 30.3 (CH_2, C6'), 31.3 (CH_2, C2'), 41.2 (CH_2, C7'), 49.2 (CH_2, C1'), 71.0 (CH_2, C2"), 113.3 (C, C9a), 115.2 (C, C4a"), 115.4 (C, C8a), 119.1 (CH, C5), 120.5 (C, C10a"), 122.7 (CH, C7"), 123.3 (CH, C10"), 126.8 (CH, C7), 128.8 (CH, C8), 130.4 [CH, C3(5) *p*-chlorophenyl], 132.0 [CH, C2(6) *p*-chlorophenyl], 132.5 (C, C1 *p*-chlorophenyl), 132.8 (CH, C8"), 135.1 (C, C9"), 138.7 (C, C4 *p*-chlorophenyl), 140.1 (C, C6), 140.5 (C, C10a), 142.0 (C, C6a"), 152.1 (C, C4a), 157.8 (C, C9), 158.5 (C, C5"), 166.4 (C, C10b"), 167.9 (C, CONH). HRMS

calcd for ($C_{39}H_{40}{}^{35}Cl_2N_4O_2$ + H^+) 667.2607, found 667.2576. Anal. ($C_{39}H_{40}Cl_2N_4O_2 \cdot 2HCl \cdot 0.5H_2O$) C, H, N.

6-Chloro-9-{{8-[5-(4-chlorophenyl)-3,4-dihydro-2*H*-pyrano[3,2-*c*]quinoline-9-carboxamido]octyl}amino}-1,2,3,4-tetrahydroacridine Dihydrochloride (20·2HCl). From crude **13** [aliquot of 243 mg of a total amount of 486 mg of the crude product obtained from 403 mg (1.10 mmol) of ester **11**] and amine **17e** (160 mg, 0.45 mmol), a yellowish oily residue (301 mg) was obtained and subjected to column chromatography [35–70 μm silica gel (20 g), hexane/AcOEt/Et_3N mixtures]. On elution with hexane/AcOEt/Et_3N 50:50:0.5, hybrid **20** (59 mg, 19% yield) was isolated as a yellowish oil: R_f = 0.42 (CH_2Cl_2/MeOH/Et_3N 98:2:0.5). **20**·2HCl: mp 169–170 ºC (CH_2Cl_2). IR (KBr) ν 3500–2500 (max at 3248, 3067, 2926, 2853, N–H, $^+$N–H and C–H st), 1633, 1582, 1570, 1539, and 1530 (C=O, ar–C–C and ar–C–N st) cm^{-1}; ^{1}H NMR (500 MHz, CD_3OD) δ 1.40–1.48 (complex signal, 8H, 3'-H_2, 4'-H_2, 5'-H_2, and 6'-H_2), 1.67 (tt, $J \approx J' \approx$ 7.0 Hz, 2H, 7'-H_2), 1.84 (tt, $J \approx J' \approx$ 7.0 Hz, 2H, 2'-H_2), 1.91–1.99 (complex signal, 4H, 2-H_2, and 3-H_2), 2.10 (tt, $J \approx J' \approx$ 6.0 Hz, 2H, 3"-H_2), 2.65 (t, J = 6.0 Hz, 2H, 1-H_2), 2.78 (t, J = 6.0 Hz, 2H, 4"-H_2), 2.98 (t, J = 6.0 Hz, 2H, 4-H_2), 3.43 (t, J = 7.0 Hz, 2H, 8'-H_2), 3.92 (t, J = 7.0 Hz, 2H, 1'-H_2), 4.61 (t, J = 5.5 Hz, 2H, 2"-H_2), 4.87 (s, NH and $^+$NH), 7.52 (dd, J = 9.5 Hz, J' = 1.5 Hz, 1H, 7-H), 7.58 [broad d, J = 8.5 Hz, 2H, 3(5)-H *p*-chlorophenyl], 7.62 [broad d, $J \approx$ 8.5 Hz, 2H, 2(6)-H *p*-chlorophenyl], 7.74 (broad s, 1H, 5-H), 7.96 (d, J = 9.0 Hz, 1H, 7"-H), 8.14 (dd, J = 9.0 Hz, J' = 2.0 Hz, 1H, 8"-H), 8.34 (d, $J \approx$ 9.5 Hz, 1H, 8-H), 8.68 (d, J = 2.0 Hz, 1H, 10"-H); ^{13}C NMR (100.6 MHz, CD_3OD) δ 21.7 (CH_2, C3"), 22.4 (CH_2, C3), 22.8 (CH_2, C2), 24.3 (CH_2, C4"), 24.7 (CH_2, C1), 27.5 (CH_2) and 27.8 (CH_2) (C3' and C6'), 29.3 (CH_2, C4), 30.1 (2 CH_2) and 30.4 (CH_2) (C4', C5', and C7'), 31.3 (CH_2, C2'), 41.1 (CH_2, C8'), 49.2 (CH_2, C1'), 69.4 (CH_2, C2"), 113.3 (C, C9a), 113.9 (C, C4a"), 115.4 (C, C8a), 119.1 (CH, C5), 120.6 (C, C10a"), 122.8 (CH, C7"), 126.7 (CH, C7), 127.1 (CH, C10"), 128.7 (CH, C8), 129.8 [CH, C3(5) *p*-chlorophenyl], 130.0 (CH, C8"), 131.7 [CH, C2(6) *p*-chlorophenyl], 133.5 (C, C1 *p*-chlorophenyl), 136.8 (C, C9"), 137.4 (C, C4 *p*-chlorophenyl), 140.1 (C, C6), 140.5 (C, C10a), 147.0 (C, C6a"), 152.0 (C, C4a), 157.8 (C, C9), 161.6 (C, C5"), 162.1 (C, C10b"), 169.0 (C, CONH). HRMS calcd for ($C_{40}H_{42}{}^{35}Cl_2N_4O_2$ + H^+) 681.2763, found 681.2730. Anal. ($C_{40}H_{42}Cl_2N_4O_2 \cdot 2HCl$) C, H, N.

6-Chloro-9-{{9-[5-(4-chlorophenyl)-3,4-dihydro-2*H*-pyrano[3,2-*c*]quinoline-9-carboxamido]nonyl}amino}-1,2,3,4-tetrahydroacridine Dihydrochloride (21·2HCl). From crude **13** [aliquot of 150 mg of a total amount of 305 mg of the crude product obtained from 236 mg (0.64 mmol) of ester **11**] and amine **17f** (121 mg, 0.32 mmol), a yellow oily residue (205 mg) was obtained and subjected to column chromatography [35–70 μm silica gel (30 g), hexane/AcOEt/Et_3N mixtures]. On elution with hexane/AcOEt/Et_3N 45:55:0.5, hybrid **21** (81 mg, 37% yield) was isolated as a yellowish oil: R_f = 0.80 (CH_2Cl_2/MeOH/Et_3N 95:5:0.5). **21**·2HCl: mp 159–160 ºC (MeOH/AcOEt 1:5). IR (KBr) ν 3500–2500 (max at 3370, 3263, 3065, 2927, 2854, N–H, $^+$N–H, O–H, and C–H st), 1633 and 1576 (C=O, ar–C–C and ar–C–N st) cm^{-1}; ^{1}H NMR (300 MHz,

CD_3OD) δ 1.24–1.48 (complex signal, 10H, 3'-H_2, 4'-H_2, 5'-H_2, 6'-H_2, and 7'-H_2), 1.66 (tt, $J \approx J' \approx$ 6.6 Hz, 2H, 8'-H_2), 1.83 (tt, $J \approx J' \approx$ 7.2 Hz, 2H, 2'-H_2), 1.90–1.98 (complex signal, 4H, 2-H_2 and 3-H_2), 2.15 (tt, $J \approx J' \approx$ 5.4 Hz, 2H, 3"-H_2), 2.66 (m, 2H, 1-H_2), 2.83 (t, J = 6.0 Hz, 2H, 4"-H_2), 2.98 (m, 2H, 4-H_2), 3.42 (tm, J = 6.6 Hz, 2H, 9'-H_2), 3.93 (t, J = 7.2 Hz, 2H, 1'-H_2), 4.73 (t, J = 5.4 Hz, 2H, 2"-H_2), 4.84 (s, NH and $^+$NH), 7.55 (dd, J = 9.3 Hz, J' = 2.1 Hz, 1H, 7-H), 7.67 [dm, J = 9.0 Hz, 2H, 3(5)-H *p*-chlorophenyl], 7.71 [dm, J = 9.0 Hz, 2H, 2(6)-H *p*-chlorophenyl], 7.75 (d, J = 2.1 Hz, 1H, 5-H), 8.07 (d, J = 9.0 Hz, 1H, 7"-H), 8.32 (dd, J = 9.0 Hz, J' = 1.8 Hz, 1H, 8"-H), 8.37 (d, J = 9.3 Hz, 1H, 8-H), 8.80 (d, J = 1.8 Hz, 1H, 10"-H); ^{13}C NMR (100.6 MHz, CD_3OD) δ 21.76 (CH_2) and 21.81 (CH_2) (C3 and C3"), 22.9 (CH_2, C2), 23.8 (CH_2, C4"), 24.7 (CH_2, C1), 27.6 (CH_2) and 28.0 (CH_2) (C3' and C7'), 29.3 (CH_2, C4), 30.16 (CH_2), 30.23 (CH_2), 30.4 (CH_2), and 30.8 (CH_2) (C4', C5', C6', and C8'), 31.3 (CH_2, C2'), 41.3 (CH_2, C9'), 49.2 (CH_2, C1'), 70.7 (CH_2, C2"), 113.3 (C, C9a), 115.0 (C, C4a"), 115.4 (C, C8a), 119.1 (CH, C5), 120.6 (C, C10a"), 123.2 (CH, C7"), 123.4 (CH, C10"), 126.8 (CH, C7), 128.8 (CH, C8), 130.3 [CH, C3(5) *p*-chlorophenyl], 131.9 [CH, C2(6) *p*-chlorophenyl], 132.4 (CH, C8"), 133.2 (C, C1 *p*-chlorophenyl), 134.9 (C, C9"), 138.4 (C, C4 *p*-chlorophenyl), 140.1 (C, C6), 140.5 (C, C10a), 142.8 (C, C6a"), 152.1 (C, C4a), 157.8 (C, C9), 159.0 (C, C5"), 165.7 (C, C10b"), 168.0 (C, CONH). HRMS calcd for ($C_{41}H_{44}{}^{35}Cl_2N_4O_2$ + H^+) 695.2914, found 695.2891. Anal. ($C_{41}H_{44}Cl_2N_4O_2 \cdot 2HCl \cdot 2.1H_2O$) C, H, N.

6-Chloro-9-{{10-[5-(4-chlorophenyl)-3,4-dihydro-2*H*-pyrano[3,2-*c*]quinoline-9-carboxamido]decyl}amino}-1,2,3,4-tetrahydroacridine Dihydrochloride (22·2HCl). From crude **13** [aliquot of 143 mg of a total amount of 305 mg of the crude product obtained from 236 mg (0.64 mmol) of ester **11**] and amine **17g** (117 mg, 0.30 mmol), a yellow oily residue (183 mg) was obtained and subjected to column chromatography [35–70 μm silica gel (18 g), hexane/AcOEt/Et_3N mixtures]. On elution with hexane/AcOEt/Et_3N 50:50:0.1 to 40:60:0.1, hybrid **22** (64 mg, 30% yield) was isolated as a yellowish oil: R_f = 0.62 (CH_2Cl_2/MeOH/Et_3N 98:2:0.5). **22**·2HCl: mp 154–155 ºC (MeOH/AcOEt 1:5). IR (KBr) ν 3500–2500 (max at 3370, 3255, 3056, 2925, 2853, N–H, $^+$N–H, O–H, and C–H st), 1633 and 1576 (C=O, ar–C–C and ar–C–N st) cm^{-1}; ^{1}H NMR (300 MHz, CD_3OD) δ 1.24–1.48 (complex signal, 12H, 3'-H_2, 4'-H_2, 5'-H_2, 6'-H_2, 7'-H_2, and 8'-H_2), 1.66 (tt, $J \approx J' \approx$ 6.6 Hz, 2H, 9'-H_2), 1.83 (tt, $J \approx J' \approx$ 7.2 Hz, 2H, 2'-H_2), 1.90–2.00 (complex signal, 4H, 2-H_2 and 3-H_2), 2.16 (tt, $J \approx J' \approx$ 6.0 Hz, 2H, 3"-H_2), 2.66 (m, 2H, 1-H_2), 2.83 (t, J = 6.0 Hz, 2H, 4"-H_2), 2.98 (m, 2H, 4-H_2), 3.43 (tm, J = 6.6 Hz, 2H, 10'-H_2), 3.93 (t, J = 7.2 Hz, 2H, 1'-H_2), 4.75 (t, J = 5.4 Hz, 2H, 2"-H_2), 4.84 (s, NH and $^+$NH), 7.55 (dd, J = 9.3 Hz, J' = 2.1 Hz, 1H, 7-H), 7.68 [dm, J = 9.0 Hz, 2H, 3(5)-H *p*-chlorophenyl], 7.72 [dm, J = 9.0 Hz, 2H, 2(6)-H *p*-chlorophenyl], 7.75 (d, J = 2.1 Hz, 1H, 5-H), 8.08 (d, J = 9.0 Hz, 1H, 7"-H), superimposed in part 8.35 (dd, J = 9.0 Hz, J' = 1.8 Hz, 1H, 8"-H), 8.37 (d, J = 9.3 Hz, 1H, 8-H), 8.82 (d, J = 1.8 Hz, 1H, 10"-H); ^{13}C NMR (100.6 MHz, CD_3OD) δ 21.7 (CH_2, C3"), 21.8 (CH_2, C3), 22.9 (CH_2, C2), 23.7 (CH_2, C4"), 24.7 (CH_2, C1), 27.7 (CH_2) and 28.1 (CH_2) (C3' and C8'), 29.3 (CH_2, C4), 30.2 (CH_2), 30.36 (CH_2), 30.45 (CH_2), 30.48 (CH_2), and 30.51 (CH_2) (C4', C5', C6', C8', and C9'),

31.3 (CH_2, C2'), 41.3 (CH_2, C10'), 49.2 (CH_2, C1'), 70.9 (CH_2, C2"), 113.3 (CH_2, C9a), 115.1 (CH_2, C4a"), 115.4 (CH, C8a), 119.1 (CH, C5), 120.5 (C, C10a"), 122.9 (CH, C7"), 123.3 (CH, C10"), 126.8 (CH, C7), 128.8 (CH, C8), 130.4 [CH, C3(5) *p*-chlorophenyl], 132.0 [CH, C2(6) *p*-chlorophenyl], 132.7 (CH, C8"), 132.8 (C, C1 *p*-chlorophenyl), 135.0 (C, C9"), 138.6 (C, C4 *p*-chlorophenyl), 140.1 (C, C6), 140.5 (C, C10a), 142.3 (C, C6a"), 152.1 (C, C4a), 157.8 (C, C9), 158.6 (C, C5"), 166.2 (C, C10b"), 168.0 (C, CONH). HRMS calcd for ($C_{42}H_{46}{}^{35}Cl_2N_4O_2$ + H^+) 709.3070, found 709.3054. Anal. ($C_{42}H_{46}Cl_2N_4O_2 \cdot 2HCl \cdot 1.25H_2O$) C, H, N.

6-Chloro-9-{{4-[3-(3,4-dihydro-5-phenyl-2*H*-pyrano[3,2-*c*]quinolin-9-yl)propanamido]butyl}amino}-1,2,3,4-tetrahydroacridine Dihydrochloride (23·2HCl). From crude **14** [580 mg of the crude product obtained from 276 mg (0.80 mmol) of ester **12**] and amine **17a** (203 mg, 0.67 mmol), a yellow oily residue (330 mg) was obtained and subjected to column chromatography [35–70 μm silica gel (33 g), hexane/AcOEt/Et_3N mixtures]. On elution with hexane/AcOEt/Et_3N 30:70:0.1, hybrid **23** (200 mg, 48% yield) was isolated as a yellowish oil: R_f = 0.20 (AcOEt/MeOH/Et_3N 98:2:0.1). **23**·2HCl: mp 179–180 ºC (MeOH/AcOEt 1:8). IR (KBr) ν 3500–2500 (max at 3338, 3236, 3055, 2929, 2858, N–H, $^+$N–H, O–H, and C–H st), 1734, 1631, and 1576 (C=O, ar–C–C and ar–C–N st) cm^{-1}; ^{1}H NMR (500 MHz, CD_3OD) δ 1.55 (tt, $J \approx J' \approx 7.0$ Hz, 2H) and 1.73 (tt, $J \approx J' \approx 7.0$ Hz, 2H) (2'-H_2 and 3'-H_2), 1.90–1.98 (complex signal, 4H, 2-H_2 and 3-H_2), 2.08 (tt, $J \approx J' \approx 5.5$ Hz, 2H, 3"-H_2), 2.60 (t, J = 7.5 Hz, 2H, 9"-CH_2-CH_2-CONH), superimposed in part 2.64 (m, 2H, 1-H_2), 2.74 (t, J = 6.0 Hz, 2H, 4"-H_2), 2.97 (m, 2H, 4-H_2), 3.12 (t, J = 7.5 Hz, 2H, 4'-H_2), 3.18 (t, $J \approx$ 7.5 Hz, 2H, 9"-CH_2-CH_2-CONH), 3.86 (t, J = 7.5 Hz, 2H, 1'-H_2), 4.59 (t, J = 5.0 Hz, 2H, 2"-H_2), 4.85 (s, NH and $^+$NH), 7.52 (dd, J = 9.0 Hz, J' = 2.0 Hz, 1H, 7-H), 7.57 [complex signal, 5H, Ar-H phenyl], 7.71 (broad d, J = 8.0 Hz, 1H, 8"-H), 7.74 (broad s, 1H, 5-H), 7.89 (d, J = 8.0 Hz, 1H, 7"-H), 8.06 (broad s, 1H, 10"-H), 8.30 (d, J = 9.0 Hz, 1H, 8-H); ^{13}C NMR (100.6 MHz, CD_3OD) δ 21.7 (CH_2, C3"), 22.3 (CH_2, C3), 22.8 (CH_2, C2), 24.2 (CH_2, C4"), 24.8 (CH_2, C1), 27.5 (CH_2) and 28.5 (CH_2) (C2' and C3'), 29.3 (CH_2, C4), 32.8 (CH_2, 9"-*C*H_2-CH_2-CONH), 38.3 (CH_2, 9"-CH_2-*C*H_2-CONH), 39.6 (CH_2, C4'), 48.7 (CH_2, C1'), 69.5 (CH_2, C2"), 113.3 (C, C9a), 113.4 (C, C4a"), 115.4 (C, C8a), 119.2 (CH, C5), 121.0 (C, C10a"), 121.7 (CH) and 125.5 (CH) (C7" and C10"), 126.8 (CH, C7), 128.7 (CH, C8), 129.7 (CH) and 130.0 (CH) [C2(6) and C3(5) phenyl], 130.9 (CH, C4 phenyl), 133.8 (CH, C8"), 137.7 (C, C1 phenyl), 140.0 (C), 140.4 (C), and 141.3 (C) (C6, C10a, and C6a"), 143.3 (C, C9"), 152.1 (C, C4a), 157.6 (C) and 159.9 (C) (C9 and C5"), 162.0 (C, C10b"), 174.8 (C, CONH). HRMS calcd for ($C_{38}H_{39}{}^{35}ClN_4O_2$ + H^+) 619.2834, found 619.2832. Anal. ($C_{38}H_{39}ClN_4O_2 \cdot 2HCl \cdot 3H_2O \cdot 0.25AcOEt$) C, H, N.

6-Chloro-9-{{5-[3-(3,4-dihydro-5-phenyl-2*H*-pyrano[3,2-*c*]quinolin-9-yl)propanamido]pentyl}amino}-1,2,3,4-tetrahydroacridine Dihydrochloride (24·2HCl). From crude **14** [427 mg of the crude product obtained from 252 mg (0.73 mmol) of ester **12**] and amine **17b** (232 mg, 0.73 mmol), a yellow oily residue (413 mg) was obtained and subjected to column chromatography [35–70 μm silica gel (41 g),

hexane/AcOEt/Et_3N mixtures]. On elution with hexane/AcOEt/Et_3N 35:65:0.1, hybrid **24** (144 mg, 31% yield) was isolated as a yellowish oil: R_f = 0.20 (AcOEt/MeOH/Et_3N 98:2:0.1). **24**·2HCl: mp 179–180 ºC (MeOH/AcOEt 1:8). IR (KBr) ν 3500–2500 (max at 3396, 3233, 3055, 2928, 2857, N–H, $^+$N–H, O–H, and C–H st), 1734, 1631 and 1577 (C=O, ar–C–C and ar–C–N st) cm^{-1}; ^1H NMR (500 MHz, CD_3OD) δ 1.42 (tt, $J = J' = 7.5$ Hz, 2H) and 1.53 (tt, $J = J' = 7.5$ Hz, 2H) (3'-H_2 and 4'-H_2), 1.84 (tt, $J = J' = 7.5$ Hz, 2H, 2'-H_2), 1.91–2.00 (complex signal, 4H, 2-H_2 and 3-H_2), 2.15 (tt, $J \approx J' \approx 5.5$ Hz, 2H, 3"-H_2), 2.62 (t, $J = 7.5$ Hz, 2H, 9"-CH_2-C*H_2*-CONH), 2.68 (m, 2H, 1-H_2), 2.83 (t, $J = 6.0$ Hz, 2H, 4"-H_2), 2.99 (m, 2H, 4-H_2), 3.16 (t, $J = 7.5$ Hz, 2H, 5'-H_2), superimposed in part 3.17 (t, $J \approx 7.5$ Hz, 2H, 9"-C*H_2*-CH_2-CONH), 3.92 (t, $J = 7.5$ Hz, 2H, 1'-H_2), 4.75 (t, $J = 5.0$ Hz, 2H, 2"-H_2), 4.83 (s, NH and $^+$NH), 7.56 (dm, $J \approx 9.0$ Hz, 1H, 7-H), 7.66–7.73 [complex signal, 5H, Ar-H phenyl], 7.76 (d, $J = 1.5$ Hz, 1H, 5-H), 7.94 (broad d, $J = 9.0$ Hz, 1H, 8"-H), 8.00 (d, $J = 9.0$ Hz, 1H, 7"-H), 8.22 (broad s, 1H, 10"-H), 8.38 (d, $J = 9.0$ Hz, 1H, 8-H); ^{13}C NMR (100.6 MHz, CD_3OD) δ 21.67 (CH_2) and 21.74 (CH_2) (C3 and C3"), 22.9 (CH_2, C2), 23.6 (CH_2, C4"), 24.8 (CH_2, C1), 24.9 (CH_2, C3'), 29.3 (CH_2, C4), 30.0 (CH_2) and 30.9 (CH_2) (C2' and C4'), 32.8 (CH_2, 9"-*C*H_2-CH_2-CONH), 38.1 (CH_2, 9"-CH_2-*C*H_2-CONH), 40.0 (CH_2, C5'), 49.0 (CH_2, C1'), 71.0 (CH_2, C2"), 113.3 (C, C9a), 114.6 (C, C4a"), 115.4 (C, C8a), 119.1 (CH, C5), 120.9 (C, C10a"), 121.1 (CH) and 122.5 (CH) (C7" and C10"), 126.8 (CH, C7), 128.8 (CH, C8), 130.2 (CH) and 130.3 (CH) [C2(6) and C3(5) phenyl], 132.7 (CH, C4 phenyl), 132.8 (C, C1 phenyl), 136.6 (CH, C8"), 138.3 (C, C6a"), 140.0 (C, C6), 140.5 (C, C10a), 143.5 (C, C9"), 152.2 (C, C4a), 157.1 (C, C5") 157.8 (C, C9), 166.3 (C, C10b"), 174.4 (C, CONH). HRMS calcd for ($C_{39}H_{41}{}^{35}ClN_4O_2$ + H^+) 633.2990, found 633.2999. Anal. ($C_{39}H_{41}ClN_4O_2$·2HCl·3H_2O) C, H, N.

6-Chloro-9-{{6-[3-(3,4-dihydro-5-phenyl-2*H*-pyrano[3,2-*c*]quinolin-9-yl)propanamido]hexyl}amino}-1,2,3,4-tetrahydroacridine Dihydrochloride (25·2HCl). From crude **14** [450 mg of the crude product obtained from 250 mg (0.72 mmol) of ester **12**] and amine **17c** (239 mg, 0.72 mmol), a yellow oily residue (477 mg) was obtained and subjected to column chromatography [35–70 μm silica gel (48 g), hexane/AcOEt/Et_3N mixtures]. On elution with hexane/AcOEt/Et_3N 45:55:0.1, hybrid **25** (117 mg, 25% yield) was isolated as a yellowish oil: R_f = 0.34 (AcOEt/MeOH/Et_3N 98:2:0.1). **25**·2HCl: mp 180–181 ºC (MeOH/AcOEt 1:8). IR (KBr) ν 3500–2500 (max at 3399, 3236, 3054, 2929, 2856, N–H, $^+$N–H, O–H, and C–H st), 1733, 1633, and 1576 (C=O, ar–C–C and ar–C–N st) cm^{-1}; ^1H NMR (500 MHz, CD_3OD) δ 1.32 (tt, $J \approx J' \approx 7.5$ Hz, 2H), 1.41 (tt, $J \approx J' \approx 7.5$ Hz, 2H), and superimposed in part 1.47 (tt, $J \approx J' \approx 7.5$ Hz, 2H) (3'-H_2, 4'-H_2, and 5'-H_2), 1.80 (tt, $J = J' = 7.5$ Hz, 2H, 2'-H_2), 1.91–1.98 (complex signal, 4H, 2-H_2 and 3-H_2), 2.13 (tt, $J = J' = 5.5$ Hz, 2H, 3"-H_2), 2.61 (t, $J = 7.5$ Hz, 2H, 9"-CH_2-C*H_2*-CONH), 2.66 (m, 2H, 1-H_2), 2.82 (t, $J = 6.0$ Hz, 2H, 4"-H_2), 2.98 (m, 2H, 4-H_2), 3.12 (t, $J = 7.0$ Hz, 2H, 6'-H_2), 3.17 (t, $J = 7.5$ Hz, 2H, 9"-C*H_2*-CH_2-CONH), 3.91 (t, $J = 7.5$ Hz, 2H, 1'-H_2), 4.72 (t, $J = 5.0$ Hz, 2H, 2"-H_2), 4.84 (s, NH and $^+$NH), 7.55 (dd, $J = 9.5$ Hz, $J' = 2.5$ Hz, 1H, 7-H), 7.63–7.71 [complex signal, 5H, Ar-H phenyl], 7.75 (d, $J = 2.5$ Hz, 1H, 5-H), 7.90 (dd, $J = 9.0$ Hz, $J' = 1.5$ Hz, 1H, 8"-H), 7.97 (d, $J = 9.0$ Hz, 1H, 7"-H), 8.19 (broad s, 1H, 10"-H),

8.36 (d, J = 9.5 Hz, 1H, 8-H); ^{13}C NMR (100.6 MHz, CD_3OD) δ 21.7 (2 CH_2, C3 and C3"), 22.9 (CH_2, C2), 23.6 (CH_2, C4"), 24.8 (CH_2, C1), 27.2 (CH_2) and 27.4 (CH_2) (C3' and C4'), 29.3 (CH_2, C4), 30.2 (CH_2, C5'), 31.2 (CH_2, C2'), 32.8 (CH_2, 9"-*C*H_2-CH_2-CONH), 38.1 (CH_2, 9"-CH_2-*C*H_2-CONH), 40.1 (CH_2, C6'), 48.9 (CH_2, C1'), 70.8 (CH_2, C2"), 113.3 (C, C9a), 114.5 (C, C4a"), 115.4 (C, C8a), 119.1 (CH, C5), 121.0 (C, C10a"), 121.6 (CH) and 122.4 (CH) (C7" and C10"), 126.8 (CH, C7), 128.8 (CH, C8), 130.2 (CH) and 130.3 (CH) [C2(6) and C3(5) phenyl], 132.5 (CH, C4 phenyl), 133.4 (C, C1 phenyl), 136.3 (CH, C8"), 138.9 (C, C6a"), 140.1 (C, C6), 140.5 (C, C10a), 143.3 (C, C9"), 152.1 (C, C4a), 157.4 (C, C5") 157.8 (C, C9), 165.8 (C, C10b"), 174.3 (C, CONH). HRMS calcd for ($C_{40}H_{43}{}^{35}ClN_4O_2$ + H^+) 647.3147, found 647.3143. Anal. ($C_{40}H_{43}ClN_4O_2$·2HCl·4H_2O) C, H, N.

6-Chloro-9-{{7-[3-(3,4-dihydro-5-phenyl-2*H*-pyrano[3,2-*c*]quinolin-9-yl)propanamido]heptyl}amino}-1,2,3,4-tetrahydroacridine Dihydrochloride (26·2HCl). From crude **14** [281 mg of the crude product obtained from 150 mg (0.43 mmol) of ester **12**] and amine **17d** (143 mg, 0.41 mmol), a yellow oily residue (299 mg) was obtained and subjected to column chromatography [35–70 μm silica gel (22 g), heptane/AcOEt/Et_3N mixtures]. On elution with heptane/AcOEt/Et_3N 10:90:0.1 to 0:100:0.1, hybrid **26** (120 mg, 44% yield) was isolated as a yellowish oil: R_f = 0.63 (AcOEt/MeOH/Et_3N 90:10:0.1). **26**·2HCl: mp 190–191 ºC (MeOH/AcOEt 2:9). IR (KBr) ν 3500–2500 (max at 3244, 3055, 2926, 2855, N–H, $^+$N–H, O–H, and C–H st), 1633 and 1576 (C=O, ar–C–C and ar–C–N st) cm^{-1}; ^{1}H NMR (500 MHz, CD_3OD) δ 1.20–1.45 (complex signal, 8H, 3'-H_2, 4'-H_2, 5'-H_2, and 6'-H_2), 1.79 (tt, J = J' = 7.0 Hz, 2H, 2'-H_2), 1.90–2.00 (complex signal, 4H, 2-H_2, and 3-H_2), 2.12 (tt, $J \approx J' \approx$ 5.5 Hz, 2H, 3"-H_2), 2.60 (t, J = 7.5 Hz, 2H, 9"-CH_2-C*H*$_2$-CONH), 2.65 (m, 2H, 1-H_2), 2.80 (t, J = 6.0 Hz, 2H, 4"-H_2), 2.98 (m, 2H, 4-H_2), 3,11 (td, $J \approx J' \approx$ 7.0 Hz, 2H, 7'-H_2), 3.15 (t, J = 7.5 Hz, 2H, 9"-C*H*$_2$-CH_2-CONH), 3.90 (t, J = 7.0 Hz, 2H, 1'-H_2), 4.69 (t, J = 5.0 Hz, 2H, 2"-H_2), 4.85 (s, NH and $^+$NH), 7.54 (broad d, J = 9.0 Hz, 1H, 7-H), 7.55–7.68 [complex signal, 5H, Ar-H phenyl], 7.76 (broad s, 1H, 5-H), 7.84 (broad d, $J \approx$ 9.0 Hz, 1H, 8"-H), 7.95 (d, J = 9.0 Hz, 1H, 7"-H), 8.15 (broad s, 1H, 10"-H), 8.36 (d, J = 9.0 Hz, 1H, 8-H); ^{13}C NMR (100.6 MHz, CD_3OD) δ 21.8 (CH_2, C3"), 21.9 (CH_2, C3), 22.9 (CH_2, C2), 23.7 (CH_2, C4"), 24.7 (CH_2, C1), 27.6 (CH_2, C3'), 27.7 (CH_2, C5'), 29.3 (CH_2, C4), 29.8 (CH_2, C4'), 30.2 (CH_2, C6'), 31.3 (CH_2, C2'), 32.8 (CH_2, 9"-*C*H_2-CH_2-CONH), 38.2 (CH_2, 9"-CH_2-*C*H_2-CONH), 40.2 (CH_2, C7'), 49.1 (CH_2, C1'), 70.6 (CH_2, C2"), 113.3 (C, C9a), 114.3 (C, C4a"), 115.4 (C, C8a), 119.1 (CH, C5), 121.0 (C, C10a"), 122.2 (CH, C7"), 122.3 (CH, C10"), 126.8 (CH, C7), 128.8 (CH, C8), 130.1 (CH) and 130.2 (CH) [C2(6) and C3(5) phenyl], 132.2 (C+CH) (C1 and C4 phenyl), 135.9 (CH, C8"), 139.5 (C, C6a"), 140.1 (C, C6), 140.5 (C, C10a), 143.0 (C, C9"), 152.1 (C, C4a), 157.8 (C, C5"), 157.9 (C, C9), 165.1 (C, C10b"), 174.3 (C, CONH). HRMS calcd for ($C_{41}H_{45}{}^{35}ClN_4O_2$ + H^+) 661.3303, found 661.3300. Anal. ($C_{41}H_{45}ClN_4O_2$·2HCl·2H_2O) C, H, N.

Solution Stability Study. 1:1 Acetonitrile/Sorensen phosphate buffer at pH 7.4 solutions of hybrid **23** at 1 mg mL^{-1} were prepared in duplicate, spliced in 10 portions of 100 μL, and incubated at 37 ºC.[1] The integrity of the compound was assessed at time points t = 0, 0.5, 1, 2, 4, 8, 12, 24, 48, and 96 h by direct injection of 5 μL of a given portion into an HPLC chromatograph (Perkin Elmer series 200 chromatograph provided with a variable λ detector, using a Kromasil® C-18 column (5 μm, 25×0.46 cm), 35:65:0.2 acetonitrile/water/trifluoroacetic acid as eluent, flow 1 mL min^{-1}, λ = 254 nm) and comparison of the resulting chromatogram with those of **23** at t = 0 (t_R = 5.05 min) and of a pure sample of its hydrolysis product **17a** (t_R = 2.33 min).

Table S1. Values of pK_a Estimated for Selected Compounds Using ACD Software.[2]

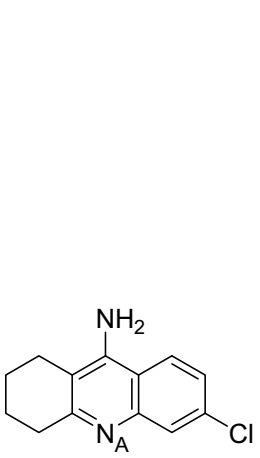

6-Chlorotacrine, **3**

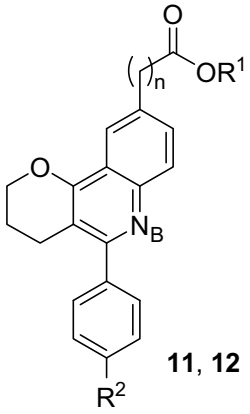

11, **12**

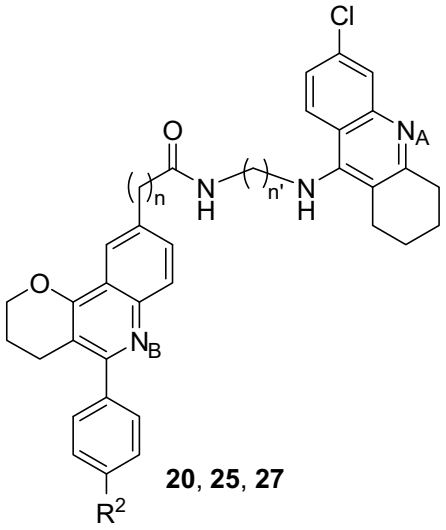

20, **25**, **27**

Compound	pK_a	
	N_A	N_B
6-Chlorotacrine	9.7	---
11 (n = 0; R^1 = Et; R^2 = Cl)	---	4.5
12 (n = 2; R^1 = Me; R^2 = H)	---	6.0
20 (n = 0; n' = 8; R^2 = Cl)	8.9	4.6
25 (n = 2; n' = 6; R^2 = H)	8.9	6.1
27 (n = 2; n' = 8; R^2 = H)	8.9	6.1

Table S2. Orientation of the Indole Ring of Trp286 (hAChE Numbering) Found in Several X-Ray Crystallographic Structures of AChE.[a]

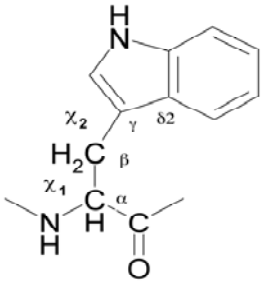

PDB code	Enzyme[b]	Ligand	χ_1: N–C_α–C_β–C_γ [c] χ_2: C_α–C_β–C_γ–$C_{\delta 2}$	Ref.[d]
Apo form				
2ACE	*Tc*AChE	—	–62.7 –89.0	75
1J06	mAChE	—	–60.1, –60.6 –78.9, –68.0	53
Catalytic site inhibitors				
1ACJ	*Tc*AChE	tacrine	–53.7 –150.8	7
1E66	*Tc*AChE	huprine X	–60.4 –83.1	69
1VOT	*Tc*AChE	(–)-huperzine A	–57.7 –95.7	76
Peripheral site inhibitors				
1N5R	mAChE	propidium	–60.9, –64.0 –83.7, –87.2	53
1J07	mAChE	decidium	–66.2, –67.4 –80.0, –77.8	53
1N5M	mAChE	gallamine	–65.6, –61.6 –82.1, –91.0	53
1B41	hAChE	fasciculin	–57.6 –83.1	78
Dual binding site inhibitors				
1ACL	*Tc*AChE	decamethonium	–64.8 –92.5	7
1EVE	*Tc*AChE	donepezil	–51.7 –83.5	77

1ZGB	*Tc*AChE	(*R*)-tacrine(10)-hupyridone	–60.0 –82.6	72
1ZGC	*Tc*AChE	(*S*)-tacrine(10)-hupyridone	–65.6,–59.4 –81.2, –80.5	72
1Q84	mAChE	*anti*-TZ2PA6	–73.0, –74.2 –74.5, –64.8	73
2CMF	*Tc*AChE	*bis*(5)-tacrine	–76.3 –87.0	70
2CKM	*Tc*AChE	*bis*(7)-tacrine	–121.4 +43.7	70
1ODC	*Tc*AChE	tacrine(8)-4-aminoquinoline	–122.4 +55.7	70
2CEK	*Tc*AChE	NF595	–118.2 +46.5	71
1Q83	mAChE	*syn*-TZ2PA6	–162.4, –163.7 –126.8, –122.2	73

[a] The orientation is measured through the dihedral angles N–C_α–C_β–C_γ and C_α–C_β–C_γ–$C_{\delta 2}$ (in degrees) of the side chain. [b] *Tc*AChE, *Torpedo californica* AChE; mAChE, mouse AChE; hAChE, human AChE. [c] If more than one monomer is present in the X-ray crystallographic structure, the dihedral angles measured for the side chain of Trp286 in each monomer are given in the Table. [d] See these references in the text.

Table S3. Best Poses (Chosen on the Basis of the Minimum Root-Mean Square Deviation (RMSD; Å) Relative to the X-ray Crystallographic Structure) for Selected Dual Binding Site Inhibitors upon Docking to Their Target Models of hAChE.

Ligand	PDB entry	RMSD	Rank order	Docked ligand[a]
Target A				
anti-TZ2PA6	1Q84	1.5	4	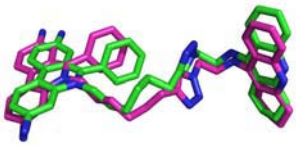
(*R*)-Tacrine(10)-hupyridone	1ZGB	1.8	10	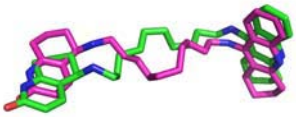
(*S*)-Tacrine(10)-hupyridone	1ZGC	1.2	3	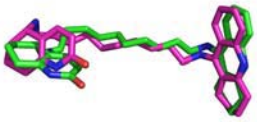
bis(5)-Tacrine	2CMF	0.9	5	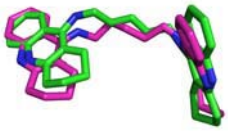
Target B				
Tacrine(8)-4-aminoquinoline	1ODC	1.5	9	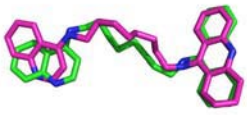
bis(7)-Tacrine	2CKM	1.3	1	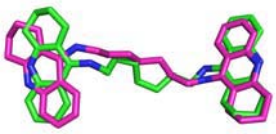

Target C				
syn-TZ2PA6	1Q83	1.8	3	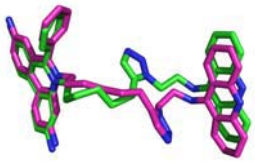

[a] The best docked pose is shown coloured by atom, and the X-ray crystallographic structure is shown in magenta.

Table S4. MM–PBSA Analysis of the Binding Affinity (kcal/mol) Determined for the Most Favorable Interaction of Compounds **20**, **25** and **27** to Targets A–C.

Compound[a]	Target	ΔG_{MM}	ΔG_{ele}^{sol}	$\Delta G_{non-polar}^{sol}$	$\Delta G_{binding}$	$\Delta\Delta G_{binding}$
20	A	–238.0	129.5	–3.7	–112.2	0.0
(ε = 2)	B	–222.2	121.2	–3.5	–104.5	7.7
	C	–229.5	116.8	–3.8	–116.5	–4.3
20	A	–167.4	30.6	–3.7	–140.5	0.0
(ε = 4)	B	–162.8	31.0	–3.6	–135.4	5.1
	C	–168.3	29.2	–3.8	–142.9	–2.4
25	A	–228.3	127.0	–3.5	–104.8	0.0
(ε = 2)	B	–229.4	127.2	–3.6	–105.8	–1.0
	C	–224.3	115.6	–3.7	–112.4	–7.6
25	A	–163.2	30.0	-3.5	–136.7	0.0
(ε = 4)	B	–161.6	32.1	-3.5	–133.0	3.7
	C	–164.9	28.9	–3.8	–139.8	–3.1
27 [b]	A	–226.2	122.3	–3.7	–106.4	0.0
(ε = 2)	B	–227.0	126.9	–3.5	–102.4	4.0
	C	–226.6	116.0	–3.9	–113.3	–6.9
27 [b]	A	–160.5	28.8	–3.6	–134.1	0.0
(ε = 4)	B	–162.4	31.2	–3.6	–133.6	0.5
	C	–168.6	27.4	–4.0	–144.0	–9.9

[a] Value of the dielectric permittivity used for the interior of the protein–ligand complex is indicated in parenthesis. [b] Corrected for the freezing of the extra conformational degrees of freedom (see Experimental Section).

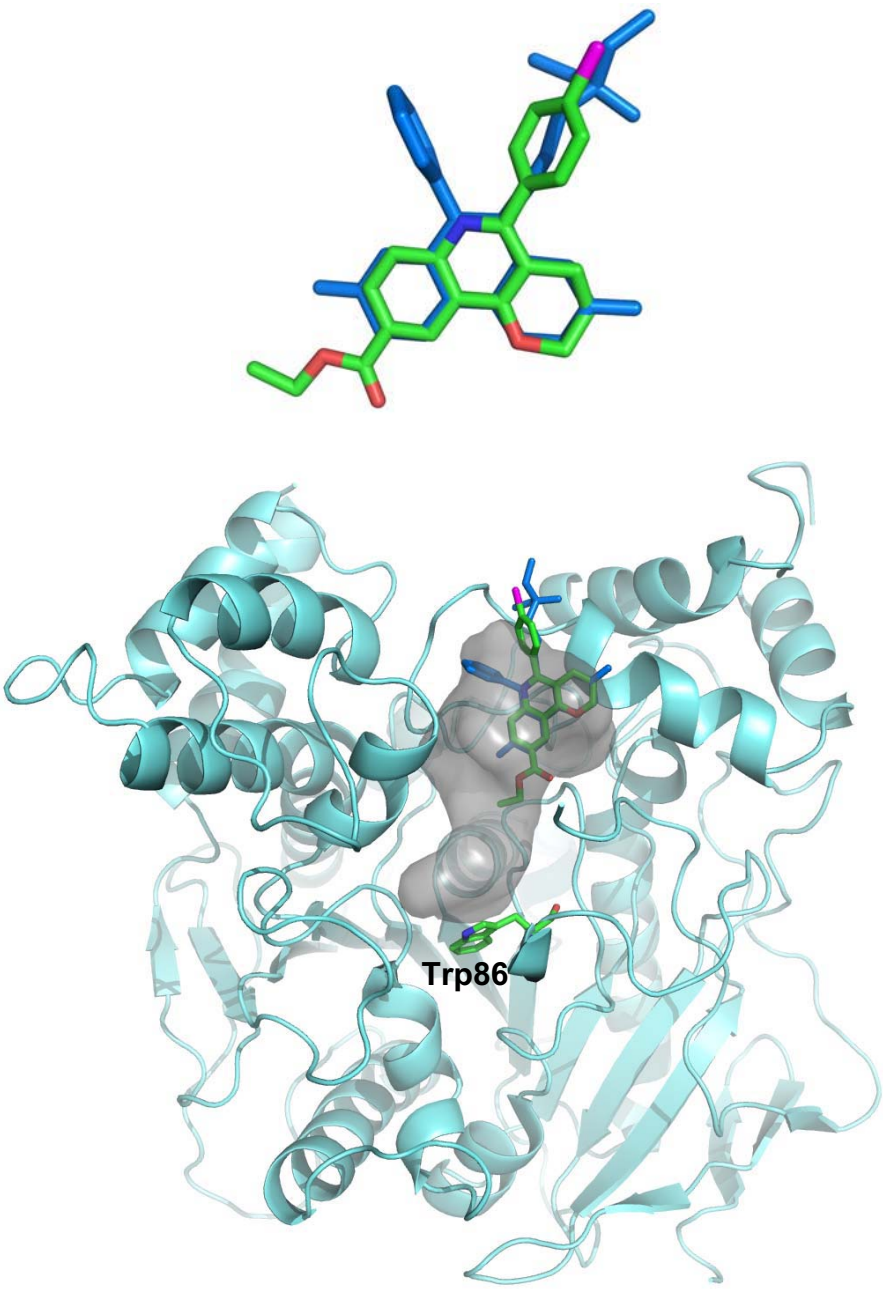

Figure S1. Superposition of the 6-phenylphenanthridinium and 5-phenylpyrano[3,2-*c*]quinoline moieties of propidium (blue) and ester **11** (coloured by atom), respectively, at the peripheral site of AChE. Trp86 at the AChE catalytic site is also shown. The gorge leading from the peripheral site to the catalytic pocket is shown in grey.

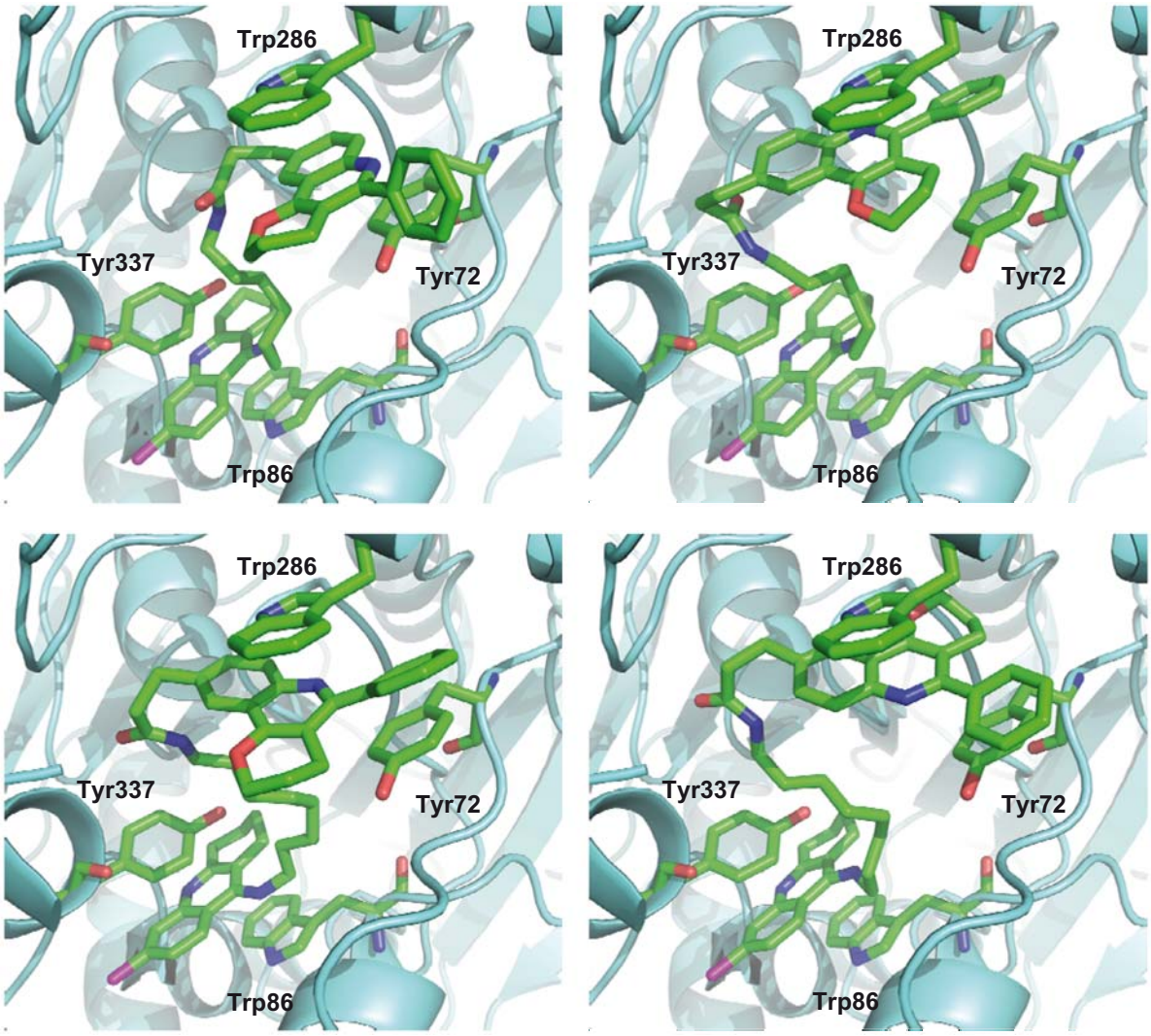

Figure S2. Representation of the most favorable binding mode of hybrids **25** (top) and **27** (bottom) (coloured by atom) determined from MM–PBSA computations performed with internal permittivities of 2 (left) and 4 (right). Relevant residues at the catalytic (Trp86 and Tyr337) and peripheral (Trp286 and Tyr72) binding sites are coloured by atom.

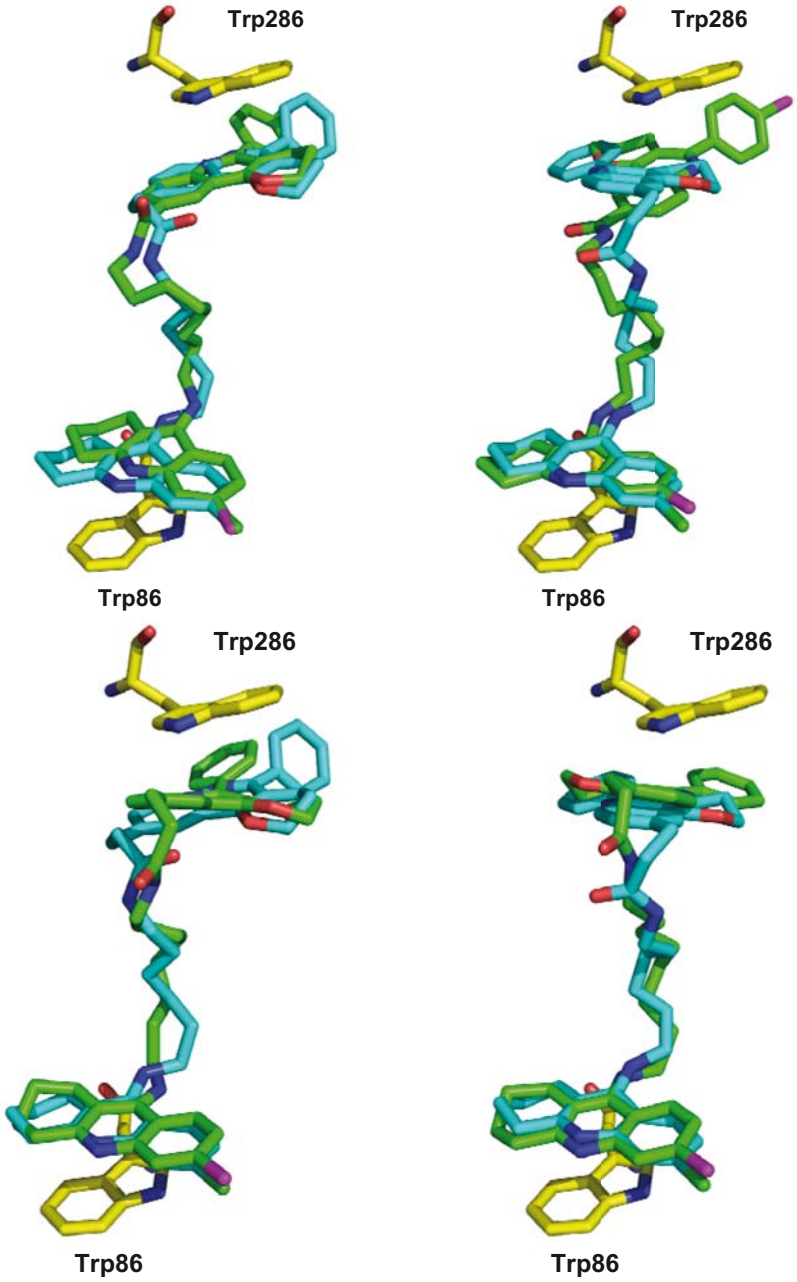

Figure S3. Superposition of the most favorable binding modes determined from MM–PBSA computations performed using internal permittivities of 2 (left) and 4 (right) for hybrids (top) **20** (coloured by atom) and **25** (blue) and (bottom) **25** (blue) and **27** (coloured by atom).

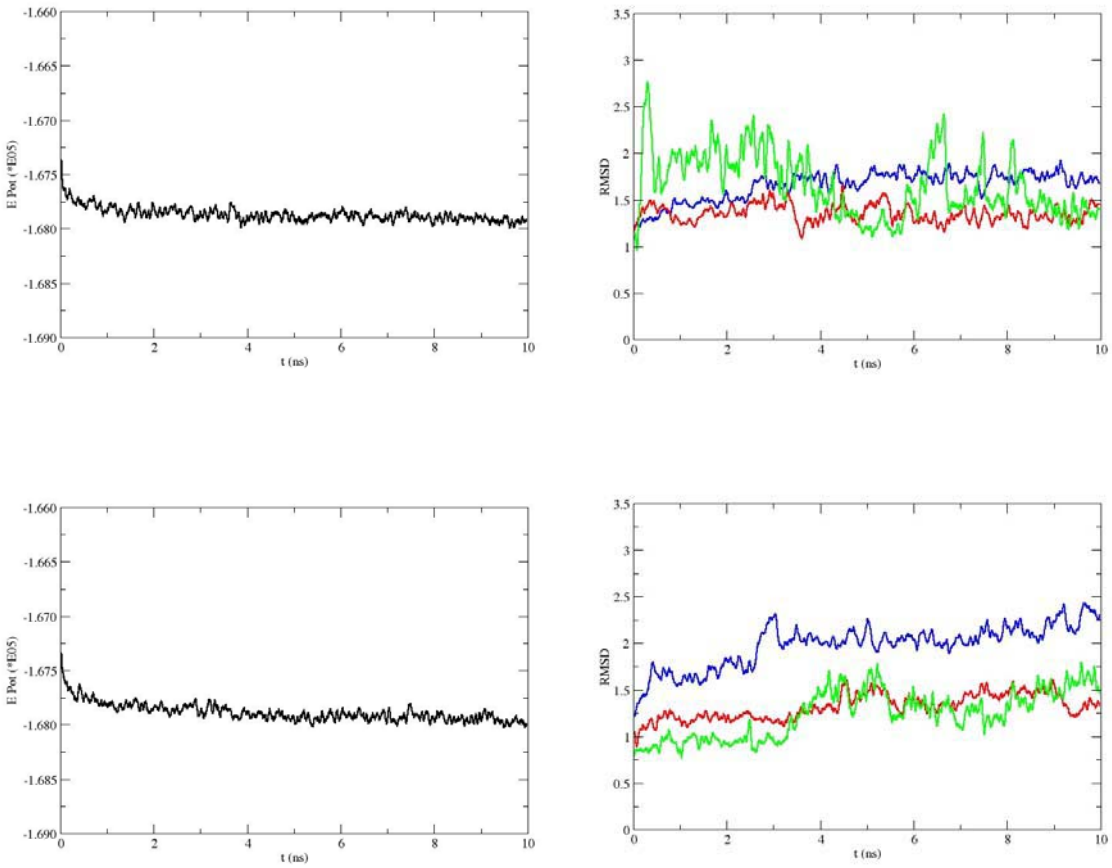

Figure S4. Time dependence of the potential energy (E Pot; kcal/mol) and positional root-mean square deviation (RMSD; Å) of the backbone atoms (blue), the heavy atoms in the binding site (including catalytic and peripheral sites and the gorge; red) and the heavy atoms of the ligand (green) for the AChE complexes with **20** (top) and **25** (bottom) along the 10 ns molecular dynamics simulations.

In Vitro Blood–Brain Barrier Permeation Assay

Table S5. Permeability (P_e 10^{-6} cm s^{-1})[a] in the PAMPA-BBB Assay for Commercial Drugs (Used in the Experiment Validation) and Pyrano[3,2-*c*]quinoline–6-Chlorotacrine Hybrids with their Predictive Penetration into the CNS.

Commercial drugs	Bibl.[b]	PBS:EtOH (80:20)	PBS:EtOH (70:30)
testosterone	17.0	27.6 ± 1.7	38.9 ± 2.4
verapamil	16.0	26.7 ± 0.4	28.3 ± 2.1
imipramine	13.0	19.2 ± 0.3	22.3 ± 1.2
desipramine	12.0	22.9 ± 0.3	24.4 ± 2.3
progesterone	9.3	n.d.	26.1 ± 2.4
promazine	8.8	13.2 ± 0.3	22.4 ± 1.5
chlorpromazine	6.5	8.5 ± 0.4	13.6 ± 0.9
clonidine	5.3	10.2 ± 0.9	14.1 ± 0.8
corticosterone	5.1	8.8 ± 0.4	6.4 ± 0.3
piroxicam	2.5	2.5 ± 0.3	3.0 ± 0.2
hydrocortisone	1.9	4.9 ± 0.2	4.9 ± 0.2
caffeine	1.3	4.7 ± 0.3	4.4 ± 0.3
lomefloxacin	1.1	4.3 ± 0.2	2.8 ± 0.1
enoxacin	0.9	4.7 ± 0.4	4.2 ± 0.3
ofloxacin	0.8	3.1 ± 0.1	2.6 ± 0.1

Compound	PBS:EtOH (80:20)	PBS:EtOH (70:30)	Prediction
18·2HCl	n.d.[c]	14.9 ± 1.1	CNS+
19·2HCl	n.d.[c]	17.7 ± 0.2	CNS+
23·2HCl	15.1 ± 0.2	n.d.	CNS+
24·2HCl	n.d.[c]	10.6 ± 0.4	CNS+
25·2HCl	13.2 ± 0.4	n.d.	CNS+
26·2HCl	n.d.[c]	10.2 ± 0.3	CNS+
27·2HCl	n.d.[c]	10.1 ± 0.4	CNS+
12	21.4 ± 0.6	n.d.	CNS+
6-chlorotacrine·HCl	19.8 ± 0.4	n.d.	CNS+

[a] Data are the mean ± SD of 3 independent experiments. [b] Taken from ref. 3. [c] Compounds **18**·2HCl, **19**·2HCl, **24**·2HCl, **26**·2HCl, and **27**·2HCl were evaluated in PBS:EtOH (70:30) because of their poor solubility in PBS:EtOH (80:20).

Assay validations were made by comparing the experimental permeability of commercial drugs with reported values, which gave a good linear correlation in each case (Figure S5).

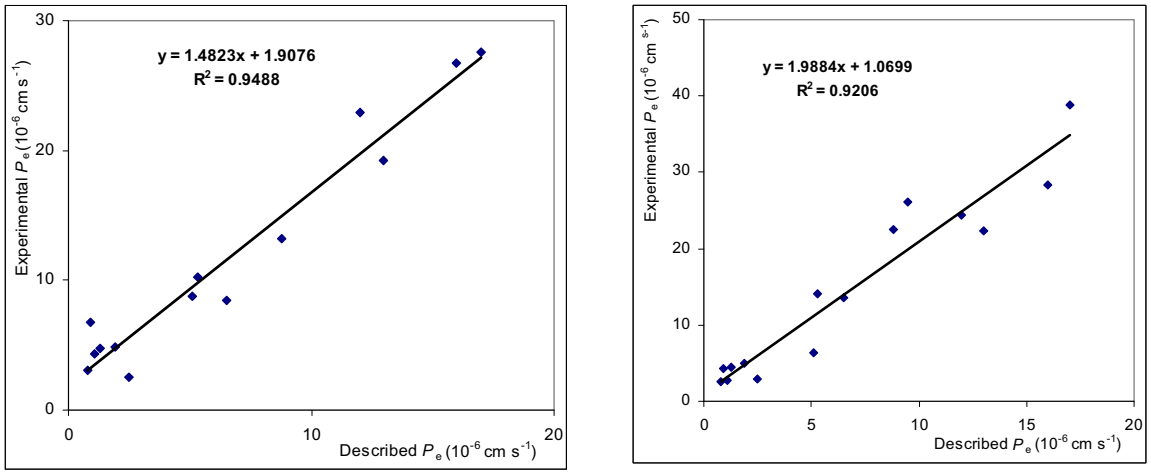

(a) (b)

Figure S5. Lineal correlation between experimental and reported permeability of commercial drugs using the PAMPA-BBB assay. (a) PBS:EtOH (80:20). (b) PBS:EtOH (70:30).

From the straight-line equations and taking into account the described limits for BBB permeation,[3] we established the ranges of permeability for these assays as shown in Table S6.

Table S6. Ranges of Permeability of PAMPA-BBB Assays (P_e, 10^{-6} cm s^{-1}).

	PBS:EtOH (80:20)	PBS:EtOH (70:30)
Compounds of high BBB permeation (CNS+)	$P_e > 7.8$	$P_e > 9.0$
Compounds of uncertain BBB permeation (CNS+/–)	$7.8 > P_e > 4.9$	$9.0 > P_e > 5.1$
Compounds of low BBB permeation (CNS–)	$P_e < 4.9$	$P_e < 5.1$

References

(1) Kerns, E. H.; Di, L. Drug-Like Properties: Concepts, Structure Design and Methods. From ADME to Toxicity Optimization; Elsevier: Amsterdam, 2008; pp 353–359.

(2) ACD/p*K*a v8.02, Advanced Chemistry Development, Inc., Toronto ON, Canada, www.acdlabs.com, 2006.

(3) Di, L.; Kerns, E. H.; Fan, K.; McConnell, O. J.; Carter, G. T. High Throughput Artificial Membrane Permeability Assay for Blood–Brain Barrier. *Eur. J. Med. Chem.* **2003**, *38*, 223–232.

Appendix

Compound	Molecular Formula	Calculated			Found		
		C	H	N	C	H	N
17a·2HCl·1.5H_2O	$C_{17}H_{22}ClN_3$·2HCl·1.5H_2O	50.57	6.74	10.41	50.49	6.24	10.05
28b·2HCl·2.75H_2O	$C_{31}H_{34}Cl_2N_4$·2HCl·2.75H_2O	56.76	6.38	8.54	56.67	6.24	8.73
28f·2HCl·1.25H_2O	$C_{35}H_{42}Cl_2N_4$·2HCl·1.25H_2O	61.36	6.84	8.18	61.06	6.81	7.79
18·2HCl·2.4H_2O	$C_{38}H_{38}Cl_2N_4O_2$·2HCl·2.4H_2O	59.29	5.87	7.28	59.66	5.59	6.83
19·2HCl·0.5H_2O	$C_{39}H_{40}Cl_2N_4O_2$·2HCl·0.5H_2O	62.49	5.78	7.47	62.11	6.02	7.28
20·2HCl	$C_{40}H_{42}Cl_2N_4O_2$·2HCl	63.67	5.88	7.42	64.04	6.07	7.14
21·2HCl·2.1H_2O	$C_{41}H_{44}Cl_2N_4O_2$·2HCl·2.1H_2O	61.06	6.27	6.95	60.79	5.87	6.92
22·2HCl·1.25H_2O	$C_{42}H_{46}Cl_2N_4O_2$·2HCl·1.25H_2O	62.65	6.32	6.96	62.66	6.15	6.91
23·2HCl·3H_2O·0.25AcOEt	$C_{38}H_{39}ClN_4O_2$·2HCl·3H_2O·0.25AcOEt	60.98	6.43	7.29	61.13	6.18	6.90
24·2HCl·3H_2O	$C_{39}H_{41}ClN_4O_2$·2HCl·3H_2O	61.62	6.50	7.37	61.52	6.60	7.03
25·2HCl·4H_2O	$C_{40}H_{43}ClN_4O_2$·2HCl·4H_2O	60.64	6.74	7.07	60.45	6.20	6.60
26·2HCl·2H_2O	$C_{41}H_{45}ClN_4O_2$·2HCl·2H_2O	63.93	6.67	7.27	63.64	6.61	7.07
27·2HCl·2.25H_2O	$C_{42}H_{47}ClN_4O_2$·2HCl·2.25H_2O	63.96	6.84	7.10	64.34	6.86	6.63

Capítol 5: ***Estudis de modelatge molecular d'híbrids donepezil–huprina amb activitat inhibitòria enfront la formació i l'agregació del pèptid βA.***

(*ChemMedChem* **2010**, *5*, 1855–1879).

5.1 Els híbrids donepezil–huprina

En vista de l'excel·lent perfil farmacològic dels híbrids donepezil–tacrina **19**–**22a**,**b** preparats en el nostre grup de recerca, particularment dels derivats indànics **21a**,**b** i **22a**,**b** pel que fa a l'efecte antiagregant del pèptid βA, i de l'elevada afinitat de les huprines pel centre actiu de l'AChE, en el Màster Experimental d'Elisabet Viayna es va plantejar la preparació d'una sèrie d'híbrids donepezil–huprina d'estructures **68**–**69a**,**b** en forma racèmica (Figura 5.1) com a una nova família d'inhibidors d'AChE de lloc d'unió dual, constituïts per una unitat d'huprina Y, **15** o d'huprina X, **16**, per a la interacció amb el centre actiu de l'AChE i el fragment de 5,6-dimetoxi-2[(4-piperidinil)metil]indà derivat del donepezil per a interaccionar amb la gorja catalítica i el lloc perifèric, separats per una cadena espaiadora constituïda per 2 o 3 grups metilè.

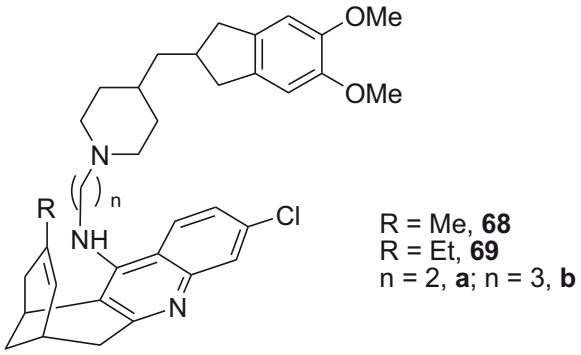

Figura 5.1 Nous híbrids donepezil–huprina com a inhibidors d'AChE de lloc d'unió dual.

D'altra banda, donada la diferència d'activitat inhibitòria de l'AChE entre els dos enantiòmers de les huprines Y i X en favor de l'enantiòmer levorotatori, de configuració (7*S*,11*S*), eutòmer de la família,[135] es va plantejar la síntesi dels enantiòmers (7*S*,11*S*) d'aquests híbrids. A més, a efectes de comparació, també es va plantejar la preparació de l'enantiòmer (7*R*,11*R*) d'algun d'aquests híbrids. Cal destacar que la síntesi d'aquests nous híbrids es va plantejar seguint la metodologia alternativa desenvolupada en aquesta Tesi Doctoral per als híbrids donepezil–tacrina (Capítol 3).

L'activitat inhibitòria de l'AChE i la BchE humanes dels nous híbrids donepezil–huprina **68**–**69a**,**b** van ser avaluats pel grup d'investigació dels Drs. Albert Badia i M. Victòria Clos fent servir el mètode Ellman.[129]

[129]Ellman, G.L.; Courtney, K.D.; Andres, B., Jr.; Featherstone, R.M. *Biochem. Pharmacol.* **1961**, *7*, 88. [135]Camps, P.; El Achab, R.; Görbig, D.M.; Morral, J.; Muñoz-Torrero, D.; Badia, A.; Baños, J.E.; Vivas, N.M.; Barril, X.; Orozco, M.; Luque F.J. *J. Med. Chem.* **1999**, *42,* 3227.

Els nous híbrids van resultat ser potents inhibidors d'hAChE, amb valors d'IC_{50} en el rang nanomolar baix. L'avaluació d'aquests compostos va permetre establir quines característiques estructurals proporcionaven una major activitat inhibitòria enfront l'hAChE, com són la presència del grup metil en la posició 9 de la unitat d'huprina o la cadena espaiadora de 3 carbonis. Com era d'esperar, els enantiòmers levorotatoris contenint una unitat derivada de la (7*S*,11*S*)-huprina Y o X són els eutòmers d'aquesta família, sent unes 2 vegades més potents que els corresponents racèmics i molt més potents que l'enantiòmer dextrorotatori.

Tot i que els nous híbrids donepezil–huprina han resultat ser potents inhibidors de l'hAChE, la seva menor activitat anticolinesteràsica respecte les huprines a partir de les quals han estat dissenyats, així com les diferències d'activitat trobades entre els híbrids 9-metil i 9-etil substituïts (Taula 5.1) semblaven indicatius d'un diferent mode d'unió amb el centre actiu de l'AChE.

Taula 5.1 Activitat inhibitòria dels híbrids donepezil–huprina enfront l'hAChE i la hBChE.[a]

Compost	IC_{50} (nM) hAChE	IC_{50} (nM) hBChE
(±)-**68a**·2HCl	18,1 ± 1,2	336 ± 21
(–)-**68a**·2HCl	13,0 ± 0,1	303 ± 12
(±)-**68b**·2HCl	5,37 ± 0,3	88 ± 2,3
(–)-**68b**·2HCl	2,61 ± 0,2	349 ± 20
(+)-**68b**·2HCl	49,9 ± 5,1	95 ± 5,3
(±)-**69a**·2HCl	48,6 ± 5,2	174 ± 9,4
(–)-**69a**·2HCl	28,6 ± 2,3	419 ± 17
(±)-**69b**·2HCl	6,32 ± 0,1	61 ± 3,2
(–)-**69b**·2HCl	3,85 ± 0,2	194 ± 9,3
donepezil·HCl	21,4 ± 2,3	7273 ± 621
(±)-**huprina Y**·HCl	0,61 ± 0,03	236 ± 44
(–)-**huprina Y**·HCl	0,43 ± 0,03	247 ± 18
(+)-**huprina Y**·HCl	13,6 ± 1,5	153 ± 31
(±)-**huprina X**·HCl	0,67 ± 0,05	15,8 ± 2,4
(–)-**huprina X**·HCl	0,27 ± 0,02	159 ± 10
(+)-**huprina X**·HCl	6,30 ± 0,5	58,3 ± 5,9

[a] Valors expressats com a mitjana ± error estàndard de la mitjana de com a mínim 4 experiments. Activitat expressada com a IC_{50} (nM) enfront l'AChE humana recombinant o BChE de sèrum humà.

D'altra banda, el grup d'investigació de la Dra. Vincenza Andrisano va determinar la inhibició de l'agregació del βA induïda per AChE i de l'agregació del βA espontània, així com la inhibició de l'enzim BACE-1. Els resultats van indicar que els nous híbrids donepezil–huprina inhibeixen significativament l'agregació del pèptid βA induïda per hAChE a una concentració de 100 μM, obtenint-se percentatges d'inhibició entre 27% i 50%. La inhibició augmenta lleugerament en presència del *linker* trimetilènic però en canvi, la presència d'un substituent metil o etil en la posició 9 de la unitat d'huprina no sembla tenir cap efecte sobre l'activitat enfront l'agregació del βA induïda per hAChE.

La necessitat d'explorar el mode d'unió d'aquests nous híbrids mitjançant tècniques computacionals per confirmar el caràcter d'inhibidors de lloc d'unió dual de l'AChE i justificar les diferències d'activitat entre els diferents compostos de la sèrie semblava clara.

5.2 Química computacional

Veure també Mètodes en química computacional (Annex 1)

L'elevat nombre d'àtoms que contenen els sistemes d'interès bioquímic i farmacològic fa inabordable en l'actualitat el tractament mecano-quàntic dels mateixos. Per això, el seu estudi s'ha d'abordar recurrint a la mecànica molecular, que suposa que les molècules poden descriure's com un conjunt de masses centrades en els nuclis atòmics units entre elles mitjançant molles. El conjunt de forces en què es troben aquestes partícules segueix un tractament clàssic, així la mecànica molecular ens permet examinar de forma eficient l'espai configuracional de sistemes amb un gran nombre d'àtoms, sempre que les propietats d'interès no suposin una redistribució important en la densitat electrònica de les molècules, com són els processos associats a la formació i ruptura d'enllaços.[136]

Per a poder aplicar la mecànica molecular s'han d'assumir tres principis fonamentals: (i) la descripció de les diferents contribucions energètiques mitjançant potencials efectius, (ii) l'additivitat dels mateixos, i (iii) la transferibilitat d'aquests potencials.[137]

[136]Leach, A.R. *Molecular Modelling: Principles and applications,* 2nd edition, **2001**, Pearson Education (Prentice Hall), Essex. [137]Schlick, T. *Molecular Modeling and Simulation. An interdisciplinary Guide,* **2002**, Springer-Verlag New York, Inc. New York.

En base al primer principi, s'assumeix que l'energia molecular pot expressar-se com una suma de potencials que representen forces físiques simples. Les contribucions energètiques es classifiquen com a termes *enllaçants*, quan describeixen les tensions de tipus mecànic originades a conseqüència de desviacions respecte el valor d'equilibri de les longituds, els angles d'enllaç i les torsions dels diedres; i els termes *no enllaçants*, que generalment es limiten a les interaccions electrostàtiques i de van der Waals.[136,137] Per tant, l'energia pot expressar-se com:

$$E_{total} = \left(\sum_{\substack{enlaces \\ i}} E_{enlace}\left(b_i\right) + \sum_{\substack{ángulos \\ i}} E_{ángulos}\left(\theta_i\right) + \sum_{\substack{diedros \\ i}} E_{died.}\left(\chi_i\right) \right)_{enlazados} + \left(\sum_{\substack{no\ enlazados \\ (i,j)i<j}} E_r\left(r_{ij}\right) \right)$$

En base al segon principi, s'assumeix que els paràmetres derivats de dades experimentals o càlculs mecano-quàntics d'estructures representatives poden utilitzar-se per ajustar els potencials efectius que descriuran les macromolècules a partir d'aquestes estructures.[136,137]

Dues tècniques d'especial utilitat en biologia en les quals s'apliquen els camps de forces són la mecànica molecular i la dinàmica molecular (DM). Ambdues tècniques comparteixen moltes característiques i la seva principal diferència estreba en la inclusió dels temps com a variable en la DM.

Les simulacions per DM es van començar a gestar en la dècada dels 50. L'any 1957, els Drs. Alder i Wainwright van utilitzar aquesta tècnica per primer cop per a simular l'evolució d'un sistema format per esferes rígides que interaccionaven en col·lisions perfectes.[138] Al llarg de les següents dècades i amb l'augment del poder de càlcul gràcies bàsicament a l'informàtica, les simulacions per DM han pasat a ser una eina essencial en el modelatge molecular. Mitjançant l'aplicació d'aquesta tècnica és possible obtenir informació estructural, termodinàmica o cinètica de processos biomoleculars, com canvis conformacionals associats a la unió de lligands, plegament de proteïnes, transport d'ions o formació d'agregats proteics, entre molts d'altres.[139]

[136]Leach, A.R. *Molecular Modelling: Principles and applications,* 2nd edition, **2001**, Pearson Education (Prentice Hall), Essex. [137]Schlick, T. *Molecular Modeling and Simulation. An interdisciplinary Guide,* **2002**, Springer-Verlag New York, Inc. New York. [138]Alder, B.J.; Wainwright, T.E. *J. Chem. Phys.* **1957**, 27, 1208. [139]Adcock, S.A.; McCammon, J.A. *Chem. Rev.* **2006**, *106*, 1589.

5.3 Modelatge molecular dels híbrids donepezil–huprina

El mode d'unió dels compostos (–)-**68a** i (–)-**68b** amb l'hAChE (cal notar la diferència d'alguns residus entre l'hAChE i la *Tc*AChE, Taula 5.2) va ser explorat mitjançant simulacions de DM de 30 ns. El posicionament inicial dels compostos va ser construït aprofitant el mode d'unió conegut de la (–)-huprina X en el complex amb *Tc*AChE obtingut per cristal·lografia de raigs X,[108] i del mode d'unió amb l'AChE dels híbrids donepezil–tacrina suggerit en la Tesi Doctoral del Dr. Axel Bidón-Chanal, del grup de recerca del Dr. F. Javier Luque.[140]

En la DM simulada per al complex entre l'hAChE i (–)-**68a** es va obtenir una trajectoria estable, com es pot observar amb els perfils d'energia potencial i de *root-mean square desviation* (RMSD) de l'esquelet de la proteïna (backbone, 1.9 Å), dels residus que delimiten la gorja catalítica (*binding site*, 2.4 Å), incloent el centre catalític, la zona intermèdia de la gorja i el lloc perifèric; i dels àtoms del lligand (1,2 Å) en el complex enzim–lligand (Figura 5.2).

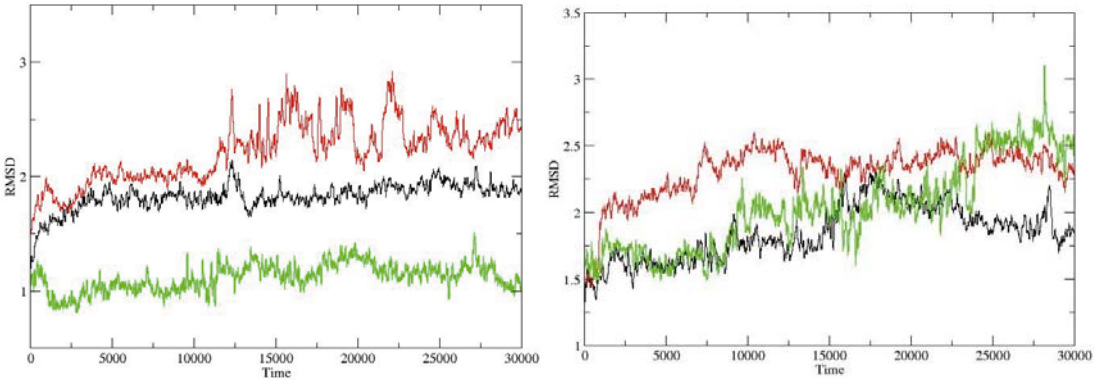

Figura 5.2 RMSDs (Å) de (–)-**68a** (esquerra) i (–)-**68b** (dreta) determinats per al *backbone* (negre), el lloc d'unió (*binding site*, vermell) i el lligand (verd) en la part mòbil de la simulació del sistema per al complex amb l'hAChE.

Per al complex amb (–)-**68b**, es van obtenir valors similars als anteriors de RMSD tant per al *backbone* com per al *binding site*. No obstant, en el cas del RMSD del lligand, aquest va anar augmentant progressivament fins a 2.5 Å durant els primers 23 ns de simulació. Després dels primers 23 ns, però, es va mantenir estable fins al final de la trajectòria. Així, el temps de relaxació necessari per a l'acomodament dels dos inhibidors en el lloc d'unió suggereix que hauria d'haver algunes diferències en les interaccions que intervenen en la unió de (–)-**68a** i (–)-**68b** amb l'hAChE.

[108]Dvir, H.; Wong, D.M.; Harel, M.; Barril, X.; Orozco, M.; Luque, F.J.; Muñoz-Torrero, D.; Camps, P.; Rosenberry, T.L.; Silman, I.; Sussman, J.L. *Biochemistry* **2002**, *41*, 2970. [140]Axel Bidón-Chanal, *Tesi Doctoral*, Universitat de Barcelona, **2007**.

Taula 5.2 Correspondència entre els residus de l'*Tc*AChE i l'hAChE

***Tc*AChE**	**hAChE**
Asp72	Asp74
Trp84	Trp86
Tyr121	Tyr124
Trp279	Trp286
Phe288	Phe295
Phe290	Phe297
Phe330	Tyr337
Phe331	Phe338
Tyr334	Tyr341
Trp432	Trp439
Met436	Met443
His440	His447

En el complex (–)-**68a**–AChE, la posició de la unitat de (–)-huprina Y en el lloc catalític gairebé coincideix amb la de la (–)-huprina X en l'estructura cristal·logràfica de raigs X del complex amb *Tc*AChE (codi PDB: 1E66, Figura 5.3). Així, el sistema heteroaromàtic de la (–)-huprina Y de (–)-**68a** interacciona mitjançant π-stacking amb l'anell de Trp86 (Trp84 en *Tc*AChE, distància mitjana: 3,8 Å). A més, també es conserva la interacció del nitrogen quinolínic protonat amb el grup carbonil de la His447. No obstant això, la interacció de π-stacking que s'observa entre l'anell heteroaromàtic de la huprina amb l'anell de benzè de la Phe330 (Tyr337 de l'hAChE) a l'estructura de raigs X no és manté en tota la seva totalitat en aquest cas. La pèrdua d'aquesta interacció es pot atribuir a la formació d'un pont de d'hidrogen entre el grup hidroxil de la Tyr337 i l'àtom de nitrogen protonat de la piperidina de (–)-**68a** (3,1 Å), la qual cosa impedeix la disposició adequada per al π-stacking de l'anell de fenol de la Tyr337 amb el sistema quinolínic de la unitat d'huprina. Al lloc perifèric, el sistema d'indà interacciona mitjançant π-stacking amb el Trp286 (Trp279 en *Tc*AChE), imitant així la interacció observada en l'estructura de raigs X del donepezil[141] (codi PDB: 1EVE). Hi ha, però, un desplaçament considerable de la posició relativa del grup indà i del grup indanona de (–)-**68a** i donepezil respectivament. L'anell de cinc membres de la unitat d'indà de (–)-**68a** ocupa la mateixa

[141]Kryger, G.; Silman, I.; Sussman, J.L. *Structure* **1999**, *7*, 297.

posició que l'anell de sis membres de la fracció d'indanona del donepezil, el que condueix a un millor apilament entre el sistema d'indà de (–)-**68a** en relació amb el de donepezil amb el Trp286. En la zona mitja de la gorja la presència de l'anell de piperidina dóna lloc a una notable reorganització estructural d'alguns residus específics. En el complex donepezil–*Tc*AChE la Tyr121 forma una interacció mediada per una molècula d'aigua amb l'àtom de nitrogen de la piperidina del donepezil. En canvi, en el complex (–)-**68a**–hAChE tal interacció es perd a causa de la nova orientació adoptada per l'anell de piperidina per formar un pont d'hidrogen amb la Tyr337. Aquesta nova orientació de l'anell piperidínic provoca el xoc amb la Tyr124 i la Phe338 (Tyr121 i Phe331 en *Tc*AChE). No obstant això, aquest xoc estèric acaba reduint-se al mínim com a conseqüència del desplaçament de la cadena lateral on estan aquests residus, que al seu torn afecta la disposició espacial de la Phe297 i la Phe295 (Phe290 i Phe288 en *Tc*AChE). Finalment, l'anell de piperidina també obliga a la distorsió de la Tyr341 (Tyr334 en *Tc*AChE), que al seu torn afecta a l'orientació espacial del Trp439 i la Met443 (Trp432 i Met436 en *Tc*AChE). Cal recalcar que aquests residus aromàtics defineixen els *pockets* d'unió que acomoden el grup etil de la posició 9 (Phe288, Phe290 i Phe331) i l'àtom de clor de la posició 3 (Trp432 i Met436) de la (–)-huprina X en *Tc*AChE (Figura 5.3).

El mode d'unió de (–)-**68b** en el centre actiu i el lloc periferic de l'hAChE conserva les interaccions essencials de (–)-**68a**, com poden ser el π-stacking amb el Trp86 i el Trp286, i el pont d'hidrogen amb la His447. No obstant això, la substitució del *linker* de dos metilens de (–)-**68a** pel linker trimetilènic de (–)-**68b** té una influència important en el posicionament de l'anell de piperidina en la part central de la gorja catalítica i dóna lloc a interaccions diferents amb els residus situats en aquesta part central. Així, la interacció per pont d'hidrogen entre (–)-**68a** i la Tyr337 es perd en (–)-**68b**. No obstant això, l'addició d'un grup metilè en el *linker* permet l'enfocament de l'anell de piperidina al grup carboxilat de l'Asp74, donant lloc a una interacció iònica, interacció que no existeix en el final de la DM amb (–)-**68a**.

D'altra banda, l'augment de la longitud del *linker* redueix al mínim el impediment estèric de l'anell de piperidina amb la Tyr124 i la Tyr341, que ocupen posicions similars a les observades en les estructures de raigs X de 1E66 i 1EVE. Per contra, l'orientació de la Tyr337 és en gran part alterada, i afecta la posició de la Phe338 en el lloc d'unió. Com a resultat, mentre que la cadena d'etil en la posició 9 de (–)-huprina X en 1E66 s'ajusta a una cavitat delimitada per la Phe288, la Phe290 i la Phe331 en *Tc*AChE (Phe295, Phe297, Phe338 en hAChE), aquest *pocket* està format per la Phe295, la Phe297 i en aquest cas la Tyr337, en el complex entre (–)-**68b** i hAChE al final dels 30 ns de DM (Figura 5.3).

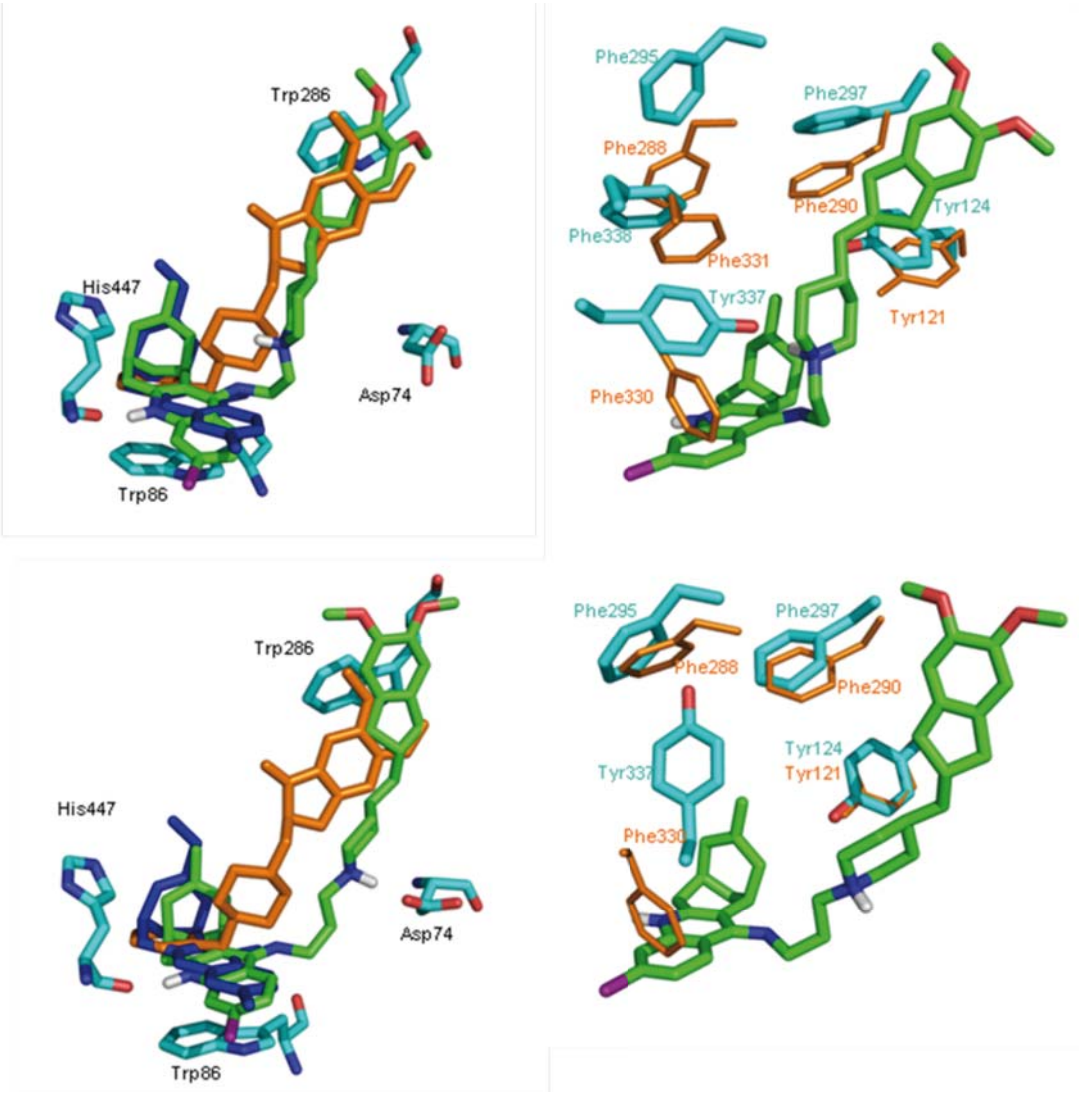

Figura 5.3 *Esquerra*: Superposició de les estructures (verd) recol·lectades al final de 30 ns de simulació de DM dels compostos (–)-**68a** (part superior) i (–)-**68b** (part inferior) amb l'hAChE, i el donepezil amb el complex obtingut per cristal·lografia de raigs X amb *Tc*AChE (taronja, codi PDB 1EVE) i (–)-huprina X (blau fosc, codi PDB: 1E66). *Dreta*: Comparació de les estructures (verd) i dels residus rellevants (cian) recol·lectades al final de 30 ns de simulació de DM dels compostos (–)-**68a** (part superior) i (–)-**68b** (part inferior) amb l'estructura obtigunda per cristal·lografia de raigs X del complex donepezil–*Tc*AChE (taronja, codi PDB: 1EVE).

Per comprovar la hipòtesi anterior, es van dur a terme càlculs d'integració termodinàmica (TI) per racionalitzar la diferència en l'afinitat d'unió entre els híbrids substituïts amb metil i etil. El canvi d'energia lliure d'unió es va determinar a partir del cicle termodinàmic que es mostra a la Figura 5.4. Aquests resultats prediuen que la conversió de metil de (–)-**68a** i (–)-**68b** a etil de (–)-**69a** i (–)-**69b,** respectivament, disminueix l'afinitat d'unió per l'enzim en 0,4 i 0,3 kcal·mol^{-1}, respectivament, resultats que convergeixen amb les dades experimentals.

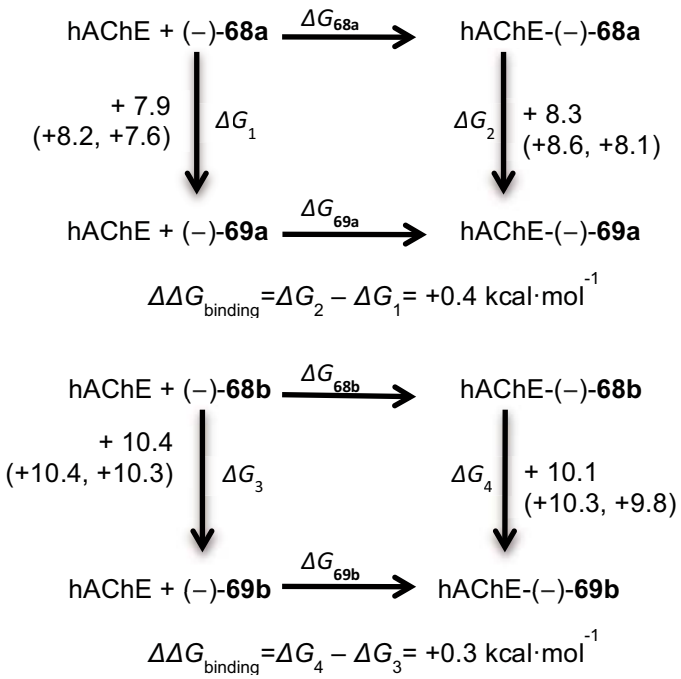

Figura 5.4 Cicle termodinàmic dels compostos (–)-**68a** i (–)-**68b**

En conjunt, aquests resultats donen suport als models estructurals derivats de les simulacions de DM. D'altra banda, aquests resultats posen de relleu la importància que la part central de la gorja catalítica té en la modulació de l'afinitat d'unió dels inhibidors de lloc d'unió dual de l'AChE.

DOI: 10.1002/cmdc.201000322

Novel Huprine Derivatives with Inhibitory Activity toward β-Amyloid Aggregation and Formation as Disease-Modifying Anti-Alzheimer Drug Candidates

Elisabet Viayna,[a] Tània Gómez,[a] Carles Galdeano,[a] Lorena Ramírez,[a] Míriam Ratia,[b] Albert Badia,[b] M. Victòria Clos,[b] Ester Verdaguer,[c] Félix Junyent,[c] Antoni Camins,[c] Mercè Pallàs,[c] Manuela Bartolini,[d] Francesca Mancini,[d] Vincenza Andrisano,[d] Mariana P. Arce,[e] María Isabel Rodríguez-Franco,[e] Axel Bidon-Chanal,[f] F. Javier Luque,[f] Pelayo Camps,[a] and Diego Muñoz-Torrero*[a]

Dedicated to Professor Carmen Nájera on the occasion of her 60th birthday.

A new family of dual binding site acetylcholinesterase (AChE) inhibitors has been designed, synthesized, and tested for their ability to inhibit AChE, butyrylcholinesterase (BChE), AChE-induced and self-induced β-amyloid (Aβ) aggregation and β-secretase (BACE-1), and to cross the blood–brain barrier. The new heterodimers consist of a unit of racemic or enantiopure huprine Y or X and a donepezil-related 5,6-dimethoxy-2-[(4-piperidinyl)methyl]indane moiety as the active site and peripheral site to mid-gorge-interacting moieties, respectively, connected through a short oligomethylene linker. Molecular dynamics simulations and kinetics studies support the dual site binding to AChE. The new heterodimers are potent inhibitors of human AChE and moderately potent inhibitors of human BChE, AChE-induced and self-induced Aβ aggregation, and BACE-1, and are predicted to be able to enter the central nervous system (CNS), thus constituting promising multitarget anti-Alzheimer drug candidates with the potential to modify the natural course of this disease.

Introduction

Alzheimer's disease (AD) represents one of the major unmet disorders in modern medicine. Current therapeutic options for AD—the acetylcholinesterase (AChE) inhibitors donepezil, rivastigmine and galantamine, and the glutamate NMDA receptor antagonist memantine—are regarded as symptomatic. The launch of the first generation of disease-modifying anti-Alzheimer drugs remains elusive, after the recent failure of the most advanced candidates in phase III clinical trials due to efficacy or safety issues.[1]

AD is a complex disorder that arises from multiple molecular defects, and it therefore involves more than one key pathogenic target. The polyetiological origin of AD renders the notion that it can be efficiently managed through single-target drugs untenable. In an attempt to fulfill the acute need for effective disease-modifying anti-Alzheimer therapies, research efforts are gradually shifting toward the rational design of drug candidates aimed at addressing multiple biological targets, preferentially those involved in the mechanisms that drive the progression of the disease.

β-Amyloid peptide (Aβ) seems to be the major culprit in triggering neuronal death and subsequent cognitive decline in AD patients. Aβ is a 39–43 amino acid peptide generated by proteolytic cleavage of the amyloid precursor protein (APP) through the sequential action of β-secretase (β-site APP cleaving enzyme or BACE-1) and γ-secretase. The aggregation of Aβ is considered to be the key event in the neuropathogenesis of AD.[2]

Fibrillar aggregated Aβ is deposited in amyloid plaques (senile plaques) in the brain of AD patients, constituting a prominent hallmark of the disease. Plaque-derived Aβ fibrils

[a] *E. Viayna, T. Gómez, C. Galdeano, L. Ramírez, Prof. P. Camps, Prof. D. Muñoz-Torrero*
Laboratori de Química Farmacèutica (Unitat Associada al CSIC)
Facultat de Farmàcia, and Institut de Biomedicina (IBUB)
Universitat de Barcelona, Av. Diagonal 643, 08028, Barcelona (Spain)
Fax: (+34) 934035941
E-mail: dmunoztorrero@ub.edu

[b] *Dr. M. Ratia, Prof. A. Badia, Prof. M. V. Clos*
Departament de Farmacologia, Terapèutica i Toxicologia
Institut de Neurociències
Universitat Autònoma de Barcelona, 08193, Bellaterra, Barcelona (Spain)

[c] *Dr. E. Verdaguer, Dr. F. Junyent, Prof. A. Camins, Prof. M. Pallàs*
Unitat de Farmacologia i Farmacognòsia
Facultat de Farmàcia, and Institut de Biomedicina (IBUB)
Universitat de Barcelona, Av. Diagonal 643, 08028, Barcelona (Spain)

[d] *Dr. M. Bartolini, Dr. F. Mancini, Prof. V. Andrisano*
Department of Pharmaceutical Sciences, Alma Mater Studiorum
Bologna University, Via Belmeloro 6, 40126 Bologna (Italy)

[e] *Dr. M. P. Arce, Prof. M. I. Rodríguez-Franco*
Instituto de Química Médica (CSIC)
Juan de la Cierva, 3, 28006, Madrid (Spain)

[f] *Dr. A. Bidon-Chanal, Prof. F. J. Luque*
Departament de Fisicoquímica
Facultat de Farmàcia, and Institut de Biomedicina (IBUB)
Universitat de Barcelona, Av. Diagonal 643, 08028, Barcelona (Spain)

Supporting information for this article is available on the WWW under http://dx.doi.org/10.1002/cmdc.201000322.

enhance oxidative stress and inflammation, leading to neuronal toxicity,[3] although over the last decade a growing body of evidence has identified non-fibrillar Aβ oligomers as the main toxic species in AD.[4] The aggregation process is highly dependent on Aβ concentration,[5] which consequently makes Aβ formation another pivotal target for AD management. Because BACE-1 is the first and rate-limiting step in Aβ generation, it is considered a good target for intervention.[6]

The so-called dual binding site acetylcholinesterase inhibitors (AChEIs) have recently emerged as a new class of anti-Alzheimer drug candidates that may have the potential to positively modify the course of AD, exhibiting both multipotency and the ability to interfere the neurotoxic cascade upstream by targeting Aβ. The primary biological target of these compounds is the enzyme AChE, with which they interact simultaneously, blocking both the active and peripheral sites, placed respectively at the bottom and the mouth of a 20-Å-long gorge.[7] This particular mode of action usually results in high AChE inhibitory potency, of interest for the management of the symptomatology of AD by compensating for the characteristic central cholinergic deficit in AD patients, and, more interestingly, in a blockade of the peripheral-site-mediated Aβ pro-aggregating action of AChE. Indeed, AChE can bind through its peripheral site to soluble Aβ, thereby promoting Aβ aggregation as an early event in the neurodegenerative cascade of AD.[8] This Aβ pro-aggregating action results in an increase in brain amyloid burden and cognitive impairment in double transgenic mice that overexpress both human APP and AChE.[9] Recently, it has been found that AChE accelerates the formation of synaptotoxic Aβ oligomers, particularly protofibrils or amylospheroids, which are responsible for the increased neurotoxicity of Aβ when complexed with AChE.[10]

To the extent that dual binding site AChEIs can block Aβ oligomerization and its subsequent neurotoxicity apart from the acetylcholine-hydrolyzing activity of AChE, this class of compounds shows promise as disease-modifying anti-Alzheimer agents. This is particularly true in some dual binding site AChEIs that have been found to be able to inhibit BACE-1 as well, a direct effect independent of their interaction with AChE.[11] The proof-of-concept of the particular pharmacological profile of dual binding site AChEIs has been obtained in two of these compounds, namely memoquin[11a] and NP-61,[12] which have been shown to decrease brain amyloid burden and increase cognitive function in animal models of AD. Some dual binding site AChEIs such as memoquin[11a] or bis(7)-tacrine, also called bis(7)-cognitin,[13] are currently undergoing preclinical evaluation, while NP-61 is currently in phase I clinical trials for AD in the UK.

So far, the sole dual binding site AChEI among the marketed anti-Alzheimer drugs is donepezil (**1**, Figure 1).[14] The dual site binding of donepezil to AChE is mediated by two aromatic stacking interactions between its benzyl and 5,6-dimethoxy-1-indanone moieties and the indole rings of Trp84 and Trp279 [*Torpedo californica* AChE (*Tc*AChE) numbering, equivalent to Trp86 and Trp286 in human AChE (hAChE)] at the catalytic and peripheral sites, respectively. Additionally, the piperidine nitrogen atom, protonated at physiological pH, establishes additional interactions with mid-gorge residues, namely cation–π interactions with the phenyl ring of Phe330 (Tyr337 in hAChE). This binding mode endows donepezil with high hAChE inhibitory activity and moderate in vitro AChE-induced Aβ aggregation inhibitory activity.

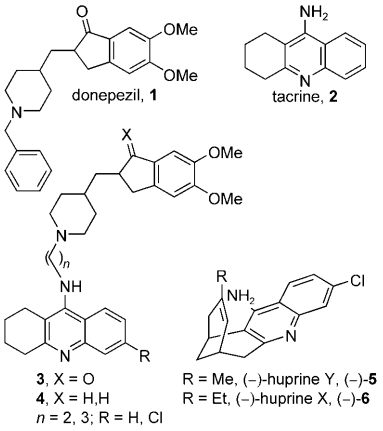

Figure 1. Structures of donepezil, tacrine, donepezil–tacrine heterodimers series **3** and **4**, and (−)-huprines Y and X.

We recently developed a family of heterodimers that bear the 5,6-dimethoxy-2-[(4-piperidinyl)methyl]-1-indanone moiety of donepezil (or the indane derivative thereof) and a unit of tacrine (**2**, Figure 1) as the peripheral to mid-gorge and active site interacting moieties, respectively. These heterodimers (series **3** and **4**, Figure 1) are more potent hAChE and AChE-induced Aβ aggregation inhibitors than the parent donepezil and tacrine.[15]

One decade ago, huprines emerged as a novel class of highly potent hAChEIs.[16] The lead huprines, the so-called huprines Y and X (**5** and **6**, respectively, Figure 1) exhibit a multitarget pharmacological profile encompassing M_1 muscarinic receptor agonistic activity, NMDA receptor antagonistic properties, and in vitro and in vivo neuroprotective effects against NMDA-, glutamate-, and 3-nitropropionic acid-induced toxicity, apart from highly potent hAChE inhibitory activity.[16e] Moreover, huprines have been shown to be effective in improving cognition after chronic treatment in normal middle-aged mice without inducing adverse effects.[17] The X-ray crystallographic structure of the complex between *Tc*AChE and (−)-huprine X (PDB ID: 1E66)[18] and biochemical studies[16c] revealed that huprines tightly bind to the active site of AChE, with one of the highest affinities reported for a reversible inhibitor. Taking into account the outstanding pharmacological profile of huprines, which could be shared by their derivatives, and their high-affinity binding to the catalytic site of AChE, huprines constitute a very attractive moiety for development as the active site interacting unit in dual binding site AChEIs.[19]

Herein we describe the synthesis, pharmacological evaluation, and molecular modeling of a novel family of dual binding site AChEIs that combine the donepezil-related 5,6-dimethoxy-2-[(4-piperidinyl)methyl]indane moiety with a unit of racemic or enantiopure huprine Y or X through an ethylene or trimethylene linker. Our pharmacological evaluation of these

novel compounds includes AChE and butyrylcholinesterase (BChE) inhibition, as well as inhibition of AChE- and self-induced Aβ aggregation and inhibition of BACE-1. Penetration of the novel heterodimers into the CNS was also assessed by using an artificial membrane assay.

Results and Discussion

Chemistry

The main difference in the pharmacological profile of heterodimers of the series **3** and **4**, which differ structurally only by the presence of an indanone or an indane system, lies in the fact that the former are more potent hAChE inhibitors (up to fourfold), whereas the latter are more potent inhibitors of hAChE-induced Aβ aggregation (1.5-fold).[15] The most valuable activity of dual binding site AChEIs is the interference with Aβ, as this could endow the compound with a potential disease-modifying effect, while inhibition of the catalytic activity of AChE would be responsible for a symptomatic action. Therefore, we selected the 5,6-dimethoxy-2-[(4-piperidinyl)methyl]indane moiety of heterodimers of series **4** as the peripheral site interacting unit of the new family of donepezil–huprine heterodimers **11**–**12a**,**b** (Scheme 1) for development, with the hope of attaining a greater Aβ anti-aggregating effect, albeit perhaps at the expense of a somewhat lower inhibitory potency toward AChE. Moreover, the lack of stereogenic centers in this moiety avoids problems related to the formation and separation of diastereomeric mixtures when combined with the chiral huprine moiety; such problems would have been present if the chiral indanone moiety of heterodimers of series **3** were used instead.

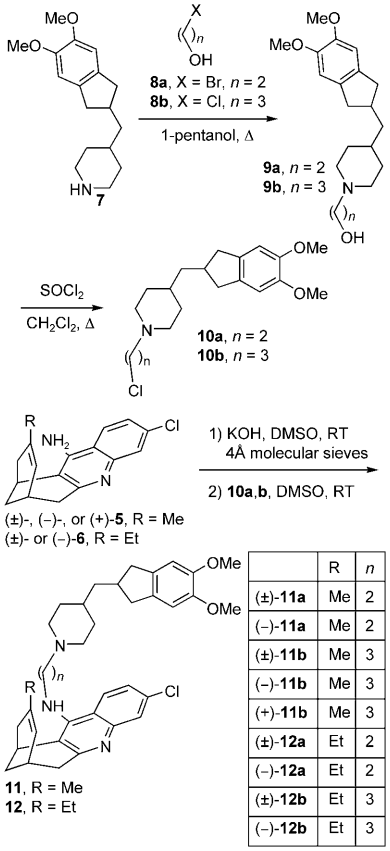

	R	n
(±)-**11a**	Me	2
(–)-**11a**	Me	2
(±)-**11b**	Me	3
(–)-**11b**	Me	3
(+)-**11b**	Me	3
(±)-**12a**	Et	2
(–)-**12a**	Et	2
(±)-**12b**	Et	3
(–)-**12b**	Et	3

Scheme 1. Synthesis of the donepezil–huprine heterodimers **11**–**12a**,**b**.

Huprines Y and X (**5** and **6**, Figure 1) were selected as the active site interacting unit of the novel heterodimers because they are the most potent huprines developed so far.[16] The eutomer of this structural class is the levorotatory enantiomer, bearing the 7*S*,11*S* configuration. Consequently, (–)-**5** and (–)-**6** were used for the preparation of the novel heterodimers, apart from the racemic compounds. Moreover, for comparison purposes the distomer (+)-**5** was used for the synthesis of one of the heterodimers.

Taking into account that tacrine and huprines, the active site interacting unit of donepezil–tacrine heterodimers of series **3** and **4** and of the novel donepezil–huprine heterodimers **11**–**12a**,**b**, respectively, occupy the same binding zone within the AChE active site,[7,18] and that the dual site binding of heterodimers of the series **3** and **4** was supported by recent molecular modeling studies,[15] the same lengths of the linker used in **3** and **4** were considered adequate to provide the necessary distance between huprine and the donepezil-related moiety for the desired dual site binding in the novel family of heterodimers.

The synthesis of donepezil–tacrine heterodimers of the series **3** and **4** involved amination of a readily available tacrine-related 4-chloroquinoline[20] with 2-aminoethanol or 3-amino-1-propanol, followed by mesylation and alkylation of the donepezil-derived piperidine.[15] The same methodology was not considered to be so useful for the synthesis of the novel donepezil–huprine heterodimers **11**–**12a**,**b** mainly because the multistep preparation of the starting huprine-related 4-chloroquinoline is hampered by issues of regioselectivity and poor yield.[19,21]

Therefore, an alternative methodology was envisioned for the novel donepezil–huprine heterodimers, which involved the use of a 4-aminoquinoline, that is, huprines Y or X themselves, instead of the aforementioned 4-chloroquinoline derivative. On the one hand, racemic huprines Y and X can be easily prepared at the multi-gram scale through a four-step sequence from bicyclo[3.3.1]nonane-3,7-dione, involving a final Friedländer condensation, which regioselectively affords huprines bearing the endocyclic carbon–carbon double bond and the quinoline system in an *anti* disposition.[16] On the other hand, enantiopure huprines Y and X can be obtained at the gram scale by chiral chromatographic resolution of the racemic compounds, namely by medium-pressure liquid chromatography using microcrystalline cellulose triacetate as the chiral stationary phase,[22] thus enabling the synthesis of donepezil–huprine heterodimers in enantiopure form.

The first step of the sequence for the synthesis of the novel donepezil–huprine heterodimers **11**–**12a**,**b** involved alkylation of the known piperidine **7**[15,23] with 2-bromoethanol or 3-chloro-1-propanol in 1-pentanol at reflux,[24] which afforded alcohols **9a** and **9b** in moderate yields (Scheme 1). Alcohols **9a** and **9b** were converted into the corresponding chloro deriva-

tives **10a** and **10b** by reaction with excess thionyl chloride, without alkaline aqueous workup to avoid the subsequent formation of cyclization by-products arising from intramolecular alkylation of the piperidine nitrogen atom. Racemic or enantiopure huprines Y and X were alkylated with the crude chloro derivatives **10a** and **10b** by using a standard procedure[25] to afford racemic or enantiopure donepezil–huprine heterodimers **11**–**12a**,**b** in moderate yields, after a tedious silica gel chromatographic purification. The novel heterodimers **11**–**12a**,**b** were fully characterized as dihydrochlorides through their spectroscopic data and elemental analyses (C, H, N, Cl).

Biological evaluation

AChE inhibition

The AChE inhibitory activity of heterodimers **11**–**12a**,**b** was assayed by the method of Ellman et al.[26] on human recombinant AChE (hAChE) (Table 1). The novel donepezil–huprine heterodimers are potent inhibitors of hAChE, exhibiting IC_{50} values in the low nanomolar range in most cases. Some clear structure–activity relationship trends are evident from the data in Table 1. The levorotatory enantiomers of these heterodimers, bearing a (7*S*,11*S*)-huprine moiety, are the eutomers in this family, being roughly twofold more potent than the corresponding racemic compounds and much more potent than the dextrorotatory enantiomers [(−)-**11b** is 19-fold more potent than (+)-**11b**]. This finding reflects the greater inhibitory activity of the levorotatory enantiomers of the parent compounds, as noted in a 23–31-fold difference between the potencies of (−)- and (+)-huprines. Moreover, the hAChE inhibitory potency of the heterodimers increases with the presence of a trimethylene linker, as the corresponding compounds are 3–8-fold more potent than their ethylene-linked counterparts. Finally, the inhibitory activity also increases with the presence of a methyl substituent at position 9 of the huprine moiety (huprine Y derivatives are ~1.5–3-fold more potent than their huprine X-based counterparts). This latter trend was a priori unexpected, because the reverse trend is found for the parent compounds [(−)-huprine Y is 1.6-fold less potent than (−)-huprine X].

Table 1. AChE and BChE inhibitory activities of the hydrochlorides of donepezil, racemic and enantiopure huprines Y and X, and the dihydrochlorides of racemic and enantiopure heterodimers **11a**,**b** and **12a**,**b**.[a]

Compd	IC_{50} [nM] hAChE	hBChE	AChE Selectivity[b]
(±)-**11a**·2HCl	18.1 ± 1.2	336 ± 21	19
(−)-**11a**·2HCl	13.0 ± 0.1	303 ± 12	23
(±)-**11b**·2HCl	5.37 ± 0.3	88 ± 2.3	16
(−)-**11b**·2HCl	2.61 ± 0.2	349 ± 20	134
(+)-**11b**·2HCl	49.9 ± 5.1	95 ± 5.3	2
(±)-**12a**·2HCl	48.6 ± 5.2	174 ± 9.4	4
(−)-**12a**·2HCl	28.6 ± 2.3	419 ± 17	15
(±)-**12b**·2HCl	6.32 ± 0.1	61 ± 3.2	10
(−)-**12b**·2HCl	3.85 ± 0.2	194 ± 9.3	50
donepezil·HCl	21.4 ± 2.3	7273 ± 621	340
(±)-huprine Y·HCl	0.61 ± 0.03	236 ± 44	387
(−)-huprine Y·HCl	0.43 ± 0.03	247 ± 18	574
(+)-huprine Y·HCl	13.6 ± 1.5	153 ± 31	11
(±)-huprine X·HCl	0.67 ± 0.05	15.8 ± 2.4	24
(−)-huprine X·HCl	0.27 ± 0.02	159 ± 10	589
(+)-huprine X·HCl	6.30 ± 0.50	58.3 ± 5.9	9

[a] Values are expressed as the mean ± SEM of at least four experiments; IC_{50}: 50% inhibitory concentration of human recombinant or human serum BChE activity. [b] $(IC_{50\ hBChE})/(IC_{50\ hAChE})$.

Overall, the most potent hAChEI of the series is (−)-**11b**, which turned out to be eightfold more potent than donepezil but, contrary to our expectations, sixfold less potent than the parent (−)-huprine Y [(−)-**5**]. Also, the most potent huprine X-based heterodimer, namely (−)-**12b**, turned out to be 14-fold less potent than the parent (−)-huprine X [(−)-**6**]. Although high hAChE inhibitory activity was retained in the novel donepezil–huprine heterodimers, the lower potency relative to the parent huprines seemed indicative of unfavorable interactions arising from the linker in the mid-gorge region or structural rearrangements that might affect the proper positioning of the huprine moiety within the catalytic site. Finally, the inhibitory activity of the most potent heterodimers, (−)-**11b** and (−)-**12b**, was in the same range as that found for the most potent compounds of the structurally related indane-bearing donepezil–tacrine heterodimers of series **4** (Figure 1, R = Cl, $n = 3$, $IC_{50} = 1.06$ nM; R = H, $n = 3$, $IC_{50} = 2.16$ nM). Nevertheless, caution should be taken in making a strict comparison because the AChE source was different, as the latter heterodimers were evaluated using human erythrocyte AChE instead of human recombinant AChE.

Molecular modeling studies of AChE inhibition

The binding mode of compounds (−)-**11a** and (−)-**11b** to hAChE was explored by means of 30 ns molecular dynamics (MD) simulations. The starting pose of the compounds was built by taking advantage of the known pose of huprine X in the X-ray crystallographic complex with *Tc*AChE,[18] and the binding pose of the related donepezil–tacrine heterodimers studied in our previous work.[15] The MD simulation run for the complex between hAChE and (−)-**11a** yielded a stable trajectory, as noted by inspection of the time evolution of both the potential energy and the root-mean-square deviation (RMSD) of the protein backbone (1.9 Å), the residues that delineate the binding cavity, including catalytic, mid-gorge, and peripheral sites (2.4 Å), and the inhibitor (1.2 Å) in the ligand–enzyme complexes (Figure 2). For the complex with (−)-**11b**, whereas similar RMSD values were obtained for the protein backbone and the binding site, the RMSD of the ligand increased to 2.5 Å after the first 23 ns and then remained stable until the end of the trajectory. The distinct relaxation times required for accommodation of the two inhibitors in the binding site suggest that there must be some differences between the interactions that mediate the binding of (−)-**11a** and (−)-**11b** to hAChE.

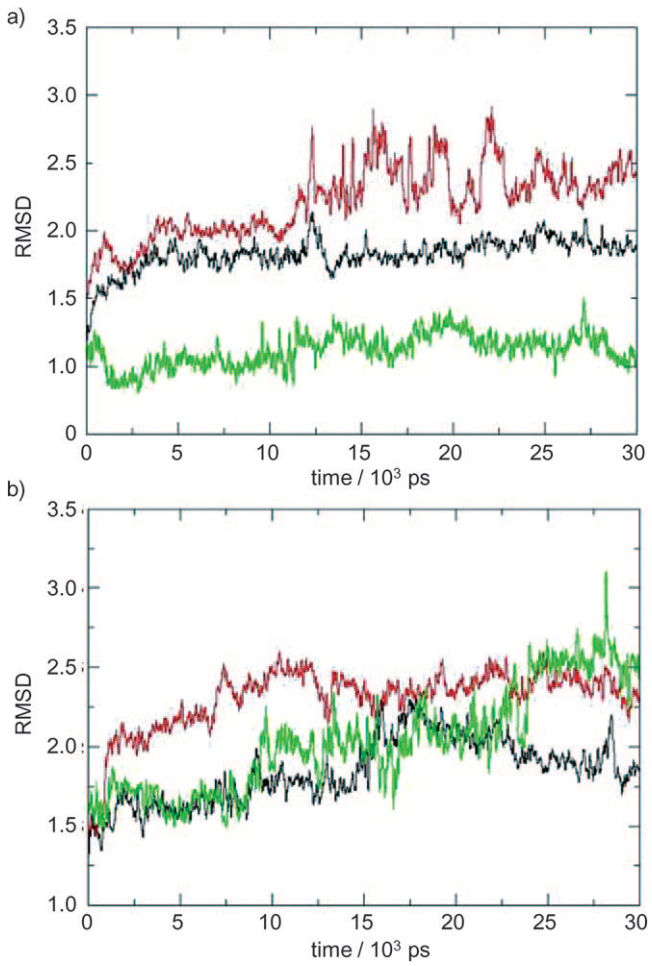

Figure 2. Time dependence of the positional RMSD (Å) of a) (−)-**11 a** and b) (−)-**11 b** determined for the backbone (black), the binding site (red), and the ligand (green) in the mobile part of the simulation system for the hAChE complex. The profiles were smoothed in 50 ps windows for the sake of clarity.

In the (−)-**11 a**–hAChE complex, binding of the huprine Y moiety at the catalytic site nearly matches the position of huprine X in the X-ray crystallographic structure of the complex with *Tc*AChE (PDB ID: 1E66) (Figure 3).[18] Thus, the heteroaromatic ring system of the huprine Y unit of (−)-**11 a** stacks against the indole ring of Trp86 (average distance: 3.8 Å), and the protonated quinoline nitrogen atom is hydrogen bonded to the carbonyl group of His447 (2.8 Å). However, the stacking of the heteroaromatic ring system of huprines against the benzene ring of Phe330 found in the X-ray structure is not maintained in the interaction of (−)-**11 a** with hAChE (note that Phe330 in *Tc*AChE is replaced by Tyr337 in hAChE). The loss of this interaction can be ascribed to the formation of a hydrogen bond between the hydroxy group of Tyr337 and the protonated piperidine nitrogen atom of (−)-**11 a** (3.1 Å), which in turn precludes the proper arrangement for the stacking of the phenol ring of Tyr337 and the quinoline system of the huprine Y unit. In the peripheral site, the indane system stacks against Trp286 (4.7 Å), thus mimicking the interaction observed in the X-ray structure of donepezil bound to *Tc*AChE (PDB ID: 1EVE).[14] There is, however, a sizable displacement in the relative position of the indane and indanone systems of (−)-**11 a** and donepezil, as the five-membered ring of the indane moiety of (−)-**11 a** occupies roughly the same position as the six-membered ring of the indanone moiety of donepezil, thus leading to better stacking between the indane system of (−)-**11 a** and Trp286 relative to that of donepezil.

In the mid-gorge region the presence of the piperidine ring gives rise to a remarkable structural rearrangement of specific residues. Thus, in the complex between donepezil and *Tc*AChE, Tyr121 forms a water-mediated interaction with the piperidine nitrogen atom of donepezil. In the (−)-**11 a**–hAChE complex, such an interaction is lost due to the new orientation adopted by the piperidine ring to form a hydrogen bond with Tyr337 (see above). In turn, this new orientation would cause the piperidine ring to collide with Tyr124 and Phe338 (Tyr121 and Phe331 in *Tc*AChE). However, the steric clash is minimized upon displacement of the side chain of those residues, which in turn affects the spatial arrangement of Phe297 and Phe295 (Phe290 and Phe288 in *Tc*AChE). Finally, the piperidine ring also forces the distortion of Tyr341 (Tyr334 in *Tc*AChE), which in turn affects the spatial orientation of Trp439 and Met443 (Trp432 and Met436 in *Tc*AChE). Notably, those residues define binding pockets that accommodate the ethyl group and chlorine atom present at positions 9 (Phe288, Phe290 and Phe331) and 3 (Trp432 and Met436) of huprine X in *Tc*AChE.

The binding of (−)-**11 b** at the catalytic and peripheral sites of hAChE retains the essential features noted for (−)-**11 a**, such as stacking against Trp86 and Trp286, and the hydrogen bond with His447. However, replacement of the ethylene linker in (−)-**11 a** by a trimethylene linker in (−)-**11 b** influences the positioning of the piperidine ring in the mid-gorge site and leads to different interactions with the neighboring residues. Thus, the hydrogen bond formed between (−)-**11 a** and Tyr337 is lost in (−)-**11 b**, whereas the additional methylene unit in the linker permits the approach of the piperidine ring to the carboxylate group of Asp74, leading to a salt bridge interaction. Moreover, the increased length of the linker minimizes the steric hindrance of the piperidine ring with both Tyr124 and Tyr341, which occupy positions similar to those observed in the X-ray structures 1E66 and 1EVE. In contrast, the orientation of Tyr337 is largely altered, and affects the positioning of Phe338 in the binding site. As a result, while the ethyl chain of huprine X in 1E66 fits a cavity delineated by Phe288, Phe290, and Phe331 in *Tc*AChE, such pocket is formed by Tyr337, Phe295, and Phe297 in the complex between (−)-**11 b** and hAChE.

The preceding findings suggest that the decrease in inhibitory potency of the novel heterodimers (−)-**11 a** and (−)-**11 b** relative to the parent huprine Y can be related to the structural distortion generated by the presence of the piperidine ring in the tether that links huprine and indane moieties. In particular, such distortion affects the pocket filled by the methyl/ethyl substituent bound at position 9 in the huprine moiety, and could thus explain the different influence exerted by the replacement of methyl by ethyl in the inhibitory potency of the heterodimers and the parent compounds (see Table 1). Thus,

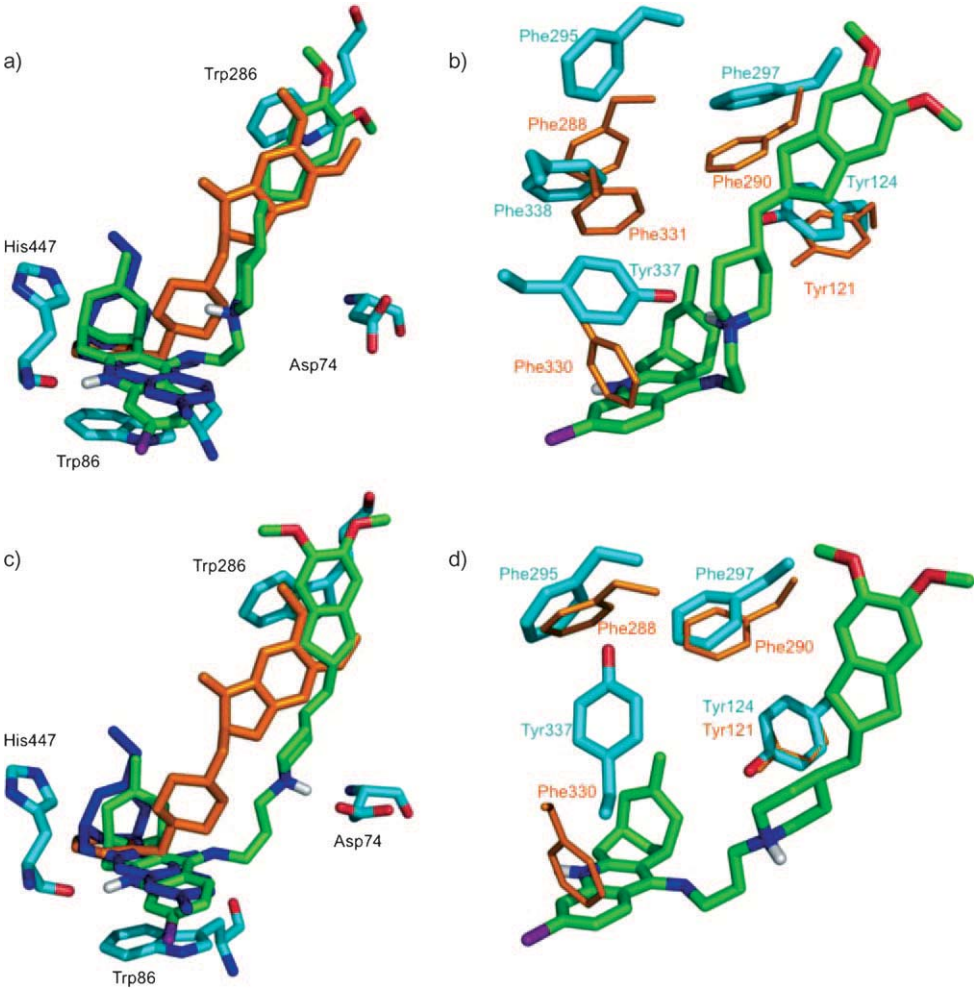

Figure 3. Superposition of the structures (green) collected at the end of the 30 ns MD simulations of compounds a) (−)-**11 a** and c) (−)-**11 b** bound to hAChE, and the X-ray crystallographic structures of *Tc*AChE with donepezil (orange, PDB ID: 1EVE) and (−)-huprine X (dark blue, PDB ID: 1E66). Comparison of the structures (green) and relevant residues (cyan) collected at the end of the 30 ns MD simulations of compounds b) (−)-**11 a** and d) (−)-**11 b** with the X-ray crystallographic structure of *Tc*AChE with donepezil (orange, PDB ID: 1EVE).

whereas replacement of methyl by ethyl in (−)-huprine increases the inhibitory potency by 1.6-fold, the reverse trend is observed for the heterodimers, with potency decreasing by ~1.5–3-fold (see Table 1).

To check the preceding hypothesis, thermodynamic integration (TI) calculations coupled with MD simulations were performed to rationalize the difference in binding affinity between methyl- and ethyl-substituted heterodimers. The change in binding free energy was determined from the thermodynamic cycle shown in Figure 4. The results predict that the conversion from methyl [(−)-**11 a**,**b**] to ethyl [(−)-**12 a**,**b**] decreases the binding affinity for the enzyme by 0.4 and 0.3 kcal mol^{-1}, respectively, which is in agreement with the experimental data. In contrast, similar calculations performed for the parent compound, (−)-huprine, predicted huprine X to be more potent than huprine Y by 0.7 kcal mol^{-1}.[16d]

As a whole, these results reflect the changes in the available experimental data originated upon replacement of methyl by ethyl at position 9, thus lending support to the structural models derived from the extended MD simulations. Moreover, these results highlight the importance of the mid-gorge site in modulating the binding affinity of dual binding site inhibitors in AChE.

Kinetic analysis of AChE inhibition

To gain further insight into the mechanism of action of this family of compounds on human recombinant AChE, a kinetics study was carried out with the most potent compound of the series: heterodimer (−)-**11 b**. Graphical analysis of the overlaid reciprocal Lineweaver–Burk plots (Figure 5) showed both increased slopes (decreased V_{max}) and intercepts (higher K_M) with increasing inhibitor concentrations. This pattern indicates mixed-type inhibition, and therefore supports the dual site binding suggested by MD simulations. Re-plots of the slope versus concentration of heterodimer (−)-**11 b** gave an estimate of the competitive inhibition constant, K_i, at 0.53 nM.

BChE inhibition

Recent evidence has shown that inhibition of BChE might be valuable in the search for anti-Alzheimer agents.[27] Consequently, the inhibitory activity toward human serum BChE (hBChE) was also assayed by the method of Ellman et al. (Table 1).[26] Huprines are selective for hAChE versus hBChE inhibition. The presence of the chlorine atom at the huprine unit, which is partly responsible for the high hAChE inhibitory activity of 4-aminoquinoline derivatives,[28] becomes detrimental for hBChE inhibition. Steric hindrance due to the proximity of the chlorine atom to the terminal methyl group of Met437 in the hBChE active site seems to account for the detrimental influence of this substituent on the hBChE inhibitory activity relative to unsubstituted 4-aminoquinolines such as tacrine,[29] which is a fivefold more potent inhibitor toward hBChE than hAChE.[15] Moreover, donepezil is very selective for hAChE versus hBChE inhibition. As expected, the huprine-based heterodimers **11**–**12 a**,**b** are more potent inhibitors of hAChE than hBChE (2–134-fold). Nevertheless, as huprines themselves, they can be considered moderately potent inhibitors of hBChE, with IC_{50} values in the nanomolar range. Following the same trends

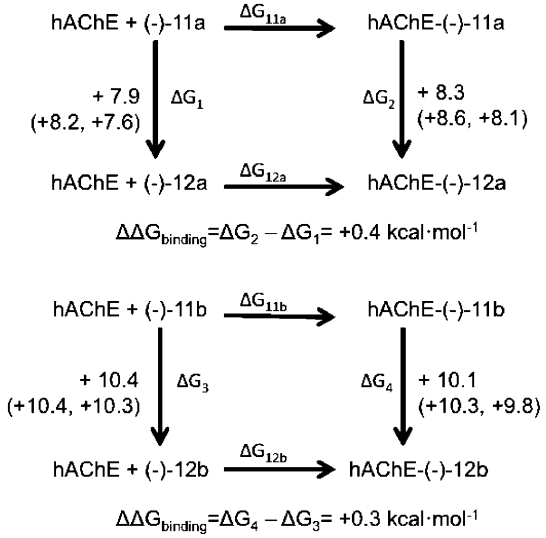

Figure 4. Thermodynamic cycle used in free energy calculations in water and in the hAChE enzyme to determine relative binding. The results for the forward and reverse mutations are given in parentheses. Values are in kcal mol^{-1}.

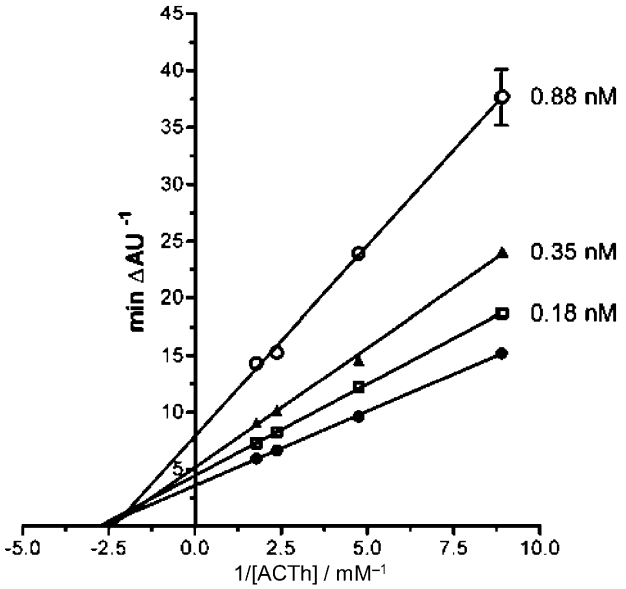

Figure 5. Kinetics study on the mechanism of AChE inhibition by heterodimer (−)-**11 b**. Overlaid Lineweaver–Burk reciprocal plots of AChE initial velocity at increasing substrate concentration (ATCh, 0.56–0.11 mM) in the absence of inhibitor and in the presence of (−)-**11 b** (0.18–0.88 nM) are shown. Lines were derived from a weighted least-squares analysis of the data points.

found in the parent huprines, the hBChE inhibitory activity of the novel heterodimers increases with the presence of an ethyl substituent at position 9 of the huprine moiety (huprine X derivatives being 1.5–2-fold more potent than their huprine Y-based counterparts) and with the presence of a dextrorotatory huprine moiety, with the 7*R*,11*R* configuration (the levorotatory enantiomers being generally two to fourfold less potent than the racemic compounds and fourfold less potent than the dextrorotatory enantiomer in the case of **11 b**). The tether length leading to higher activity turned out to be that corresponding to a trimethylene linker, the corresponding heterodimers being 1.2–4-fold more potent than their ethylene-linked counterparts. Overall, the most potent hBChEI among these heterodimers was (±)-**12 b**, which is 119-fold more potent than donepezil, but fourfold less potent than the parent (±)-huprine X [(±)-**6**]. Slightly lower inhibitory potencies were found for (±)-**11 b** and (+)-**11 b**.

Inhibition of AChE-induced Aβ aggregation

Regarding the potential interference of the new heterodimers with Aβ, they were first tested for their ability to inhibit AChE-induced aggregation of $A\beta_{1-40}$, by using a thioflavin T fluorescence method.[30] The Aβ anti-aggregating effect of racemic and enantiopure (−)- and (+)-huprines Y and X, was also determined, while that of donepezil was already described.[30] The new heterodimers significantly inhibit, at a concentration of 100 μM, hAChE-induced Aβ aggregation, with percentages of inhibition ranging from 25 to 50% (Table 2). In all cases, the inhibitory activity was higher than that of the dual binding site AChEI donepezil (22%), likely a result of better dual site binding to AChE, and in most cases also higher than those of the parent huprines, which exhibited remarkable inhibitory activity (12–37%). Although (−)-huprine X has been shown to bind tightly to the AChE active site,[18] kinetics studies have demonstrated that this compound interferes with the binding of the peripheral site AChEI propidium to AChE.[16c] The binding ge-

Table 2. Aβ aggregation and BACE-1 inhibitory activities of the hydrochlorides of donepezil, racemic and enantiopure huprines Y and X, and the dihydrochlorides of racemic and enantiopure heterodimers **11 a,b** and **12 a,b**.[a]

Compd	AChE-induced $A\beta_{1-40}$ aggregation [%][b]	$A\beta_{1-42}$ self-induced aggregation [%][c]	BACE-1 [%][d]
(±)-**11 a**·2 HCl	44.2 ± 1.0	26.0 ± 2.0	14.3 ± 7.6[e]
(−)-**11 a**·2 HCl	31.1 ± 0.4	16.3 ± 0.5	24.6 ± 3.0[e]
(±)-**11 b**·2 HCl	44.5 ± 1.8	28.5 ± 0.4	29.1 ± 2.9[e]
(−)-**11 b**·2 HCl	41.5 ± 2.4	29.0 ± 2.0	30.8 ± 4.1[e]
(+)-**11 b**·2 HCl	24.9 ± 2.4	29.9 ± 1.3	13.1 ± 4.7[e]
(±)-**12 a**·2 HCl	35.7 ± 3.2	16.3 ± 0.5	19.2 ± 2.2[e]
(−)-**12 a**·2 HCl	27.3 ± 2.6	20.9 ± 0.3	12.5 ± 0.7[e]
(±)-**12 b**·2 HCl	49.8 ± 0.4	20.9 ± 0.3	18.0 ± 9.0[e]
(−)-**12 b**·2 HCl	43.8 ± 0.8	23.6 ± 4.0	14.9 ± 3.9[e]
donepezil·HCl	22[f]	< 5[g]	–[h]
(±)-huprine Y·HCl	37.5 ± 0.5	ND[i]	ND[i]
(−)-huprine Y·HCl	25.1 ± 4.9	10.2 ± 6.5	14.0 ± 0.1[j]
(+)-huprine Y·HCl	11.6 ± 1.7	13.2 ± 1.9	13.6 ± 2.3[j]
(±)-huprine X·HCl	34.1 ± 0.2	25.5 ± 2.1	15.7 ± 3.8[j]
(−)-huprine X·HCl	28.9 ± 0.2	25.4 ± 1.2	21.8 ± 7.2[j]
(+)-huprine X·HCl	21.5 ± 1.4	22.9 ± 0.4	16.7 ± 0.6[j]

[a] Values are expressed as the mean ± SEM from two independent measurements, each performed in duplicate. [b] Inhibitor concentration: 100 μM. [c] Inhibitor concentration: 10 μM ([Aβ]/[I] = 5:1). [d] Inhibitor concentration: 5 μM. [e] Human recombinant BACE-1 (Sigma), substrate M-2420 (Bachem). [f] Data from Ref. [30]. [g] Data from Ref. [31a]. [h] IC_{50} = 11.3 ± 0.9 μM. [i] Not determined. [j] Human recombinant BACE-1 (Invitrogen), substrate Panvera Peptide (Invitrogen).

ometry and added molecular volume of huprines, when bound to the active site, could explain the decreased affinity of peripheral site ligands such as propidium,[16c] as well as Aβ.

The AChE-induced Aβ aggregation inhibitory activity of the novel heterodimers **11**–**12a**,**b** slightly increased with the presence of a trimethylene linker (up to 1.6-fold relative to the ethylene-linked counterparts) and a unit of racemic huprine, while the presence of a methyl or ethyl substituent at position 9 of the huprine moiety had essentially no effect on this activity. Overall, the most potent compounds were the trimethylene-linked heterodimers (±)-**11b**, (−)-**11b**, (±)-**12b**, and (−)-**12b**, as well as the ethylene-linked heterodimer (±)-**11a**, all of which showed percentages of inhibition between 40 and 50%, which are in the same range as those of the structurally related heterodimers of series **3** and **4** (Figure 1).

Inhibition of Aβ self-aggregation

A number of dual binding site AChE inhibitors have been found to exhibit significant inhibitory activity toward Aβ self-aggregation.[11a,29a,31] Analogously, the new donepezil–huprine heterodimers significantly inhibit the self-induced Aβ aggregation when tested at a concentration fivefold lower than that of Aβ, with percentages of inhibition ranging from 16 to 30% (Table 2). In all cases, this effect was higher than that of donepezil (<5%) and (−)- and (+)-huprine Y (10 and 13%, respectively), while similar to that of racemic and enantiopure huprine X (23–25%). Contrary to the trend found for the parent huprines, the Aβ anti-aggregating action of the novel heterodimers slightly increased with the presence of a methyl group at position 9 of the huprine moiety (1.2–1.6-fold relative to the ethyl-substituted counterparts). Also, this activity slightly increased with the presence of a trimethylene linker (1.1–1.8-fold relative to the ethylene-linked counterparts), while it generally remained insensitive to the configuration of the huprine moiety.

The strongest inhibitors of spontaneous Aβ aggregation among known dual binding site AChEIs show potencies in the low micromolar range.[11a,31a,d,e] The expected IC_{50} values for most of the heterodimers of this family must be clearly below 50 μM, so that they could be considered moderate inhibitors of $A\beta_{1-42}$ self-aggregation.

Inhibition of BACE-1

BACE-1 constitutes a prime therapeutic target for disease-modifying anti-Alzheimer drugs, as it is involved in the initial and rate-limiting step of the proteolytic cleavage of APP to Aβ; its inhibition should decrease all forms of Aβ. Indeed, Aβ generation, amyloid pathology, and cognitive deficits are abrogated in BACE-1-deficient bigenic mice overexpressing APP.[5b] However, BACE-1 has other substrates in addition to APP, and so its complete inhibition might lead to serious side effects. Thus, although initial studies on BACE-1-deficient mice indicated no adverse phenotype,[32] some subtle effects on both peripheral and central myelin formation have recently been found.[33] This mechanism-based toxicity, more importantly present in inhibitors of the more promiscuous γ-secretase, requires some selectivity or a balanced inhibition, which could be reached by mild inhibition or by simultaneously addressing multiple targets in order to minimize harmful side effects.[3a] Indeed, the degree of decrease in Aβ synthesis that secretase inhibitors have to achieve to affect the progression of AD is a matter of debate, and partial inhibition of BACE-1 has been proposed to provide therapeutic benefits with limited mechanism-based adverse effects.[5b] Thus, heterozygous BACE-1 knockout APP transgenic mice with only 15% reduction of brain Aβ show a dramatic decrease in brain amyloid burden at old age.[34]

Although highly active in vitro peptide inhibitors with poor pharmacokinetics are known, development of potent brain-permeable inhibitors is turning out to be a difficult task. Indeed, so far only one BACE-1 inhibitor, namely CTS-21166, has reached clinical trials. Therefore, there is still an increasing need for small organic BACE-1 inhibitors that are able to cross the blood–brain barrier (BBB).[35] As previously mentioned, some dual binding site AChEIs such as bis(7)-tacrine[11c,36] and some derivatives thereof,[11b] lipocrine,[37] memoquin,[11a] AP2243,[38] and some pyrano[3,2-*c*]quinoline-6-chlorotacrine heterodimers[31f] exhibit significant BACE-1 inhibitory activity, which is independent of their action on the primary target, AChE.

Thus, the BACE-1 inhibitory activity of this novel family of dual binding site AChEIs was screened at a single concentration (5 μM) by a fluorimetric assay, which is considered predictive of activity in cell culture.[39] All of the heterodimers exhibited significant BACE-1 inhibition (12–31%). The substitution pattern leading to greater BACE-1 inhibition involved the presence of a methyl substituent at position 9 of the huprine moiety (1.3–2.1-fold more potent than the ethyl-substituted counterparts) and a trimethylene linker (1.1–2-fold more potent than the ethylene-linked counterparts), while a clear trend regarding the configuration of the huprine moiety was not found. The most potent BACE-1 inhibitors, that is, heterodimers (±)-**11b**, (−)-**11b**, and (−)-**11a**, are more potent inhibitors than the parent huprines, and roughly equipotent to donepezil ($IC_{50} = 11.3 \pm 0.9$ μM) when evaluated under the same assay conditions. Indeed, heterodimer (−)-**11b** exhibited an IC_{50} value of 11.0 ± 0.59 μM, thus constituting a moderate BACE-1 inhibitor.

In vitro blood–brain barrier permeation assay

Successful CNS drugs must overcome the biological hurdle of BBB penetration. To predict the brain penetration of the donepezil–huprine heterodimers described herein, we used the widely known PAMPA-BBB assay,[40] which was successfully applied by us to different classes of anti-Alzheimer compounds.[31f,41] The in vitro permeability (P_e) of racemic **11**–**12a**,**b**, and of the parent huprines Y and X and donepezil through a lipid extract of porcine brain were determined by using phosphate-buffered saline (PBS)/EtOH (80:20 or 70:30, depending on the solubility of compounds). At each solvent mixture, assay validation was made by comparing the experimental permeability with the reported values of 15 commercial

drugs that gave a good linear correlation: $P_{e(exp.)} = 1.48 P_{e(lit.)} + 1.91$ ($R^2 = 0.95$) for PBS/EtOH (80:20) and $P_{e(exp.)} = 2.15 P_{e(lit.)} + 1.13$ ($R^2 = 0.93$) for PBS/EtOH (70:30) (see tables 1 and 2 and figure 3 of the Supporting Information). From these equations and taking into account the limits established by Di et al. for BBB permeation,[40] we established that compounds with permeability values greater than 7.8×10^{-6} cm s^{-1} (PBS/EtOH, 80:20) or 9.7×10^{-6} cm s^{-1} (PBS/EtOH, 70:30) should cross the BBB. All tested heterodimers, as well as the parent huprines and donepezil, showed permeability values over the above limits (Table 3), pointing out that they could cross the BBB and reach their pharmacological targets located in the CNS, as has been confirmed for huprines in in vivo and ex vivo studies,[16d,17] and, of course, for donepezil during clinical use.

Table 3. Permeability results from the PAMPA-BBB assay for the donepezil–huprine heterodimers, huprines Y and X, and donepezil, with their predicted penetration into the CNS.

Compd	P_e [10^{-6} cm s^{-1}][a]	Prediction
(±)-**11a**·2 HCl[b]	15.2 ± 0.1	CNS +
(±)-**11b**·2 HCl[b]	11.4 ± 0.2	CNS +
(±)-**12a**·2 HCl[b]	21.3 ± 0.4	CNS +
(±)-**12b**·2 HCl[c]	17.1 ± 0.4	CNS +
donepezil·HCl[c]	25.2 ± 0.2	CNS +
(±)-huprine Y·HCl[c]	18.2 ± 0.1	CNS +
(±)-huprine X·HCl[c]	17.8 ± 0.1	CNS +

[a] Values are expressed as the mean ± SD of three independent experiments. [b] Compound dissolved in PBS/EtOH (70:30). [c] Compound dissolved in PBS/EtOH (80:20).

Conclusions

We have synthesized a new family of donepezil–huprine heterodimers designed to simultaneously interact with the peripheral, mid-gorge, and active sites of hAChE, with the aim of attaining high hAChE inhibitory activity and more importantly of interfering with AChE-induced Aβ aggregation; the former effect is of interest for the management of the symptomatology of AD, and the latter for the modification of AD progression. The novel heterodimers are potent inhibitors of hAChE and moderately potent inhibitors of hAChE-induced Aβ aggregation, and are clearly superior to the parent donepezil in both activities. They are also more potent than the parent huprines as hAChE-induced Aβ aggregation inhibitors, but are less potent than huprines for hAChE inhibition. This fact could be ascribed to the structural distortion within hAChE generated by the presence of the piperidine ring in the linker of the heterodimers. The hAChE and hAChE-induced Aβ aggregation inhibitory activity of the novel heterodimers compares with that found for the most potent compounds of the structurally related indane-bearing donepezil–tacrine heterodimers of series **4**. Interestingly, the novel heterodimers also exhibit a significant inhibitory activity toward hBChE and Aβ self-aggregation, are able to block Aβ formation through inhibition of BACE-1, and have been predicted to be able to cross the BBB and enter the CNS. Although it remains to be proven if the novel heterodimers share other activities of the parent huprines such as modulation of cholinergic or NMDA receptors or neuroprotective effects, their multitarget pharmacological and pharmacokinetic profile described herein make these heterodimers very promising disease-modifying anti-Alzheimer drug candidates.

Experimental Section

Chemistry

Melting points were determined in open capillary tubes with a MFB 595010M Gallenkamp melting point apparatus. ^{1}H NMR (400 MHz) and ^{13}C NMR (100.6 MHz) spectra, as well as 500 MHz ^{1}H NMR spectra were recorded on Varian Mercury 400 and Varian Inova 500 spectrometers, respectively. Chemical shifts (δ) are reported in ppm relative to internal tetramethylsilane, and coupling constants are reported in Hertz (Hz). Assignments given for the NMR spectra of the new compounds were carried out by comparison with the NMR data of the previously described heterodimer **4** (X = H,H; R = Cl; $n = 3$) and huprines **5** and **6**, as model compounds, which in turn, were assigned on the basis of DEPT, COSY ^{1}H/^{1}H (standard procedures), and COSY ^{1}H/^{13}C (gHSQC and gHMBC sequences) experiments. IR spectra were run on a PerkinElmer Spectrum RX I spectrophotometer. Absorption values are expressed as wavenumbers (cm^{-1}); only significant absorption bands are given. Column chromatography was performed on silica gel 60 AC.C (35–70 mesh, SDS, ref. 2000027) or with Biotage FLASH 40M Silica equipment (KP-Sil™ 40–63 μm, 40 × 150 mm cartridges). Thin-layer chromatography was performed with aluminum-backed sheets with silica gel 60 F_{254} (Merck, ref. 1.05554), and spots were visualized with UV light and 1% aqueous solution of $KMnO_4$. Optical rotations were measured on a PerkinElmer model 241 polarimeter. The specific rotation was not corrected for the presence of solvent of crystallization. Analytical-grade solvents were used for crystallization, while pure synthesis-grade solvents were used in the reactions, extractions, and column chromatography. For characterization purposes, the new heterodimers were transformed into the corresponding dihydrochlorides, and recrystallized. The analytical samples of all of the new heterodimers which were subjected to pharmacological evaluation possess a purity ≥ 95% as evidenced by their elemental analyses. Notably, as previously reported for some tacrine-related dimeric compounds,[42] the new heterodimers described herein have the ability to retain water molecules, which cannot be removed after drying the analytical samples at 65 °C, 30 Torr for 4 days. Thus, the elemental analyses of these compounds showed the presence of variable amounts of water, which have been indicated in the corresponding compound formulas. NMR spectra of all of the new compounds were performed at the Serveis Científico-Tècnics of the University of Barcelona, while elemental analyses and high-resolution mass spectrometry were carried out at the Microanalysis Service of the IIQAB (CSIC, Barcelona, Spain) with a Carlo Erba model 1106 analyzer, and at the Serveis Científico-Tècnics of the University of Barcelona with an LC–MSD TOF Agilent Technologics spectrometer.

2-{[1-(2-Hydroxyethyl)piperidin-4-yl]methyl}-5,6-dimethoxyindane (9a). A mixture of piperidine **7** (970 mg, 3.53 mmol, 1 equiv) and 2-bromoethanol, **8a** (0.5 mL, 0.88 g, 7.05 mmol, 2 equiv) in 1-pentanol was heated under reflux for 48 h. The resulting suspension was allowed to cool to room temperature, diluted with EtOAc (60 mL) and extracted with aqueous 1 N HCl (3 × 20 mL). The combined aqueous phases were washed with EtOAc (4 × 20 mL), alkalinized with NaOH pellets (pH 12), and extracted with CH_2Cl_2 (3 ×

30 mL). The combined organic extracts were dried with anhydrous Na_2SO_4 and concentrated in vacuo to give a grey solid residue (861 mg), which was subjected to column chromatography (35–70 μm silica gel, CH_2Cl_2/MeOH/50% aq NH_4OH mixtures as eluent). On elution with CH_2Cl_2/MeOH/50% aq NH_4OH 92:8:0.5, alcohol **9a** (616 mg, 55%) was isolated as a white solid. On elution with CH_2Cl_2/MeOH/50% aq NH_4OH 90:10:0.5→80:20:0.5, starting piperidine **7** (193 mg) [68% yield of alcohol **9a** based on reacted piperidine **7**] was recovered.

9a: R_f = 0.27 (CH_2Cl_2/MeOH/50% aq NH_4OH 8.5:1.5:0.05); mp: 78–79 °C (CH_2Cl_2/MeOH/50% aq NH_4OH 92:8:0.5); ^{1}H NMR (400 MHz, $CDCl_3$): δ = 1.24 [dddd, $J \approx J' \approx J'' \approx$ 12.4 Hz, J''' = 3.2 Hz, 2H, piperidine 3(5)-H_{ax}], superimposed in part 1.30–1.44 (m, 1H, piperidine 4-H), 1.44 (dd, $J = J'$ = 6.8 Hz, 2H, 2-CH_2), 1.72 [br d, J = 12.0 Hz, 2H, piperidine 3(5)-H_{eq}], 2.05 [ddd, $J = J'$ = 11.6 Hz, J'' = 1.6 Hz, 2H, piperidine 2(6)-H_{ax}], superimposed in part 2.46–2.61 [complex signal, 3H, indane 1(3)-H_a and 2-H], 2.51 (t, J = 5.2 Hz, 2H, NC$H_2$$CH_2$OH), 2.90 [br d, J = 11.6 Hz, 2H, piperidine 2(6)-H_{eq}], 2.96 [dd, J = 14.0 Hz, J' = 7.2 Hz, 2H, indane 1(3)-H_b], 3.60 (t, J = 5.2 Hz, 2H, NCH_2CH_2OH), 3.84 [s, 6H, indane 5(6)-OCH_3], 6.73 [s, 2H, indane 4(7)-H], the signal corresponding to the OH group was not observed; ^{13}C NMR (100.6 MHz, $CDCl_3$): δ = 32.7 [CH_2, piperidine C3(5)], 34.5 (CH, piperidine C4), 37.7 (CH, indane C2), 39.5 [CH_2, indane C1(3)], 42.8 (CH_2, 2-CH_2), 53.8 [CH_2, piperidine C2(6)], 56.0 [CH_3, indane 5(6)-OCH_3], 57.8 (CH_2, NCH_2CH_2OH), 59.5 (CH_2, NCH_2CH_2OH), 107.9 [CH, indane C4(7)], 134.9 [C, indane C3a(7a)], 147.8 [C, indane C5(6)]; IR (KBr): $\tilde{\nu}$ = 3514 cm^{-1} (O-H st); Anal. calcd for $C_{19}H_{29}NO_3$: C 71.44, H 9.15, N 4.38, found: C 71.41, H 9.09, N 4.36.

2-{[1-(3-Hydroxypropyl)piperidin-4-yl]methyl}-5,6-dimethoxyindane (9b). It was prepared as described for **9a**. From piperidine **7** (1.09 g, 3.96 mmol, 1 equiv) and 3-chloro-1-propanol, **8b** (0.7 mL, 0.79 g, 8.37 mmol, 2 equiv), a grey solid residue (1.02 g) was obtained and subjected to column chromatography (35–70 μm silica gel, CH_2Cl_2/MeOH/50% aq NH_4OH mixtures as eluent). On elution with CH_2Cl_2/MeOH/50% aq NH_4OH 92:8:0.5, alcohol **9b** (577 mg, 44%) was isolated as a white solid. On elution with CH_2Cl_2/MeOH/50% aq NH_4OH 90:10:0.5 to 85:15:0.5, starting piperidine **7** (78 mg) [47% of alcohol **9b** based on reacted piperidine **7**] was recovered.

9b: R_f = 0.29 (CH_2Cl_2/MeOH/50% aq NH_4OH 9:1:0.05); mp: 85–86 °C (CH_2Cl_2/MeOH/50% aq NH_4OH 92:8:0.5); ^{1}H NMR (400 MHz, $CDCl_3$): δ = 1.22 [dddd, $J \approx J' \approx J'' \approx$ 12.4 Hz, J''' = 3.6 Hz, 2H, piperidine 3(5)-H_{ax}], superimposed in part 1.30–1.41 (m, 1H, piperidine 4-H), 1.42 (dd, $J = J'$ = 6.4 Hz, 2H, 2-CH_2), 1.67–1.76 [complex signal, 4H, $NCH_2CH_2CH_2$OH and piperidine 3(5)-H_{eq}], 1.92 [br dd, $J \approx J' \approx$ 11.2 Hz, 2H, piperidine 2(6)-H_{ax}], 2.45–2.55 [complex signal, 3H, indane 1(3)-H_a and 2-H], 2.58 (t, J = 5.6 Hz, 2H, NC$H_2$$CH_2CH_2$OH), 2.95 [dd, J = 14.0 Hz, J' = 7.6 Hz, 2H, indane 1(3)-H_b], 3.05 [br d, J = 11.2 Hz, 2H, piperidine 2(6)-H_{eq}], 3.79 (t, J = 5.6 Hz, 2H, $NCH_2CH_2CH_2$OH), 3.83 [s, 6H, indane 5(6)-OCH_3], 6.72 [s, 2H, indane 4(7)-H], the signal corresponding to the OH group was not observed; ^{13}C NMR (100.6 MHz, $CDCl_3$): δ = 27.1 (CH_2, $NCH_2CH_2CH_2$OH), 32.6 [CH_2, piperidine C3(5)], 34.4 (CH, piperidine C4), 37.7 (CH, indane C2), 39.4 [CH_2, indane C1(3)], 42.6 (CH_2, 2-CH_2), 54.2 [CH_2, piperidine C2(6)], 56.0 [CH_3, indane 5(6)-OCH_3], 59.3 (CH_2, $NCH_2CH_2CH_2$OH), 64.8 (CH_2, $NCH_2CH_2CH_2$OH), 107.8 [CH, indane C4(7)], 134.9 [C, indane C3a(7a)], 147.8 [C, indane C5(6)]; IR (KBr): $\tilde{\nu}$ = 3172 cm^{-1} (O-H st); Anal. calcd for $C_{20}H_{31}NO_3$: C 72.04, H 9.37, N 4.20, found: C 72.06, H 9.25, N 4.16.

2-{[1-(2-Chloroethyl)piperidin-4-yl]methyl}-5,6-dimethoxyindane (10a). $SOCl_2$ (6.43 mL, 10.5 g, 88.2 mmol, 50 equiv) was added dropwise to a 5 °C solution of alcohol **9a** (566 mg, 1.77 mmol, 1 equiv) in CH_2Cl_2 (25 mL). The reaction mixture was heated under reflux for 4 h, cooled to room temperature and evaporated in vacuo. The resulting light-brown solid residue was taken in CH_2Cl_2 (5×10 mL) and evaporated in vacuo to give crude **9a**·HCl (671 mg), which was used in the next step without further purification.

2-{[1-(3-Chloropropyl)piperidin-4-yl]methyl}-5,6-dimethoxyindane (10b). It was prepared as described for **10a**. From alcohol **9b** (694 mg, 2.08 mmol, 1 equiv) and $SOCl_2$ (7.6 mL, 12.4 g, 104 mmol, 50 equiv), crude **10b**·HCl (825 mg) was obtained and used in the next step without further purification.

General procedure for the reaction of ω-chloroalkylpiperidines 10 with huprines 5 and 6. A solution of huprine **5** or **6** (1 mmol) in anhydrous DMSO (4.5 mL) was prepared by heating at 70 °C in a water bath, was allowed to cool to room temperature, and was added to a mixture of powdered KOH (343 mg of a 85% purity reagent, 5.2 mmol) and 4 Å molecular sieves (~600 mg). The resulting mixture was stirred thoroughly at room temperature for 2 h and then treated, dropwise, with a solution of ω-chloroalkylpiperidine **10** (1.2 mmol) in DMSO (1.5–5 mL), previously prepared by heating at 70 °C in a water bath. The reaction mixture was stirred thoroughly at room temperature for 3–5 days, diluted with water (30–100 mL), and extracted with CH_2Cl_2 (4×20 mL). The combined organic extracts were washed with water (3×30 mL), dried with anhydrous Na_2SO_4, and evaporated at reduced pressure to give a brown solid or oily residue, which was subjected to column chromatography [35–70 μm silica gel or Biotage FLASH 40M Silica equipment (KP-Sil™ 40–63 μm, 40×150 mm cartridges), CH_2Cl_2/MeOH/50% aq NH_4OH or hexane/EtOAc/Et_3N mixtures as eluent].

The isolated donepezil–huprine heterodimers **11**–**12** were transformed into the corresponding dihydrochlorides as follows: A solution of the free base (1 mmol) in CH_2Cl_2 (10–50 mL) was filtered through a 0.45 μm PTFE filter and treated with an excess of a methanolic solution of HCl (9 mmol). The solution was concentrated in vacuo to dryness and the solid residue was recrystallized from MeOH/EtOAc mixtures and/or dried at 65 °C, 30 Torr for 4 days.

(±)-3-Chloro-12-[(2-{4-[(5,6-dimethoxyindan-2-yl)methyl]piperidin-1-yl}ethyl)amino]-6,7,10,11-tetrahydro-9-methyl-7,11-methanocycloocta[*b*]quinoline [(±)-11a]. From (±)-**5** (235 mg, 0.83 mmol) and crude **10a** [aliquot of 371 mg of a total amount of 671 mg of the crude product obtained from 566 mg (1.77 mmol) of alcohol **9a**], a brown solid residue (384 mg) was obtained and subjected to column chromatography [35–70 μm silica gel (50 g), CH_2Cl_2/MeOH/50% aq NH_4OH 99:1:0.4], to afford successively heterodimer (±)-**11a** (103 mg, 21%) as a light-yellow solid, a mixture (±)-**11a**/(±)-**5** in an approximate ratio 64:36 (^{1}H NMR) [114 mg, 36% total yield of (±)-**11a**], and starting huprine (±)-**5** (47 mg) [58% total yield of (±)-**11a** based on reacted (±)-**5**].

(±)-**11a**: R_f = 0.64 (CH_2Cl_2/MeOH/50% aq NH_4OH 9:1:0.05).

(±)-**11a**·2HCl: mp: 200–202 °C (CH_2Cl_2/MeOH 6:7); ^{1}H NMR (500 MHz, CD_3OD): δ = 1.53 (t, J = 7.0 Hz, 2H, indane 2-CH_2), 1.58 (s, 3H, 9-CH_3), 1.66 [m, 2H, piperidine 3(5)-H_{ax}], 1.72–1.80 (br signal, 1H, piperidine 4-H), 1.93 (d, J = 18.5 Hz, 1H, 10-H_{endo}), superimposed in part 1.97 (dm, $J \approx$ 13.0 Hz, 1H, 13-H_{syn}), 2.06 [br d, J = 14.5 Hz, 2H, piperidine 3(5)-H_{eq}], superimposed in part 2.10 (dm, J = 13.0 Hz, 1H, 13-H_{anti}), 2.53 [br d, J = 14.0 Hz, 2H, indane 1(3)-H_{cis}], superimposed in part 2.48–2.60 (m, 1H, indane 2-H), superimposed in part 2.60 (br dd, $J \approx$ 18.5 Hz, J' = 5.0 Hz, 1H, 10-H_{exo}), 2.78 (m, 1H,

7-H), 2.92 (dm, $J=18.0$ Hz, 1H, 6-H_{endo}), 3.00 [dd, $J\approx14.0$ Hz, $J'\approx7.0$ Hz, 2H, indane 1(3)-H_{trans}], 3.11 [br t, $J=11.5$ Hz, 2H, piperidine 2(6)-H_{ax}], 3.24 (dd, $J=18.0$ Hz, $J'=5.5$ Hz, 1H, 6-H_{exo}), 3.60 (m, 1H, 11-H), superimposed in part 3.62 (m, 2H, $NHCH_2CH_2N$), 3.68–3.76 [br signal, 2H, piperidine 2(6)-H_{eq}], 3.77 [s, 6H, indane 5(6)-OCH_3], 4.42 (t, $J=6.5$ Hz, 2H, $NHCH_2CH_2N$), 4.84 (s, NH and $^+$NH), 5.58 (br d, $J=4.5$ Hz, 1H, 8-H), 6.78 [s, 2H, indane 4(7)-H], 7.64 (dd, $J=9.0$ Hz, $J'=2.0$ Hz, 1H, 2-H), 7.81 (d, $J\approx2.0$ Hz, 1H, 4-H), 8.35 (d, $J=9.0$ Hz, 1H, 1-H); ^{13}C NMR (100.6 MHz, CD_3OD): $\delta=23.4$ (CH_3, 9-CH_3), 27.5 (CH, C11), 27.8 (CH, C7), 29.1 (CH_2, C13), 30.9 [CH_2, piperidine C3(5)], 33.4 (CH, piperidine C4), 36.2 (CH_2, C10), 36.6 (CH_2, C6), 38.9 (CH, indane C2), 40.3 [CH_2, indane C1(3)], 43.0 (CH_2, $NHCH_2CH_2N$), 43.9 (CH_2, indane 2-CH_2), 54.9 [CH_2, piperidine C2(6)], 56.7 [CH_3, indane 5(6)-OCH_3], 57.2 (CH_2, $NHCH_2CH_2N$), 109.7 [CH, indane C4(7)], 116.0 (C) and 119.3 (C) (C11a and C12a), 119.4 (CH, C4), 125.1 (CH, C8), 127.5 (CH, C2), 129.0 (CH, C1), 134.7 (C, C9), 136.3 [C, indane C3a(7a)], 140.4 (C, C3), 140.8 (C, C4a), 149.4 [C, indane C5(6)], 152.5 (C, C5a), 157.1 (C, C12); IR (KBr): $\tilde{\nu}=3500$–2500 (max at 3417, 3256, 3055, 3001, 2928, 2835, N-H, $^+$N-H, O-H, and C-H st), 1630, 1581, and 1504 cm^{-1} (ar-C-C and ar-C-N st); HRMS *m/z* $[M+H]^+$ calcd for $C_{36}H_{44}{}^{35}ClN_3O_2$: 586.3194, found: 586.3207; Anal. calcd for $C_{36}H_{44}ClN_3O_2\cdot2HCl\cdot3H_2O$: C 60.63, H 7.35, N 5.89, Cl 14.91, found: C 60.90, H 7.05, N 5.93, Cl 15.06.

(−)-(7*S*,11*S*)-3-Chloro-12-[(2-{4-[(5,6-dimethoxyindan-2-yl)methyl]piperidin-1-yl}ethyl)amino]-6,7,10,11-tetrahydro-9-methyl-7,11-methanocycloocta[*b*]quinoline [(−)-11a]. From (−)-**5** (>99% *ee*, 295 mg, 1.04 mmol) and crude **10a** [aliquot of 473 mg of a total amount of 2.50 g of the crude product obtained from 2.20 g (6.90 mmol) of alcohol **9a**] with a reaction time of 5 days, a brown solid residue (686 mg) was obtained and subjected to column chromatography [35–70 μm silica gel (68 g), CH_2Cl_2/MeOH/50% aq NH_4OH mixtures]. On elution with CH_2Cl_2/MeOH/50% aq NH_4OH 99:1:0.2 to 98:2:0.2, heterodimer (−)-**11a** (106 mg, 17%) and a mixture (−)-**11a**/(−)-**5** in an approximate ratio 55:45 (^{1}H NMR) [210 mg, 36% total yield of (−)-**11a**, 54% total yield of (−)-**11a** based on reacted huprine (−)-**5**] were successively isolated as a colorless oil and a yellowish oil, respectively.

(−)-**11a**·2HCl: mp: 228–230 °C (CH_2Cl_2/MeOH 4:1); $[\alpha]_{20}^{D}=-139$ ($c=0.96$ in MeOH); the ^{1}H and ^{13}C NMR spectra were identical to those reported above for (±)-**11a**·2HCl; IR (KBr): $\tilde{\nu}=3600$–2500 (max at 3551, 3388, 3342, 3229, 3056, 2928, 2842, 2701, N-H, $^+$N-H, O-H, and C-H st), 1629, 1582, and 1505 cm^{-1} (ar-C-C and ar-C-N st); HRMS *m/z* $[M+H]^+$ calcd for $C_{36}H_{44}{}^{35}ClN_3O_2$: 586.3194, found: 586.3193; Anal. calcd for $C_{36}H_{44}ClN_3O_2\cdot2HCl\cdot2H_2O$: C 62.20, H 7.25, N 6.04, Cl 15.30, found: C 62.45, H 7.20, N 6.19, Cl 15.13.

(±)-3-Chloro-12-[(3-{4-[(5,6-dimethoxyindan-2-yl)methyl]piperidin-1-yl}propyl)amino]-6,7,10,11-tetrahydro-9-methyl-7,11-methanocycloocta[*b*]quinoline [(±)-11b]. From (±)-**5** (311 mg, 1.09 mmol) and crude **10b** [aliquot of 508 mg of a total amount of 825 mg of the crude product obtained from 694 mg (2.08 mmol) of alcohol **9b**], a brown solid residue (641 mg) was obtained. After three successive purifications by column chromatography [35–70 μm silica gel (65 g), CH_2Cl_2/MeOH/50% aq NH_4OH 99:1:0.2 to 92:8:0.2 + Biotage FLASH 40M Silica equipment, CH_2Cl_2/MeOH/50% aq NH_4OH 98:2:0.2 + Biotage FLASH 40M Silica equipment, CH_2Cl_2/MeOH/50% aq NH_4OH 100:0:0.2 to 95:5:0.2], a mixture (±)-**5**/(±)-**11b** in an approximate ratio 38:62 (^{1}H NMR) (152 mg) and heterodimer (±)-**11b** [136 mg, 21% isolated yield, 35% total yield, 43% total yield based on reacted huprine (±)-**5**] were isolated as a yellowish solid and oil, respectively.

(±)-**11b**: $R_f=0.59$ (CH_2Cl_2/MeOH/50% aq NH_4OH 9:1:0.05).

(±)-**11b**·2HCl: mp: 184–186 °C (MeOH/EtOAc 1:8); ^{1}H NMR (500 MHz, CD_3OD): $\delta=1.51$ (m, 2H, indane 2-CH_2), superimposed in part 1.55 [m, 2H, piperidine, 3(5)-H_{ax}], 1.58 (s, 3H, 9-CH_3), 1.70–1.80 (br signal, 1H, piperidine 4-H), 1.92 (d, $J=17.5$ Hz, 1H, 10-H_{endo}), superimposed in part 1.97 (dm, $J\approx13.0$ Hz, 1H, 13-H_{syn}), 2.04 [br d, $J=14.5$ Hz, 2H, piperidine 3(5)-H_{eq}], 2.09 (dm, $J=13.0$ Hz, 1H, 13-H_{anti}), 2.37 (m, 2H, $NHCH_2CH_2CH_2N$), 2.52 [br d, $J=13.0$ Hz, 2H, indane 1(3)-H_{cis}], superimposed in part 2.48–2.59 (m, 1H, indane 2-H), superimposed in part 2.62 (br dd, $J\approx17.5$ Hz, $J'=4.0$ Hz, 1H, 10-H_{exo}), 2.77 (m, 1H, 7-H), 2.88 (d, $J=18.0$ Hz, 1H, 6-H_{endo}), 2.99 [dd, $J\approx13.0$ Hz, $J'=8.0$ Hz, 2H, indane 1(3)-H_{trans}], superimposed in part 3.00 [m, 2H, piperidine 2(6)-H_{ax}], 3.22 (dd, $J=18.0$ Hz, $J'=5.5$ Hz, 1H, 6-H_{exo}), 3.27 (m, 2H, $NHCH_2CH_2CH_2N$), 3.54 (m, 1H, 11-H), 3.58–3.66 [br signal, 2H, piperidine 2(6)-H_{eq}], 3.77 [s, 6H, indane 5(6)-OCH_3], 4.08 (t, $J=7.0$ Hz, 2H, $NHCH_2CH_2CH_2N$), 4.85 (s, NH and $^+$NH), 5.58 (br d, $J=5.0$ Hz, 1H, 8-H), 6.78 [s, 2H, indane 4(7)-H], 7.60 (dd, $J=9.5$ Hz, $J'=2.0$ Hz, 1H, 2-H), 7.78 (d, $J=2.0$ Hz, 1H, 4-H), 8.41 (d, $J=9.5$ Hz, 1H, 1-H); ^{13}C NMR (100.6 MHz, CD_3OD): $\delta=23.5$ (CH_3, 9-CH_3), 26.2 (CH_2, $NHCH_2CH_2CH_2N$), 27.4 (CH, C11), 27.9 (CH, C7), 29.3 (CH_2, C13), 30.9 [CH_2, piperidine C3(5)], 33.6 (CH, piperidine C4), 36.1 (CH_2, C10), 36.4 (CH_2, C6), 38.8 (CH, indane C2), 40.3 [CH_2, indane C1(3)], 43.0 (CH_2, indane 2-CH_2), 46.6 (CH_2, $NHCH_2CH_2CH_2N$), 54.3 [CH_2, piperidine C2(6)], 55.3 (CH_2, $NHCH_2CH_2CH_2N$), 56.7 [CH_3, indane 5(6)-OCH_3], 109.7 [CH, indane C4(7)], 115.8 (C) and 118.3 (C) (C11a and C12a), 119.2 (CH, C4), 125.1 (CH, C8), 127.2 (CH, C2), 129.4 (CH, C1), 134.7 (C, C9), 136.3 [C, indane C3a(7a)], 140.3 (C, C3), 140.9 (C, C4a), 149.4 [C, indane C5(6)], 151.8 (C, C5a), 156.9 (C, C12); IR (KBr): $\tilde{\nu}=3600$–2500 (max at 3417, 3252, 3060, 2995, 2928, 2835, N-H, $^+$N-H, O-H, and C-H st), 1630, 1581, and 1504 cm^{-1} (ar-C-C and ar-C-N st); HRMS *m/z* $[M+H]^+$ calcd for $C_{37}H_{46}{}^{35}ClN_3O_2$: 600.3351, found: 600.3358; Anal. calcd for $C_{37}H_{46}ClN_3O_2\cdot2HCl\cdot2H_2O$: C 62.66, H 7.39, N 5.93, Cl 15.00, found: C 62.29, H 7.19, N 5.71, Cl 15.05.

(−)-(7*S*,11*S*)-3-Chloro-12-[(3-{4-[(5,6-dimethoxyindan-2-yl)methyl]piperidin-1-yl}propyl)amino]-6,7,10,11-tetrahydro-9-methyl-7,11-methanocycloocta[*b*]quinoline [(−)-11b]. From (−)-**5** **(>99% *ee*, 200 mg, 0.70 mmol) and crude 10b** [aliquot of 276 mg of a total amount of 1.29 g of the crude product obtained from 1.30 g (3.90 mmol) of alcohol **9b**], a brown oily residue (415 mg) was obtained and subjected to column chromatography [35–70 μm silica gel (42 g), CH_2Cl_2/MeOH/50% aq NH_4OH 99:1:0.2], to afford successively a mixture (−)-**5**/(−)-**11b** in an approximate ratio 22:78 (^{1}H NMR) (65 mg) and heterodimer (−)-**11b** [64 mg, 15% isolated yield, 27% total yield, 29% total yield based on reacted (−)-**5**] as yellowish oils.

(−)-**11b**·2HCl: mp: 206–208 °C (CH_2Cl_2/MeOH 5:1); $[\alpha]_{20}^{D}=-139$ ($c=0.11$ in MeOH); the ^{1}H and ^{13}C NMR spectra were identical to those reported above for (±)-**11b**·2HCl; IR (KBr): $\tilde{\nu}=3600$–2500 (max at 3371, 3232, 3119, 3055, 2924, 2856, 2646, N-H, $^+$N-H, O-H, and C-H st), 1630, 1582, and 1502 cm^{-1} (ar-C-C and ar-C-N st); HRMS *m/z* $[M+H]^+$ calcd for $C_{37}H_{46}{}^{35}ClN_3O_2$: 600.3351, found: 600.3344; Anal. calcd for $C_{37}H_{46}ClN_3O_2\cdot2HCl\cdot3.5H_2O$: C 60.36, H 7.53, N 5.71, Cl 14.45, found: C 60.07, H 7.29, N 5.34, Cl 14.79.

(+)-(7*R*,11*R*)-3-Chloro-12-[(3-{4-[(5,6-dimethoxyindan-2-yl)methyl]piperidin-1-yl}propyl)amino]-6,7,10,11-tetrahydro-9-methyl-7,11-methanocycloocta[*b*]quinoline [(+)-11b]. From (+)-**5** **(>99% *ee*, 283 mg, 0.99 mmol) and crude 10b** [aliquot of 461 mg of a total amount of 1.29 g of the crude product obtained from 1.30 g (3.90 mmol) of alcohol **9b**], a brown oily residue (590 mg) was obtained and subjected to column chromatography [35–70 μm silica gel (59 g), hexane/EtOAc/Et_3N 50:50:0.2], to afford successively starting (+)-**5** (41 mg) as a yellowish solid, a mixture

(+)-**5**/(+)-**11b** in an approximate ratio 35:65 (^{1}H NMR) (20 mg), and heterodimer (+)-**11b** [279 mg, 47% isolated yield, 49% total yield, 59% total yield based on reacted (+)-**5**] as yellowish oils.

(+)-**11b**·2HCl: mp: 198–199 °C (MeOH/EtOAc 2:13); $[\alpha]_{20}^{D}=+140$ ($c=0.82$ in MeOH); the ^{1}H and ^{13}C NMR spectra were identical to those reported above for (±)-**11b**·2HCl; IR (KBr): $\tilde{\nu}=3600$–2500 (max at 3400, 3220, 3119, 3061, 3014, 2920, 2897, 2833, 2628, 2552, N-H, $^+$N-H, O-H, and C-H st), 1630, 1605, 1583, and 1504 cm^{-1} (ar-C-C and ar-C-N st); HRMS *m/z* $[M+H]^+$ calcd for $C_{37}H_{46}{}^{35}ClN_3O_2$: 600.3351, found: 600.3352; Anal. calcd for $C_{37}H_{46}ClN_3O_2{\cdot}2HCl{\cdot}2.5H_2O$: C 61.88, H 7.44, N 5.85, Cl 14.81, found: C 62.14, H 7.22, N 5.81, Cl 14.38.

(±)-3-Chloro-12-[(2-{4-[(5,6-dimethoxyindan-2-yl)methyl]piperidin-1-yl}ethyl)amino]-9-ethyl-6,7,10,11-tetrahydro-7,11-methanocycloocta[*b*]quinoline [(±)-12a]. From (±)-**6** (322 mg, 1.08 mmol) and crude **10a** [aliquot of 464 mg of a total amount of 503 mg of the crude product obtained from 396 mg (1.24 mmol) of alcohol **9a**], a brown solid residue (549 mg) was obtained and subjected to column chromatography [35–70 μm silica gel (55 g), CH_2Cl_2/MeOH/50% aq NH_4OH mixtures]. On elution with CH_2Cl_2/MeOH/50% aq NH_4OH 99:1:0.2 to 95:5:0.2, heterodimer (±)-**12a** (181 mg, 28%) was isolated as a yellowish solid.

(±)-**12a**: $R_f=0.58$ (CH_2Cl_2/MeOH/50% aq NH_4OH 9:1:0.05).

(±)-**12a**·2HCl: mp: 222–225 °C (MeOH/EtOAc 2:9); ^{1}H NMR (500 MHz, CD_3OD): $\delta=0.91$ (t, $J=7.5$ Hz, 3H, 9-CH_2CH_3), 1.52 (m, 2H, indane 2-CH_2), 1.55–1.68 [br signal, 2H, piperidine 3(5)-H_{ax}], 1.70–1.80 (br signal, 1H, piperidine 4-H), 1.86 (dq, $J=15.0$ Hz, $J'=7.5$ Hz, 1H) and 1.89 (dq, $J=15.0$ Hz, $J'=7.5$ Hz, 1H) (9-CH_2CH_3), 1.93 (d, $J=18.0$ Hz, 1H, 10-H_{endo}), 1.99 (dm, $J=13.0$ Hz, 1H, 13-H_{syn}), 2.05 [br d, $J=13.5$ Hz, 2H, piperidine 3(5)-H_{eq}], 2.11 (dm, $J\approx13.0$ Hz, 1H, 13-H_{anti}), 2.52 [br d, $J=13.0$ Hz, 2H, indane 1(3)-H_{cis}], superimposed in part 2.48–2.60 (m, 1H, indane 2-H), 2.63 (br dd, $J\approx18.0$ Hz, $J'=4.5$ Hz, 1H, 10-H_{exo}), 2.81 (m, 1H, 7-H), 2.92 (br d, $J=18.0$ Hz, 1H, 6-H_{endo}), 2.99 [dd, $J=13.0$ Hz, $J'=7.0$ Hz, 2H, indane 1(3)-H_{trans}], 3.04–3.15 [br signal, 2H, piperidine 2(6)-H_{ax}], 3.25 (dd, $J=18.0$ Hz, $J'=5.5$ Hz, 1H, 6-H_{exo}), 3.57 (m, 1H, 11-H), superimposed in part 3.61 (m, 2H, $NHCH_2CH_2N$), 3.64–3.74 [br signal, 2H, piperidine 2(6)-H_{eq}], 3.77 [s, 6H, indane 5(6)-OCH_3], 4.41 (t, $J=6.0$ Hz, 2H, $NHCH_2CH_2N$), 4.84 (s, NH and $^+$NH), 5.59 (br d, $J=5.5$ Hz, 1H, 8-H) 6.78 [s, 2H, indane 4(7)-H], 7.63 (dd, $J=9.0$ Hz, $J'=2.0$ Hz, 1H, 2-H), 7.81 (d, $J=2.0$ Hz, 1H, 4-H), 8.35 (d, $J=9.0$ Hz, 1H, 1-H); ^{13}C NMR (100.6 MHz, CD_3OD): $\delta=12.5$ (CH_3, 9-CH_2CH_3), 27.5 (CH, C11), 27.8 (CH, C7), 29.4 (CH_2, C13), 30.9 (CH_2, 9-CH_2CH_3), 31.0 [CH_2, piperidine C3(5)], 33.5 (CH, piperidine C4), 35.1 (CH_2, C10), 36.3 (CH_2, C6), 38.9 (CH, indane C2), 40.3 [CH_2, indane C1(3)], 43.1 (CH_2, $NHCH_2CH_2N$), 43.9 (CH_2, indane 2-CH_2), 54.9 [CH_2, piperidine C2(6)], 56.7 [CH_3, indane 5(6)-OCH_3], 57.1 (CH_2, $NHCH_2CH_2N$), 109.7 [CH, indane C4(7)], 116.0 (C) and 119.3 (C) (C11a and C12a), 119.5 (CH, C4), 123.4 (CH, C8), 127.5 (CH, C2), 128.9 (CH, C1), 136.3 [C, indane C3a(7a)], 140.2 (C, C9), 140.4 (C, C3), 140.8 (C, C4a), 149.4 [C, indane C5(6)], 152.6 (C, C5a), 157.1 (C, C12); IR (KBr): $\tilde{\nu}=3600$–2500 (max at 3402, 3256, 3226, 3056, 2925, 2851, 2707, 2651, N-H, $^+$N-H, O-H, and C-H st), 1629, 1582, 1557, and 1505 cm^{-1} (ar-C-C and ar-C-N st); HRMS *m/z* $[M+H]^+$ calcd for $C_{37}H_{46}{}^{35}ClN_3O_2$: 600.3351, found: 600.3358; Anal. calcd for $C_{37}H_{46}ClN_3O_2{\cdot}2HCl{\cdot}1.5H_2O$: C 63.47, H 7.34, N 6.00, Cl 15.19, found: C 63.51, H 7.18, N 5.94, Cl 15.21.

(−)-(7*S*,11*S*)-3-Chloro-12-[(2-{4-[(5,6-dimethoxyindan-2-yl)methyl]piperidin-1-yl}ethyl)amino]-9-ethyl-6,7,10,11-tetrahydro-7,11-methanocycloocta[*b*]quinoline [(−)-12a]. From (−)-**6** (>99% *ee*, 303 mg, 1.02 mmol) and crude **10a** [aliquot of 413 mg of a total amount of 2.50 g of the crude product obtained from 2.20 g (6.90 mmol) of alcohol **9a**], a brown solid residue (555 mg) was obtained and subjected to column chromatography [35–70 μm silica gel (55 g), CH_2Cl_2/MeOH/50% aq NH_4OH mixtures]. On elution with CH_2Cl_2/MeOH/50% aq NH_4OH 99:1:0.2 to 98:2:0.2, heterodimer (−)-**12a** (110 mg, 18%) and a mixture (−)-**12a**/(−)-**6** in an approximate ratio 68:32 (^{1}H NMR) [156 mg, 35% total yield of (−)-**12a**, 43% total yield of (−)-**12a** based on reacted huprine (−)-**6**] were successively isolated as colorless and yellowish oils, respectively.

(−)-**12a**·2HCl: mp: 251–252 °C (CH_2Cl_2/MeOH 4:1); $[\alpha]_{20}^{D}=-140$ ($c=1.39$ in MeOH); the ^{1}H and ^{13}C NMR spectra were identical to those reported above for (±)-**12a**·2HCl; IR (KBr): $\tilde{\nu}=3500$–2500 (max at 3402, 3220, 3117, 3047, 2927, 2904, 2837, 2718, 2677, 2642, 2505, N-H, $^+$N-H, O-H, and C-H st), 1631, 1601, 1582, and 1502 cm^{-1} (ar-C-C and ar-C-N st); HRMS *m/z* $[M+H]^+$ calcd for $C_{37}H_{46}{}^{35}ClN_3O_2$: 600.3351, found: 600.3353; Anal. calcd for $C_{37}H_{46}ClN_3O_2{\cdot}2HCl{\cdot}1.75H_2O$: C 63.06, H 7.37, N 5.96, Cl 15.09, found: C 63.03, H 7.27, N 5.94, Cl 14.50.

(±)-3-Chloro-12-[(3-{4-[(5,6-dimethoxyindan-2-yl)methyl]piperidin-1-yl}propyl)amino]-9-ethyl-6,7,10,11-tetrahydro-7,11-methanocycloocta[*b*]quinoline [(±)-12b]. From (±)-**6** (230 mg, 0.77 mmol) and crude **10b** [aliquot of 358 mg of a total amount of 1.69 g of the crude product obtained from 1.33 g (3.99 mmol) of alcohol **9b**], a brown solid residue (412 mg) was obtained and subjected to column chromatography [Biotage FLASH 40 M Silica equipment, CH_2Cl_2/MeOH/50% aq NH_4OH mixtures]. On elution with CH_2Cl_2/MeOH/50% aq NH_4OH 99:1:0.2 to 97:3:0.2, a mixture (±)-**6**/(±)-**12b** in an approximate ratio 10:90 (^{1}H NMR) (138 mg) and heterodimer (±)-**12b** [97 mg, 21% isolated yield, 47% total yield, 50% total yield based on reacted huprine (±)-**6**] were successively isolated as yellowish oil and solid, respectively.

(±)-**12b**: $R_f=0.59$ (CH_2Cl_2/MeOH/50% aq NH_4OH 9:1:0.05).

(±)-**12b**·2HCl: mp: 210–211 °C (MeOH/EtOAc 1:8); ^{1}H NMR (500 MHz, CD_3OD): $\delta=0.91$ (t, $J=7.5$ Hz, 3H, 9-CH_2CH_3), 1.46–1.60 [complex signal, 4H, indane 2-CH_2 and piperidine 3(5)-H_{ax}], 1.70–1.78 (br signal, 1H, piperidine 4-H), 1.84–1.92 (complex signal, 2H, 9-CH_2CH_3), 1.94 (d, $J=18.0$ Hz, 1H, 10-H_{endo}), superimposed in part 1.97 (br d, $J\approx12.5$ Hz, 1H, 13-H_{syn}), 2.04 [br d, $J=13.5$ Hz, 2H, piperidine 3(5)-H_{eq}], 2.11 (dm, $J=12.5$ Hz, 1H, 13-H_{anti}), 2.36 (m, 2H, $NHCH_2CH_2CH_2N$), 2.52 [br d, $J=13.0$ Hz, 2H, indane 1(3)-H_{cis}], superimposed in part 2.48–2.58 (m, 1H, indane 2-H), 2.62 (br dd, $J\approx18.0$ Hz, $J'\approx4.0$ Hz, 1H, 10-H_{exo}), 2.80 (m, 1H, 7-H), 2.88 (d, $J\approx18.0$ Hz, 1H, 6-H_{endo}), 2.99 [dd, $J\approx13.0$ Hz, $J'\approx7.0$ Hz, 2H, indane 1(3)-H_{trans}], superimposed in part 3.04 [m, 2H, piperidine 2(6)-H_{ax}], 3.23 (dd, $J=18.0$ Hz, $J'=5.5$ Hz, 1H, 6-H_{exo}), superimposed in part 3.27 (m, 2H, $NHCH_2CH_2CH_2N$), 3.54 (m, 1H, 11-H), 3.58–3.66 [m, 2H, piperidine 2(6)-H_{eq}], 3.77 [s, 6H, indane 5(6)-OCH_3], 4.08 (t, $J=7.0$ Hz, 2H, $NHCH_2CH_2CH_2N$), 4.84 (s, NH and $^+$NH), 5.59 (br d, $J=5.0$ Hz, 1H, 8-H), 6.78 [s, 2H, indane 4(7)-H], 7.60 (dd, $J\approx9.5$ Hz, $J'=1.5$ Hz, 1H, 2-H), 7.78 (d, $J=1.5$ Hz, 1H, 4-H), 8.40 (d, $J=9.5$ Hz, 1H, 1-H); ^{13}C NMR (100.6 MHz, CD_3OD): $\delta=12.5$ (CH_3, 9-CH_2CH_3), 26.2 (CH_2, $NHCH_2CH_2CH_2N$), 27.3 (CH, C11), 27.8 (CH, C7), 29.5 (CH_2, C13), 30.87 (CH_2) and 30.92 (CH_2) [9-CH_2CH_3 and piperidine C3(5)], 33.6 (CH, piperidine C4), 34.9 (CH_2, C10), 36.2 (CH_2, C6), 38.8 (CH, indane C2), 40.3 [CH_2, indane C1(3)], 43.0 (CH_2, indane 2-CH_2), 46.5 (CH_2, $NHCH_2CH_2CH_2N$), 54.3 [CH_2, piperidine C2(6)], 55.3 (CH_2, $NHCH_2CH_2CH_2N$), 56.7 [CH_3, indane 5(6)-OCH_3], 109.7 [CH, indane C4(7)], 115.8 (C) and 118.3 (C) (C11a and C12a), 119.2 (CH, C4), 123.3 (CH, C8), 127.2 (CH, C2), 129.3 (CH, C1), 136.3 [C, indane C3a(7a)], 140.2 (C, C9), 140.3 (C, C3), 140.8 (C, C4a), 149.4 [C,

indane C5(6)], 151.8 (C, C5a), 156.8 (C, C12); IR (KBr): $\tilde{\nu}$ = 3600–2500 (max at 3372, 3254, 3120, 3055, 2926, 2837, 2723, N-H, $^{+}$N-H, O-H, and C-H st), 1630, 1583, and 1503 cm^{-1} (ar-C-C and ar-C-N st); HRMS *m/z* $[M+H]^{+}$ calcd for $C_{38}H_{48}{}^{35}ClN_3O_2$: 614.3507, found: 614.3515. Anal. calcd for $C_{38}H_{48}ClN_3O_2 \cdot 2\,HCl \cdot 2.5\,H_2O$: C 62.33, H 7.57, N 5.74, Cl 14.53, found: C 62.11; H 7.19, N 5.59; Cl 14.79.

(−)-(7*S*,11*S*)-3-Chloro-12-[(3-{4-[(5,6-dimethoxyindan-2-yl)methyl]piperidin-1-yl}propyl)amino]-9-ethyl-6,7,10,11-tetrahydro-7,11-methanocycloocta[*b*]quinoline [(−)-12 b]. From (−)-**6** (> 99% *ee*, 311 mg, 1.04 mmol) and crude **10 b** [aliquot of 408 mg of a total amount of 1.29 g of the crude product obtained from 1.30 g (3.90 mmol) of alcohol **9 b**], a brown oily residue (610 mg) was obtained. After two successive purifications by column chromatography [35–70 μm silica gel (76 g), CH_2Cl_2/MeOH/50% aq NH_4OH 99:1:0.2 + 35–70 μm silica gel (45 g), hexane/EtOAc/Et_3N 50:50:0.2], starting huprine (−)-**6** (143 mg) and heterodimer (−)-**12 b** [151 mg, 24%, 44% based on reacted huprine (−)-**6**] were isolated as a yellowish solid and oil, respectively.

(−)-**12 b**·2 HCl: mp: 234–236 °C (CH_2Cl_2/MeOH 5:2); $[\alpha]_{20}^{D} = -136$ (*c* = 0.10 in MeOH); the ^{1}H and ^{13}C NMR spectra were identical to those reported above for (±)-**12 b**·2 HCl; IR (KBr): $\tilde{\nu}$ = 3600–2500 (max at 3419, 3129, 3064, 2925, 2852, N-H, $^{+}$N-H, O-H, and C-H st), 1629, 1583, and 1505 cm^{-1} (ar-C-C and ar-C-N st); HRMS *m/z* $[M+H]^{+}$ calcd for $C_{38}H_{48}{}^{35}ClN_3O_2$: 614.3507, found: 614.3501; Anal. calcd for $C_{38}H_{48}ClN_3O_2 \cdot 2\,HCl \cdot 3\,H_2O$: C 61.58, H 7.61, N 5.67, Cl 14.35, found: C 61.56, H 7.43, N 5.41, Cl 14.10.

Biological evaluation

AChE and BChE inhibition assay. AChE and BChE inhibitory activity was evaluated spectrophotometrically by the method of Ellman et al.,[26] using human recombinant AChE and human serum BChE. The reactions took place in a final volume of 300 μL 0.1 M PBS pH 8.0, containing 0.02 U mL^{-1} AChE or BChE and 333 μM 5,5′-dithiobis(2-nitrobenzoic) acid (DTNB) solution used to produce the yellow anion of 5-thio-2-nitrobenzoic acid. Inhibition curves were performed in duplicate using at least 10 increasing concentrations of inhibitor and pre-incubating for 20 min at 37 °C. One duplicate sample without inhibitor was always present to yield 100% AChE or BChE activity. Substrates, acetylthiocholine iodide (450 μM) or butyrylthiocholine iodide (300 μM) were then added, and the reaction was developed for 5 min at 37 °C. The color production was measured at λ = 412 nm using a labsystems Multiskan spectrophotometer.

Data from concentration–inhibition experiments of the inhibitors were calculated by nonlinear regression analysis using the GraphPad Prism program package (GraphPad Software; San Diego, CA, USA), which gave estimates of the IC_{50} value (concentration of drug effecting 50% inhibition of enzyme activity). Results are expressed as the mean ± SEM of at least four experiments performed in duplicate. DTNB, acetylthiocholine iodide, butyrylthiocholine iodide, and enzymes were purchased from Sigma.

Kinetic analysis of AChE inhibition. To obtain estimates of the mechanism of action of (−)-**11 b**, reciprocal plots of 1/velocity versus 1/[substrate] were constructed at relatively low concentration of substrate (0.563–0.112 mM) by using Ellman's method[26] and human recombinant AChE (Sigma, Milan, Italy). Three concentrations of (−)-**11 b** were selected for this study: 0.18, 0.35, and 0.88 nM. The plots were assessed by a weighted least-squares analysis that assumed the variance of the velocity (*v*) to be a constant percentage of *v* for the entire data set. Data analysis was performed with GraphPad Prism 4.03 software (GraphPad Software Inc.).

Slopes of the obtained reciprocal plots were then plotted against (−)-**11 b** concentration in a similar weighted analysis, and K_i was determined as the intercept on the negative *x*-axis.

AChE-induced $A\beta_{1-40}$ aggregation inhibition assay. Thioflavin T (Basic Yellow 1), human recombinant AChE lyophilized powder, 1,1,1,3,3,3-hexafluoro-2-propanol (HFIP), were purchased from Sigma Chemicals. Absolute DMSO over molecular sieves was from Fluka. Water was deionized and doubly distilled. $A\beta_{1-40}$, supplied as trifluoroacetate salt, was purchased from Bachem AG (Switzerland). $A\beta_{1-40}$ (2 mg mL^{-1}) was dissolved in HFIP and lyophilized. The 1 mM solutions of tested inhibitors were prepared by dissolution in methanol.

Aliquots of 2 μL $A\beta_{1-40}$ peptide, lyophilized from 2 mg mL^{-1} HFIP solution and dissolved in DMSO, were incubated for 24 h at room temperature in 0.215 M sodium phosphate buffer (pH 8.0) at a final concentration of 230 μM. For co-incubation experiments, aliquots (16 μL) of hAChE (final concentration 2.30 μM, Aβ/AChE molar ratio 100:1) and AChE in the presence of 2 μL of the tested inhibitor (final inhibitor concentration: 100 μM) in 0.215 M sodium phosphate buffer pH 8.0 solution were added. Blanks containing $A\beta_{1-40}$ alone, human recombinant AChE alone, and $A\beta_{1-40}$ plus tested inhibitors in 0.215 M sodium phosphate buffer (pH 8.0) were prepared. The final volume of each vial was 20 μL. Each assay was run in duplicate. To quantify amyloid fibril formation, the thioflavin T fluorescence method was then applied.[30] After incubation, samples were diluted to a final volume of 2.0 mL with 50 mM glycine-NaOH buffer (pH 8.5) containing 1.5 μM thioflavin T. A 300 s time scan of fluorescence intensity was carried out (λ_{ex} = 446 nm; λ_{em} = 490 nm, FP-6200 fluorimeter, Jasco Europe), and values at plateau were averaged after subtracting the background fluorescence of 1.5 μM thioflavin T solution. The percent inhibition of the AChE-induced aggregation due to the presence of the tested compound was calculated by the following expression: $100-(IF_i/IF_o \times 100)$, in which IF_i and IF_o are the fluorescence intensities obtained for Aβ plus AChE in the presence and absence of inhibitor, respectively, minus the fluorescence intensities due to the respective blanks.

$A\beta_{1-42}$ self-aggregation inhibition assay. As reported in a previously published protocol,[43] HFIP pretreated $A\beta_{1-42}$ samples (Bachem AG, Switzerland) were solubilized with a mixture of $CH_3CN/Na_2CO_3/NaOH$ (48.4:48.4:3.2). Experiments were performed by incubating the peptide in 10 mM phosphate buffer (pH 8.0) containing 10 mM NaCl, at 30 °C for 24 h (final Aβ concentration: 50 μM) with and without inhibitor (10 μM, Aβ/inhibitor = 5:1). Blanks containing the tested inhibitors were also prepared and tested. Following the same procedure previously described for the AChE-induced $A\beta_{1-40}$ aggregation inhibition assay to quantify amyloid fibrils formation, the thioflavin T fluorescence method was used.[30] The fluorescence intensities were compared, and the percent inhibition due to the presence of the inhibitor was calculated from the fluorescence intensities obtained for $A\beta_{1-42}$ in the presence and in the absence of inhibitor, respectively.

BACE-1 inhibition assay. BACE-1 (Sigma, Italy) inhibition studies were performed by employing a peptide mimicking APP sequence as substrate (M-2420, Bachem; Switzerland). The following procedure was employed: 5 μL test compound (or DMSO) were pre-incubated with 175 μL of the enzyme (*c* = 17.2 nM) for 1 h at room temperature. The substrate (3 μM) was then added and left to react for 15 min. The fluorescence signal was read at λ_{em} = 405 nm (λ_{ex} = 320 nm). The fluorescence intensities with and without inhibi-

tor were compared and the percent inhibition due to the presence of test compounds was calculated. The percent inhibition due to the presence of increasing test compound concentration was calculated from the fluorescence intensities obtained for BACE-1 in the presence and in the absence of inhibitor, respectively.

To demonstrate inhibition of BACE-1 activity a peptidomimetic inhibitor (β-secretase inhibitor IV, Calbiochem, UK) was serially diluted into the reaction wells ($IC_{50} = 0.013$ μM).

For compounds that showed fluorescence interferences with the previous assay conditions, a different enzyme source and substrate was used for testing the BACE-1 inhibition. In brief, purified baculovirus-expressed BACE-1 in 50 mM Tris (pH 7.5), 10% glycerol and rhodamine-derivative substrate (Panvera peptide) were purchased from Invitrogen (Milan, Italy). Stock solutions of the test compounds were prepared in DMSO and diluted with 50 mM sodium acetate buffer (pH 4.5). Specifically, 20 μL of BACE-1 enzyme (11.7 nM, final concentration) were incubated with 20 μL of test compound for 60 min. To start the reaction, 20 μL of Panvera peptide (0.25 μM, final concentration) were added to each well. The mixture was incubated at 37 °C for 60 min. To stop the reaction, 20 μL of BACE-1 stop solution (sodium acetate, 2.5 M) were added to each well. The spectrofluorimetric assay was subsequently performed by reading the fluorescence signal at $\lambda = 590$ nm. The DMSO concentration in the final mixture was maintained $< 5\%$ (*v/v*) to guarantee no significant loss of enzyme activity. Additional measurements were performed in the presence of a detergent (CHAPS, 0.1% *w/v*) to check for nonspecific effects.[44]

Molecular modeling. The binding modes of compounds (−)-**11 a** and (−)-**11 b** were explored by means of 30 ns MD simulations performed for their complexes to hAChE. The simulation protocol was based on the computational strategy used in our previous studies,[15] which is briefly summarized here. MD simulations were run using the PMEMD module of Amber9 and the parm99SB parameters for the protein. The enzyme was modeled in its physiologically active form with neutral His440 and deprotonated Glu327, which together with Ser200 form the catalytic triad. The standard ionization state at neutral pH was considered for the rest of ionizable residues with the exception of Asp392 and Glu443, which were neutral, and His471, which was protonated, according to previous studies.[45] The charge distribution of the inhibitors was determined from a fit HF/6-31G(d) electrostatic potential obtained with Gaussian 03[46] using the RESP procedure.[47] The starting pose of the compounds was built up taking advantage of the known pose of huprine X in the X-ray crystallographic complex with *Tc*AChE[18] and the binding pose of the related donepezil–tacrine heterodimers studied in our previous work.[15] Six Na^+ cations were added to neutralize the negative charge of the system with the XLEAP module of Amber9.[48] The system was immersed in a box of TIP3P[49] water molecules, preserving the crystallographic waters inside the binding cavity. The final systems contained the protein–ligand complex, Na^+ cations, and ~20000 water molecules.

The geometry of the system was minimized in four steps. First, the position of hydrogen atoms was optimized using 3000 steps of steepest descent algorithm. Then, water molecules were refined through 2000 steps of steepest descent followed by 3000 steps of conjugate gradient. Next, the ligand, water molecules, and counterions were optimized with 2000 steps of steepest descent and 4000 steps of conjugate gradient, and finally the whole system was optimized with 3000 steps of steepest descent and 7000 steps of conjugate gradient. Thermalization of the system was performed in five steps of 20 ps, increasing the temperature from 100 K up to 298 K. Then, a series of 30 ns trajectories were run for the two compounds using a time step of 1 fs. SHAKE was used for those bonds containing hydrogen atoms, in conjunction with periodic boundary conditions at constant pressure (1 atm) and temperature (298 K), Particle-Mesh Ewald for the treatment of long-range electrostatic interactions, and a cutoff of 11 Å for nonbonded interactions.

Free energy calculations were performed using thermodynamic integration (TI) as implemented in the SANDER module of the Amber9 package to investigate the effect of replacing the methyl group at position 9 by an ethyl group on the binding affinity of (−)-**11 b** and (−)-**12 b**. Calculations were carried out using the Sander module of Amber9 package. The alchemical mutation was performed for the inhibitors in water and in the enzyme. The starting structures for the TI computations in the enzyme were taken from the last snapshot of the previous MD simulations. To carry out the alchemical transformation in water, a 1 ns MD simulation was run for the compound in aqueous solution before starting TI calculations for the inhibitor in solution. In this latter case, the simulated system contained two chloride anions to neutralize the positive charge of the inhibitor, and ~2100 TIP3P water molecules. The mutations involved both forward (methyl→ethyl) and reverse (ethyl→methyl) calculations in both aqueous solution and in the enzyme. To this end, the final structures obtained at the end of the forward TI calculation were equilibrated for 5 ns before starting the reverse mutation. The numerical integration was performed by using a five-point quadrature strategy with λ values of 0.04691, 0.23076, 0.5, 0.76923, and 0.95308. The time step was 1 fs, and the simulated time for every λ value was 2 ns. Thus, the total sampling time for each alchemical free energy change calculation was 14 ns. This simulation protocol sufficed to obtain equilibrated values of $\delta V/\delta\lambda$ during the last 1 ns, which were used to compute the change in free energy associated to the alchemical transformation.

In vitro PAMPA-BBB permeation assay. Prediction of the brain penetration was evaluated using a parallel artificial membrane permeation assay (PAMPA), in a similar manner as described previously.[40,41] Commercial drugs, PBS at pH 7.4, and dodecane were purchased from Sigma, Aldrich, Acros, and Fluka. Millex filter units (PVDF membrane, diameter 25 mm, pore size 0.45 μm) were acquired from Millipore. The porcine brain lipid (PBL) was obtained from Avanti Polar Lipids. The donor microplate was a 96-well filter plate (PVDF membrane, pore size 0.45 μm) and the acceptor microplate was an indented 96-well plate, both from Millipore. The acceptor 96-well microplate was filled with 170 μL PBS/EtOH (80:20 or 70:30), and the filter surface of the donor microplate was impregnated with 4 μL porcine brain lipid (PBL) in dodecane (20 mg mL^{-1}). Compounds were dissolved in PBS/EtOH (80:20 or 70:30) at 100 μg mL^{-1}, filtered through a Millex filter, and then added to the donor wells (170 μL). The donor filter plate was carefully put on the acceptor plate to form a sandwich, which was left undisturbed for 120 min at 25 °C. After incubation, the donor plate was carefully removed, and the concentration of compounds in the acceptor wells was determined by UV/Vis spectroscopy. Every sample was analyzed at five wavelengths, in four wells and at least in three independent runs, and the results are given as the mean ± SD. In each experiment, 15 quality control standards of known BBB permeability were included to validate the analysis set.

Acknowledgements

Financial support from the Ministerio de Ciencia e Innovación (CTQ2008-03768/PPQ, SAF2009-10553, SAF2009-13093, SAF2006-01249, SAF2008-05595), Generalitat de Catalunya (2005-SGR00180, 2009-SGR00249), Instituto de Salud Carlos III (PI080400), University of Bologna (RFO), MIUR (PRIN 2007), and COST D34, and a fellowship for C.G. (IBUB) are acknowledged.

Keywords: β-amyloid peptides · β-secretase · acetylcholinesterase · drug design · inhibitors

[1] a) R. C. Green, L. S. Schneider, D. A. Amato, A. P. Beelen, G. Wilcock, E. A. Swabb, K. H. Zavit, *JAMA J. Am. Med. Assoc.* **2009**, *302*, 2557 – 2564; b) M. G. Sullivan, *Clin. Psychiatry News* **2007**, *35*, 27; c) I. Melnikova, *Nat. Rev. Drug Discovery* **2007**, *6*, 341 – 342.

[2] a) D. J. Selkoe, *Nat. Cell Biol.* **2004**, *6*, 1054 – 1061; b) J. Coomaraswamy, E. Kilger, H. Wölfing, C. Schäfer, S. A. Kaeser, B. M. Wegenast-Braun, J. K. Hefendehl, H. Wolburg, M. Mazzela, J. Ghiso, M. Goedert, H. Akiyama, F. Garcia-Sierra, D. P. Wolfer, P. M. Mathews, M. Jucker, *Proc. Natl. Acad. Sci. USA* **2010**, *107*, 7969 – 7974.

[3] a) M. Bartolini, V. Andrisano, *ChemBioChem* **2010**, *11*, 1018 – 1035; b) M. Citron, *Nat. Rev. Drug Discovery* **2010**, *9*, 387 – 398.

[4] a) D. M. Walsh, D. J. Selkoe, *J. Neurochem.* **2007**, *101*, 1172 – 1184; b) W. Cerpa, M. C. Dinamarca, N. C. Inestrosa, *Curr. Alzheimer Res.* **2008**, *5*, 233 – 243.

[5] a) L. De Kimpe, W. Scheper, *Curr. Med. Chem.* **2010**, *17*, 198 – 212; b) B. De Strooper, R. Vassar, T. Golde, *Nat. Rev. Neurol.* **2010**, *6*, 99 – 107.

[6] C. E. Hunt, A. J. Turner, *FEBS J.* **2009**, *276*, 1845 – 1859.

[7] M. Harel, I. Schalk, L. Ehret-Sabatier, F. Bouet, M. Goeldner, C. Hirth, P. H. Axelsen, I. Silman, J. L. Sussman, *Proc. Natl. Acad. Sci. USA* **1993**, *90*, 9031 – 9035.

[8] a) N. C. Inestrosa, A. Alvarez, C. A. Pérez, R. D. Moreno, M. Vicente, C. Linker, O. I. Casanueva, C. Soto, J. Garrido, *Neuron* **1996**, *16*, 881 – 891; b) G. V. De Ferrari, M. A. Canales, I. Shin, L. M. Weiner, I. Silman, N. C. Inestrosa, *Biochemistry* **2001**, *40*, 10447 – 10457.

[9] a) T. Rees, P. I. Hammond, H. Soreq, S. Younkin, S. Brimijoin, *Neurobiol. Aging* **2003**, *24*, 777 – 787; b) T. M. Rees, A. Berson, E. H. Sklan, L. Younkin, S. Younkin, S. Brimijoin, H. Soreq, *Curr. Alzheimer Res.* **2005**, *2*, 291 – 300.

[10] a) N. C. Inestrosa, M. C. Dinamarca, A. Alvarez, *FEBS J.* **2008**, *275*, 625 – 632; b) M. C. Dinamarca, J. P. Sagal, R. A. Quintanilla, J. A. Godoy, M. S. Arrázola, N. C. Inestrosa, *Mol. Neurodegener.* **2010**, *5*, 4.

[11] a) A. Cavalli, M. L. Bolognesi, S. Capsoni, V. Andrisano, M. Bartolini, E. Margotti, A. Cattaneo, M. Recanatini, C. Melchiorre, *Angew. Chem.* **2007**, *119*, 3763 – 3766; *Angew. Chem. Int. Ed.* **2007**, *46*, 3689 – 3692; b) M. L. Bolognesi, M. Bartolini, F. Mancini, G. Chiriano, L. Ceccarini, M. Rosini, A. Milelli, V. Tumiatti, V. Andrisano, C. Melchiorre, *ChemMedChem* **2010**, *5*, 1215 – 1220; c) H. Fu, J. Dou, W. Li, W. Cui, S. Mak, Q. Hu, J. Luo, C. S. C. Lam, Y. Pang, M. B. H. Youdim, Y. Han, *Eur. J. Pharmacol.* **2009**, *623*, 14 – 21.

[12] E. García-Palomero, P. Muñoz, P. Usan, P. Garcia, C. De Austria, R. Valenzuela, L. Rubio, M. Medina, A. Martínez, *Neurodegener. Dis.* **2008**, *5*, 153 – 156.

[13] a) W. M. Li, K. K. W. Kan, P. R. Carlier, Y. P. Pang, Y. F. Han, *Curr. Alzheimer Res.* **2007**, *4*, 386 – 396; b) L. Zhang, H. Yu, W. M. Li, M. C. Cheung, Y. P. Pang, Z. M. Gu, K. Chan, Y. T. Wang, Z. Zuo, Y. F Han, *Int. J. Pharm.* **2008**, *357*, 85 – 94.

[14] G. Kryger, I. Silman, J. L. Sussman, *Structure* **1999**, *7*, 297 – 307.

[15] P. Camps, X. Formosa, C. Galdeano, T. Gómez, D. Muñoz-Torrero, M. Scarpellini, E. Viayna, A. Badia, M. V. Clos, A. Camins, M. Pallàs, M. Bartolini, F. Mancini, V. Andrisano, J. Estelrich, M. Lizondo, A. Bidon-Chanal, F. J. Luque, *J. Med. Chem.* **2008**, *51*, 3588 – 3598.

[16] a) A. Badia, J. E. Baños, P. Camps, J. Contreras, D. M. Görbig, D. Muñoz-Torrero, M. Simon, N. M. Vivas, *Bioorg. Med. Chem.* **1998**, *6*, 427 – 440; b) P. Camps, R. El Achab, D. M. Görbig, J. Morral, D. Muñoz-Torrero, A. Badia, J. E. Baños, N. M. Vivas, X. Barril, M. Orozco, F. J. Luque, *J. Med. Chem.* **1999**, *42*, 3227 – 3242; c) P. Camps, B. Cusack, W. D. Mallender, R. El Achab, J. Morral, D. Muñoz-Torrero, T. L. Rosenberry, *Mol. Pharmacol.* **2000**, *57*, 409 – 417; d) P. Camps, R. El Achab, J. Morral, D. Muñoz-Torrero, A. Badia, J. E. Baños, N. M. Vivas, X. Barril, M. Orozco, F. J. Luque, *J. Med. Chem.* **2000**, *43*, 4657 – 4666; e) D. Muñoz-Torrero, P. Camps, *Expert Opin. Drug Discovery* **2008**, *3*, 65 – 81, and references therein.

[17] M. Ratia, L. Giménez-Llort, P. Camps, D. Muñoz-Torrero, M. V. Clos, A. Badia, *Pharmacol. Biochem. Behav.* **2010**, *95*, 485 – 493.

[18] H. Dvir, D. M. Wong, M. Harel, X. Barril, M. Orozco, F. J. Luque, D. Muñoz-Torrero, P. Camps, T. L. Rosenberry, I. Silman, J. L. Sussman, *Biochemistry* **2002**, *41*, 2970 – 2981.

[19] P. Camps, X. Formosa, D. Muñoz-Torrero, J. Petrignet, A. Badia, M. V. Clos, *J. Med. Chem.* **2005**, *48*, 1701 – 1704.

[20] a) M. K. Hu, C. F. Lu, *Tetrahedron Lett.* **2000**, *41*, 1815 – 1818; b) E. T. Michalson, S. D'Andrea, J. P. Freeman, J. Szmuszkovicz, *Heterocycles* **1990**, *30*, 415 – 425.

[21] C. Ronco, G. Sorin, F. Nachon, R. Foucault, L. Jean, A. Romieu, P. Y. Renard, *Bioorg. Med. Chem.* **2009**, *17*, 4523 – 4536.

[22] P. Camps, J. Contreras, M. Font-Bardia, J. Morral, D. Muñoz-Torrero, X. Solans, *Tetrahedron: Asymmetry* **1998**, *9*, 835 – 849.

[23] K. V. S. R. K. Reddy, J. M. Babu, P. A. Kumar, E. R. R. Chandrashekar, V. T. Mathad, S. Eswaraiah, M. S. Reddy, K. Vyas, *J. Pharm. Biomed. Anal.* **2004**, *35*, 1047 – 1058.

[24] a) D. Galanakis, C. A. Davis, C. R. Ganellin, P. M. Dunn, *J. Med. Chem.* **1996**, *39*, 359 – 370; b) P. R. Carlier, E. S. H. Chow, Y. Han, J. Liu, J. El Yazal, Y. P. Pang, *J. Med. Chem.* **1999**, *42*, 4225 – 4231.

[25] Y. P. Pang, P. Quiram, T. Jelacic, F. Hong, S. Brimijoin, *J. Biol. Chem.* **1996**, *271*, 23646 – 23649.

[26] G. L. Ellman, K. D. Courtney, B. Andres, Jr., R. M. Featherstone, *Biochem. Pharmacol.* **1961**, *7*, 88 – 95.

[27] a) E. Giacobini, *Pharmacol. Res.* **2004**, *50*, 433 – 440; b) R. M. Lane, S. G. Potkin, A. Enz, *Int. J. Neuropsychopharmacol.* **2006**, *9*, 101 – 124.

[28] a) V. E. Gregor, M. R. Emmerling, C. Lee, C. J. Moore, *Bioorg. Med. Chem. Lett.* **1992**, *2*, 861 – 864; b) M. Recanatini, A. Cavalli, F. Belluti, L. Piazzi, A. Rampa, A. Bisi, S. Gobbi, P. Valenti, V. Andrisano, M. Bartolini, V. Cavrini, *J. Med. Chem.* **2000**, *43*, 2007 – 2018.

[29] a) P. Muñoz-Ruiz, L. Rubio, E. García-Palomero, I. Dorronsoro, M. del Monte-Millán, R. Valenzuela, P. Usán, C. de Austria, M. Bartolini, V. Andrisano, A. Bidon-Chanal, M. Orozco, F. J. Luque, M. Medina, A. Martínez, *J. Med. Chem.* **2005**, *48*, 7223 – 7233; b) L. Savini, A. Gaeta, C. Fattorusso, B. Catalanotti, G. Campiani, L. Chiasserini, C. Pellerano, E. Novellino, D. McKissic, A. Saxena, *J. Med. Chem.* **2003**, *46*, 1 – 4.

[30] M. Bartolini, C. Bertucci, V. Cavrini, V. Andrisano, *Biochem. Pharmacol.* **2003**, *65*, 407 – 416.

[31] a) M. L. Bolognesi, R. Banzi, M. Bartolini, A. Cavalli, A. Tarozzi, V. Andrisano, A. Minarini, M. Rosini, V. Tumiatti, C. Bergamini, R. Fato, G. Lenaz, P. Hrelia, A. Cattaneo, M. Recanatini, C. Melchiorre, *J. Med. Chem.* **2007**, *50*, 4882 – 4897; b) Y. E. Kwon, J. Y. Park, K. T. No, J. H. Shin, S. K. Lee, J. S. Eun, J. H. Yang, T. Y. Shin, D. K. Kim, B. S. Chae, J. Y. Leem, K. H. Kim, *Bioorg. Med. Chem.* **2007**, *15*, 6596 – 6607; c) M. Rosini, E. Simoni, M. Bartolini, A. Cavalli, L. Ceccarini, N. Pascu, D. W. McClymont, A. Tarozzi, M. L. Bolognesi, A. Minarini, V. Tumiatti, V. Andrisano, I. R. Mellor, C. Melchiorre, *J. Med. Chem.* **2008**, *51*, 4381 – 4384; d) V. Tumiatti, A. Milelli, A. Minarini, M. Rosini, M. L. Bolognesi, M. Micco, V. Andrisano, M. Bartolini, F. Mancini, M. Recanatini, A. Cavalli, C. Melchiorre, *J. Med. Chem.* **2008**, *51*, 7308 – 7312; e) M. L. Bolognesi, M. Bartolini, M. Rosini, V. Andrisano, C. Melchiorre, *Bioorg. Med. Chem. Lett.* **2009**, *19*, 4312 – 4315; f) P. Camps, X. Formosa, C. Galdeano, D. Muñoz-Torrero, L. Ramírez, E. Gómez, N. Isambert, R. Lavilla, A. Badia, M. V. Clos, M. Bartolini, F. Mancini, V. Andrisano, M. P. Arce, M. I. Rodríguez-Franco, O. Huertas, T. Dafni, F. J. Luque, *J. Med. Chem.* **2009**, *52*, 5365 – 5379.

[32] S. L. Roberds, J. Anderson, G. Basi, M. J. Bienkowski, D. G. Branstetter, K. S. Chen, S. B. Freedman, N. L. Frigon, D. Games, K. Hu, K. Johnson-Wood, K. E. Kappenman, T. T. Kawabe, I. Kola, R. Kuehn, M. Lee, W. Liu, R. Motter, N. F. Nichols, M. Power, D. W. Robertson, D. Schenk, M. Schoor, G. M. Shopp, M. E. Shuck, S. Sinha, K. A. Svensson, G. Tatsuno, H. Tintrup, J. Wijsman, S. Wright, L. McConlogue, *Hum. Mol. Genet.* **2001**, *10*, 1317 – 1324.

[33] M. Willem, A. N. Garratt, B. Novak, M. Citron, S. Kaufmann, A. Rittger, B. DeStrooper, P. Saftig, C. Birchmeier, C. Haass, *Science* **2006**, *314*, 664 – 666.

[34] L. McConlogue, M. Buttini, J. P. Anderson, E. F. Brigham, K. S. Chen, S. B. Freedman, D. Games, K. Johnson-Wood, M. Lee, M. Zeller, W. Liu, R. Motter, S. Sinha, *J. Biol. Chem.* **2007**, *282*, 26326 – 26334.
[35] R. Jakob-Roetne H. Jacobsen, *Angew. Chem.* **2009**, *121*, 3074 – 3105; *Angew. Chem. Int. Ed.* **2009**, *48*, 3030 – 3059.
[36] H. Fu, W. Li, J. Luo, N. T. K. Lee, M. Li, K. W. K. Tsim, Y. Pang, M. B. H. Youdim, Y. Han, *Biochem. Biophys. Res. Commun.* **2008**, *366*, 631 – 636.
[37] M. Rosini, V. Andrisano, M. Bartolini, C. Melchiorre, WO 2006/080043A2, **2006**.
[38] L. Piazzi, A. Cavalli, F. Colizzi, F. Belluti, M. Bartolini, F. Mancini, M. Recanatini, V. Andrisano, A. Rampa, *Bioorg. Med. Chem. Lett.* **2008**, *18*, 423 – 426.
[39] S. Hanessian, H. Yun, Y. Hou, G. Yang, M. Bayrakdarian, E. Therrien, N. Moitessier, S. Roggo, S. Veenstra, M. Tintelnot-Blomley, J. M. Rondeau, C. Ostermeier, A. Strauss, P. Ramage, P. Paganetti, U. Neumann, C. Betschart, *J. Med. Chem.* **2005**, *48*, 5175 – 5190.
[40] L. Di, E. H. Kerns, K. Fan, O. J. McConnell, G. T. Carter, *Eur. J. Med. Chem.* **2003**, *38*, 223 – 232.
[41] a) M. I. Rodríguez-Franco, M. I. Fernández-Bachiller, C. Pérez, B. Hernández-Ledesma, B. Bartolomé, *J. Med. Chem.* **2006**, *49*, 459 – 462; b) M. I. Fernández-Bachiller, C. Pérez, N. E. Campillo, J. A. Páez, G. C. González-Muñoz, P. Usán, E. García-Palomero, M. G. López, M. Villarroya, A. G. García, A. Martínez, M. I. Rodríguez-Franco, *ChemMedChem* **2009**, *4*, 828 – 841; c) J. Marco-Contelles, R. León, C. de Los Ríos, A. Samadi, M. Bartolini, V. Andrisano, O. Huertas, X. Barril, F. J. Luque, M. I. Rodríguez-Franco, B. López, M. G. López, A. G. García, M. C. Carreiras, M. Villarroya, *J. Med. Chem.* **2009**, *52*, 2724 – 2732; d) M. I. Fernández-Bachiller, C. Pérez, G. C. González-Muñoz, S. Conde, M. G. López, M. Villarroya, A. G. García, M. I. Rodríguez-Franco, *J. Med. Chem.* **2010**, *53*, 4927 – 4937.
[42] F. Aguado, A. Badía, J. E. Baños, F. Bosch, C. Bozzo, P. Camps, J. Contreras, M. Dierssen, C. Escolano, D. M. Görbig, D. Muñoz-Torrero, M. D. Pujol, M. Simón, M. T. Vázquez, N. M. Vivas, *Eur. J. Med. Chem.* **1994**, *29*, 205 – 221.
[43] M. Bartolini, C. Bertucci, M. L. Bolognesi, A. Cavalli, C. Melchiorre, V. Andrisano, *ChemBioChem* **2007**, *8*, 2152 – 2161.
[44] A. J. Ryan, N. M. Gray, P. N. Lowe, C. W. Chung, *J. Med. Chem.* **2003**, *46*, 3448 – 3451.
[45] S. T. Wlodek, J. Antosiewicz, J. A. McCammon, T. P. Straatsma, M. K. Gilson, J. M. Briggs, C. Humblet, J. L. Sussman, *Biopolymers* **1996**, *38*, 109 – 117.
[46] M. J. Frisch, G. W. Trucks, H. B. Schlegel, G. E. Scuseria, M. A. Robb, J. R. Cheeseman, J. A. Montgomery, Jr., T. Vreven, K. N. Kudin, J. C. Burant, J. M. Millam, S. S. Iyengar, J. Tomasi, V. Barone, B. Mennucci, M. Cossi, G. Scalmani, N. Rega, G. A. Petersson, H. Nakatsuji, M. Hada, M. Ehara, K. Toyota, R. Fukuda, J. Hasegawa, M. Ishida, T. Nakajima, Y. Honda, O. Kitao, H. Nakai, M. Klene, X. Li, J. E. Knox, H. P. Hratchian, J. B. Cross, V. Bakken, C. Adamo, J. Jaramillo, R. Gomperts, R. E. Stratmann, O. Yazyev, A. J. Austin, R. Cammi, C. Pomelli, J. W. Ochterski, P. Y. Ayala, K. Morokuma, G. A. Voth, P. Salvador, J. J. Dannenberg, V. G. Zakrzewski, S. Dapprich, A. D. Daniels, M. C. Strain, O. Farkas, D. K. Malick, A. D. Rabuck, K. Raghavachari, J. B. Foresman, J. V. Ortiz, Q. Cui, A. G. Baboul, S. Clifford, J. Cioslowski, B. B. Stefanov, G. Liu, A. Liashenko, P. Piskorz, I. Komaromi, R. L. Martin, D. J. Fox, T. Keith, M. A. Al-Laham, C. Y. Peng, A. Nanayakkara, M. Challacombe, P. M. W. Gill, B. Johnson, W. Chen, M. W. Wong, C. Gonzalez, J. A. Pople, *Gaussian 03*, revision B.04, Gaussian, Inc.: Pittsburgh, PA (USA), **2003**.
[47] C. I. Bayly, P. Cieplak, W. D. Cornell, P. A. Kollman, *J. Phys. Chem.* **1993**, *97*, 10269 – 10280.
[48] D. A. Case, T. A. Darden, T. E. Cheatham III, C. L. Simmerling, J. Wang, R. E. Duke, R. Luo, K. M. Merz, D. A. Pearlman, M. Crowley, R. C. Walker, W. Zhang, B. Wang, S. Hayik, A. Roitberg, G. Seabra, K. F. Wong, F. Paesani, X. Wu, S. Brozell, V. Tsui, H. Gohlke, L. Yang, C. Tan, J. Mongan, V. Hornak, G. Cui, P. Beroza, D. H. Mathews, C. Schafmeister, W. S. Ross, P. A. Kollman, AMBER version 9, University of California San Francisco, CA (USA), **2006**.
[49] W. L. Jorgensen, J. Chandrasekhar, J. D. Madura, R. W. Impey, M. L. Klein, *J. Chem. Phys.* **1983**, *79*, 926 – 935.

Received: July 30, 2010
Revised: September 1, 2010
Published online on September 21, 2010

CHEMMEDCHEM
Chemistry & Drug Discovery

Supporting Information

Novel Huprine Derivatives with Inhibitory Activity toward β-Amyloid Aggregation and Formation as Disease-Modifying Anti-Alzheimer Drug Candidates

Elisabet Viayna,[a] Tània Gómez,[a] Carles Galdeano,[a] Lorena Ramírez,[a] Míriam Ratia,[b] Albert Badia,[b] M. Victòria Clos,[b] Ester Verdaguer,[c] Félix Junyent,[c] Antoni Camins,[c] Mercè Pallàs,[c] Manuela Bartolini,[d] Francesca Mancini,[d] Vincenza Andrisano,[d] Mariana P. Arce,[e] María Isabel Rodríguez-Franco,[e] Axel Bidon-Chanal,[f] F. Javier Luque,[f] Pelayo Camps,[a] and Diego Muñoz-Torrero*[a]

cmdc_201000322_sm_miscellaneous_information.pdf

Figure 1. Time (ps) evolution of selected interactions between the inhibitor (–)-**11a** and residues in the binding site of hAChE. Distances are in Å. Average values were taken from the snapshots sampled in the last 5 ns.

His447 (C=O) --- Quinolinyl nitrogen

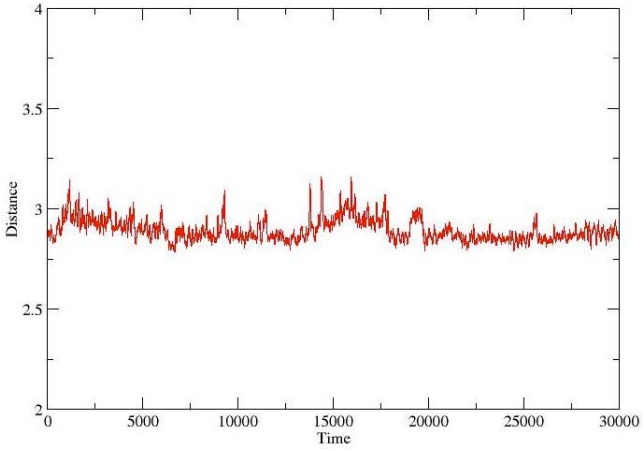

Tyr337 (OH)---Piperidinyl nitrogen

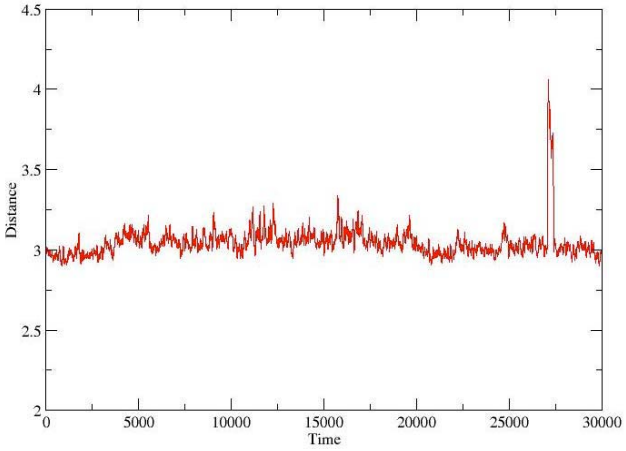

Stacking Trp286 --- Indane moiety

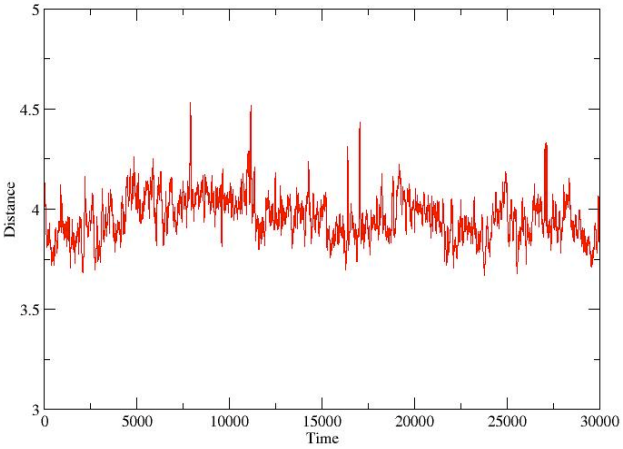

Stacking Trp86 --- (–)-Huprine moiety

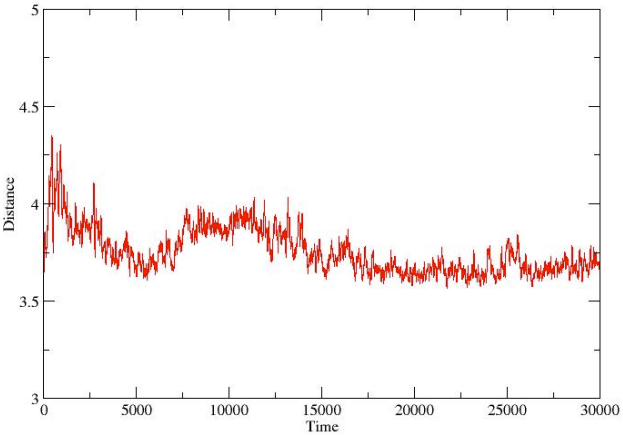

Figure 2. Time (ps) evolution of selected interactions between the inhibitor (–)-**11b** and residues in the binding site of hAChE. Distances are in Å. Average values were taken from the snapshots sampled in the last 5 ns.

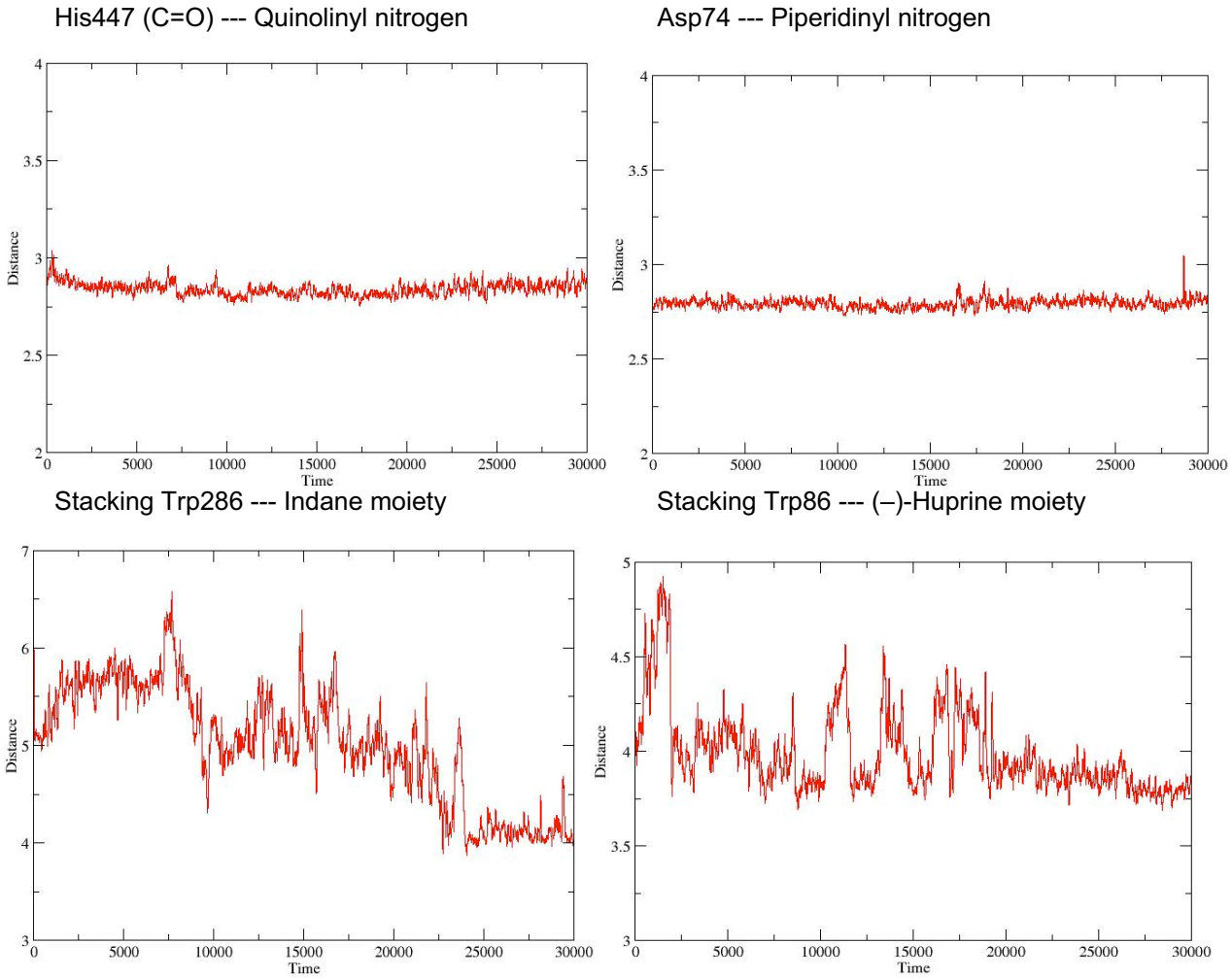

***In vitro* evaluation of the brain penetration of donepezil–huprine hybrids 11a,b and 12a,b, donepezil, huprine Y and huprine X using the PAMPA–BBB assay**

Table 1. Permeability (P_e 10^{-6} cm s^{-1})[a] in the PAMPA-BBB assay for commercial drugs (used in the experiment validation) and compounds **11a**,**b**, **12a**,**b**, donepezil, huprine Y and huprine X with their predictive penetration into the CNS.

Commercial drugs	Bibl.[b]	PBS:EtOH (80:20)	PBS:EtOH (70:30)
Testosterone	17.0	27.6 ± 1.7	42.1 ± 1.7
Verapamil	16.0	26.7 ± 0.4	30.9 ± 2.1
Imipramine	13.0	19.2 ± 0.3	24.4 ± 1.2
Desipramine	12.0	22.9 ± 0.3	27.0 ± 1.6
Progesterone	9.3	n.d.	26.0 ± 0.2
Promazine	8.8	13.2 ± 0.3	23.0 ± 1.8
Chlorpromazine	6.5	8.5 ± 0.4	14.5 ± 0.7
Clonidine	5.3	10.2 ± 0.9	18.4 ± 0.8
Corticosterone	5.1	8.8 ± 0.4	7.6 ± 0.4
Piroxicam	2.5	2.5 ± 0.3	3.1 ± 0.1
Hydrocortisone	1.9	4.9 ± 0.2	4.9 ± 0.2
Caffeine	1.3	4.7 ± 0.3	4.8 ± 0.3
Lomefloxacin	1.1	4.3 ± 0.2	2.7 ± 0.1
Enoxacin	0.9	4.7 ± 0.4	4.1 ± 0.2
Ofloxacin	0.8	3.1 ± 0.1	2.6 ± 0.03

Compd.	PBS:EtOH (80:20)	PBS:EtOH (70:30)	Prediction
(±)-**11a**	n.d.[c]	15.2 ± 0.1	CNS+
(±)-**11b**	n.d.[c]	11.4 ± 0.2	CNS+
(±)-**12a**	n.d.[c]	21.3 ± 0.4	CNS+
(±)-**12b**	17.1 ± 0.4	n.d.	CNS+
Donepezil	25.2 ± 0.2	n.d.	CNS+
(±)-Huprine Y	18.2 ± 0.1	n.d.	CNS+
(±)-Huprine X	17.8 ± 0.1	n.d.	CNS+

[a] Data are the mean ± standard deviation of three independent experiments. [b] Taken from ref. [40]. [c] Compounds evaluated in PBS:EtOH (70:30) because of their poor solubility in PBS:EtOH (80:20).

At each solvent mixture, assay validation was made by comparing the experimental permeability with the reported values of the commercial drugs that gave a good lineal correlation (Figure 3).

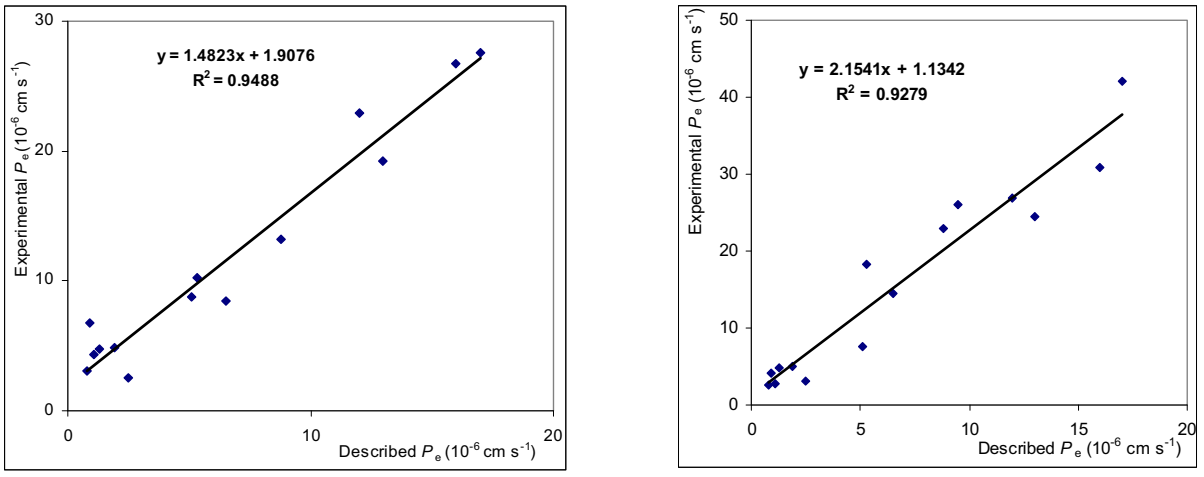

(a) (b)

Figure 3. Lineal correlation between experimental and reported permeability of commercial drugs using the PAMPA-BBB assay. (a) PBS:EtOH (80:20). (b) PBS:EtOH (70:30).

From these straight-line equations and taking into account the limits established by Di et al. for BBB permeation,[41] we established the ranges of permeability for these assays as shown in Table 2.

Table 2. Ranges of permeability of PAMPA-BBB assays (P_e, 10^{-6} cm s^{-1}).

	PBS:EtOH (80:20)	PBS:EtOH (70:30)
Compounds of high BBB permeation (CNS+)	$P_e > 7.8$	$P_e > 9.7$
Compounds of uncertain BBB permeation (CNS+/–)	$7.8 > P_e > 4.9$	$9.7 > P_e > 5.4$
Compounds of low BBB permeation (CNS–)	$P_e < 4.9$	$P_e < 5.4$

Capítol 6: ***Síntesi i modelatge molecular d'híbrids huprina–tacrina com a compostos anti-amiloidogènics amb potencial interès enfront la malaltia d'Alzheimer i les malalties priòniques.***

(J. Med. Chem. **2012**, *55,* 661–669).

6.1 Antecedents dels híbrids huprina–tacrina

De cara a incrementar encara més l'afinitat i la potència inhibitòria enfront l'AChE de les huprines i per tal d'inhibir l'agregació del pèptid βA, a la Tesi Doctoral del Dr. Xavier Formosa[113] es va decidir complementar el *binding estès* de les huprines en el lloc actiu de l'AChE amb la interacció simultània amb el lloc perifèric. Així es va combinar en una mateixa estructura una unitat d'huprina Y, **15**, amb una de tacrina, **1**, o de 6-clorotacina, **43**, a través de *linkers* de diferent longitud, amb l'objectiu que la subunitat d'huprina Y interaccionés amb el centre actiu de l'enzim i que la subunitat de tacrina, **1**, o 6-clorotacrina, **43**, interaccionés amb el lloc perifèric.

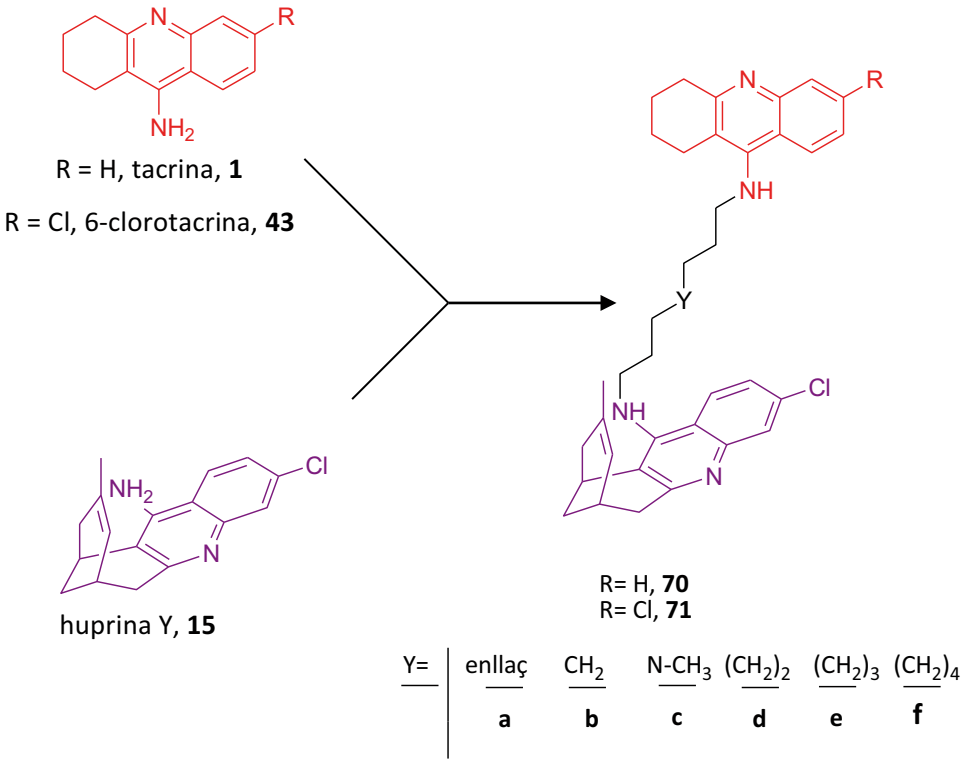

Figura 6.1 Disseny dels híbrids huprina–tacrina descrits en la Tesi Doctoral del Dr. Xavier Formosa.

Tots els nous híbrids sintetitzats van resultar clarament més actius com a inhibidors de l'hAChE que la tacrina i la (−)-huperzina A, i similars a la *rac*-huprina Y, exhibint tots ells valors nanomolars o subnanomolars d'IC_{50}.[142] El patró de substitució en la unitat de tacrina semblava tenir poca influència en l'activitat inhibidora de l'hAChE la qual cosa semblava indicativa de que aquesta interacciona al lloc perifèric, mentre que la longitud de cadena del *linker* per a

[113]Xavier Formosa, *Tesi Doctoral*, Universitat de Barcelona, **2006**. [142]Camps, P.; Formosa, X.; Muñoz-Torrero, D.; Petrignet, J.; Badia, A.; Clos, M.V. *J. Med. Chem.* **2005**, *48*, 1701.

una activitat òptima era l'equivalent a 7 o 8 metilens. La presència d'un grup amino protonable (**70c** i **71c**) en el *linker va* comportar un modest augment en l'activitat inhibidora de l'hAChE. A més, tots ells van resultar ser potents inhibidors de la hBChE, presentant valors d'IC_{50} en el rang nanomolar baix, sent més potents que la tacrina, la (−)-huperzina A i la (±)-huprina.

Recents estudis han posat de manifest un efecte antiagregant del pèptid βA molt significatiu d'aquests híbrids (23**–**67% en el cas de l'efecte antiagregant induït per AChE a 100 μM de l'inhibidor i 23**–**47% en el cas de l'agregació espontània a 10 μM). Aquests nous híbrids també s'han assajat enfront BACE-1, presentant els compostos més potents valors d'IC_{50} en el rang micromolar baix.

A més, s'ha pogut determinar una activitat inhibitòria sobre l'agregació d'un pèptid priònic que sembla estar relacionada amb la modulació de l'AChE. La proteïna priònica, al igual que el pèptid βA, tendeix a formar agregats d'amiloide rics en làmines β. Recentment, els Profs. Clos i Salmona han descobert que l'enzim AChE accelera l'agregació de dos pèptids priònics ($PrP_{106-126}$ i PrP_{82-146}) de forma depenent de la concentració, amb un perfil de dependència molt similar al descrit pel Prof. Inestrosa per a l'efecte proagregant de l'AChE sobre el βA.[143,144] S'ha observat que l'efecte proagregant de l'AChE sobre el $PrP_{106-126}$ pot ser bloquejat per inhibidors de lloc perifèric com el propidi (87% d'inhibició a 100 μM), però no per inhibidors de lloc actiu com la tacrina o la (–)-huperzina A (16% i 15% d'inhibició, respectivament).[143] La inhibició de l'agregació del $PrP_{106-126}$ per l'inhibidor de lloc perifèric propidi, va fer pensar que els inhibidors d'AChE de lloc d'unió dual, que també bloquejen el lloc perifèric, també podrien inhibir l'agregació del $PrP_{106-126}$ induïda per AChE. Efectivament, els híbrids huprina**–**tacrina **70d** i **71d** inhibeixen aquesta agregació en un percentatge idèntic a l'observat amb el propidi, presentant per aquesta activitat antiagregant valors d'IC_{50} en el rang nanomolar (69 i 263 nM, respectivament).

[143]Pera, M.; Román, S.; Ratia, M.; Camps, P.; Muñoz-Torrero, D.; Colombo, L.; Manzoni, C; Salmona, M.; Badia, A.; Clos, M.V. *Biochem. Biophys. Res. Commun.* **2006**, *346*, 89. [144]Pera, M.; Martínez-Otero, A.; Colombo, L.; Salmona, M.; Ruiz-Molina, D.; Badia, A.; Clos, M.V. *Mol. Cell. Neurosci.* **2009**, *40*, 217.

6.1.1 Antecedents de la síntesi d'híbrids huprina–tacrina en forma enantiopura

Tenint en compte que aquests híbrids contenen una unitat d'huprina, i donat que les huprines presenten una gran diferència d'activitat inhibitòria de l'AChE entre els dos enantiòmers, en la Tesi Doctoral de Xavier Formosa es va plantejar l'obtenció en forma enantiopura dels híbrids amb cadena heptametilènica (7*S*,11*S*)-**70b**, (7*R*,11*R*)-**70b**, (7*S*,11*S*)-**71b** i (7*R*,11*R*)-**71b** amb l'objectiu d'avaluar la seva activitat farmacològica, i determinar si existien difèrencies d'activitat entre els enantiòmers, per completar així les relacions estructura−activitat d'aquesta nova família estructural.

Així, en un primer moment es va pensar en l'obtenció del híbrids enantiopurs mitjançant resolució cromatogràfica dels corresponents compostos racèmics mitjançant una metodologia descrita en el nostre grup de recerca, i usada en la separació de les huprines.[103,105,135,145] Diversos intents de resolució cromatogràfica de (±)-**71b** a escala preparativa amb un MPLC equipat amb una columna de triacetat de cel·lulosa microcristal·lí sota diferents condicions cromatogràfiques van resultar infructuosos analitzant les fraccions amb un HPLC equipat amb una columnna *Chiralcel® OD-H* que contenia *tris*(3,5-dimetilfenilcarbamat) de cel·lulosa com a fase estacionària quiral.[113]

El fet que els enantiòmers de (±)-**70b** i (±)-**71b** s'haguessin pogut separar per HPLC a escala analítica usant *tris*(3,5-dimetilfenilcarbamat) de cel·lulosa com a fase estacionària quiral, ens va suggerir que l'ús d'una columna de similars característiques a escala preparativa ens podria proporcionar de forma satisfactòria els compostos enantiopurs. Amb aquest propòsit es va contactar amb el grup de la Dr. Cristina Minguillón (Universitat de Barcelona), que usant una columna preparativa que contenia *tris*(3,5-dimetilfenilcarbamat) d'amilosa (*Chiralpak® IA*) com a fase estacionària quiral va aconseguir separar els enantiomers de (±)-**71b**. No obstant, aquests enantiòmers es van obtenir en quantitats molt reduïdes (4 i 5 mg), cosa que feia molt difícil la seva caracterització química i l'avaluació farmacològica dels mateixos. Això va fer pensar en obtenir els híbrids (7*S*,11*S*)-**70b**, (7*R*,11*R*)-**70b**, (7*S*,11*S*)-**71b** i (7*R*,11*R*)-**71b** mitjançant una síntesi asimètrica a partir de les corresponents huprines enantiopures.

---

[103]Camps, P.; El Achab, R.; Morral, J.; Muñoz-Torrero, D.; Badia, A.; Baños, J.E.; Vivas, N.M.; Barril, X.; Orozco, M.; Luque, F.J. *J. Med. Chem.* **2000**, *43*, 4657. [105]Camps, P.; Cusack, B.; Mallender, W.D.; El Achab, R.; Morral, J.; Muñoz-Torrero, D.; Rosenberry, T.L. *Mol. Pharmacol.* **2000**, *57*, 409. [113]Xavier Formosa, *Tesi Doctoral*, Universitat de Barcelona, 2006. [135]Camps, P.; El Achab, R.; Görbig, D.M.; Morral, J.; Muñoz-Torrero, D.; Badia, A.; Baños, J.E.; Vivas, N.M.; Barril, X.; Orozco, M.; Luque F.J. *J. Med. Chem.* **1999**, *42,* 3227. [145]Camps, P.; Contreras, J.; Font-Bardia, M.; Morral, J.; Muñoz-Torrero, D.; Solans, X. *Tetrahedron: Asymmetry* **1998**, *9*, 3227.

6.2 Síntesi dels híbrids huprina–tacrina enantiopurs

6.2.1 Preparació de la (±)-huprina Y, (±)-15

En el moment d'iniciar aquesta Tesi Doctoral, al nostre grup no hi havia una quantitat important d'huprina Y en forma racèmica, ni tampoc de cap dels enantiòmers. Per aquest motiu, el primer objectiu que es va plantejar a la present Tesi Doctoral va ser la síntesi d'huprina Y racèmica i la posterior separació dels seus enantiòmers.

La preparació de la (±)-huprina Y, com a molècula precursora dels nous híbrids tacrina–huprina, es va dur a terme a través de la metodologia desenvolupada al grup de recerca ja fa anys[101,103,105] introduint-ne petites modificacions, especialment a nivell de purificació, que simplifiquessin el procés. La preparació de la (±)-huprina Y, (±)-**15**, implicava la síntesi de l'enona intermèdia (±)-**79** (Esquema 6.1).

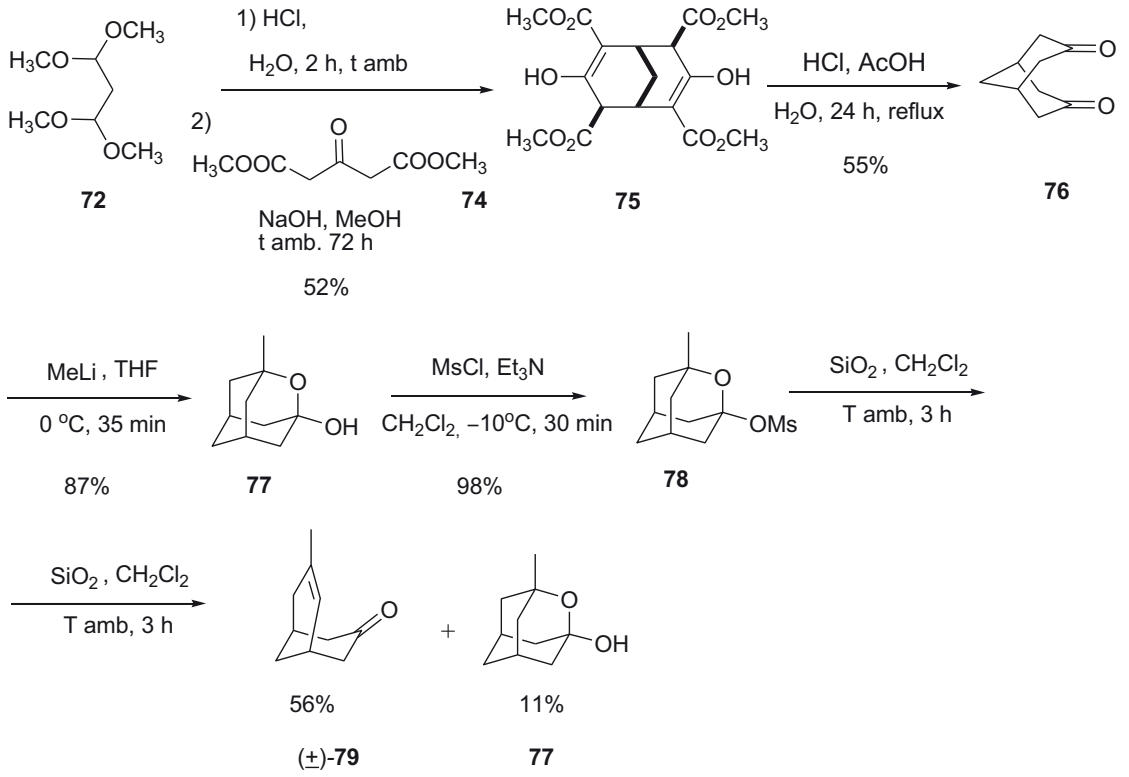

Esquema 6.1

La reacció de malondialdehid, **73**, obtingut *in situ* per hidròlisi àcida de l'1,1,3,3-tetrametoxipropà, **72**, amb 2 equivalents d'acetondicarboxilat de dimetil, **74**, en presència de

[101]Badia, A.; Baños, J.E.; Camps, P.; Contreras, J.; Görbig, D.M.; Muñoz-Torrero, D.; Simon, M.; Vivas, N.M. *Bioorg. Med. Chem.* **1998**, *6*, 427. [103]Camps, P.; El Achab, R.; Morral, J.; Muñoz-Torrero, D.; Badia, A.; Baños, J.E.; Vivas, N.M.; Barril, X.; Orozco, M.; Luque, F.J. *J. Med. Chem.* **2000**, *43*, 4657. [105]Camps, P.; Cusack, B.; Mallender, W.D.; El Achab, R.; Morral, J.; Muñoz-Torrero, D.; Rosenberry, T.L. *Mol. Pharmacol.* **2000**, *57*, 409.

NaOH a temperatura ambient, va proporcionar, després de 3 dies de reacció, el tetraèster desitjat **75** amb un 52% de rendiment. La posterior hidròlisi i descarboxilació de **75** amb una mescla d'HCl i AcOH, escalfant a reflux, durant 24 h va permetre l'obtenció de la dicetona **76** amb un 55% de rendiment, la qual va ser utilitzada en la següent reacció sense cap purificació posterior.

La síntesi de l'oxadaamantanol **77** es va dur a terme per addició nucleòfila de MeLi sobre la dicetona **76**, en el si de THF a 0 ^{o}C, durant 35 min. Així es va obtenir amb un 87% de rendiment l'oxaadamantanol **77**, el qual es va usar directament en la següent reacció sense cap purificació posterior. El tractament de **77** amb clorur de metansulfonil en presència de Et_3N a −10 ^{o}C, durant 30 min va proporcionar el mesilat **78**, amb un 98% de rendiment. La posterior fragmentació de **78**, induïda per gel de sílice, seguida de purificació per cromatografia en columna a través de gel de sílice, va proporcionar l'enona (±)-**79** amb un 56% de rendiment, juntament amb una petita quantitat d'oxaadamantanol **77** (11%, Esquema 6.1).

La reacció de condensació de tipus Friedländer entre l'enona (±)-**79** i el 2-amino-4-clorobenzonitril, **42**, utilitzant $AlCl_3$ com a catalitzador àcid de Lewis, en el si de dicloroetà, escalfant a reflux durant 7 h, seguit de cristal·lització del cru de reacció d'una mescla d'AcOEt / hexà 9:1, va proporcionar (±)-**15** amb un 48% de rendiment global (Esquema 6.2). Cal destacar que la purificació final de la huprina Y resultava així molt més pràctica i econòmica, tot i que quelcom menys eficient, que per cromatografia en columna a través de gel de sílice com s'havia fet tradicionalment al grup de recerca (66% de rendiment global).

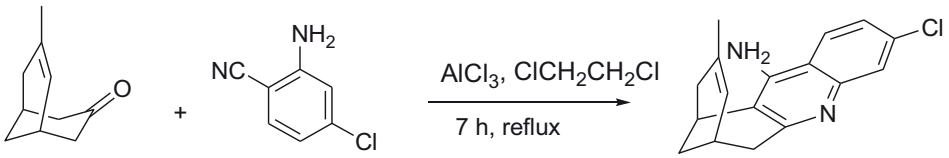

(±)-**79** **42** 48% (±)-**15**

Esquema 6.2

6.2.2 Separació dels enantiòmers d'huprina Y

La naturalesa quiral de les huprines i la interessant activitat anticolinesteràsica mostrada per la major part d'elles, va fer que fa uns anys, el nostre grup de recerca abordés la preparació dels enantiòmers d'algunes de les huprines que havien presentat major activitat biològica, amb l'objectiu de determinar si existien diferències d'activitat entre elles.

Entre les diferents metodologies assajades per a la preparació d'huprines en forma enantiopura s'incloïen (i) intents de síntesi de les enones precursores enantiopures per

fragmentacions enantioselectives de mesilats de 3-alquil-2-oxa-1-adamantil amb bases quirals, (ii) resolució cinètica d'enones racèmiques mitjançant hidroxilació asimètrica de Sharpless o epoxidació asimètrica de Jacobsen, o (iii) resolució d'huprines racèmiques mitjançant cristal·lització de sals diastereomèriques derivades d'àcids quirals enantiopurs. Únicament una metodologia basada en una síntesi asimètrica de les enones precursores, que es basava en la desprotonació enantioselectiva del monoacetal precursor derivat de la dicetona **76** i etilenglicol seguida de la reacció de l'enolat format amb *N*-feniltriflimida, i una altra metodologia basada en la resolució cromatogràfica d'huprines racèmiques van permetre assolir exitosament l'objectiu plantejat.[145]

En aquesta Tesi Doctoral es va accedir a les huprines en forma enantiopura mitjançant la resolució cromatogràfica a escala preparativa de les corresponents mescles racèmiques per MPLC utilitzant triacetat de cel·lulosa microcristal·lí com a fase estacionària quiral.

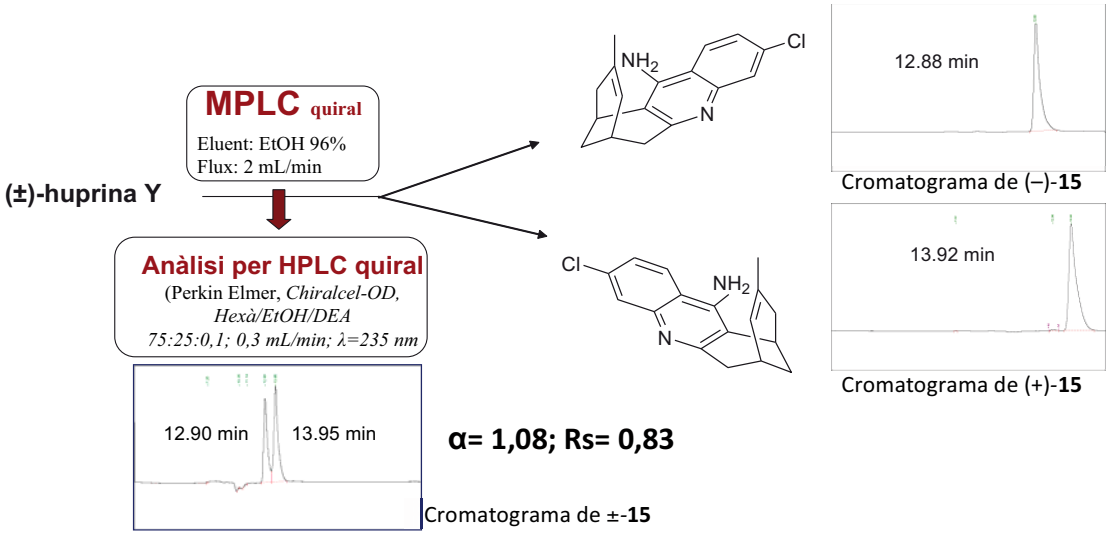

Figura 6.2 Resolució cromatogràfica de la (±)-huprina Y, (±)-**15.**

Per tal de determinar l'excés enantiomèric de les fraccions obtingudes per MPLC quiral es va posar a punt un nou mètode analític amb l'HPLC, ja que el mètode usat fins al moment requeria temps d'anàlisi superior (temps de retenció al voltant d'1 h). Així, l'anàlisi es va dur a terme amb l'ajut d'un cromatògraf líquid Perkin Elmer, proveït amb un detector de longitud d'ona (λ) variable Perkin Elmer *series 200*, i usant una columna *Chiralcel® OD* que contenia *tris*(3,5-dimetilfenilcarbamat) de cel·lulosa com a fase estacionària quiral, en lloc de la columna *Chiralcel® OD-H* que s'havia fet servir anteriorment al grup de recerca (Figura 6.2).

Les condicions que van resultar òptimes per a l'anàlisi per HPLC quiral de les fraccions

[145]Camps, P.; Contreras, J.; Font-Bardia, M.; Morral, J.; Muñoz-Torrero, D.; Solans, X. *Tetrahedron: Asymmetry* **1998**, *9*, 3227.

en el MPLC implicaven l'ús com a dissolvent d'una mescla hexà / EtOH / DEA (Et_2NH) en proporció 75:25:0,1, amb un flux de 0,3 mL/min i determinant les absorbàncies a una λ de 235 nm. Partint d'una quantitat total de 3,8 g de (±)-**15**, es va obtenir, després de successives separacions mitjançant l'ús de l'MPLC quiral, 1,4 g de (–)-**15** i 1,3 g de (+)-**15** amb un excés enantiomèric de >99% en ambdos casos.

6.2.3 Síntesi dels híbrids finals

La síntesi del nous híbrids enantiopurs desitjats (7*S*,11*S*)-**70b**, (7*R*,11*R*)-**70b**, (7*S*,11*S*)-**71b** i (7*R*,11*R*)-**71b** es va realitzar fent servir la metodologia sintètica desenvolupada a la Tesi Doctoral del Dr. Xavier Formosa per a la síntesi dels híbris huprina–tacrina racèmics**.** L'alquilació de la tacrina, **1**, o la 6-clorotacrina, **43**, amb dibromoheptà, **80**, es va realitzar en presència de KOH en el si de DMSO i tamís molecular de 4 Å a temperatura ambient durant 24 h. Així, es van obtenir els productes **81** i **82** amb un rendiment del 38% i 37%, respectivament, després de purificació dels corresponents crus de reacció per cromatogràfia en columna de gel de sílice, que va permetre la separació de subproductes de dimerització i β-eliminació. Cal recalcar que en la primera etapa de reacció cal desprotonar l'amina primària durant 2 hores amb la corresponent base. Per intentar afavorir aquesta reacció, durant la primera hora es va escalfar la mescla de reacció amb un *heat-gun.* Encara que en aquest cas no es va augmentar el rendiment, en altres alquilacions amb dibromoalcans, aquesta estrategia va ser més exitosa (Esquema 6.3).[142]

R = H, **1**R
R = Cl, **43**

R = H, **81** (38%)
R = Cl, **82** (37%)

Esquema 6.3

Finalment, els haloderivats **81** i **82** es van usar per a l'alquilació de la (±)-huprina Y, (±)-**15**, en les condicions de reacció comentades anteriorment, però amb un temps de reacció major (70 h). Així, es van preparar satisfactòriament, amb uns rendiments de baixos a moderats després de purificació per cromatografia en columna, els híbrids huprina**–**tacrina enantiopurs plantejats (Esquema 6.4). A efectes de caracterització i també per a la posterior avaluació farmacològica, els nous híbrids (7*S*,11*S*)-**70b**, (7*R*,11*R*)-**70b**, (7*S*,11*S*)-**71b** i (7*R*,11*R*)-**71b** es van

[142]Camps, P.; Formosa, X.; Muñoz-Torrero, D.; Petrignet, J.; Badia, A.; Clos, M.V. *J. Med. Chem.* **2005**, *48*, 1701.

transformar, per tractament amb un excés d'una dissolució metanòlica d'HCl, en els corresponents dihidroclorurs. Aquests compostos van ser caracteritzats a través de les seves dades espectroscòpiques, espectre de masses d'alta resolució, anàlisi elemental i HPLC quiral.

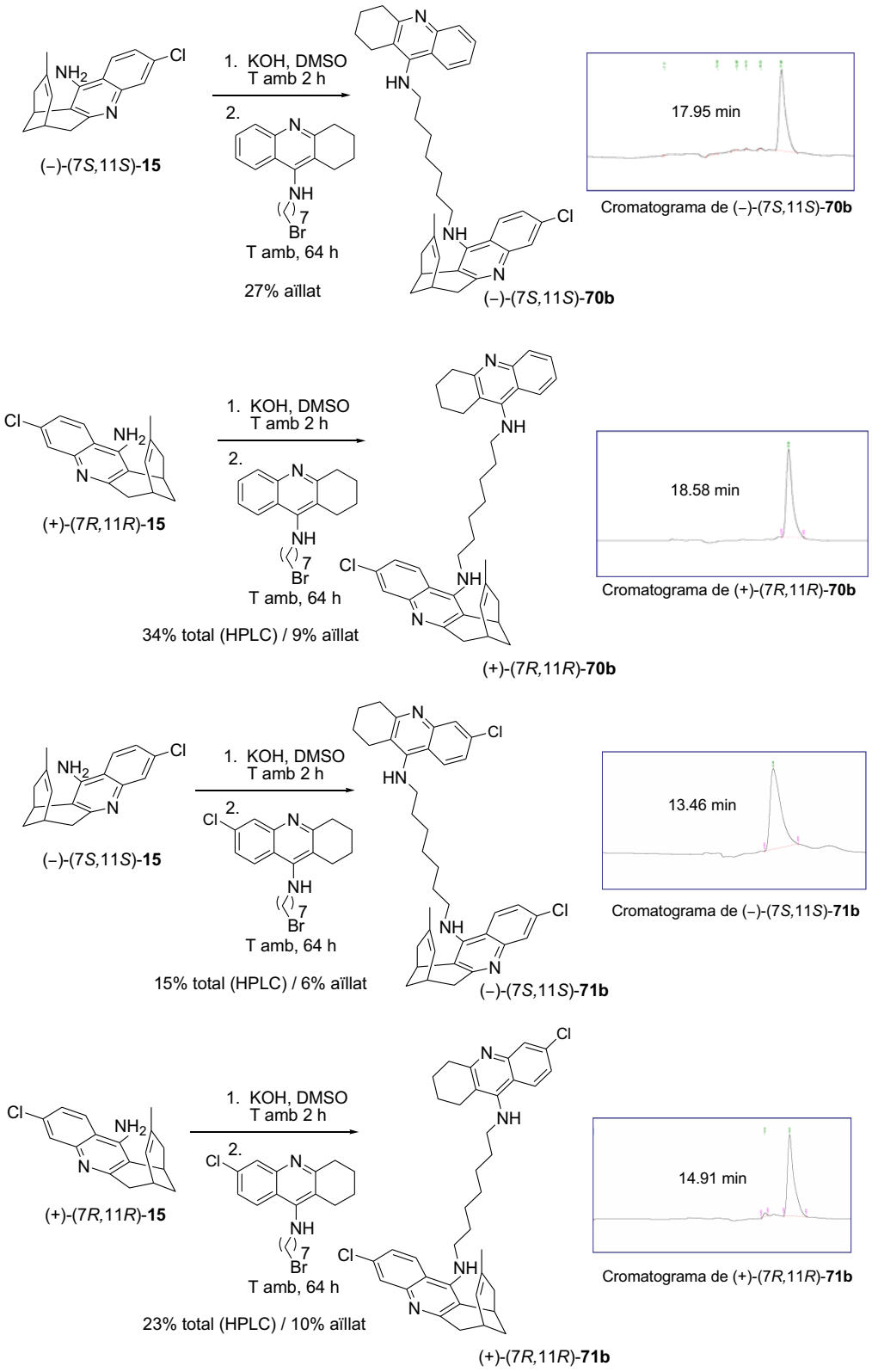

Esquema 6.4

La metodologia emprada per a l'anàlisi cromatogràfica d'aquests nous híbrids va ser la mateixaque l'emprada per a l'anàlisi de la (±)-huprina Y (hexà / EtOH / DEA en proporció 75:25:0,1, amb un flux de 0,3 mL/min i determinant les absorbàncies a una λ de 235 nm; Esquema 6.4).

6.3 Estudis de modelatge molecular. Dinàmica molecular

El mecanisme d'acció de l'híbrid huprina**–**tacrina (–)-**71b** amb l'AChE va ser estudiat mitjançant simulacions de DM (veure Annex 1). L'orientació inicial de l'inhibidor en la gorja catalítica de l'AChE va ser construïda a partir del coneixement de l'estructura de raigs X dels complexos de diferents lligands amb l'AChE, principalment, del complex entre l'AChE de *Torpedo californica* amb la *bis*(7)**–**tacrina (codi PDB: 2CKM).[79] En (–)-**71b** tant la unitat d'huprina com la unitat de 6-clorotacrina podrien interaccionar amb qualsevol dels dos lloc d'unió de l'enzim, mimetitzant la interacció de les dues unitats de tacrina de *bis*(7)-tacrina amb el Trp84 (lloc catalític; Trp86 en l'hAChE) i el Trp279 (lloc perifèric; Trp286 en l'hAChE). Tenint en compte la superior activitat de la (–)-huprina Y respecte a la de 6-clorotacrina (31 cops més potent enfront l'hAChE recombinant), la unitat d'huprina Y de (–)-**71b** va ser situada en el lloc catalític de l'enzim, mentre que la unitat de 6-clorotacrina es va situar al lloc perifèric.

Des d'un punt de vista estructural, la part de 4-aminoquinolina de la (–)-huprina X en l'estructura cristall amb *Tc*AChE (codi PDB: 1E66)[108] se superposa de forma quasi bé igual amb: (i) la tacrina en l'estructura complexada amb *Tc*AChE (codi PDB: 1ACJ);[37] i (ii) amb la unitat de tacrina de l'híbrid *bis*(7)**–**tacrina que ocupa la part catalítica de l'enzim en l'estructura de 2CKM. Aquesta distribució permet al sistema carbocíclic de la (–)-huprina X acomodar-se en un *pocket* definit pels residus Phe288, Phe290 i Phe331 (*Tc*AChE). A més, l'àtom de clor de la posició 3 se situa en una butxaca hidrofòbica delineada pel Trp432 i la Met436 (*Tc*AChE). Cal doncs esperar una situació similar en el lloc catalític per a la unitat d'huprina Y de (–)-**71b.**

Si ens centrem en el lloc perifèric de l'enzim, es podrien considerar dues orientacions diferents que es diferencien entre elles per la rotació de 180 ^{o} al voltant de l'eix N---N de l'anell central

[37]Harel, M.; Schalk, I.; Ehret-Sabatier, L.; Bouet, F.; Goeldner, M.; Hirth, C.; Axelsen, P.; Silman, I.; Sussman, J.L. *Proc. Natl. Acad. Sci. U.S.A.* **1993**, *90*, 9031. [79]Rydberg, E.H.; Brumshtein, B.; Greenblatt, H.M.; Harry, M.; Wong, D.M.; Shaya, D.; Williams, L.D.; Carlier, P.R.; Pang, Y.-P.; Silman, I.; Sussman, J.L. *J. Med. Chem.* **2006**, *49*, 5491..[108]Dvir, H.; Wong, D.M.; Harel, M.; Barril, X.; Orozco, M.; Luque, F.J.; Muñoz-Torrero, D.; Camps, P.; Rosenberry, T.L.; Silman, I.; Sussman, J.L. *Biochemistry* **2002**, *41*, 2970

de la unitat de 6-clorotacrina de (–)-**71b.** Així, tindríem un primer mode d'unió on l'àtom de clor estaria exposat directament al solvent (mode d'unió **A**) i un altre mode d'unió alternatiu on l'àtom de clor estaria orientat cap a l'interior del lloc perifèric (mode d'unió **B**). En ambdues orientacions la unitat de 6-clorotacrina podria apilar-se amb el Trp286 i la Tyr72 (Trp279 i Tyr70 en *Tc*AChE). No obstant, l'estructura *pseudo*-planar de l'unitat de 6-clorotacrina i la facilitat d'accés a la zona perifèrica fan que sigui difícil discernir *a priori* entre els dos arranjaments possibles (mode d'unió **A** i mode d'unió **B**) a la zona perifèrica.

Després de 34 ns de simulació de DM dels dos modes d'unió plantejats per a (–)-**71b** amb l'hAChE, l'orientació **A** sembla ser la més favorable, tant per l'integritat estructural com per l'estabilitat energètica després de la recol·lecció d'estructures al llarg dels 34 ns de trajectòria (Figures 6.3 i 6.4). El RMSD del *backbone* de la proteïna en l'orientació **A** està al voltant de 1,9 Å, mentre que el RMSD determinat per als residus que delimiten la gorja catalítica, incloent el lloc catalític, la part central de la gorja (*mid-gorge*) i el lloc perifèric, és lleugerament inferior (1,4 Å) (Figura 6.3). L'anell heteroaromàtic de la unitat de (–)-huprina interacciona mitjançant π-stacking amb el grup indol del Trp86 (distància mitjana 4,0 Å) i amb l'anell de fenol de la Tyr337 (Phe330 en *Tc*AChE, distància mitjana 3,8 Å). A més, aquest complex està estabilitzat per una interacció de pont d'hidrogen entre l'àtom de nitrogen quinolínic protonat i el grup carbonil de la His447 (2,9 Å). D'altra banda, la unitat de 6-clorotacrina manté les interaccions de π-stacking amb els anells aromàtics del Trp286 i la Tyr72 (distàncies mitjanes de 3,7 i 3,8 Å, respectivament), que s'observen en 2CKM.

No s'observen interaccions específiques entre el *linker* heptametilènic i els residus situats en la *mid-gorge*. És important recalcar que l'integritat estructural del *binding site* està suportada per una xarxa de ponts d'hidrogen entre diferents residus de l'hAChE, com ara el pont d'hidrogen entre Asp74 i els residus Tyr341 i Thr79, el pont d'hidrogen entre Tyr72 i Thr75, i finalment el pont mediat per una molècula d'aigua entre Tyr337 i Tyr124.

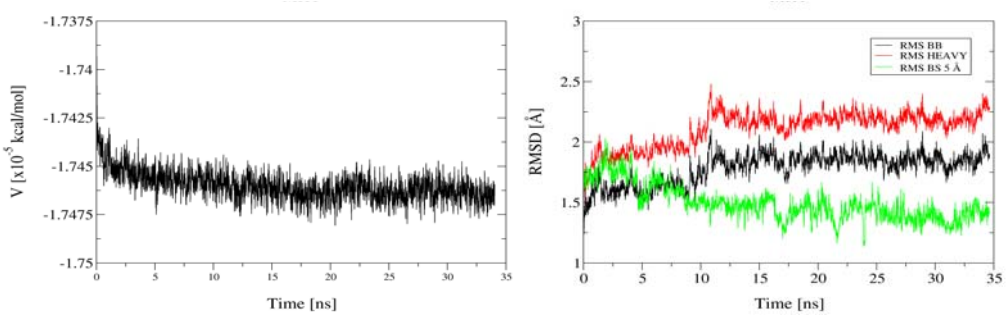

Figura 6.3 *Esquerra:* Evolució en el temps de l'energia potencial del mode d'unio **A** de (–)-**71b**. *Dreta:* RMSD determinat per als àtoms del *backbone* (BB), tots els atoms pesats de l'enzim (HEAVY) i els àtoms pesats del *binding site*, (BS; definit com qualsevol residu a $\leq$ 5 Å de qualsevol àtom del lligand) del mode d'unió **A** de (–)-**71b** .

Si es compara amb l'estructura de raigs X del complex *Tc*AChE**–***bis*(7)**–**tacrina, és important destacar la semblança entre l'esquelet de (–)-**71b** modelat i la *bis*(7)**–**tacrina en l'estructura de raigs X (Figura 6.4), com s'observa en la similar posició dels anells heteroaromàtics i de la cadena heptametilènica. En general l'anàlisi estructural dóna suport al mode d'unió **A** proposat per a (–)-**71b** amb l'hAChE.

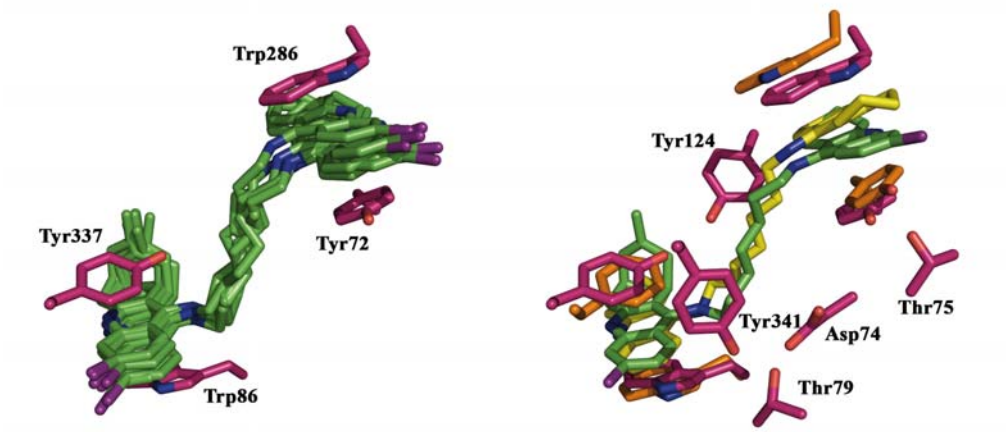

Figure 6.4 Representació del mode d'unió de (**–**)-**71b** (verd) en la gorja catalítica de l'enzim hAChE. *Esquerra*: Superposició dels *snapshots* a l'inici i al final de 34 ns de trajectòria de DM, i els *snapshots* recol·lectats cada 5 ns al llarg de la DM. *Dreta*: Superposició de la *bis*(7)**–**tacrina (groc) i (–)-**71b** en l'últim snapshot de la trajectòria. Els residus de l'últim snapshot de (–)-**71b** es mostren en magenta i els de l'estructura de raigs X de 2CKM en taronja.

Quan s'examina el mode d'unió **B**, el perfil de RMSD mostra l'existència de un reajustament estructural molt més gran en els residus que delimiten el lloc d'unió, en el qual l'estructura del lligand i dels residus claus del *binding site* estan visiblement distorsionats (Figura 6.5).

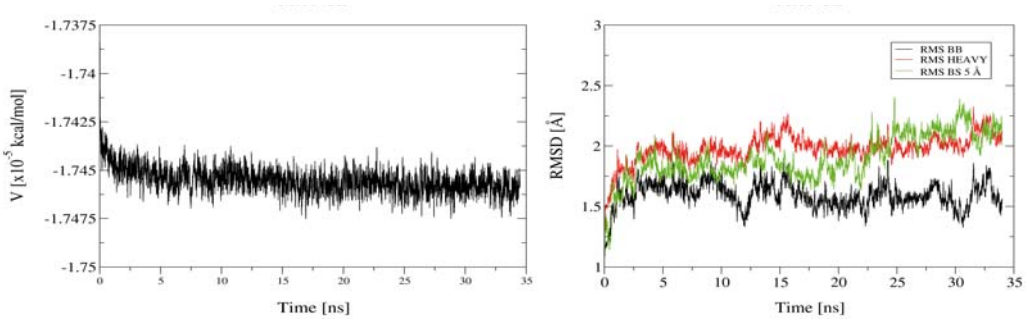

Figura 6.5 *Esquerra:* Evolució en el temps de l'energia potencial del mode d'unio **B** de (–)-**71b** . *Dreta:* RMSD determinat per als àtoms del *backbone* (BB), tots els atoms pesats de l'enzim (HEAVY) i els àtoms pesats del *binding site*, (BS; definit com qualsevol residu a $\leq$ 5 Å de qualsevol àtom del lligand) del mode d'unió **B** de (–)-**71b** .

Aquest efecte pot ser causat per interaccions no favorables entre l'àtom de clor de la unitat de 6-clorotacrina, i el grup carboxilat i carbonílic de Glu285 i Val282, respectivament, les quals

tendeixen a desplaçar la unitat de 6-clorotacrina del lloc perifèric de l'enzim. Aquest desplaçament en el lloc perifèric es propaga a la cadena d'unió heptametilènica, la qual adopta una disposició plegada, clarament diferent de l'orientació lineal de la cadena de *bis*(7)**–**tacrina o del mode d'unió **A**. Com a resultat, hi ha un xoc estèric en la zona mitja de l'enzim amb la Phe338 (Phe331 en *Tc*AChE, Figura 6.6), que canvia la seva orientació, i com a conseqüència queda afectat l'apilament de la unitat d'huprina Y amb Tyr337. L'apilament amb el Trp86 és manté fins als 20 ns de la simulació. No obstant, aquesta interacció s'altera als 22 ns i es perd de forma total als 25 ns de la DM (la distància entre els anells de la unitat d'huprina i del Trp86 s'aproxima als 6 Å; Figura 6.6).

6.3.1 *Càlculs Solvent Interaction Energies (SIE)*

Des d'un punt de vista energètic, la superior estabilitat estructural del mode d'unió **A** també s'observa en les afinitats d'unió estimades amb el mètode *Solvent Interaction Energies* (SIE), [146,147] el qual és una variant del mètode MM/PBSA, parametritzat mitjançant la relació entre la calibració de les contribucions d'energia lliure amb les afinitats d'unió experimentals per diversos complexos lligand–receptor. Els càlculs de SIE es van realitzar amb 100 snapshots recol·lectats de forma uniforme durant els últims 5 ns de les trajectòries per als modes **A** i **B**. Mentre que l'afinitat d'unió es preveu que sigui de **–**14,4 ± 0,3 kcal·mol^{-1} per al mode d'unió **A**, aquesta es desestabilitza unes 1,6 kcal·mol^{-1} ($\Delta G_{binding}$= **–**12,8 ± 0,5 kcal·mol^{-1}) per al mode d'unió **B,** reforçant així la integritat del mode d'unió **A** per al complex hAChE-(–)-**71b**.

[146]Naïm, M.; Bhat, S.; Rankin, K.N.; Dennis, S.; Chowdhury, S.F.; Siddiqi, I.; Drabik, P.; Sulea, T.; Bayly, C.I.; Jakalian, A.; Purisima, E.O. *J. Chem. Inf. Model*. **2007**, *47*, 122. [147]Cui, Q.; Sulea, T.; Schrag, J.D.; Munger, C.; Hung, M.-N.; Nam, M.; Cygler, M.; Purisima, E.O. *J. Mol. Biol.* **2008**, *379*, 787.

MODE UNIÓ B – 20 ns

MODE UNIÓ B – 34 ns

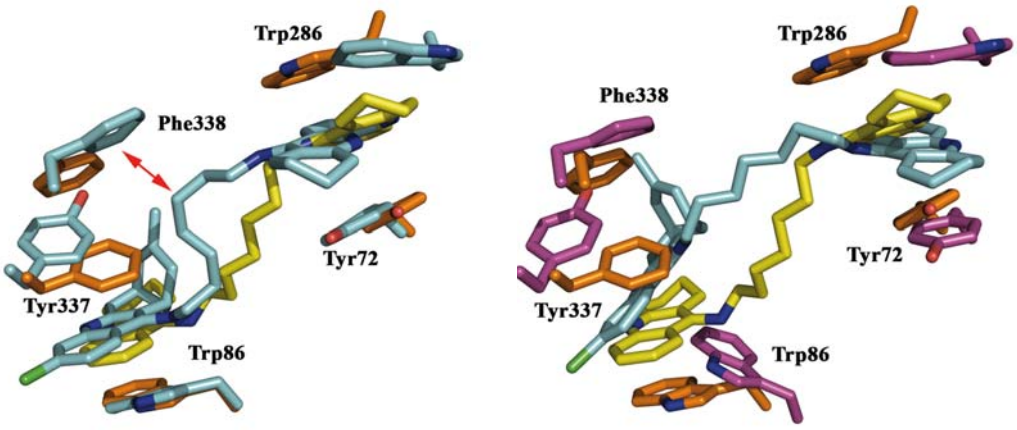

Figura 6.6 *Esquerra*: Representació del mode d'unió de (–)-**71b** en la gorja catalítica de l'AChE en l'orientació **B** als 20 ns de trajectòria (cian) i la *bis*(7)**–**tacrina (groc) en 2CKM. Els residus de l'estructura cristall de 2CKM es mostren en taronja. *Dreta:* Representació del mode d'unió de (–)-**71b** en la gorja catalítica de l'hAChE en l'orientació **B** a l'últim *snapshot* de la trajectòria (lligand en cian i residus en magenta) i la *bis*(7)**–**tacrina (groc) en 2CKM. En taronja es mostren els residus de l'estructura cristall de 2CKM.

Journal of Medicinal Chemistry

Article

pubs.acs.org/jmc

Huprine–Tacrine Heterodimers as Anti-Amyloidogenic Compounds of Potential Interest against Alzheimer's and Prion Diseases

Carles Galdeano,[†,‡] Elisabet Viayna,[†,‡] Irene Sola,[†,‡] Xavier Formosa,[†] Pelayo Camps,[†,‡] Albert Badia,[§] M. Victòria Clos,[§] Júlia Relat,[§] Míriam Ratia,[§] Manuela Bartolini,[∥] Francesca Mancini,[∥] Vincenza Andrisano,[∥] Mario Salmona,[⊥] Cristina Minguillón,[†] Gema C. González-Muñoz,[@] M. Isabel Rodríguez-Franco,[@] Axel Bidon-Chanal,[#] F. Javier Luque,[‡,#] and Diego Muñoz-Torrero*[,†,‡]

[†]Laboratori de Química Farmacèutica (Unitat Associada al CSIC), Facultat de Farmàcia, Universitat de Barcelona, Av. Diagonal 643, E-08028 Barcelona, Spain

[‡]Institut de Biomedicina (IBUB), Universitat de Barcelona, Barcelona, Spain

[§]Departament de Farmacologia, de Terapèutica i de Toxicologia, Institut de Neurociències, Universitat Autònoma de Barcelona, E-08193 Bellaterra, Barcelona, Spain

[∥]Department of Pharmaceutical Sciences, Alma Mater Studiorum, Bologna University, Via Belmeloro 6, I-40126 Bologna, Italy

[⊥]Department of Molecular Biochemistry and Pharmacology, Istituto di Ricerche Farmacologiche "Mario Negri", Milan, Italy

[@]Instituto de Química Médica (IQM-CSIC), Juan de la Cierva, 3, E-28006 Madrid, Spain

[#]Departament de Fisicoquímica, Facultat de Farmàcia, Universitat de Barcelona, Av. Diagonal 643, E-08028 Barcelona, Spain

Supporting Information

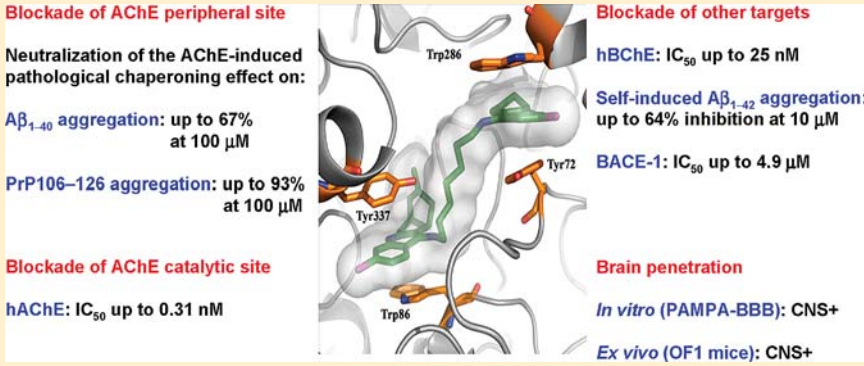

ABSTRACT: A family of huprine–tacrine heterodimers has been developed to simultaneously block the active and peripheral sites of acetylcholinesterase (AChE). Their dual site binding for AChE, supported by kinetic and molecular modeling studies, results in a highly potent inhibition of the catalytic activity of human AChE and, more importantly, in the in vitro neutralization of the pathological chaperoning effect of AChE toward the aggregation of both the β-amyloid peptide (Aβ) and a prion peptide with a key role in the aggregation of the prion protein. Huprine–tacrine heterodimers take on added value in that they display a potent in vitro inhibitory activity toward human butyrylcholinesterase, self-induced Aβ aggregation, and β-secretase. Finally, they are able to cross the blood–brain barrier, as predicted in an artificial membrane model assay and demonstrated in ex vivo experiments with OF1 mice, reaching their multiple biological targets in the central nervous system. Overall, these compounds are promising lead compounds for the treatment of Alzheimer's and prion diseases.

INTRODUCTION

Alzheimer's disease (AD) and prion diseases are fatal progressive neurodegenerative disorders with a devastating albeit very different impact on humans. Worldwide, it is estimated that 35 million people suffer dementia, most cases being due to AD,[1] whereas prion diseases affect approximately one individual in 1 million people each year.[2] Although relatively rare, the emergence of variant Creutzfeldt-Jakob disease in the human population likely due to the consumption of contaminated beef products has attracted much scientific and public interest. The devastating nature and public health concerns posed by Alzheimer's and prion diseases render the development of effective drugs against these disorders an acute clinical need.[3]

Very interestingly, despite the significant differences in incidence, as well as in clinical symptomatology and disease evolution, AD and prion diseases share common hallmarks and

Received: June 28, 2011
Published: December 19, 2011

similar pathogenic mechanisms,[4,5] among them oxidative stress, excessive transition metal ions, and prominently aggregation and accumulation in the brain of a β-sheet rich protein as fibrillar amyloid deposits, namely the β-amyloid peptide (Aβ) in AD, a 39−43-amino acid peptide arising from the proteolytic cleavage of the amyloid precursor protein (APP) by the sequential action of the enzymes β-secretase (BACE-1) and γ-secretase, and the scrapie prion protein (PrP^{Sc}), a conformationally altered isoform of the 209-amino acid normal cellular prion protein (PrP^{C}).[2,5,6] Consequently, similar therapeutic approaches against Alzheimer's and prion diseases could be envisaged, including antioxidants, β-sheet breakers, and metal chelators.[4,6,7]

Because aggregation of misfolded Aβ or PrP^{Sc} is widely accepted to be a key event in the early pathogenesis of Alzheimer's and prion diseases,[2,8] anti-AD and anti-prion drug discovery is to a large extent driven by the design of Aβ and prion protein aggregation inhibitors. Thus, Aβ aggregation inhibitors have been extensively studied in the past,[9] whereas the design of prion protein anti-aggregating compounds is becoming increasingly popular,[10] by disruption of protein−protein interactions through a direct action on the protein prone to aggregation. However, the conversion of soluble Aβ or PrP^{C} into each pathological β-sheet rich conformer and their subsequent aggregation can be promoted by the action of pathological chaperones.[3] Indeed, apolipoprotein E (apoE),[11] α1-antichymotrypsin,[11] C1q complement factor,[12] and acetylcholinesterase (AChE)[13] have been reported to accelerate Aβ aggregation in vitro. Very interestingly, a critical dependence of Aβ deposition in plaques on the presence of apoE and AChE has also been confirmed in vivo in transgenic mice models of AD.[14,15] The pathological chaperoning effect of apoE and AChE seems to be initiated by the binding to Aβ through hydrophobic interactions to form stable complexes that are prone to aggregation.[13,16,17] Inhibition of the pathological chaperoning effect of these molecules by blockade of these hydrophobic interactions has emerged as a promising approach to reducing the level of protein aggregation and modifying disease progression at a very early stage.[8] Binding of AChE to Aβ is proposed to be mediated by the AChE peripheral site,[16] located at the mouth of a 20 Å narrow gorge at the bottom of which the catalytic site is placed. Thus, compounds able to block either the AChE peripheral site or simultaneously both the catalytic and peripheral sites [dual-binding site AChE inhibitors (AChEIs)] have emerged as promising new drug candidates for mitigating the pathological chaperoning effect of AChE. The proof of concept of this approach has been obtained from a few dual-binding site AChEIs,[18−20] which have been shown to reduce brain amyloid load and improve cognition in animal models of AD. One of them, Noscira's NP-61, is currently in phase I clinical trials for AD in the United Kingdom.

It remains to be determined whether a similar approach can be used against prion diseases. A first step in this direction has been the recent discovery of a similar pathological chaperoning effect of AChE toward prion peptide aggregation. Thus, AChE has been reported to promote in vitro the aggregation of PrP106−126,[21] one of the key domains involved in the aggregation and conformational change of the prion protein, and PrP82−146, the main component of the amyloid plaques found in patients with Gerstmann-Sträussler-Scheinker disease, accelerating oligomer and amyloid fibril formation.[22] Not unlike the interaction with Aβ, the PrP pro-aggregating action of AChE seems to reside in its peripheral site, as addition of the specific peripheral site inhibitor propidium iodide results in the inhibition of AChE-induced PrP106−126 and PrP82−146 aggregation. Thus, at 100 μM, propidium iodide inhibits the AChE-induced aggregation of Aβ,[23] PrP106−126,[21] and PrP82−146[22] by 82, 87, and 78%, respectively. However, because of its DNA−RNA intercalating properties and the presence of two quaternary nitrogen atoms, which prevents its entry into the central nervous system (CNS), propidium iodide does not have any therapeutic applicability. Alternatively, dual-binding site AChEIs should also be able to inhibit the AChE-induced PrP aggregation, although no example of such a class of compounds with this activity has been reported.

Recently, we described a short series of dual-binding site AChEIs,[24] consisting of a unit of racemic huprine Y [(±)-**6** (Scheme 1)], a high-affinity reversible AChEI,[25] and a unit of tacrine [**1** (Scheme 1)], a known AChEI with reported affinity for both the active and peripheral sites of AChE,[26] or its 6-chloro-substituted analogue, 6-chlorotacrine (**2**), connected through a linker of suitable length. These racemic huprine−tacrine heterodimers exhibited a very potent inhibitory activity toward human erythrocyte AChE and human serum butyrylcholinesterase (BChE),[24] although their mechanism of action, i.e., the dual-site binding to AChE, as well as their anti-amyloidogenic effects remained to be determined.

Scheme 1. Synthesis of the Huprine−Tacrine Heterodimers

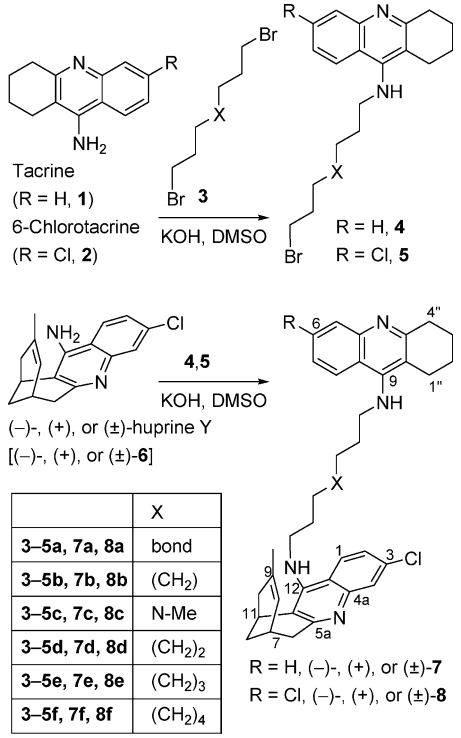

	X
3–5a, 7a, 8a	bond
3–5b, 7b, 8b	(CH_2)
3–5c, 7c, 8c	N-Me
3–5d, 7d, 8d	$(CH_2)_2$
3–5e, 7e, 8e	$(CH_2)_3$
3–5f, 7f, 8f	$(CH_2)_4$

Herein, we describe the synthesis of several enantiopure huprine−tacrine heterodimers and new longer racemic homologues, as well as a thorough pharmacological evaluation of the new heterodimers and those previously reported, including, on one hand, the determination of their inhibitory activity toward AChE-induced Aβ and PrP aggregation and toward human recombinant AChE. The mechanism of action responsible for these activities has been studied by means of molecular dynamics simulations and kinetic studies. On the

dx.doi.org/10.1021/jm200840c | J. Med. Chem. 2012, 55, 661−669

Table 1. Inhibitory Activities of the Dihydrochlorides or Trihydrochlorides of Huprine−Tacrine Heterodimers and Reference Compounds toward AChE and AChE-Induced $A\beta_{1-40}$ and PrP106−126 Aggregation, BChE, Self-Induced $A\beta_{1-42}$ Aggregation, and BACE-1[a]

compd	hAChE IC_{50} (nM)[b]	AChE-induced $A\beta_{1-40}$ aggregation[c] (%)	AChE-induced PrP106−126 aggregation[c] (%)	hBChE IC_{50} (nM)[b]	$A\beta_{1-42}$ self-induced aggregation[d] (%)	BACE-1 inhibition[e] (%)
(±)-**7a**	0.89 ± 0.07	44.4 ± 1.3	90.9 ± 2.0	24.6 ± 1.5	44.4 ± 7.0	na[f]
(±)-**7b**	1.89 ± 0.19	56.9 ± 5.1	89.1 ± 2.5	87.1 ± 4.2	51.5 ± 3.1	na[f]
(−)-**7b**	1.33 ± 0.07	66.4 ± 1.3	91.1 ± 1.3	133 ± 4.1	60.8 ± 6.4	na[f]
(+)-**7b**	6.84 ± 0.48	56.5 ± 3.0	83.5 ± 3.4	139 ± 5.2	57.0 ± 7.2	na[f]
(±)-**7c**	0.42 ± 0.04	38.8 ± 3.7	92.4 ± 0.6	44.2 ± 1.3	28.1 ± 6.4	na[f]
(±)-**7d**	1.38 ± 0.13	66.9 ± 1.3[g]	87.3 ± 2.8[h]	74.2 ± 5.7	63.7 ± 4.0	na[f]
(±)-**7e**	3.53 ± 0.37	57.8 ± 0.4	87.2 ± 2.9	43.3 ± 4.2	53.7 ± 0.9	26.5 ± 1.6
(±)-**7f**	4.19 ± 0.39	54.1 ± 0.3	93.4 ± 1.2	26.6 ± 2.5	33.3 ± 4.9	34.8 ± 2.5[i]
(±)-**8a**	0.74 ± 0.07	30.0 ± 3.7	91.9 ± 1.4	75.2 ± 2.6	30.9 ± 2.2	18.5 ± 3.5
(±)-**8b**	4.02 ± 0.27	44.2 ± 5.7	84.5 ± 3.9	73.3 ± 6.0	37.0 ± 5.7	40.9 ± 0.4
(−)-**8b**	2.04 ± 0.24	42.7 ± 1.1	79.4 ± 8.3	86.8 ± 4.2	32.2 ± 2.7	40.0 ± 2.8[j]
(+)-**8b**	11.5 ± 1.08	44.9 ± 2.2	83.1 ± 5.5	47.4 ± 4.4	45.5 ± 3.6	41.8 ± 0.7[k]
(±)-**8c**	0.31 ± 0.02	35.2 ± 2.9	87.5 ± 2.2	51.3 ± 4.6	38.6 ± 5.5	na[f]
(±)-**8d**	1.32 ± 0.09	47.2 ± 1.4	87.2 ± 2.6[l]	35.1 ± 3.8	30.3 ± 0.2	46.6 ± 3.1[m]
(±)-**8e**	3.26 ± 0.19	23.5 ± 0.4	91.7 ± 2.5	27.2 ± 2.3	36.3 ± 4.0	41.6 ± 1.0[n]
(±)-**8f**	9.09 ± 0.92	23.4 ± 2.3	90.4 ± 1.3	76.6 ± 4.9	29.3 ± 4.7	40.3 ± 0.1[o]
(±)-**6**	0.69 ± 0.03	17.1 ± 4.5	69.0 ± 1.3	175 ± 6.3	nd[p]	nd[p]
(−)-**6**	0.43 ± 0.03	24.7 ± 1.3	nd[p]	nd[p]	11.5 ± 5.2	14.0 ± 0.1
(+)-**6**	13.6 ± 1.50	9.1 ± 3.6	nd[p]	nd[p]	13.2 ± 1.9	13.6 ± 2.3
1	317 ± 15.3	5.2 ± 2.9	16.2 ± 1.7	24.5 ± 0.6	5.6 ± 1.6	na[f]

[a]Values are expressed as means ± the standard error of the mean (SEM) of at least four experiments (n = 4), each performed in duplicate (AChE and BChE inhibition), three experiments (n = 3), each performed in duplicate (AChE-induced, self-induced $A\beta$ aggregation, and BACE-1 inhibition), or three experiments (n = 3), each performed in triplicate (AChE-induced PrP106−126 aggregation inhibition). [b]IC_{50} inhibitory concentration of human recombinant AChE or human serum BChE. [c]Percent inhibition with inhibitor at 100 μM. [d]Percent inhibition with inhibitor at 10 μM (5:1 [$A\beta$]:[I]). [e]Percent inhibition with inhibitor at 5 μM, and human recombinant BACE-1 (Sigma) and substrate M-2420 (Bachem) (for huprine−tacrine heterodimers) or human recombinant BACE-1 (Invitrogen) and substrate Panvera Peptide (Invitrogen) (for reference compounds). [f]Not active. [g]IC_{50} = 61.3 ± 5.4 μM. [h]IC_{50} = 68.7 ± 1.0 nM. [i]IC_{50} = 7.3 ± 0.8 μM. [j]IC_{50} = 5.7 ± 0.5 μM. [k]IC_{50} = 5.9 ± 1.1 μM. [l]IC_{50} = 263 ± 50 nM. [m]IC_{50} = 4.9 ± 0.6 μM. [n]IC_{50} = 5.8 ± 1.2 μM. [o]IC_{50} = 6.6 ± 0.1 μM. [p]Not determined.

other hand, other anti-amyloidogenic activities such as the inhibitory activities toward $A\beta$ self-induced aggregation and BACE-1 as well as the BChE inhibitory activity have been evaluated for the whole family of huprine−tacrine heterodimers. Finally, the penetration of these compounds into the brain has been assessed using an artificial membrane assay and ex vivo experiments.

RESULTS AND DISCUSSION

Chemistry. The previously described huprine−tacrine heterodimers bear a unit of racemic huprine Y and a hexa-, hepta-, 4-methyl-4-azahepta-,[27] or octamethylene linker [(±)-**7a−d** and (±)-**8a−d** (Scheme 1)]. With regard to the interaction with the catalytic site of AChE, it is well established that the eutomer in the family of huprines is the levorotatory enantiomer, bearing the 7*S*,11*S* configuration.[25,28,29]

In this work, we have synthesized the new longer nona- and decamethylene-linked homologues in racemic form [(±)-**7e**, (±)-**7f**, (±)-**8e**, and (±)-**8f**], as well as the enantiopure (−)-(7*S*,11*S*)- and (+)-(7*R*,11*R*)-heptamethylene-linked heterodimers (−)-**7b**, (+)-**7b**, (−)-**8b**, and (+)-**8b** (Scheme 1), to determine if longer tether lengths could lead to improved blockade of the AChE peripheral site upon dual-site binding to the enzyme and to assess potential differences in potency between the enantiomers of huprine−tacrine heterodimers with respect to the different biological activities to be tested.

As previously described,[24] the synthesis of the new huprine−tacrine heterodimers was envisaged by nucleophilic substitution of α,ω-dihaloalkanes with 4-aminoquinoline derivatives tacrine or 6-chlorotacrine and huprine Y. Alternative procedures based on the high-temperature nucleophilic aromatic substitution of 4-chloroquinoline derivatives with α,ω-diaminoalkanes[30] or Pd-catalyzed amination reactions[31,32] were discarded because they required the use of a huprine-related 4-chloroquinoline precursor not readily available.[24]

Thus, alkylation of tacrine (**1**) or 6-chlorotacrine (**2**)[33] with 1,9-dibromononane or 1,10-dibromodecane in the presence of KOH in DMSO[26] afforded bromoalkyltacrines **4e,f** and **5e,f** in moderate yields (Scheme 1). Alkylation of racemic huprine Y,[34] (±)-**6**, with **4e,f** and **5e,f** under similar reaction conditions, followed by purification via silica gel column chromatography, afforded the racemic heterodimers (±)-**7e,f** and (±)-**8e,f** in moderate to good yields.

Different attempts to chromatographically resolve (±)-**8b** at preparative scale by medium-pressure liquid chromatography (MPLC) using microcrystalline cellulose triacetate as the chiral stationary phase[34] under different conditions were fruitless. Eventually, we managed to set up a novel methodology that allowed the resolution of (±)-**8b**, based on preparative high-performance liquid chromatography (HPLC) using amylose tris(3,5-dimethylphenylcarbamate) as the chiral selector in the stationary phase and a 100:0.2 acetonitrile/Et_2NH mixture as the eluent, which afforded (−)-**8b** and (+)-**8b** in >99 and 97% ee, respectively, albeit in insufficient amounts to allow their complete chemical and pharmacological characterization. Alternatively, enantiopure heterodimers (−)- and (+)-**7b** and (−)- and (+)-**8b** were prepared at a more suitable scale (decigram scale) and in good yields by chromatographic

dx.doi.org/10.1021/jm200840c | J. Med. Chem. 2012, 55, 661−669

resolution of huprine Y, (±)-**6**, by our previously described methodology,[34] followed by alkylation of the obtained enantiopure (−)- or (+)-**6** with bromoheptyltacrine **4b** or **5b**, respectively (Scheme 1).

The novel huprine−tacrine heterodimers were fully characterized as dihydrochlorides via their spectroscopic data and elemental analyses. Pharmacological evaluation of the complete family of huprine−tacrine heterodimers was conducted from their dihydrochloride or trihydrochloride salts.

Pharmacology and Molecular Modeling. *Inhibition of Human AChE and AChE-Induced Aβ and PrP Aggregation. AChE Inhibition.* Huprine−tacrine heterodimers were rationally designed to hit AChE as their primary biological target, in a dual-site binding fashion, which should endow these compounds with the ability to block the enzyme catalytic activity and, more interestingly, the pathological chaperoning effect of AChE toward both Aβ and PrP aggregation. The AChE inhibitory activity of the novel heterodimers (±)-**7e,f**, (±)-**8e,f**, (−)-**7b**, (+)-**7b**, (−)-**8b**, and (+)-**8b** was assayed by the method of Ellman et al.[35] on human recombinant AChE (hAChE) (Table 1). Also, the previously synthesized heterodimers (±)-**7a−d** and (±)-**8a−d**, which had been evaluated using human erythrocyte AChE, were re-evaluated using the more readily available human recombinant enzyme.

All the huprine−tacrine heterodimers are very potent inhibitors of human recombinant AChE, exhibiting IC_{50} values in the subnanomolar to low nanomolar range. The presence or absence of a chlorine atom at position 6 of the tacrine unit does not seem to have a clear effect on hAChE inhibitory activity, thus suggesting that the tacrine unit is binding at the AChE peripheral site, rather than the active site. Conversely, some clear trends were found regarding the length and nature of the linker of these heterodimers. On one hand, the inhibitory activity was maximal when a chain of six methylenes was present and decreased in the longer homologues, heterodimers (±)-**7a** and (±)-**8a** being 5- and 12-fold more potent than decamethylene-linked heterodimers (±)-**7f** and (±)-**8f**, respectively. A second peak of activity was found for octamethylene-linked heterodimers (±)-**7d** and (±)-**8d**, which turned out to be 3- and 7-fold more potent than (±)-**7f** and (±)-**8f**, respectively. On the other hand, replacement of the central methylene group of the tether chain of heptamethylene-linked compounds (±)-**7b** and (±)-**8b** with a protonatable methylamino group, (±)-**7c** and (±)-**8c**, respectively, resulted in 5- and 13-fold increased hAChE inhibitory potency, respectively. These results are in agreement with those reported by Savini et al. for a series of tacrine homodimers and may be ascribed to additional cation−π interactions with some midgorge aromatic residues, which would act as a third recognition site within the active site gorge of AChE, apart from the active and peripheral sites.[27] As expected, the levorotatory (7*S*,11*S*)-huprine-based heterodimers are the eutomers with regard to hAChE inhibition, compounds (−)-**7b** and (−)-**8b** being 5−6-fold more potent than the dextrorotatory enantiomers.

Overall, the most potent huprine−tacrine heterodimers are (±)-**7c** and (±)-**8c**, which turned out to be ∼2- and ∼750−1000-fold more potent than the parent (±)-huprine Y and tacrine, respectively, and (±)-**7a** and (±)-**8a**, which were roughly equipotent to (±)-huprine Y and around 400-fold more potent than tacrine.

AChE-Induced Aβ Aggregation Inhibition. The ability of the huprine−tacrine heterodimers to block the chaperoning effect of AChE toward $A\beta_{1-40}$ aggregation was assessed using a thioflavin T fluorescent method,[23] and the parent racemic and enantiopure huprines and tacrine as reference compounds (Table 1). Huprine−tacrine heterodimers, at 100 μM, exhibited a significant inhibitory activity toward hAChE-induced Aβ aggregation, with percentages of inhibition ranging from 39 to 67% in the tacrine-based heterodimers and from 23 to 47% in the chlorotacrine-based heterodimers. All heterodimers are clearly more potent Aβ anti-aggregating compounds than the parent huprine Y and tacrine. The structural features leading to a stronger Aβ anti-aggregating effect are the presence of an unsubstituted tacrine unit and an octamethylene linker, heterodimer (±)-**7d** being the most potent of the family (IC_{50} = 61.3 ± 5.4 μM.). In contrast with the trends found regarding hAChE inhibition, (i) the presence of a protonatable amino group within the linker seems to be detrimental for the AChE-induced Aβ aggregation inhibitory activity and (ii) there are no significant differences in Aβ anti-aggregating activity between enantiomeric huprine−tacrine heterodimers.

AChE-Induced PrP106−126 Aggregation Inhibition. The ability of the huprine−tacrine heterodimers to block the chaperoning effect of AChE toward PrP106−126 aggregation was assessed through fluorescence microscopy analysis using a peptide containing a coumarin fluorescent probe (coumarin PrP106−126) and bovine AChE.[21] The parent racemic and enantiopure huprines as well as tacrine were also evaluated as reference compounds (Table 1). All the huprine−tacrine heterodimers, at 100 μM, turned out to be potent inhibitors of the AChE-induced PrP106−126 aggregation with percentages of inhibition generally higher than 80%, and, therefore, without significant differences between compounds bearing an unsubstituted or chloro-substituted tacrine unit, between different tether lengths, or between enantiomers. To the best of our knowledge, this is the first report of a family of dual-binding site AChEIs able to neutralize the pathological chaperoning effect of AChE toward both Aβ and PrP aggregation.

Even though huprine−tacrine heterodimers are more potent Aβ and PrP anti-aggregating compounds than the parent tacrine and huprine Y, the latter compound exhibits a remarkable inhibitory activity (17 and 69% inhibition of AChE-induced Aβ and PrP106−126 aggregation, respectively). Indeed, huprine X, the 9-ethyl-substituted analogue of huprine Y, has recently been reported to decrease by 40% levels of insoluble $A\beta_{1-40}$ in the hippocampus of a transgenic mouse model of AD.[36] (−)-Huprine X has been shown to tightly bind to the AChE active site,[29] but kinetic studies have demonstrated that this compound also interferes with the binding of the peripheral site AChEI propidium to AChE.[25] The binding geometry and added molecular volume of huprines, when bound to the active site, could therefore account for the decreased affinity of peripheral site ligands such as propidium, which could also be the case for Aβ and PrP.

The potent and greater (relative to the parent huprine Y and tacrine) inhibitory activity of huprine−tacrine heterodimers toward hAChE and AChE-induced Aβ and PrP aggregation might be ascribed to dual-site binding to the enzyme.

Kinetic Analysis of AChE Inhibition. To gain insight into the mechanism of action of the huprine−tacrine heterodimers, responsible for AChE inhibition as well as AChE-induced Aβ and PrP aggregation, we conducted both kinetic analysis and molecular modeling studies of the interaction of selected compounds with hAChE. The mechanism of AChE inhibition

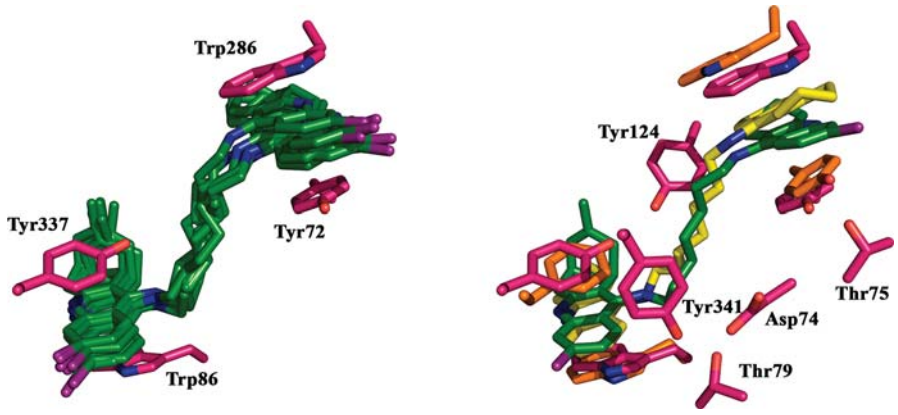

Figure 1. Representation of the mode of binding of (−)-**8b** (green) in the catalytic gorge of hAChE. The left panel shows the superposition of the snapshots at the beggining and end of the 34 ns trajectory, and of the snapshots taken every 5 ns. The right panel shows the superposition of bis(7)-tacrine (yellow) and (−)-**8b** in the final snapshot of the trajectory (magenta) and X-ray structure 2CKM (orange). The side chains of selected residues are also shown (hydrogens omitted for the sake of clarity).

was investigated in vitro using compound (−)-**8b**. Graphical analysis of the overlaid reciprocal Lineweaver−Burk plots (Figure S2 of the Supporting Information) showed both increasing slopes (decreased V_{max}) and increasing intercepts (higher K_m) at increasing inhibitor concentrations, this pattern being indicative of a mixed-type inhibition. Thus, this kinetic study supported the dual-site binding to AChE as the mechanism of action of this compound. Replots of the slope versus concentration of (−)-**8b** give an estimate of the competitive inhibition constant, K_i, of 1.51 nM.

Molecular Modeling Studies. The mechanism of action of huprine−tacrine heterodimer (−)-**8b** on AChE was further studied by molecular dynamics (MD) simulations. To this end, the orientation of the inhibitor in the catalytic gorge of AChE was modeled by taking advantage of the X-ray structural data available for distinct AChE−ligand complexes. The X-ray structure of the complex between *Torpedo californica* AChE (*Tc*AChE) and the heptamethylene-linked bis(4-aminoquinoline)-based compound bis(7)-tacrine (PDB entry 2CKM)[37] was used as template to orient (−)-**8b**. Both huprine and 6-chlorotacrine units in (−)-**8b** should be capable of interacting simultaneously at both catalytic and peripheral sites of the enzyme, thus mimicking the interaction of the two tacrine units of bis(7)-tacrine with Trp84 (catalytic site; Trp86 in hAChE) and Trp279 (peripheral site; Trp286 in hAChE). Taking into account the larger hAChE inhibitory activity of (−)-huprine Y relative to that of 6-chlorotacrine (31-fold more potent against recombinant hAChE, as the experimentally measured IC_{50} of 6-chlorotacrine is 13.2 nM), we placed the huprine Y moiety of (−)-**8b** in the catalytic site and its 6-chlorotacrine unit in the peripheral site. From a structural viewpoint, the 4-aminoquinoline unit of (−)-huprine X bound to *Tc*AChE (PDB entry 1E66)[29] superposes well with the corresponding unit of tacrine in its complex with *Tc*AChE (PDB entry 1ACJ),[38] and with the tacrine moiety of bis(7)-tacrine that fills the active site in 2CKM. This arrangement permits the carbobicyclic system of (−)-huprine X to be accommodated in a pocket defined by aromatic residues Phe288, Phe290, and Phe331, whereas the chlorine atom at position 3 fills a hydrophobic pocket delineated by Trp432 and Met436 (Figure S3 of the Supporting Information). A similar arrangement might be expected for the binding of the huprine moiety of (−)-**8b** to the catalytic site. With regard to the peripheral site interacting unit, two orientations that differ by a 180° rotation around the N−N axis of the central ring of the 6-chlorotacrine unit of (−)-**8b** were considered (Figure S3 of the Supporting Information), namely, a first binding mode in which the chlorine atom was oriented toward the aqueous solvent (denoted as binding mode **A**) and an alternative binding mode in which the chlorine atom was oriented toward the interior of the peripheral site (denoted as binding mode **B**). In both orientations, the 6-chlorotacrine moiety would stack against Trp279 and Tyr70 (Trp286 and Tyr72, respectively, in hAChE). However, the pseudoplanar structure of the 6-chlorotacrine moiety and the large accessibility of the peripheral site make it difficult to discern a priori between the two arrangements in the peripheral site.

After 34 ns MD simulations of these two alternative modes of binding of (−)-**8b** to hAChE, orientation **A** seemed to be the most favorable. The reliability of this binding mode is supported by the structural integrity and energetic stability of the snapshots collected from the trajectory (Figure 1 and Figure S4 of the Supporting Information). The root-mean-square deviation (rmsd) of the protein backbone amounts to 1.9 Å, which is slightly larger than the rmsd determined for the set of residues that delineate the binding cavity, including catalytic, midgorge, and peripheral sites (1.4 Å). The heteroaromatic ring system of the (−)-huprine moiety is firmly stacked against the indole ring of Trp86 (average distance of 4.0 Å) and the phenol ring of Tyr337 (average distance of 3.8 Å). Moreover, the stacked complex is further stabilized by the hydrogen bond between the protonated quinoline nitrogen atom and the carbonyl group of His447 (2.9 Å). On the other hand, the 6-chlorotacrine unit remains stacked against the aromatic rings of Trp286 and Tyr72 (average distances of 3.7 and 3.8 Å, respectively). Even though there are no specific interactions between the heptamethylene linker and the residues in the midgorge, it is worth noting that the structural integrity of the binding site is assisted by a network of transient hydrogen bonds between different residues, namely, hydrogen bonds between Asp74 and Tyr341 and Thr79, a hydrogen bond between Tyr72 and Thr75, and finally a water-mediated bridge between Tyr337 and Tyr124. Compared to the X-ray structure of the *Tc*AChE−bis(7)-tacrine complex, it is worth noting the global resemblance found between the skeleton of (−)-**8b** in the modeled complex and bis(7)-tacrine in the X-ray structure (Figure 1), as noted in the similar position of the heteroaromatic rings and the heptamethylene linker. Overall,

dx.doi.org/10.1021/jm200840c | *J. Med. Chem.* 2012, 55, 661−669

the structural analysis supports the stability of binding mode **A** proposed for (−)-**8b** in hAChE.

When the alternative binding mode **B** was examined, the rmsd profile revealed the occurrence of much larger structural readjustment in the residues that delineate the binding site (Figure S5 of the Supporting Information), which is clearly visible in the distorted structure of the ligand and relevant residues in the binding site (Figure S6 of the Supporting Information). This effect can be ascribed to the unfavorable interactions between the chlorine atom of the 6-chlorotacrine unit and the carboxylate and carbonyl groups of Glu285 and Val282, respectively, which tend to displace the tacrine unit from the peripheral site. Such displacement alters the arrangement of the side chain, which in turn leads to steric clashes in the midgorge and is propagated to the catalytic site (Figure S7 of the Supporting Information).

From an energetic point of view, the larger structural stability of binding mode **A** is also reflected in the binding affinities predicted using the solvent interaction energy (SIE) technique, which is a variant of the MM/PBSA method carefully parametrized by calibrating the (free) energy contributions against experimental binding affinities.[39] The SIE calculations were performed for 100 snapshots evenly taken during the last 5 ns of the trajectories. Whereas the binding affinity ($\Delta G_{binding}$) is predicted to be −14.4 ± 0.3 kcal/mol for binding mode **A**, it is destabilized by 1.6 kcal/mol ($\Delta G_{binding}$ = −12.8 ± 0.5 kcal/mol) for binding mode **B**, thus reinforcing the integrity of binding mode **A** for the AChE−(−)-**8b** complex.

BChE Inhibition. Other activities of interest in the context of AD treatment such as BChE, self-induced Aβ aggregation, and BACE-1 inhibition have been also evaluated (Table 1).

There is a growing appreciation of an important role of BChE in dementia, where this enzyme seems to exert a compensatory effect in response to a great decrease in brain AChE activity as AD progresses.[40] In this light, the inhibitory activity of the huprine−tacrine heterodimers on human serum BChE (hBChE) was assayed by the method of Ellman et al. (Table 1).[35]

(±)-Huprine Y inhibits hAChE 250-fold more potently than hBChE. The presence of the chlorine atom at position 3 of the aminoquinoline moiety of huprines, which is in part responsible for its high hAChE inhibitory activity,[29] becomes detrimental for hBChE inhibition. A steric hindrance between the chlorine atom and the side chain of Met437 in the hBChE active site seems to account for the detrimental effect of this substituent on the hBChE inhibitory activity of chloro-substituted 4-aminoquinolines relative to unsubstituted counterparts such as tacrine,[27,41] which turned out to be 13-fold more potent toward hBChE than hAChE. As huprines, huprine−tacrine heterodimers are selective inhibitors of hAChE, exhibiting inhibitory potencies 4−105-fold higher toward hAChE than toward hBChE, albeit still maintaining potent hBChE inhibitory activity, with IC_{50} values in the nanomolar range (Table 1). No clear trends were found regarding the influence of the presence or absence of a chlorine atom at the tacrine unit or the length of the linker on the hBChE inhibitory activity. The presence of a methylamino group in the linker seemed to be beneficial for this activity, compounds (±)-**7c** and (±)-**8c** being 3- and 1.5-fold more potent than (±)-**7b** and (±)-**8b**, respectively, with an equivalent tether length. The (+)-(7*R*,11*R*)-enantiomer of heterodimer **8b** is more potent than the levorotatory enantiomer, but in the case of **7b**, both enantiomers turned out to be equipotent. The most potent huprine−tacrine heterodimers as hBChE inhibitors, i.e., (±)-**7a**, (±)-**7f**, and (±)-**8e**, are 6−7-fold more potent than (±)-huprine Y and equipotent with respect to tacrine.

Aβ Self-Aggregation Inhibition. The inhibitory activity of huprine−tacrine heterodimers on Aβ self-induced aggregation was also evaluated using a thioflavin T-based fluorometric assay.[42] Huprine−tacrine heterodimers significantly inhibit the self-induced Aβ aggregation when tested at a concentration 5-fold lower than that of Aβ, exhibiting percentages of inhibition ranging from 28 to 64%, clearly higher than those found for the parent huprine Y and tacrine (Table 1). The presence of an unsubstituted tacrine unit leads to a higher potency, heterodimers **7** being ∼1.5−2-fold more potent than their 6-chlorotacrine-based counterparts **8**. In the first series, the inhibitory activity toward Aβ self-aggregation peaks at a tether length of eight methylenes whereas the presence of a methylamino group in the linker is detrimental to this activity, and no difference in potency was found for enantiomers. In the 6-chlorotacrine-based series, the length of the linker and the presence of a methylamino group in the linker had a weaker influence on this activity, but a significant difference in potency was found for both enantiomers of compound **8b**, in favor of the dextrorotatory enantiomer.

It is worth noting that the most potent huprine−tacrine heterodimers toward Aβ self-induced aggregation, i.e., compounds (±)-**7b**, (−)-**7b**, (+)-**7b**, (±)-**7d**, and (±)-**7e**, have IC_{50} values below or close to 10 μM.

As a final remark, considering the overall inhibitory activity of huprine−tacrine heterodimers on AChE-induced and self-induced Aβ aggregation, the possibility that the inhibitory activity against self-induced Aβ aggregation does not partially contribute to the inhibitory action against the AChE-induced one cannot be unequivocally excluded.

BACE-1 Inhibition. BACE-1 is involved in the first and rate-limiting step of formation of Aβ from APP. Because Aβ aggregation is partially a concentration-dependent event, reduction of brain Aβ levels by inhibition of BACE-1 might be of utmost importance for a disease-modifying anti-Alzheimer therapeutic approach.[43] Indeed, brain Aβ production, amyloid pathology, and cognitive deficits are abrogated in BACE-1 knockout mice overexpressing APP.[44] Some concerns about potential mechanism-based toxicity,[45] which might be prevented by a partial inhibition of BACE-1, have arisen. Encouragingly, heterozygous BACE-1 knockout APP transgenic mice with an only 15% reduction in the level of brain Aβ showed a dramatic reduction in brain amyloid burden at old age.[44]

The ability of the huprine−tacrine heterodimers to inhibit in vitro human recombinant BACE-1 was determined at a single concentration (5 μM) using a fluorometric assay.[46] 6-Chlorotacrine-based heterodimers were found to exhibit an important BACE-1 inhibitory activity, with percentages of inhibition ranging from 18 to 47% at 5 μM (Table 1), clearly higher than that of huprine Y and tacrine. In this series, neither the length of the linker nor the configuration of the huprine moiety in the enantiopure heterodimers had an influence on BACE-1 inhibitory activity, most of these heterodimers displaying very similar percentages of inhibition between 40 and 47%, whereas only the presence of a methylamino group in the linker was clearly detrimental for BACE-1 inhibition. Conversely, with the sole exception of the longer homologues (±)-**7e** and (±)-**7f**, heterodimers bearing an unsubstituted tacrine unit were inactive toward BACE-1.

The IC_{50} for BACE-1 inhibition was determined for most of the active heterodimers, namely, (±)-**7f**, (−)-**8b**, (+)-**8b**, and (±)-**8d**−**f**, and found to lie within the range from 5 to 7 μM (Table 1). Thus, huprine−tacrine heterodimers exhibit a BACE-1 inhibitory activity very similar to that found for the prototypic dual-binding site AChEI bis(7)-tacrine (IC_{50} = 7.5 μM)[47] and can be considered moderately potent inhibitors of BACE-1. Moreover, on the basis of the structural similarity between huprine−tacrine heterodimers and bis(7)tacrine, which was found to reduce BACE-1 intracellular activity at a concentration of 1 μM,[47] we are confident that these heterodimers can be active in more complex biological systems, being able to cross the cell membrane and therefore exerting the same activity in cell cultures.

Brain Penetration. In Vitro Blood−Brain Barrier Permeation Assay. The development of drugs intented to act in the CNS has to contend with the need to efficiently cross the BBB. Brain penetration of the huprine−tacrine heterodimers was predicted using a parallel artificial membrane permeation assay, namely the widely known PAMPA−BBB assay.[48] The in vitro permeability (P_e) of racemic huprine−tacrine heterodimers through a lipid extract of porcine brain was determined by using a 70:30 phosphate-buffered saline (PBS)/EtOH mixture. The assay was validated by comparing the experimental permeability with the reported values of 15 commercial drugs that gave a good linear correlation: $P_e(\text{exp}) = 1.99P_e(\text{lit.}) + 1.07$ ($R^2 = 0.92$) (Tables S1 and S2 and Figure S8 of the Supporting Information). From this equation and taking into account the limits established by Di et al. for BBB permeation,[48] we established that compounds with permeability values of $>9.0 \times 10^{-6}$ cm/s should cross the BBB. All the huprine−tacrine heterodimers showed permeability values above this limit, with the sole exceptions of (±)-**7e** and (±)-**8c**, for which an uncertain BBB permeation has been predicted (Tables S1 and S2 of the Supporting Information). In general, heterodimers bearing a 6-chloro-substituted tacrine unit seem to be more brain permeable than their counterparts bearing an unsubstituted tacrine unit. Also, brain permeability increases with an increase in tether length, heterodimers (±)-**7f** and (±)-**8f** being the most permeable of each series. Not unexpectedly, introduction of a protonatable methylamino group into the linker leads to a decreased permeability relative to that of the corresponding heterodimer with an oligomethylene linker of equivalent length.

These results reveal that most huprine−tacrine heterodimers could cross the BBB and reach their multiple pharmacological targets located in the CNS, which has been confirmed for huprines in in vivo[36] and ex vivo[28] studies.

Ex Vivo Brain Penetration Study. To confirm the brain permeability of the huprine−tacrine heterodimers predicted by the PAMPA−BBB assay, compounds (±)-**7d** and (±)-**8d** were subjected to an ex vivo determination of their AChE inhibitory activity using the same methodology and conditions previously set up for huprines.[28] In this assay, huprine−tacrine heterodimers were administered intraperitoneally (ip) to OF1 mice at a single dose of 10 μmol/kg 20 min before the animals were sacrificed, and the percentage of brain AChE inhibition versus untreated controls was measured. Heterodimers (±)-**7d** and (±)-**8d** were found to inhibit mouse brain AChE activity by 30.0 ± 3.3 and 28.5 ± 3.7%, respectively, relative to control nontreated animals. The parent (±)-huprine Y had been reported to inhibit brain AChE activity under these conditions by 59.2 ± 8.2%. The lower potency of (±)-**7d** and (±)-**8d** relative to that of the parent huprine Y could be ascribed, in part, to their slightly lower potency found in vitro (Table 1), but also to the fact that in this assay we used the experimental conditions that were optimized for huprines. Irrespective of the fact that perhaps a greater activity could be observed for huprine−tacrine heterodimers (±)-**7d** and (±)-**8d** under optimized conditions, their significant inhibition of brain mouse AChE after their ip administration clearly demonstrates that they are able to cross the BBB in vivo.

CONCLUSION

We have developed a family of 16 heterodimeric compounds consisting of a unit of racemic or enantiopure huprine Y linked to a unit of tacrine or 6-chlorotacrine through an oligomethylene chain of 6−10 methylene groups or a 4-methyl-4-azaheptamethylene chain. These huprine−tacrine heterodimers have been designed to simultaneously interact with both the active and peripheral sites of AChE and in some cases also with aromatic residues at the midgorge of the enzyme. The dual-site binding of these compounds to hAChE results in a highly potent inhibition of the catalytic activity of hAChE and, more importantly, in an in vitro neutralization of the pathological chaperoning effect of this enzyme toward Aβ and PrP aggregation. To the best of our knowledge, this is the first report of a structural family exhibiting this dual anti-amyloidogenic action. Because Aβ aggregation and PrP aggregation are key early pathogenic events in AD and prion diseases, the dual action of huprine−tacrine heterodimers is of great interest for a potential disease-modifying treatment of these disorders. Additionally, huprine−tacrine heterodimers have been found to display other pharmacological effects resulting from their action on biological targets other than AChE, namely, a potent inhibitory activity on BChE and a significant inhibitory activity toward self-induced Aβ aggregation and BACE-1, which should reinforce their symptomatic and disease-modifying effects, respectively, in the context of AD treatment, even though it should be noted that more balanced activities at the different targets would be desirable. Huprine−tacrine heterodimers are able to cross the BBB, as predicted by the PAMPA−BBB assay and demonstrated for two selected compounds in ex vivo experiments, thereby having access to their different biological targets in the CNS, from which a plethora of pharmacological effects result. Taken together, the data show that huprine−tacrine heterodimers can be considered very promising lead compounds for AD and prion diseases.

EXPERIMENTAL SECTION

The analytical samples of all of the huprine−tacrine heterodimers that were subjected to pharmacological evaluation possess a purity of ≥95% as evidenced by their elemental analyses. Enantiopure huprine−tacrine heterodimers possess an enantiomeric excess of >99% as evidenced by chiral HPLC. The synthetic procedure for the preparation of the huprine−tacrine heterodimers is exemplified through the synthesis of (−)-**7b**.

(−)-(7*S*,11*S*)-3-Chloro-6,7,10,11-tetrahydro-9-methyl-12-({7-[(1,2,3,4-tetrahydroacridin-9-yl)amino]heptyl}amino)-7,11-methanocycloocta[*b*]quinoline Dihydrochloride [(−)-7b·2HCl] from (−)-Huprine Y. A mixture of finely powdered KOH (85% pure reagent, 225 mg, 3.42 mmol, 1.6 equiv), (−)-huprine Y [(−)-**6**][34] (323 mg, 1.14 mmol, 1 equiv), and 4 Å molecular sieves (approximately 690 mg) in dry DMSO (4 mL) was thoroughly stirred for 1 h and heated with a heatgun every 10 min and for an additional 1 h at room temperature. The resulting mixture was added dropwise over 2 h to a

dx.doi.org/10.1021/jm200840c | J. Med. Chem. 2012, 55, 661−669

mixture of haloalkyltacrine **4b** (515 mg, 1.37 mmol, 1.2 equiv) in dry DMSO (5 mL). The reaction mixture was vigorously stirred at room temperature for 3 days, diluted with water (200 mL), treated with NaOH pellets until an alkaline pH was reached, and extracted with AcOEt (3 × 160 mL). The combined organic extracts were washed with water (3 × 150 mL), dried with anhydrous Na_2SO_4, and evaporated at reduced pressure to give a brown oily residue (549 mg), which was subjected to column chromatography (35−70 mesh silica gel, 100:0.2 CH_2Cl_2/50% aqueous NH_4OH mixture). Starting (−)-**6** (63 mg), β-elimination byproduct (25 mg), a mixture of β-elimination byproduct and heterodimer (−)-**7b** in a ratio of 1:99 (285 mg), and pure heterodimer (−)-**7b** (85 mg, 13% isolated yield, 56% total yield) were consecutively separated as yellowish oils.

A solution of (−)-**7b** (85 mg, 0.15 mmol) in CH_2Cl_2 (10 mL) was filtered through a polytetrafluoroethylene 0.45 μm filter and treated with an excess of a methanolic solution of HCl (0.65 N, 2.0 mL, 1.3 mmol), and the resulting solution was concentrated in vacuo to dryness. The solid was taken in MeOH (0.6 mL) and precipitated upon addition of AcOEt (1.6 mL). The precipitated solid was separated and dried at 65 °C and 15 Torr for 4 days to give (−)-**7b**·2HCl·2.75H_2O (75 mg) as a light brown solid: $[\alpha]^{20}_D = -139$ (c = 0.30, MeOH); >99% ee by chiral HPLC on the liberated base [CHIRALCEL OD-H column, 90:10:0.1 hexane/EtOH/Et_2NH mixture, flow rate of 0.2 mL/min, λ = 254 nm; (−)-**7b**, t_R = 55.27 min, k'_1 = 2.54; (+)-**7b**, t_R = 61.77 min, k'_2 = 2.96; α = 1.16, res. = 6.7]; mp 237−239 °C (3:8 MeOH/AcOEt); IR (KBr) ν 3600−2500 (maxima at 3405, 3234, 3049, 2927, 2855, and 2773 cm^{-1}; N^+-H, N-H, and C-H st), 1628, 1617, 1583, 1572, 1534 (ar-C-C and ar-C-N st) cm^{-1}. The ^1H and ^{13}C NMR spectra were identical to those described for (±)-**7b**·2HCl.[24] HRMS calcd for $C_{37}H_{43}{}^{35}ClN_4$ + H: 579.3249. Found: 579.3240. Anal. ($C_{37}H_{43}ClN_4$·2HCl·2.75H_2O) C, H, N, Cl.

■ ASSOCIATED CONTENT

Supporting Information

Experimental procedures (chemistry and biochemical, brain penetration, and molecular modeling studies), fluorescence micrographs of the effect of huprine−tacrine heterodimers on AChE-induced coumarin−PrP106−126 aggregation, and figures displaying additional data from kinetic, molecular dynamics, and PAMPA−BBB studies. This material is available free of charge via the Internet at http://pubs.acs.org.

■ AUTHOR INFORMATION

Corresponding Author

*Phone: +34+934024533. Fax: +34+934035941. E-mail: dmunoztorrero@ub.edu.

■ ACKNOWLEDGMENTS

Financial support from the Ministerio de Ciencia e Innovación (MICINN) and FEDER (CTQ2008-03768/PPQ, SAF2009-10553, SAF2008-05595, and SAF2006-01249), Generalitat de Catalunya (GC) (2005SGR00180, 2009SGR1396, 2009SGR0843, and 2009SGR249), EU's 7FP funding (BISNES, NMP-2007-1.1-1, GA no. 214538), and fellowships for C.G. (IBUB) and E.V. (GC) are acknowledged. We thank Isabel Delgado for technical support.

■ ABBREVIATIONS

Aβ, β-amyloid peptide; AChE, acetylcholinesterase; AChEI, acetylcholinesterase inhibitor; AD, Alzheimer's disease; apoE, apolipoprotein E; APP, amyloid precursor protein; BACE-1, β-secretase; BBB, blood−brain barrier; BChE, butyrylcholinesterase; CNS, central nervous system; hAChE, human acetylcholinesterase; hBChE, human butyrylcholinesterase; MD, molecular dynamics; PAMPA, parallel artificial membrane permeation assay; PBS, phosphate-buffered saline; PDB, Protein Data Bank; PrP^C, cellular prion protein; PrP^{Sc}, scrapie prion protein; SIE, solvent interaction energy; *Tc*AChE, *T. californica* acetylcholinesterase

■ REFERENCES

(1) Wimo, A.; Prince, M. *World Alzheimer Report 2010. The global economic impact of dementia*; Alzheimer's Disease International (http://www.alz.co.uk).

(2) Cobb, N. J.; Surewicz, W. K. Prion diseases and their biochemical mechanisms. *Biochemistry* **2009**, *48*, 2574−2585.

(3) Wisniewski, T.; Sigurdsson, E. M. Therapeutic approaches for prion and Alzheimer's disease. *FEBS J.* **2007**, *274*, 3784−3798.

(4) Barnham, K. J.; Cappai, R.; Beyreuther, K.; Masters, C. L.; Hill, A. F. Delineating common molecular mechanisms in Alzheimer's and prion diseases. *Trends Biochem. Sci.* **2006**, *31*, 465−472.

(5) Soto, C. Protein misfolding and disease; protein refolding and therapy. *FEBS Lett.* **2001**, *498*, 204−207.

(6) Soto, C.; Kascsak, R. J.; Saborío, G. P.; Aucouturier, P.; Wisniewski, T.; Prelli, F.; Kascsak, R.; Mendez, E.; Harris, D. A.; Ironside, J.; Tagliavini, F.; Carp, R. I.; Frangione, B. Reversion of prion protein conformational changes by synthetic β-sheet breaker peptides. *Lancet* **2000**, *355*, 192−197.

(7) Zhang, H.-Y. Same causes, same cures. *Biochem. Biophys. Res. Commun.* **2006**, *351*, 578−581.

(8) Bartolini, M.; Andrisano, V. Strategies for the inhibition of protein aggregation in human diseases. *ChemBioChem* **2010**, *11*, 1018−1035.

(9) Re, F.; Airoldi, C.; Zona, C.; Masserini, M.; La Ferla, B.; Quattrocchi, N.; Nicotra, F. β amyloid aggregation inhibitors: Small molecules as candidate drugs for therapy of Alzheimer's disease. *Curr. Med. Chem.* **2010**, *17*, 2990−3006.

(10) Tran, H. N. A.; Bongarzone, S.; Carloni, P.; Legname, G.; Bolognesi, M. L. Synthesis and evaluation of a library of 2,5-bisdiamino-benzoquinone derivatives as probes to modulate protein-protein interactions in prions. *Bioorg. Med. Chem. Lett.* **2010**, *20*, 1866−1868.

(11) Ma, J.; Yee, A.; Brewer, H. B. Jr.; Das, S.; Potter, H. Amyloid-associated proteins α1-antichymotrypsin and apolipoprotein E promote assembly of Alzheimer β-protein into filaments. *Nature* **1994**, *372*, 92−94.

(12) Boyett, K. W.; DiCarlo, G.; Jantzen, P. T.; Jackson, J.; O'Leary, C.; Wilcock, D.; Morgan, D.; Gordon, M. N. Increased fibrillar β-amyloid in response to human C1q injections into hippocampus and cortex of APP + PS1 transgenic mice. *Neurochem. Res.* **2003**, *28*, 83−93.

(13) Inestrosa, N. C.; Alvarez, A.; Pérez, C. A.; Moreno, R. D.; Vicente, M.; Linker, C.; Casanueva, O. I.; Soto, C.; Garrido, J. Acetylcholinesterase accelerates assembly of amyloid-β-peptides into Alzheimer's fibrils: Possible role of the peripheral site of the enzyme. *Neuron* **1996**, *16*, 881−891.

(14) Bales, K. R.; Verina, T.; Cummins, D. J.; Du, Y.; Dodel, R. C.; Saura, J.; Fishman, C. E.; DeLong, C. A.; Piccardo, P.; Petegnief, V.; Ghetti, B.; Paul, S. M. Apolipoprotein E is essential for amyloid deposition in the APPV717F transgenic mouse model of Alzheimer's disease. *Proc. Natl. Acad. Sci. U.S.A.* **1999**, *96*, 15233−15238.

(15) Rees, T. M.; Berson, A.; Sklan, E. H.; Younkin, L.; Younkin, S.; Brimijoin, S.; Soreq, H. Memory deficits correlating with acetylcholinesterase splice shift and amyloid burden in doubly transgenic mice. *Curr. Alzheimer Res.* **2005**, *2*, 291−300.

(16) De Ferrari, G. V.; Canales, M. A.; Shin, I.; Weiner, L. M.; Silman, I.; Inestrosa, N. C. A structural motif of acetylcholinesterase that promotes amyloid β-peptide fibril formation. *Biochemistry* **2001**, *40*, 10447−10457.

(17) Naslund, J.; Thyberg, J.; Tjernberg, L. O.; Wernstedt, C.; Karlstrom, A. R.; Bogdanovic, N.; Gandy, S. E.; Lannfelt, L.; Terenius, L.; Nordstedt, C. Characterization of stable complexes involving

apolipoprotein E and the amyloid β peptide in Alzheimer's disease brain. *Neuron* **1995**, *15*, 219−228.
(18) Cavalli, A.; Bolognesi, M. L.; Capsoni, S.; Andrisano, V.; Bartolini, M.; Margotti, E.; Cattaneo, A.; Recanatini, M.; Melchiorre, C. A small molecule targeting the multifactorial nature of Alzheimer's disease. *Angew. Chem., Int. Ed.* **2007**, *46*, 3689−3692.
(19) García-Palomero, E.; Muñoz, P.; Usan, P.; Garcia, P.; De Austria, C.; Valenzuela, R.; Rubio, L.; Medina, M.; Martínez, A. Potent β-amyloid modulators. *Neurodegener. Dis.* **2008**, *5*, 153−156.
(20) Spuch, C.; Antequera, D.; Fernandez-Bachiller, M. I.; Rodríguez-Franco, M. I.; Carro, E. A new tacrine-melatonin hybrid reduces amyloid burden and behavioral deficits in a mouse model of Alzheimer's disease. *Neurotoxic. Res.* **2010**, *17*, 421−431.
(21) Pera, M.; Román, S.; Ratia, M.; Camps, P.; Muñoz-Torrero, D.; Colombo, L.; Manzoni, C.; Salmona, M.; Badia, A.; Clos, M. V. Acetylcholinesterase triggers the aggregation of PrP 106−126. *Biochem. Biophys. Res. Commun.* **2006**, *346*, 89−94.
(22) Pera, M.; Martínez-Otero, A.; Colombo, L.; Salmona, M.; Ruiz-Molina, D.; Badia, A.; Clos, M. V. Acetylcholinesterase as an amyloid enhancing factor in PrP82−146 aggregation process. *Mol. Cell. Neurosci.* **2009**, *40*, 217−224.
(23) Bartolini, M.; Bertucci, C.; Cavrini, V.; Andrisano, V. β-Amyloid aggregation induced by human acetylcholinesterase: Inhibition studies. *Biochem. Pharmacol.* **2003**, *65*, 407−416.
(24) Camps, P.; Formosa, X.; Muñoz-Torrero, D.; Petrignet, J.; Badia, A.; Clos, M. V. Synthesis and pharmacological evaluation of huprine-tacrine heterodimers: Subnanomolar dual binding site acetylcholinesterase inhibitors. *J. Med. Chem.* **2005**, *48*, 1701−1704.
(25) Camps, P.; Cusack, B.; Mallender, W. D.; El Achab, R.; Morral, J.; Muñoz-Torrero, D.; Rosenberry, T. L. Huprine X is a novel high-affinity inhibitor of acetylcholinesterase that is of interest for the treatment of Alzheimer's disease. *Mol. Pharmacol.* **2000**, *57*, 409−417.
(26) Pang, Y.-P.; Quiram, P.; Jelacic, T.; Hong, F.; Brimijoin, S. Highly potent, selective, and low cost bis-tetrahydroaminacrine inhibitors of acetylcholinesterase. *J. Biol. Chem.* **1996**, *271*, 23646−23649.
(27) Savini, L.; Gaeta, A.; Fattorusso, C.; Catalanotti, B.; Campiani, G.; Chiasserini, L.; Pellerano, C.; Novellino, E.; McKissic, D.; Saxena, A. Specific targeting of acetylcholinesterase and butyrylcholinesterase recognition sites. Rational design of novel, selective, and highly potent cholinesterase inhibitors. *J. Med. Chem.* **2003**, *46*, 1−4.
(28) Camps, P.; El Achab, R.; Morral, J.; Muñoz-Torrero, D.; Badia, A.; Baños, J. E.; Vivas, N. M.; Barril, X.; Orozco, M.; Luque, F. J. New tacrine-huperzine A hybrids (huprines): Highly potent tight-binding acetylcholinesterase inhibitors of interest for the treatment of Alzheimer's disease. *J. Med. Chem.* **2000**, *43*, 4657−4666.
(29) Dvir, H.; Wong, D. M.; Harel, M.; Barril, X.; Orozco, M.; Luque, F. J.; Muñoz-Torrero, D.; Camps, P.; Rosenberry, T. L.; Silman, I.; Sussman, J. L. 3D Structure of *Torpedo californica* acetylcholinesterase complexed with huprine X at 2.1 Å resolution: Kinetic and molecular dynamics correlates. *Biochemistry* **2002**, *41*, 2970−2981.
(30) Carlier, P. R.; Chow, E. S.-H.; Han, Y.; Liu, J.; El Yazal, J.; Pang, Y.-P. Heterodimeric tacrine-based acetylcholinesterase inhibitors: Investigating ligand-peripheral site interactions. *J. Med. Chem.* **1999**, *42*, 4225−4231.
(31) Ma, M.; Mehta, J.; Williams, L. D.; Carlier, P. R. Pd-catalyzed amination as an alternative to nucleophilic aromatic substitution for the synthesis of *N*-alkyltacrines and analogs. *Tetrahedron Lett.* **2011**, *52*, 916−919.
(32) Ronco, C.; Jean, L.; Outaabout, H.; Renard, P.-Y. Palladium-catalyzed preparation of *N*-alkylated tacrine and huprine compounds. *Eur. J. Org. Chem.* **2011**, 302−310.
(33) Gregor, V. E.; Emmerling, M. R.; Lee, C.; Moore, C. J. The synthesis and *in vitro* acetylcholinesterase and butyrylcholinesterase inhibitory activity of tacrine (Cognex®) derivatives. *Bioorg. Med. Chem. Lett.* **1992**, *2*, 861−864.
(34) Camps, P.; Contreras, J.; Font-Bardia, M.; Morral, J.; Muñoz-Torrero, D.; Solans, X. Enantioselective synthesis of tacrine-huperzine A hybrids. Preparative chiral MPLC separation of their racemic mixtures and absolute configuration assignments by X-ray diffraction analysis. *Tetrahedron: Asymmetry* **1998**, *9*, 835−849.
(35) Ellman, G. L.; Courtney, K. D.; Andres, V. Jr.; Featherstone, R. M. A new and rapid colorimetric determination of acetylcholinesterase activity. *Biochem. Pharmacol.* **1961**, *7*, 88−95.
(36) Hedberg, M. M.; Clos, M. V.; Ratia, M.; Gonzalez, D.; Unger Lithner, C.; Camps, P.; Muñoz-Torrero, D.; Badia, A.; Giménez-Llort, L.; Nordberg, A. Effect of huprine X on β-amyloid, synaptophysin and α7 neuronal nicotinic acetylcholine receptors in the brain of 3xTg-AD and APPswe transgenic mice. *Neurodegener. Dis.* **2010**, *7*, 379−388.
(37) Rydberg, E. H.; Brumshtein, B.; Greenblatt, H. M.; Wong, D. M.; Shaya, D.; Williams, L. D.; Carlier, P. R.; Pang, Y.-P.; Silman, I.; Sussman, J. L. Complexes of alkylene-linked tacrine dimers with *Torpedo californica* acetylcholinesterase: Binding of bis(5)-tacrine produces a dramatic rearrangement in the active site gorge. *J. Med. Chem.* **2006**, *49*, 5491−5500.
(38) Harel, M.; Schalk, I.; Ehret-Sabatier, L.; Bouet, F.; Goeldner, M.; Hirth, C.; Axelsen, P. H.; Silman, I.; Sussman, J. L. Quaternary ligand binding to aromatic residues in the active-site gorge of acetylcholinesterase. *Proc. Natl. Acad. Sci. U.S.A.* **1993**, *90*, 9031−9035.
(39) Cui, Q.; Sulea, T.; Schrag, J. D.; Munger, C.; Hung, M.-N.; Nam, M.; Cygler, M.; Purisima, E. O. Molecular dynamics-solvated interaction energy studies of protein-protein interactions: The MP1-p14 scaffolding complex. *J. Mol. Biol.* **2008**, *379*, 787−802.
(40) Lane, R. M.; Potkin, S. G.; Enz, A. Targeting acetylcholinesterase and butyrylcholinesterase in dementia. *Int. J. Neuropsychopharmacol.* **2006**, *9*, 101−124.
(41) Elsinghorst, P. W.; Cieslik, J. S.; Mohr, K.; Tränkle, C.; Gütschow, M. First gallamine-tacrine hybrid: Design and characterization at cholinesterases and the M_2 muscarinic receptor. *J. Med. Chem.* **2007**, *50*, 5685−5695.
(42) Bartolini, M.; Bertucci, C.; Bolognesi, M. L.; Cavalli, A.; Melchiorre, C.; Andrisano, V. Insight into the kinetic of amyloid β(1−42) peptide self-aggregation: Elucidation of inhibitors' mechanism of action. *ChemBioChem* **2007**, *8*, 2152−2161.
(43) De Strooper, B.; Vassar, R.; Golde, T. The secretases: Enzymes with therapeutic potential in Alzheimer's disease. *Nat. Rev. Neurol.* **2010**, *6*, 99−107.
(44) McConlogue, L.; Buttini, M.; Anderson, J. P.; Brigham, E. F.; Chen, K. S.; Freedman, S. B.; Games, D.; Johnson-Wood, K.; Lee, M.; Zeller, M.; Liu, W.; Motter, R.; Sinha, S. Partial reduction of BACE1 has dramatic effects on Alzheimer plaque and synaptic pathology in APP transgenic mice. *J. Biol. Chem.* **2007**, *282*, 26326−26334.
(45) Hu, X.; Hicks, C. W.; He, W.; Wong, P.; Macklin, W. B.; Trapp, B. D.; Yan, R. BACE1 modulates myelination in the central and peripheral nervous system. *Nat. Neurosci.* **2006**, *9*, 1520−1525.
(46) Hanessian, S.; Yun, H.; Hou, Y.; Yang, G.; Bayrakdarian, M.; Therrien, E.; Moitessier, N.; Roggo, S.; Veenstra, S.; Tintelnot-Blomley, M.; Rondeau, J.-M.; Ostermeier, C.; Strauss, A.; Ramage, P.; Paganetti, P.; Neumann, U.; Betschart, C. Structure-based design, synthesis, and memapsin 2 (BACE) inhibitory activity of carbocyclic and heterocyclic peptidomimetics. *J. Med. Chem.* **2005**, *48*, 5175−5190.
(47) Fu, H.; Li, W.; Luo, J.; Lee, N. T. K.; Li, M.; Tsim, K. W. K.; Pang, Y.; Youdim, M. B. H.; Han, Y. Promising anti-Alzheimer's dimer bis(7)-tacrine reduces β-amyloid generation by directly inhibiting BACE-1 activity. *Biochem. Biophys. Res. Commun.* **2008**, *366*, 631−636.
(48) Di, L.; Kerns, E. H.; Fan, K.; McConnell, O. J.; Carter, G. T. High throughput artificial membrane permeability assay for blood-brain barrier. *Eur. J. Med. Chem.* **2003**, *38*, 223−232.

Supporting Information for

Huprine–Tacrine Heterodimers as Anti-Amyloidogenic Compounds of Potential Interest Against Alzheimer's and Prion Diseases

Carles Galdeano,[†,‡] Elisabet Viayna,[†,‡] Irene Sola,[†,‡] Xavier Formosa,[†] Pelayo Camps,[†,‡] Albert Badia,[§] M. Victòria Clos,[§] Júlia Relat,[§] Míriam Ratia,[§] Manuela Bartolini,[#] Francesca Mancini,[#] Vincenza Andrisano,[#] Mario Salmona,[⊥] Cristina Minguillón,[†] Gema C. González-Muñoz,[◊] M. Isabel Rodríguez-Franco,[◊] Axel Bidon-Chanal,[//] F. Javier Luque,[//,‡] and Diego Muñoz-Torrero[*,†,‡]*

[†] Laboratori de Química Farmacèutica (Unitat Associada al CSIC), Facultat de Farmàcia, Universitat de Barcelona, Av. Diagonal 643, E-08028, Barcelona, Spain; [‡] Institut de Biomedicina (IBUB), Universitat de Barcelona, Barcelona, Spain; [§] Departament de Farmacologia, de Terapèutica i de Toxicologia, Institut de Neurociències, Universitat Autònoma de Barcelona, E-08193, Bellaterra, Barcelona, Spain; [#] Department of Pharmaceutical Sciences, Alma Mater Studiorum, Bologna University, Via Belmeloro 6, I-40126, Bologna, Italy; [⊥] Department of Molecular Biochemistry and Pharmacology, Istituto di Ricerche Farmacologiche "Mario Negri", Milan, Italy; [◊] Instituto de Química Médica (IQM-CSIC), Juan de la Cierva, 3, E-28006, Madrid, Spain; [//] Departament de Fisicoquímica, Facultat de Farmàcia, Universitat de Barcelona, Av. Diagonal 643, E-08028, Barcelona, Spain

Table of Contents

Experimental procedures

Chemistry. **General Methods**. Melting points were determined in open capillary tubes with a MFB 595010M Gallenkamp melting point apparatus. 300 MHz ^{1}H/75.4 MHz ^{13}C NMR spectra and 400 MHz ^{1}H/100.6 MHz ^{13}C NMR spectra were recorded on Varian Gemini 300 and Varian Mercury 400 spectrometers, respectively. The chemical shifts are reported in ppm (δ scale) relative to internal tetramethylsilane, and coupling constants are reported in Hertz (Hz). Assignments given for the NMR spectra of the new compounds have been carried out by comparison with the NMR data of tacrine, 6-chlorotacrine, and 9-[(6-bromohexyl)amino]-1,2,3,4-tetrahydroacridine, as model compounds, which in turn, were assigned on the basis of DEPT, COSY ^{1}H/^{1}H (standard procedures), and COSY ^{1}H/^{13}C (gHSQC or gHMBC sequences) experiments. The *syn* (*anti*) notation of the protons at position 13 of the huprine moiety of the heterodimers means that the corresponding proton at position 13 is on the same (different) side of the quinoline moiety with respect to the cyclohexene ring. IR spectra were run on a Perkin-Elmer Spectrum RX I spectrophotometer. Absorption values are expressed as wave-numbers (cm^{-1}); only significant absorption bands are given. The chromatographic resolution of heterodimer (±)-**8b** was carried out on a HP1100 Agilent Technologies HPLC equipment, furnished with a column containing amylose tris(3,5-dimethylphenylcarbamate) (300 mm × 10 mm) and using CH_3CN/Et_2NH 100:0.2 as eluent, flow 10 mL min^{-1}, λ = 254 nm. Optical rotations

were measured on a Perkin-Elmer model 241 polarimeter. The specific rotation has not been corrected for the presence of solvent of crystallization. Column chromatography was performed on silica gel 60 AC.C (35−70 mesh, SDS, ref 2000027). Thin-layer chromatography was performed with aluminum-backed sheets with silica gel 60 F_{254} (Merck, ref 1.05554), and spots were visualized with UV light and 1% aqueous solution of $KMnO_4$. NMR spectra of all of the new compounds were performed at the Centres Científics i Tecnològics of the University of Barcelona (CCiTUB), while elemental analyses and high resolution mass spectra were carried out at the Mycroanalysis Service of the IIQAB (CSIC, Barcelona, Spain) with a Carlo Erba model 1106 analyzer, and at the CCiTUB with a LC/MSD TOF Agilent Technologies spectrometer, respectively. The analytical samples of all of the huprine−tacrine heterodimers which were subjected to pharmacological evaluation possess a purity ≥95% as evidenced by their elemental analyses. Enantiopure huprine−tacrine heterodimers possess an enantiomeric excess >99% as evidenced by chiral HPLC.

9-[(9-Bromononyl)amino]-1,2,3,4-tetrahydroacridine (4e). A mixture of finely powdered KOH (85% purity reagent, 0.91 g, 16.2 mmol, 1.6 equiv), a solution of tacrine (**1**) (2.00 g, 10.1 mmol, 1 equiv) in dry DMSO (10 mL) (previously prepared by heating at 70 ºC in a water bath), and 4 Å molecular sieves (approximately 1 g) was thoroughly stirred at room temperature for 2 h. To the resulting mixture 1,9-dibromononane (**3e**) (2.00 mL, 2.90 g, 10.1 mmol, 1 equiv) was added, and the reaction mixture was vigorously stirred at room temperature for 15 h. Then, it was diluted with water (200 mL) and extracted with

AcOEt (4×100 mL). The combined organic extracts were washed with water (3×100 mL), dried with anhydrous Na_2SO_4 and evaporated at reduced pressure to give a brown oily residue (3.80 g), which was subjected to column chromatography (70–200 mesh silica gel, hexane/AcOEt mixtures). On elution with hexane/AcOEt 50:50 to 25:75, a 91:9 (^{1}H NMR) mixture of compound **4e** and the β-elimination byproduct (138 mg) and pure **4e** (1.48 g, 39% total yield) were consecutively isolated as yellowish oils; $R_{f(\mathbf{4e})}$ 0.25 (AcOEt/MeOH 4:1).

For characterization purposes, an analytical sample of the hydrobromide of **4e** was prepared by treatment of a solution of **4e** (238 mg, 0.59 mmol) in MeOH (10 mL) with 45% aqueous HBr (0.2 mL, 1.11 mmol, 1.9 equiv), followed by evaporation of the solvents at reduced pressure and recrystallization of the resulting solid (290 mg) from MeOH/AcOEt 1:12 (6.5 mL). After drying of the obtained solid at 80 ºC / 1 Torr for 2 days, **4e**·HBr·1/2H_2O (160 mg) was obtained as a light orange solid.

4e·HBr: mp 138–139 ºC (MeOH/AcOEt 1:12); IR (KBr) ν 3500–2500 (max at 3290, 3049, 3014, 2927, 2852, and 2779, N^+-H, N-H, and C-H st), 1629, 1589, 1575, and 1521 (ar-C-C and ar-C-N st) cm^{-1}; ^{1}H NMR (300 MHz, CD_3OD) δ 1.28–1.48 (complex signal, 10H, 3'-H_2, 4'-H_2, 5'-H_2, 6'-H_2, and 7'-H_2), 1.76–1.88 (complex signal, 4H, 2'-H_2 and 8'-H_2), 1.92–2.02 (complex signal, 4H, 2-H_2 and 3-H_2), 2.71 (m, 2H, 1-H_2), 3.02 (m, 2H, 4-H_2), 3.43 (t, *J*=6.6 Hz, 2H, 9'-H_2), 3.96 (t, *J*=7.5 Hz, 2H 1'-H_2), 4.87 (s, NH and NH^+), 7.59 (ddd, *J*=9.0 Hz, *J'*=6.9 Hz, *J''*=1.5 Hz, 1H, 7-H), 7.76 (dd, *J*=8.4 Hz, *J'*≈1.5 Hz, 1H, 5-H), 7.86 (ddd, *J*=8.4 Hz, *J'*=6.9 Hz, *J''*=1.2 Hz, 1H, 6-H), 8.40 (d, *J*=9.0 Hz, 1H, 8-H); ^{13}C

NMR (75.4 MHz, CD_3OD) δ 21.8 (CH_2, C3), 23.0 (CH_2, C2), 25.0 (CH_2, C1), 27.6 (CH_2), 29.0 (CH_2), 29.6 (CH_2), 30.1 (CH_2), and 30.3 (CH_2) (C3', C4', C5', C6', and C7'), 29.3 (CH_2, C4), 31.5 (CH_2, C2'), 33.9 (CH_2, C8'), 34.5 (CH_2, C9'), 49.1 (CH_2, C1'), 112.8 (C, C9a), 117.0 (C, C8a), 120.0 (CH, C5), 126.3 (CH, C7), 126.5 (CH, C8), 134.0 (CH, C6), 139.6 (C, C10a), 151.5 (C, C4a), 157.9 (C, C9). Anal. ($C_{22}H_{31}BrN_2 \cdot HBr \cdot 1/2H_2O$) C, H, N.

9-[(9-Bromononyl)amino]-6-chloro-1,2,3,4-tetrahydroacridine (5e). A mixture of finely powdered KOH (85% purity reagent, 1.36 g, 20.6 mmol, 1.6 equiv), 6-chlorotacrine (**2**) (3.00 g, 12.9 mmol, 1 equiv), 4 Å molecular sieves (approximately 1.5 g) in dry DMSO (30 mL) was thoroughly stirred for 1 h heating with a heatgun every 10 min and for one additional hour at room temperature. The resulting mixture was added dropwise during 2 h to a mixture of 1,9-dibromononane (**3e**) (3.1 mL, 4.43 g, 15.5 mmol, 1.2 equiv) and 4 Å molecular sieves in dry DMSO (30 mL). The reaction mixture was vigorously stirred at room temperature for 24 h, treated with 10 N NaOH (50 mL), diluted with water (150 mL), and extracted with AcOEt (3×150 mL). The combined organic extracts were washed with water (3×150 mL), dried with anhydrous Na_2SO_4 and evaporated at reduced pressure to give a brown oily residue (4.64 g), which was subjected to column chromatography (35–70 mesh silica gel, CH_2Cl_2/MeOH/50% aqueous NH_4OH mixtures, gradient elution). On elution with CH_2Cl_2/50% aqueous NH_4OH 100:0.2, bromoalkyltacrine **5e** (1.06 g, 19% isolated yield) was obtained as a yellow oil. On elution with CH_2Cl_2/MeOH/50% aqueous NH_4OH 100:0:0.2 to 90:10:0.2, a mixture **5e**/**2** in a ratio 37:63 (^{1}H NMR) (2.36 g, 45%

total yield of **5e**) was separated as a yellow oil; $R_{f(\mathbf{5e})}$ 0.70 (CH_2Cl_2/MeOH/25% aqueous NH_4OH 9:1:0.05).

A solution of **5e** (155 mg, 0.35 mmol) in MeOH (20 mL) was treated with 45% aqueous HBr (0.12 mL, 1.11 mmol, 1.9 equiv) and evaporated at reduced pressure. The resulting solid (180 mg) was recrystallized from MeOH/AcOEt 1:40 (4.1 mL). After drying of the obtained solid at 80 ºC / 1 Torr for 2 days, **5e**·0.9HBr (143 mg) was obtained as a light green solid.

5e·HBr: mp 136–137 ºC (MeOH/AcOEt 1:40); IR (KBr) ν 3500–2500 (max at 3258, 3119, 3047, 3007, 2925, 2854, and 2793, N^+-H, N-H, and C-H st), 1628, 1602, 1582, 1567, and 1521 (ar-C-C and ar-C-N st) cm^{-1}; ^{1}H NMR (300 MHz, CD_3OD) δ 1.25–1.44 (complex signal, 10H, 3'-H_2, 4'-H_2, 5'-H_2, 6'-H_2, and 7'-H_2), 1.80–1.84 (complex signal, 4H, 2'-H_2 and 8'-H_2), 1.85–2.00 (complex signal, 4H, 2-H_2 and 3-H_2), 2.68 (m, 2H, 1-H_2), 3.00 (m, 2H, 4-H_2), 3.43 (t, J=6.6 Hz, 2H, 9'-H_2), 3.94 (t, J=7.2 Hz, 2H 1'-H_2), 4.86 (s, NH and NH^+), 7.56 (dd, J=9.3 Hz, J'=2.1 Hz, 1H, 7-H), 7.76 (d, $J\approx$2.1 Hz, 1H, 5-H), 8.39 (d, J=9.3 Hz, 1H, 8-H); ^{13}C NMR (75.4 MHz, CD_3OD) δ 21.8 (CH_2, C3), 22.9 (CH_2, C2), 24.8 (CH_2, C1), 27.6 (CH_2, C3'), 29.1 (CH_2, C5'), 29.4 (CH_2, C4), 29.6 (CH_2), 30.1 (CH_2), and 30.3 (CH_2) (C4', C6', and C7'), 31.3 (CH_2) and 33.9 (CH_2) (C2' and C9'), 34.5 (CH_2, C8'), 49.2 (CH_2, C1'), 113.3 (C) and 115.4 (C) (C8a and C9a), 119.1 (CH, C5), 126.7 (CH, C7), 128.8 (CH, C8), 140.0 (C, C6), 140.4 (C, C10a), 152.0 (C, C4a), 157.7 (C, C9). Anal. ($C_{22}H_{30}BrClN_2$·0.9HBr) C, H, N.

9-[(10-Bromodecyl)amino]-1,2,3,4-tetrahydroacridine (4f). It was prepared as described for **4e**. From a solution of tacrine (**1**) (3.00 g, 15.2 mmol, 1 equiv) in dry DMSO (7 mL) and 1,10-dibromodecane (**3f**) (4.08 mL, 5.45 g, 18.2 mmol, 1.2 equiv), a brown oily residue (6.64 g) was obtained and purified by column chromatography (35−70 mesh silica gel, CH_2Cl_2/MeOH mixtures, gradient elution). On elution with CH_2Cl_2/MeOH 97:3 to 95:5, bromoalkyltacrine **4f** (2.15 g, 34% yield) was isolated as a yellowish oil; $R_{f(\mathbf{4f})}$ 0.45 (CH_2Cl_2/MeOH/25% aqueous NH_4OH 9:1:0.05).

A solution of **4f** (109 mg, 0.26 mmol) in MeOH (5 mL) was treated with 45% aqueous HBr (0.09 mL, 0.50 mmol, 1.9 equiv) and evaporated at reduced pressure. The resulting solid (131 mg) was recrystallized from MeOH/AcOEt 1:10 (2.2 mL). After drying of the obtained solid at 80 ºC / 1 Torr for 2 days, **4f**·HBr (106 mg) was obtained as a light brown solid.

4f·HBr: mp 145−146 ºC (MeOH/AcOEt 1:10); IR (KBr) ν 3500–2500 (max at 3299, 3050, 3009, 2924, 2851, 2795, and 2660, N^+-H, N-H, and C-H st), 1630, 1590, 1574, and 1519 (ar-C-C and ar-C-N st) cm^{-1}; ^1H NMR (400 MHz, CD_3OD) δ 1.28−1.46 (complex signal, 12H, 3'-H_2, 4'-H_2, 5'-H_2, 6'-H_2, 7'-H_2, and 8'-H_2), 1.77−1.88 (complex signal, 4H, 2'-H_2 and 9'-H_2), 1.92−2.10 (complex signal, 4H, 2-H_2 and 3-H_2), 2.71 (t, *J*=5.4 Hz, 2H, 1-H_2), 3.03 (t, *J*=5.6 Hz, 2H, 4-H_2), 3.42 (t, *J*=6.6 Hz, 2H, 10'-H_2), 3.96 (t, *J*=7.4 Hz, 2H 1'-H_2), 4.84 (s, NH and NH^+), 7.59 (ddd, *J*=8.4 Hz, *J'*=6.8 Hz, *J''*=1.2 Hz, 1H, 7-H), 7.78 (dd, *J*=8.4 Hz, *J'*=1.2 Hz, 1H, 5-H), 7.85 (ddd, *J*≈8.4 Hz, *J'*=6.8 Hz, *J''*=0.8 Hz, 1H, 6-H), 8.39 (d, *J*≈8.4 Hz, 1H, 8-H); ^{13}C NMR (100.6 MHz, CD_3OD) δ 21.8 (CH_2, C3), 23.0 (CH_2, C2),

24.9 (CH_2, C1), 27.6 (CH_2), 29.1 (CH_2), 29.7 (CH_2), 30.2 (CH_2), 30.38 (CH_2), and 30.40 (CH_2) (C3', C4', C5', C6', C7', and C8'), 29.3 (CH_2, C4), 31.5 (CH_2, C2'), 33.9 (CH_2, C9'), 34.5 (CH_2, C10'), 49.1 (CH_2, C1'), 112.8 (C, C9a), 117.0 (C, C8a), 120.1 (CH, C5), 126.3 (CH, C7), 126.5 (CH, C8), 134.1 (CH, C6), 139.7 (C, C10a), 151.6 (C, C4a), 158.0 (C, C9). Anal. ($C_{23}H_{33}BrN_2 \cdot HBr$) C, H, N.

9-[(10-Bromodecyl)amino]-6-chloro-1,2,3,4-tetrahydroacridine (5f). It was prepared as described for **4e**. From a solution of 6-chlorotacrine (**2**) (2.00 g, 8.60 mmol, 1 equiv) in dry DMSO (30 mL) and 1,10-dibromodecane (**3f**) (2.40 mL, 3.20 g, 10.7 mmol, 1.2 equiv), a brown oily residue (4.76 g) was obtained and purified by column chromatography (35–70 mesh silica gel, CH_2Cl_2 / MeOH mixtures, gradient elution). On elution with CH_2Cl_2/MeOH 96:4 to 95:5, mixtures of bromoalkyltacrine **5f** and the β-elimination byproduct in the ratio 79:21 (^{1}H NMR, 451 mg), 95:5 (260 mg), and 96:4 (561 mg) (29% total yield of **5f**) were consecutively isolated as yellowish oils; $R_{f(\mathbf{5f})}$ 0.79 (CH_2Cl_2/MeOH/25% aqueous NH_4OH 9:1:0.05).

A solution of a 96:4 mixture of **5f** and the β-elimination byproduct (44 mg, 0.10 mmol) in MeOH (5 mL) was treated with 45% aqueous HBr (0.03 mL, 0.17 mmol, 1.7 equiv) and evaporated at reduced pressure. The resulting solid (55 mg) was recrystallized from CH_3CN (2 mL). After drying of the obtained solid at 80 ºC / 1 Torr for 2 days, **5f**·HBr·3/4H_2O (20 mg) was obtained as a yellowish solid.

5f·HBr: mp 129–130 ºC (CH_3CN); IR (KBr) ν 3500–2500 (max at 3252, 3125, 3045, 3012, 2924, 2852, and 2795, N^+-H, N-H, and C-H st), 1629, 1586, 1569, and 1523 (ar-C-C

and ar-C-N st) cm^{-1}; ^1H NMR (400 MHz, CD_3OD) δ 1.28–1.48 (complex signal, 12H, 3'-H_2, 4'-H_2, 5'-H_2, 6'-H_2, 7'-H_2, and 8'-H_2), 1.78–1.88 (complex signal, 4H, 2'-H_2 and 9'-H_2), 1.92–2.00 (complex signal, 4H, 2-H_2 and 3-H_2), 2.68 (t, *J*=5.2 Hz, 2H, 1-H_2), 3.00 (t, *J*=5.8 Hz, 2H, 4-H_2), 3.43 (t, *J*=6.6 Hz, 2H, 10'-H_2), 3.95 (t, *J*=7.2 Hz, 2H 1'-H_2), 4.85 (s, NH and NH^+), 7.57 (dd, *J*=9.2 Hz, *J'*=2.0 Hz, 1H, 7-H), 7.77 (d, *J*=2.0 Hz, 1H, 5-H), 8.39 (d, *J*≈9.2 Hz, 1H, 8-H); ^{13}C NMR (100.6 MHz, CD_3OD) δ 21.8 (CH_2, C3), 22.9 (CH_2, C2), 24.7 (CH_2, C1), 27.6 (CH_2, C3'), 29.1 (CH_2, C5'), 29.3 (CH_2, C4), 29.7 (CH_2), 30.2 (CH_2), and 30.4 (2 CH_2) (C4', C6', C7', and C8'), 31.3 (CH_2) and 33.9 (CH_2) (C2' and C10'), 34.5 (CH_2, C9'), 49.2 (CH_2, C1'), 113.4 (C) and 115.5 (C) (C8a and C9a), 119.1 (CH, C5), 126.8 (CH, C7), 128.8 (CH, C8), 140.2 (C, C6), 140.6 (C, C10a), 152.1 (C, C4a), 157.9 (C, C9). Anal. ($C_{23}H_{32}BrClN_2 \cdot HBr \cdot 3/4H_2O$) C, H, N.

3-Chloro-6,7,10,11-tetrahydro-9-methyl-12-{{9-[(1,2,3,4-tetrahydroacridin-9-yl)amino]nonyl}amino}-7,11-methanocycloocta[*b*]quinoline dihydrochloride [(±)-7e·2HCl]. It was prepared as described for **5e**. From a solution of (±)-huprine Y [(±)-**6**] (362 mg, 1.27 mmol, 1 equiv) in dry DMSO (5 mL) and a solution of haloalkyltacrine **4e** (616 mg, 1.53 mmol, 1.2 equiv) in dry DMSO (7.5 mL), and using a reaction time of 4 days, a brown oily residue (832 mg) was obtained and purified by column chromatography (35–70 mesh silica gel, CH_2Cl_2/MeOH/50% aqueous NH_4OH mixtures, gradient elution). On elution with CH_2Cl_2/50% aqueous NH_4OH 100:0.2, a mixture of starting (±)-**6**, β-elimination byproduct and heterodimer (±)-**7e** (120 mg) in an approximate ratio 43:13:44 (^1H NMR) was separated. On elution with CH_2Cl_2/MeOH/50% aqueous NH_4OH 100:0:0.2

to 99:1:0.2, heterodimer (±)-**7e** (593 mg, 77% isolated yield; 84% total yield) was isolated as a yellowish oil; R_f 0.47 (CH_2Cl_2/MeOH/25% aqueous NH_4OH 9:1:0.05).

A solution of (±)-**7e** (466 mg, 0.77 mmol) in CH_2Cl_2 (20 mL) was filtered through a polytetrafluoroethylene (PTFE) 0.45 μm filter, and treated with an excess of a methanolic solution of HCl (0.65 N, 10.6 mL, 6.9 mmol) and the resulting solution was concentrated in vacuo to dryness. The solid was taken in MeOH (0.8 mL) and precipitated upon addition of AcOEt (6.2 mL). The precipitated solid was separated, triturated with pentane (3×2 mL) and dried at 65 ºC/15 Torr for 4 days, to give (±)-**7e**·2HCl·H_2O (497 mg) as a yellowish solid.

(±)-**7e**·2HCl: mp 184–185 ºC (MeOH); IR (KBr) ν 3500–2500 (max at 3383, 3231, 3047, 2925, 2854, and 2793, N^+-H, N-H, and C-H st), 1628, 1582, and 1511 (ar-C-C and ar-C-N st) cm^{-1}; ^{1}H NMR (400 MHz, CD_3OD) δ 1.32–1.47 (complex signal, 10H, 3'-H_2, 4'-H_2, 5'-H_2, 6'-H_2, and 7'-H_2), 1.58 (s, 3H, 9-CH_3), 1.80–2.02 (complex signal, 10H, 10-H_{endo}, 13-H_{syn}, 2'-H_2, 8'-H_2, 2"-H_2, and 3"-H_2), 2.08 (broad d, *J*=10.4 Hz, 1H, 13-H_{anti}), 2.55 (broad d, *J*=16.0 Hz, 1H, 10-H_{exo}), 2.71 (m, 2H, 1"-H_2), 2.77 (m, 1H, 7-H), 2.87 (d, *J*=17.6 Hz, 1H, 6-H_{endo}), 3.02 (m, 2H, 4"-H_2), 3.20 (dd, *J*=17.6 Hz, *J'*=4.4 Hz, 1H, 6-H_{exo}), 3.46 (m, 1H, 11-H), 3.90–4.40 (complex signal, 4H, 1'-H_2 and 9'-H_2), 4.85 (s, NH and NH^+), 5.58 (broad d, *J*=4.0 Hz, 1H, 8-H), 7.51–7.61 (complex signal, 2H, 2-H and 7"-H), 7.77 (s, 1H, 4-H), superimposed in part 7.78 (d, *J*≈8.4 Hz, 1H, 5"-H), 7.84 (dd, *J*=8.4 Hz, *J'*=6.4 Hz, 1H, 6"-H), 8.35–8.42 (complex signal, 2H, 1-H and 8"-H); ^{13}C NMR (100.6 MHz, CD_3OD) δ 21.9 (CH_2, C3"), 23.0 (CH_2, C2"), 23.5 (CH_3, 9-CH_3), 24.9 (CH_2, C1"), 27.3 (CH, C11),

27.75 (CH_2) and 27.84 (CH + CH_2, C7, C3', and C7'), 29.3 (2 CH_2, C13 and C4"), 30.2 (CH_2), 30.3 (CH_2), and 30.5 (CH_2) (C4', C5', and C6'), 31.3 (CH_2) and 31.6 (CH_2) (C2' and C8'), 36.07 (CH_2) and 36.13 (CH_2) (C6 and C10), 49.2 (CH_2) and 49.7 (CH_2) (C1' and C9'), 112.8 (C), 115.6 (C), 117.0 (C), and 117.6 (C) (C11a, C12a, C8a", and C9a"), 119.1 (CH) and 120.1 (CH) (C4 and C5"), 125.2 (CH, C8), 126.3 (CH, C7"), 126.5 (CH, C8"), 126.7 (CH, C2), 129.5 (CH, C1), 134.1 (CH, C6"), 134.5 (C, C9), 139.8 (C), 140.2 (C), and 141.0 (C) (C3, C4a, and C10a"), 151.2 (C) and 151.7 (C) (C5a and C4a"), 156.9 (C) and 158.0 (C) (C12 and C9"). Anal. ($C_{39}H_{47}ClN_4 \cdot 2HCl \cdot H_2O$) C, H, N, Cl.

3-Chloro-6,7,10,11-tetrahydro-9-methyl-12-{{9-[(6-chloro-1,2,3,4-tetrahydroacridin-9-yl)amino]nonyl}amino}-7,11-methanocycloocta[*b*]quinoline dihydrochloride [(±)-8e·2HCl]. It was prepared as described for **5e**. From a solution of **(±)-**huprine Y [(±)-**6**] (300 mg, 1.05 mmol, 1 equiv) in dry DMSO (4 mL) and a solution of haloalkyltacrine **5e** (512 mg, 1.17 mmol, 1.1 equiv) in dry DMSO (6 mL), and using a reaction time of 4 days, a brown oily residue (726 mg) was obtained and purified by column chromatography (35−70 mesh silica gel, CH_2Cl_2/50% aqueous NH_4OH 100:0.2) to give a mixture of starting (±)-**6** and heterodimer (±)-**8e** (266 mg) in an approximate ratio 5:95 (^{1}H NMR) and heterodimer (±)-**8e** (200 mg, 30% isolated yield; 67% total yield) were consecutively isolated as yellowish oils; $R_{f[(\pm)\text{-}\mathbf{8e}]}$ 0.41 (CH_2Cl_2/MeOH/25% aqueous NH_4OH 9:1:0.05).

A solution of (±)-**8e** (200 mg, 0.31 mmol) in CH_2Cl_2 (10 mL) was filtered through a PTFE 0.45 μm filter, and treated with an excess of a methanolic solution of HCl (0.65 N, 4.3 mL,

2.80 mmol) and the resulting solution was concentrated in vacuo to dryness. The solid was taken in MeOH (0.65 mL) and precipitated upon addition of AcOEt (4.6 mL). The precipitated solid was separated, triturated with pentane (3×1 mL) and dried at 65 ºC/15 Torr for 4 days, to give (±)-**8e**·2HCl·H_2O (224 mg) as a yellowish solid.

(±)-**8e**·2HCl: mp 188–189 ºC (MeOH/AcOEt 1:10); IR (KBr) ν 3600–2500 (max at 3383, 3210, 3106, 3058, 2925, and 2844, N^+-H, N-H, and C-H st), 1633, 1582, and 1526 (ar-C-C and ar-C-N st) cm^{-1}; ^1H NMR (400 MHz, CD_3OD) δ 1.30–1.46 (complex signal, 10H, 3'-H_2, 4'-H_2, 5'-H_2, 6'-H_2, and 7'-H_2), 1.57 (s, 3H, 9-CH_3), 1.78–2.00 (complex signal, 10H, 10-H_{endo}, 13-H_{syn}, 2'-H_2, 8'-H_2, 2"-H_2, and 3"-H_2), 2.07 (dm, *J*=12.4 Hz, 1H, 13-H_{anti}), 2.54 (broad d, *J*=18.0 Hz, 1H, 10-H_{exo}), 2.67 (m, 2H, 1"-H_2), 2.77 (m, 1H, 7-H), 2.87 (broad d, *J*=17.6 Hz, 1H, 6-H_{endo}), 3.00 (m, 2H, 4"-H_2), 3.20 (dd, *J*=17.6 Hz, *J'*=5.6 Hz, 1H, 6-H_{exo}), 3.45 (m, 1H, 11-H), 3.93 (t, *J*=7.6 Hz, 2H) and 3.97 (t, *J*=6.8 Hz, 2H) (1'-H_2 and 9'-H_2), 4.84 (s, NH and NH^+), 5.58 (m, 1H, 8-H), 7.54 (dm, *J*=9.2 Hz, 2H, 2-H and 7"-H), 7.78 (d, *J*=2.0 Hz, 1H) and 7.79 (d, *J*=2.0 Hz, 1H) (4-H and 5"-H), 8.37 (d, *J*=9.2 Hz, 1H) and 8.38 (d, *J*=9.2 Hz, 1H) (1-H and 8"-H); ^{13}C NMR (100.6 MHz, CD_3OD) δ 21.7 (CH_2, C3"), 22.8 (CH_2, C2"), 23.5 (CH_3, 9-CH_3), 24.7 (CH_2, C1"), 27.2 (CH, C11), 27.7 (CH_2) and 27.8 (CH + CH_2) (C7, C3', and C7'), 29.3 (2 CH_2, C13 and C4"), 30.1 (CH_2), 30.2 (CH_2), and 30.4 (CH_2) (C4', C5', and C6'), 31.2 (CH_2) and 31.3 (CH_2) (C2' and C8'), 36.0 (CH_2, C10), 36.1 (CH_2, C6), 113.3 (C), 115.4 (C), 115.6 (C), and 117.6 (C) (C11a, C12a, C8a", and C9a"), 119.1 (2 CH, C4 and C5"), 125.1 (CH, C8), 126.6 (CH) and 126.7 (CH) (C2 and C7"), 128.7 (CH) and 129.4 (CH) (C1 and C8"), 134.5 (C, C9), 140.1 (C) and 140.2 (C)

(C3 and C6"), 140.5 (C) and 141.0 (C) (C4a and C10a"), 151.3 (C) and 152.1 (C) (C5a and C4a"), 156.8 (C) and 157.8 (C) (C12 and C9"), the signals corresponding to C1' and C9', superimposed with some signals of CD_3OD, could not be distinguished. Anal. ($C_{39}H_{46}Cl_2N_4 \cdot 2HCl \cdot H_2O$) C, H, N, Cl.

3-Chloro-6,7,10,11-tetrahydro-9-methyl-12-{{10-[(1,2,3,4-tetrahydroacridin-9-yl)amino]decyl}amino}-7,11-methanocycloocta[*b*]quinoline dihydrochloride [(±)-7f·2HCl]. It was prepared as described for **4e**. From a solution of (±)-huprine Y [(±)-**6**] (398 mg, 1.40 mmol, 1 equiv) in dry DMSO (7 mL) and a solution of haloalkyltacrine **4f** (700 mg, 1.68 mmol, 1.2 equiv) in dry DMSO (2 mL), and using a reaction time of 64 h, a brown oily residue (815 mg) was obtained and purified by column chromatography (35–70 mesh silica gel, CH_2Cl_2/MeOH mixtures, gradient elution). On elution with CH_2Cl_2/MeOH 95:5, heterodimer (±)-**7f** (472 mg, 54% yield) was isolated as a yellowish oil; R_f 0.37 (CH_2Cl_2/MeOH/25% aqueous NH_4OH 9:1:0.05).

A solution of (±)-**7f** (261 mg, 0.42 mmol) in CH_2Cl_2 (10 mL) was treated with an excess of a methanolic solution of HCl (0.48 N, 5.2 mL, 2.50 mmol) and the resulting solution was concentrated in vacuo to dryness. The solid (263 mg) was recrystallized from MeOH (1 mL) and dried at 65 ºC/15 Torr for 4 days, to give (±)-**7f**·2HCl·$2H_2O$ (147 mg) as a light brown solid.

(±)-**7f**·2HCl: mp 226–227 ºC (MeOH); IR (KBr) ν 3500–2500 (max at 3399, 3242, 3045, 2926, 2853, and 2791, N^+-H, N-H, and C-H st), 1631, 1583, and 1522 (ar-C-C and ar-C-N st) cm^{-1}; ^1H NMR (400 MHz, CD_3OD) δ 1.28–1.47 (complex signal, 12H, 3'-H_2, 4'-H_2, 5'-

H_2, 6'-H_2, 7'-H_2, and 8'-H_2), 1.58 (s, 3H, 9-CH_3), 1.78–2.01 (complex signal, 10H, 10-H_{endo}, 13-H_{syn}, 2'-H_2, 9'-H_2, 2"-H_2, and 3"-H_2), 2.08 (dm, *J*=12.8 Hz, 1H, 13-H_{anti}), 2.55 (broad dd, *J*=17.6 Hz, *J'*=4.4 Hz, 1H, 10-H_{exo}), 2.71 (m, 2H, 1"-H_2), 2.76 (m, 1H, 7-H), 2.88 (d, *J*=18.0 Hz, 1H, 6-H_{endo}), 3.03 (m, 2H, 4"-H_2), 3.20 (dd, *J*=18.0 Hz, *J'*=5.6 Hz, 1H, 6-H_{exo}), 3.46 (m, 1H, 11-H), 3.95 (t *J*=7.2 Hz, 2H) and 3.98 (t *J*=7.2 Hz, 2H) (1'-H_2 and 10'-H_2), 4.85 (s, NH and NH^+), 5.58 (broad d, *J*=4.8 Hz, 1H, 8-H), 7.53 (dd, *J*=9.2 Hz, *J'*=2.0 Hz, 1H, 2-H), 7.57 (ddd, *J*=8.8 Hz, *J'*=6.8 Hz, *J''*=1.2 Hz, 1H, 7"-H), superimposed 7.782 (m, 1H, 5"-H), 7.783 (d, *J*=2.0 Hz, 1H, 4-H), 7.84 (dd, *J*=8.4 Hz, *J'*=7.6 Hz, 1H, 6"-H), 8.36–8.41 (complex signal, 2H, 1-H and 8"-H); ^{13}C NMR (100.6 MHz, CD_3OD) δ 21.9 (CH_2, C3"), 23.0 (CH_2, C2"), 23.5 (CH_3, 9-CH_3), 24.9 (CH_2, C1"), 27.3 (CH, C11), 27.7 (CH_2), 27.8 (CH_2), and 27.9 (CH_2) (C7, C3', and C8'), 29.3 (2 CH_2, C13 and C4"), 30.2 (CH_2), 30.3 (CH_2), 30.48 (CH_2), and 30.52 (CH_2) (C4', C5', C6', and C7'), 31.3 (CH_2) and 31.5 (CH_2) (C2' and C9'), 36.07 (CH_2) and 36.11 (CH_2) (C6 and C10), 49.1 (CH_2) and 49.6 (CH_2) (C1' and C10'), 112.8 (C), 115.6 (C), 117.0 (C), and 117.6 (C) (C11a, C12a, C8a", and C9a"), 119.2 (CH) and 120.1 (CH) (C4 and C5"), 125.2 (CH, C8), 126.3 (CH, C7"), 126.5 (CH, C8"), 126.6 (CH, C2), 129.5 (CH, C1), 134.1 (CH, C6"), 134.5 (C, C9), 139.8 (C), 140.1 (C), and 141.0 (C) (C3, C4a, and C10a"), 151.3 (C) and 151.7 (C) (C5a and C4a"), 156.9 (C) and 158.0 (C) (C12 and C9"). Anal. ($C_{40}H_{49}ClN_4 \cdot 2HCl \cdot 2H_2O$) C, H, N, Cl.

3-Chloro-6,7,10,11-tetrahydro-9-methyl-12-{{10-[(6-chloro-1,2,3,4-tetrahydroacridin-9-yl)amino]decyl}amino}-7,11-methanocycloocta[*b*]quinoline

dihydrochloride [(±)-8f·2HCl]. It was prepared as described for **4e**. From a solution of (±)-huprine Y [(±)-**6**] (400 mg, 1.41 mmol, 1 equiv) in dry DMSO (6 mL) and a solution of haloalkyltacrine **5f** (821 mg, 1.74 mmol, 1.2 equiv) in dry DMSO (2 mL), and using a reaction time of 60 h, a brown oily residue (926 mg) was obtained and purified by column chromatography (35–70 mesh silica gel, CH_2Cl_2/MeOH mixtures, gradient elution). On elution with CH_2Cl_2/MeOH 95:5, heterodimer (±)-**8f** (428 mg, 46% yield) was isolated as a colorless oil; R_f 0.64 (CH_2Cl_2/MeOH/25% aqueous NH_4OH 9:1:0.05).

A solution of (±)-**8f** (136 mg, 0.21 mmol) in MeOH (10 mL) was treated with an excess of a methanolic solution of HCl (0.48 N, 2.60 mL, 1.25 mmol) and the resulting solution was concentrated in vacuo to dryness. The solid (162 mg) was recrystallized from MeOH/AcOEt 1:10 (5.5 mL) and dried at 65 ºC/15 Torr for 4 days, to give (±)-**8f**·2HCl·$4H_2O$ (123 mg) as a yellowish solid.

(±)-**8f**·2HCl: mp 226–227 ºC (MeOH/AcOEt 1:10); IR (KBr) ν 3600–2500 (max at 3397, 3233, 3048, 2925, 2853, and 2791, N^+-H, N-H, and C-H st), 1630, 1582, and 1514 (ar-C-C and ar-C-N st) cm^{-1}; ^1H NMR (400 MHz, CD_3OD) δ 1.28–1.49 (complex signal, 12H, 3'-H_2, 4'-H_2, 5'-H_2, 6'-H_2, 7'-H_2, and 8'-H_2), 1.58 (s, 3H, 9-CH_3), 1.78–2.01 (complex signal, 10H, 10-H_{endo}, 13-H_{syn}, 2'-H_2, 9'-H_2, 2"-H_2, and 3"-H_2), 2.08 (dm, J=10.0 Hz, 1H, 13-H_{anti}), 2.55 (broad d, J=16.4 Hz, 1H, 10-H_{exo}), 2.68 (m, 2H, 1"-H_2), 2.77 (m, 1H, 7-H), 2.88 (broad d, J=17.2 Hz, 1H, 6-H_{endo}), 3.01 (m, 2H, 4"-H_2), 3.20 (broad d, $J\approx$17.2 Hz, 1H, 6-H_{exo}), 3.46 (m, 1H, 11-H), 3.92–4.00 (complex signal, 4H, 1'-H_2 and 10'-H_2), 4.85 (s, NH and NH^+), 5.58 (m, 1H, 8-H), 7.53 (m, 1H) and 7.54 (m, 1H) (2-H and 7"-H), 7.785 (m,

1H) and 7.793 (m, 1H) (4-H and 5”-H), 8.38 (m, 1H) and 8.39 (m, 1H) (1-H and 8”-H); ^{13}C NMR (100.6 MHz, CD_3OD) δ 21.8 (CH_2, C3”), 22.9 (CH_2, C2”), 23.5 (CH_3, 9-CH_3), 24.8 (CH_2, C1”), 27.3 (CH, C11), 27.7 (CH_2) and 27.8 (CH + CH_2) (C7, C3’, and C8’), 29.4 (2 CH_2, C13 and C4”), 30.27 (CH_2), 30.30 (CH_2), 30.49 (CH_2), and 30.53 (CH_2) (C4’, C5’, C6’, and C7’), 31.3 (CH_2) and 31.4 (CH_2) (C2’ and C9’), 36.07 (CH_2, C10), 36.13 (CH_2, C6), 49.2 (CH_2) and 49.7 (CH_2) (C1’ and C10’), 113.3 (C), 115.4 (C), 115.6 (C), and 117.6 (C) (C11a, C12a, C8a”, and C9a”), 119.1 (2 CH, C4 and C5”), 125.2 (CH, C8), 126.6 (CH) and 126.8 (CH) (C2 and C7”), 128.8 (CH) and 129.5 (CH) (C1 and C8”), 134.5 (C, C9), 140.1 (C) and 140.2 (C) (C3 and C6”), 140.5 (C) and 141.0 (C) (C4a and C10a”), 151.2 (C) and 152.1 (C) (C5a and C4a”), 156.9 (C) and 157.8 (C) (C12 and C9”). Anal. ($C_{40}H_{48}Cl_2N_4 \cdot 2HCl \cdot 4H_2O$) C, H, N, Cl.

Preparative resolution of (±)-3-chloro-6,7,10,11-tetrahydro-9-methyl-12-{{7-[(6-chloro-1,2,3,4-tetrahydroacridin-9-yl)amino]heptyl}amino}-7,11-methanocycloocta[*b*]quinoline [(±)-8b] by chiral HPLC: (–)-(7*S*,11*S*)-8b and (+)-(7*R*,11*R*)-8b. The chromatographic resolution of (±)-**8b** was carried out by using the above described HPLC equipment. The sample of (±)-**8b** (40 mg) was introduced as free base using CH_3CN/Et_2NH 100:0.2 (10 mL min^{-1}) as eluent. The chromatographic fractions were analyzed by chiral HPLC [HP1100 Agilent Technologies HPLC equipment with a CHIRALPAK® IA column containing the chiral stationary phase amylose tris(3,5-dimethylphenylcarbamate) immobilized on 5 μm silica gel, the isocratic mobile phase was a mixture of CH_3CN/Et_2NH 100:0.2, flow 1 mL min^{-1}, λ = 254 nm; (**–**)-**8b**, t_R=38.68 min,

k'_1=9.87; (+)-**8b**, t_R=59.08 min, k'_2=15.60; α=1.58; res.=10.0] and combined conveniently. In this way, (–)-(7*S*,*11*S)-**8b** (4 mg, >99% ee) and (+)-(7*R*,*11*R)-**8b** (5 mg, 97% ee) were obtained. The remaining product consisted of mixtures of both enantiomers with lower ee.

(+)-(7*R*,11*R*)-3-Chloro-6,7,10,11-tetrahydro-9-methyl-12-{{7-[(1,2,3,4-tetrahydroacridin-9-yl)amino]heptyl}amino}-7,11-methanocycloocta[*b*]quinoline dihydrochloride [(+)-7b·2HCl] from (+)-huprine Y. It was prepared as described for **5e**. From a solution of (+)-huprine Y [(+)-**6**][1] (280 mg, 0.99 mmol, 1 equiv) in dry DMSO (4 mL) and a solution of haloalkyltacrine **4b** (446 mg, 1.19 mmol, 1.2 equiv] in dry DMSO (5 mL), and using a reaction time of 3 days, a brown oily residue (490 mg) was obtained and purified by column chromatography (35–70 mesh silica gel, CH_2Cl_2/50% aqueous NH_4OH 100:0.2). Starting (+)-**6** (26 mg), a mixture of β-elimination byproduct and heterodimer (+)-**7b** in a ratio 1:99 (83 mg) and pure heterodimer (+)-**7b** (222 mg, 39% isolated yield; 53% total yield) were consecutively separated as yellowish oils.

A solution of (+)-**7b** (145 mg, 0.25 mmol) in CH_2Cl_2 (10 mL) was filtered through a PTFE 0.45 μm filter, and treated with an excess of a methanolic solution of HCl (0.65 N, 3.5 mL, 2.28 mmol) and the resulting solution was concentrated in vacuo to dryness. The solid was taken in MeOH (0.4 mL) and precipitated upon addition of AcOEt (2.2 mL). The precipitated solid was separated and dried at 65 ºC/15 Torr for 4 days, to give (+)-**7b**·2HCl·2H_2O (125 mg) as a light brown solid: $[\alpha]^{20}_D$ = +139 (*c*=0.34, MeOH), >99% ee by chiral HPLC on the liberated base (see above); mp 219–221 ºC (MeOH/AcOEt 2:11); IR (KBr) ν 3600–2500 (max at 3395, 3236, 3049, 2927, 2854, and 2773, N^+-H, N-H, and C-H

st), 1629, 1582, 1571, 1560, and 1522 (ar-C-C and ar-C-N st) cm^{-1}; the ^{1}H and ^{13}C NMR spectra were identical to those described for (±)-**7b**·2HCl.[2] HRMS calcd for $C_{37}H_{43}{}^{35}ClN_4$ + H, 579.3249; found, 579.3241. Anal. ($C_{37}H_{43}ClN_4$·2HCl·2H_2O) C, H, N, Cl.

(–)-(7*S*,11*S*)-3-Chloro-12-{{7-[(6-chloro-1,2,3,4-tetrahydroacridin-9-yl)amino]heptyl}amino}-6,7,10,11-tetrahydro-9-methyl-7,11-methanocycloocta[*b*]quinoline dihydrochloride [(–)-8b·2HCl] from (–)-huprine Y. It was prepared as described for **5e**. From a solution of (–)-huprine Y [(–)-**6**][1] (315 mg, 1.11 mmol, 1 equiv) in dry DMSO (3.5 mL) and a solution of haloalkyltacrine **5b** [552 mg, 1.33 mmol, 1.2 equiv] in dry DMSO (3.5 mL), and using a reaction time of 3 days, a brown oily residue (672 mg) was obtained and purified by column chromatography (35−70 mesh silica gel, CH_2Cl_2/50% aqueous NH_4OH 100:0.2). β-Elimination byproduct (48 mg), mixtures of starting (–)-**6** and heterodimer (–)-**8b** in the ratio 46:54 (46 mg) and 5:95 (250 mg) (^{1}H NMR), and pure heterodimer (–)-**8b** (239 mg, 35% isolated yield; 74% total yield) were consecutively separated as yellowish oils.

A solution of (–)-**8b** (239 mg, 0.39 mmol) in CH_2Cl_2 (20 mL) was filtered through a PTFE 0.45 μm filter, and treated with an excess of a methanolic solution of HCl (0.65 N, 5.4 mL, 3.51 mmol) and the resulting solution was concentrated in vacuo to dryness. The solid was dried at 65 ºC/15 Torr for 4 days, to give (–)-**8b**·2HCl·1.5H_2O (237 mg) as a yellowish solid: $[\alpha]^{20}_D$ = −152 (*c*=0.33, MeOH), >99% ee by chiral HPLC on the liberated base [CHIRALCEL OD-H column, hexane/EtOH/Et_2NH 90:10:0.1, flow 0.2 mL min^{-1}, λ = 254 nm; (–)-**8b**, t_R=41.85 min, k'_1=1.67; (+)-**8b**, t_R=46.23 min, k'_2=1.95, α=1.17, res.=5.7]; mp

218–220 ºC; IR (KBr) ν 3600–2500 (max at 3405, 3229, 3046, 3005, 2927, 2855, 2768, and 2746, N^+-H, N-H, and C-H st), 1630, 1581, and 1510 (ar-C-C and ar-C-N st) cm^{-1}; the ^1H and ^{13}C NMR spectra were identical to those described for (±)-**8b**·2HCl.[2] HRMS calcd for $C_{37}H_{42}{}^{35}Cl_2N_4$ + H, 613.2859; found, 613.2863. Anal. ($C_{37}H_{42}Cl_2N_4$·2HCl·1.5H_2O) C, H, N, Cl.

(+)-(7*R*,11*R*)-3-Chloro-12-{{7-[(6-chloro-1,2,3,4-tetrahydroacridin-9-yl)amino]heptyl}amino}-6,7,10,11-tetrahydro-9-methyl-7,11-methanocycloocta[*b*]quinoline dihydrochloride [(+)-8b·2HCl] from (+)-huprine Y. It was prepared as described for **5e**. From a solution of (+)-huprine Y [(+)-**6**][1] (343 mg, 1.21 mmol, 1 equiv) in dry DMSO (3.5 mL) and a solution of haloalkyltacrine **5b** [impurified by 7% (^1H NMR) of its β-elimination byproduct, 634 mg, 1.44 mmol, 1.2 equiv] in dry DMSO (4 mL), and using a reaction time of 3 days, a brown oily residue (723 mg) was obtained and purified by column chromatography (35–70 mesh silica gel, CH_2Cl_2/50% aqueous NH_4OH 100:0.2). β-Elimination byproduct (55 mg), starting (+)-**6** (61 mg), and pure heterodimer (+)-**8b** (356 mg, 48% yield) were consecutively separated as yellowish oils.

A solution of (+)-**8b** (356 mg, 0.58 mmol) in CH_2Cl_2 (25 mL) was filtered through a PTFE 0.45 μm filter, and treated with an excess of a methanolic solution of HCl (0.65 N, 8.0 mL, 5.20 mmol) and the resulting solution was concentrated in vacuo to dryness. The solid was dried at 65 ºC/15 Torr for 4 days, to give (+)-**8b**·2HCl·1.5H_2O (358 mg) as a yellowish solid: $[\alpha]^{20}_D$ = +150 (*c*=0.36, MeOH), >99% ee by chiral HPLC on the liberated base (see above); mp 226–228 ºC; IR (KBr) ν 3600–2500 (max at 3395, 3226, 3045, 3011, 2925,

2854, and 2742, N^+-H, N-H, and C-H st), 1628, 1617, 1582, 1574, 1558, 1537, and 1521 (ar-C-C and ar-C-N st) cm^{-1}; the ^1H and ^{13}C NMR spectra were identical to those described for (±)-**8b**·2HCl.[2] HRMS calcd for $C_{37}H_{42}{}^{35}Cl_2N_4$ + H, 613.2859; found, 613.2863. Anal. ($C_{37}H_{42}Cl_2N_4$·2HCl·1.5H_2O) C, H, N, Cl.

Biochemical Studies. AChE and BChE Inhibition Assay. AChE and BChE inhibitory activity was evaluated spectrophotometrically by the method of Ellman[3] using human recombinant AChE and human serum BChE. The reactions took place in a final volume of 300 μL of 0.1 M phosphate-buffered solution pH 8.0, containing 0.02 units mL^{-1} of AChE or BChE and 333 μM 5,5'-dithiobis(2-nitrobenzoic) acid (DTNB) solution used to produce the yellow anion of 5-thio-2-nitrobenzoic acid. Inhibition curves were performed in duplicates using at least 10 increasing concentrations of inhibitor and preincubated for 20 min at 37 ºC. One duplicate sample without inhibitor was always present to yield 100% of AChE or BChE activities. Then substrates, acetylthiocholine iodide (450 μM) or butyrylthiocholine iodide (300 μM), were added and the reaction was developed for 5 min at 37 ºC. The color production was measured at 414 nm using a labsystems Multiskan spectrophotometer.

Data from concentration−inhibition experiments of the inhibitors were calculated by non-linear regression analysis, using the GraphPad Prism program package (GraphPad Software; San Diego, USA), which gave estimates of the IC_{50} (concentration of drug producing 50% of enzyme activity inhibition). Results are expressed as mean ± S.E.M. of at

least 4 experiments performed in duplicate. DTNB, acetylthiocholine, butyrylthiocholine, and enzymes were purchased from Sigma.

AChE-Induced $A\beta_{1-40}$ Aggregation Inhibition Assay. Thioflavin T (Basic Yellow 1), human recombinant AChE lyophilized powder, 1,1,1,3,3,3-hexafluoro-2-propanol (HFIP), were purchased from Sigma Chemicals. Absolute DMSO over molecular sieves was from Fluka. Water was deionized and doubly distilled. $A\beta_{1-40}$, supplied as trifluoroacetate salt, was purchased from Bachem AG (Bubendorf, Switzerland). $A\beta_{1-40}$ (2 mg mL^{-1}) was dissolved in HFIP and lyophilized. The 1 mM solutions of tested inhibitors were prepared by dissolution in MeOH.

Aliquots of 2 μL $A\beta_{1-40}$ peptide, lyophilized from 2 mg mL^{-1} HFIP solution and dissolved in DMSO, were incubated for 24 h at room temperature in 0.215 M sodium phosphate buffer (pH 8.0) at a final concentration of 230 μM. For co-incubation experiments aliquots (16 μL) of hAChE (final concentration 2.30 μM, Aβ/AChE molar ratio 100:1) and AChE in the presence of 2 μL of the tested inhibitor (final inhibitor concentration 100 μM) in 0.215 M sodium phosphate buffer pH 8.0 solution were added. Blanks containing $A\beta_{1-40}$ alone, human recombinant AChE alone, and $A\beta_{1-40}$ plus tested inhibitors in 0.215 M sodium phosphate buffer (pH 8.0) were prepared. The final volume of each vial was 20 μL. Each assay was run in duplicate. For IC_{50} determination, increasing concentrations of tested inhibitor were used in order to get % inhibition in the range of 20–80%. To quantify amyloid fibril formation, the thioflavin T fluorescence method was then applied.[4] Fluorescence intensities due to β-sheet conformation were monitored for 300

s at λ_{em} = 490 nm (λ_{exc} = 446 nm). The percent inhibition of the AChE-induced aggregation due to the presence of the tested compound was calculated by the following expression: 100 – ($IF_i/IF_o \times 100$) where IF_i and IF_o are the fluorescence intensities obtained for Aβ plus AChE in the presence and in the absence of inhibitor, respectively, minus the fluorescence intensities due to the respective blanks.

AChE-Induced PrP106–126 Aggregation Inhibition Assay. The peptide corresponding to the 106–126 segment (KTNMKHMAG-AAAAGAVVGGLG) of the human prion protein and a scrambled sequence thereof (NGAKALMGGHGATKVMVGAAA) were synthesized using solid-phase chemistry with a 433A instrument (Applied Biosystems). Fmoc (9-fluorenylmethoxycarbonyl) was used as the protective group for amine residues, and 1-hydroxybenzotriazole and *N*,*N*-dicyclohexylcarbodiimide as activators of carboxylic residues. Fluorescent peptides were synthesized using Fmoc-K(methoxycoumarin)-OH and a single coumarin moiety was introduced into K106 and K109 residues in the wild type and scrambled sequences, respectively. Peptides were purified by HPLC as previously described;[5] their purity being always above 99.5%.

Coumarin-PrP106–126 was incubated in 100 mM Tris–HCl, pH 7.0 at a final concentration of 500 μM, in the presence of bovine AChE (Sigma; 2.5 μM) and inhibitors at a concentration of 100 μM, for 48 h at room temperature. Parallel control samples devoid of inhibitors or in the presence of inhibitors without AChE were always run. After incubation for 48 h at room temperature samples were centrifuged at 13,000 × g for 10 min

to separate the aggregates from the soluble peptide[6] and immediately deep-frozen and stored at −20 ºC until analysis. To quantify coumarin-PrP106−126 aggregation, peptide pellets were washed several times with 100 mM TRIS-HCl, pH 7.0, and suspended in 10 μL of the same buffer, placed on gelatin-coated slides and finaly analyzed by fluorescence microscopy (Olympus BXJ1; DAPI filter). Three images of each replicate were selected (at least three experiments were run in triplicate) and the maximum size of aggregates (MSA, μm^2) of each image was determined using a standard-image analysis program (Leica Qwin).[7] This area was used to quantify the inhibitory effect of drugs on the AChE-induced PrP106−126 aggregation (control: PrP106−126 = 2500 ± 275 μm^2; AChE: PrP106−126 + AChE = 50496 ± 498 μm^2). Results are expressed as mean ± S.E.M. of at least three experiments performed in triplicate.

Kinetic Analysis of AChE Inhibition. To obtain estimates of the competitive inhibition constant K_i, reciprocal plots of 1/V versus 1/[S] were constructed at relatively low concentration of substrate (below 0.5 mM). The plots were assessed by a weighted least square analysis that assumed the variance of V to be a constant percentage of V for the entire data set. Slopes of these reciprocal plots were then plotted against the concentration of (−)-**8b** (range 0–2.67 nM) in a weighted analysis and K_i was determined as the intersect on the negative x-axis. Data analysis was performed with GraphPad Prism 4.03 software (GraphPad Software Inc.).

$A\beta_{1-42}$ Self-Aggregation Inhibition Assay. As reported in a previously published protocol,[8] HFIP pretreated $A\beta_{1-42}$ samples (Bachem AG, Switzerland) were first solubilized

with a CH_3CN/0.3 mM Na_2CO_3/250 mM NaOH (48.4:48.4:3.2) mixture to obtain a 500 μM solution. Experiments were performed by incubating the peptide in 10 mM phosphate buffer (pH = 8.0) containing 10 mM NaCl, at 30 °C for 24 h (final Aβ concentration 50 μM) with and without inhibitor (10 μM, Aβ/inhibitor = 5/1). Blanks containing the tested inhibitors were also prepared and tested. To quantify amyloid fibrils formation, the thioflavin T fluorescence method was used.[4] After incubation, samples were diluted to a final volume of 2.0 mL with 50 mM glycine–NaOH buffer (pH 8.5) containing 1.5 μM thioflavin T. A 300-second-time scan of fluorescence intensity was carried out (λ_{exc} = 446 nm; λ_{em} = 490 nm, FP-6200 fluorometer, Jasco Europe), and values at plateau were averaged after subtracting the background fluorescence of 1.5 μM thioflavin T solution. The fluorescence intensities were compared and the percent inhibition due to the presence of the inhibitor was calculated by the following formula: $100 - (IF_i/IF_o \times 100)$ where IF_i and IF_o are the fluorescence intensities obtained for $A\beta_{1-42}$ in the presence and in the absence of inhibitor, respectively.

β-Secretase (BACE-1) Inhibition Assay. BACE-1 (Sigma, Italy) inhibition studies were performed by employing a peptide mimicking APP sequence as substrate (M-2420, Bachem; Switzerland). The following procedure was employed: 5 μL of test compound (or DMSO) were pre-incubated with 175 μL of the enzyme (c=17.2 nM) for 1 h at room temperature. The substrate (3 μM) was then added and left to react for 15 min. The fluorescence signal was read at λ_{em}=405 nm (λ_{exc}=320 nm). The fluorescence intensities with and without inhibitor were compared and the percent inhibition due to the presence of

test compounds was calculated. The % inhibition due to the presence of increasing test compound concentration was calculated from the fluorescence intensities obtained for BACE-1 in the presence and in the absence of inhibitor, respectively.

For compounds that showed fluorescence interferences with the previous assay conditions a different enzyme source and substrate was used for testing the BACE-1 inhibition. In brief, purified Baculovirus-expressed BACE-1 in 50 mM Tris (pH 7.5), 10 % glycerol and rhodamine-derivative substrate (Panvera peptide) were purchased from Invitrogen (Milan, Italy). Stock solutions of the test compounds were prepared in DMSO and diluted with 50 mM sodium acetate buffer (pH 4.5). Specifically, 20 μL of BACE-1 enzyme (11.7 nM, final concentration) were incubated with 20 μL of test compound for 60 min. To start the reaction, 20 μL of Panvera peptide (0.25 μM, final concentration) were added to each well. The mixture was incubated at 37 °C for 60 min. To stop the reaction, 20 μL of BACE-1 stop solution (sodium acetate, 2.5 M) were added to each well. The spectrofluorometric assay was subsequently performed by reading the fluorescence signal at 590 nm. The DMSO concentration in the final mixture was maintained below 5 % (v/v) to guarantee no significant loss of enzyme activity. Additional measurements were performed in the presence of a detergent (CHAPS, 0.1 % w/v) to check for nonspecific effects.[9]

Inhibition curves were obtained for (±)-**7f**, (−)-**8b**, (+)-**8b**, and (±)-**8d**–**f** by plotting the % inhibition versus the logarithm of inhibitor concentration in the assay solution. The linear regression parameters were determined for each curve and the IC_{50} extrapolated (GraphPad

Prism 4.0 GraphPad Software Inc.). To demonstrate inhibition of BACE-1 activity a peptido-mimetic inhibitor (β-secretase inhibitor IV, Calbiochem, UK) was serially diluted into the reactions' wells (IC_{50}=0.013 μM).

***In Vitro* BBB Permeation Assay.** Prediction of the brain penetration was evaluated using a parallel artificial membrane permeation assay (PAMPA-BBB), in a similar manner as described previously.[10–17] Commercial drugs, phosphate buffered saline solution at pH 7.4 (PBS), and dodecane were purchased from Sigma, Aldrich, Acros, and Fluka. Millex filter units (PVDF membrane, diameter 25 mm, pore size 0.45 μm) were acquired from Millipore. The porcine brain lipid (PBL) was obtained from Avanti Polar Lipids. The donor microplate was a 96-well filter plate (PVDF membrane, pore size 0.45 μm) and the acceptor microplate was an indented 96-well plate, both from Millipore. The acceptor 96-well microplate was filled with 170 μL of PBS:EtOH 70:30 and the filter surface of the donor microplate was impregnated with 4 μL of porcine brain lipid (PBL) in dodecane (20 mg mL^{-1}). Compounds were dissolved in PBS:EtOH 70:30 at 100 μg mL^{-1}, filtered through a Millex filter, and then added to the donor wells (170 μL). The donor filter plate was carefully put on the acceptor plate to form a sandwich, which was left undisturbed for 240 min at 25 ºC. After incubation, the donor plate was carefully removed and the concentration of compounds in the acceptor wells was determined by UV spectroscopy. Every sample was analysed at five wavelengths, in four wells and, at least, in three independent runs, and the results are given as the mean ± standard deviation. In each

experiment, 15 quality control standards of known BBB permeability were included to validate the analysis set.

***Ex Vivo* AChE Inhibition Assay.** Groups of 10 OF1 mice were treated i.p. with each compound at 10 μmol kg^{-1}. The animals were sacrificed 20 min later and brains were quickly removed and frozen on dry ice. Residual AChE activitity was determined as previously described by the method of Ellman[3] using brain homogenate preparations as a source of the enzyme. Percent of inhibition was calculated by comparing AChE activity in brain of the drug-treated mice with activity from untreated controls.

The protocol described above was approved by the Animals Ethics Committee of the Universitat Autònoma de Barcelona and comply with the current laws of Spain, which are in accordance with the European Community Council Directive of 24 November 1986 (86/609/EEC). All efforts were made to minimise animal suffering and to reduce the number of animals used.

Molecular Modeling. Molecular Dynamics Simulations. The binding mode of compound (–)-**8b** was explored by means of 34 ns molecular dynamics (MD) simulations performed for their complexes to hAChE. The simulation protocol was based on the computational strategy used in our previous studies,[10,18] which is briefly summarized here. MD simulations were run using the PMEMD module of Amber9[19] and the parm99SB parameters for the protein. Models of the bonded ligands were built up using the X-ray crystallographic structure of the hAChE–*bis*(7)-tacrine complex (PDB code 2CKM).[20] *Bis*(7)-tacrine was removed from the structure and truncated residues were reconstructed.

The enzyme was modeled in its physiological active form with neutral His440 and deprotonated Glu327, which together with Ser200 form the catalytic triad. The standard ionization state at neutral pH was considered for the rest of ionizable residues with the exception of Asp392 and Glu443, which were neutral, and His471, which was protonated, according to previous studies.[21] The charge distribution of the inhibitor was determined by fitting the HF/6-31G(d) electrostatic potential obtained with Gaussian'03[22] and using the RESP procedure.[23] The starting pose of the compounds was built up taking advantage of the known pose of *bis*(7)-tacrine (2CKM)[20] and (–)-huprine X (1E66)[24] in the X-ray crystallographic complex with *Tc*AChE. Six Na^+ cations were added to neutralize the negative charge of the system with the XLEAP module of Amber9.[19] The system was hydrated by centering a octahedron of 12 Å of TIP3P[25] water molecules at the inhibitor, preserving the crystallographic waters inside the binding cavity. The final systems contained the protein–ligand complex, Na^+ cations and around 17000 water molecules.

The geometry of the system was minimized in four steps. First, the position of hydrogen atoms was optimized using 3000 steps of steepest descent algorithm. Then, water molecules were refined through 2000 steps of steepest descent followed by 3000 steps of conjugate gradient. Next, the ligand, water molecules, and counterions were optimized with 2000 steps of steepest descent and 4000 steps of conjugate gradient, and finally the whole system was optimized with 3000 steps of steepest descent and 7000 steps of conjugate gradient. Thermalization of the system was performed in four steps of 25 ps, incrementing the temperature from 100 K up to 298 K. Then, a series of 25 ns trajectories were run for the

two compounds using a time step of 1 fs. SHAKE was used for those bonds containing hydrogen atoms, in conjunction with periodic boundary conditions at constant pressure (1 atm) and temperature (298 K), Particle-Mesh Ewald for the treatment of long-range electrostatic interactions, and a cutoff of 11 Å for nonbonded interactions. The structural analysis was performed using in house software and standard codes (PTRAJ module) of Amber-9.

SIE Calculations. The solvent interaction energies (SIE) technique developed by Purisima and co-workers[26,27] was used to estimate the interaction free energies for the two binding modes of (–)-**8b**. Briefly, the SIE method is formally related to the MM/PBSA strategy, as it estimates the binding free energy by combining the interaction energy between ligand and protein target determined by using a classical force field, and a solvation term calculated by using a continuum model that includes electrostatic and non-electrostatic components. Nevertheless, the method has been carefully parametrized by calibrating those (free) energy contributions in the context of a binding calculation through the inclusion of appropriate parameters chosen to reproduce the absolute binding free energies for a set of protein-ligand complexes. In particular, binding affinities have been estimated using Eq. 1,

$$\Delta G_{binding} = \alpha\left(E_{ele} + E_{vW} + \Delta G^{sol}_{ele} + \Delta G^{sol}_{n-ele}\right) + C \qquad (1)$$

where the terms in parenthesis stand for the electrostatic (E_{ele}) and van der Waals (E_{vW}) components of the ligand–protein interaction energy, the electrostatic term (ΔG^{sol}_{ele}) due to the solvent reaction field, the non-electrostatic (ΔG^{sol}_{n-ele}) component of the solvation free

energy, which is related to the solvent accesible surface (SA; $\Delta G^{sol}_{non-ele} = \gamma \Delta SA$), and the parameters α, γ and C account for the enthalpy–entropy compensation correction (α = 0.1048), the surface tension (γ = 0.0129 kcal mol^{-1} Å^{-2}) and a fitting constant (C = –2.89 kcal mol^{-1}).

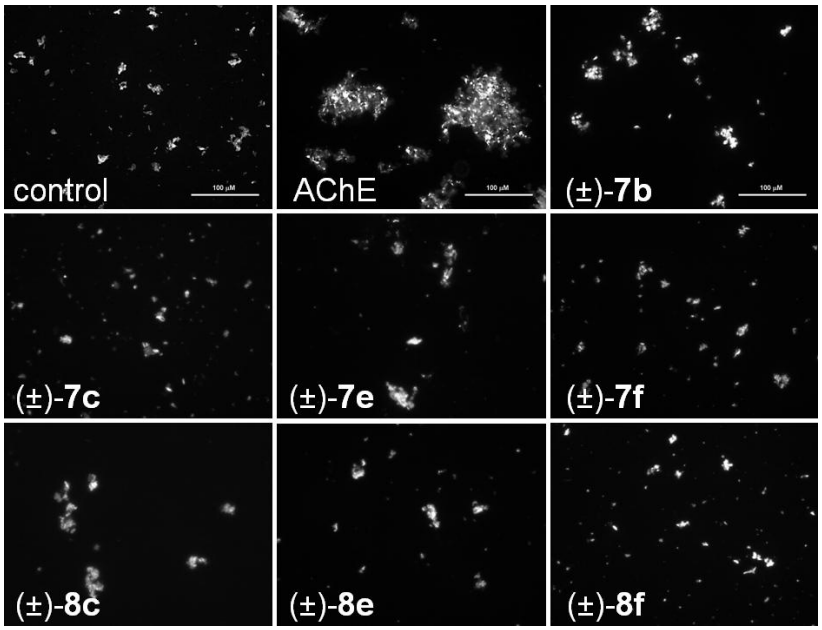

Figure S1. Fluorescence micrographs of aggregates generated in vitro by coumarin-PrP106–126 (500 μM): control, PrP106–126 + AChE (2.5 μM), and PrP106–126 + AChE + inhibitors (100 μM), following 48 h of incubation. Magnification 10×; scale bar 100 μm.

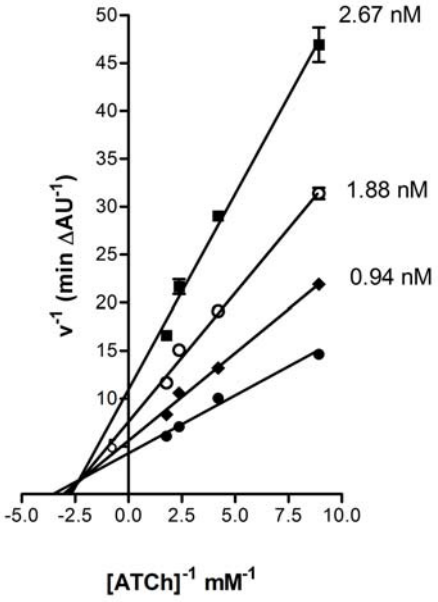

Figure S2. Kinetic study on the mechanism of AChE inhibition by (–)-**8b**. Overlaid Lineweaver-Burk reciprocal plots of AChE initial velocity at increasing substrate concentration (ATCh, <0.5 mM) in the absence of inhibitor and in the presence of (–)-**8b** (0–2.67 nM) are shown. Lines were derived from a weighted least-squares analysis of the data points.

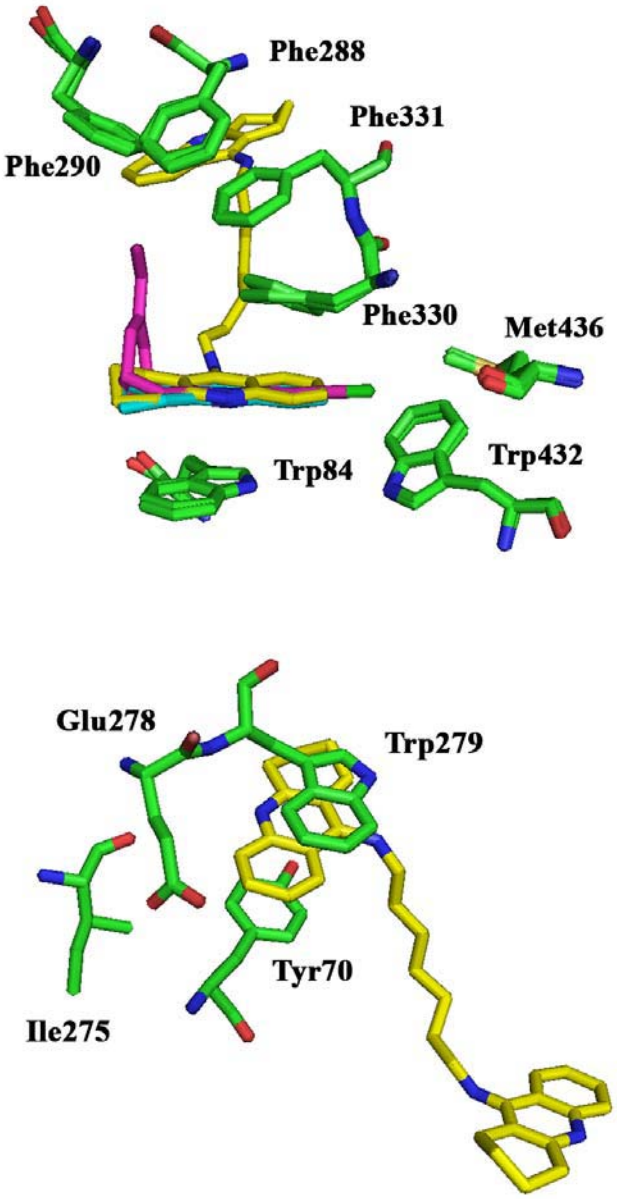

Figure S3. Structural details of the binding mode of *bis*(7)-tacrine (yellow), huprine X (magenta) and tacrine (blue) in their complexes to *Tc*AChE. Selected residues (numbered as found in *Tc*AChE) in the binding site of the enzyme are shown in green.

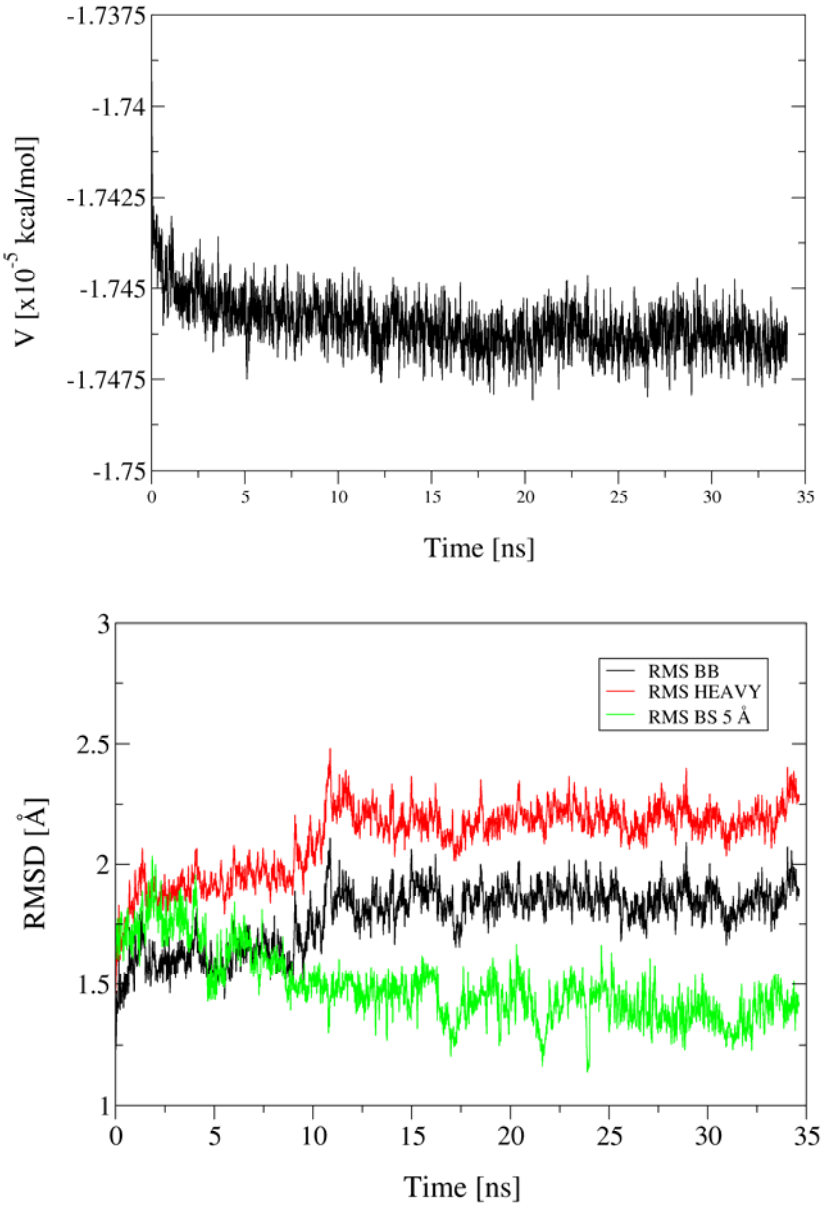

Figure S4. Time evolution of the (top) potential energy and (bottom) RMSD determined for the backbone (BB) atoms, all heavy atoms in the enzyme, and the heavy atoms of the residues that delineate the binding site (BS; defined as the set of residues at less than 5 Å from any atom of the inhibitor) for the binding mode **A** of (–)-**8b**.

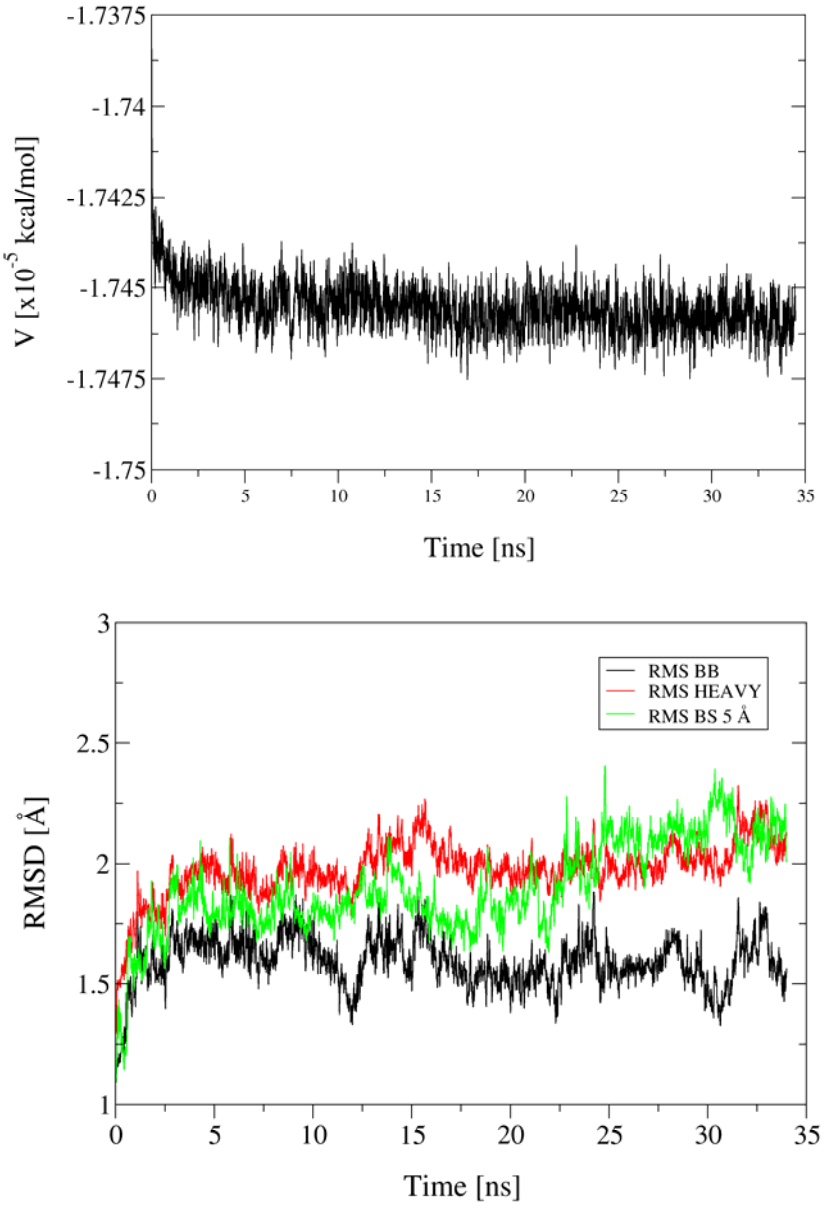

Figure S5. Time evolution of the (*top*) potential energy and (*bottom*) RMSD determined for the backbone (BB) atoms, all heavy atoms in the enzyme, and the heavy atoms of the residues that delineate the binding site (BS; defined as the set of residues at less than 5 Å from any atom of the inhibitor) for the binding mode **B** of (–)-**8b**.

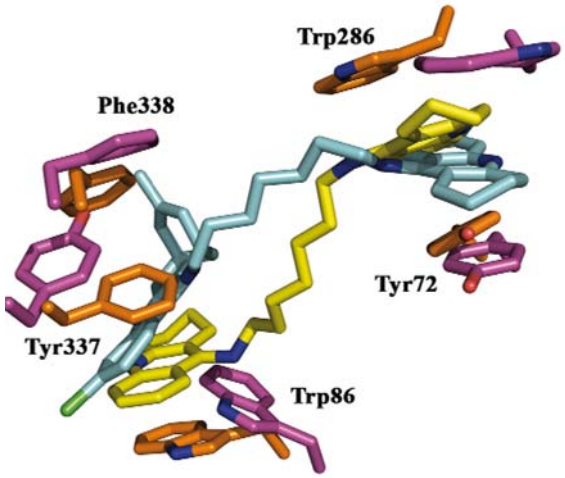

Figure S6. Representation of the binding mode of (–)-**8b** in the catalytic gorge of AChE for the orientation **B** of the 6-chlorotacrine unit in the peripheral site after superposition of the final snapshot of the trajectory (magenta) and the X-ray structure (orange) 2CKM. *Bis*(7)-tacrine is shown in yellow, and (–)-**8b** in cyan. The side chains of selected residues are also shown (hydrogens are omitted for the sake of clarity).

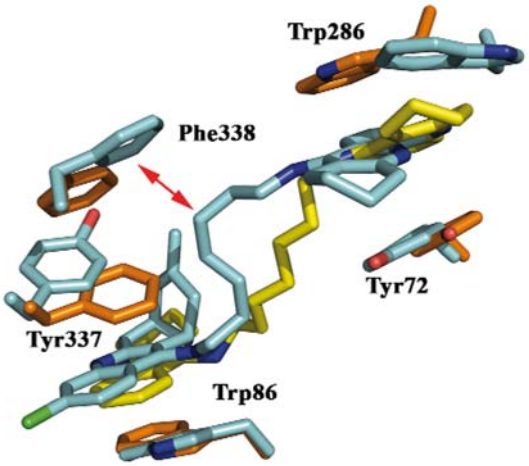

Figure S7. Representation of the binding mode of (–)-**8b** in the catalytic gorge of AChE for the orientation **B** of the 6-chlorotacrine unit in the peripheral site at 20 ns of the trajectory (cyan) and of *bis*(7)-tacrine (yellow) in 2CKM. The side chains of selected residues are also shown (hydrogens are omitted for the sake of clarity). The displacement of the 6-chlorotacrine unit in the peripheral site is propagated to the heptamethylene linker, which adopts a curved fold instead of the rather linear arrangement seen in *bis*(7)-tacrine. As a result, there is steric clash (red arrow) with the side chain of Phe338 (Phe331 in *Tc*AChE; see Figure S3), which changes its orientation, and subsequently affects the stacking of the huprine moiety with Tyr337 (Phe330 in *Tc*AChE; see Figure S3). The stacking with Trp86 (Trp84 in *Tc*AChE; see Figure S3) is still retained at this time (20 ns) of the simulation. However, this interaction is altered at 22 ns and the stacking is lost at 25 ns (the distance between the rings of huprine moiety and Trp86 is close to 6 Å).

In Vitro Blood–Brain Barrier Permeation Assay

Table S1. Permeability (P_e 10^{-6} cm s^{-1})[a] in the PAMPA-BBB Assay for Commercial Drugs (Used in the Experiment Validation), Huprine–Tacrine Heterodimers and Huprine Y with their Predictive Penetration into the CNS.

Commercial drugs	Lit.[b]	P_e (exp.)	Compound	P_e (exp.)	Prediction
Testosterone	17.0	38.9 ± 2.4	(±)-**7a**·2HCl	10.7 ± 0.5	CNS+
Verapamil	16.0	28.3 ± 2.1	(±)-**7b**·2HCl	12.5 ± 0.8	CNS+
Imipramine	13.0	22.3 ± 1.2	(±)-**7c**·3HCl	11.4 ± 0.4	CNS+
Desipramine	12.0	24.4 ± 2.3	(±)-**7d**·2HCl	10.2 ± 0.5	CNS+
Progesterone	9.3	26.1 ± 2.4	(±)-**7e**·2HCl	6.0 ± 0.3	CNS+/–
Promazine	8.8	22.4 ± 1.5	(±)-**7f**·2HCl	16.3 ± 1.5	CNS+
Chlorpromazine	6.5	13.6 ± 0.9	(±)-**8a**·2HCl	12.0 ± 0.7	CNS+
Clonidine	5.3	14.1 ± 0.8	(±)-**8b**·2HCl	20.9 ± 0.5	CNS+
Corticosterone	5.1	6.4 ± 0.3	(±)-**8c**·3HCl	7.0 ± 0.6	CNS+/–
Piroxicam	2.5	3.0 ± 0.2	(±)-**8d**·2HCl	21.1 ± 1.2	CNS+
Hydrocortisone	1.9	4.9 ± 0.2	(±)-**8e**·2HCl	15.6 ± 0.1	CNS+
Caffeine	1.3	4.4 ± 0.3	(±)-**8f**·2HCl	29.1 ± 2.0	CNS+
Lomefloxacin	1.1	2.8 ± 0.1	(±)-huprine Y·HCl	18.2 ± 0.1[b]	CNS+
Enoxacin	0.9	4.2 ± 0.3			
Ofloxacin	0.8	2.6 ± 0.1			

[a] Values are expressed as the mean ± standard deviation of three independent experiments. Heterodimers dissolved in PBS:EtOH 70:30. [b] Taken from ref. 12, compound dissolved in PBS:EtOH 80:20.

Assay validations were made by comparing the experimental permeability of commercial drugs with reported values, which gave a good linear correlation in each case (Figure S8).

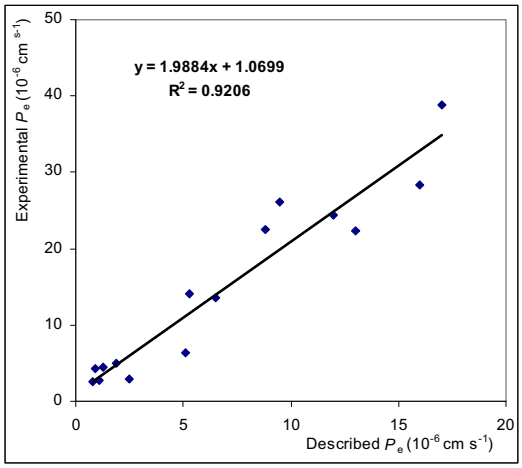

Figure S8. Linear correlation between experimental and reported permeability of commercial drugs using the PAMPA-BBB assay with PBS:EtOH 70:30.

From this straight-line equation and taking into account the limits established by Di *et al.* for BBB permeation,[12] we established the ranges of permeability for these assays as shown in Table S2.

Table S2. Ranges of Permeability of PAMPA-BBB Assay, using PBS:EtOH 70:30 (P_e, 10^{-6} cm s^{-1}).

	P_e (10^{-6} cm s^{-1})
Compounds of high BBB permeation (CNS+)	$P_e > 9.0$
Compounds of uncertain BBB permeation (CNS+/–)	$9.0 > P_e > 5.1$
Compounds of low BBB permeation (CNS–)	$P_e < 5.1$

References

(1) Camps, P.; Contreras, J.; Font-Bardia, M.; Morral, J.; Muñoz-Torrero, D.; Solans, X. Enantioselective synthesis of tacrine–huperzine A hybrids. Preparative chiral MPLC separation of their racemic mixtures and absolute configuration assignments by X-ray diffraction analysis. *Tetrahedron: Asymmetry* **1998**, *9*, 835–849.

(2) Camps, P.; Formosa, X.; Muñoz-Torrero, D.; Petrignet, J.; Badia, A.; Clos, M. V. Synthesis and pharmacological evaluation of huprine–tacrine heterodimers: Subnanomolar dual binding site acetylcholinesterase inhibitors. *J. Med. Chem.* **2005**, *48*, 1701–1704.

(3) Ellman, G. L.; Courtney, K. D.; Andres, V., Jr.; Featherstone, R. M. A new and rapid colorimetric determination of acetylcholinesterase activity. *Biochem. Pharmacol.* **1961**, *7*, 88–95.

(4) Bartolini, M.; Bertucci, C.; Cavrini, V.; Andrisano, V. β-Amyloid aggregation induced by human acetylcholinesterase: Inhibition studies. *Biochem. Pharmacol.* **2003**, *65*, 407–416.

(5) De Gioia, L.; Selvaggini, C.; Ghibaudi, E.; Diomede, L.; Bugiani, O.; Forloni, G.; Tagliavini, F.; Salmona, M. Conformational polymorphism of the amyloidogenic and neurotoxic peptide homologous to residues 106–126 of the prion protein. *J. Biol. Chem.* **1994**, *269*, 7859–7862.

(6) Selvaggini, C.; De Gioia, L.; Cantu, L.; Ghibaudi, E.; Diomede, L.; Passerini, F.; Forloni, G.; Bugiani, O.; Tagliavini, F.; Salmona, M. Molecular characteristics of a protease-resistant, amyloidogenic and neurotoxic peptide homologous to residues 106–126 of the prion protein. *Biochem. Biophys. Res. Commun.* **1993**, *194*, 1380–1386.

(7) Pera, M.; Román, S.; Ratia, M.; Camps, P.; Muñoz-Torrero, D.; Colombo, L.; Manzoni, C.; Salmona, M.; Badia, A.; Clos, M. V. Acetylcholinesterase triggers the aggregation of PrP 106–126. *Biochem. Biophys. Res. Commun.* **2006**, *346*, 89–94.

(8) Bartolini, M.; Bertucci, C.; Bolognesi, M. L.; Cavalli, A.; Melchiorre, C.; Andrisano, V. Insight into the kinetic of amyloid beta (1–42) peptide self-aggregation: Elucidation of inhibitors' mechanism of action. *ChemBioChem* **2007**, *8*, 2152–2161.

(9) Ryan, A. J.; Gray, N. M.; Lowe, P. N.; Chung, C. W. Effect of detergent on "promiscuous" inhibitors. *J. Med. Chem.* **2003**, *46*, 3448–3451.

(10) Viayna, E.; Gómez, T.; Galdeano, C.; Ramírez, L.; Ratia, M.; Badia, A.; Clos, M. V.; Verdaguer, E.; Junyent, F.; Camins, A.; Pallàs, M.; Bartolini, M.; Mancini, F.; Andrisano, V.; Arce, M. P.; Rodríguez-Franco, M. I.; Bidon-Chanal, A.; Luque, F. J.; Camps, P.; Muñoz-Torrero, D. Novel huprine derivatives with inhibitory activity toward β-amyloid aggregation and formation as disease-modifying anti-Alzheimer drug candidates. *ChemMedChem* **2010**, *5*, 1855–1870.

(11) Camps, P.; Formosa, X.; Galdeano, C.; Muñoz-Torrero, D.; Ramírez, L.; Gómez, E.; Isambert, N.; Lavilla, R.; Badia, A.; Clos, M. V.; Bartolini, M.; Mancini, F.; Andrisano, V.; Arce, M. P.; Rodríguez-Franco, M. I.; Huertas, O.; Dafni, T.; Luque, F. J. Pyrano[3,2-*c*]quinoline−6-chlorotacrine hybrids as a novel family of acetylcholinesterase and β-amyloid-directed anti-Alzheimer compounds. *J. Med. Chem.* **2009**, *52*, 5365−5379.

(12) Di, L.; Kerns, E. H.; Fan, K.; McConnell, O. J.; Carter, G. T. High throughput artificial membrane permeability assay for blood−brain barrier. *Eur. J. Med. Chem.* **2003**, *38*, 223−232.

(13) Rodríguez-Franco, M. I.; Fernández-Bachiller, M. I.; Pérez, C.; Hernández-Ledesma, B.; Bartolomé, B. Novel tacrine−melatonin hybrids as dual-acting drugs for Alzheimer disease, with improved acetylcholinesterase inhibitory and antioxidant properties. *J. Med. Chem.* **2006**, *49*, 459−462.

(14) Fernández-Bachiller, M. I.; Pérez, C.; Campillo, N. E.; Páez, J. A.; González-Muñoz, G. C.; Usán, P.; García-Palomero, E.; López, M. G.; Villarroya, M.; García, A. G.; Martínez, A.; Rodríguez-Franco, M. I. Tacrine–melatonin hybrids as multifunctional agents for Alzheimer's disease, with cholinergic, antioxidant, and neuroprotective properties. *ChemMedChem* **2009**, *4*, 828−841.

(15) Marco-Contelles, J.; León, R.; de los Ríos, C.; Samadi, A.; Bartolini, M.; Andrisano, V.; Huertas, O.; Barril, X.; Luque, F. J.; Rodríguez-Franco, M. I.; López, B.; López, M. G.; García, A. G.; Carreiras, M. C.; Villarroya, M. Tacripyrines, the first tacrine−dihydropyridine hybrids, as multitarget-directed ligands for the treatment of Alzheimer's disease. *J. Med. Chem.* **2009**, *52*, 2724−2732.

(16) Arce, M. P.; Rodríguez-Franco, M. I.; González-Muñoz, G. C.; Pérez, C.; López, B.; Villarroya, M.; López, M. G.; García, A. G.; Conde, S. Neuroprotective and cholinergic properties of multifunctional glutamic acid derivatives for the treatment of Alzheimer's disease. *J. Med. Chem.* **2009**, *52*, 7249−7257.

(17) Fernández-Bachiller, M. I.; Pérez, C.; González-Muñoz, G. C.; Conde, S.; López, M. G.; Villarroya, M.; García, A. G.; Rodríguez-Franco, M. I. Novel tacrine–8-hydroxyquinoline hybrids as multifunctional agents for the treatment of Alzheimer's disease, with neuroprotective, cholinergic, antioxidant, and copper-complexing properties. *J. Med. Chem.* **2010**, *13*, 4927−4937.

(18) Camps, P.; Formosa, X.; Galdeano, C.; Gómez, T.; Muñoz-Torrero, D.; Scarpellini, M.; Viayna, E.; Badia, A.; M. V. Clos, M. V.; Camins, A.; Pallàs, M.; Bartolini, M.; Mancini, F.; Andrisano, V.; Estelrich, J.; Lizondo, M.; Bidon-Chanal, A.; Luque, F. J. Novel donepezil-based inhibitors of acetyl- and butyrylcholinesterase and acetylcholinesterase-induced β-amyloid aggregation. *J. Med. Chem*. **2008**, *51*, 3588−3598.

(19) AMBER, version 9; Case, D. A.; Darden, T. A.; Cheatham, T. E. III; Simmerling, C.L.; Wang, J.; Duke, R. E.; Luo, R.; Merz, K. M.; Pearlman, D.A.; Crowley, M.; Walker, R. C.; Zhang, W.; Wang, B.; Hayik, S; Roitberg, A.; Seabra, G.; Wong, K.

F.; Paesani, F.; Wu, X.; Brozell, S.; Tsui, V.; Gohlke, H.; Yang, L.; Tan, C.; Mongan, J.; Hornak, V.; Cui, G.; Beroza, P.; Mathews, D. H.; Schafmeister, C.; Ross, W. S.; Kollman, P. A. University of California: San Francisco, 2006.

(20) Rydberg, E. H.; Brumshtein, B.; Greenblatt, H. M.; Wong, D. M.; Shaya, D.; Williams, L. D.; Carlier, P. R.; Pang, Y.-P.; Silman, I.; Sussman, J. L. Complexes of alkylene-linked tacrine dimers with *Torpedo californica* acetylcholinesterase: Binding of bis(5)-tacrine produces a dramatic rearrangement in the active site gorge. *J. Med. Chem.* **2006**, *49*, 5491–5500.

(21) Wlodek, S. T.; Antosiewicz, J.; McCammon, J. A.; Straatsma, T. P.; Gilson, M. K.; Briggs, J. M.; Humblet, C.; Sussman, J. L. Binding of tacrine and 6-chlorotacrine to acetylcholinesterase. *Biopolymers* **1996**, *38*, 109–117.

(22) Gaussian 03; Revision B.04; Frisch, M. J.; Trucks, G. W.; Schlegel, H. B.; Scuseria, G. E.; Robb, M. A.; Cheeseman, J. R.; Montgomery, J. A., Jr.; Vreven, T.; Kudin, K. N.; Burant, J. C.; Millam, J. M.; Iyengar, S. S.; Tomasi, J.; Barone, V.; Mennucci, B.; Cossi, M.; Scalmani, G.; Rega, N.; Petersson, G. A.; Nakatsuji, H.; Hada, M.; Ehara, M.; Toyota, K.; Fukuda, R.; Hasegawa, J.; Ishida, M.; Nakajima, T.; Honda, Y.; Kitao, O.; Nakai, H.; Klene, M.; Li, X.; Knox, J. E.; Hratchian, H. P.; Cross, J. B.; Adamo, C.; Jaramillo, J.; Gomperts, R.; Stratmann, R. E.; Yazyev, O.; Austin, A. J.; Ortiz, J. V.; Cui, Q.; Baboul, A. G.; Clifford, S.; Cioslowski, J.; Stefanov, B. B.; Liu, G.; Liashenko, A.; Piskorz, P.; Komaromi, I.; Martin, R. L.; Fox, D. J.; Keith, T.; Al-Laham, M. A.; Peng, C. Y.; Nanayakkara, A.; Challacombe, M.; Gill, P. M. W.; Johnson, B.; Chen, W.; Wong, M. W.; Gonzalez, C.; Pople, J. A. Gaussian, Inc., Pittsburgh PA, 2003.

(23) Bayly, C. I.; Cieplak, P.; Cornell, W.; Kollman, P. A. A well-behaved electrostatic potential based method using charge restraints for deriving atomic charges: the RESP model. *J. Phys. Chem.* **1993**, *97*, 10269–10280.

(24) Dvir, H.; Wong, D. M.; Harel, M.; Barril, X.; Orozco, M.; Luque, F. J.; Muñoz-Torrero, D.; Camps, P.; Rosenberry, T. L.; Silman, I.; Sussman, J. L. 3D Structure of *Torpedo californica* acetylcholinesterase complexed with huprine X at 2.1 Å resolution: Kinetic and molecular dynamics correlates. *Biochemistry* **2002**, *41*, 2970–2981.

(25) Jorgensen, W. L.; Chandrasekhar, J.; Madura, J. D.; Impey, R. W.; Klein, M. L. Comparison of simple potential functions for simulating liquid water. *J. Chem. Phys.* **1983**, *79*, 926–935.

(26) Naïm, M.; Bhat, S.; Rankin, K. N.; Dennis, S.; Chowdhury, S. F.; Siddiqi, I.; Drabik, P.; Sulea, T.; Bayly, C. I.; Jakalian, A.; Purisima, E. O. Solvated interaction energy (SIE) for scoring protein-ligand binding affinities. 1. Exploring the parameter space. *J. Chem. Inf. Model*. **2007**, *47*, 122–133.

(27) Cui, Q.; Sulea, T.; Schrag, J. D.; Munger, C.; Hung, M.-N.; Nam, M.; Cygler, M.; Purisima, E. O. Molecular dynamics-solvated interaction energy studies of protein-protein interactions: the MP1- p14 scaffolding complex. *J. Mol. Biol.* **2008**, *379*, 787–802.

Appendix

Compound	Molecular Formula	Calculated				Found			
		C	H	N	Cl	C	H	N	Cl
4e·HBr·1/2H_2O	$C_{22}H_{31}BrN_2$·HBr·1/2H_2O	53.56	6.74	5.68		53.84	7.13	5.68	
4f·HBr	$C_{23}H_{33}BrN_2$·HBr	55.43	6.88	5.62		55.20	6.85	5.51	
5e·0.9HBr	$C_{22}H_{30}BrClN_2$·0.9HBr	51.74	6.10	5.49		51.81	6.46	5.46	
5f·HBr·3/4H_2O	$C_{23}H_{32}BrClN_2$·HBr·3/4H_2O	50.57	6.37	5.13		50.44	6.44	4.98	
(−)-**7b**·2HCl·2.75H_2O	$C_{37}H_{43}ClN_4$·2HCl·2.75H_2O	63.33	7.25	7.98	15.16	63.28	6.84	7.88	15.53
(+)-**7b**·2HCl·2H_2O	$C_{37}H_{43}ClN_4$·2HCl·2H_2O	64.58	7.18	8.14	15.45	64.36	6.81	8.01	15.66
(±)-**7e**·2HCl·H_2O	$C_{39}H_{47}ClN_4$·2HCl·H_2O	67.09	7.36	8.02	15.23	66.72	7.23	7.76	15.21
(±)-**7f**·2HCl·2H_2O	$C_{40}H_{49}ClN_4$·2HCl·2H_2O	65.79	7.59	7.67	14.56	65.75	7.45	7.53	14.84
(−)-**8b**·2HCl·1.5H_2O	$C_{37}H_{42}Cl_2N_4$·2HCl·1.5H_2O	62.28	6.64	7.85	19.87	62.09	6.48	7.68	20.08
(+)-**8b**·2HCl·1.5H_2O	$C_{37}H_{42}Cl_2N_4$·2HCl·1.5H_2O	62.28	6.64	7.85	19.87	62.22	6.56	7.56	19.91
(±)-**8e**·2HCl·H_2O	$C_{39}H_{46}Cl_2N_4$·2HCl·H_2O	63.94	6.88	7.65	19.36	63.65	6.68	7.55	20.09
(±)-**8f**·2HCl·4H_2O	$C_{40}H_{48}Cl_2N_4$·2HCl·4H_2O	60.00	7.30	7.00	17.71	59.66	6.94	6.82	18.32

Resum i conclusions

Capítol 3. Síntesi d'híbrids donepezil–tacrina com a agents anticolinesteràsics i antiagregants del pèptid βA. *(J. Med. Chem.* **2008,** *51,* 3588–3598).

1. S'han resintetitzat els híbrids donepezil–tacrina **20a**,**b**–**22a**,**b** utilitzant una metodologia basada en l'aminació de les 4-cloroquinolines **23** i **24** amb el corresponent aminoalcohol, seguit de conversió dels alcohols **26a**,**b** i **27a**,**b** en els seus mesilats, i la seva reacció amb les piperidines **30** o **31**. Les dues primeres etapes tenen lloc amb excel·lents rendiments i no impliquen purificació cromatogràfica. No obstant, els rendiments de l'última etapa són de baixos a moderats i l'aïllament dels productes finals requereix una tediosa purificació per cromatografía en columna. Respecte a la metodologia posada a punt prèviament en el grup, s'ha millorat l'aïllament dels alcohols intermedis, a través d'extraccions àcid–base en lloc d'eliminar per microdestil·lació a pressió reduïda l'excés de l'aminoalcohol i el 1-pentanol usat com a dissolvent en la reacció d'obtenció dels mateixos. A més, s'ha duplicat el rendiment global d'obtenció de dos dels heterodímers i s'ha desenvolupat un mètode de síntesi alternatiu de la piperidina **31**, independent de la donació externa de donepezil que en els treballs inicials havia possibilitat la síntesi de les piperidines **30** i **31**.

2. S'ha desenvolupat una via alternativa d'accés als híbrids donepezil–tacrina **22a** i **22b** basada en l'alquilació inicial de la piperidina **31** amb 2-bromoetanol o 3-cloro-1-propanol, seguit de conversió de l'alcohol resultant en el corresponent cloroderivat, el qual s'ha d'aïllar sense tractament bàsic en el final de reacció, i alquilació final de la 6-clorotacrina amb aquest cloroderivat cru. Aquesta via no funciona quan el fragment derivat del donepezil presenta un sistema d'indanona. Els rendiments globals d'obtenció dels híbrids **22a** i **22b** són una mica més baixos que els obtinguts a través de la via anterior.

Capítol 4. Disseny, síntesi i avaluació farmacològica d'híbrids pirano[3,2-c]quinolina–6-clorotacrina com a una nova família de compostos anti–Alzheimer. (*J. Med. Chem* **2009**, *52,* 5365–5379).

1. S'han dissenyat i sintetitzat dues sèries d'híbrids d'estructura general **64** i **65**, que presenten una unitat de 6-clorotacrina unida amb un sistema tricíclic reminiscent del propidi, a través d'un *linker* de longitud variable que conté un grup amido. Aquests compostos s'han obtingut per reacció de les aminoalquiltacrines **50** amb els àcids carboxílics **66**·HCl i **67**·HCl. Les aminoalquiltacrines **50** s'han preparat amb rendiments de moderats a bons, seguint un procediment descrit basat en l'aminació de 6,9-dicloro-1,2,3,4-tetrahidroacridina, **24**, amb α,ω-diaminoalcans comercials, **62**, mentre que els àcids **66**·HCl i **67**·HCl s'han preparat per hidròlisi bàsica dels nous èsters **44** i **45** prèviament sintetitzats pel grup de recerca del Dr. Rodolfo Lavilla. Tot i que la seqüència de síntesi dels nous híbrids és curta, els baixos rendiments sobretot de l'última etapa, així com la tediosa purificació dels productes finals per cromatografia en columna a través de gel de sílice, fan difícil accedir a quantitats importants de **64c**–**g** i **65a-e 64**.

2. L'avaluació farmacològica dels nous híbrids sintetitzats (**64c**–**g i 65a-e**) va ser realitzada per mi mateix al laboratori dels Profs. Albert Badia i Victòria Clos de la Universitat Autònoma de Barcelona, posant de manifest que aquests compostos són potents inhibidors de l'AChE bovina i humana (IC_{50} en el rang nanomolar baix), mentre que no són gaire potents enfront la BChE. Tots els híbrids assajats són inhibidors molt més potents de l'AChE bovina i humana que els èsters **44** i **45** (assajats com a models d'interacció amb el lloc perifèric de l'enzim) i d'activitat comparable a 6-clorotacrina (model d'interacció amb el lloc actiu). Així, la incorporació del fragment tricíclic dels èsters **44** i **45** en els híbrids **64c**–**g** i **65a-e** no comporta una pèrdua significativa de potència inhibitòria respecte a la 6-clorotacrina. Els híbrids **65a-e** són lleugerament menys potents que els híbrids **64c**–**g** enfront a la BChE, pero més potents enfront a l'hAChE. En cap cas el desplaçament en dues unitats del grupo amido en el *linker* de **65a-e** respecte **64c**–**g** produeix un augment de potència tant important com l'observat en els compostos relacionats desenvolupats per la Dra. Ana Martínez (Instituto de Química Mèdica, Madrid).

Capítol 5. Estudis de modelatge molecular d'híbrids donepezil–huprina amb activitat inhibitòria enfront la formació i l'agregació del pèptid βA. (*ChemMedChem* **2010**, *5*, 1855–1879).

1. Els estudis de modelatge molecular dels híbrids (–)-**68a** i (–)-**68b** han confirmat el seu caràcter d'inhibidors de lloc d'unió dual, justificant la seva elevada potència inhibitòria no només per la interacció amb el centre actiu i el lloc perifèric, sinó també per interaccions addicionals amb residus de la gorja catalítica de l'AChE. Les porcions de dimetoxiindà i aminoquinolina estableixen interaccions de tipus π-stacking amb els sistemes d'indol dels residus de triptòfan característics del lloc perifèric i del lloc actiu. La variació de la cadena espaiadora de dos a tres metilens comporta una variació en el mode d'unió a l'enzim. Així, en (–)-**68b** l'addició d'un grup metilè en el *linker* permet l'enfocament de l'anell de piperidina al grup carboxilat de l'Asp74, donant lloc a una interacció per pont salí, interacció que no existeix amb (–)-**68a.**

2. El canvi d'energia lliure d'unió estimat amb càlculs d'integració termodinàmica permet racionalitzar la diferència en l'afinitat d'unió entre els híbrids substituïts amb metil i etil. Així, la conversió de metil de (–)-**68a** i (–)-**68b** a etil de (–)-**69a** i (–)-**69b** disminueix l'afinitat d'unió per l'enzim en 0,4 i 0,3 kcal mol^{-1}, respectivament, resultats que convergeixen amb les dades experimentals.

Capítol 6. Síntesi i modelatge molecular d'híbrids huprina–tacrina com a compostos anti-amilodiogènics amb potencial interès enfront la malaltia d'Alzheimer i les malalties priòniques. *(J. Med. Chem.* **2012**, *55*, 661–669).

1. S'ha preparat la huprina Y, (±)-**15**, en forma racèmica i en quantitat suficient, seguint la metodologia desenvolupada pel nostre grup però introduint petites modificacions, especialment a nivell de purificació, per simplificar el procés. S'han trobat unes condicions de cristal·lització que han permès obtenir la huprina Y pura amb rendiment moderat, permetent la seva preparació amb una única purificació per cromatografia en columna per a l'obtenció de l'enona (±)-**79**.

2. S'han obtingut els dos enantiòmers de la huprina Y en forma enantiopura a escala multigram mitjançant resolució cromatogràfica del compostos racèmics per MPLC quiral. L'excés enantiomèric de les fraccions obtingudes per MPLC quiral s'ha determinat mitjançant l'aplicació d'un mètode analític desenvolupat per a HPLC quiral.

3. S'han sintetitzat els híbrids huprina–tacrina (7*S*,11*S*)-**70b**, (7*R*,11*R*)-**70b**, (7*S*,11*S*)-**71b** i (7*R*,11*R*)-**71b** en forma enantiopura, en tots els casos en quantitat suficient per a la seva caracterització química i farmacològica.

4. El mecanisme d'acció de l'heterodímer huprina**–**tacrina (–)-**71b** amb l'AChE ha estat estudiat mitjançant simulacions de DM que han confirmat el seu caràcter d'inhibidors de lloc d'unió dual. Pel que fa a la interacció amb el lloc perifèric de l'enzim, es van considerar dues orientacions diferents que es diferencien per la rotació de 180 ^{0} al voltant de l'eix N---N de l'anell central de la unitat de 6-clorotacrina de (–)-**71b.** Tant l'estabilitat estructural al llarg de la simulació de DM com l'afinitat d'unió estimada amb càlculs SIE reforcen un mode d'unió on l'àtom de clor de la unitat de 6-clorotacrina està exposat directament al solvent.

Bibliografia

1. Alzheimer A. *Allegemeine Zeitschrift für Psychiatrie und Psychisch-Gerichtliche Medizin* **1907**, *64*, 146.
2. Launer, L.J.; Fratiglioni, L.; Andersen, K.; Breteler, M.M.B.; Copeland, R.J.M.; Dartigues, J.-F.; Lobo, A.; Martinez-Lage, J.; Soininen, H.; Hofman, A. En "*Alzheimer's Disease and Related Disorders: Etiology, Pathogenesis and Therapeutics*"; Iqbal, K.; Swaab, D.F.; Winblad, B.; Wisniewski, H.M. Eds. John Wiley & Sons, New York, **1999**.
3. Alzheimer's Disease International. *World Alzheimer Report: The benefits of early diagnosis and intervention* **2011**.
4. Walsh, D.M.; Selkoe, D.J. *Neuron* **2004**, *44*, 181.
5. Cummings, J.L.; Askin-Edgar, S. *CNS Drugs* **2000**, *13*, 385.
6. Leonard, B.E. *Hum. Psychopharmacol.* **1998**, *13*, 83.
7. Lahiri, D.K.; Farlow, M.R.; Sambamurti, K.; Greig, N.H.; Giacobini, E.; Schneider, L.S. *Curr. Drug Targets* **2003**, *4*, 97.
8. Goate, A.; Chartier-Harlin, N.C.; Mullan, M.; Brown, J.; Crawford, F.; Fidani, L.; Giuffra, L.; Haynes, A.; Irving, N.; James, L.; Mant, R.; Newton, P.; Rooke, K.; Roques, P.; Talbot, C.; Pericak-Vance, M.; Roses, A.; Williamson, R.; Rossor, M.; Owen, M.; Hardy, J. *Nature* **1991**, *349*, 704.
9. Sherrington, R.; Rogaev, E.I.; Liang, Y.; Rogaeva, E.A.; Levesque, G.; Ikeda, M.; Chi, H.; Lin, C.; Li, G.; Holman, K.; Tsuda, T.; Mar, L.; Foncin, J.-F.; Bruni, A.C.; Montesi, M.P.; Sorbi, S.; Rainero, I.; Pinessi, L.; Nee, L.; Chumakov, I.; Pollen, D.; Brookes, A.; Sanseau, P.; Polinsky, R.J.; Wasco, W.; Da Silva, H.A.R.; Haines, J.L.; Pericak-Vance, M.A.; Tanzi, R.E.; Roses, A.D.; Fraser, P.E.; Rommens, J.M.; St Geroge-Hyslop, P.H. *Nature* **1995**, *375*, 754.
10. Levy-Lehad, E.; Wijsman, E.M.; Nemens, E.; Anderson, A.L.; Goddard, K.A.B.; Weber, J.L.; Bird, T.D.; Schellenberg, G.D. *Science* **1995**, *269*, 970.
11. Klafki, H-W.; Staufenbiel, M.; Kornhuber, J.; Wiltfang, J. *Brain* **2006**, *129*, 743.
12. Castellani, R.J.; Zhu, X.; Lee, H-G.; Moreira, P.I.; Perry, G.; Smith, M.A. *Expert Rev. Neurother*. **2007**, 7, 473.
13. Hardy, J.; Allsop, D.; *Trends Pharm. Sci*. **1991**, *12*, 383.
14. Hardy, J. *Curr. Alzheimer Res*. **2006**, *3*, 71.
15. Coughlan, C.M.; Breen, K.C; *Pharmacol. Therapeut* **2000**, *86*, 111.
16. Inestrosa, N.C., *Las incomunicaciones del Alzheimer*, Atenea Impresores Ltda. **2007**.
17. Goedert, M. *Trends Neurosci.* **1993**, *16,* 460.
18. Schubert, S.; Behl, C.; Lesley, R.; Brack, A.; Dargusch, R.; Sagara, Y.; Kumura, H. *Proc. Natl. Acad. Sci. USA* **1995**, *92*, 1989.
19. Olanow, C.W. *Trends Neurosci.* **1993**, *16*, 439.
20. Eikelenboom, P.; Zhan, S.-S.; van Gool, W.A.; Allsop, D. *Trends Pharmacol. Sci.* **1994**, *15*, 447.
21. Melnikova, I. *Nat. Rev. Drug Discovery* **2007**, *6*, 341.
22. Skovronsky, D.M.; Lee, V.M.-Y.; Trojanowski, J.Q. *Annu. Rev. Pathol. Mech. Dis*. **2006**, *1*, 151.
23. Yamin, G.; Ono, K.; Inayathullah, M.; Teplow, D.B. *Curr. Pharm. Design* ***2008***, *14*, 3231.
24. Ghosh, A.K.; Gemma, S.; Tang, J. *Neurotherapeutics* **2008**, *5*, 399.
25. Silvestri R. *Med. Res. Rev.* **2009**, *29*, 295.
26. Buee, L.; Bussiere, T.; Buee-Scherrer, V.; Delacourte, A.; Hof, P.R. *Brain Res. Rev.* **2000**, *33*, 95.
27. Carreiras, M.C.; Marco, J.L.; *Curr. Pharm. Design* **2004**, *10*, 3167.
28. Saura, J.; Luque, J.L.; Cesura, A.M.; Da Prada, M.; Chan-Palay, V.; Huber, G.; Loffler, J.; Richards, J.G. *Neurosci.* **1994**, *62*, 15.
29. Good, P.F.; Werner, P.; Hsu, A.; Olanow, C.W.; Perl, D.P. *Am. J. Pathol.* **1996**, *149*, 21.
30. Ebadi, M.; Sharma, S.; Shavadi, S.; El Refaey, K. *J. Neurosci. Res.* **2002**, *67*, 285.
31. Rogawski, M.A. *Amino Acids* **2000**, *19*, 133.
32. Cutler, N.R.; Sramek, J.J. *Prog. Neuro-Psychopharmacol. Biol. Psychiat.* **2001**, *25*, 27.
33. D. Knopman, *Clin. Neuropharmacol.* **2003**, *26*, 93-101.
34. Youdim, M.B.; Buccafusco, J. J. *Trends Pharmacol. Sci.* **2005**, *26*, 27.
35. Camps, P.; Muñoz-Torrero, D. *Mini-Rev. Med. Chem* **2002**, *2*, 11.
36. Sussman, J.L.; Harel, M.; Frolow, F.; Oefner, C.; Goldman, A.; Toker, L.; Silman, I. *Science* **1991**, *253*, 872
37. Harel, M.; Schalk, I.; Ehret-Sabatier, L.; Bouet, F.; Goeldner, M.; Hirth, C.; Axelsen, P.; Silman, I.; Sussman, J.L. *Proc. Natl. Acad. Sci. U.S.A.* **1993**, *90*, 9031.
38. Greenblatt, H.M.; Kryger, G.; Lewis, T.; Silman, I.; Sussman, J. *FEBS Lett.* **1999**, *463*, 321.
39. Giacobini, E. *Neurochem. Res.* **2000**, *25*, 1185.

40. Muñoz-Torrero, D. *Neuroprotección en la enfermedad de Alzheimer*; Edicomplet **2007**, Madrid.
41. Akaike, A. *Alzheimer Dis. Assoc. Disord.* **2006**, *20(Suppl. 1)*, S8.
42. Geerts, H. *Brain. Res. Bull.* **2005**, *64*, 519.
43. Akasofu, S.; Kimura, M.; Kosasa, T.; Ogura, H.; Sawada, K. *Eur. J. Pharmacol.* **2006**, *530*, 215.
44. Kimura, M.; Akasofu, S.; Ogura, H.; Sawada, K. *Brain Res.* **2005**, *1047*, 72.
45. Kimura, M.; Komatsu, H.; Ogura, H.; Sawada, K. *Neurosci. Lett.* **2005**, *391*, 17–21.
46. Arias, E.; Gallego-Sandín, S.; Villarroya, M.; García, A.G.; López, M.G. *J. Pharmacol. Exp. Ther.* **2005**, *315*, 1346.
47. Meunier, J.; Ieni, J.; Maurice, T. *Br. J. Pharmacol.* **2006**, *149*, 998.
48. Zhang, H.Y.; Tang, X.C. *Neurosci. Lett.* **2000**, *292*, 41.
49. Meunier, J.; Ieni, J.; Maurice, T. *J. Pharmacol. Exp. Ther.* **2006**, *317*, 1307.
50. Riepe, M.W. *Eur. J. Neurol.* **2005**, *12(Suppl. 3)*, 3.
51. Zhou, J.; Fu, Y. ; Tang, X.C. *Neurosci. Lett.* **2001**, *306*, 53.
52. Sobrado, M.; Roda, J.M.; López, M.G.; Egea, J.; García, A.G. *Neurosci. Lett.* **2004**, *365*, 132.
53. Sabbagh, M.N.; Farlow, M.R.; Relkin, N.; Beach, T.G. *Alzheimers & Dementia* **2006**, *2*, 118.
54. Bullock, R.; Dengiz, A. *Int. J. Clin. Pract.* **2005**, *59*, 817.
55. Modrego, P.J. *Curr. Med. Chem.* **2006**, *13*, 3417.
56. Jack, C.R. Jr.; Petersen, R.C.; Xu, Y.; O-Brien, P.C.; Smith, G.E.; Ivnik, R.J.; Tangalos, E.G.; Kokmen, E. *Neurology* **1998**, *51*, 993.
57. Mori, E.; Lee, K.; Yasuda, M.; Hashimoto, M.; Kazui, H.; Hirono, N.; Matsui, M.. *Ann. Neurol.* **2002**, *51*, 209.
58. Hashimoto, M.; Kazui, H.; Matsumoto, K.; Nakano, Y.; Yasuda, M.; Mori, E. *Am. J. Psychiatry* **2005**, *162*, 676.
59. Krishnan, K.R.; Charles, H.C.; Doraiswamy, P.M.; Mintzer, J.; Weiler, R.; Yu, X.; Perdomo, C.; Ieni, J.R.; Rogers, S. *Am. J. Psychiatry* **2003**, *160*, 2003.
60. Wang, X.-D.; Chen, X.-Q.; Yang, H.-H.; Hu, G.-Y. *Neurosci. Lett.* **1999**, *272*, 21.
61. Takada-Takatori, Y.; Kume, T.; Sugimoto, M.; Katsui, H.; Sugimoto, H.; Akaike, A. *Neuropharmacology* **2006**, *51*, 474.
62. Nitsch, R.M.; Slack, B.E.; Wurtman, R.J.; Growdon, J.H. *Science* **1992**, *258*, 304.
63. Lahiri, D.K.; Rogers, J.T.; Greig, N.H.; Sambamurti, K. *Curr. Pharm. Des.* **2004**, *10*, 3111.
64. Chong, Y.H.; Suh, Y.H. *Life Sci.* **1996**, *59*, 545.
65. Zimmermann, M.; Gardoni, F.; Marcello, E.; Colciaghi, F.; Borroni, B.; Padovani, A.; Cattabeni, F.; DiLuca, M. *J. Neurochem.* **2004**, *90*, 1489.
66. Borroni, B.; Colciaghi, F.; Pastorino, L.; Pettenati, C.; Cottini, E.; Rozzini, L.; Monastero, R.; Lenzi, G.L.; Cattabeni, F.; DiLuca, M.; Padovani, A. *Arch. Neurol.* **2001**, *58*, 442.
67. Zimmermann, M.; Borroni, B.; Cattabeni, F.; Padovani, A.; Di Luca, M. *Neurobiol. Dis.* **2005**, *19*, 237.
68. Inestrosa, N.C.; Alvarez, A.; Pérez, C.A.; Moreno, R.D.; Vicente, M.; Linker, C.; Casanueva, O.I.; Soto, C.; Garrido, C. *Neuron.* **1996**, 16, 81.
69. Alvarez, A.; Alarcón, R.; Opazo, C.; Campos, E.O.; Muñoz, F.J.; Calderón, F.H.; Dajas, F.; Gentry, M.K.; Doctor, B.P.; De Mello, F.G.; Inestrosa, N.C. S *J. Neurosci.* **1998**, *18*, 3213
70. Reyes, A.E.; Chacón, M.A.; Dinamarca, M.C.; Cerpa, W.; Morgan, C.; Inestrosa, N.C. *Am. J. Pathol.* **2004**, *164*, 2163.
71. Rees, T.; Hammond, P.I.; Soreq, H.; Younkin, S.; Brimijoin, S. *Neurobiol. Aging* **2003**, *24*, 777
72. Rees, T.M.; Berson, A.; Sklan, E.H.; Younkin, S.; Brimiojin, S.; Soreq, H. *Curr. Alzheimer Res.* **2005**, *2*, 291.
73. De Ferrari, G.V.; Canales, M.A.; Shin, I.; Weiner, L.M.; Silman, I.; Inestrosa, N.C. *Biochemistry* **2001**, *40*, 10447.
74. Taylor, P., Lappi, S. *Biochemistry* **1975**, *14,* 1989.
75. Muñoz-Torrero. D.; Camps, P. *Curr. Med. Chem.* **2006**, *13*, 399.
76. Bartolini, M.; Bertucci, C.; Cavrini, V.; Andrisano, V. *Biochem. Pharmacol.* **2003**, *65*, 407.
77. Pang. Y.-P.; Quiram. P.; Jelacic. T.; Hong. F.; Brimijoin. S. *J. Biol. Chem.* **1996**, *271*, 23646.
78. Carlier, P.R.; Han, Y.F.; Chow, E.S.-H.; Li, C.P.-L.; Wang, H.; Lieu, T.X.; Wong, H.S.; Pang, Y.-P. *Bioorg. Med. Chem.* **1999**, *7*, 351.
79. Rydberg, E.H.; Brumshtein, B.; Greenblatt, H.M.; Harry, M.; Wong, D.M.; Shaya, D.; Williams, L.D.; Carlier, P.R.; Pang, Y.-P.; Silman, I.; Sussman, J.L. *J. Med. Chem.* **2006**, *49*, 5491.

80. Bolognesi, M.L.; Cavalli, A.; Valgimigli, L.; Bartolini, M.; Rosini, M.; Andrisano, V.; Recanatini, M.; Mechiorre, C. *J. Med. Chem.* **2007**, *50*, 6446.
81. Xiao, X.Q.; Lee, N.T.-K.; Carlier, P.R.; Pang, Y.-P.; Han, Y.F. *Neurosci. Lett.* **2000**, *290*, 197.
82. Li, W.; Pi, R.; Chan, H.H.N.; Fu, H.; Lee, N.T.K.; Tsang, H.W.; Pu, Y.; Chang, D.C.; Li, C.; Luo, J.; Xiong, K.; Li, Z.; Xue, H.; Carlier, P.R.; Pang, Y.-P.; Tsim, K.W.K.; Li, M.; Han, Y. *J. Biol. Chem.* **2005**, *280*, 18179.
83. Fu, H.; Li. W.; Lao, Y.; Luo, J.; Lee, N.T.K.; Kan, K.K.W.; Tsang, H.W.; Tsim, K.W.K.; Pang, Y.-P.; Li, Z.; Chang, D.C.; Li, M.; Han, Y. *J. Neurochem.* **2006**, *98*, 1400.
84. Han, Y.-F.; Wu, D.-C.; Xiao, X.-Q.; Chen, P.M.Y.; Chung, W.; Lee, N.T.K.; Pang, Y.-P.; Carlier, P.R. *Neurosci. Lett.* **2000**, *288*, 95. *Corrigendum in Neurosci. Lett.* **2000**, *290*, 84.
85. Castro, A.; Martinez, A. *Mini-Rev. Med. Chem.* **2001**, *1*, 267.
86. Du, D.-M.; Carlier, P.R. *Curr. Pharm. Des.* **2004**, *10*, 3141.
87. Li, W.M.; Kan, K.K.W.; Carlier, P.R.; Pang, Y.P.; Han, Y.F. *Curr. Alzheimer Res.* **2007**, *4*, 386.
88. Recanatini, M.; Valenti, P. *Curr. Pharm. Des.* **2004**, *10*, 3157.
89. Castro, A.; Martinez, A. *Curr. Pharm. Des.* **2006**, *12*, 4377.
90. Holzgrabe, U.; Kapková, P.; Alptüzün, V.; Scheiber, J.; Kugelmann, E. *Expert Opin. Ther. Targets* **2007**, *11*, 161.
91. Musial, A.; Bajda, M.; Malawska, B. *Curr. Med. Chem.* **2007**, *14*, 2654.
92. Haviv, H.; Wong, D.M.; Silman, I.; Sussman, J.L. *Curr. Top. Med. Chem.* **2007**, *7*, 375
93. Cavalli, A.; Bolognesi, M.L.; Minarini, A.; Rosini, M.; Tumiatti, V.; Recanatini, M.; Melchiorre, C. *J. Med. Chem.* **2008**, *51*, 347.
94. Piazzi, L.; Rampa, A.; Bisi, A.; Gobbi, S.; Belluti, F.; Cavalli, A.; Bartolini, M.; Andrisano, V.; Valenti, P.; Recanatini, M. *J. Med. Chem.* **2003**, *46*, 2279.
95. Piazzi, L.; Cavalli, A.; Colizzi, F.; Belluti, F.; Bartolini, M.; Mancini, F.; Recanatini, M.; Andrisano, V.; Rampa, A. *Bioorg. Med. Chem. Lett.* **2008**, *18*, 423.
96. Muñoz-Ruiz, P.; Rubio, L.; García-Palomero, E.; Dorronsoro, I.; del Monte-Millán, M.; Valenzuela, R.; Usán, P.; de Austria, C.; Bartolini, M.; Andrisano, V.; Bidon-Chanal, A.; Orozco, M.; Luque, F.J.; Medina, M.; Martínez, A. *J. Med. Chem.* **2005**, *48*, 7223.
97. Cavalli, A.; Bolognesi, M.L.; Capsoni, S.; Andrisano, V.; Bartolini, M.; Margotti, E.; Cattaneo, A.; Recanatini, M.; Melchiorre, C. *Angew. Chem. Int. Ed.* **2007**, *46*, 3689.
98. Bolognesi, M.L.; Banzi, R.; Bartolini, M.; Cavalli, A.; Tarozzi, A.; Andrisano, V.; Minarini, A.; Rosini, M.; Tumiatti, V.; Bergamini, C.; Fato, R.; Lenaz, G.; Hrelia, P.; Cattaneo, A.; Recanatini, M.; Melchiorre, C. *J. Med. Chem.* **2007**, *50*, 4882.
99. Vericat, J.A.; Muñoz, P.; Windisch, M.; Hutter-Paier, B.; Medina, M.; Martinez, A. *5th Neurobiology of Aging Conference*, San Diego, USA, 2004.
100. http://www.noscira.es.
101. Badia, A.; Baños, J.E.; Camps, P.; Contreras, J.; Görbig, D.M.; Muñoz-Torrero, D.; Simon, M.; Vivas, N.M. *Bioorg. Med. Chem.* **1998**, *6*, 427.
102. Muñoz-Torrero, D.; Camps, P. *Expert Opin. Drug Discovery* **2008**, *3*, 65.
103. Camps, P.; El Achab, R.; Morral, J.; Muñoz-Torrero, D.; Badia, A.; Baños, J.E.; Vivas, N.M.; Barril, X.; Orozco, M.; Luque, F.J. *J. Med. Chem.* **2000**, *43*, 4657.
104. Alcalá, M.M.; Vivas, N.M.; Hospital, S.; Camps, P.; Muñoz-Torrero, D.; Badia, A. *Neuropharmacol.* **2003**, *44*, 749.
105. Camps, P.; Cusack, B.; Mallender, W.D.; El Achab, R.; Morral, J.; Muñoz-Torrero, D.; Rosenberry, T.L. *Mol. Pharmacol.* **2000**, *57*, 409.
106. Roman, S.; Vivas, N.M.; Badia, A.; Clos, M.V. *Neurosci. Lett.* **2002**, *325*, 103.
107. Canudas, A.M.; Pubill, D.; Sureda, F.X.; Verdaguer, E.; Camps, P.; Muñoz-Torrero, D.; Jiménez, A.; Camins, A.; Pallàs, M. *Exp. Neurol.* **2003**, *180*, 123.
108. Dvir, H.; Wong, D.M.; Harel, M.; Barril, X.; Orozco, M.; Luque, F.J.; Muñoz-Torrero, D.; Camps, P.; Rosenberry, T.L.; Silman, I.; Sussman, J.L. *Biochemistry* **2002**, *41*, 2970.
109. Hedberg, M.M; Clos, M.V.; Ratia, M.; Gonzalez, D.; Unger Lithner, C.; Camps, P.; Muñoz-Torrero, D.; Badia, A.; Giménez-Llort, L.; Nordberg, A. *Neurodegene. Dis.* **2010**, *7*, 379.
110. Shao, D.; Zou, C.; Luo, C.; Tang, X.; Li, Y. *Bioorg. Med. Chem. Lett.* **2004**, *14*, 4639.
111. Alonso, D.; Dorronsoro, I.; Rubio, L.; Muñoz, P.; García-Palomero, E.; Del Monte, M.; Bidon-Chanal, A.; Orozco, M.; Luque, F.J.; Castro, A.; Medina, M.; Martínez, A. *J. Med. Chem.* **2005**, *48*, 7223.
112. Scarpellini, M. *Màster Experimental*, Universitat de Barcelona, 2006.

113. Xavier Formosa, *Tesi Doctoral*, Universitat de Barcelona, 2006.
114. Camps, P.; Muñoz-Torrero, D.; Formosa, X.; Scarpellini, M. Patent P200601045, WO2007/122274A1
115. Kawakami, H.; Ohuchi, R.; Kitano, M.; Ono, K. EP 0 268 871 A1, 1988.
116. Giacobini, E. *Neurochem. Res.* **2003**, *28*, 515.
117. De Ferrari, G.V.; Mallender, W.D.; Inestrosa, N.C.; Rosenberry, T.L. *J. Biol. Chem.* **2001**, *276*, 23282.
118. Hu, M.-K.; Lu, C.-F. *Tetrahedron Lett.* **2000**, *41*, 1815.
119. Hu, M.-K.; Wu, L.-J.; Hsiao, G.; Yen, M.-H. *J. Med. Chem.* **2002**, *45*, 2277.
120. Crossland, R.K.; Servis, K.L. *J. Org. Chem.* **1970**, *35*, 3195.
121. Sugimoto, H.; Iimura, Y.; Yamanishi, Y.; Yamatsu, K. *J. Med. Chem.* **1995**, *38*, 4821.
122. Elati, C.R.; Kolla, N.; Chalamala, S.R.; Vankawala, P.J.; Sundaram, V.; Vurimidi, H.; Mathad, V.T. *Synth. Commun.* **2006**, *36*, 169.
123. Reddy, K.V.S.R.K.; Babu, J.M.; Kumar, P.A.; Chandrashekar, E.R.R.; Mathad, V.T.; Eswaraiah, S.; Reddy, M.S.; Vyas, K. *J. Pharm. Biomed. Anal.* **2004**, *35*, 1047.
124. Bolognesi, M.L.; Andrisano, V.; Bartolini, M.; Banzi, R.; Melchiorre, C. *J. Med. Chem*. **2005**, *48,* 24.
125. Bourne, Y.; Kolb, H.C.; Radic, Z.; Sharpless, K.B.; Taylor, P.; Marchot, P. *Proc. Natl. Acad. Sci. U.S.A* **2004**, *101*, 1449.
126. Jiménez, O.; de la Rosa, G.; Lavilla, R. *Angew. Chem., Int. Ed.* **2005**, *44*, 6521.
127. Bourne, Y.; Taylor, P.; Radic, Z.; Marchot, P. *EMBO J.* **2003**, *22*, 1.
128. Carlier, P.R.; Chow, E.S.-H.; Han, Y.; Liu, J.; El Yazal, J.; Pang, Y.-P. *J. Med. Chem.* **1999**, *42*, 4225
129. Ellman, G.L.; Courtney, K.D.; Andres, B., Jr.; Featherstone, R.M. *Biochem. Pharmacol.* **1961**, *7*, 88.
130. Miao, Y.; He, N.; Zhu, J.-J. *Chem. Rev.* **2010,** *110,* 5216.
131. Rackonczay, Z. *Neuromethods, Neurotransmitter Enzymes*; Humana Press: NJ, **1986;** p. 319**.**
132. Viayna, E.; Gómez, T.; Galdeano, C.; Ramírez, L.; Ratia, M.; Badia, A.; Clos, M. V.; Verdaguer, E.; Junyent, F.; Camins, A.; Pallàs, M.; Bartolini, M.; Mancini, F.; Andrisano, V.; Arce, M. P.; Rodríguez-Franco, M. I.; Bidon-Chanal, A.; Luque, F. J.; Camps, P.; Muñoz-Torrero, D. *ChemMedChem* **2010**, *5*, 1855.
133. *Stability testing of New Drugs Substances and Products* (**2002**) Proceedings of the International Conference on Harmonization (ICH), IFPMA, Geneva, Switzerland.
134. Álvarez-Lueje, A.; Valenzuela, C.; Squella, J.A.; Nuñez-Vergara, J.L. *J. AOAC Int.* **2005**, *88*, 1631.
135. Camps, P.; El Achab, R.; Görbig,D.M.; Morral, J.; Muñoz-Torrero, D.; Badia, A.; Baños, J.E.; Vivas, N.M.; Barril, X.; Orozco, M.; Luque F.J. *J. Med. Chem.* **1999**, *42,* 3227.
136. Leach, A. R. *Molecular Modelling: Principles and applications,* 2nd edition, **2001**, Pearson Education (Prentice Hall), Essex.
137. Schlick, T. *Molecular Modeling and Simulation. An interdisciplinary Guide,* **2002**, Springer-Verlag New York, Inc. New York.
138. Alder, B. J.; Wainwright, T. E. *J. Chem. Phys.* **1957**, 27, 1208.
139. Adcock, S. A.; McCammon, J. A. *Chem. Rev.* **2006**, *106*, 1589
140. Axel Bidón-Chanal, *Tesi Doctoral*, Universitat de Barcelona, **2007**.
141. Kryger, G.; Silman, I.; Sussman, J. L. *Structure* **1999**, *7*, 297.
142. Camps, P.; Formosa, X.; Muñoz-Torrero, D.; Petrignet, J.; Badia, A.; Clos, M.V. *J. Med. Chem.* **2005**, *48*, 1701.
143. Pera, M.; Román, S.; Ratia, M; Camps, P; Muñoz-Torrero, D.; Colombo, L.; Manzoni, C; Salmona, M.; Badia, A.; Clos, M.V. *Biochem. Biophys. Res. Commun.* **2006**, *346*, 89.
144. Pera, M.; Martínez-Otero, A.; Colombo, L.; Salmona, M.; Ruiz-Molina, D.; Badia, A.; Clos, M.V. *Mol. and Cell. Neurosci.* **2009**, *40*, 217.
145. Camps, P.; Contreras, J.; Font-Bardia, M.; Morral, J.; Muñoz-Torrero, D.; Solans, X. *Tetrahedron: Asymmetry* **1998**, *9*, 3227.
146. Naïm, M.; Bhat, S.; Rankin, K. N.; Dennis, S.; Chowdhury, S. F.; Siddiqi, I.; Drabik, P.; Sulea, T.; Bayly, C. I.; Jakalian, A.; Purisima, E. O. *J. Chem. Inf. Model*. **2007**, *47*, 122.
147. Cui, Q.; Sulea, T.; Schrag, J. D.; Munger, C.; Hung, M.-N.; Nam, M.; Cygler, M.; Purisima, E. O. *J. Mol. Biol.* **2008**, *379*, 787.

Annex 1: Mètodes en química computacional

A1.1 Camps de forces

El conjunt de paràmetres i equacions utilitzats per a descriure l'energia potencial d'un sistema mitjançant la mecànica molecular es coneix amb el nom de camp de forces.[a1-a4] Existeixen en l'actualitat diversos tipus de camps de forces que es diferencien bàsicament en el nombre de termes utilitzats per a calcular l'energia del sistema, així com en la forma en què s'han obtingut els paràmetres individuals presents en cadascuna d'aquestes contribucions. Tot i així, tots ells comparteixen en major o menor mesura la forma de calcular cada terme en particular; s'utilitzen potencials armònics per a descriure els enllaços i els angles, sèries de Fourier per a les torsions, i les interaccions entre parells d'àtoms no enllaçats es descriuen mitjançant una funció del tipus Lennard-Jones (van der Waals) i una funció coulòmbica (electrostàtic).

Els camps de forces actuals es poden subdividir en tres classes diferents:

Classe I: aquells camps que no contenen termes creuats i en què els termes de flexió i torsió s'aproximen mitjançant funcions armòniques; exemples d'aquests camps serien AMBER[a5] i CHARMM.[a6]

Classe II: desenvolupats per a reproduir les propietats de molècules petites aïllades, per la qual cosa és necessari incloure termes creuats i on els termes de flexió i torsió es descriuen mitjançant polinomis d'ordre superior o sèries de Fourier; aquesta classe inclou els camps de forces MM3[a7] i CFF93.[a8]

Classe III: del mateix tipus que l'anterior, però amb termes addicionals per a descriure fenòmens d'hiperconjugació i electronegativitat, com per exemple el camp de forces MM4.[a9]

En el següent apartat explicarem breument las característiques dels camps de forces més senzills (classe I; concretament el formalisme que segueix AMBER) que han estat els usats en aquesta Tesi Doctoral.

[a1]Leach, A.R. *Molecular Modelling: Principles and applications,* 2nd edition, **2001**, Pearson Education (Prentice Hall), Essex. [a2]Schlick, T. *Molecular Modeling and Simulation. An interdisciplinary Guide,* **2002**, Springer-Verlag New York, Inc. New York. [a3]Frenkel, D.; Smit, B. *Understanding Molecular Simulation* **2002**, Academic Press. [a4]McCammon, J.A.; Harvey, S.C. *Dynamics of Proteins and Nucleic Acids* **1987**, Cambridge University Press, Cambridge. [a5]Weiner, P.K.; Kollman, P.A. *J. Comp. Chem.* **1981**, *2*, 287. [a6]Brooks, B.R.; Bruccoleri, R.E.; Olafson, B.D.; States, D.J.; Swaminathan, S.; Karplus, M. *J. Comp. Chem.* **1983**, *4*, 187. [a7]Allinger, N.L.; Yuh, Y.H.; Lii, J-H. *J. Am. Chem. Soc.* **1989**, *111*, 8551. [a8]Hwang, M.-J.; Stockfisch, T.P.; Hagler, A.T. *J. Am. Chem. Soc.* **1994**, *116*, 2515. [a9]Allinger, N.L.; Chen, K.; Lii, J-H, *J. Comp. Chem.* **1996**, *17*, 642.

A1.2 El camp de força AMBER

Els camps de forces de la família AMBER són uns dels més usats per a sistemes macromoleculars d'interès biològic. La seva primera versió es va desenvolupar l'any 1984[a10] i incloïa sis termes corresponents a les contribucions de tensió, flexió, torsió, interaccions de van der Waals, electroestàtiques i ponts d'hidrogen. Posteriorment, l'any 1995 es va publicar una segona generació, coneguda com PARM94,[a11] on cal destacar la desaparició del terme de pont d'hidrogen. Posteriors ajustaments van millorar els resultats obtinguts per a la descripció de pèptids, proteïnes i especialment àcids nucleics, donant lloc a les versions PARM96, PARM98, PARM99, PARM03 i versions modificades com PARMSB o PARMSBC0.

Aquests nous models, segons els propis autors, poden ser considerats com a "minimalistes" en la seva forma funcional, amb els termes de tensió i flexió representats per una simple expressió armònica que en situacions pròximes a les d'equilibri s'aproximen bastant bé a les curves de potencial de Morse que descriuen l'energia potencial d'un enllaç. Així, la llei de Hooke per a un oscil·lador armònic és el model més simple que pot utilitzar-se per a descriure les deformacions dels enllaços covalents. Representant l'enllaç entre dos àtoms com una molla que els manté units i que permet cert desplaçament mutu en forma d'elongació del mateix, l'energia potencial vindrà descrita per:

$$E_{vib} = \sum_{enl} K_{vib}\left(r - r_{eq}\right)^2 \qquad \text{[Eq. A1.1]}$$

on r és la distància d'enllaç, r_{eq} la distància de referència (normalment la d'equilibri) i K_{vib} és la constant de força associada.

El potencial més senzill que es pot utilitzar per a descriure les deformacions en els angles d'enllaç és el que es deriva de l'aplicació de la llei de Hooke per a un oscil·lador armònic:

$$E_{ang} = \sum_{enl} K_{ang}\left(\theta - \theta_{eq}\right)^2 \qquad \text{[Eq. A1.2]}$$

sent K_{ang} la constant de força associada i θ_{eq} el valor de refèrencia per a l'angle entre tres àtoms units per enllaços covalents.

[a10] Weiner, S.J.; Kollman, P.A.; Case, D.A.; Singh, U.C.; Ghio, C.; Alagona, G.; Profeta, S.; Weiner, P. *J. Am. Chem. Soc*. **1984,** *106*, 765. [a11] Cornell, W.D.; Cieplak, P.; Bayly, C.I.; Gould, I.R.; Merz, K.M.; Ferguson, D.M.; Spellmeyer, D.C.; Fox, T.; Caldwell, J.W.; Kollman, P.A. *J. Am. Chem. Soc*. **1995**, *117*, 5179.

Per a descriure les torsions es precisa utilitzar una expressió més complexa, doncs per expressar la periodicitat del perfil d'energia s'utilitzen expressions periòdiques en sèrie de Fourier, que poden dependre només dels dos àtoms centrals implicats en el diedre o bé ser específiques de tots els diedres que defineixen la torsió:

$$E_{tor} = \sum_{tor}\sum_{n}\frac{V_n}{2}\left(1+\cos\left(n\phi-\phi_0\right)\right) \qquad \text{[Eq. A1.3]}$$

on V_n representa la barrera de torsió associada a cada terme de la funció, n la periodicitat del terme, ϕ l'angle diedre i ϕ_0 l'angle de fase.

Per arribar a descriure bé les energies i geometries és necessari, en la majoria de casos, afegir una funció per a descriure les *torsions impròpies,* a fi de mantenir la planaritat o la quiralitat de certs grups. Aquest terme sol es pot descriure mitjançant una expressió semblant a la torsió convencional :

$$E_{tor} = \sum_{tor}\sum_{n}\frac{V_n}{2}\left(1+\cos\left(2\xi_n-180\right)\right) \qquad \text{[Eq. A1.4]}$$

on V_n representa la constant de força de cada terme de la funció, n la periodicitat del terme i ξ l'angle diedre.

Per últim queden el termes *no enllaçants*, corresponents a interaccions de van der Waals i electrostàtiques. El terme de van der Waals està descrit mitjançant un potencial *6-12* del tipus Lennard-Jones.[a1-a4] Aquesta expressió està formada per la suma de dos termes, un repulsiu per a les distàncies curtes entre àtoms i un altre atractiu per a les distàncies superiors. Podem representar les interaccions atractives a curta distància com a fruit de les forces dispersives i evitant la fusió d'àtoms no units de càrrega oposada:

$$E_{vdw} = \sum_{i}\sum_{j>i}\left(\frac{A_{ij}}{r_{ij}^{12}}-\frac{B_{ij}}{r_{ij}^{6}}\right) \qquad \text{[Eq. A1.5]}$$

on A_{ij} i B_{ij} són constants per a cada par d'àtoms relacionats amb els seus radis de van der Waals i r_{ij} és la distància entre ells.

[a1]Leach, A.R. *Molecular Modelling: Principles and applications,* 2nd edition, **2001**, Pearson Education (Prentice Hall), Essex. [a2]Schlick, T. *Molecular Modeling and Simulation. An interdisciplinary Guide,* **2002**, Springer-Verlag New York, Inc. New York. [a3]Frenkel, D.; Smit, B. *Understanding Molecular Simulation* **2002**, Academic Press. [a4]McCammon, J.A.; Harvey, S.C. *Dynamics of Proteins and Nucleic Acids* **1987**, Cambridge University Press, Cambridge.

Finalment, les interaccions electrostàtiques estan descrites mitjançant un potencial coulòmbic basat en la interacció de càrregues puntuals, i l'energia ve donada per l'equació:

$$E_{ele} = \sum_i \sum_{j>i} \frac{q_i q_j}{4\pi\varepsilon_0 r_{ij}} \qquad \text{[Eq. A1.6]}$$

sent q_i i q_j les càrregues puntuals de cada àtom, r_{ij} la distància entre àtoms i ε la constant dielèctrica del medi.

En la majoria dels camps de forces, les càrregues puntuals fraccionals s'obtenen mitjançant un ajustament del potencial electrostàtic molecular calculat quànticament a partir de la funció d'ona Hartree-Fock obtinguda utilitzant una base *6-31G(d)*. En el camp de forces d'AMBER, les càrregues es deriven amb el mètode RESP[a12] (Restrained Electrostatic Potential), que usa restriccions hiperbòliques sobre la càrrega dels àtoms pesats, evitant que l'ajustament no restringit al potencial condueixi a solucions en què les càrregues dels àtoms interns adoptin valors sense sentit químic.

A1.3 Mecànica i dinàmica molecular

Dues tècniques d'especial utilitat en biologia en les quals s'apliquen els camps de forces són la mecànica molecular i la dinàmica molecular (DM). Les dues tècniques comparteixen moltes característiques i la seva principal diferència estreba en la inclusió dels temps com a variable en la dinàmica molecular.

A1.3.1 Mecànica molecular: minimització d'energia

L'energia potencial que descriu els estats conformacionals d'una molècula és funció de les coordenades cartesianes associades a la posició de cada àtom en l'espai. Així, es pot associar cada estructura a un punt en una hipersuperfície d'energia potencial. En aquesta hipersuperfície poden existir molts punts de mínima energia que es corresponent amb estats

[a12] Bayly, C. I.; Cieplak, P.; Cornell, D.W.; Kollman, P.A. *J. Phys. Chem.* **1993**, *79*, 10269.

configuracionals estables del sistema anomenats *mínims locals*. El punt que té l'energía més baixa es coneix amb el nom de *mínim global*.[a1-a3]

Existeixen diverses classes de mètodes per a identificar els punts corresponents a mínims en la superfície d'energia potencial, que es diferencien en la utilització de la informació continguda en el gradient i/o l'hessiana, de cara a traçar el camí fins al mínim d'energia.

Mètodes com *Simplex* o *Seqüencial* són mètodes no derivatius. En el primer es localitza el mínim mitjançant l'exploració de la superfície d'energia potencial amb desplaçaments geomètrics dels vèrtexs d'una figura formada per n+1 variables de la funció a minimitzar. Per a l'exploració de la superfície s'utilitzen tres tipus de moviments: reflexió, expansió i contracció. En el mètode *Seqüencial* s'explora la superficie d'energia potencial de forma rotatòria per a totes les variables de la funció. Prenent com a partida una variable, es calcula el valor de la funció en dos punts situats a $x+\delta x$ *i* $x+2\delta x$. A continuació s'ajusta una paràbola als tres punts i es calcula el mínim d'aquesta a partir del qual es canvia de variable i així succesivament fins arribar al mínim.[a2]

D'altra banda, els mètodes *derivatius* es classifiquen per l'ordre de les derivades que s'utilitzen. Normalment és preferible usar combinacions. Es comença per un mètode que utilitzi primeres derivades per a aproximar-se al mínim i es refina l'estructura per algun mètode que calculi o aproximi les segones derivades. Dins dels mètodes que utilitzen primeres derivades es troben els mètodes *steepest-descent (SD)* i *conjugate gradient (CG)*.[a1,a2] En el primer la direcció de búsqueda és paral·lela al gradient, i la progressió fins al mínim es realitza amb un amplada de pas variable segons si el valor de la funció és menor o major que el punt anterior. En el segon mètode, els gradients en cada punt del camí a seguir per arribar al mínim són ortogonals, mentre que les direccions a seguir per a passar d'un punt a un altre són conjugades a les direccions dels passos previs. D'aquesta forma s'aconsegueix major eficàcia quant s'està prop del mínim, tot i que la convergència és més lenta en regions apartades. L'estratègia més comuna és combinar els dos mètodes: *SD* al principi de l'optimització i *CG* en les etapes finals.

Per a sistemes petits és possible aplicar els mètodes que calculen explícitament segones derivades. Entre aquests mètodes es troben el mètode Newton-Raphson i les seves variants i

[a1]Leach, A.R. *Molecular Modelling: Principles and applications,* 2nd edition, **2001**, Pearson Education (Prentice Hall), Essex. [a2]Schlick, T. *Molecular Modeling and Simulation. An interdisciplinary Guide,* **2002**, Springer-Verlag New York, Inc. New York. [a3]Frenkel, D.; Smit, B. *Understanding Molecular Simulation* **2002**, Academic Press.

els mètodes quasi-newtonians.[a2] Tots ells són eficaços quan la funció d'energia potencial depèn d'un nombre relativament petit de variables, ja que s'ha de calcular l'hessiana del sistema a cada pas, per la qual cosa els requisits computacionals són molt més grans.

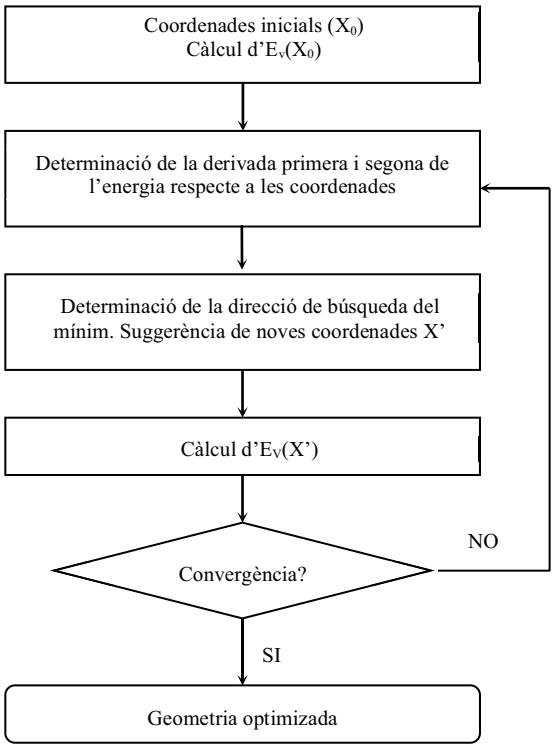

Figura A1.1 Algoritme bàsic dels mètodes de mecànica molecular

A1.3.2 Dinàmica molecular

Per a aplicar la DM és necessari tenir informació espacial de l'estructura de la molècula que es vol estudiar. Aquesta informació ha de contenir la situació en l'espai en forma de coordenades de cada àtom. Aplicant les lleis de Newton al sistema s'obté una trajectòria que conté les diferents conformacions que adopta la molècula al llarg del temps de simulació.

La segona equació de Newton per a una partícula *i*, amb massa m_i, i la posició de la qual en l'espai ve donada pel vector ***r*** de tres dimensions, és:

$$\frac{dp_i}{dt} = F_i \qquad \text{[Eq. A1.7]}$$

[a2]Schlick, T. *Molecular Modeling and Simulation. An interdisciplinary Guide,* **2002**, Springer-Verlag New York, Inc. New York.

on F_i és la força que actua sobre l'àtom *i*, i la quantitat de movimient p_i ve donada per:

$$m_i \frac{dr_i}{dt} = p_i \qquad \text{[Eq. A1.8]}$$

$$F_i = -\frac{dV}{dr_i} \qquad \text{[Eq. A1.9]}$$

on r_i indica el vector posició de l'àtom *i*, *t* representa el temps, i *V* és el potencial total, que s'avalua a partir del camp de forces.

Si es coneix la posició de la partícula a un temps donat *t*, llavors la seva posició després d'un increment petit i finit *Δt* vindrà donada per una expansió en sèrie de Taylor al voltant del punt d'origen. Prenent només la component del vector ***r*** en una dimensió (*x* en aquest cas), l'expansió en sèrie resulta de la forma:

$$x(t + \Delta t) = x(t) + \frac{dx(t)}{dt}\Delta t + \frac{d^2x(t)}{dt^2}\frac{\Delta t^2}{2} + \ldots \qquad \text{[Eq. A1.10]}$$

on apareix la posició de la partícula a un temps donat *x(t)*, la seva velocitat $\frac{dx(t)}{dt}$ i la seva acceleració $\frac{d^2x(t)}{dt^2}$.

Si es trunca la sèrie de Taylor en el segon ordre, la integració de les equacions del moviment es pot portar a terme de forma numèrica amb aquestes tres variables.

A1.3.3 Algoritme d'integració i temps d'integració

En sistemes formats per múltiples partícules sota la influència d'un potencial continu, la força que actua sobre una partícula serà funció de les posicions de totes les altres partícules del sistema i canviarà en variar la seva posició, així com la de qualsevol altra partícula del sistema. Aquest fenòmen, conegut com *problema de molts cossos*, és degut a que el moviment de les partícules està acoblat.[a1] En conseqüència, la integració de les equacions del moviment s'ha de realitzar de forma diferencial per mètodes de diferències finites on l'etapa d'integració ha de ser sempre menor que el movimient més ràpid del sistema (en l'escala del femtosegon en sistemes biològics, Taula A1.1).

A nivell pràctic hi ha desenvolupats diferentes mètodes. En l'algoritme de Verlet,[a13] per

[a1] Leach, A.R. *Molecular Modelling: Principles and applications,* 2nd edition, **2001**, Pearson Education (Prentice Hall), Essex. [a13] Verlet, L. *Phys. Rev.* **1967**, *159*, 98.

exemple, s'utilitzen les posicions i les acceleracions a un temps donat *t* i les posicions a un temps $t-\delta t$ per a calcular les posicions en el següent pas, $t+\delta t$. Això implica que les velocitats no tenen per què calcular-se i per tant els requisits d'emmagatzematge i càlcul no són massa elevats.

El problema d'aquest algoritme recau en la precisió amb què s'obtenen les coordenades per a les noves posicions, ja que aquestes s'obtenen per la següent equació, on se suma un valor molt petit a la diferència entre dos valors molt superiors:

$$\mathbf{r}(t+\delta t) = 2\mathbf{r}(t) - \mathbf{r}(t-\delta t) + \delta t^2 \mathbf{a}(t) \qquad \text{[Eq. A1.11]}$$

Taula A1.1 Relació entre els intervals de temps de fenòmens característics de molècules i sistemes biomoleculars i els mètodes teòrics existents.

event	extensió espacial (nm)	amplitud (nm)	temps (s)	simulació apropiada
vibració de la distància d'enllaç	0,2–0,5	0,001–0,01	10^{-14}–10^{-13}	Mètodes QM
vibració elàstica d'un domini globular	1,0–2,0	0,005–0,05	10^{-12}–10^{-11}	DM convencional
rotació de cadenes exposades a solvent	0,5–1,0	0,5–1,0	10^{-11}–10^{-10}	DM convencional
oscil·lació torsional de grups interns	0,5–1,0	0,05	10^{-11}–10^{-19}	DM convencional
hinge bending (moviment relatiu de dominis globulars)	1,0–2,0	0,1–0,5	10^{-11}–10^{-7}	Dinàmica de Langevin, mètodes d'ampli mostreig?
rotació de cadenes laterals internes	0,5	0,5	10^{-4}–1	mètodes d'ampli mostreig?
transicions al·lostèriques	0,5–0,4	0,1–0,5	10^{-5}–1	mètodes d'ampli mostreig?
desnaturalització local	0,5–1,0	0,5–1,0	10^{-5}–10^{1}	mètodes d'ampli mostreig?
moviments de loops	1,0–5,0	1,0–5,0	10^{-9}–10^{-5}	Dinàmica Browniana
moviments de cos rígid (hèlixs)		1,0–5,0	10^{-9}–10^{-6}	mètodes d'ampli mostreig?
transicions hèlix–enrollat		>5,0	10^{-7}–10^{4}	mètodes d'ampli mostreig?
associació de proteïnes	>>1,0			Dinàmica Browniana

Existeixen diverses variants del mètode de Verlet que es diferencien principalment en la forma en què s'obtenen les noves posicions, com per exemple l'algoritme de velocitats de Verlet [a14] o el de Beeman,[a15] però la variant de l'algoritme de Verlet més extesa és el mètode leap-frog (Figura A1.2).[a16] En aquest, les posicions a *t+δt* s'obtenen a partir de les *velocitats* a $t + \frac{1}{2}\delta t$ mitjançant les equacions :

$$\mathbf{r}\left(t + \delta t\right) = \mathbf{r}\left(t\right) + \delta t\mathbf{v}\left(t + \tfrac{1}{2}\delta t\right) \qquad \text{[Eq. A1.12]}$$

$$\mathbf{v}\left(t + \tfrac{1}{2}\delta t\right) = \mathbf{v}\left(t - \tfrac{1}{2}\delta t\right) + \delta t\mathbf{a}\left(t\right) \qquad \text{[Eq. A1.13]}$$

D'aquesta forma, s'eviten els problemes de precisió de l'algoritme de Verlet i a més poden obtenir-se les velocitats, tot i que desfasades respecte de les posicions $\frac{1}{2}\delta t$. Les velocitats a un temps donat *t* s'obtenen per l'equació:

$$\mathbf{v}\left(t\right) = \frac{1}{2}\left[\mathbf{v}\left(t + \tfrac{1}{2}\delta t\right) + \mathbf{v}\left(t - \tfrac{1}{2}\delta t\right)\right] \qquad \text{[Eq. A1.14]}$$

Finalment cal destacar els mètodes d'integració, com els de predicció–correcció, on les posicions, velocitats i acceleracions s'obtenen per expansió en sèrie de Taylor. El valor de les acceleracions es compara amb l'obtingut a partir de les forces, per a corregir i obtenir les noves posicions. Això fa que els requisits d'emmagatzematge i càlcul siguin majors que en l'algoritme de Verlet i les seves variants abans esmentades.

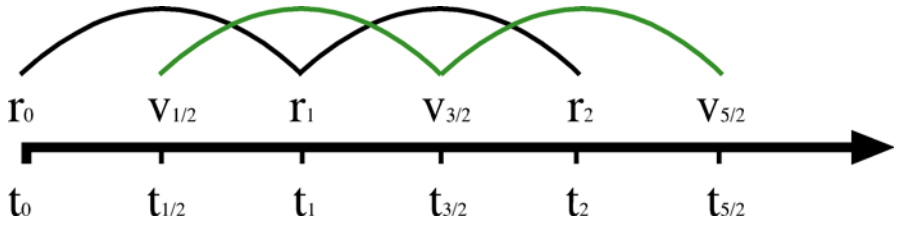

Figura A1.2 Representació esquemàtica de l'algoritme *leap-frog*.

[a14] Swope, W.C.; Anderson, H.C.; Berens, P.H.; Wilson, K.R. *J. Chem. Phys.* **1982**, *76*, 3271. [a15]Beeman, D. *J. Comp. Phys.* **1976**, *20*, 130. [a16]Hockney, R.W. *Meth. Comp. Phys.* **1970**, *9*, 136.

Com s'ha comentat anteriorment, el temps d'integració hauria de ser de l'ordre del femtosegon. Això representa que per poder tenir un nanosegon de trajectòria és necessari realitzar 10^6 pasos amb tot el cost computacional i temporal que això requereix.
Una de les opcions més utilitzades per a augmentar el pas d'integració és aplicar restriccions al sistema, com SHAKE,[a17] que fixa les distàncies d'enllaç entre àtoms i per tant permet duplicar el pas d'integració.

A1.3.4 Condicions de simulació

El punt inicial de qualsevol simulació és sempre una configuració inicial. Aquesta estructura podrà obtenir-se de dades experimentals de raigs-X, RMN o d'un model teòric, i precisa d'un conjunt de velocitats inicials, que s'assignaran a l'atzar seguint una distribució de tipus Maxwell-Boltzmann, tal que l'energia cinètica associada es correspondrà a l'energia tèrmica diana per a la temperatura de treball. Finalment, es requereix fixar les condicions de simulació: el nombre de partícules (N), el volum (V), la temperatura (T), la pressió (P) o l'energia total del sistema (E). En funció de la combinació de les mateixes es pot distingir entre varis col·lectius:

-microcanònic (NVE)
-isotèrmic–isobàric (NPT)
-canònic (NVT)

sent NPT i NVT els més usats en DM de proteïnes.

En treballar sota condicions NPT s'haurà de controlar tant la temperatura com la pressió. En el cas de la temperatura existeixen diferents opcions. La primera de elles seria el re-escalat de les velocitats mitjançant l'aplicació d'un factor. Una altra alternativa seria mantenir la temperatura acoblada a un bany tèrmic extern fixat a la temperatura desitjada. Aquests banys actuen com a font d'energia tèrmica, afegint o eliminant calor del sistema en funció de les necessitats. Les velocitats són també re-escalades periòdicament, en funció de la diferència de temperatura entre el bany i el sistema. Els mètodes més coneguts són el de Berendsen[a18] i el

[a17]Ryckaert, J.P.; Cicotti, G.; Berendsen, H.J.C. *J. Comp. Phys.* **1977**, *23*, 327. [a18]Berendsen, H.J.C.; Postma, J.P.M.; van Gunsteren, W.F.; Di Nola, A.; Haak, J.R. *J. Chem. Phys.* **1984**, *81*, 3684.

Nosé-Hoover.[a19] Mètodes similars són usats per a mantenir la pressió. Típicament es calcula el de virial per a determinar la pressió interna i aquesta s'acobla a un pistó que garantitza equilibri amb la pressió externa, augmentant o disminuint el volum de sistemes simulats.

La imposibilitat de simular sistemas infinits juntament amb l'ús de potencials continus planteja diferents problemes en portar a terme una simulació. Els sistemes estan necessàriament confinants en un espai finit, per la qual cosa les partícules ubicades en els límits del sistema interaccionaran amb les parets d'aquest. Per a sistemes petits això significa que la major part de las partícules del sistema es troben sota la influència de les parets. Si es vol obtenir propietats macroscòpiques a partir de sistemes model, necessàriament ha d'eliminar-se d'alguna manera l'efecte de les parets.[a1,a2] D'altra banda, donat que cada partícula interacciona amb totes les altres, seria necessari calcular N(N-1) pars d'interaccions no enllaçants a cada pas, augmentant de forma desmesurada el temps de càlcul necessari.

El primer problema pot minimitzar-se si s'utilizen condicions periòdiques de contorn, per les quals es confinen les partícules del sistema en una caixa que es replica en totes les direccions de l'espai. Durant la simulació, si una partícula abandona la caixa central, la seva imatge en una altra caixa entrarà en la caixa central pel costat oposat, mantenint constant el número de partícules d'aquesta caixa.

Per al segon problema és suficient tenir en compte la forma del potencial que s'està utilitzant. El terme de van der Waals cau ràpidament amb la distància de tal forma que a una distància interatòmica de 2.5σ (sent σ la distància entre àtoms, per la qual el potencial té valor nul), el seu valor és l'1% del que pren a la distància d'equilibri, cosa que provoca que a distàncies suficientment grans pot despreciar-se. Així, pot restringir-se el càlcul de les interaccions *no enllaçants* tallant a una distància donada pel potencial (*cut-off*) i usant el mètode de la mínima imatge. D'aquesta forma les interaccions d'aquesta classe es calculen entre una partícula i totes aquelles que es troben en un radi arbitrari al seu voltant escollint les imatges de les partícules que estan més a prop.

D'altra banda, el potencial electrostàtic cau amb la distància a *1/r*, per la qual cosa no es pot negligir a distàncies grans si es vol evitar artefactes en sistemes carregats, com proteïnes i àcids nucleics.[a1,a2] El mètode més utilitzat per a resoldre aquest tipus de problemes és el mètode de sumes de Ewald.[a20]

[a1]Leach, A.R. *Molecular Modelling: Principles and applications,* 2nd edition, **2001**, Pearson Education (Prentice Hall), Essex. [a2]Schlick, T. *Molecular Modeling and Simulation. An interdisciplinary Guide,* **2002**, Springer-Verlag New York, Inc. New York. [a19]Hoover, W.G. *Phys. Rev. A.* **1985**, *31*, 1695.[a20] Ewald, P.P. *Ann. Phys*. **1921**, *64*, 253.

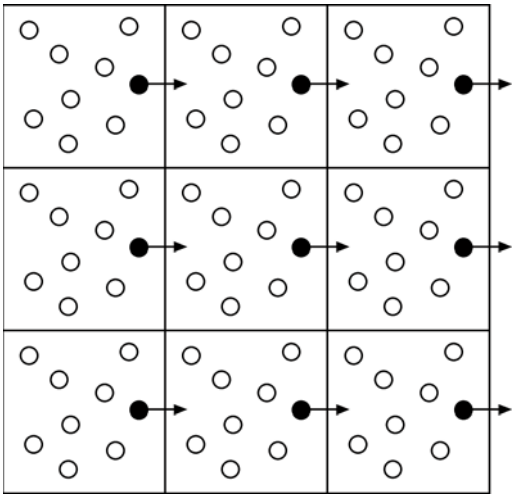

Figura A1.3 Representació esquemàtica de les condicions periòdiques de contorn

En ell, es transforma el càlcul de la sumatòria de totes les interaccions electrostàtiques possibles en dos termes de convergència molt més ràpids: un que engloba les interaccions a curta distància (espai directe), que són calculades mitjançant un potencial coulòmbic modificat, i un altre en què s'inclou la resta (espai recíproc), que es calcula per sumes vectorials. Una variant més eficaç d'aquest mètode és el Particle Mesh Ewald,[a21] en el qual s'optimitiza el càlcul de l'espai recíproc mitjançant la interpolació *B-spline* de les càrregues puntuals a malles tridimensionals. Aquestes malles són posteriorment tractades mitjançant transformades de Fourier, les quals redueixen notablement el cost computacional.

A1.4 Càlcul d'energies lliures

L'energia lliure és possiblement la propietat termodinàmica més important. D'una banda, modula la possiblitat de trobar un sistema en un estat determinat, i d'una altra banda, determina que sigui factible la realització de qualsevol procés. Normalment s'expressa per mitjà de la funció de Helmholtz, *A* (colectiu NVT), o mitjançant la funció de Gibbs, *G* (colectiu NPT).

L'energia lliure és una magnitud extremadament difícil de calcular teòricament en sistemes macromoleculars amb molts graus de llibertat i gran quantitat de configuracions de mínima energia separades per petites barreres energètiques. Per això, es requereix un correcte

[a21] Darden, T.L.; York, D.; Pedersen, L. *J. Chem. Phys.* **1993**, *98*, 10089.

mostreig d'aquelles regions de l'espai de fase del sistema que més contribueixen a l'energia lliure. No obstant, des d'un punt de vista computacional és més senzill realitzar càlculs d'energia lliure entre dos estats que presenten poques diferències entre ells. Per tal fi, s'han proposat diferents mètodes, sent els més emprats la *Perturbació de l'Energia Lliure* i la *Integració Termodinàmica.*

A1.4.1 Perturbació de l'energia lliure

Imaginen dos estats definits, *X i Y,* que venen descrits pels Hamiltonians H_x *i* H_y, respectivament. La diferència d'energia entre aquests estats pot descriure's com:

$$\Delta G = G_Y - G_x = -k_B T \ln (Q^Y / Q^X) \qquad \text{[Eq. A1.15]}$$

sent Q la funció de partició, K_b la constant de Boltzman i T la temperatura.
L'equació anterior pot ser escrita en termes d'un conjunt promedi de configuracions com:[a22]

$$\Delta G = -k_B T \ln \{ \exp [- (H_x - H_Y) / k_B T] \}_0 \qquad \text{[Eq. A1.16]}$$
$$\Delta G = -k_B T \ln \{ \exp [- (H_x - H_Y) / k_B T] \}_1$$

on el subíndex *0* o *1* indica que el promig de configuracions representatives s'ha de realitzar sobre l'estat inicial *X* o final *Y.*
L'aplicació directa de les expressions anteriors no proporcionarà una estimació precisa de la diferència d'energia lliure si no existeix solapament entre els espais de fase dels dos estats. Això pot solucionar-se introduint estats intermedis que permetin dur a terme una transformació gradual entre *X* i *Y* mitjançant un paràmetre d'acoblament λ, cosa que permet transformar gradualment el hamiltonià H_x en H_y:

$$H_\lambda = \lambda H_x + (1 - \lambda) H_Y \qquad \text{[Eq. A1.17]}$$

La diferència d'energia lliure entre els estats *X* i *Y* es pot finalment obtenir mitjançant la suma de les energies de cadascun del passos:

[a22] Zwanzig, R.W. *J. Chem. Phys.* **1954**, *22*, 1420.

$$\Delta G_X - \Delta G_Y = -k_B T \sum \ln \{ \exp [- (H_\lambda - H_{\lambda+\Delta\lambda}) / k_B T] \}_\lambda \quad \text{[Eq. A1.18]}$$

La qualitat del càlcul pot verificar-se realitzant la perturbació en ambdues direccions, de *X* a *Y* i viceversa (idealment amb un nombre d'etapes suficientment elevat perquè la diferència d'energia entre cadascuna de elles sigui de l'ordre de $K_B T$), sent la histèresi obtinguda una mesura de la convergència del càlcul.

A1.4.2 Integració termodinàmica

Un procediment alternatiu és la integració termodinàmica, que emplea la següent integral per al càlcul de l'energia lliure existent entre els estats *X* i *Y*.

$$\Delta G_{X \to Y} = \int_{\lambda=0}^{\lambda=1} \left({}^{\delta H}/_{\delta \lambda} \right) \lambda \, d\lambda \quad \text{[Eq. A1.19]}$$

Aquesta integral, a la pràctica, es resol realizant una sèrie de simulacions corresponents a valors discrets de λ entre 0 i 1, calculant per a cadascun d'aquests valors el promig. Finalment, la diferència d'energia lliure entre *X* i *Y* pot obtenir-se mitjançant diferències finites aplicades a cadascuna de les etapes de la integració.

A1.4.3 Cicles termodinàmics

En el marc del disseny de fàrmacs, un problema central es la predicció de afinitats relatives per a una sèrie de molècules relacionades estructuralment que interaccionin enfront un mateix receptor. També sol ser comú l'estudi de l'efecte que mutacions puntuals en aquest receptor puguin tenir en la interacció amb el fàrmac. En aquest tipus de problemes els càlculs de diferències d'energia lliure poden resultar una eina molt potent si es combinen amb cicles termodinàmics. Mitjançant aquesta tècnica es poden calcular diferencies d'energia lliure de processos reals a través de rutes fictícies que no tenen sentit físic directe.

Per al càlcul de la diferència d'energia lliure d'un receptor amb dos lligands relacionats estructuralment es pot establir el següent cicle termodinàmic (Figura A1.4).

Explicat d'una altra forma, l'afinitat relativa entre els dos lligands correspon a $\Delta\Delta G = \Delta G_2 - \Delta G_1$. Donat que la interacció del lligand amb el receptor provocarà canvis estructurals tant a nivell de receptor com en la reorganització del solvent, aquests canvis són difícils d'avaluar degut a

la impossibitat d'obtenir un bon mostreig representatiu del receptor en estat lliure i unit. No obstant, l'ús del cicle termodinàmic permet expressar de manera equivalent $\Delta\Delta G=\Delta G_3-\Delta G_4$, on ΔG_3 reflexa la diferència d'energies lliures entre lligands en solució, mentre que ΔG_4 correspon a la diferència d'energia lliure entre els mateixos units al receptor. Si bé aquests processos no corresponen a un procés físic real de laboratori, és factible abordar el seu càlcul per simulació, ja que en ser petites les diferències existents entre lligands, els espais configuracionals han de ser semblants, permetent avaluar les diferències d'energia lliure per les tècniques comentades anteriorment.

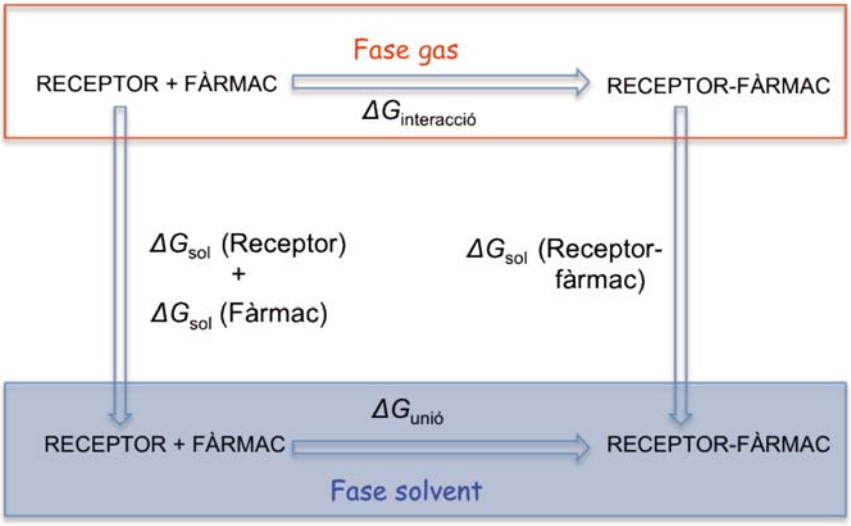

$$\Delta G_{union} = \Delta G_{inter} + \Delta G_{sol}(R\text{-}F) - \Delta G_{sol}(R) - \Delta G_{sol}(F) = \Delta G_{inter} + \Delta\Delta G_{sol}$$

Figura A1.4 Cicle termodinàmic

A1.5 Càlculs SIE

El mètode SIE (Solvent Interaction Energies) va ser desenvolupat per Purisima i col·laboradors [a23,a24] i està formalment relacionat amb el mètode MM/PBSA, que estima l'energia lliure d'interacció entre un lligand i una proteïna diana determinada mitjançant l'ús d'un camp de força clàssic, i un terme de solvatació calculat utilitzant un model continu que inclou els components electrostàtics i no electrostàtics. El mètode SIE ha estat acuradament parametritzat per la calibració de les diferents aportacions energètiques en el context d'un

[a23]Naïm, M.; Bhat, S.; Rankin, K.N.; Dennis, S.; Chowdhury, S.F.; Siddiqi, I.; Drabik, P.; Sulea, T.; Bayly, C. I.; Jakalian, A.; Purisima, E.O. *J. Chem. Inf. Model*. **2007**, *47*, 122. [a24]Cui, Q.; Sulea, T.; Schrag, J.D.; Munger, C.; Hung, M.-N.; Nam, M.; Cygler, M.; Purisima, E.O. *J. Mol. Biol.* **2008**, *379*, 787.

càlcul d'unió a través de la inclusió dels paràmetres adequats per reproduir l'energia lliure d'unió absoluta d'un conjunt de complexos proteïna–lligand. En particular, les afinitats d'unió s'han calculat utilitzant l'equació:

$$\Delta G_{binding} = \alpha\left(E_{ele} + E_{vW} + \Delta G_{ele}^{sol} + \Delta G_{n-ele}^{sol}\right) + C \qquad \text{[Eq. A1.20]}$$

on es representa l'energia electrostàtica (E_{ele}), l'energia de van der Waals (E_{vW}), el terme electrostàtic (ΔG_{ele}^{sol}) solvatat, el terme no-electrostàtic (ΔG_{n-ele}^{sol}) de l'energia de solvatació lliure, que es relaciona amb la superfície accessible al dissolvent (SA; $\Delta G_{n-ele}^{sol} = \gamma\ \Delta SA$), i els paràmetres α, γ, factors de correció de l'entalpia–entropia (α= 0,1048) i la tensió superficial (γ = 0,0129 kcal mol^{-1} A^{-2}) i una constant (C = –2.89 kcal mol^{-1}).

A1.6 Bibliografia Annex 1

a1. Leach, A.R. *Molecular Modelling: Principles and applications,* 2nd edition, **2001**, Pearson Education (Prentice Hall), Essex.
a2. Schlick, T. *Molecular Modeling and Simulation. An interdisciplinary Guide,* **2002**, Springer-Verlag New York, Inc. New York.
a3. Frenkel, D.; Smit, B. *Understanding Molecular Simulation* **2002**, Academic Press.
a4. McCammon, J.A.; Harvey, S.C. *Dynamics of Proteins and Nucleic Acids* **1987**, Cambridge University Press, Cambridge
a5. Weiner, P.K.; Kollman, P. A. *J. Comp. Chem.* **1981**, *2*, 287.
a6. Brooks, B.R.; Bruccoleri, R.E.; Olafson, B.D.; States, D.J.; Swaminathan, S.; Karplus, M. *J. Comp. Chem.* **1983**, *4*, 187.
a7. Allinger, N. L.; Yuh, Y. H.; Lii, J-H.; *J. Am. Chem. Soc.* **1989**, *111*, 8551.
a8. Hwang, M.-J.; Stockfisch, T.P.; Hagler, A.T. *J. Am. Chem. Soc.* **1994**, *116*, 2515.
a9. Allinger, N. L.; Chen, K.; Lii, J-H, *J. Comp. Chem.* **1996**, *17*, 642.
a10. Weiner, S. J.; Kollman, P.A.; Case, D.A.; Singh, U.C.; Ghio, C.; Alagona, G.; Profeta, S.; Weiner, P. *J. Am. Chem. Soc*. **1984,** *106*, 765.
a11. Cornell, W.D.; Cieplak, P.; Bayly, C.I.; Gould, I.R.; Merz, K.M.; Ferguson, D.M.; Spellmeyer, D.C.; Fox, T.; Caldwell, J.W.; Kollman, P.A. *J. Am. Chem. Soc*. **1995**, *117*, 5179.
a12. Bayly, C.I.; Cieplak, P.; Cornell, D.W.; Kollman, P.A. *J. Phys. Chem.* **1993**, *79*, 10269.
a13. Verlet, L. *Phys. Rev.* **1967**, *159*, 98.
a14. Swope, W.C.; Anderson, H.C.; Berens, P.H.; Wilson, K.R. *J. Chem. Phys.* **1982**, *76*, 3271.
a15. Beeman, D. *J. Comp. Phys.* **1976**, *20*, 130.
a16. Hockney, R.W. *Meth. Comp. Phys.* **1970**, *9*, 136.
a17. Ryckaert, J.P.; Cicotti, G.; Berendsen, H.J.C. *J. Comp. Phys.* **1977**, *23*, 327.
a18. Berendsen, H.J.C.; Postma, J.P.M.; van Gunsteren, W.F.; Di Nola, A.; Haak, J.R. *J. Chem. Phys.* **1984**, *81*, 3684.
a19. Hoover, W.G. *Phys. Rev. A.* **1985**, *31*, 1695.
a20. Ewald, P.P. *Ann. Phys*. **1921**, *64*, 253.
a21. Darden, T.L.; York, D.; Pedersen, L. *J. Chem. Phys.* **1993**, *98*, 10089.
a22. Zwanzig, R. W. *J. Chem. Phys.* **1954**, *22*, 1420.

a23. Naïm, M.; Bhat, S.; Rankin, K.N.; Dennis, S.; Chowdhury, S.F.; Siddiqi, I.; Drabik, P.; Sulea, T.; Bayly, C.I.; Jakalian, A.; Purisima, E.O. *J. Chem. Inf. Model*. **2007**, *47*, 122.
a24. Cui, Q.; Sulea, T.; Schrag, J. D.; Munger, C.; Hung, M.-N.; Nam, M.; Cygler, M.; Purisima, E.O. *J. Mol. Biol.* **2008**, *379*, 787.

Annex 2: Altres publicacions i patents

- Camps, P.; Domingo, L.R.; Formosa, X.; **Galdeano, C.**; González, D.; Muñoz-Torrero, D.; Segalés, S.; Font-Bardia, M.; Solans, X. Highly diastereoselective one-pot synthesis of spiro{cyclopenta[*a*]indene-2,2'-indene}diones from 1-indanones and aromatic aldehydes. *Journal of Organic Chemistry* **2006**, *71*, 2464–3471.

- Camps, P.; Formosa, X.; **Galdeano, C.;** Gómez, T.; Muñoz-Torrero, D.; Ramírez, L.; Viayna, E.; Gómez, E.; Isambert, N.; Lavilla, R.; Badia, A.; Clos, M. V.; Bartolini, M.; Mancini, F.; Andrisano, V.; Bidon-Chanal, A.; Huertas, O.; Dafni, T.; Luque, F. J. Tacrine-based dual binding site acetylcholinesterase inhibitors as potential disease-modifying anti-Alzheimer drug candidates. *Chemico-Biological Interactions* **2010**, *187*, 411–415.

- **Galdeano, C**.; Viayna, E.; Arroyo, P.; Bidon-Chanal, A.; Blas, J. R.; Muñoz-Torrero, D.; Luque, F. J. Structural determinants of the multifunctional profile of dual binding site acetylcholinesterase inhibitors as anti-Alzheimer agents. *Current Pharmaceutical Design* **2010**, *16*, 2818–2836.

- Defaux, J.; Sala, M.; Formosa, X.; **Galdeano, C**.; Taylor, M. C.; Alobaid, W. A. A.; Kelly, J. M.; Wright, C. W.; Camps, P.; Muñoz-Torrero, D. Huprines as a new family of dual acting trypanocidal-antiplasmodial agents. *Bioorganic & Medicinal Chemistry* **2011**, *19*, 1702–1707.

- Camps, P.; **Galdeano, C**.; Muñoz-Torrero, D.; Rull, J.; Calvet, T.; Font-Bardia, M. Diastereoselective preparation of (*S*)-(1,4,4-trimethylpyrrolidin-2-yl)amine, a new chiral 1,2-diamine for thiourea type organocatalysts. *Tetrahedron: Asymmetry* **2011,** *22,* 745–751.

- Muñoz-Torrero, D.; Pera, M.; Relat, J.; Ratia, M.; **Galdeano, C**.; Viayna, E.; Sola, I.; Formosa, X.; Camps, P.; Badia, A.; Clos, M.V. Expanding the multipotent profile of huprine-tacrine heterodimers as disease-modifying anti-Alzheimer agents. *Neurodegenerative Diseases* **2012**, *8*, (DOI: 10.1159/000333225).

- Muñoz-Torrero, D.; Camps, P.; Gómez, T.; Viayna, E.; **Galdeano, C**. Compuestos multifuncionales modificadores de la enfermedad de Alzheimer para el tratamiento de esta enfermedad. WO 011/076969 A1, SPAIN, **2010**.